IRREVERSIBLE THERMODYNAMICS AND HYDRODYNAMICS OF BIOLOGICAL MEMBRANES

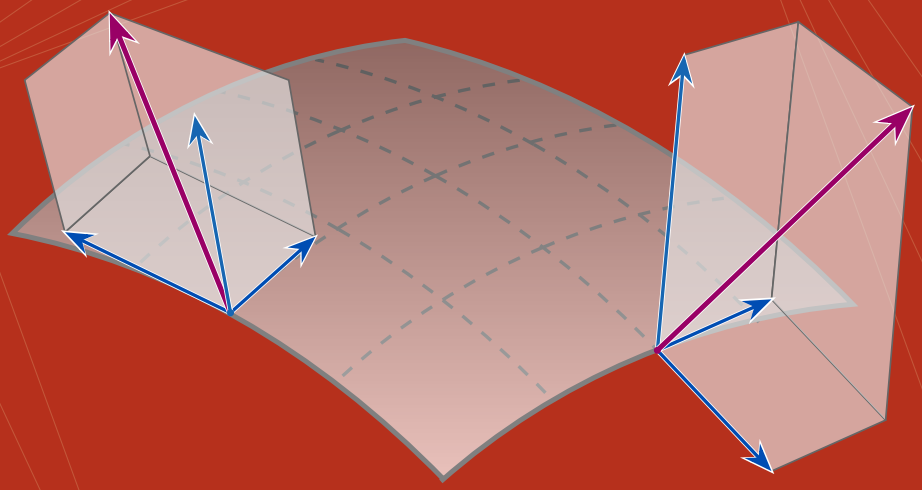

Amaresh Sahu
Kranthi K. Mandadapu

IRREVERSIBLE THERMODYNAMICS AND HYDRODYNAMICS OF BIOLOGICAL MEMBRANES

Thesis by
Amaresh Sahu

In Partial Fulfillment of the Requirements
for the Degree of
Doctor of Philosophy

University of California at Berkeley
Berkeley, California, USA

August 2022

amaresh-sahu.github.io/papers/a-sahu-thesis.pdf

Committee in charge:

Professor Kanthi K. Mandadapu, Chair
Professor Clayton J. Radke
Professor Per-Olof Persson
Professor Karthik Shekhar

ABSTRACT

This thesis is concerned with developing a wholistic description of biological membranes: fascinating materials that make up the boundary of the cell, as well as many of the cell's internal organelles. Our formulation of the theory of such materials relies on two well-known concepts: differential geometry and irreversible thermodynamics. The setting of differential geometry allows us to describe curves and surfaces, which in this case are embedded in the three-dimensional Euclidean space, while irreversible thermodynamics provides a theoretical framework to develop constitutive relations between the various thermodynamic forces and fluxes in a system. Both concepts are well-known, and are reviewed in Part A.

We build on these classic results in Part B, and develop the theory of irreversible thermodynamics for arbitrarily curved and deforming lipid membranes. In particular, we treat the membrane as a two-dimensional surface, in which lipids flow in-plane as a two-dimensional fluid while the membrane bends out-of-plane as an elastic shell. We then obtain the fundamental balance laws of mass, linear momentum, angular momentum, energy, and entropy, as well as the second law of thermodynamics. Finally, we apply the framework of irreversible thermodynamics to determine appropriate constitutive relations, and substitute them into the balance laws to obtain the equations governing membrane dynamics. Our main result is to present the equations of motion and appropriate boundary conditions for three systems of increasing complexity: (*i*) a compressible, inviscid membrane, (*ii*) a compressible, viscous membrane, and (*iii*) an incompressible, viscous membrane.

Part C of this thesis focuses on applications of the single-component theory. We begin by specializing the general governing equations to three commonly observed geometries in biological systems: planar sheets, spherical vesicles, and cylindrical tubes. A scaling analysis of the resultant equations reveals membrane dynamics are governed by two dimensionless numbers. The well-known Föppl–von Kármán number, Γ, compares tension forces to the familiar elastic bending forces, while a new dimensionless quantity—which we name the Scriven–Love number, $\mathcal{SL}$—compares out-of-plane forces arising from the in-plane, intramembrane viscous stresses to bending forces. Calculations of non-negligible Scriven–Love numbers in various biological processes and *in vitro* experiments show in-plane intramembrane viscous flows cannot generally be ignored when analyzing lipid membrane behavior, and can never be ignored in lipid membrane tubes. Moreover, a stability analysis indicates membrane tubes are unstable above a critical value of Γ, while $\mathcal{SL}$ governs the spatiotemporal evolution of the deforming membrane. We close by investigating a novel hydrodynamic instability in which an initially local disturbance to an unstable tube yields propagating fronts, which leave a thin atrophied tube in their wake. Depending on the value of the Föppl–von Kármán number Γ, the thin tube is connected to the unperturbed regions via oscillatory or monotonic shape transitions—reminiscent of recent experimental observations on the retraction and atrophy of axons.

Berkeley, California A. S.
August 2022

ACKNOWLEDGMENTS

Even after six years as a graduate student, it is still hard to believe my time at Berkeley has officially come to an end. I have many people to thank for making my doctoral experience so enjoyable.

First and foremost, I would like to thank my Ph.D. advisor, Prof. Kranthi Mandadapu. Kranthi and I first met over seven years ago, in April 2015, when I was a software engineer in San Francisco and he was a postdoc in theoretical chemistry at Berkeley. At the time, I sought a research opportunity (on the side of my day job) to strengthen my application to graduate programs. Kranthi and I were introduced by our mutual acquaintance, Michelle Liu: my friend and lab partner from undergrad, who was also studying theoretical chemistry at Berkeley—and whose office was adjacent to Kranthi's.

Kranthi and I started off by exchanging a few emails, and I began reading papers on dynamical phase transitions in glasses. Then, on one fateful Monday at the end of April, I took the train after work to meet him. I don't remember much from our initial discussion, though it ended with Kranthi mentioning another one of his research interests: biological membranes. I distinctly recall him saying the phrase "Christoffel symbols" and talking about how one had to use differential geometry to describe the kinematics and dynamics of such materials. [‡] From that point on, I was hooked.

Over the next year, I spent my nights and weekends thinking about biological membranes. Kranthi and I discussed weekly, in the evenings: after the workday was over, I took the train from San Francisco to Berkeley, and we met at the *Berkeley Espresso* coffee shop—which was closer to the train station than his office was. In the hours discussing material time derivatives, phenomenological coefficients, and entropy production, I experienced the pleasure of developing a theory. It is hard to describe how transformative these discussions were, as it was through them I found my calling as a scientist. For the many late nights in *Berkeley Espresso,* and the countless hours spent discussing since then, I also offer my most sincere appreciation to Kranthi's wife, Deepthi—for the patience she had, and continues to have, for the both of us.

It is a pleasure to thank my co-workers. Yannick Omar and I developed numerical methods to simulate the dynamics of biological membranes, and his expertise with both theory and simulation was invaluable. Alec Glisman was an undergrad during the two years we worked together, and it was satisfying to see him form a scientific philosophy as we linearized and non-dimensionalized the membrane equations. Sho Takatori and I started a collaboration after a chance encounter: when Sho interviewed at Berkeley, he presented unpublished experimental data that sparked my interest. Almost a year later, we set out to quantitatively describe his measurements, and it was exciting to combine our perspectives to arrive at an understanding together. [†] Finally, I thank Joël Tchoufag for the many intellectual adven-

[‡] Relevant concepts from differential geometry, including Christoffel symbols, are presented in Chapter II.

[†] Our work together was independent of this thesis, and so is not discussed here. Details can be found in S.C. Takatori and A. Sahu. "Active contact forces drive nonequilibrium fluctuations in membrane vesicles". *Phys. Rev. Lett.* **124** (2020), 158102. arXiv: 1911.01337.

tures. He joined the group shortly after I did, and though we discussed science often, it wasn't until the end of my third year that we started working together. The following 12 months were my most productive at Berkeley, and my biggest regret from graduate school is that Joël and I didn't start working together sooner.

Kranthi's research group, and his connections to Berkeley, played an important role in my doctoral experience. Clay Batton and I were the group's first graduate students, and together we attracted Muhammad Hasyim the following year. I fondly remember those early days. Since then, the lab has grown considerably, and I appreciate how the philosophy of slow and careful science remains constant. This methodology underlies the ongoing theoretical advancements by Yannick, Ahmad Alkadri, and Joshua Fernandes; I continue to learn about membrane behavior from all of them. Within the chemical engineering community more broadly, I am grateful for my interactions with Profs. Carlo Carraro, Clay Radke, Susan Muller, David Limmer, Bryan McCloskey, and Karthik Shekhar. It was also a pleasure to meet with and receive advice from Kranthi's own Ph.D. advisor, Prof. Panayiotis Papadopoulos, who was always a calm voice of reason.

I owe much to those who shaped me before my time at Berkeley, and who in turn had a profound impact on my academic career. Through their example, my parents—Urmila and Devaraj Sahu—instilled in me the value of hard, honest work. My older brother, Ashutosh, passed down his insights, while my younger brother, Vikash, was always there when I needed him—including in my first year at Berkeley, when I couldn't locate the bug in an in-house membrane code.[‡] I thank my best friends from high school, Richard Zhao, Anshu Rustagi, and Bryan Huang, for teaching me much that school could not; their influences are clearly reflected in the person I am today. Hannah Guan was available throughout my journey to lend her perspective, which I will always value. Eric An continues to be a constant in my life; without his encouragement in undergrad, I may not have graduated with a physics minor. My roommates and closest friends at Princeton, Akhil Reddy and Sagar Vijay, helped me realize what true determination can result in. They continue to inspire me with their own excellence. Finally, Prof. Howard Stone was a wonderful advisor during my undergraduate years, and his enthusiasm for fluid mechanics and scaling laws was infectious. It was also on his recommendation that I sought a research advisor while working in San Francisco, and so in some ways Howard guided me to Kranthi.

I close by thanking my wife, Sarah. She helped me realize I was lost in the months after Princeton, and it was only with her love that I found my way. The long journey to this thesis began in an effort to make her proud; my hope now at the close is that I succeeded. I cannot express enough my gratitude for her constant love and support over the last decade, and I dedicate this thesis to her.

[‡]See the Acknowledgments, on page 1075, of Y.A.D. Omar et al. "Non-axisymmetric shapes of biological membranes from locally induced curvature". *Biophys. J.* **119** (2020), 1065–1077.

For Sarah

Contents

Part B Theory

Chapter I

Introduction and Overview

> *I took a good clear piece of Cork, and . . . cut a piece off, . . . examining it very diligently with a Microscope . . . I could exceedingly plainly perceive it to be all perforated and porous, much like a Honey-comb . . . these pores, or cells, were not very deep, but consisted of a great many little boxes . . . these . . . were indeed the first microscopical pores I ever saw, and perhaps, that were ever seen, for I had not met with any Writer or Person, that had made any mention of them before this . . .*
>
> —Robert Hooke, 1665 [‡]

Biological membranes are unique materials comprised of lipids and proteins, which make up the boundary of the cell and many of the cell's internal organelles. A primary component of such membranes are phospholipid molecules, which have a hydrophilic head group and two hydrophobic tails—for which a bilayer is energetically favorable in an aqueous environment (see Fig. 1). One important feature of lipid bilayers is that they are essentially two-dimensional: bilayers are roughly five nanometers thick, but their other two spatial dimensions can span tens of microns. Moreover, the bilayer structure allows biological membranes to act as protective barriers, as their hydrophobic interior prevents ions, proteins, and other water-soluble compounds from passing through them. In this manner, biological membranes serve an essential role in separating the cell from its surroundings, and also compartmentalizing many of the cell's internal organelles.

While biological membranes are often viewed as simply being static, semipermeable barriers protecting their internal contents, they in fact play a dynamic role in many cellular processes. Endocytosis, for example, begins when proteins in the surrounding fluid bind to the cell membrane's constituent lipids and proteins at a specific location. The bound proteins locally induce a shallow invagination, to which additional proteins are recruited. A mature bud eventually develops, and then pinches off into a membrane-bound vesicle that enters the cell. [†] This vesicular membrane contains lipids and proteins that were previously on the cell boundary, and furthermore the vesicle may enclose nutrients or other cargo. Endocytosis is

[‡]R. Hooke. *Micrographia: or, Some Physiological Descriptions of Minute Bodies made by Magnifying Glasses. With Observations and Inquiries thereupon.* London: Royal Society of London, 1665

[†]M.K. Higgins and H.T. McMahon. "Snap-shots of clathrin-mediated endocytosis". *Trends Biochem. Sci.* **27** (2002), 257–263.

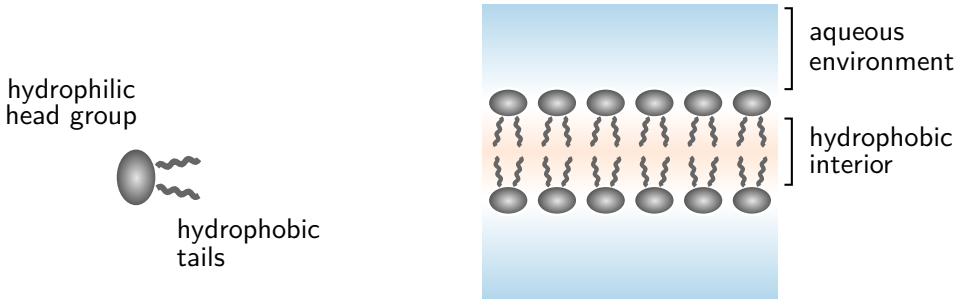

(a) phospholipid molecule (b) lipid bilayer

Figure 1: Schematics of (a) a generic phospholipid molecule and (b) a portion of the lipid bilayer. Phospholipid molecules are amphiphilic, with a hydrophilic head group and two hydrophobic, fatty acid tails. In an aqueous environment, a bilayer is energetically favorable. Moreover, the bilayer structure gives rise to the material's in-plane fluidity and out-of-plane elasticity.

thus a key process in transferring nutrients to the cell, regulating the expression of proteins on the cell surface, and maintaining cell homeostasis. [‡]

Another dynamic behavior of biological membranes is the rearrangement of the many types of constituent lipids and proteins to form heterogeneous domains. For example, T cell receptors form specific patterns at the immunological synapse when detecting antigens [†, *]—a phenomenon which is sensitive to the rates of receptor binding and unbinding. [§, ♯] It is also well-known that membrane lipids can phase separate into liquid-ordered (L_o) and liquid-disordered (L_d) domains, which coexist in many biological settings. [‖, ∀] A first-order phase transition separates the two phases, and the associated line tension of the interface is relevant when characterizing membrane behavior. For instance, in phase-separated systems, either the L_o or L_d domains were observed to bulge outward to reduce the line tension between the two phases. [◇, $] The boundary between L_o and L_d domains is also relevant in the fusion of HIV-containing vesicles with target immune cells, as (*i*) fusion proteins primarily reside at

[‡]H.T. McMahon and E. Boucrot. "Molecular mechanism and physiological functions of clathrin-mediated endocytosis". *Nat. Rev. Mol. Cell Bio.* **12** (2011), 517–533.

[†]S.Y. Qi, J.T. Groves, and A.K. Chakraborty. "Synaptic pattern formation during cellular recognition". *Proc. Natl. Acad. Sci. U.S.A.* **98** (2001), 6548–6553.

[*]A. Carlson and L. Mahadevan. "Elastohydrodynamics and kinetics of protein patterning in the immunological synapse". *PLoS. Comput. Biol.* **11** (2015), 1–16.

[§]M.M. Davis et al. "Ligand recognition by $\alpha\beta$ T cell receptors". *Annu. Rev. Immunol.* **16** (1998), 523–544.

[♯]K. Matsui et al. "Kinetics of T-cell receptor binding to peptide/I-Ek complexes: Correlation of the dissociation rate with T-cell responsiveness". *Proc. Natl. Acad. Sci. U.S.A.* **91** (1994), 12862–12866.

[‖]S.L. Veatch and S.L. Keller. "Seeing spots: Complex phase behavior in simple membranes". *BBA-Mol. Cell Res.* **1746** (2005), 172–185.

[∀]S.L. Veatch et al. "Critical fluctuations in plasma membrane vesicles". *ACS Chem. Biol.* **3** (2008), 287–293.

[◇]S.L. Veatch and S.L. Keller. "Separation of liquid phases in giant vesicles of ternary mixtures of phospholipids and cholesterol". *Biophys. J.* **85** (2003), 3074–3083.

[$]T. Baumgart, S.T. Hess, and W.W. Webb. "Imaging coexisting fluid domains in biomembrane models coupling curvature and line tension". *Nature* **425** (2003), 821–824.

the interface between the two phases, and (*ii*) fusion is believed to be favorable because it reduces the total line tension energy between the two phases. [‡]

In the aforementioned phenomena, and in biological systems more generally, lipid membranes often undergo morphological shape changes over several seconds, in which deformations occur over hundreds of nanometers. Over such length and time scales, biological membranes behave as unique materials in which lipids flow in-plane as a two-dimensional fluid, while the entire membrane bends out-of-plane as an elastic shell. To understand this constitutive behavior, we again consider the bilayer structure, as shown in Fig. 1. We first recognize lipids and proteins are free to move around within the plane of the membrane: such displacements maintain the separation between the hydrophobic interior and the surrounding fluid, and thus do not cost energy. Moreover, under physiological conditions, there is no in-plane restoring force to return lipids and proteins to a prior configuration—as evident from experimental investigations of the in-plane diffusion and coarsening of multi-component membranes. [†, *] The in-plane movement of lipids is thus irreversible, and biological membranes have an in-plane fluidity.

The out-of-plane elasticity of lipid membranes can also be understood from the bilayer structure. In particular, the out-of-plane movement of individual lipids is energetically costly because it exposes the membrane's hydrophobic interior to the surrounding, aqueous environment. Accordingly, out-of-plane membrane deformations are largely restricted to shape changes over longer length scales, for which the relative out-of-plane displacement between adjacent phospholipid molecules remains small. The resultant deformations tend to compress one of the bilayer leaflets and stretch the other—both of which cost energy, in a manner reminiscent of the bending of elastic beams and shells. [§] In particular, the out-of-plane displacement of lipids during a deformation is reversible, as the lipids can be returned to their original configuration via an elastic restoring force. [♯] With this understanding, we recognize that over longer length and time scales, biological membranes deform in the out-of-plane direction as an elastic shell.

Despite experimental evidence for the dynamic nature and unique constitution of biological membranes, the physical mechanisms underlying membrane behavior remain poorly understood. Accordingly, theoretical efforts are required to gain deeper insights into the many biological phenomena involving lipid membranes—some of which are described above. The goal of this thesis is to develop a comprehensive theory of lipid membrane behavior, with a particular emphasis on how the in-plane and out-of-plane dynamics are coupled in giving rise to a variety of complex biological phenomena. In what follows, we present our systematic developments.

[‡]S.-T. Yang, V. Kiessling, and L.K. Tamm. "Line tension at lipid phase boundaries as driving force for HIV fusion peptide-mediated fusion". *Nat. Commun.* **7** (2016), 11401–11409.

[†]P. Cicuta, S.L. Keller, and S.L. Veatch. "Diffusion of liquid domains in lipid bilayer membranes". *J. Phys. Chem. B* **111** (2007), 3328–3331. arXiv: `cond-mat/0611492`.

[*]C.A. Stanich et al. "Coarsening dynamics of domains in lipid membranes". *Biophys. J.* **105** (2013), 444–454.

[§]P.M. Naghdi. "Finite Deformation of Elastic Rods and Shells". *Proceedings of the IUTAM Symposium on Finite Elasticity.* Ed. by D.E. Carlson and R.T. Shield. Dordrecht: Springer Netherlands, 1982, pp. 47–103.

[♯]E.A. Evans. "Bending resistance and chemically induced moments in membrane bilayers". *Biophys. J.* **14** (1974), 923–931.

1. The goals of this thesis

In developing a lipid membrane theory, the phenomena we seek to describe motivate certain choices for our models. For example, to describe membrane deformations over several seconds and hundreds to thousands of nanometers, we employ the balance law formalism of continuum mechanics. [‡] Next, because biological membranes are so thin relative to their other spatial dimensions, they are treated as a single two-dimensional surface embedded in the surrounding, three-dimensional space. In doing so, we implicitly assume no slip between the two bilayer leaflets as the membrane deforms. At this point, we realize that biological membranes are capable of undergoing arbitrarily large morphological shape transitions—for which it is prohibitively difficult to use standard Cartesian, cylindrical, and spherical coordinate systems to describe the membrane surface. Moreover, we seek to apply balance laws on this highly curved surface, which is itself deforming over time. These issues are addressed by employing the techniques of differential geometry, with which the membrane evolution and associated balance laws can naturally be expressed. The basic concepts of differential geometry are reviewed in Chapter II.

Another complexity in developing biological membrane models lies in the nontrivial coupling between in-plane and out-of-plane behaviors—with some being elastic, and others being dissipative. In fact, all of the membrane phenomena described above involve the out-of-plane elastic bending being fully coupled to the irreversible processes of (*i*) the in-plane flow of lipids, (*ii*) the in-plane diffusion of lipids and proteins, and (*iii*) the binding of peripheral proteins to the membrane surface. While comprehensive models are needed to fully understand the complex behavior of biological membranes, developing such models is difficult because of the aforementioned coupling between various processes. Prior theoretical efforts instead focused on the dynamics about specific geometries, [†, *, §] or considered surface flows on a stationary membrane and their coupling to the hydrodynamics of the surrounding fluid. [♯, ‖] In addition, more general geometric frameworks relying on variational methods were also established. [∀, ◇, $] However, while the formulation of models from variational models is theoretically sound, the techniques involved are not easily extendable to model the coupling between membrane bending, lipid flow, species diffusion, and chemical reactions.

[‡] P. Chadwick. *Continuum Mechanics: Concise Theory and Problems*. 2nd ed. Mineola: Dover, 1999.

[†] N. Dan, P. Pincus, and S.A. Safran. "Membrane-induced interactions between inclusions". *Langmuir* **9** (1993), 2768–2771.

[*] T.R. Powers, G. Huber, and R.E. Goldstein. "Fluid-membrane tethers: Minimal surfaces and elastic boundary layers". *Phys. Rev. E* **65** (2002), 041901. arXiv: `cond-mat/0201290`.

[§] J.K. Sigurdsson, F.L.H. Brown, and P.J. Atzberger. "Hybrid continuum-particle method for fluctuating lipid bilayer membranes with diffusing protein inclusions". *J. Comp. Phys.* **252** (2013), 65–85.

[♯] J.K. Sigurdsson and P.J. Atzberger. "Hydrodynamic coupling of particle inclusions embedded in curved lipid bilayer membranes". *Soft Matter* **12** (2016), 6685–6707. arXiv: `1601.06461`.

[‖] B.J. Gross and P.J. Atzberger. "Hydrodynamic flows on curved surfaces: Spectral numerical methods for radial manifold shapes". *J. Comp. Phys.* **371** (2018), 663–689. arXiv: `1803.07594`.

[∀] R. Capovilla and J. Guven. "Stresses in lipid membranes". *J. Phys. A: Math. Gen.* **35** (2002), 6233–6247. arXiv: `cond-mat/0203148`.

[◇] A. Agrawal and D.J. Steigmann. "Modeling protein-mediated morphology in biomembranes". *Biomech. Model. Mechan.* **8** (2009), 371–379.

[$] M. Rahimi and M. Arroyo. "Shape dynamics, lipid hydrodynamics, and the complex viscoelasticity of bilayer membranes". *Phys. Rev. E* **86** (2012), 11932–11946.

In our prior work, [‡] we developed comprehensive membrane models through the framework of irreversible thermodynamics, within a differential geometric setting. In doing so, we determined the coupling between all the reversible and irreversible processes mentioned thus far. In general, irreversible thermodynamics provides a natural way to determine the fluxes and stresses in any system, as demonstrated in Chapter III—where we review the most relevant concepts of this framework in the context of a three-dimensional, bulk material. In doing so, we demonstrate how the equations governing a Newtonian fluid and linear elastic solid can both be obtained from a single application of the theory. While none of the results of this chapter are new, many of the ideas will be useful when developing a lipid membrane theory in Part B. We note that only single-component membranes are considered in this thesis, and we direct interested readers to our earlier study [‡] for the equations governing biological membranes in more complicated settings. Given the limited scope of the presentation in this thesis, it is important to mention we were not the first to present the equations governing a single-component, arbitrarily curved and deforming lipid membrane. In fact, three prior independent investigations [†, *, §] arrived at these equations via different methods—with the timeline of previous efforts discussed in Chapter IV.

After the single-component membrane equations are systematically obtained, we investigate the hydrodynamic stability of these equations in Part C. We focus on the three predominantly observed membrane geometries in biological systems: flat patches, spherical vesicles, and cylindrical tubes—each of which is a static solution to the governing membrane equations. For each geometry, the linearized dynamical equations about the base configuration are determined, and then subsequently non-dimensionalized via a scaling analysis. We close our investigation of each morphology by examining the membrane's hydrodynamic stability, i.e. its response to infinitesimal perturbations. The general findings of our analysis are summarized in Chapter VI, with Chapters VII, VIII, and IX respectively containing the detailed calculations for flat patches, spherical vesicles, and cylindrical tubes.

References

[1] A. Agrawal and D.J. Steigmann. "Modeling protein-mediated morphology in biomembranes". *Biomech. Model. Mechan.* **8** (2009), 371–379

[2] M. Arroyo and A. DeSimone. "Relaxation dynamics of fluid membranes". *Phys. Rev. E* **79** (2009), 31915–31931

[3] T. Baumgart, S.T. Hess, and W.W. Webb. "Imaging coexisting fluid domains in biomembrane models coupling curvature and line tension". *Nature* **425** (2003), 821–824

[‡] A. Sahu et al. "Irreversible thermodynamics of curved lipid membranes". *Phys. Rev. E* **96** (2017), 042409. arXiv: 1701.06495

[†] D. Hu, P. Zhang, and W. E. "Continuum theory of a moving membrane". *Phys. Rev. E* **75** (2007), 041605.

[*] M. Arroyo and A. DeSimone. "Relaxation dynamics of fluid membranes". *Phys. Rev. E* **79** (2009), 31915–31931.

[§] P. Rangamani et al. "Interaction between surface shape and intra-surface viscous flow on lipid membranes". *Biomech. Model. Mechan.* **12** (2012), 833–845.

[4] R. Capovilla and J. Guven. "Stresses in lipid membranes". *J. Phys. A: Math. Gen.* **35** (2002), 6233–6247. arXiv: cond-mat/0203148

[5] A. Carlson and L. Mahadevan. "Elastohydrodynamics and kinetics of protein patterning in the immunological synapse". *PLoS. Comput. Biol.* **11** (2015), 1–16

[6] P. Chadwick. *Continuum Mechanics: Concise Theory and Problems*. 2nd ed. Mineola: Dover, 1999

[7] P. Cicuta, S.L. Keller, and S.L. Veatch. "Diffusion of liquid domains in lipid bilayer membranes". *J. Phys. Chem. B* **111** (2007), 3328–3331. arXiv: cond-mat/0611492

[8] N. Dan, P. Pincus, and S.A. Safran. "Membrane-induced interactions between inclusions". *Langmuir* **9** (1993), 2768–2771

[9] M.M. Davis et al. "Ligand recognition by $\alpha\beta$ T cell receptors". *Annu. Rev. Immunol.* **16** (1998), 523–544

[10] E.A. Evans. "Bending resistance and chemically induced moments in membrane bilayers". *Biophys. J.* **14** (1974), 923–931

[11] B.J. Gross and P.J. Atzberger. "Hydrodynamic flows on curved surfaces: Spectral numerical methods for radial manifold shapes". *J. Comp. Phys.* **371** (2018), 663–689. arXiv: 1803.07594

[12] M.K. Higgins and H.T. McMahon. "Snap-shots of clathrin-mediated endocytosis". *Trends Biochem. Sci.* **27** (2002), 257–263

[13] R. Hooke. *Micrographia: or, Some Physiological Descriptions of Minute Bodies made by Magnifying Glasses. With Observations and Inquiries thereupon*. London: Royal Society of London, 1665

[14] D. Hu, P. Zhang, and W. E. "Continuum theory of a moving membrane". *Phys. Rev. E* **75** (2007), 041605

[15] K. Matsui et al. "Kinetics of T-cell receptor binding to peptide/I-Ek complexes: Correlation of the dissociation rate with T-cell responsiveness". *Proc. Natl. Acad. Sci. U.S.A.* **91** (1994), 12862–12866

[16] H.T. McMahon and E. Boucrot. "Molecular mechanism and physiological functions of clathrin-mediated endocytosis". *Nat. Rev. Mol. Cell Bio.* **12** (2011), 517–533

[17] P.M. Naghdi. "Finite Deformation of Elastic Rods and Shells". *Proceedings of the IUTAM Symposium on Finite Elasticity*. Ed. by D.E. Carlson and R.T. Shield. Dordrecht: Springer Netherlands, 1982, pp. 47–103

[18] T.R. Powers, G. Huber, and R.E. Goldstein. "Fluid-membrane tethers: Minimal surfaces and elastic boundary layers". *Phys. Rev. E* **65** (2002), 041901. arXiv: cond-mat/0201290

[19] S.Y. Qi, J.T. Groves, and A.K. Chakraborty. "Synaptic pattern formation during cellular recognition". *Proc. Natl. Acad. Sci. U.S.A.* **98** (2001), 6548–6553

[20] M. Rahimi and M. Arroyo. "Shape dynamics, lipid hydrodynamics, and the complex viscoelasticity of bilayer membranes". *Phys. Rev. E* **86** (2012), 11932–11946

[21] P. Rangamani et al. "Interaction between surface shape and intra-surface viscous flow on lipid membranes". *Biomech. Model. Mechan.* **12** (2012), 833–845

[22] A. Sahu et al. "Irreversible thermodynamics of curved lipid membranes". *Phys. Rev. E* **96** (2017), 042409. arXiv: 1701.06495

[23] J.K. Sigurdsson and P.J. Atzberger. "Hydrodynamic coupling of particle inclusions embedded in curved lipid bilayer membranes". *Soft Matter* **12** (2016), 6685–6707. arXiv: 1601.06461

[24] J.K. Sigurdsson, F.L.H. Brown, and P.J. Atzberger. "Hybrid continuum-particle method for fluctuating lipid bilayer membranes with diffusing protein inclusions". *J. Comp. Phys.* **252** (2013), 65–85

[25] C.A. Stanich et al. "Coarsening dynamics of domains in lipid membranes". *Biophys. J.* **105** (2013), 444–454

[26] S.L. Veatch and S.L. Keller. "Seeing spots: Complex phase behavior in simple membranes". *BBA-Mol. Cell Res.* **1746** (2005), 172–185

[27] S.L. Veatch and S.L. Keller. "Separation of liquid phases in giant vesicles of ternary mixtures of phospholipids and cholesterol". *Biophys. J.* **85** (2003), 3074–3083

[28] S.L. Veatch et al. "Critical fluctuations in plasma membrane vesicles". *ACS Chem. Biol.* **3** (2008), 287–293

[29] S.-T. Yang, V. Kiessling, and L.K. Tamm. "Line tension at lipid phase boundaries as driving force for HIV fusion peptide-mediated fusion". *Nat. Commun.* **7** (2016), 11401–11409

Part A

Basic Concepts

Chapter II

Differential Geometry

> *In order to describe their mechanics, it is essential to give serious consideration to the differential geometry of time-dependent surfaces.*
>
> —Allen M. Waxman, 1984 [‡]

A characteristic feature of lipid membranes is that their thickness, roughly five nanometers, is much smaller than either of their other two spatial dimensions—typically hundreds of nanometers to tens of microns. Consequently, within our continuum description, lipid membranes are modeled as two-dimensional surfaces embedded in the Euclidean 3-space $\mathbb{R}^3$. Lipid membranes can also undergo arbitrarily large shape deformations, and we seek to develop balance laws and determine the equations of motion on such configurations. It is therefore necessary to describe the geometry of an arbitrarily curved surface, for which we turn to the formalism of differential geometry. This chapter is meant to call attention to the most relevant features of the subject, but for those seeking a deeper understanding we refer the reader to the works by S. Carroll [†] and D.J. Struik. [*] We assume the reader is familiar with the general concepts of vectors and tensors.

1. The geometry of curves

The description of a one-dimensional curve embedded in $\mathbb{R}^3$ is well-known from vector calculus, yet we review several concepts here due to their utility in understanding the more complicated geometry of surfaces. Suppose we have a curve $\mathcal{C}$ parametrized by a general variable θ, such that the position of the curve $\boldsymbol{x}$ is given by

$$\boldsymbol{x} = \boldsymbol{x}(\theta) \ . \tag{1}$$

Equation (1) indicates that for any value of the parameter θ, the position of a point on the curve, $\boldsymbol{x}$, is specified in $\mathbb{R}^3$. A schematic of such a curve is depicted in Fig. 1.

It is a well-known result of vector calculus that for a curve of the form given in Eq. (1), the quantity $\mathrm{d}\boldsymbol{x}/\mathrm{d}\theta$ is a vector tangent to the curve. For example, if the curve represents the

[‡] A.M. Waxman. "Dynamics of a couple-stress fluid membrane". *Studies Appl. Math.* **70** (1984), 63–86.
[†] S. Carroll. "Lecture notes on general relativity". *arXiv preprint* (1997). arXiv: gr-qc/9712019.
[*] D.J. Struik. *Lectures on Classical Differential Geometry*. 2nd ed. New York: Dover, 1988.

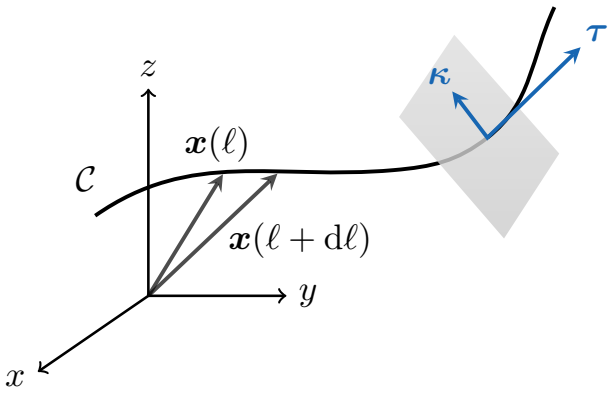

Figure 1: A schematic of a curve $\mathcal{C}$ in $\mathbb{R}^3$. The curve is arc length parametrized, such that $\theta = \ell$. At a single point, the unit tangent $\boldsymbol{\tau}$ and curvature vector $\boldsymbol{\kappa}$ are shown. Note $\boldsymbol{\kappa}$ lies in the plane normal to $\boldsymbol{\tau}$, depicted in light gray.

trajectory of a point particle parametrized by the time t, the quantity $\mathrm{d}\boldsymbol{x}/\mathrm{d}t$ is the velocity of the particle—which points in the direction of the curve. In another example, consider a curve parametrized by its arc length ℓ, for which $(\mathrm{d}\ell)^2 = \mathrm{d}\boldsymbol{x} \cdot \mathrm{d}\boldsymbol{x}$.. The unit tangent to the curve, $\boldsymbol{\tau}$, satisfies $\boldsymbol{\tau} \cdot \boldsymbol{\tau} = 1$ and is given by

$$\boldsymbol{\tau} := \frac{\mathrm{d}\boldsymbol{x}}{\mathrm{d}\ell} \, . \tag{2}$$

The unit tangent to the curve only carries information about the curve's orientation, and changes in $\boldsymbol{\tau}$ along the length of the curve $\mathcal{C}$ indicate the curve is bending. Accordingly, we define the curvature vector $\boldsymbol{\kappa}$ as

$$\boldsymbol{\kappa} := \frac{\mathrm{d}\boldsymbol{\tau}}{\mathrm{d}\ell} \, . \tag{3}$$

Both the unit tangent $\boldsymbol{\tau}$ and curvature vector $\boldsymbol{\kappa}$ are depicted in Fig. 1. Intuitively, for a straight line the unit tangent $\boldsymbol{\tau}$ will not change along the length of the curve, and so the curvature vector $\boldsymbol{\kappa} = \mathbf{0}$. Furthermore, by taking the derivative of the identity $\boldsymbol{\tau} \cdot \boldsymbol{\tau} = 1$ with respect to ℓ, we find $\boldsymbol{\kappa} \cdot \boldsymbol{\tau} = 0$, such that the curvature vector lies entirely in the plane normal to the curve.

As mentioned earlier, we presented the well-known description of a parametrized curve in $\mathbb{R}^3$ to review familiar concepts and develop an intuition which will aid in the study of surface geometries. Indeed, when analyzing a surface it is often helpful to consider a curve on the surface and then recall the above concepts. Two especially useful results are as follows: (i) the derivative of a position vector field with respect to a parametric variable yields a vector tangent to the curve, and (ii) the derivative of the tangent vector with respect to a parametric variable quantifies the curvature.

2. The geometry of surfaces

Just as the position of a curve is parametrized by a single variable θ, the position of a two-dimensional surface is parametrized by two variables—which we denote θ^1 and θ^2. Ac-

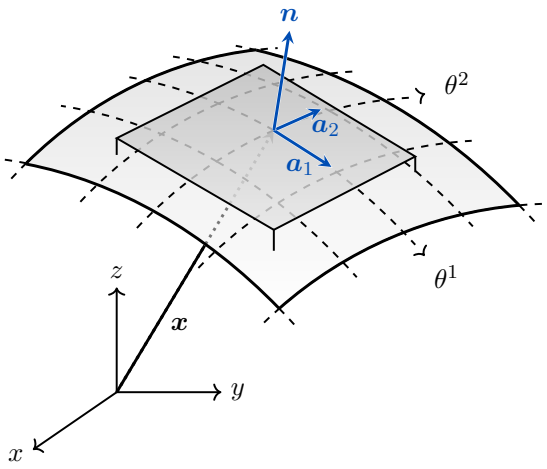

Figure 2: A schematic of a parametrized surface. Lines of constant θ^α are depicted with dotted lines, and the tangent plane at a particular point $\boldsymbol{x}$ is shown in gray. The tangent plane is defined by the two in-plane basis vectors $\boldsymbol{a}_1$ and $\boldsymbol{a}_2$, which in turn define the unit normal to the surface $\boldsymbol{n}$.

cordingly, the position of the surface is written as

$$\boldsymbol{x} \;=\; \boldsymbol{x}(\theta^1, \theta^2) \;. \tag{4}$$

As a shorthand from now on, α and other Greek indices span the set $\{1, 2\}$, such that θ^α refers to both θ^1 and θ^2, and the position in Eq. (4) can be written as $\boldsymbol{x} = \boldsymbol{x}(\theta^\alpha)$.

With the surface position given in Eq. (4), we construct curves of constant θ^α by holding either θ^1 or θ^2 fixed and allowing the other coordinate to vary (Fig. 2). These curves will in general not be arc length parametrized, so the vectors $\partial\boldsymbol{x}/\partial\theta^\alpha$ will be tangent to the curve but in general will not be normalized. We denote the tangent vectors induced by the parametrization as

$$\boldsymbol{a}_\alpha \;:=\; \boldsymbol{x}_{,\alpha} \;, \tag{5}$$

where here and from now on we use the shorthand $(\,\cdot\,)_{,\alpha} := \partial(\,\cdot\,)/\partial\theta^\alpha$ to denote the partial derivative with respect to θ^α.

Now consider two curves—one of constant θ^1 and one of constant θ^2—crossing at a point $\boldsymbol{x}$. Because θ^1 and θ^2 parametrize the surface, the tangent vectors $\boldsymbol{a}_1$ and $\boldsymbol{a}_2$ at that point are linearly independent and thus form a basis of the tangent plane at $\boldsymbol{x}$, as shown in Fig. 2. The basis vectors $\{\boldsymbol{a}_\alpha\}$ play a fundamental role in describing the geometry of a surface, and we now describe several of their important properties.

(a). The metric tensor

For a general surface, the change in position $\mathrm{d}\boldsymbol{x}$ resulting from differential changes in the parametrized values $\mathrm{d}\theta^\alpha$ is given by

$$\mathrm{d}\boldsymbol{x} \;=\; \sum_{\alpha=1}^{2} \boldsymbol{x}_{,\alpha}\,\mathrm{d}\theta^\alpha \;=\; \boldsymbol{a}_\alpha\,\mathrm{d}\theta^\alpha \;, \tag{6}$$

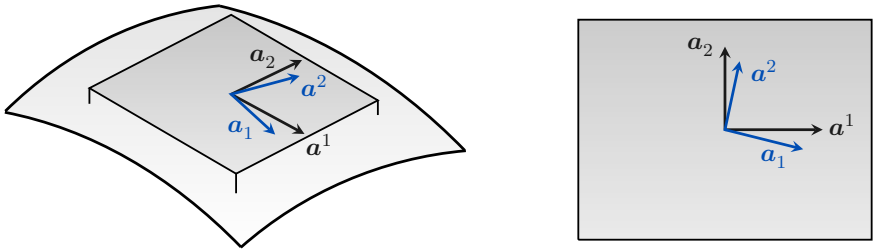

(a) (b)

Figure 3: The relationship between the covariant and contravariant bases vectors. In (a), the in-plane basis vectors are portrayed on the tangent plane above a surface. In (b), we zoom in on the tangent plane. Note $\boldsymbol{a}^1$ and $\boldsymbol{a}_2$, as well as $\boldsymbol{a}_1$ and $\boldsymbol{a}^2$, are required to be orthogonal.

where in the second equality we substituted Eq. (5) and introduced the Einstein summation convention—in which indices repeated in a superscript and subscript are always summed over. We use this convention throughout for notational convenience. To find the length of the differential element in Eq. (6), we calculate

$$|\mathrm{d}\boldsymbol{x}|^2 \;=\; \mathrm{d}\boldsymbol{x}\cdot\mathrm{d}\boldsymbol{x} \;=\; \boldsymbol{a}_\alpha \mathrm{d}\theta^\alpha \cdot \boldsymbol{a}_\beta \mathrm{d}\theta^\beta \;=\; a_{\alpha\beta}\,\mathrm{d}\theta^\alpha\,\mathrm{d}\theta^\beta \;. \tag{7}$$

In the last term of Eq. (7) we introduced the metric tensor $a_{\alpha\beta}$ (sometimes referred to as the covariant metric tensor), defined as

$$a_{\alpha\beta} \;:=\; \boldsymbol{a}_\alpha \cdot \boldsymbol{a}_\beta \tag{8}$$

and so-called because it relates changes in the parametrization to a length measured on the surface. Note that as the indices 'α' and 'β' span the set $\{1,2\}$, the metric tensor has four components: $a_{11} = \boldsymbol{a}_1\cdot\boldsymbol{a}_1$, $a_{12} = a_{21} = \boldsymbol{a}_1\cdot\boldsymbol{a}_2$, and $a_{22} = \boldsymbol{a}_2\cdot\boldsymbol{a}_2$.

The basis vectors $\{\boldsymbol{a}_\alpha\}$ at any point on the surface define a tangent plane to the surface, and we correspondingly define a dual basis $\{\boldsymbol{a}^\alpha\}$ such that

$$\boldsymbol{a}^\alpha \cdot \boldsymbol{a}_\beta \;=\; \delta^\alpha_\beta \;, \tag{9}$$

where δ^α_β is the Kronecker delta given by $\delta^1_1 = \delta^2_2 = 1$ and $\delta^1_2 = \delta^2_1 = 0$. The geometric relationship between the $\{\boldsymbol{a}_\alpha\}$ and $\{\boldsymbol{a}^\alpha\}$ bases is shown in Fig. 3. Note in particular $\boldsymbol{a}_1$ need not be orthogonal to $\boldsymbol{a}_2$, and $\boldsymbol{a}^1$ need not be orthogonal to $\boldsymbol{a}^2$. The $\{\boldsymbol{a}^\alpha\}$ basis is also known as the contravariant basis. We explain the notion of contravariance, as well as the reason for our raising and lowering Greek indices, in the next section. As $\boldsymbol{a}^\alpha$ is a vector in the tangent plane, we can decompose it in the $\{\boldsymbol{a}_\lambda\}$ basis as

$$\boldsymbol{a}^\alpha \;=\; a^{\alpha\lambda}\boldsymbol{a}_\lambda \;, \tag{10}$$

where $a^{\alpha\lambda}$ is an unknown quantity we solve for. On substituting Eqs. (8) and (10) into Eq. (9), we find

$$a^{\alpha\lambda}a_{\lambda\beta} \;=\; \delta^\alpha_\beta \;, \qquad \text{for which} \qquad \left(a^{\alpha\beta}\right) \;=\; \left(a_{\alpha\beta}\right)^{-1} \;. \tag{11}$$

In Eq. (11), $(a_{\alpha\beta})^{-1}$ denotes the matrix inverse of $a_{\alpha\beta}$. We have thus determined the form of $a^{\alpha\beta}$, which is called the contravariant metric tensor. It can additionally be calculated as

$$a^{\alpha\beta} \;=\; \boldsymbol{a}^{\alpha} \cdot \boldsymbol{a}^{\beta} \;. \tag{12}$$

By applying the matrix inverse $(a^{\alpha\lambda})^{-1}$ to both sides of Eq. (10) and substituting Eq. (11), we obtain the relation

$$\boldsymbol{a}_{\alpha} \;=\; a_{\alpha\beta}\, \boldsymbol{a}^{\beta} \;. \tag{13}$$

(b). The notions of covariance and contravariance

In this section we explain our notation, in which Greek indices can be either raised or lowered, and the closely related concepts of covariant and contravariant quantities. An arbitrary vector $\boldsymbol{t}$ in the tangent plane can be expressed in the $\{\boldsymbol{a}_{\alpha}\}$ basis as

$$\boldsymbol{t} \;=\; t^{\alpha} \boldsymbol{a}_{\alpha} \;, \tag{14}$$

and as per the definition of a vector, $\boldsymbol{t}$ is invariant to our choice of the parametrization θ^{α}. The basis vectors $\boldsymbol{a}_{\alpha}$, however, clearly depend on the choice of parametrization [see Eq. (5)]. Accordingly, the vector components t^{α} must depend on θ^{α} in an inverse sense, such that under a change of coordinates the vector $\boldsymbol{t}$ does not change. In general, raised and lowered indices indicate how a quantity transforms—thus, for example, θ^{α} and t^{α} transform in the same way. We proceed to describe these ideas in detail.

Consider a change of the parametrization from unprimed to primed coordinates

$$\theta^{\alpha} \;\to\; \theta^{\alpha'} \;, \tag{15}$$

in which we use primed coordinates to indicate a different parametrization of the surface. Under the coordinate transformation in Eq. (15), the basis vectors $\boldsymbol{a}_{\alpha}$ are transformed to the primed coordinates according to

$$\boldsymbol{a}_{\alpha'} \;=\; \frac{\partial \boldsymbol{x}}{\partial \theta^{\alpha'}} \;=\; \frac{\partial \boldsymbol{x}}{\partial \theta^{\alpha}} \frac{\partial \theta^{\alpha}}{\partial \theta^{\alpha'}} \;=\; \frac{\partial \theta^{\alpha}}{\partial \theta^{\alpha'}}\, \boldsymbol{a}_{\alpha} \;, \tag{16}$$

where $\partial\theta^{\alpha}/\partial\theta^{\alpha'}$ is the 2×2 matrix representing the coordinate transformation. As mentioned earlier, for the vector $\boldsymbol{t}$ to be invariant to a change of coordinates, the components t^{α} must transform in an inverse manner to $\boldsymbol{a}_{\alpha}$. The coordinate transformation in Eq. (15) is invertible, so we write the inverse transformation matrix as

$$\left(\frac{\partial \theta^{\alpha}}{\partial \theta^{\alpha'}}\right)^{-1} \;=\; \frac{\partial \theta^{\alpha'}}{\partial \theta^{\alpha}} \;, \qquad \text{such that} \qquad t^{\alpha'} \;=\; \frac{\partial \theta^{\alpha'}}{\partial \theta^{\alpha}}\, t^{\alpha} \;. \tag{17}$$

With Eqs. (16) and (17), we find the vector $\boldsymbol{t}$ can be expressed as

$$\boldsymbol{t} \;=\; t^{\alpha'} \boldsymbol{a}_{\alpha'} \;=\; t^{\beta} \frac{\partial \theta^{\alpha'}}{\partial \theta^{\beta}} \frac{\partial \theta^{\alpha}}{\partial \theta^{\alpha'}} \boldsymbol{a}_{\alpha} \;=\; t^{\beta} \frac{\partial \theta^{\alpha}}{\partial \theta^{\beta}} \boldsymbol{a}_{\alpha} \;=\; t^{\alpha} \delta^{\alpha}_{\beta}\, \boldsymbol{a}_{\alpha} \;=\; t^{\alpha} \boldsymbol{a}_{\alpha} \;, \tag{18}$$

and is thus invariant to a change of coordinates.

In general, every quantity with a single Greek index will transform under a change of coordinates. As we have seen, such quantities can transform in the same way as the basis vectors $\boldsymbol{a}_\alpha$, or in the opposite way. Those which "co-vary," or transform in the same way, are termed covariant, while those which "contra-vary," or transform in the opposite way, are termed contravariant. The notions of covariance and contravariance are essential because physical, measurable quantities are invariant to our choice of coordinates. Furthermore, our notation automatically dictates whether an indexed quantity is covariant or contravariant—consider, for example, expanding the vector $\boldsymbol{t}$ in the $\{\boldsymbol{a}^\alpha\}$ basis as

$$\boldsymbol{t} = t_\alpha \boldsymbol{a}^\alpha \,. \tag{19}$$

Based on the index placement alone, t_α is a covariant quantity while $\boldsymbol{a}^\alpha$ is a contravariant one. As our notation dictates which basis we are working in, we will often refer to t^α as a contravariant vector and t_α as a covariant vector, with the basis implied.

The notions of covariance and contravariance apply to the components of a tensor as well. A general second-order tensor $\boldsymbol{T}$ defined in the tangent plane can be written equivalently as

$$\boldsymbol{T} = T^{\alpha\beta}\,\boldsymbol{a}_\alpha \otimes \boldsymbol{a}_\beta = T^\alpha{}_\beta\,\boldsymbol{a}_\alpha \otimes \boldsymbol{a}^\beta = T_\alpha{}^\beta\,\boldsymbol{a}^\alpha \otimes \boldsymbol{a}_\beta = T_{\alpha\beta}\,\boldsymbol{a}^\alpha \otimes \boldsymbol{a}^\beta \,, \tag{20}$$

where $\otimes$ denotes the outer or dyadic product between two vectors. We therefore refer to the covariant tensor components $T_{\alpha\beta}$, the contravariant tensor components $T^{\alpha\beta}$, and the mixed tensor components $T^\alpha{}_\beta$ and $T_\alpha{}^\beta$. The tensor components transform under Eq. (15) as expected given the placement of the indices, as for example

$$T^{\alpha'}{}_{\beta'} = \frac{\partial\theta^\beta}{\partial\theta^{\beta'}}\frac{\partial\theta^{\alpha'}}{\partial\theta^\alpha}\,T^\alpha{}_\beta \,. \tag{21}$$

Just as in the case of vectors, we often refer to $T^{\alpha\beta}$ as a contravariant tensor, as the basis is implied. We have already done so in calling $a_{\alpha\beta}$ the covariant metric tensor and $a^{\alpha\beta}$ the contravariant metric tensor.

It will often be useful to convert a covariant quantity into a contravariant quantity and vice versa, for which we use the metric tensor $a_{\alpha\beta}$ and contravariant metric tensor $a^{\alpha\beta}$. The covariant and contravariant components of an in-plane vector $\boldsymbol{t}$ are related by

$$t^\alpha = a^{\alpha\beta}\,t_\beta \qquad \text{and} \qquad t_\alpha = a_{\alpha\beta}\,t^\beta \,. \tag{22}$$

Equation (22) holds for any covariant and contravariant quantities, as already seen in Eqs. (10) and (13). Just as the metric tensor $a_{\alpha\beta}$ and dual metric tensor $a^{\alpha\beta}$ convert between covariant indices and contravariant indices in Eq. (22), the indices of tensors are raised and lowered according to

$$T^\alpha{}_\beta = T^{\alpha\lambda}\,a_{\lambda\beta} \qquad \text{and} \qquad T^{\alpha\beta} = T^\alpha{}_\lambda\,a^{\lambda\beta} \,. \tag{23}$$

Note that a covariant tensor $S_{\alpha\beta}$ is symmetric if $S_{\alpha\beta} = S_{\beta\alpha}$. If one index is then raised, the order of the indices is not important and the tensor may be written as S^α_β.

(c). The Christoffel symbols and the covariant derivative

At this point, we consider how the partial derivatives of covariant and contravariant quantities transform under Eq. (15). Note the partial derivative of the position $\boldsymbol{x}$ with respect to θ^α gave the covariant vectors $\boldsymbol{a}_\alpha$, and in general the partial derivative of an invariant quantity will be covariant. We seek to determine how the partial derivative acts on the components of a vector, and whether the resultant quantity transforms as the components of a tensor. To this end, we calculate how $t^\alpha_{\ ,\beta}$ transforms under the coordinate transformation in Eq. (15) and find

$$\begin{aligned} t^{\alpha'}_{\ ,\beta'} &= \frac{\partial}{\partial\theta^{\beta'}}\left[\overbrace{\frac{\partial\theta^{\alpha'}}{\partial\theta^\alpha}\,t^\alpha}^{=t^{\alpha'}}\right] \\ &= \frac{\partial\theta^\beta}{\partial\theta^{\beta'}}\frac{\partial}{\partial\theta^\beta}\left[\frac{\partial\theta^{\alpha'}}{\partial\theta^\alpha}\,t^\alpha\right] \\ &= \frac{\partial\theta^\beta}{\partial\theta^{\beta'}}\frac{\partial\theta^{\alpha'}}{\partial\theta^\alpha}\,t^\alpha_{\ ,\beta} + t^\alpha\frac{\partial\theta^\beta}{\partial\theta^{\beta'}}\frac{\partial}{\partial\theta^\beta}\left[\frac{\partial\theta^{\alpha'}}{\partial\theta^\alpha}\right]. \end{aligned} \tag{24}$$

In Eq. (24), we started by writing out how $t^{\alpha'}$ transformed in the first line, used the chain rule to get to the second line, and used the product rule to get to third line. If $t^\alpha_{\ ,\beta}$ were to transform as a tensor, only the first term in the third line of Eq. (24) would remain, as was the case for $T^\alpha{}_\beta$ in Eq. (21). Consequently, $t^\alpha_{\ ,\beta}$ is not a tensor, and by similar arguments we can show $t_{\alpha,\beta}$ is not a tensor either.

While the partial derivatives of covariant and contravariant vectors are non-tensorial, it is possible to add quantities to the partial derivatives such that they transform appropriately. Such quantities are called Christoffel symbols, denoted $\Gamma^\alpha_{\beta\mu}$, and are defined according to

$$\Gamma^\alpha_{\beta\mu} := \frac{1}{2}a^{\alpha\nu}\left(a_{\nu\beta,\mu} + a_{\nu\mu,\beta} - a_{\beta\mu,\nu}\right), \tag{25}$$

and are equivalently calculated as

$$\Gamma^\alpha_{\beta\mu} = \boldsymbol{a}^\alpha\cdot\boldsymbol{a}_{\beta,\mu} = -\boldsymbol{a}^\alpha_{\ ,\mu}\cdot\boldsymbol{a}_\beta\,. \tag{26}$$

The covariant derivative, denoted $(\,\cdot\,)_{;\alpha}$, is defined as

$$t^\alpha_{\ ;\beta} := t^\alpha_{\ ,\beta} + \Gamma^\alpha_{\beta\mu}t^\mu \qquad \text{and} \qquad t_{\alpha;\beta} := t_{\alpha,\beta} - \Gamma^\mu_{\alpha\beta}t_\mu \tag{27}$$

for contravariant and covariant vectors, respectively. Importantly, $t^\alpha_{\ ;\beta}$ and $t_{\alpha;\beta}$ now obey the tensor transformation law [cf. Eq. (21)]

We provide several useful relations involving the covariant derivative. First, the covariant derivative of the covariant and contravariant metric tensor is zero, written as

$$a_{\alpha\beta;\mu} = 0 \qquad \text{and} \qquad a^{\alpha\beta}_{\ ;\mu} = 0\,. \tag{28}$$

Furthermore, when operating on an invariant quantity the covariant derivative reduces to the partial derivative, such that

$$\phi_{;\alpha} = \phi_{,\alpha} \qquad \text{and} \qquad \boldsymbol{v}_{;\alpha} = \boldsymbol{v}_{,\alpha} \tag{29}$$

for an arbitrary scalar field ϕ and arbitrary vector field $\boldsymbol{v}$. Finally, we introduce the surface Laplacian operator Δ_{s} (also called the Laplace–Beltrami operator), defined as

$$\Delta_{\mathrm{s}}(\,\cdot\,) \;:=\; a^{\alpha\beta}\,(\,\cdot\,)_{;\alpha\beta}\;. \tag{30}$$

(d). The unit normal vector

Because the two-dimensional surface under consideration is embedded in $\mathbb{R}^3$, we can construct a unit vector normal to the surface at every point. The unit normal, denoted $\boldsymbol{n}$, is also orthogonal to the tangent plane and is constructed from the in-plane basis vectors $\boldsymbol{a}_1$ and $\boldsymbol{a}_2$ according to (see Fig. 2)

$$\boldsymbol{n} \;:=\; \frac{\boldsymbol{a}_1 \times \boldsymbol{a}_2}{|\boldsymbol{a}_1 \times \boldsymbol{a}_2|}\;. \tag{31}$$

We simplify the denominator of Eq. (31) by calculating

$$\begin{aligned} |\boldsymbol{a}_1 \times \boldsymbol{a}_2|^2 \;&=\; \big(\boldsymbol{a}_1 \times \boldsymbol{a}_2\big) \cdot \big(\boldsymbol{a}_1 \times \boldsymbol{a}_2\big) \\ &=\; \big(\boldsymbol{a}_1 \cdot \boldsymbol{a}_1\big)\,\big(\boldsymbol{a}_2 \cdot \boldsymbol{a}_2\big) \;-\; \big(\boldsymbol{a}_1 \cdot \boldsymbol{a}_2\big)\,\big(\boldsymbol{a}_2 \cdot \boldsymbol{a}_1\big) \\ &=\; a_{11}\,a_{22} \;-\; a_{12}\,a_{21} \\ &=\; \det a_{\alpha\beta}\;, \end{aligned} \tag{32}$$

such that $\boldsymbol{n}$ can be written as

$$\boldsymbol{n} \;=\; \frac{\boldsymbol{a}_1 \times \boldsymbol{a}_2}{\sqrt{\det a_{\alpha\beta}}}\;. \tag{33}$$

With a unit normal $\boldsymbol{n}$ at every point on the surface, the sets $\{\boldsymbol{a}_1, \boldsymbol{a}_2, \boldsymbol{n}\}$ and $\{\boldsymbol{a}^1, \boldsymbol{a}^2, \boldsymbol{n}\}$ form bases of $\mathbb{R}^3$ such that any general vector $\boldsymbol{v}$ can be decomposed as

$$\boldsymbol{v} \;=\; v^\alpha \boldsymbol{a}_\alpha \;+\; v\boldsymbol{n} \;=\; v_\alpha \boldsymbol{a}^\alpha \;+\; v\boldsymbol{n}\;. \tag{34}$$

In Eq. (34), v^α and v_α are the contravariant and covariant components, respectively, of the vector $\boldsymbol{v}$ while v is the normal component and is invariant to a change in the surface parametrization. We can furthermore define the surface identity tensor $\boldsymbol{i}$ in the tangent plane and identity tensor $\mathbf{1}$ in $\mathbb{R}^3$, respectively, as

$$\boldsymbol{i} \;:=\; \boldsymbol{a}^\alpha \otimes \boldsymbol{a}_\alpha \qquad \text{and} \qquad \mathbf{1} \;:=\; \boldsymbol{i} \;+\; \boldsymbol{n} \otimes \boldsymbol{n}\;. \tag{35}$$

(e). The curvature of a surface

The derivatives of the unit normal $\boldsymbol{n}$ in the θ^α directions contain information about the curvature of the surface. We accordingly define the curvature tensor $\boldsymbol{b}$ as

$$\boldsymbol{b} \;:=\; -\boldsymbol{n}_{,\alpha} \otimes \boldsymbol{a}^\alpha\;, \tag{36}$$

where the dyadic product ensures $\boldsymbol{b}$ is an invariant quantity. Taking the partial derivative of both sides of the identity $\boldsymbol{n} \cdot \boldsymbol{n} = 1$ with respect to θ^α gives $\boldsymbol{n} \cdot \boldsymbol{n}_{,\alpha} = 0$, so $\boldsymbol{n}_{,\alpha}$ lies entirely in the tangent plane. We expand $\boldsymbol{n}_{,\alpha}$ in the $\{\boldsymbol{a}^\beta\}$ basis as

$$\boldsymbol{n}_{,\alpha} \;=\; -b_{\beta\alpha}\boldsymbol{a}^\beta\;, \tag{37}$$

substitute Eq. (37) into Eq. (36), and swap the dummy indices 'α' and 'β' to obtain

$$\boldsymbol{b} \;=\; b_{\alpha\beta}\,\boldsymbol{a}^{\alpha} \otimes \boldsymbol{a}^{\beta} \;. \tag{38}$$

The covariant components of the curvature tensor, $b_{\alpha\beta}$, can be obtained by contracting Eq. (37) with $\boldsymbol{a}_{\mu}$—yielding $\boldsymbol{a}_{\mu} \cdot \boldsymbol{n}_{,\alpha} = -b_{\alpha\beta}\boldsymbol{a}^{\beta} \cdot \boldsymbol{a}_{\mu} = -b_{\alpha\beta}\delta^{\beta}_{\mu} = -b_{\alpha\mu}$. By rearranging dummy indices, we find

$$b_{\alpha\beta} \;=\; -\boldsymbol{n}_{,\beta} \cdot \boldsymbol{a}_{\alpha} \;=\; -\big(\underbrace{\boldsymbol{n} \cdot \boldsymbol{a}_{\alpha}}_{=\,0}\big)_{,\beta} + \boldsymbol{n} \cdot \boldsymbol{a}_{\alpha,\beta} \;=\; \boldsymbol{n} \cdot \boldsymbol{x}_{,\alpha\beta} \;, \tag{39}$$

where we used the orthogonality of $\boldsymbol{n}$ and $\boldsymbol{a}_{\beta}$, as well as the relation $\boldsymbol{a}_{\beta} = \boldsymbol{x}_{,\beta}$. Equation (39) shows the surface curvature is connected to the second derivative of the position with respect to the parametrization; the analogous result for curves was presented in Eq. (3). Moreover, Eq. (39) indicates the curvature tensor is symmetric. We note Eq. (37) is called the Weingarten equation, and plays an important role in calculating the gradients of vectors and tensors—as will be discussed in §2 (g). The curvature tensor obeys the relations

$$b_{\alpha\mu;\beta} \;=\; b_{\beta\mu;\alpha} \;, \tag{40}$$

which are known as the Mainardi–Codazzi equations (stated without proof here). In two dimensions, the only nontrivial equations are $b_{12;2} = b_{22;1}$ and $b_{21;1} = b_{11;2}$.

With the metric and curvature tensors we calculate the mean and Gaussian curvatures of the surface. The mean curvature H is defined as

$$H \;:=\; \frac{1}{2}\,\mathrm{tr}\,\boldsymbol{b} \;=\; \frac{1}{2}\,a^{\alpha\beta}b_{\alpha\beta} \;, \tag{41}$$

and the Gaussian curvature K is defined as

$$K \;:=\; \det \boldsymbol{b} \;=\; \frac{1}{2}\,\varepsilon^{\alpha\beta}\,\varepsilon^{\mu\nu}\,b_{\alpha\mu}\,b_{\beta\nu} \;=\; \frac{\det(b_{\alpha\beta})}{\det(a_{\alpha\beta})} \;, \tag{42}$$

where the Levi–Civita tensor $\varepsilon^{\alpha\beta}$ is given by $\varepsilon^{12} = -\varepsilon^{21} = 1/\sqrt{\det(a_{\alpha\beta})}$ and $\varepsilon^{11} = \varepsilon^{22} = 0$. We also introduce the cofactor of curvature $\bar{b}^{\alpha\beta}$, defined as

$$\bar{b}^{\alpha\beta} \;:=\; 2Ha^{\alpha\beta} - b^{\alpha\beta} \;, \qquad \text{or equivalently} \qquad \bar{b}^{\alpha\beta} \;=\; \varepsilon^{\alpha\mu}\varepsilon^{\beta\nu}b_{\mu\nu} \;, \tag{43}$$

where $b^{\alpha\beta} = a^{\alpha\mu}a^{\beta\nu}b_{\mu\nu}$ are the contravariant components of the curvature tensor. We use the cofactor of curvature as a matter of convenience, because it satisfies

$$\bar{b}^{\alpha\beta}_{\;;\beta} \;=\; 0 \;. \tag{44}$$

The Gaussian curvature is related to the metric, curvature, and cofactor of curvature tensors via

$$\bar{b}^{\alpha\mu}\,b^{\beta}_{\mu} \;=\; K\,a^{\alpha\beta} \qquad \text{and} \qquad \bar{b}^{\alpha\beta}\,b_{\alpha\beta} \;=\; 2K \;. \tag{45}$$

The Gaussian curvature also plays an important role in breaking the commutativity of the covariant derivative, as we now demonstrate. We introduce the Riemann–Christoffel tensor $R^{\alpha}{}_{\beta\mu\nu}$, given by the relations

$$R^{\alpha}{}_{\beta\mu\nu} \;=\; a^{\alpha\lambda}R_{\lambda\beta\mu\nu} \qquad \text{and} \qquad R_{\alpha\beta\mu\nu} \;=\; K\big(a_{\alpha\mu}a_{\beta\nu} \,-\, a_{\alpha\nu}a_{\beta\mu}\big) \;. \tag{46}$$

Equation (46) is K.F. Gauss' *Theorema Egregium.*[‡] The Riemann–Christoffel tensor contains information about how covariant derivatives commute, as shown in the relations

$$v_{\alpha;\beta\mu} = v_{\alpha;\mu\beta} + R^{\nu}{}_{\alpha\beta\mu} v_\nu \qquad \text{and} \qquad v^{\alpha}_{;\beta\mu} = v^{\alpha}_{;\mu\beta} - R^{\alpha}{}_{\nu\beta\mu} v^\nu \,. \tag{47}$$

It is also useful to define the Ricci curvature tensor $R_{\alpha\beta}$ as the contraction of the first and third indices of the Riemann–Christoffel tensor, which is found to be

$$R_{\alpha\beta} := R^{\mu}{}_{\alpha\mu\beta} = a^{\mu\nu} R_{\mu\alpha\nu\beta} = K a_{\alpha\beta} \,. \tag{48}$$

With Eqs. (47) and (48), we find

$$v^{\alpha}_{;\alpha\beta} = v^{\alpha}_{;\beta\alpha} - K v_\beta \,, \tag{49}$$

indicating nonzero Gaussian curvatures break the commutativity of the covariant derivative. Equation (49) is useful when obtaining the in-plane equations of motion governing biological membranes, as viscous forces arise in part from two derivatives of the in-plane velocity.

(f). Considerations at the edge of a surface

When describing an arbitrary surface patch $\mathcal{P}$, the surface boundary will not in general be aligned with one of the in-plane basis vectors $\boldsymbol{a}_\alpha$. It is thus useful to define a new basis on the patch boundary $\partial\mathcal{P}$. Consider the tangent plane at a point $\boldsymbol{x}_\mathrm{b} = \boldsymbol{x}(\theta^\alpha_\mathrm{b})$ on $\partial\mathcal{P}$, with normal vector $\boldsymbol{n}$ (see Fig. 4). We define in-plane orthonormal basis vectors $\boldsymbol{\tau}$ and $\boldsymbol{\nu}$, where $\boldsymbol{\tau}$ is tangent to the boundary while $\boldsymbol{\nu}$ is orthogonal to $\boldsymbol{\tau}$. Both $\boldsymbol{\tau}$ and $\boldsymbol{\nu}$ are orthogonal to the surface normal $\boldsymbol{n}$, as they lie in the tangent plane. If the surface boundary is parametrized by its arc length ℓ, the in-plane unit tangent $\boldsymbol{\tau}$ and unit normal $\boldsymbol{\nu}$ are defined as [cf. §1]

$$\boldsymbol{\tau} := \frac{\mathrm{d}\boldsymbol{x}_\mathrm{b}}{\mathrm{d}\ell} = \boldsymbol{a}_\alpha \frac{\mathrm{d}\theta^\alpha_\mathrm{b}}{\mathrm{d}\ell} \qquad \text{and} \qquad \boldsymbol{\nu} := \boldsymbol{\tau} \times \boldsymbol{n} \,. \tag{50}$$

The orthonormal basis $\{\boldsymbol{\tau}, \boldsymbol{\nu}, \boldsymbol{n}\}$ at position $\boldsymbol{x}_\mathrm{b}$ on the boundary $\partial\mathcal{P}$ is depicted in Fig. 4.

With a new set of basis vectors on the patch boundary, it is convenient to relate $\boldsymbol{\nu}$ and $\boldsymbol{\tau}$ to the covariant and contravariant basis vectors $\boldsymbol{a}_\alpha$ and $\boldsymbol{a}^\alpha$. To this end, we decompose $\boldsymbol{\nu}$ and $\boldsymbol{\tau}$ in the $\{\boldsymbol{a}_\alpha\}$ basis as

$$\boldsymbol{\nu} = \nu^\alpha \boldsymbol{a}_\alpha \qquad \text{and} \qquad \boldsymbol{\tau} = \tau^\alpha \boldsymbol{a}_\alpha \,, \tag{51}$$

such that $\tau^\alpha = \mathrm{d}\theta^\alpha_\mathrm{b}/\mathrm{d}\ell$ [cf. Eq. $(50)_1$]. By swapping repeated indices in Eq. (51) and contracting the two relations with $\boldsymbol{a}^\alpha$ we find

$$\boldsymbol{a}^\alpha \cdot \boldsymbol{\nu} = \nu^\alpha \qquad \text{and} \qquad \boldsymbol{a}^\alpha \cdot \boldsymbol{\tau} = \tau^\alpha \,. \tag{52}$$

As $\{\boldsymbol{\nu}, \boldsymbol{\tau}\}$ is a basis of the tangent space, we express the surface identity tensor $\boldsymbol{i}$ (35) as

$$\boldsymbol{i} := \boldsymbol{\nu} \otimes \boldsymbol{\nu} + \boldsymbol{\tau} \otimes \boldsymbol{\tau} \,. \tag{53}$$

[‡]K.F. Gauss. *General investigations of curved surfaces of 1827 and 1825.* Transl. by J.C. Morehead and A.M. Hiltebeitel. Princeton: Princeton University Library, 1902.

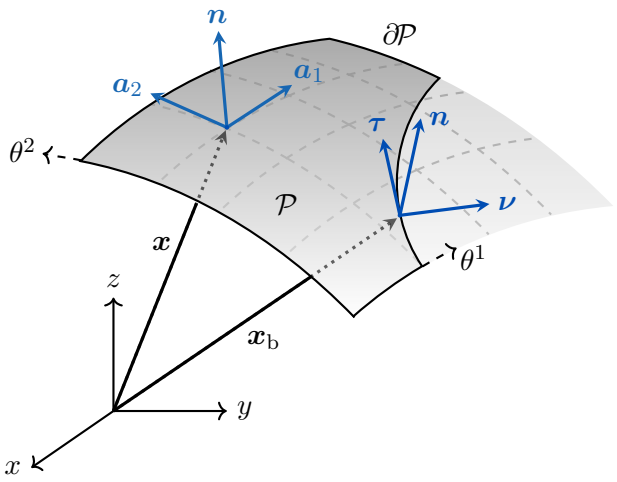

Figure 4: A schematic of a patch of surface $\mathcal{P}$. At each point $\boldsymbol{x}$ on the patch we define the in-plane vectors $\boldsymbol{a}_1$ and $\boldsymbol{a}_2$ as well as the normal vector to the plane $\boldsymbol{n}$. The set $\{\boldsymbol{a}_1, \boldsymbol{a}_2\}$ constitutes a basis for the tangent plane at any location, while the set $\{\boldsymbol{a}_1, \boldsymbol{a}_2, \boldsymbol{n}\}$ forms a basis of $\mathbb{R}^3$. At every point $\boldsymbol{x}_\mathrm{b} = \boldsymbol{x}(\theta^\alpha_\mathrm{b})$ on the patch boundary $\partial\mathcal{P}$, we define the in-plane unit tangent $\boldsymbol{\tau}$ and unit normal $\boldsymbol{\nu}$—which also form a basis of the tangent plane.

Accordingly, with Eqs. (51) and (52), we find

$$\boldsymbol{a}^\alpha \;=\; \boldsymbol{i}\,\boldsymbol{a}^\alpha \;=\; \boldsymbol{\nu}(\boldsymbol{\nu}\cdot\boldsymbol{a}^\alpha) + \boldsymbol{\tau}(\boldsymbol{\tau}\cdot\boldsymbol{a}^\alpha) \;=\; \nu^\alpha\boldsymbol{\nu} + \tau^\alpha\boldsymbol{\tau}\;. \tag{54}$$

By substituting Eq. (54) into the expression of the curvature tensor $\boldsymbol{b}$ in Eq. (38), we obtain

$$\begin{aligned}\boldsymbol{b} \;&=\; b_{\alpha\beta}\left(\nu^\alpha\boldsymbol{\nu} + \tau^\alpha\boldsymbol{\tau}\right)\otimes\left(\nu^\beta\boldsymbol{\nu} + \tau^\beta\boldsymbol{\tau}\right)\\ &=\; b_{\alpha\beta}\,\nu^\alpha\nu^\beta\,\boldsymbol{\nu}\otimes\boldsymbol{\nu} \;+\; b_{\alpha\beta}\,\tau^\alpha\tau^\beta\,\boldsymbol{\tau}\otimes\boldsymbol{\tau} \;+\; b_{\alpha\beta}\,\nu^\alpha\tau^\beta\,\boldsymbol{\nu}\otimes\boldsymbol{\tau} \;+\; b_{\alpha\beta}\,\tau^\alpha\nu^\beta\,\boldsymbol{\tau}\otimes\boldsymbol{\nu}\\ &=\; \kappa_\nu\,\boldsymbol{\nu}\otimes\boldsymbol{\nu} \;+\; \kappa_\tau\,\boldsymbol{\tau}\otimes\boldsymbol{\tau} \;+\; \xi\left(\boldsymbol{\nu}\otimes\boldsymbol{\tau} + \boldsymbol{\tau}\otimes\boldsymbol{\nu}\right)\;.\end{aligned} \tag{55}$$

In Eq. (55), the normal curvatures in the $\boldsymbol{\nu}$ and $\boldsymbol{\tau}$ directions, κ_ν and κ_τ, are calculated as

$$\kappa_\nu \;:=\; b_{\alpha\beta}\,\nu^\alpha\nu^\beta \;=\; \bar{b}^{\alpha\beta}\,\tau_\alpha\tau_\beta \qquad\text{and}\qquad \kappa_\tau \;:=\; b_{\alpha\beta}\,\tau^\alpha\tau^\beta \;=\; \bar{b}^{\alpha\beta}\,\nu_\alpha\nu_\beta\;, \tag{56}$$

respectively. Additionally, the twist on the boundary ξ is defined as

$$\xi \;:=\; b_{\alpha\beta}\,\nu^\alpha\tau^\beta\;. \tag{57}$$

We can thus express the curvature tensor $\boldsymbol{b}$ in the orthonormal basis $\{\boldsymbol{\nu}, \boldsymbol{\tau}\}$ as

$$\boldsymbol{b} \;=\; \begin{pmatrix}\kappa_\nu & \xi\\ \xi & \kappa_\tau\end{pmatrix}\;. \tag{58}$$

The components κ_ν and κ_τ are the magnitudes of the curvature vector $\boldsymbol{\kappa}$ (3) for curves in the $\boldsymbol{\nu}$ and $\boldsymbol{\tau}$ directions along the surface, respectively, while the twist ξ accounts for how, for example, the normal to a curve along $\boldsymbol{\nu}$ changes in the $\boldsymbol{\tau}$ direction. We also find, based on the relations $H = \frac{1}{2}\operatorname{tr}\boldsymbol{b}$ (41) and $K = \det\boldsymbol{b}$ (42), that the mean and Gaussian curvatures at the membrane boundary can be written as

$$H \;=\; \frac{1}{2}\left(\kappa_\nu \;+\; \kappa_\tau\right) \qquad\text{and}\qquad K \;=\; \kappa_\nu\,\kappa_\tau - \xi^2\;. \tag{59}$$

(g). The variation of the basis vectors

To conclude our discussion, we note that for an arbitrarily curved surface, the basis vectors $\boldsymbol{a}_\alpha$ and $\boldsymbol{n}$ will in general vary along the surface. We calculate $\boldsymbol{n}_{,\alpha}$ by recognizing $\boldsymbol{n}\cdot\boldsymbol{n}=1$, such that taking the partial derivative of both sides yields $\boldsymbol{n}\cdot\boldsymbol{n}_{,\alpha}=0$ and thus $\boldsymbol{n}_{,\alpha}$ has components only in the tangent plane. We already recognized how $\boldsymbol{n}_{,\alpha}$ is connected to the curvature tensor through the Weingarten equation (39), which is more often written as

$$\boldsymbol{n}_{,\alpha} \;=\; -b_\alpha^\beta\,\boldsymbol{a}_\beta\;. \tag{60}$$

To calculate the covariant derivative of $\boldsymbol{a}_\alpha$, we first calculate

$$\boldsymbol{a}_{\alpha;\beta}\cdot\boldsymbol{n} \;=\; \big(\underbrace{\boldsymbol{a}_\alpha\cdot\boldsymbol{n}}_{=0}\big)_{;\beta} - \boldsymbol{a}_\alpha\cdot\underbrace{\boldsymbol{n}_{,\beta}}_{=\boldsymbol{n}_{;\beta}} \;=\; b_{\alpha\beta}\;, \tag{61}$$

where in the first equality we used the product rule as well as the equality of covariant and partial derivative for invariant quantities, while in the second equality we used the result of Eq. (39). We next calculate

$$\boldsymbol{a}_{\alpha;\beta}\cdot\boldsymbol{a}^\mu \;=\; \boldsymbol{a}_{\alpha,\beta}\cdot\boldsymbol{a}^\mu \;-\; \Gamma^\nu_{\alpha\beta}\,\underbrace{\boldsymbol{a}_\nu\cdot\boldsymbol{a}^\mu}_{=\delta^\mu_\nu} \;=\; \Gamma^\mu_{\alpha\beta} \;-\; \Gamma^\mu_{\alpha\beta} \;=\; 0\;, \tag{62}$$

where we used the definition of the covariant derivative (27) and the Christoffel symbols (26). With these two results we find

$$\boldsymbol{a}_{\alpha;\beta} \;=\; b_{\alpha\beta}\,\boldsymbol{n}\;, \tag{63}$$

which is known as the Gauss equation.

The Gauss (63) and Weingarten (60) equations are of tremendous practical importance when calculating the gradients of vectors and tensors on a surface. Consider, for example, the partial derivative of the general vector $\boldsymbol{v}$ given in Eq. (34), which we calculate as

$$\begin{aligned}\boldsymbol{v}_{,\alpha} \;&=\; \boldsymbol{v}_{;\alpha} \;=\; \big(v^\beta\boldsymbol{a}_\beta \;+\; v\boldsymbol{n}\big)_{;\alpha}\\ &=\; v^\beta_{;\alpha}\boldsymbol{a}_\beta \;+\; v^\beta\boldsymbol{a}_{\beta;\alpha} \;+\; v_{,\alpha}\boldsymbol{n} \;+\; v\boldsymbol{n}_{,\alpha}\\ &=\; \big(v^\beta_{;\alpha} \;-\; vb^\beta_\alpha\big)\boldsymbol{a}_\beta \;+\; \big(v_{,\alpha} \;+\; v^\beta b_{\beta\alpha}\big)\boldsymbol{n}\;.\end{aligned} \tag{64}$$

In Eq. (64), we used the equivalence of partial and covariant derivatives for invariant quantities, then used the product rule in the second line, and substituted the Gauss (63) and Weingarten (60) equations in the third line.

(h). Examples

To demonstrate how the tools described above are used in practice, we work through two examples involving geometries in which biological membranes are frequently observed. In the first case, we describe the geometry of an unperturbed sphere. In the second case, we describe a slightly deformed planar surface, which remains in one-to-one correspondence with a plane. The well-known parametrization used in the latter is attributed to G. Monge [‡], and called the Monge parametrization.

[‡] G. Monge. *Application de l'analyse à la géométrie*. Paris: Bernard, 1807.

EXAMPLE 1: SPHERICAL GEOMETRY

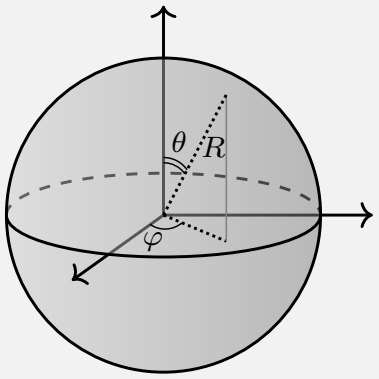

Consider a spherical surface with polar angle θ and azimuthal angle φ, such that the surface position is given by

$$\boldsymbol{x}(\theta,\varphi) \,=\, R\,\boldsymbol{e}_r(\theta,\varphi)\ ,$$

where R is the sphere radius. We choose the parametrization $\theta^1 = \theta$ and $\theta^2 = \varphi$, such that the in-plane basis vectors are given by

$$\boldsymbol{a}_1 \,=\, \frac{\partial \boldsymbol{x}}{\partial\theta} \,=\, R\,\frac{\partial \boldsymbol{e}_r}{\partial\theta} \,=\, R\,\boldsymbol{e}_\theta$$

and

$$\boldsymbol{a}_2 \,=\, \frac{\partial \boldsymbol{x}}{\partial\varphi} \,=\, R\,\frac{\partial \boldsymbol{e}_r}{\partial\varphi} \,=\, R\sin\theta\,\boldsymbol{e}_\varphi\ .$$

The normal vector $\boldsymbol{n}$ is calculated to be

$$\boldsymbol{n} \,=\, \frac{\boldsymbol{a}_1\times\boldsymbol{a}_2}{|\boldsymbol{a}_1\times\boldsymbol{a}_2|} \,=\, \frac{R^2\sin\theta\,(\boldsymbol{e}_\theta\times\boldsymbol{e}_\varphi)}{R^2\sin\theta\,|\boldsymbol{e}_\theta\times\boldsymbol{e}_\varphi|} \,=\, \boldsymbol{e}_r\ ,$$

as expected. Note that if we switched our parametrization such that $\theta^1 = \varphi$ and $\theta^2 = \theta$, the normal would point towards the center rather than outwards. For our purposes, we will always choose a surface parametrization for which the normal points outwards. We calculate $\boldsymbol{a}_1\cdot\boldsymbol{a}_1 = R^2$, $\boldsymbol{a}_1\cdot\boldsymbol{a}_2 = 0$, and $\boldsymbol{a}_2\cdot\boldsymbol{a}_2 = R^2\sin^2\theta$, such that the covariant metric tensor is given by

$$a_{\alpha\beta} = \begin{pmatrix} R^2 & 0 \\ 0 & R^2\sin^2\theta \end{pmatrix}\ .$$

Next, we calculate

$$\boldsymbol{x}_{,11} \,=\, \boldsymbol{a}_{1,1} \,=\, R\,\frac{\partial \boldsymbol{e}_\theta}{\partial\theta} \,=\, -R\,\boldsymbol{e}_r\ ,$$

$$\boldsymbol{x}_{,12} \,=\, \boldsymbol{x}_{,21} \,=\, \boldsymbol{a}_{1,2} \,=\, R\,\frac{\partial \boldsymbol{e}_\theta}{\partial\varphi} \,=\, R\cos\theta\,\boldsymbol{e}_\varphi\ ,$$

and

$$\boldsymbol{x}_{,22} \,=\, \boldsymbol{a}_{2,2} \,=\, R\sin\theta\,\frac{\partial \boldsymbol{e}_\varphi}{\partial\varphi} \,=\, -R\sin\theta\,\big(\cos\theta\,\boldsymbol{e}_\theta \,+\, \sin\theta\,\boldsymbol{e}_r\big)\ .$$

With these relations, we calculate the curvature tensor through the relation $b_{\alpha\beta} = \boldsymbol{n} \cdot \boldsymbol{x}_{,\alpha\beta}$, and obtain

$$b_{\alpha\beta} = \begin{pmatrix} -R & 0 \\ 0 & -R\sin^2\theta \end{pmatrix} .$$

We then determine the contravariant metric and curvature tensors according to $a^{\alpha\beta} = (a_{\alpha\beta})^{-1}$ and $b^{\alpha\beta} = a^{\alpha\mu}a^{\beta\nu}b_{\mu\nu}$, for which

$$a^{\alpha\beta} = \begin{pmatrix} R^{-2} & 0 \\ 0 & R^{-2}\csc^2\theta \end{pmatrix} \qquad \text{and} \qquad b^{\alpha\beta} = \begin{pmatrix} -R^{-3} & 0 \\ 0 & -R^{-3}\csc^2\theta \end{pmatrix} .$$

At this point, we calculate the mean curvature as

$$\begin{aligned} H \;&=\; \frac{1}{2}\,a^{\alpha\beta}b_{\alpha\beta} \;=\; \frac{1}{2}\Big\{ \underbrace{a^{11}b_{11}}_{=R^{-2}\cdot(-R)} + \underbrace{a^{12}b_{12}}_{=0} + \underbrace{a^{21}b_{21}}_{=0} + \underbrace{a^{22}b_{22}}_{=R^{-2}\csc^2\theta\cdot(-R\sin^2\theta)} \Big\} \\ &=\; -\frac{1}{R} , \end{aligned}$$

and the Gaussian curvature as

$$K \;=\; \frac{\det(b_{\alpha\beta})}{\det(a_{\alpha\beta})} \;=\; \frac{R^2\sin^2\theta}{R^4\sin^2\theta} \;=\; \frac{1}{R^2} .$$

Finally, by using the relation $\Gamma^{\alpha}_{\beta\mu} = \boldsymbol{a}^{\alpha} \cdot \boldsymbol{a}_{\beta,\mu}$, we find a sphere has four non-zero Christoffel symbols—given by

$$\Gamma^1_{22} \;=\; \boldsymbol{a}^1 \cdot \boldsymbol{a}_{2,2} \;=\; R^{-1}\boldsymbol{e}_\theta \cdot (-R\sin\theta\cos\theta\,\boldsymbol{e}_\theta - R\sin^2\theta\,\boldsymbol{e}_r) \;=\; -\sin\theta\cos\theta ,$$

$$\Gamma^2_{12} \;=\; \boldsymbol{a}^2 \cdot \boldsymbol{a}_{1,2} \;=\; R^{-1}\csc\theta\,\boldsymbol{e}_\varphi \cdot R\cos\theta\,\boldsymbol{e}_\varphi \;=\; \cot\theta ,$$

and

$$\Gamma^2_{21} \;=\; \boldsymbol{a}^2 \cdot \boldsymbol{a}_{2,1} \;=\; \boldsymbol{a}^2 \cdot \boldsymbol{a}_{1,2} \;=\; \Gamma^2_{12} \;=\; \cot\theta .$$

We note here that Christoffel symbols are symmetric in the lower two indices, as can be seen from how they are calculated.

Example 2: Monge Parametrization

Consider a nearly planar surface lying above the x–y plane, such that the position of the surface can be specified everywhere as the height $h(x, y)$ above each point (x, y) in the plane. We choose the parametrization $\theta^1 = x$ and $\theta^2 = y$, such that the position of the surface is given by

$$\boldsymbol{x} \;=\; x\boldsymbol{e}_1 \,+\, y\boldsymbol{e}_2 \,+\, h(x,y)\boldsymbol{e}_3 \;=\; \theta^\alpha \boldsymbol{e}_\alpha \,+\, h(\theta^\alpha)\boldsymbol{e}_3 \;,$$

where $\boldsymbol{e}_i$ are unit vectors in the i^{th} direction in $\mathbb{R}^3$. In choosing such a parametrization, we have implicitly assumed there is no point (x, y) for which two heights exist—as would be the case for a sphere or cylinder. Thus the Monge parametrization is generally used in the limit of small deformations, where $h \ll 1$, such that no tubes or buds form. In this example, we will first consider a general height h and then afterwards take the small deformation limit.

For the chosen parametrization, the in-plane basis vectors $\boldsymbol{a}_\alpha$ are given by

$$\boldsymbol{a}_\alpha \;=\; \boldsymbol{x}_{,\alpha} \;=\; \boldsymbol{e}_\alpha \,+\, h_{,\alpha}\boldsymbol{e}_3 \;.$$

We then calculate

$$\boldsymbol{a}_1 \times \boldsymbol{a}_2 \;=\; \big(\boldsymbol{e}_1 \,+\, h_{,x}\boldsymbol{e}_3\big) \times \big(\boldsymbol{e}_2 \,+\, h_{,y}\boldsymbol{e}_3\big) \;=\; \boldsymbol{e}_3 \,-\, h_{,x}\boldsymbol{e}_1 \,-\, h_{,y}\boldsymbol{e}_2 \;=\; \boldsymbol{e}_3 \,-\, h_{,\alpha}\boldsymbol{e}_\alpha$$

and

$$|\boldsymbol{a}_1 \times \boldsymbol{a}_2| \;=\; \sqrt{1 \,+\, (h_{,x})^2 \,+\, (h_{,y})^2} \;,$$

for which the unit normal $\boldsymbol{n}$ is found to be

$$\boldsymbol{n} \;=\; \frac{\boldsymbol{a}_1 \times \boldsymbol{a}_2}{|\boldsymbol{a}_1 \times \boldsymbol{a}_2|} \;=\; \frac{\boldsymbol{e}_3 \,-\, h_{,\alpha}\boldsymbol{e}_\alpha}{\sqrt{1 + (h_{,x})^2 + (h_{,y})^2}} \;.$$

With the basis vectors $\{\boldsymbol{a}_\alpha, \boldsymbol{n}\}$, we calculate the metric tensor as

$$a_{\alpha\beta} \;=\; \boldsymbol{a}_\alpha \cdot \boldsymbol{a}_\beta \;=\; \big(\boldsymbol{e}_\alpha \,+\, h_{,\alpha}\boldsymbol{e}_3\big) \cdot \big(\boldsymbol{e}_\beta \,+\, h_{,\beta}\boldsymbol{e}_3\big) \;=\; \delta_{\alpha\beta} \,+\, h_{,\alpha}h_{,\beta} \;.$$

Next, we recognize $\boldsymbol{x}_{,\alpha\beta} = \boldsymbol{a}_{\alpha,\beta} = (\boldsymbol{e}_\alpha + h_{,\alpha}\boldsymbol{e}_3)_{,\beta} = h_{,\alpha\beta}\,\boldsymbol{e}_3$, from which we calculate the curvature tensor via the relation $b_{\alpha\beta} = \boldsymbol{n} \cdot \boldsymbol{x}_{,\alpha\beta}$ as

$$b_{\alpha\beta} \;=\; \frac{h_{,\alpha\beta}}{\sqrt{1 + (h_{,x})^2 + (h_{,y})^2}} \;.$$

As we have seen in this and the previous example, it is evident that once a parametrization θ^α is chosen and the position $\boldsymbol{x}$ is known, all of the geometric quantities can be calculated.

At this point, we choose to work in the small deformation limit where $|h_{,\alpha}| \ll 1$ to simplify further calculations. Keeping terms to second order in h, the in-plane basis vectors and metric tensor are unchanged. The normal vector simplifies to

$$\boldsymbol{n} \;=\; \left(1 \;-\; \frac{1}{2}\Big[(h_{,x})^2 \;+\; (h_{,y})^2\Big]\right)\boldsymbol{e}_3 \;-\; h_{,\alpha}\boldsymbol{e}_\alpha \;,$$

and consequently the curvature tensor simplifies to

$$b_{\alpha\beta} \;=\; \boldsymbol{n}\cdot\boldsymbol{x}_{,\alpha\beta} \;=\; \boldsymbol{n}\cdot h_{,\alpha\beta}\,\boldsymbol{e}_3 \;=\; h_{,\alpha\beta} \;.$$

From the metric tensor $a_{\alpha\beta}$ we calculate the contravariant metric tensor as

$$a^{\alpha\beta} \;=\; \big(a_{\alpha\beta}\big)^{-1} \;=\; \delta_{\alpha\beta} \;-\; h_{,\alpha}h_{,\beta} \;+\; \mathcal{O}(h^3) \;.$$

To lowest order in h, the mean curvature H is calculated to be

$$H \;=\; \frac{1}{2}\Big(h_{,xx} \;+\; h_{,yy}\Big) \;=\; \frac{1}{2}\,\Delta_{\mathrm{s}}h \;,$$

where for nearly planar systems the surface Laplacian is given by

$$\Delta_{\mathrm{s}}(\,\cdot\,) \;=(\,\cdot\,)_{,xx} \;+\; (\,\cdot\,)_{,yy} \;.$$

Again to lowest order in h, the Gaussian curvature K is found to be

$$K \;=\; h_{,xx}\,h_{,yy} \;-\; (h_{,xy})^2 \;,$$

which is the determinant of the Hessian matrix $h_{,\alpha\beta}$. These results, valid for small deformations, give an intuition about the geometric description of the surface.

References

[1] S. Carroll. "Lecture notes on general relativity". *arXiv preprint* (1997). arXiv: gr-qc/9712019

[2] K.F. Gauss. *General investigations of curved surfaces of 1827 and 1825*. Transl. by J.C. Morehead and A.M. Hiltebeitel. Princeton: Princeton University Library, 1902

[3] G. Monge. *Application de l'analyse à la géométrie*. Paris: Bernard, 1807

[4] D.J. Struik. *Lectures on Classical Differential Geometry*. 2nd ed. New York: Dover, 1988

[5] A.M. Waxman. "Dynamics of a couple-stress fluid membrane". *Studies Appl. Math.* **70** (1984), 63–86

Chapter III

Irreversible Thermodynamics

> *Classical thermodynamics has solved the problem of the competition between randomness and organization for equilibrium situations. How then is it possible to extend these results to dissipative systems? What part of the energy flow may be used to create and maintain some structure in such systems?*
>
> —Ilya R. Prigogine, 1955 [‡]

In arriving at a continuum description of any material, an essential requirement is to determine the form of the stresses in said material. In doing so, one captures how forces are transmitted between different portions of the body. Experiments are used to determine the material stresses whenever possible. For example, measurements of the stress versus strain in three-dimensional elastic solids and stress versus strain rate in three-dimensional Newtonian fluids yield the well-known stress tensors of the aforementioned materials. For lipid membranes, however, it is prohibitively difficult to perform the analogous experiments. Accordingly, other techniques are required in order to determine the form of the membrane stresses.

In this work, we employ the framework of *irreversible thermodynamics* [†] to determine the equations governing lipid membrane systems. The present chapter serves to introduce the most important concepts of the framework by considering two more familiar systems: a bulk [*] Newtonian fluid and a bulk elastic solid. In doing so, we show how a single continuum description can be used to describe both fluids and solids. Moreover, we demonstrate how within the framework of irreversible thermodynamics, one can obtain the governing equations of two different materials by choosing the appropriate form of the Helmholtz free energy, and with knowledge of the dissipative phenomena within the system. None of the results here are new: the unified description of fluids and solids was first presented by K.K. Mandadapu, [§]

[‡]I. Prigogine. *Introduction to Thermodynamics of Irreversible Processes*. 3rd ed. New York: Interscience Publishers, 1967.

[†]The framework also goes by the name *non-equilibrium thermodynamics*.

[*]Throughout this work, we will use 'bulk' synonymously with 'three-dimensional.'

[§]K.K. Mandadapu. "Homogeneous Non-Equilibrium Molecular Dynamics Methods for Calculating the Heat Transport Coefficient of Solids and Mixtures". PhD thesis. University of California, Berkeley, 2011.

who extended the seminal works of I. PRIGOGINE,[‡] L. ONSAGER,[†,*] S.R. DE GROOT,[§] and P. MAZUR.[§]

The chapter is organized as follows. We begin by presenting the canonical kinematic description of continuum systems. Next, the local forms of the balance of mass, linear momentum, and angular momentum are obtained. At this point, rather than postulating the form of the stress tensor for a given material, we develop local forms of the first and second laws of thermodynamics. By relating the rate of change of internal energy and entropy via the Helmholtz free energy, we combine the aforementioned balance laws into a single equation. Only then do we differentiate between fluid and solid materials: the fundamental thermodynamic variables describing a fluid are its density and temperature, while those of an elastic solid are its deformation gradient and temperature. With the fundamental thermodynamic variables, and our knowledge that fluid flow is dissipative and elastic deformations are reversible, we follow the standard techniques of irreversible thermodynamics to obtain general relations for the stress tensor of a fluid and solid. By then proposing a form of the Helmholtz free energy and substituting the resultant fluid and solid stresses into the linear momentum balance, we respectively obtain the Navier–Stokes and Cauchy–Navier equations.

1. The kinematics of a bulk material

We begin by describing the kinematics of a general continuum material. Consider an abstract body $\mathscr{B}$ as a collection of material points. At any time t, we define the configuration of the body to be the domain $\mathcal{Q} \subset \mathbb{R}^3$ occupied by $\mathscr{B}$, of which we consider an arbitrary region $\mathcal{R} \subseteq \mathcal{Q}$. The position of any point within the region $\mathcal{R}$ is given by

$$\boldsymbol{x} = x_i \boldsymbol{e}_i \ , \qquad \text{with} \qquad x_i = \boldsymbol{x} \cdot \boldsymbol{e}_i \ . \tag{1}$$

In Eq. (1), summation is implied over repeated Roman indices, which span the set $\{1, 2, 3\}$. Here, $\{\boldsymbol{e}_i\}$ is an orthonormal basis of $\mathbb{R}^3$. The configuration of the body $\mathscr{B}$ at time t, or equivalently $\mathcal{R}(t)$, is called the *current configuration*. We next consider the configuration of $\mathscr{B}$ at an arbitrary reference time t_0, for which we are concerned with the region $\mathcal{R}_0 := \mathcal{R}(t_0)$. The position of any point in $\mathcal{R}_0$ is written as

$$\boldsymbol{X} = X_A \boldsymbol{E}_A \ , \qquad \text{with} \qquad X_A = \boldsymbol{X} \cdot \boldsymbol{E}_A \tag{2}$$

and the orthonormal basis $\{\boldsymbol{E}_A\}$ not necessarily equal to $\{\boldsymbol{e}_i\}$. We follow the standard notation in which quantities in the *reference configuration* $\mathcal{R}_0$ either have a subscript '0' or are capitalized.

We seek to describe how the body evolves over time from its reference configuration $\mathcal{R}_0$ to its current configuration $\mathcal{R}(t)$. To this end, we define the motion $\hat{\boldsymbol{\chi}} : \mathbb{R}^3 \times \mathbb{R} \to \mathbb{R}^3$ mapping the reference position $\boldsymbol{X}$ to the current position $\boldsymbol{x}$, as a function of time t. Formally, we write

$$\boldsymbol{x} = \hat{\boldsymbol{\chi}}(\boldsymbol{X}, t) \qquad \text{or equivalently} \qquad x_i = \hat{\chi}_i(X_A, t) \ . \tag{3}$$

[‡]Prigogine, *Introduction to Thermodynamics of Irreversible Processes*.

[†]L. Onsager. "Reciprocal relations in irreversible processes. I.". *Phys. Rev.* **37** (1931), 405–426.

[*]L. Onsager. "Reciprocal relations in irreversible processes. II.". *Phys. Rev.* **38** (1931), 2265–2279.

[§]S.R. de Groot and P. Mazur. *Non-Equilibrium Thermodynamics*. New York: Dover, 1984

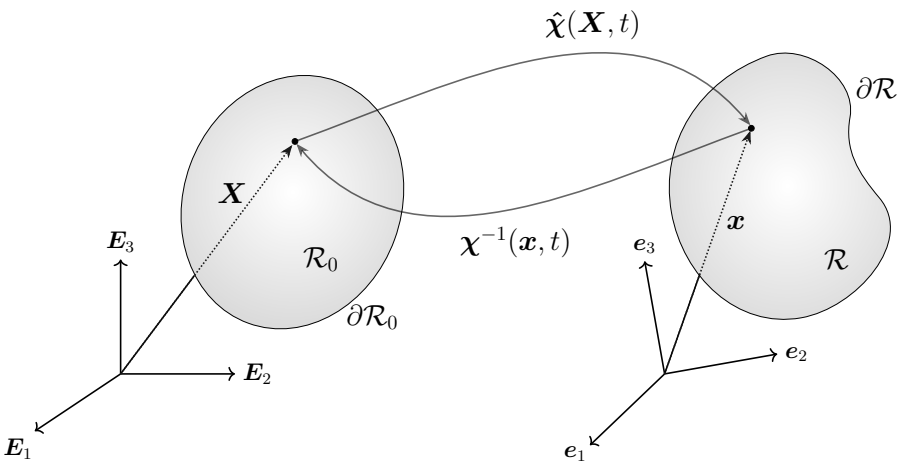

Figure 1: A schematic of the mappings $\hat{\boldsymbol{\chi}}(\boldsymbol{X},t)$ and $\boldsymbol{\chi}^{-1}(\boldsymbol{x},t)$ between the reference (left) and current (right) configurations.

As all configurations can be mapped to the reference configuration, the reference position $\boldsymbol{X}$ labels material points, while $\hat{\boldsymbol{\chi}}$ tracks those material points over time. We additionally introduce the inverse mapping $\boldsymbol{\chi}^{-1} : \mathbb{R}^3 \times \mathbb{R} \to \mathbb{R}^3$ as

$$\boldsymbol{X} \,=\, \boldsymbol{\chi}^{-1}(\boldsymbol{x},t) \qquad \text{or equivalently} \qquad X_A \,=\, \chi_A^{-1}(x_i,t)\;. \tag{4}$$

A schematic of the reference and current configurations, and the mapping between them, is illustrated in Fig. 1.

With the motion $\hat{\boldsymbol{\chi}}$ of the material over time, we describe the kinematics of the body. The deformation gradient

$$\hat{\boldsymbol{F}}(\boldsymbol{X},t) \,:=\, \frac{\partial\hat{\boldsymbol{\chi}}}{\partial\boldsymbol{X}}\;, \qquad \text{or equivalently} \qquad \hat{F}_{iA}(X_B,t) \,=\, \frac{\partial\hat{\chi}_i}{\partial X_A}\;, \tag{5}$$

describes the change in distance between neighboring points as the material deforms. In Eq. (5) and from now on, a 'hat' accent indicates we are using a *Lagrangian description*, in which the function depends on the reference position $\boldsymbol{X}$ and time t. Note the deformation gradient is a so-called two-point tensor: as $\hat{\boldsymbol{F}} = \hat{F}_{iA}\,\boldsymbol{e}_i \otimes \boldsymbol{E}_A$, it has one 'leg' in the current configuration and one 'leg' in the reference configuration. When the material deforms, the relative volume change of an infinitesimal element of the body $\mathscr{B}$ is captured by the Jacobian $\tilde{J}$, given by

$$\tilde{J} \,=\, \hat{J}(\boldsymbol{X},t) \,=\, \det\Big(\hat{\boldsymbol{F}}(\boldsymbol{X},t)\Big) \,=\, \frac{\mathrm{d}v}{\mathrm{d}V}\;, \tag{6}$$

where $\mathrm{d}v$ is a differential volume element in the current configuration and $\mathrm{d}V$ is the volume of that same element in the reference configuration (we will comment on our use of the 'tilde' accent below). The velocity $\tilde{\boldsymbol{v}}$ is the rate of change of position of a material point, and is given by

$$\tilde{\boldsymbol{v}} \,=\, \hat{\boldsymbol{v}}(\boldsymbol{X},t) \,=\, \frac{\partial}{\partial t}\Big(\hat{\boldsymbol{\chi}}(\boldsymbol{X},t)\Big)\;. \tag{7}$$

The acceleration $\tilde{\boldsymbol{c}}$ is similarly expressed as [‡]

$$\tilde{\boldsymbol{c}} \;=\; \hat{\boldsymbol{c}}(\boldsymbol{X},t) \;=\; \frac{\partial}{\partial t}\Big(\hat{\boldsymbol{v}}(\boldsymbol{X},t)\Big) \;=\; \frac{\partial^2}{\partial t^2}\Big(\hat{\boldsymbol{\chi}}(\boldsymbol{X},t)\Big)\;, \tag{8}$$

i.e. the rate of change of velocity of a material point.

While Eqs. (6)–(8) are useful to study solid materials, in fluid descriptions quantities are often expressed in terms of the current configuration. We formally define the velocity as a function of the current position $\boldsymbol{x}$ and time t as

$$\tilde{\boldsymbol{v}} \;=\; \boldsymbol{v}(\boldsymbol{x},t) \;=\; \hat{\boldsymbol{v}}\big(\boldsymbol{\chi}^{-1}(\boldsymbol{x},t),t\big)\;, \tag{9}$$

where here and from now on a quantity with a 'hat' accent depends on $\boldsymbol{X}$ and t, a quantity with no accent depends on $\boldsymbol{x}$ and t, and a quantity with a 'tilde' accent can refer to either description. We then calculate the acceleration $\boldsymbol{c}$ as the material time derivative of the velocity, given by

$$\begin{aligned}\tilde{\boldsymbol{c}} \;=\; \boldsymbol{c}(\boldsymbol{x},t) &= \frac{\partial}{\partial t}\Big(\boldsymbol{v}(\boldsymbol{x},t)\Big)\Big|_{\boldsymbol{X}} \\ &= \frac{\partial}{\partial t}\Big(\boldsymbol{v}(\boldsymbol{x},t)\Big) \;+\; \left[\frac{\partial}{\partial \boldsymbol{x}}\Big(\boldsymbol{v}(\boldsymbol{x},t)\Big)\right]\frac{\partial}{\partial t}\Big(\hat{\boldsymbol{\chi}}(\boldsymbol{X},t)\Big) \\ &= \frac{\partial \boldsymbol{v}}{\partial t} \;+\; (\boldsymbol{\nabla}\boldsymbol{v})\boldsymbol{v}\;.\end{aligned} \tag{10}$$

In the last line in Eq. (10), we introduced the shorthand $\boldsymbol{\nabla}(\,\cdot\,) := [\partial(\,\cdot\,)/\partial \boldsymbol{x}]|_t$ for the spatial gradient in the current configuration. Often, we use a 'dot' accent to indicate a material time derivative in the *Eulerian description*, where quantities are written in terms of the current position $\boldsymbol{x}$ and time t. For example, $\boldsymbol{c}(\boldsymbol{x},t) = \dot{\boldsymbol{v}}(\boldsymbol{x},t)$. By introducing the velocity gradient

$$\boldsymbol{L} \;:=\; \frac{\partial}{\partial \boldsymbol{x}}\Big(\boldsymbol{v}(\boldsymbol{x},t)\Big)\;, \qquad \text{or equivalently} \qquad L_{ij} \;=\; \frac{\partial v_i}{\partial x_j}\;, \tag{11}$$

Eq. (10) can also [†] be written as $\boldsymbol{c}(\boldsymbol{x},t) = \partial \boldsymbol{v}/\partial t + \boldsymbol{L}\boldsymbol{v}$. The relationship between the velocity and deformation gradient is obtained by taking the material time derivative of the latter, for which we find

$$\begin{aligned}\frac{\mathrm{d}\tilde{\boldsymbol{F}}}{\mathrm{d}t} \;&=\; \frac{\partial}{\partial t}\Big(\hat{\boldsymbol{F}}(\boldsymbol{X},t)\Big) \;=\; \frac{\partial}{\partial t}\left[\frac{\partial}{\partial \boldsymbol{X}}\Big(\hat{\boldsymbol{\chi}}(\boldsymbol{X},t)\Big)\right] \;=\; \frac{\partial}{\partial \boldsymbol{X}}\left[\frac{\partial}{\partial t}\Big(\hat{\boldsymbol{\chi}}(\boldsymbol{X},t)\Big)\right] \\ &=\; \frac{\partial}{\partial \boldsymbol{X}}\Big(\hat{\boldsymbol{v}}(\boldsymbol{X},t)\Big) \;=\; \frac{\partial}{\partial \boldsymbol{X}}\Big(\boldsymbol{v}(\boldsymbol{x},t)\Big) \;=\; \left[\frac{\partial}{\partial \boldsymbol{x}}\Big(\boldsymbol{v}(\boldsymbol{x},t)\Big)\right]\frac{\partial}{\partial \boldsymbol{X}}\Big(\hat{\boldsymbol{\chi}}(\boldsymbol{X},t)\Big)\;,\end{aligned} \tag{12}$$

[‡]The acceleration is denoted $\boldsymbol{c}$ rather than $\boldsymbol{a}$ to avoid notational confusion with the vectors $\boldsymbol{a}_\alpha$ in subsequent sections, following P.M. Naghdi. "The Theory of Shells and Plates". *Linear Theories of Elasticity and Thermoelasticity: Linear and Nonlinear Theories of Rods, Plates, and Shells*. Ed. by C. Truesdell. Berlin, Heidelberg: Springer, 1973, pp. 425–640.

[†]In fluid mechanics, the result of Eq. (10) is often written as $\boldsymbol{a} = \partial \boldsymbol{v}/\partial t + (\boldsymbol{v}\cdot\boldsymbol{\nabla})\boldsymbol{v}$. However, in understanding $\boldsymbol{\nabla}\boldsymbol{v}$ to be the velocity gradient tensor $\boldsymbol{L}$, we prefer to express the acceleration as in Eq. (10).

such that

$$\frac{\mathrm{d}\tilde{\boldsymbol{F}}}{\mathrm{d}t} = \tilde{\boldsymbol{L}}\tilde{\boldsymbol{F}} \ , \qquad \text{or equivalently} \qquad \frac{\mathrm{d}\tilde{F}_{iA}}{\mathrm{d}t} = \tilde{L}_{ij}\tilde{F}_{jA} \ . \tag{13}$$

Equations (9), (10), and (12) show how to switch between Lagrangian and Eulerian descriptions, and take material time derivatives in the latter. In particular, for any scalar function $\tilde{f}$,

$$\tilde{f} = f(\boldsymbol{x},t) = f\big(\hat{\boldsymbol{\chi}}(\boldsymbol{X},t),t\big) = \hat{f}(\boldsymbol{X},t) \ , \tag{14}$$

and furthermore

$$\frac{\mathrm{d}\tilde{f}}{\mathrm{d}t} = \frac{\partial \hat{f}}{\partial t} \qquad \Leftrightarrow \qquad \frac{\mathrm{d}\tilde{f}}{\mathrm{d}t} = \frac{\partial f}{\partial t}\Big|_{\boldsymbol{X}} = \frac{\partial f}{\partial t} + \frac{\partial \hat{\boldsymbol{\chi}}}{\partial t} \cdot \frac{\partial f}{\partial \boldsymbol{x}} = \frac{\partial f}{\partial t} + \boldsymbol{v} \cdot \boldsymbol{\nabla} f \ . \tag{15}$$

Note that in general, some care must be applied when taking the material time derivative of vectorial and tensorial quantities.

2. The balance laws

The formulation of global and local forms of various balance laws is an essential component of any continuum mechanical formulation. Before obtaining the relevant balance laws, however, we provide several results which will be used repeatedly. With Eq. (6), integrals over the body can be expressed in either the current or reference configurations as

$$\int_{\mathcal{R}} f(\boldsymbol{x},t)\ \mathrm{d}v \ = \int_{\mathcal{R}_0} \hat{f}(\boldsymbol{X},t)\, \hat{J}(\boldsymbol{X},t)\ \mathrm{d}V \ , \tag{16}$$

where the functions f and $\hat{f}$ are related by Eq. (14). Taking the total time derivative of both sides of Eq. (16) yields

$$\begin{aligned}
\frac{\mathrm{d}}{\mathrm{d}t}\bigg(\int_{\mathcal{R}} f(\boldsymbol{x},t)\ \mathrm{d}v \bigg) \ &= \ \frac{\mathrm{d}}{\mathrm{d}t}\bigg(\int_{\mathcal{R}_0} \hat{f}(\boldsymbol{X},t)\, \hat{J}(\boldsymbol{X},t)\ \mathrm{d}V \bigg) \\
&= \int_{\mathcal{R}_0} \bigg[\frac{\partial}{\partial t}\Big(\hat{f}(\boldsymbol{X},t)\Big) \hat{J}(\boldsymbol{X},t) \ + \ \hat{f}(\boldsymbol{X},t) \frac{\partial}{\partial t}\Big(\hat{J}(\boldsymbol{X},t)\Big) \bigg] \ \mathrm{d}V \\
&= \int_{\mathcal{R}_0} \bigg(\frac{\mathrm{d}\hat{f}}{\mathrm{d}t}\, \hat{J} \ + \ \hat{f}\, \frac{\mathrm{d}\hat{J}}{\mathrm{d}t} \bigg) \ \mathrm{d}V \\
&= \int_{\mathcal{R}} \bigg(\dot{f} \ + \ f\, \frac{\dot{J}}{J} \bigg) \ \mathrm{d}v \ .
\end{aligned} \tag{17}$$

In going from the first to the second line in Eq. (17), we recognized the domain of integration $\mathcal{R}_0$ is constant and brought the time derivative inside the integral. In the third line, quantities are equivalently expressed in terms of the material derivative via Eq. (15), and in the fourth line we mapped quantities back to the current configuration. By using the matrix identity $\partial(\det \hat{\boldsymbol{F}})/\partial t = \det \hat{\boldsymbol{F}}\ \mathrm{tr}\,(\hat{\boldsymbol{F}}^{-1}\, \partial \hat{\boldsymbol{F}}/\partial t)$, where $\hat{J} = \det \hat{\boldsymbol{F}}$ (6), we find

$$\frac{\partial \hat{J}}{\partial t} \ = \ \hat{J}\ \mathrm{tr}\left(\hat{\boldsymbol{F}}^{-1} \frac{\partial \hat{\boldsymbol{F}}}{\partial t} \right) \ = \ \hat{J}\ \mathrm{tr}\left(\hat{\boldsymbol{F}}^{-1} \hat{\boldsymbol{L}} \hat{\boldsymbol{F}} \right) \ = \ \hat{J}\ \mathrm{tr}\left(\hat{\boldsymbol{L}} \hat{\boldsymbol{F}} \hat{\boldsymbol{F}}^{-1} \right) \ = \ \hat{J}\ \mathrm{tr}\, \hat{\boldsymbol{L}} \ , \tag{18}$$

such that

$$\dot{J} \;=\; J\,\operatorname{tr}\boldsymbol{L} \;=\; J\,\boldsymbol{\nabla}\cdot\boldsymbol{v}\;. \tag{19}$$

By Substituting Eq. (19) into Eq. (17), we obtain the well-known Reynolds Transport Theorem, given by

$$\frac{\mathrm{d}}{\mathrm{d}t}\left(\int_{\mathcal{R}} f(\boldsymbol{x},t)\;\mathrm{d}v\right) \;=\; \int_{\mathcal{R}}\left(\dot{f} \;+\; f\,\boldsymbol{\nabla}\cdot\boldsymbol{v}\right)\mathrm{d}v\;. \tag{20}$$

At this point, we provide two additional results without proof. The first is the divergence theorem, which can be written as

$$\int_{\partial\mathcal{R}} f\,\boldsymbol{n}\,\mathrm{d}a \;=\; \int_{\mathcal{R}} \boldsymbol{\nabla} f\,\mathrm{d}v\;, \tag{21}$$

where $\mathrm{d}a$ is a differential area element on the region boundary $\partial\mathcal{R}$, with outward pointing normal $\boldsymbol{n}$. The second is the localization theorem, which states

$$\int_{\mathcal{R}} f\,\mathrm{d}v \;=\; 0 \quad \forall\;\mathcal{R}\subseteq\mathcal{Q} \qquad \text{if and only if} \qquad f \;=\; 0 \;\text{ in }\mathcal{Q}\;, \tag{22}$$

and is useful in converting global equations to their local forms.

(a). The balance of mass

For the body $\mathscr{B}$ under consideration, we assume a mass density $\rho(\boldsymbol{x},t)$ in the current configuration, which is expressed in the reference configuration as $\hat{\rho}(\boldsymbol{X},t)$. We furthermore define $\hat{\rho}_0(\boldsymbol{X}) := \hat{\rho}(\boldsymbol{X}, t = t_0)$ to be the mass density, at the reference time t_0, in the reference configuration. In the region $\mathcal{R}(t)$, which tracks the same material points over time, the total mass of the material is conserved. The global form of the balance of mass is then given by

$$\frac{\mathrm{d}}{\mathrm{d}t}\left(\int_{\mathcal{R}} \rho(\boldsymbol{x},t)\;\mathrm{d}v\right) \;=\; 0\;. \tag{23}$$

By applying the Reynolds Transport Theorem (20) to Eq. (23), we obtain

$$\int_{\mathcal{R}}\left(\dot{\rho} \;+\; \rho\,\boldsymbol{\nabla}\cdot\boldsymbol{v}\right)\mathrm{d}v \;=\; 0\;. \tag{24}$$

As Eq. (24) is true for any $\mathcal{R}\subseteq\mathcal{Q}$, we apply the localization theorem (22) and find the local form of the balance of mass to be

$$\dot{\rho} \;+\; \rho\,\boldsymbol{\nabla}\cdot\boldsymbol{v} \;=\; 0\;. \tag{25}$$

By expanding the material time derivative with Eq. (15) and rearranging terms, Eq. (25) can also be written as

$$\frac{\partial\rho}{\partial t} \;+\; \boldsymbol{\nabla}\cdot\left(\rho\boldsymbol{v}\right) \;=\; 0\;. \tag{26}$$

Additionally, for an incompressible material, the density is ρ is constant—for which

$$\boldsymbol{\nabla}\cdot\boldsymbol{v} \;=\; 0\;, \tag{27}$$

often called the incompressibility condition.

While Eq. (25) was obtained by considering only quantities in the current configuration, we find another useful relation by expressing the total mass in the reference configuration. In particular, as the total mass of the body $\mathscr{B}$ does not change in time, we have

$$\int_{\mathcal{R}} \rho(\boldsymbol{x},t)\,\mathrm{d}v \;=\; \int_{\mathcal{R}_0} \hat{\rho}_0(\boldsymbol{X})\,\mathrm{d}V\;. \tag{28}$$

By mapping the left-hand side of Eq. (28) to the reference configuration according to Eq. (14), we obtain

$$\int_{\mathcal{R}_0} \hat{\rho}(\boldsymbol{X},t)\,\hat{J}(\boldsymbol{X},t)\,\mathrm{d}V \;=\; \int_{\mathcal{R}_0} \hat{\rho}_0(\boldsymbol{X})\,\mathrm{d}V\;, \tag{29}$$

thus implying the Jacobian $\tilde{J}$ is given by

$$\tilde{J} \;=\; \hat{J}(\boldsymbol{X},t) \;=\; \frac{\hat{\rho}_0(\boldsymbol{X})}{\hat{\rho}(\boldsymbol{X},t)}\;, \tag{30}$$

in addition to the form of the Jacobian presented in Eq. (6).

We end by substituting $f = \rho u$, for some arbitrary quantity u, into Eq. (20) to find

$$\frac{\mathrm{d}}{\mathrm{d}t}\Big(\int_{\mathcal{R}} \rho u\,\mathrm{d}v\Big) \;=\; \int_{\mathcal{R}} \Big[\rho\dot{u} + u\big(\underbrace{\dot{\rho} + \rho\,\boldsymbol{\nabla}\cdot\boldsymbol{v}}_{=0}\big)\Big]\,\mathrm{d}v \;=\; \int_{\mathcal{R}} \rho\dot{u}\,\mathrm{d}v\;. \tag{31}$$

In going from the second to third term in Eq. (31), we substituted the local form of the balance of mass (25). As we will see, Eq. (31) will be used frequently in our balance law developments.

(b). The balance of linear momentum

According to Newton's second law, the rate of change of momentum of an object is equal to the sum of all external forces acting on said object. For a continuum material, the external forces can be classified as either body forces acting on the entire volume, or boundary forces acting on the surface of the body. Denoting $\boldsymbol{f}$ to be the body force per unit volume and $\boldsymbol{t}$ to be the traction, or boundary force per unit area of the surface, the global form of the balance of linear momentum is given by

$$\frac{\mathrm{d}}{\mathrm{d}t}\Big(\int_{\mathcal{R}} \rho\boldsymbol{v}\,\mathrm{d}v\Big) \;=\; \int_{\mathcal{R}} \boldsymbol{f}\,\mathrm{d}v \;+\; \int_{\partial\mathcal{R}} \boldsymbol{t}\,\mathrm{d}a\;, \tag{32}$$

where $\int_{\mathcal{R}} \rho\boldsymbol{v}\,\mathrm{d}v$ is the total linear momentum of the body.

To simplify Eq. (32), it is necessary to convert the last term from a surface integral to a volume integral. To this end, we introduce two results. The first is known as either Cauchy's

Hypothesis or Noll's Theorem, [‡] given by

$$\boldsymbol{t}(\boldsymbol{x}, t; \partial\mathcal{R}) \;=\; \boldsymbol{t}(\boldsymbol{x}, t; \boldsymbol{n}) \tag{33}$$

and indicating the traction $\boldsymbol{t}$ depends on the region boundary only through the unit normal $\boldsymbol{n}$. The second is Cauchy's Lemma, which states

$$\boldsymbol{t}(\boldsymbol{x}, t; -\boldsymbol{n}) \;=\; -\boldsymbol{t}(\boldsymbol{x}, t; \boldsymbol{n}) \;. \tag{34}$$

Using Eqs. (33) and (34), one arrives at Cauchy's Theorem—written as

$$\boldsymbol{t}(\boldsymbol{x}, t; \boldsymbol{n}) \;=\; \boldsymbol{T}(\boldsymbol{x}, t)\boldsymbol{n} \;, \qquad \text{or equivalently} \qquad t_i \;=\; T_{ij} n_j \;, \tag{35}$$

where $\boldsymbol{T} = T_{ij}\, \boldsymbol{e}_i \otimes \boldsymbol{e}_j$ is the Cauchy stress tensor and is independent of the orientation of the surface. Upon substituting Eq. (35) into (32), we obtain

$$\frac{\mathrm{d}}{\mathrm{d}t}\left(\int_{\mathcal{R}} \rho \boldsymbol{v} \; \mathrm{d}v \right) \;=\; \int_{\mathcal{R}} \boldsymbol{f} \; \mathrm{d}v \;+\; \int_{\partial\mathcal{R}} \boldsymbol{T}\boldsymbol{n} \; \mathrm{d}a \;. \tag{36}$$

With Eq. (36), we apply Eq. (31) to the first term and the divergence theorem (21) to the last term and find

$$\int_{\mathcal{R}} \rho \dot{\boldsymbol{v}} \; \mathrm{d}v \;=\; \int_{\mathcal{R}} \boldsymbol{f} \; \mathrm{d}v \;+\; \int_{\mathcal{R}} \boldsymbol{\nabla} \cdot \boldsymbol{T} \; \mathrm{d}v \;, \tag{37}$$

where $\boldsymbol{\nabla} \cdot \boldsymbol{T} = T_{ij,j}\, \boldsymbol{e}_i$ and $(\,\cdot\,)_{,j} := \partial(\,\cdot\,)/\partial x_j$. Finally, by applying the localization theorem (22), we obtain the local form of the balance of linear momentum as

$$\rho \dot{\boldsymbol{v}} \;=\; \boldsymbol{f} \;+\; \boldsymbol{\nabla} \cdot \boldsymbol{T} \;, \qquad \text{or equivalently} \qquad \rho \dot{v}_i \;=\; f_i \;+\; T_{ij,j} \;. \tag{38}$$

Equation (38) is also known as the Cauchy momentum equation.

(c). The balance of angular momentum

In this section, we determine the local form of the balance of angular momentum, and its consequences on the symmetry of the stress tensor $\boldsymbol{T}$. We begin with the global statement, written as

$$\frac{\mathrm{d}}{\mathrm{d}t}\left(\int_{\mathcal{R}} \boldsymbol{x} \times \rho \boldsymbol{v} \; \mathrm{d}v \right) \;=\; \int_{\mathcal{R}} \boldsymbol{x} \times \boldsymbol{f} \; \mathrm{d}v \;+\; \int_{\partial\mathcal{R}} \boldsymbol{x} \times \boldsymbol{t} \; \mathrm{d}a \;, \tag{39}$$

where we assume the angular momentum of a body is only altered via the moments of external forces. While it is not considered here, J.S. Dahler and L.E. Scriven [†] discussed how the balance laws are extended to the case with internal angular momentum degrees of freedom.

[‡]Equation (33) was introduced in 1823 [A.-L. Cauchy. "Recherches sur l'équilibre et le mouvement intérieur des corps solides ou fluides, élastiques ou non élastiques". *Bulletin de la Société Philomatique* (1823), 9–13], but was proved only in 1957 [W. Noll. "The Foundations of Classical Mechanics in the Light of Recent Advances in Continuum Mechanics". *The Axiomatic Method.* Ed. by L. Henkin, P. Suppes, and A. Tarski. Studies in Logic and the Foundations of Mathematics. Amsterdam: North-Holland Publishing Co., 1959, pp. 266–281]. We acknowledge the succinct summary of these accounts, both historical and technical, by A. Gupta at http://home.iitk.ac.in/~ag/ME321/stress.pdf.

[†]J.S. Dahler and L.E. Scriven. "Angular momentum of continua". *Nature* **192** (1961), 36–37.

We now follow a similar procedure to our previous balance law developments. We apply Eq. (31) to the first term in Eq. (39), recognize $\dot{\boldsymbol{x}} = \boldsymbol{v}$ and $\boldsymbol{v} \times \boldsymbol{v} = \boldsymbol{0}$, and obtain

$$\int_{\mathcal{R}} \boldsymbol{x} \times \rho \dot{\boldsymbol{v}} \, \mathrm{d}v \;=\; \int_{\mathcal{R}} \boldsymbol{x} \times \boldsymbol{f} \, \mathrm{d}v \;+\; \int_{\partial\mathcal{R}} \boldsymbol{x} \times \boldsymbol{t} \, \mathrm{d}a \;. \tag{40}$$

Next, we substitute Eq. (35) into the last term in Eq. (40) and simplify by switching to indicial notation. To do so, we introduce the components of the three-dimensional Levi–Civita tensor, ϵ_{ijk}, in which $\epsilon_{123} = +1$, $\epsilon_{321} = -1$, and cyclic permutations of the indices yield an identical value. All other components of the Levi–Civita tensor are zero, such that for example $\boldsymbol{x} \times \boldsymbol{v} = \epsilon_{ijk}\, x_j\, v_k\, \boldsymbol{e}_i$. The i^{th} component of the last term of Eq. (40) then simplifies to

$$\begin{aligned} \int_{\partial\mathcal{R}} \epsilon_{ijk}\, x_j\, t_k \, \mathrm{d}a \;&=\; \int_{\partial\mathcal{R}} \epsilon_{ijk}\, x_j\, T_{k\ell}\, n_\ell \, \mathrm{d}a \;=\; \int_{\mathcal{R}} \Big(\epsilon_{ijk}\, x_j\, T_{k\ell}\Big)_{,\ell} \, \mathrm{d}v \\ &=\; \int_{\mathcal{R}} \epsilon_{ijk} \Big(\underbrace{x_{j,\ell}}_{=\delta_{j\ell}}\, T_{k\ell} \;+\; x_j\, T_{k\ell,\ell} \Big) \, \mathrm{d}v \;=\; \int_{\mathcal{R}} \epsilon_{ijk} \Big(T_{kj} \;+\; x_j\, T_{k\ell,\ell} \Big) \, \mathrm{d}v \;. \end{aligned} \tag{41}$$

In Eq. (41), we substituted Cauchy's Theorem (35), used the divergence theorem (21) to go from the second to the third term, then expanded the derivative and used the identity $x_{j,l} = \delta_{jl}$, where the Kronecker delta $\delta_{ij} = 1$ if $i = j$ and $\delta_{ij} = 0$ otherwise. The i^{th} component of Eq. (40) can then be written as

$$\int_{\mathcal{R}} \epsilon_{ijk}\, x_j\, \rho \dot{v}_k \, \mathrm{d}v \;=\; \int_{\mathcal{R}} \epsilon_{ijk}\, x_j\, f_k \, \mathrm{d}v \;+\; \int_{\mathcal{R}} \epsilon_{ijk} \Big(T_{kj} \;+\; x_j\, T_{k\ell,\ell} \Big) \, \mathrm{d}v \;, \tag{42}$$

upon which application of the localization theorem (22) yields

$$\epsilon_{ijk}\, x_j\, \rho \dot{v}_k \;=\; \epsilon_{ijk}\, x_j\, f_k \;+\; \epsilon_{ijk} \big(T_{kj} \;+\; x_j\, T_{k\ell,\ell} \big) \;, \tag{43}$$

namely the i^{th} component of the local form of the balance of angular momentum.

At this point, we recognize that by taking the cross product of the position $\boldsymbol{x}$ with Eq. (38) and subtracting the i^{th} component of the result from Eq. (43), we obtain

$$\epsilon_{ijk}\, T_{kj} \;=\; 0 \;, \tag{44}$$

which implies the stress tensor is symmetric—written as

$$T_{ij} \;=\; T_{ji} \qquad \text{or equivalently} \qquad \boldsymbol{T} \;=\; \boldsymbol{T}^{\mathrm{T}} \;. \tag{45}$$

(d). The balance of mechanical power

While mechanical power is not a fundamentally conserved quantity, its description is useful in our later thermodynamic developments. We begin by contracting the local form of the linear momentum balance (38) with the velocity $\boldsymbol{v}$, and integrating over the region $\mathcal{R}$ to obtain

$$\int_{\mathcal{R}} \boldsymbol{v} \cdot \rho \dot{\boldsymbol{v}} \, \mathrm{d}v \;=\; \int_{\mathcal{R}} \boldsymbol{v} \cdot \boldsymbol{f} \, \mathrm{d}v \;+\; \int_{\mathcal{R}} \boldsymbol{v} \cdot \big(\boldsymbol{\nabla} \cdot \boldsymbol{T} \big) \, \mathrm{d}v \;. \tag{46}$$

With Eq. (31), the left-hand side of Eq. (46) can be written as

$$\int_{\mathcal{R}} \boldsymbol{v}\cdot\rho\dot{\boldsymbol{v}}\,\mathrm{d}v \;=\; \frac{\mathrm{d}}{\mathrm{d}t}\Big(\int_{\mathcal{R}} \frac{\rho\boldsymbol{v}\cdot\boldsymbol{v}}{2}\,\mathrm{d}v\Big)\;, \tag{47}$$

i.e. the time derivative of the total kinetic energy. Additionally, the last term in Eq. (46) can be simplified by using indicial notation, with which we find

$$\begin{aligned}\int_{\mathcal{R}} \boldsymbol{v}\cdot(\boldsymbol{\nabla}\cdot\boldsymbol{T})\,\mathrm{d}v \;&=\; \int_{\mathcal{R}} v_i\,T_{ij,j}\,\mathrm{d}v\\ &=\; \int_{\mathcal{R}} \Big[\big(v_i\,T_{ij}\big)_{,j} \;-\; v_{i,j}\,T_{ij}\Big]\,\mathrm{d}v\\ &=\; \int_{\partial\mathcal{R}} v_i\,T_{ij}\,n_j\,\mathrm{d}a \;-\; \int_{\mathcal{R}} L_{ij}\,T_{ij}\,\mathrm{d}v\;.\end{aligned} \tag{48}$$

In Eq. (48), we began by distributing the spatial derivative, used the divergence theorem (21) on the first term, and substituted the velocity gradient L_{ij} (11) into the second term. According to the traction decomposition (35), $T_{ij}n_j = t_i$. The last term in the third line of Eq. (48) is simplified by recognizing the stress tensor is symmetric (45), such that only the symmetric portion of L_{ij} remains:

$$\begin{aligned}L_{ij}T_{ij} \;&=\; \frac{1}{2}\Big(\underbrace{L_{ij} \;+\; L_{ji}}_{=:\,2D_{ij}}\Big)T_{ij} \;+\; \frac{1}{2}\Big(L_{ij} \;-\; L_{ji}\Big)T_{ij}\\ &=\; D_{ij}\,T_{ij} \;+\; \frac{1}{2}\Big(\underbrace{L_{ij}T_{ij} \;-\; L_{ji}T_{ij}}_{=\,0}\Big)\\ &=\; D_{ij}\,T_{ij}\;.\end{aligned} \tag{49}$$

Here, we define $\boldsymbol{D}$ as the symmetric portion of the velocity gradient tensor $\boldsymbol{L} = \boldsymbol{\nabla}\boldsymbol{v}$, whose components are given by

$$D_{ij} \;:=\; \frac{1}{2}\Big(v_{i,j} \;+\; v_{j,i}\Big) \;=\; \frac{1}{2}\Big(L_{ij} \;+\; L_{ji}\Big)\;. \tag{50}$$

Denoting the double contraction of two tensors as $\boldsymbol{D}:\boldsymbol{T} = \mathrm{tr}(\boldsymbol{D}\boldsymbol{T}^{\mathrm{T}}) = D_{ij}T_{ij}$, Eq. (48) can be equivalently expressed as

$$\int_{\mathcal{R}} \boldsymbol{v}\cdot(\boldsymbol{\nabla}\cdot\boldsymbol{T})\,\mathrm{d}v \;=\; \int_{\partial\mathcal{R}} v_i\,t_i\,\mathrm{d}a \;-\; \int_{\mathcal{R}} D_{ij}\,T_{ij}\,\mathrm{d}v \;=\; \int_{\partial\mathcal{R}} \boldsymbol{v}\cdot\boldsymbol{t}\,\mathrm{d}a \;-\; \int_{\mathcal{R}} \boldsymbol{D}:\boldsymbol{T}\,\mathrm{d}v\;. \tag{51}$$

Finally, with Eqs. (47) and (51), we rewrite Eq. (46) as

$$\frac{\mathrm{d}}{\mathrm{d}t}\Big(\int_{\mathcal{R}} \frac{\rho\boldsymbol{v}\cdot\boldsymbol{v}}{2}\,\mathrm{d}v\Big) \;+\; \int_{\mathcal{R}} \boldsymbol{D}:\boldsymbol{T}\,\mathrm{d}v \;=\; \int_{\mathcal{R}} \boldsymbol{v}\cdot\boldsymbol{f}\,\mathrm{d}v \;+\; \int_{\partial\mathcal{R}} \boldsymbol{v}\cdot\boldsymbol{t}\,\mathrm{d}a\;. \tag{52}$$

Equation (52) is the mechanical power balance: the left-hand side contains the time derivative of the kinetic energy and the internal power of the body, with the latter capturing the rate of work done by internal forces on material elements; the right-hand side captures the work done by external forces on the body.

3. A thermodynamic description of a bulk material

In equilibrium thermodynamics, a material is assumed to be uniform throughout its domain, such that no spatial derivatives exist. As a consequence, one often speaks of global thermodynamic quantities, such as the total internal energy U, entropy S, or temperature T. In the study of non-equilibrium materials, on the other hand, it is of fundamental importance to describe how such quantities vary in space and time. As a result, we introduce thermodynamic fields, such as the internal energy per unit mass $u(\boldsymbol{x}, t)$, the entropy per unit mass $s(\boldsymbol{x}, t)$, and the temperature field $T(\boldsymbol{x}, t)$. In this section, we use our continuum description and balance law framework to develop local forms of the first and second laws of thermodynamics, as well as the local form of the balance of entropy.

(a). The first law: The balance of energy

According to the first law of thermodynamics, the total energy of a body $\mathscr{B}$ changes if either heat is supplied to the body or work is done on the body. The latter is described by the right-hand side of the mechanical power balance (52), while the former is captured by two terms. The first term involves the heat flux $\boldsymbol{J}_{\mathrm{q}}$, which describes the flow of energy per unit area per unit time; the second involves an external heat source per unit mass $r(\boldsymbol{x}, t)$, supplied in the volume of the body. We define $e(\boldsymbol{x}, t)$ to be the total energy per unit mass, such that the total energy of the body is given by $\int_{\mathcal{R}} \rho e \, \mathrm{d}v$. The global form of the first law of thermodynamics is then given by

$$\frac{\mathrm{d}}{\mathrm{d}t}\left(\int_{\mathcal{R}} \rho e \, \mathrm{d}v \right) = \int_{\mathcal{R}} \rho r \, \mathrm{d}v - \int_{\partial\mathcal{R}} \boldsymbol{J}_{\mathrm{q}} \cdot \boldsymbol{n} \, \mathrm{d}a + \int_{\mathcal{R}} \boldsymbol{v} \cdot \boldsymbol{f} \, \mathrm{d}v + \int_{\partial\mathcal{R}} \boldsymbol{v} \cdot \boldsymbol{t} \, \mathrm{d}a \,, \tag{53}$$

where the heat flux $\boldsymbol{J}_{\mathrm{q}}$ is defined to be positive when heat is leaving the system.

We now simplify Eq. (53) to obtain the local form of the balance of internal energy. To this end, the total energy per unit mass e can be decomposed into the kinetic energy per unit mass $\frac{1}{2}\boldsymbol{v} \cdot \boldsymbol{v}$ and the internal energy per unit mass u,[‡] for which

$$\rho e = \rho u + \frac{\rho \boldsymbol{v} \cdot \boldsymbol{v}}{2} \,. \tag{54}$$

Substituting Eq. (54) into Eq. (53), applying Eq. (31) to the resulting left-hand side, and applying the divergence theorem (21) to the heat flux term yields

$$\int_{\mathcal{R}} \left(\rho \boldsymbol{v} \cdot \dot{\boldsymbol{v}} + \rho \dot{u} \right) \mathrm{d}v = \int_{\mathcal{R}} \rho r \, \mathrm{d}v - \int_{\mathcal{R}} \boldsymbol{\nabla} \cdot \boldsymbol{J}_{\mathrm{q}} \, \mathrm{d}v + \int_{\mathcal{R}} \boldsymbol{v} \cdot \boldsymbol{f} \, \mathrm{d}v + \int_{\partial\mathcal{R}} \boldsymbol{v} \cdot \boldsymbol{t} \, \mathrm{d}a \,. \tag{55}$$

By subtracting the mechanical power balance (52) from Eq. (55) and then applying the localization theorem (22), we find the local form of the first law of thermodynamics—written as

$$\rho \dot{u} = \rho r - \boldsymbol{\nabla} \cdot \boldsymbol{J}_{\mathrm{q}} + \boldsymbol{D} : \boldsymbol{T} \,. \tag{56}$$

According to Eq. (56), the internal energy changes due to a heat supply, a flow of heat, and internal work done on the system, respectively.

[‡]For simplicity, we neglect potential energy contributions, i.e. those due to gravity or electric fields. However, such contributions can be easily incorporated.

(b). The second law and the balance of entropy

While the second law of thermodynamics is generally stated in its global form, we seek a local description within our irreversible thermodynamic formulation. To this end, we define the entropy per unit mass, $s(\boldsymbol{x}, t)$, such that the total entropy of the body $\mathscr{B}$ is $\int_{\mathcal{R}} \rho s \, \mathrm{d}v$, which can change in one of three ways. First, entropy can flow across the system boundary, as accounted for by the entropy flux $\boldsymbol{J}_{\mathrm{s}}(\boldsymbol{x}, t)$—which has units of entropy per area per time, and is defined to be positive when entropy is flowing out of the system. Second, entropy can be locally absorbed or emitted, for which we introduce the rate of external entropy supply per unit mass $\eta_{\mathrm{e}}(\boldsymbol{x}, t)$ throughout the volume of the body. By definition, the entropy flux and supply both describe the redistribution of entropy which has already been created; we capture the entropy generated at a specific location with the internal entropy production per unit mass, $\eta_{\mathrm{i}}(\boldsymbol{x}, t)$. According to this classification, the second law of thermodynamics can be written as

$$\int_{\mathcal{R}} \rho \eta_{\mathrm{i}} \, \mathrm{d}v \geq 0 \quad \forall \, \mathcal{R} \subseteq \mathcal{Q} \, , \qquad \text{for which} \qquad \rho \eta_{\mathrm{i}} \geq 0 \tag{57}$$

according to the localization theorem (22). Equation $(57)_2$ is the local form of the second law of thermodynamics.

With the aforementioned definitions, we describe how the entropy in a body can change over time. The global form of the balance of entropy is given by

$$\frac{\mathrm{d}}{\mathrm{d}t}\left(\int_{\mathcal{R}} \rho s \, \mathrm{d}v \right) = - \int_{\partial \mathcal{R}} \boldsymbol{J}_{\mathrm{s}} \cdot \boldsymbol{n} \, \mathrm{d}a + \int_{\mathcal{R}} \rho \eta_{\mathrm{e}} \, \mathrm{d}v + \int_{\mathcal{R}} \rho \eta_{\mathrm{i}} \, \mathrm{d}v \, . \tag{58}$$

Applying Eq. (31) to the left-hand side of Eq. (58) and the divergence theorem (21) to the boundary integral, we obtain

$$\int_{\mathcal{R}} \rho \dot{s} \, \mathrm{d}v = - \int_{\mathcal{R}} \boldsymbol{\nabla} \cdot \boldsymbol{J}_{\mathrm{s}} \, \mathrm{d}v + \int_{\mathcal{R}} \rho \eta_{\mathrm{e}} \, \mathrm{d}v + \int_{\mathcal{R}} \rho \eta_{\mathrm{i}} \, \mathrm{d}v \, , \tag{59}$$

for which application of the localization theorem (22) yields the local form of the balance of entropy, written as

$$\rho \dot{s} = - \boldsymbol{\nabla} \cdot \boldsymbol{J}_{\mathrm{s}} + \rho \eta_{\mathrm{e}} + \rho \eta_{\mathrm{i}} \, . \tag{60}$$

(c). The choice of thermodynamic potential

At this point, within the framework of irreversible thermodynamics, we seek to determine the form of the internal entropy production $\rho \eta_{\mathrm{i}}$. However, in the equations obtained thus far, the internal entropy production only appears in the local form of the second law of thermodynamics (57) and the entropy balance (60). To obtain an expression for $\rho \eta_{\mathrm{i}}$, we recognize the natural thermodynamic potential for continuum materials is the Helmholtz free energy—which depends on the temperature and the appropriate measure of deformation. [‡] We accordingly introduce the Helmholtz free energy per unit mass $\psi(\boldsymbol{x}, t)$, given by

$$\psi := u - T s \, , \tag{61}$$

[‡]Mandadapu, "Homogeneous Non-Equilibrium Molecular Dynamics Methods for Calculating the Heat Transport Coefficient of Solids and Mixtures".

where $\tilde{T} = T(\boldsymbol{x}, t)$ is the local temperature field of the body. By taking the material time derivative of Eq. (61) and multiplying by ρ, we obtain

$$\rho\dot{\psi} \;=\; \rho\dot{u} \;-\; \rho\dot{T}s \;-\; \rho T\dot{s}\;. \tag{62}$$

Substituting the local forms of the first law of thermodynamics (56) and the entropy balance (60) into Eq. (62) and rearranging terms yields

$$\rho\dot{s} \;=\; -\boldsymbol{\nabla}\cdot\boldsymbol{J}_{\mathrm{s}} \;+\; \rho\eta_{\mathrm{e}} \;+\; \rho\eta_{\mathrm{i}} \;=\; \frac{1}{T}\Big(\rho r \;-\; \boldsymbol{\nabla}\cdot\boldsymbol{J}_{\mathrm{q}} \;+\; \boldsymbol{D}:\boldsymbol{T} \;-\; \rho\dot{T}s \;-\; \rho\dot{\psi}\Big)\;. \tag{63}$$

Importantly, Eq. (63) involves thermodynamic quantities, velocity gradients, and the material stresses. As we will see, upon a choice of the fundamental thermodynamic variables for the Helmholtz free energy, the entropy flux, external entropy supply, and internal entropy production are determined. Irreversible thermodynamics then provides a procedure with which to determine the material stresses.

The developments thus far described a general continuum material. However, different materials are described by different fundamental thermodynamic variables, and further analysis relies on knowledge of the material of interest. To demonstrate the generality of our framework, we at this point separately consider two materials: a Newtonian fluid and an elastic solid.

4. The case of a Newtonian fluid

We begin by considering a bulk Newtonian fluid. As discussed previously, we first choose the fundamental thermodynamic variables for the Helmholtz free energy, from which we determine the form of the internal entropy production. We then take advantage of the local form of the second law of thermodynamics to arrive at an expression for the fluid stresses.

(a). The internal entropy production

In equilibrium thermodynamics, the Helmholtz free energy of a fluid depends on the temperature T and volume V. In our continuum description of an out-of-equilibrium system, the analogous quantities are the temperature field $T(\boldsymbol{x}, t)$ and mass density $\rho(\boldsymbol{x}, T)$,[‡] such that

$$\tilde{\psi} \;=\; \psi(\rho, T)\;. \tag{64}$$

By substituting Eq. (64) into Eq. (63), we obtain

$$\rho\dot{s} \;=\; -\boldsymbol{\nabla}\cdot\boldsymbol{J}_{\mathrm{s}} + \rho\eta_{\mathrm{e}} + \rho\eta_{\mathrm{i}} \;=\; \frac{1}{T}\left\{\rho r - \boldsymbol{\nabla}\cdot\boldsymbol{J}_{\mathrm{q}} + \boldsymbol{D}:\boldsymbol{T} - \rho\dot{T}\left(s + \frac{\partial\psi}{\partial T}\right) - \rho\,\frac{\partial\psi}{\partial\rho}\,\dot{\rho}\right\}\;. \tag{65}$$

We now make several simplifications. First, though the system is globally out of equilibrium, we make the *local equilibrium assumption.*[†] In any physical system, each continuum

[‡]The Helmholtz free energy density may instead be expressed as a function of the specific volume $\bar{v} = 1/\rho$.

[†]Prigogine, *Introduction to Thermodynamics of Irreversible Processes*.

point $\boldsymbol{x}$ describes a large number of constituent molecules in a neighborhood about $\boldsymbol{x}$. As there is a large separation in length and time scales of the microscopic and macroscopic dynamics, we posit that at any point $\boldsymbol{x}$ the usual thermodynamic relations hold. For example, for a fluid the entropy density $s(\rho, T)$ and pressure $p(\rho, T)$ are given by

$$s(\rho, T) \;=\; -\left(\frac{\partial \psi}{\partial T}\right)_{\rho} \qquad \text{and} \qquad p(\rho, T) \;=\; \rho^2 \left(\frac{\partial \psi}{\partial \rho}\right)_{T} , \tag{66}$$

where we recognize $p = -(\partial \psi / \partial \bar{v})_T$ for specific volume $\bar{v} = 1/\rho$. In following the terminology introduced by other authors, we will from now on refer to Eq. $(66)_1$ as the local equilibrium assumption. By substituting Eq. (66) into Eq. (65), we obtain

$$\rho \dot{s} \;=\; -\boldsymbol{\nabla} \cdot \boldsymbol{J}_{\mathrm{s}} \,+\, \rho \eta_{\mathrm{e}} \,+\, \rho \eta_{\mathrm{i}} \;=\; \frac{1}{T} \left\{ \rho r \,-\, \boldsymbol{\nabla} \cdot \boldsymbol{J}_{\mathrm{q}} \,+\, \boldsymbol{D} : \boldsymbol{T} \,-\, \frac{p \dot{\rho}}{\rho} \right\} . \tag{67}$$

Next, we rewrite the heat flux term in Eq. (67) as

$$-\,\frac{\boldsymbol{\nabla} \cdot \boldsymbol{J}_{\mathrm{q}}}{T} \;=\; -\boldsymbol{\nabla} \cdot \left(\frac{\boldsymbol{J}_{\mathrm{q}}}{T}\right) \,-\, \frac{\boldsymbol{\nabla} T \cdot \boldsymbol{J}_{\mathrm{q}}}{T^2} . \tag{68}$$

Finally, we introduce the identity tensor $\boldsymbol{I} := \delta_{ij}\, \boldsymbol{e}_i \otimes \boldsymbol{e}_j$, such that the local form of the mass balance (25) can be expressed as $\dot{\rho} = -\rho \boldsymbol{\nabla} \cdot \boldsymbol{v} = -\rho\, \boldsymbol{D} : \boldsymbol{I}$. Substituting this result, along with Eq. (68), into Eq. (67) leads to

$$\begin{aligned} \rho \dot{s} \;&=\; -\boldsymbol{\nabla} \cdot \boldsymbol{J}_{\mathrm{s}} \,+\, \rho \eta_{\mathrm{e}} \,+\, \rho \eta_{\mathrm{i}} \\ &=\; -\boldsymbol{\nabla} \cdot \left(\frac{\boldsymbol{J}_{\mathrm{q}}}{T}\right) \,+\, \frac{\rho r}{T} \,-\, \frac{\boldsymbol{\nabla} T \cdot \boldsymbol{J}_{\mathrm{q}}}{T^2} \,+\, \frac{1}{T}\, \boldsymbol{D} : \Big(\boldsymbol{T} \,+\, p \boldsymbol{I}\Big) . \end{aligned} \tag{69}$$

At this stage, we determine the form of the various terms in the entropy balance. From dimensional arguments, Eq. (69) reveals

$$\boldsymbol{J}_{\mathrm{s}} \;=\; \frac{\boldsymbol{J}_{\mathrm{q}}}{T} , \tag{70}$$

i.e. the entropy flux and heat flux through the body are related by a factor of the temperature. Moreover, as the external entropy supply captures a local change in entropy by the body's surroundings, we find

$$\rho \eta_{\mathrm{e}} \;=\; \frac{\rho r}{T} , \tag{71}$$

which similarly states the relation between the heat supply and corresponding entropy supply. Finally, the remaining terms contribute to the internal entropy production, which is given by

$$\rho \eta_{\mathrm{i}} \;=\; -\,\frac{\boldsymbol{\nabla} T \cdot \boldsymbol{J}_{\mathrm{q}}}{T^2} \,+\, \frac{1}{T}\, \boldsymbol{D} : \Big(\boldsymbol{T} \,+\, p \boldsymbol{I}\Big) \;\geq\; 0 . \tag{72}$$

(b). The thermodynamic fluxes and forces

With the form of the internal entropy production, irreversible thermodynamics provides a method to calculate the stresses in a material. Before doing so, we make several observations regarding Eq. (72). First, when the entire system is in thermodynamic equilibrium, there are no temperature gradients, no velocity gradients, and the entropy production is zero. When the body is not in thermodynamic equilibrium, either $\boldsymbol{\nabla} T \neq \mathbf{0}$, $\boldsymbol{D} \neq \mathbf{0}$, or both; in any of these cases, we expect entropy to be produced. Moreover, in the aforementioned scenarios there is a driven response in the system: a temperature gradient drives a heat flux, while a velocity gradient drives a momentum flux.

In the language of irreversible thermodynamics, temperature and velocity gradients are *thermodynamic forces*, which lead to corresponding *thermodynamic fluxes*. Denoting the former as $\{X_k\}$ and the latter as $\{J_k\}$, the internal entropy production is of the general form

$$\rho \eta_{\mathrm{i}} = \sum_k J_k \cdot X_k \geq 0 \,, \tag{73}$$

where X_k and J_k can be scalar, vector, or tensor quantities. We posit that if the system is close to equilibrium, then the thermodynamic fluxes and forces are linearly related, [‡, †] and can be expressed as

$$J_i = \sum_k L_{ik} X_k \,. \tag{74}$$

In Eq. (74), L_{ik} are known as *phenomenological coefficients*. [*] We substitute Eq. (74) into Eq. (73) to find

$$\rho \eta_{\mathrm{i}} = \sum_{i,k} L_{ik} X_i X_k \geq 0 \quad \forall \, \{X_i\} \,, \tag{75}$$

implying the matrix $[L_{ik}]$ of the phenomenological coefficients is positive semidefinite. We also note the phenomenological coefficients are symmetric, i.e. $L_{ik} = L_{ki}$, when the microscopic dynamics are time-reversal symmetric. [§, ♯]

In the internal entropy production of a bulk fluid (72), there are two thermodynamic forces: $-\boldsymbol{\nabla} T/T^2 = \boldsymbol{\nabla}(1/T)$ and $\boldsymbol{D}/T$. However, as the temperature $T > 0$ everywhere, we treat $-\boldsymbol{\nabla} T$ and $\boldsymbol{D}$ as the thermodynamic forces, with $\boldsymbol{J}_{\mathrm{q}}$ and $(\boldsymbol{T} + p\boldsymbol{I})$ the corresponding fluxes. Thus, according to Eq. (74) we find

$$\boldsymbol{J}_{\mathrm{q}} = -\boldsymbol{\kappa} \boldsymbol{\nabla} T + \boldsymbol{\alpha} \boldsymbol{D} \tag{76}$$

and

$$\boldsymbol{T} + p\boldsymbol{I} = \boldsymbol{\mu} \boldsymbol{D} - \boldsymbol{\beta} \boldsymbol{\nabla} T \,. \tag{77}$$

[‡] Prigogine, *Introduction to Thermodynamics of Irreversible Processes*.

[†] de Groot and Mazur, *Non-Equilibrium Thermodynamics*.

[*] Though the phenomenological coefficients describe transport at the continuum scale, they also capture how an equilibrium system relaxes from spontaneous thermal fluctuations, according to the celebrated Onsager regression hypothesis. [§, ♯]

[§] Onsager, "Reciprocal relations in irreversible processes. I."

[♯] Onsager, "Reciprocal relations in irreversible processes. II."

In Eqs. (76) and (77), we recognize $\boldsymbol{\kappa}$ to be the second-order thermal conductivity tensor connecting temperature gradients to heat fluxes, while $\boldsymbol{\mu}$ is the fourth-order viscosity tensor describing the irreversible fluid stresses arising from velocity gradients. The third-order tensors $\boldsymbol{\alpha}$ and $\boldsymbol{\beta}$ describe cross-coupling between heat and momentum transport, with the symmetry of the phenomenological coefficients implying $\alpha_{ijk} = \beta_{jki}$.

If the fluid is isotropic, the phenomenological coefficients are isotropic as well. It was recently shown that in d dimensions, any isotropic tensor can be expressed as a linear combination of terms involving only the Kronecker delta δ_{ij} and the d-dimensional Levi–Civita tensor—in this case ϵ_{ijk} for $d = 3$.[‡] Thus, the most general forms of the tensors $\boldsymbol{\kappa}$, $\boldsymbol{\alpha}$, $\boldsymbol{\beta}$, and $\boldsymbol{\mu}$ in three dimensions are given by

$$\kappa_{ij} \;=\; \kappa\,\delta_{ij}\;, \tag{78}$$

$$\alpha_{ijk} \;=\; \alpha\,\epsilon_{ijk}\;, \tag{79}$$

$$\beta_{ijk} \;=\; \beta\,\epsilon_{ijk}\;, \tag{80}$$

and

$$\mu_{ijk\ell} \;=\; \nu\,\delta_{ij}\delta_{k\ell} \;+\; \mu\big(\delta_{ik}\delta_{j\ell} \;+\; \delta_{i\ell}\delta_{jk}\big) \;-\; \xi\big(\delta_{ik}\delta_{j\ell} \;-\; \delta_{i\ell}\delta_{jk}\big)\;. \tag{81}$$

Additionally, to respect the required symmetry $\alpha_{ijk} = \beta_{jki}$, we find $\alpha = \beta$, such that

$$\alpha_{ijk} \;=\; \beta_{ijk} \;=\; \alpha\,\epsilon_{ijk}\;. \tag{82}$$

By substituting Eqs. (78)–(82) into Eqs. (76) and (77) and noting $D_{ij} = D_{ji}$, we obtain

$$\boldsymbol{J}_{\mathrm{q}} \;=\; -\kappa\boldsymbol{\nabla}T \;+\; \alpha\,\epsilon_{ijk}\,D_{jk}\,\boldsymbol{e}_i \tag{83}$$

and

$$\boldsymbol{T} \;+\; p\boldsymbol{I} \;=\; 2\mu\boldsymbol{D} \;+\; \nu\big(\boldsymbol{D}:\boldsymbol{I}\big)\boldsymbol{I} \;-\; \alpha\,\epsilon_{ijk}\,T_{,k}\,\boldsymbol{e}_i\otimes\boldsymbol{e}_j\;. \tag{84}$$

In Eq. (84), all quantities are symmetric except for the last term, which is antisymmetric—thus implying the coefficient $\alpha = 0$. Equations (83) and (84) then simplify to

$$\boldsymbol{J}_{\mathrm{q}} \;=\; -\kappa\boldsymbol{\nabla}T \tag{85}$$

and

$$\boldsymbol{T} \;=\; -p\boldsymbol{I} \;+\; 2\mu\boldsymbol{D} \;+\; \nu\big(\boldsymbol{D}:\boldsymbol{I}\big)\boldsymbol{I}\;, \tag{86}$$

from which we recognize κ is the scalar thermal conductivity. At this point, it is useful to partition $\boldsymbol{D}$ into deviatoric [traceless, superscript '(d)'] and isotropic [superscript '(i)'] components as

$$\boldsymbol{D} \;=\; \underbrace{\left(\boldsymbol{D} \;-\; \frac{1}{3}\,(\boldsymbol{D}:\boldsymbol{I})\right)}_{\boldsymbol{D}^{(\mathrm{d})}} \;+\; \underbrace{\left(\frac{1}{3}\,(\boldsymbol{D}:\boldsymbol{I})\,\boldsymbol{I}\right)}_{\boldsymbol{D}^{(\mathrm{i})}}\;. \tag{87}$$

[‡]J.M. Epstein and K.K. Mandadapu. "Time-reversal symmetry breaking in two dimensional nonequilibrium viscous fluids". *Phys. Rev. E* **101** (2020), 052614. arXiv: 1907.10041.

By substituting Eq. (87) into Eq. (86), rearranging terms, and defining

$$\lambda := \frac{2\mu}{3} + \nu \,, \tag{88}$$

we find the stress tensor is given by

$$\begin{aligned} \boldsymbol{T} &= -p\boldsymbol{I} + 2\mu\boldsymbol{D}^{(\mathrm{d})} + \lambda\big(\boldsymbol{D}^{(\mathrm{i})} : \boldsymbol{I}\big)\boldsymbol{I} \\ &= -p\boldsymbol{I} + \mu\left[\big(\boldsymbol{\nabla}\boldsymbol{v}\big) + \big(\boldsymbol{\nabla}\boldsymbol{v}\big)^{\mathrm{T}} - \frac{2}{3}\big(\boldsymbol{\nabla}\cdot\boldsymbol{v}\big)\,\boldsymbol{I}\right] + \lambda\big(\boldsymbol{\nabla}\cdot\boldsymbol{v}\big)\boldsymbol{I} \,, \end{aligned} \tag{89}$$

thus revealing μ is the shear viscosity and λ is the dilational viscosity.[‡] Finally, by substituting Eqs. (85) and (89) into Eq. (72) and noting $(\boldsymbol{D} : \boldsymbol{I})^2 = 3\boldsymbol{D}^{(\mathrm{i})} : \boldsymbol{D}^{(\mathrm{i})}$, we find

$$\rho\eta_{\mathrm{i}} = \frac{\kappa\boldsymbol{\nabla}T\cdot\boldsymbol{\nabla}T}{T^2} + \frac{1}{T}\left(2\mu\boldsymbol{D}^{(\mathrm{d})} : \boldsymbol{D}^{(\mathrm{d})} + 3\lambda\,\boldsymbol{D}^{(\mathrm{i})} : \boldsymbol{D}^{(\mathrm{i})}\right) \geq 0 \,. \tag{90}$$

As we can construct processes in which $\boldsymbol{\nabla}T$, $\boldsymbol{D}^{(\mathrm{d})}$, and $\boldsymbol{D}^{(\mathrm{i})}$ are specified arbitrarily, Eq. (90) reveals $\kappa > 0$, $\mu > 0$, and $\lambda > 0$.

Equations (85) and (89) present one of the main results of our introduction to irreversible thermodynamics. Namely, in the *linear irreversible regime*, for which Eq. (74) is valid, we recover the heat flux $\boldsymbol{J}_{\mathrm{q}}$ of Fourier's first law, and also obtain the well-known stress tensor of an isotropic Newtonian fluid. Thus, irreversible thermodynamics provides a framework to determine the thermodynamic fluxes in an out-of-equilibrium system. We close our discussion by proposing a form of the Helmholtz free energy density for both compressible and incompressible fluids.

The case of a compressible fluid

Thus far, our fluid developments assumed a general Helmholtz free energy density $\psi(\rho, T)$. To propose a form of ψ for an isotropic compressible fluid, we recognize the total Helmholtz free energy W is given by

$$W = \int_{\mathcal{R}} \rho\psi \,\mathrm{d}v = \int_{\mathcal{R}_0} \hat{\rho}\hat{\psi}\hat{J} \,\mathrm{d}V \,. \tag{91}$$

To energetically penalize deviations in the volume of a material element with respect to the reference configuration, we posit

$$W = \int_{\mathcal{R}_0} \frac{1}{2}\,k_{\mathrm{c}}\left(\hat{J}-1\right)^2 \mathrm{d}V \,, \tag{92}$$

in which k_{c} is a compressibility modulus with units of energy per volume. By comparing Eqs. (91) and (92), and recognizing $\hat{J} = \hat{\rho}_0/\hat{\rho}$ (30), we find

$$\psi = \frac{1}{2}\,\frac{k_{\mathrm{c}}}{\rho_0}\left(J-1\right)^2 \,. \tag{93}$$

[‡]The phenomenological coefficient λ is also known as the *bulk viscosity* or *second coefficient of viscosity*.

At this point, we recognize $p = -k_{\mathrm{c}}(J-1)$ according to Eq. $(66)_2$, for which the stress tensor $\boldsymbol{T}$ is given by

$$\begin{aligned}\boldsymbol{T} &= k_{\mathrm{c}}\big(J-1\big)\boldsymbol{I} + 2\mu\boldsymbol{D}^{(\mathrm{d})} + \lambda\big(\boldsymbol{D}^{(\mathrm{i})} : \boldsymbol{I}\big)\boldsymbol{I} \\ &= k_{\mathrm{c}}\big(J-1\big)\boldsymbol{I} + \mu\left[\big(\boldsymbol{\nabla}\boldsymbol{v}\big) + \big(\boldsymbol{\nabla}\boldsymbol{v}\big)^{\mathrm{T}} - \frac{2}{3}\big(\boldsymbol{\nabla}\cdot\boldsymbol{v}\big)\boldsymbol{I}\right] + \lambda\big(\boldsymbol{\nabla}\cdot\boldsymbol{v}\big)\boldsymbol{I}\,.\end{aligned} \tag{94}$$

Substituting Eq. (94) into Eq. (38) and including the local form of the mass balance (25) yields the compressible Navier–Stokes equations, written as

$$\dot{\rho} + \rho\boldsymbol{\nabla}\cdot\boldsymbol{v} = 0 \qquad \text{and} \qquad \rho\dot{\boldsymbol{v}} = \boldsymbol{f} - k_{\mathrm{c}}\frac{\rho_0}{\rho^2}\boldsymbol{\nabla}\rho + \mu\nabla^2\boldsymbol{v} + \left(\frac{\mu}{3}+\lambda\right)\boldsymbol{\nabla}\big(\boldsymbol{\nabla}\cdot\boldsymbol{v}\big)\,. \tag{95}$$

The case of an incompressible fluid

When the fluid is incompressible, $\rho = \rho_0 =$ constant, such that $\boldsymbol{\nabla}\cdot\boldsymbol{v} = 0$ and $J = 1$. The total Helmholtz free energy W now enforces the incompressibility constraint $J-1=0$ with the Lagrange multiplier $\Pi = \Pi(\boldsymbol{x},t)$, for which

$$W = \int_{\mathcal{R}_0} -\Pi\left(\hat{J}-1\right)\mathrm{d}V\,, \tag{96}$$

and correspondingly

$$\psi = -\Pi\left(\frac{1}{\rho} - \frac{1}{\rho_0}\right)\,. \tag{97}$$

From Eq. (97), we calculate $p = \rho^2(\partial\psi/\partial\rho) = \Pi$, thus revealing the hydrodynamic pressure is a Lagrange multiplier enforcing the incompressibility of the fluid. In this case, by including the incompressibility constraint, we arrive at the Navier–Stokes equations of an incompressible Newtonian fluid, given by

$$\boldsymbol{\nabla}\cdot\boldsymbol{v} = 0 \qquad \text{and} \qquad \rho\dot{\boldsymbol{v}} = \boldsymbol{f} - \boldsymbol{\nabla}p + \mu\nabla^2\boldsymbol{v}\,. \tag{98}$$

5. The case of an elastic solid

We end our discussion of irreversible thermodynamics for bulk materials by considering an elastic solid. We follow a similar procedure to that of a Newtonian fluid, except in this case deformations of the material are reversible and do not lead to internal entropy production. We close by presenting the stress tensor of an elastic solid, which in the limit of infinitesimal strains yields the Cauchy–Navier equations when substituted into the linear momentum balance.

(a). The internal entropy production

When deforming a solid from its reference configuration, the energy required to do so depends not only on the relative change in volume of the material, but also on the direction in which

it deforms. For example, in general it does not take the same amount of energy to compress the object isotropically as it does to shear the solid, with the latter preserving the volume of the material. The state of the deformed material is captured by the deformation gradient $\tilde{\boldsymbol{F}}$, and thus the Helmholtz free energy per unit mass is of the functional form

$$\tilde{\psi} \;=\; \psi(\boldsymbol{F}, T) \;. \tag{99}$$

Note that while we usually express the deformation gradient as a function of the reference position, in this analysis all of our balance laws are written in terms of the current position and so we write $\tilde{\boldsymbol{F}} = \boldsymbol{F}(\boldsymbol{x}, t)$. Substituting Eq. (99) into Eq. (63) yields

$$\rho\dot{s} \;=\; -\boldsymbol{\nabla}\!\cdot\!\boldsymbol{J}_{\rm s} + \rho\eta_{\rm e} + \rho\eta_{\rm i} \;=\; \frac{1}{T}\left\{\rho r - \boldsymbol{\nabla}\!\cdot\!\boldsymbol{J}_{\rm q} + \boldsymbol{D}:\boldsymbol{T} - \rho\dot{T}\left(s + \frac{\partial\psi}{\partial T}\right) - \rho\,\frac{\partial\psi}{\partial\boldsymbol{F}} : \dot{\boldsymbol{F}}^{\rm T}\right\}. \tag{100}$$

For an elastic solid, the local equilibrium assumption is given by [cf. Eq. (66)]

$$s(\boldsymbol{F}, T) \;=\; -\left(\frac{\partial\psi}{\partial T}\right)_{\boldsymbol{F}} . \tag{101}$$

Upon substituting Eq. (101) into Eq. (100), we obtain

$$\rho\dot{s} \;=\; -\boldsymbol{\nabla}\cdot\boldsymbol{J}_{\rm s} \;+\; \rho\eta_{\rm e} \;+\; \rho\eta_{\rm i} \;=\; \frac{1}{T}\left\{\rho r \;-\; \boldsymbol{\nabla}\cdot\boldsymbol{J}_{\rm q} \;+\; \boldsymbol{D}:\boldsymbol{T} \;-\; \rho\,\frac{\partial\psi}{\partial\boldsymbol{F}} : \dot{\boldsymbol{F}}^{\rm T}\right\}. \tag{102}$$

The last term in Eq. (102) is simplified by recognizing $\dot{\boldsymbol{F}} = \boldsymbol{L}\boldsymbol{F}$ (13), for which

$$\begin{aligned}\frac{\partial\psi}{\partial\boldsymbol{F}} : \dot{\boldsymbol{F}}^{\rm T} \;&=\; \frac{\partial\psi}{\partial\boldsymbol{F}} : \Big(\boldsymbol{L}\boldsymbol{F}\Big)^{\rm T} \;=\; \frac{\partial\psi}{\partial\boldsymbol{F}} : \Big(\boldsymbol{F}^{\rm T}\boldsymbol{L}^{\rm T}\Big) \\ &=\; \mathrm{tr}\left\{\frac{\partial\psi}{\partial\boldsymbol{F}}\Big(\boldsymbol{F}^{\rm T}\boldsymbol{L}^{\rm T}\Big)\right\} \;=\; \mathrm{tr}\left\{\left(\frac{\partial\psi}{\partial\boldsymbol{F}}\,\boldsymbol{F}^{\rm T}\right)\boldsymbol{L}^{\rm T}\right\} \;=\; \left(\frac{\partial\psi}{\partial\boldsymbol{F}}\,\boldsymbol{F}^{\rm T}\right) : \boldsymbol{L}^{\rm T} \;.\end{aligned} \tag{103}$$

By substituting Eq. (103) into Eq. (102), rewriting the heat flux term as in Eq. (68), and recognizing $\boldsymbol{D}:\boldsymbol{T} = \boldsymbol{T}:\boldsymbol{L}^{\rm T}$ due to the symmetry of the stress tensor (45), we obtain

$$\begin{aligned}\rho\dot{s} \;&=\; -\boldsymbol{\nabla}\cdot\boldsymbol{J}_{\rm s} \;+\; \rho\eta_{\rm e} \;+\; \rho\eta_{\rm i} \\ &=\; -\boldsymbol{\nabla}\cdot\left(\frac{\boldsymbol{J}_{\rm q}}{T}\right) \;+\; \frac{\rho r}{T} \;-\; \frac{\boldsymbol{\nabla}T\cdot\boldsymbol{J}_{\rm q}}{T^2} \;+\; \frac{1}{T}\left(\boldsymbol{T} \;-\; \rho\,\frac{\partial\psi}{\partial\boldsymbol{F}}\,\boldsymbol{F}^{\rm T}\right) : \boldsymbol{L}^{\rm T} \;.\end{aligned} \tag{104}$$

As in the analysis of a bulk fluid, we now use Eq. (104) to determine the various terms in the entropy balance. We once again find

$$\boldsymbol{J}_{\rm s} \;=\; \frac{\boldsymbol{J}_{\rm q}}{T} \tag{105}$$

and

$$\rho\eta_{\rm e} \;=\; \frac{\rho r}{T} \;, \tag{106}$$

however in this case the internal entropy production is given by

$$\rho\eta_{\rm i} \;=\; -\frac{\boldsymbol{\nabla}T\cdot\boldsymbol{J}_{\rm q}}{T^2} \;+\; \frac{1}{T}\left(\boldsymbol{T} \;-\; \rho\,\frac{\partial\psi}{\partial\boldsymbol{F}}\,\boldsymbol{F}^{\rm T}\right) : \boldsymbol{L}^{\rm T} \;\geq\; 0 \;. \tag{107}$$

(b). The thermodynamic fluxes and forces

The internal entropy production of a solid (107) is similar in form to that of a Newtonian fluid (72). Due to the temperature T being positive, we treat $-\boldsymbol{\nabla} T$ and $\boldsymbol{L}^{\mathrm{T}}$ as thermodynamic forces, with $\boldsymbol{J}_{\mathrm{q}}$ and $(\boldsymbol{T} - \rho[\partial\psi/\partial\boldsymbol{F}]\boldsymbol{F}^{\mathrm{T}})$ being the corresponding thermodynamic fluxes. In the linear irreversible regime, we find

$$\boldsymbol{J}_{\mathrm{q}} \,=\, -\boldsymbol{\kappa}\boldsymbol{\nabla} T \,+\, \alpha\, \epsilon_{ijk}\, L_{jk}\, \boldsymbol{e}_i \tag{108}$$

and

$$\boldsymbol{T} \,=\, \rho\, \frac{\partial \psi}{\partial \boldsymbol{F}}\, \boldsymbol{F}^{\mathrm{T}} \,+\, \boldsymbol{\mu}\boldsymbol{L}^{\mathrm{T}} \,-\, \alpha\, \epsilon_{ijk}\, T_{,k}\, \boldsymbol{e}_i \otimes \boldsymbol{e}_j \ , \tag{109}$$

where the cross-coupling coefficients are identical in structure to those of the Newtonian fluid. As before, we recognize that the symmetry of the stress tensor and antisymmetry of the Levi–Civita symbol require $\alpha = 0$ in Eq. (109), such that the heat flux and stress tensor are respectively given by

$$\boldsymbol{J}_{\mathrm{q}} \,=\, -\boldsymbol{\kappa}\boldsymbol{\nabla} T \tag{110}$$

and

$$\boldsymbol{T} \,=\, \rho \frac{\partial \psi}{\partial \boldsymbol{F}} \boldsymbol{F}^{\mathrm{T}} \,+\, \boldsymbol{\mu}\boldsymbol{L}^{\mathrm{T}} \ . \tag{111}$$

Equation (110) is again the general form of Fourier's first law. In Eq. (111), we recognize $\boldsymbol{\mu}$ captures an irreversible flux of momentum resulting from velocity gradients in the material. However, an elastic solid by definition deforms reversibly, implying $\boldsymbol{\mu} = \boldsymbol{0}$. Thus, for an elastic solid with Helmholtz free energy of the form given in Eq. (99), the stress tensor is given by

$$\boldsymbol{T} \,=\, \rho\, \frac{\partial \psi}{\partial \boldsymbol{F}}\, \boldsymbol{F}^{\mathrm{T}} \ . \tag{112}$$

Equation (112) is the usual form of the stress tensor of a hyperelastic material. [‡]

The case of infinitesimal strains

The result of Eq. (112) is valid for a wide range of materials; we conclude by considering the simplest example: an isotropic solid in which the strains are infinitesimal. In this case, we choose the bases in the current and reference configurations to be equal, i.e. $\{\boldsymbol{E}_A\} = \{\boldsymbol{e}_i\}$, and introduce the displacement field $\hat{\boldsymbol{u}} = \hat{u}_i\, \boldsymbol{e}_i$ satisfying

$$\hat{\boldsymbol{\chi}}(\boldsymbol{X}, t) \,=\, \boldsymbol{X} \,+\, \hat{\boldsymbol{u}}(\boldsymbol{X}, t) \ . \tag{113}$$

The deformation gradient can then be written as

$$\hat{\boldsymbol{F}} \,=\, \boldsymbol{I} \,+\, \frac{\partial \hat{\boldsymbol{u}}}{\partial \boldsymbol{X}} \ . \tag{114}$$

In the limit of infinitesimal strains, $|\partial\hat{\boldsymbol{u}}/\partial\boldsymbol{X}| \ll 1$ and $|\partial\boldsymbol{u}/\partial\boldsymbol{x}| \ll 1$, such that

$$\frac{\partial \hat{\boldsymbol{u}}}{\partial \boldsymbol{X}} \,=\, \frac{\partial \boldsymbol{u}}{\partial \boldsymbol{x}}\, \frac{\partial \hat{\boldsymbol{\chi}}}{\partial \boldsymbol{X}} \,=\, \frac{\partial \boldsymbol{u}}{\partial \boldsymbol{x}}\, \hat{\boldsymbol{F}} \,=\, \frac{\partial \boldsymbol{u}}{\partial \boldsymbol{x}} \left(\boldsymbol{I} \,+\, \frac{\partial \hat{\boldsymbol{u}}}{\partial \boldsymbol{X}} \right) \,=\, \frac{\partial \boldsymbol{u}}{\partial \boldsymbol{x}} \,+\, \mathcal{O}\left(\left| \frac{\partial \hat{\boldsymbol{u}}}{\partial \boldsymbol{X}} \right|^2 \right) \ . \tag{115}$$

[‡] R.W. Ogden. *Non-Linear Elastic Deformations*. New York: Dover, 1997.

Equation (115) indicates gradients of the displacement with respect to the reference and current positions are equal to first order. We thus define the *infinitesimal strain tensor*

$$\boldsymbol{\varepsilon} := \frac{1}{2}\Big[(\boldsymbol{\nabla u}) + (\boldsymbol{\nabla u})^{\mathrm{T}} \Big] , \tag{116}$$

which to first order satisfies

$$\boldsymbol{F}^{\mathrm{T}}\boldsymbol{F} = \boldsymbol{F}\boldsymbol{F}^{\mathrm{T}} = 2\boldsymbol{\varepsilon} + \boldsymbol{I} . \tag{117}$$

At this point, we have a simplified kinematic description of the material. We choose the total Helmholtz free energy to be quadratic in the strains, which for an isotropic material is written as

$$W = \int_{\mathcal{R}_0} \left[\mu \boldsymbol{\varepsilon} : \boldsymbol{\varepsilon} + \frac{\lambda}{2} (\boldsymbol{\varepsilon} : \boldsymbol{I})^2 \right] \mathrm{d}V . \tag{118}$$

In Eq. (118), μ and λ are the Lamé coefficients: μ penalizes shearing modes while λ penalizes volume changes relative to the reference configuration. With Eqs. (91) and (118), we find the Helmholtz free energy per unit mass to satisfy

$$\rho_0 \psi = \mu \boldsymbol{\varepsilon} : \boldsymbol{\varepsilon} + \frac{\lambda}{2} (\boldsymbol{\varepsilon} : \boldsymbol{I})^2 . \tag{119}$$

By substituting Eq. (119) into Eq. (112) and taking advantage of Eq. (117), we find the stress tensor $\boldsymbol{T}$ is given by

$$\boldsymbol{T} = 2\mu \boldsymbol{\varepsilon} + \lambda (\boldsymbol{\varepsilon} : \boldsymbol{I}) \boldsymbol{I} . \tag{120}$$

Finally, substituting Eq. (120) into the linear momentum balance (38) and including the mass balance (30) yields the well-known Cauchy–Navier equations—written in terms of the displacement $\boldsymbol{u}$ as

$$\rho = \rho_0 (1 - \boldsymbol{\nabla} \cdot \boldsymbol{u}) \qquad \text{and} \qquad \rho \ddot{\boldsymbol{u}} = \boldsymbol{f} + \mu \nabla^2 \boldsymbol{u} + (\lambda + \mu) \boldsymbol{\nabla} (\boldsymbol{\nabla} \cdot \boldsymbol{u}) . \tag{121}$$

Note Eq. (121) is similar in structure to the Navier–Stokes equations of a compressible fluid [cf. Eq. (95)].

References

[1] A.-L. Cauchy. “Recherches sur l’équilibre et le mouvement intérieur des corps solides ou fluides, élastiques ou non élastiques”. *Bulletin de la Société Philomatique* (1823), 9–13

[2] J.S. Dahler and L.E. Scriven. “Angular momentum of continua”. *Nature* **192** (1961), 36–37

[3] S.R. de Groot and P. Mazur. *Non-Equilibrium Thermodynamics*. New York: Dover, 1984

[4] J.M. Epstein and K.K. Mandadapu. “Time-reversal symmetry breaking in two dimensional nonequilibrium viscous fluids”. *Phys. Rev. E* **101** (2020), 052614. arXiv: 1907.10041

[5] K.K. Mandadapu. "Homogeneous Non-Equilibrium Molecular Dynamics Methods for Calculating the Heat Transport Coefficient of Solids and Mixtures". PhD thesis. University of California, Berkeley, 2011

[6] P.M. Naghdi. "The Theory of Shells and Plates". *Linear Theories of Elasticity and Thermoelasticity: Linear and Nonlinear Theories of Rods, Plates, and Shells*. Ed. by C. Truesdell. Berlin, Heidelberg: Springer, 1973, pp. 425–640

[7] W. Noll. "The Foundations of Classical Mechanics in the Light of Recent Advances in Continuum Mechanics". *The Axiomatic Method*. Ed. by L. Henkin, P. Suppes, and A. Tarski. Studies in Logic and the Foundations of Mathematics. Amsterdam: North-Holland Publishing Co., 1959, pp. 266–281

[8] R.W. Ogden. *Non-Linear Elastic Deformations*. New York: Dover, 1997

[9] L. Onsager. "Reciprocal relations in irreversible processes. I.". *Phys. Rev.* **37** (1931), 405–426

[10] L. Onsager. "Reciprocal relations in irreversible processes. II.". *Phys. Rev.* **38** (1931), 2265–2279

[11] I. Prigogine. *Introduction to Thermodynamics of Irreversible Processes*. 3rd ed. New York: Interscience Publishers, 1967

Part B

Theory

List of important symbols

$\mathbf{1}$	identity tensor in $\mathbb{R}^3$
a	current membrane area
A	reference membrane area
$\boldsymbol{a}_\alpha$	in-plane covariant basis vectors
$\boldsymbol{a}^\alpha$	in-plane contravariant basis vectors
$\boldsymbol{a}_{\alpha,\beta}$	partial derivative of $\boldsymbol{a}_\alpha$ w.r.t. θ^β
$\boldsymbol{a}_{\alpha;\beta}$	covariant derivative of $\boldsymbol{a}_\alpha$ w.r.t. θ^β
$a_{\alpha\beta}$	covariant metric
$a^{\alpha\beta}$	contravariant metric
$\dot{a}_{\alpha\beta}$	material time derivative of metric
$b_{\alpha\beta}$	covariant curvature components
$b^{\alpha\beta}$	contravariant curvature components
$\dot{b}_{\alpha\beta}$	material time derivative of curvature
$\bar{b}^{\alpha\beta}$	cofactor of curvature
$\boldsymbol{c}$	membrane acceleration
$\boldsymbol{d}$	director field
Δ_s	surface Laplacian operator
e	total energy per mass
$\varepsilon^{\alpha\beta}$	Levi–Civita tensor
η	in-plane bulk viscosity coefficient
η_e	external entropy per mass
η_i	internal entropy per mass
$\boldsymbol{f}$	body force per area
$\boldsymbol{F}$	force at membrane boundary
$\boldsymbol{F}_i$	force on the i^{th} corner of the membrane boundary
$\Gamma^\alpha_{\beta\mu}$	Christoffel symbols of the 2nd kind
H	mean curvature
$\boldsymbol{i}$	surface identity tensor
J	Jacobian determinant
J^k	thermodynamic flux
$\boldsymbol{J}_\mathrm{q}$	in-plane heat flux
$\boldsymbol{J}_\mathrm{s}$	in-plane entropy flux
k_b	mean bending modulus
k_g	Gaussian bending modulus
k_c	compression modulus
K	Gaussian curvature
κ	scalar thermal conductivity
$\kappa^{\alpha\beta}$	thermal conductivity components
ℓ	arc length parametrization of a curve
L^{ik}	phenomenological coefficient matrix
λ	surface tension
$\boldsymbol{m}$	bending moment per length
m_ν	component of $\boldsymbol{m}$ in the $\boldsymbol{\nu}$ direction
m_τ	component of $\boldsymbol{m}$ in the $\boldsymbol{\tau}$ direction
M	boundary moment in $\boldsymbol{\nu}$ direction
$\boldsymbol{M}$	director traction
$M^{\alpha\beta}$	bending moment components
$\boldsymbol{\mu}$	couple-stress tensor
$\boldsymbol{n}$	normal vector to membrane surface
$N^{\alpha\beta}$	in-plane stress components
$\boldsymbol{\nu}$	in-plane unit normal on $\partial\mathcal{P}$
$\omega^{\alpha\beta}$	out-of-plane dissipation components
$[\![p]\!]$	pressure drop across membrane
$\mathcal{P}$	membrane patch
$\partial\mathcal{P}$	membrane patch boundary
$\pi^{\alpha\beta}$	in-plane dissipation components
ψ	Helmholtz free energy per mass, as a function of $a_{\alpha\beta}$ and $b_{\alpha\beta}$
$\bar{\psi}$	Helmholtz free energy per mass, as a function of ρ, H, and K
r	heat source or sink per mass
ρ	areal mass density
s	entropy per mass
S^α	out-of-plane stress components
$\boldsymbol{\sigma}$	Cauchy stress tensor
$\sigma^{\alpha\beta}$	moment-free in-plane stresses
$\boldsymbol{T}$	boundary traction
$\boldsymbol{T}^\alpha$	stress vector across $\theta^\alpha = \text{const.}$
θ^α	surface-fixed coordinates
$\boldsymbol{\tau}$	in-plane unit tangent on $\partial\mathcal{P}$
u	internal energy per mass
$\boldsymbol{v}$	membrane velocity
w	total membrane energy per area
w_c	compression energy density
w_H	Helfrich energy per area
W	total membrane energy
$\boldsymbol{x}$	membrane position in $\mathbb{R}^3$
$\boldsymbol{x}_\mathrm{b}$	position of membrane boundary
X_k	thermodynamic force
ξ^α	convected coordinates
ζ	in-plane shear viscosity coefficient

Chapter IV

Introduction and Overview

> *The first part of the growth of a physical science consists in the discovery of a system of quantities on which its phenomena may be conceived to depend. The next stage is the discovery of the mathematical form of the relations between these quantities. After this, the science may be treated as a mathematical science . . .*
>
> —James C. Maxwell, 1869 [‡]

From a theoretical perspective, lipid membranes are fascinating and unique materials. Lipids flow in-plane as a two-dimensional fluid, the membrane bends out-of-plane as an elastic shell, multi-component membranes can phase separate at low temperatures, and various proteins bind to the membrane surface and locally induce curvature. Moreover, all of the aforementioned phenomena are highly coupled. As lipids flow in-plane across curved membrane morphologies, additional out-of-plane forces are generated and compete with their bending counterparts. When membranes phase separate, line tensions energetically penalize phase boundaries and favor domain coarsening—yet domains also bulge out-of-plane to reduce the line tension penalty, resulting in energetic barriers to domains coming together. If proteins bind to the membrane surface and locally induce curvature, additional in-plane stresses and out-of-plane forces ensue, leading to a rich variety of dynamics and morphologies. Comprehensive membrane models that include all these effects, and especially their coupling to one another, are needed to fully understand the diverse and complex physical behaviors of biological membranes.

A major complexity arises when developing lipid membrane theories because the surface on which we apply continuum and thermodynamic balance laws is itself arbitrarily curved and deforming over time. Thus, significant technical challenges emerge even when considering the simplest system: a membrane comprised of only a single type of phospholipid molecule, in which no phase transitions nor chemical reactions occur. Consequently, though we previously derived a non-equilibrium thermodynamic framework incorporating all of the aforementioned processes in arbitrary geometries, [†] the present work seeks to provide a wholistic perspective by discussing only the thermodynamics and hydrodynamics of

[‡]J.C. Maxwell. "Remarks on the mathematical classification of physical quantities". *Proc. London Math. Soc.* **1** (1871), 224–233.

[†]A. Sahu et al. "Irreversible thermodynamics of curved lipid membranes". *Phys. Rev. E* **96** (2017), 042409. arXiv: 1701.06495.

single-component lipid membranes. For the remainder of this chapter, we discuss the relevant history in the development of such models. At the close of this theoretical introduction, we motivate our systematic investigation of single-component membranes with increasingly complex constitutive behaviors.

From a continuum perspective, single-component lipid membranes are characterized by lipids flowing in-plane as a viscous fluid while the membrane deforms out-of-plane as a thin elastic shell. Accordingly, the theory of such materials incorporates results and techniques from investigations of two-dimensional viscous fluids, as well as solid plates and shells. In what follows, we present what we believe to be the most significant contributions to these two disparate fields, through the lens of developing an understanding of biological membranes. We then provide a historical account of the development of single-component lipid membrane theory, and conclude this introductory chapter with a summary of the major theoretical developments of the present work.

1. The investigation of viscous fluid films

Consider an arbitrarily curved and deforming viscous fluid film, lying between two bulk phases (either vapor or liquid). Following our developments and notation from Chapters II and III, we decompose the material acceleration $\boldsymbol{c} = \dot{\boldsymbol{v}}$ into in-plane and out-of-plane components as $\boldsymbol{c} = c^\alpha \boldsymbol{a}_\alpha + c\boldsymbol{n}$. Similarly, we decompose the total body force $\boldsymbol{f}$ acting on the fluid film by its surroundings as $\boldsymbol{f} = f^\alpha \boldsymbol{a}_\alpha + f\boldsymbol{n}$. If the fluid film is area-incompressible, then the in-plane equations of motion are given by

$$\underbrace{\rho c^\alpha}_{\text{inertia}} = \underbrace{a^{\alpha\beta}\lambda_{,\beta}}_{\substack{\text{tension}\\ \text{gradients}}} + \underbrace{\pi^{\beta\alpha}_{;\beta}}_{\substack{\text{viscous}\\ \text{shear forces}}} + \underbrace{f^\alpha}_{\substack{\text{external}\\ \text{forces}}} , \tag{1}$$

where $\rho = \rho(\theta^\alpha, t)$ is the mass per unit area, $\lambda = \lambda(\theta^\alpha, t)$ is the surface tension, and $\pi^{\alpha\beta}$ are the in-plane viscous stresses. Equation (1) is similar to the incompressible Navier–Stokes equations [Chapter III, Eq. (98)], where a negative gradient in pressure is replaced by a positive gradient in surface tension. The out-of-plane equation of motion is also found to be

$$\underbrace{\rho c}_{\text{inertia}} = \underbrace{2\lambda H}_{\substack{\text{tension–curvature}\\ \text{coupling}}} + \underbrace{\pi^{\alpha\beta} b_{\alpha\beta}}_{\substack{\text{viscous–curvature}\\ \text{coupling}}} + \underbrace{f}_{\substack{\text{external}\\ \text{forces}}} . \tag{2}$$

We will see in Chapter V how Eqs. (1) and (2) are a limiting case of the lipid membrane equations when no elastic bending energy is stored in the membrane. For now, we provide a historical perspective on how the terms in the in-plane and out-of-plane equations arose.

Let us begin by considering a static soap bubble. As there is no material motion, there are no inertial or viscous forces. Moreover, when the surrounding bulk medium is stationary, it serves only to apply a pressure drop $[\![p]\!]$ across the fluid surface. The in-plane equation (1) yields $\lambda_{,\beta} = 0$, for which the surface tension is constant, while the force balance in the normal direction (2) simplifies to the well-known Young–Laplace equation [‡, †]

$$0 = [\![p]\!] + 2\lambda H , \tag{3}$$

[‡] T. Young. "III. An essay on the cohesion of fluids". *Philos. Trans. R. Soc.* **95** (1805), 65–87.

[†] P.S. Laplace. *Traité Mécanique Céleste*. Vol. 4. Supplément au Livre X. Paris: Gauthier-Villars, 1805.

in which a pressure drop is balanced by tension–curvature coupling forces.

Next, we discuss the dynamics of the interface between two fluid phases, which motivated much of the early work on what is now called *interfacial hydrodynamics* or *interfacial rheology.* In the latter portion of the 19th century, J. Thomson [‡] and later C.G.M. Marangoni [†] observed that surface tension gradients at the fluid–fluid interface would drive flows in the surrounding bulk phases—a phenomena now known as the Marangoni effect. To describe the dynamics of such flows, we first recognize fluid–fluid boundaries are not material interfaces: while a surface tension λ characterizes the energy per area of the phase boundary, there is no mass at the interface. However, a force balance on the interface again yields Eqs. (1) and (2), where in this case $\rho = 0$. If we additionally assume the interface itself has no surface viscosity, then $\pi^{\alpha\beta} = 0$ and the governing equations simplify to

$$0 = a^{\alpha\beta}\lambda_{,\beta} + f^{\alpha} \qquad \text{and} \qquad 0 = 2\lambda H + f \,. \tag{4}$$

In Eq. (4), $\boldsymbol{f} = f^{\alpha}\boldsymbol{a}_{\alpha} + f\boldsymbol{n}$ is the jump in normal traction exerted by the surrounding bulk fluid on the interface. We can thus understand Eq. $(4)_1$ in one of two ways. First, if in-plane tension gradients exist and $\lambda_{,\beta} \neq 0$, then $f^{\alpha} \neq 0$—for which in-plane forces, caused by viscous flows in the surrounding fluid, are required. From another perspective, we recognize viscous flows in the bulk phases cause an in-plane traction jump at the interface, which in turn drives surface tension gradients to maintain a force balance.

In 1913, J. Boussinesq [*] investigated how spherical liquid droplets would fall in a fluid medium under the influence of gravity. To explain some of his experimental observations, Boussinesq hypothesized the existence of a *surface viscosity,* which was a property of the fluid–fluid interface itself. Such a notion was expanded upon by C.V. Sternling and Scriven in 1959 in their studies of interfacial turbulence at a nearly planar interface. [§] In a parallel effort, Scriven incorporated the effects of in-plane viscous stresses on the mechanics and dynamics of arbitrarily curved and deforming fluid interfaces [♯] to arrive at Eqs. (1) and (2). These developments marked a major shift towards our current understanding of such materials, and Scriven's equations were incorporated into the last chapter of the monograph by R. Aris [‖] as well as a later text on interfacial rheology. [∀] All three of these works, however, contain errors in their expressions for the inertial terms, as discussed and corrected by A.M. Waxman. [♢] For those readers interested in recent develops involving interfacial phenomena and fluid interfaces, we recommend the insightful perspective by H.A. Stone. [$]

[‡] J. Thomson. "On certain curious motions observable at the surfaces of wine and other alcoholic liquors". *Philos. Mag.* **10** (1855), 330–333.

[†] C. Marangoni. "Ueber die Ausbreitung der Tropfen einer Flüssigkeit auf der Oberfläche einer anderen". *Ann. Phys. Chem.* **219** (1871), 337–354.

[*] J. Boussinesq. "Sur l'existence d'une viscosité superficielle, dans la mince couche de transition séparant un liquide d'un autre fluide contigu". *Ann. Chim. Phys.* **29** (1913), 349–357.

[§] C.V. Sternling and L.E. Scriven. "Interfacial turbulence: Hydrodynamic instability and the Marangoni effect". *A.I.Ch.E. J.* **5** (1959), 514–523.

[♯] L.E. Scriven. "Dynamics of a fluid interface: Equation of motion for Newtonian surface fluids". *Chem. Eng. Sci.* **12** (1960), 98–108.

[‖] R. Aris. *Vectors, Tensors, and the Basic Equations of Fluid Mechanics.* New York: Dover, 1989.

[∀] D.A. Edwards, H. Brenner, and D.T. Wasan. *Interfacial Transport Processes and Rheology*. Butterworth Heinemann Series in Chemical Engineering. Boston: Butterworth-Heinemann, 1991.

[♢] A.M. Waxman. "Dynamics of a couple-stress fluid membrane". *Studies Appl. Math.* **70** (1984), 63–86.

[$] H.A. Stone. "Interfaces: in fluid mechanics and across disciplines". *J. Fluid Mech.* **645** (2010), 1–25.

2. The investigation of solid plates and shells

Over the same time period in which the behavior of fluid films was being investigated, there was considerable effort to understand the mechanics and dynamics of elastic structures in which one spatial dimension (the thickness) was much smaller than the other two. In considering elastic plates, which shear in-plane and deform out-of-plane, G. KIRCHHOFF [‡] began with the three-dimensional equations of linear elasticity and arrived at the corresponding two-dimensional equations when deformations are small. In doing so, Kirchhoff made two assumptions regarding how elements of the material deform relative to the material's mid-plane:

1. A linear element of the material (a filament) which is normal to the mid-plane prior to deformation remains straight and normal to the mid-plane after deformation, and

2. All elements of the mid-plane do not undergo any strain.

Shortly afterwards, A.E.H. LOVE studied the behavior of thin elastic shells, in which material elements can rotate and translate in all directions. By making the same assumptions as Kirchhoff, Love began with the equations of three-dimensional linear elasticity and obtained the two-dimensional elastic shell equations—again in the limit of small deformations. [†] The above assumptions have accordingly become known as the *Kirchhoff–Love assumptions*, and the corresponding materials are called *Kirchhoff–Love shells*. A detailed account of the development of elastic theories prior to 1890 is provided in the Historical Introduction of the seminal monograph by Love. [*]

As it turns out, there were some limitations in Love's development of the two-dimensional elastic shell equations. One advancement was made by the brothers E. and F. COSSERAT, [§] who approximated an elastic shell as a two-dimensional surface endowed with a triad of rigid, orthogonal vectors at every location—meant to capture rotations and stretches of the material independent of the overall deformation. The theory of such materials, now know as *Cosserat surfaces,* was significantly advanced in the latter half of the 20$^{\text{th}}$ century. [♯] For the purpose of describing shells and plates, a single independent vector at each location—known as a *director field*—was found to be sufficient. [‖, ∀] In the case where the director field is of unit length and constrained to lie in the direction normal to the surface, as we assume when developing the lipid membrane theory in Chapter V, the state of stress in the two-dimensional material is captured by the Cauchy stress tensor

$$\boldsymbol{\sigma} \;=\; N^{\alpha\beta}\boldsymbol{a}_\alpha \otimes \boldsymbol{a}_\beta \;+\; S^{\alpha}\boldsymbol{a}_\alpha \otimes \boldsymbol{n}\;. \tag{5}$$

[‡] G. Kirchhoff. "Über das Gleichgewicht und die Bewegung einer elastischen Schiebe". *Crelles J.* **40** (1850), 51–88.

[†] A.E.H. Love. "The small free vibrations and deformation of a thin elastic shell". *Phil. Trans. R. Soc. London* **179** (1888), 491–546.

[*] A.E.H. Love. *A Treatise on the Mathematical Theory of Elasticity.* 4th ed. New York: Dover, 1944.

[§] E. Cosserat and F. Cosserat. *Théorie des Corps Déformables.* Paris: A. Hermann et Fils, 1909.

[♯] J.L. Ericksen and C. Truesdell. "Exact theory of stress and strain in rods and shells". *Arch. Ration. Mech. Anal.* **1** (1958), 295–323.

[‖] C. Truesdell and R. Toupin. "The classical field theories". *Principles of Classical Mechanics and Field Theory.* Ed. by S. Flügge. Berlin, Heidelberg: Springer, 1960, pp. 226–858.

[∀] An illustration of a director field, in the context of lipid membranes, is provided in Fig. 3 of Chapter V.

Here, $N^{\alpha\beta}$ captures in-plane stresses and S^{α} captures out-of-plane elastic shear forces across the shell thickness. For elastic shells, both $N^{\alpha\beta}_{\text{el}}$ and S^{α}_{el} are calculated from the Helmholtz free energy per unit mass ψ_{el}. Moreover, given the stress components and our assumption regarding the director field, the in-plane and out-of-plane governing equations were found to be given by [‡]

$$\underbrace{\rho c^{\alpha}}_{\substack{\text{inertia}}} = \underbrace{N^{\beta\alpha}_{\text{el};\beta}}_{\substack{\text{in-plane}\\ \text{elastic forces}}} - \underbrace{S^{\beta}_{\text{el}} b^{\alpha}_{\beta}}_{\substack{\text{shear–curvature}\\ \text{coupling}}} + \underbrace{f^{\alpha}}_{\substack{\text{external}\\ \text{forces}}} \tag{6}$$

and

$$\underbrace{\rho c}_{\substack{\text{inertia}}} = \underbrace{N^{\alpha\beta}_{\text{el}} b_{\alpha\beta}}_{\substack{\text{in-plane–curvature}\\ \text{coupling}}} + \underbrace{S^{\alpha}_{\text{el};\alpha}}_{\substack{\text{shear}\\ \text{gradients}}} + \underbrace{f}_{\substack{\text{external}\\ \text{forces}}}, \tag{7}$$

respectfully. A comprehensive discussion of the above equations, as well as their extension to surfaces with more complicated director fields, is given by P.M. Naghdi. [†]

At this point, we observe that Eqs. (6) and (7) bear a strong resemblance to the fluid film equations, namely Eqs. (1) and (2). In fact, the latter pair is recovered from the former if we replace $N^{\alpha\beta}_{\text{el}}$ and S^{α}_{el} with the in-plane stresses and out-of-plane shear forces of a fluid film: $N^{\alpha\beta}_{\text{fl}} = \lambda a^{\alpha\beta} + \pi^{\alpha\beta}$ and $S^{\alpha}_{\text{fl}} = 0$. Moreover, our irreversible thermodynamic analysis in Chapter V demonstrates how both sets of equations can be obtained within a single framework—just as we found the three-dimensional fluid and solid equations in Chapter III.

3. The development of a lipid membrane theory

As noted previously, a single-component lipid membrane has qualities of both a two-dimensional viscous fluid film and a thin elastic shell. In what follows, we divide the development of the general, dynamical lipid membrane equations into two time periods: (*i*) the early years, from 1970–1980, in which efforts largely focused on understanding lipid membrane energetics, and (*ii*) the later years, from 1980 onwards, during which the dynamical lipid membrane equations were developed. Our historical account is focused on contributions towards describing the behavior of arbitrarily curved and deforming lipid membranes, and so here we do not discuss the many works investigating more specific membrane phenomena.

(a). The early years: 1970–1980

Just as theories of both fluid films and elastic shells reached a finalized form in the 1960's, there were three significant developments towards quantitatively describing lipid membrane behavior. First, P.B. Canham sought to explain the biconcave shape in human red blood

[‡]A.E. Green, P.M. Naghdi, and W.L. Wainwright. "A general theory of a Cosserat surface". *Arch. Ration. Mech. Anal.* **20** (1965), 287–308.

[†]P.M. Naghdi. "The Theory of Shells and Plates". *Linear Theories of Elasticity and Thermoelasticity: Linear and Nonlinear Theories of Rods, Plates, and Shells*. Ed. by C. Truesdell. Berlin, Heidelberg: Springer, 1973, pp. 425–640.

cells, [‡] and in doing so correctly recognized (*i*) there is an energetic penalty for membrane bending, as lipids in one leaflet are compressed while lipids in the other leaflet are stretched, (*ii*) the membrane will elastically resist in-plane isotropic stretching or compression, and (*iii*) lipids flow as a viscous fluid in response to in-plane shear stresses, during which no elastic energy is stored in the membrane. Accordingly, Canham proposed that the elastic energy required to bend a lipid membrane is given by [†]

$$W_{\text{Canham}} = \kappa_{\text{b}} \int \left(2H^2 - K\right) \, \mathrm{d}a \, , \tag{8}$$

where κ_{b} is a bending modulus with units of energy. The minimum energy shapes, according to Eq. (8), were calculated numerically and then compared to experimental observations. However, no dynamical equations governing membrane behavior were provided.

In an independent effort just a few years later, W. Helfrich [*] proposed an elastic energy for lipid membranes by considering three effects: (*i*) stretching of a local area element, (*ii*) tilt of lipids relative to the unit normal to the surface, and (*iii*) curvature of the surface. Moreover, while Canham simply posited a form of the bending energy, Helfrich used symmetry arguments to obtain the lowest-order term for each of the aforementioned effects. When lipid tilt is neglected, the total energy is written (in our notation [§]) as

$$W_{\text{Helfrich}} = \frac{\kappa_{\text{s}}}{2} \int \left(J - 1\right)^2 \, \mathrm{d}a + \frac{\kappa_{\text{b}}}{2} \int \left(2H - C_0\right)^2 \, \mathrm{d}a + \kappa_{\text{g}} \int K \, \mathrm{d}a \, , \tag{9}$$

where J captures the relative, local area change with respect to the unstretched membrane. In Eq. (9), κ_{s} is the stretching modulus, which has units of energy per area, such that the first term on the right-hand side accounts for the total stretching energy. Importantly, Helfrich found the bending modulus multiplying the square of the mean curvature [denoted κ_{b} to be consistent with Eq. (8)] need not be equal to the modulus multiplying the Gaussian curvature (here denoted κ_{g}). The quantity C_0 is the so-called *spontaneous curvature* and arises when the two monolayer leaflets are in different chemical environments. Interestingly, though Helfrich recognized the connection between Eq. (9) and Naghdi's (at the time) recent developments in thin elastic shells, he chose not to proceed via Naghdi's well-established methods. Instead, Helfrich used variational methods to obtain the Euler–Lagrange equations governing axisymmetric, equilibrium membrane shapes, and later extended his calculations to obtain the general equations governing arbitrarily curved equilibrium membrane morphologies. [♯]

Around the same time, in the early 1970's, E.A. Evans investigated the behavior of biological membranes (often those of red blood cells) via micropipette aspiration methods, and

[‡] P.B. Canham. "The minimum energy of bending as a possible explanation of the biconcave shape of the human red blood cell". *J. Theor. Biol.* **26** (1970), 61–81.

[†] Canham chose to express his result in terms of the two principal radii of curvature R_1 and R_2, which are related to the mean and Gaussian curvature by $2H = (1/R_1) + (1/R_2)$ and $K = 1/(R_1 R_2)$.

[*] W. Helfrich. "Elastic properties of lipid bilayers: Theory and possible experiments". *Z. Naturforsch. C* **28** (1973), 693–699.

[§] The equations in Helfrich's manuscript are expressed in terms of a locally orthogonal coordinate system, and so look quite different, yet are equivalent to the ones provided here.

[♯] O.-Y. Zhong-can and W. Helfrich. "Bending energy of vesicle membranes: General expressions for the first, second, and third variation of the shape energy and applications to spheres and cylinders". *Phys. Rev. A* **39** (1989), 5280–5288.

sought to characterize the bending modulus κ_b in Canham's proposed membrane energy (8). By considering the mechanics of two monolayer leaflets as the membrane is deformed, Evans arrived at an expression for the bending modulus in terms of the stretching moduli of the two individual leaflets, and the membrane thickness. [‡] Moreover, in examining the effect of asymmetric chemical interactions in the two leaflets, Evans expressed the spontaneous curvature C_0 in Eq. (9) in terms of the change in free energy of each leaflet due to chemical interactions. As Evans was unaware of Helfrich's developments at that time, the connection between the two results was not made until several years later. [†]

(b). The later years: 1980–

At the start of the 1980's, Helfrich had obtained the general Euler–Lagrange equations governing equilibrium membrane shapes. [*] However, the Euler–Lagrange equations by construction include only thermodynamically reversible phenomena, and thus do not contain viscous forces arising from the in-plane flow of lipids. In an effort to provide a dynamical description of such systems, Waxman [§] applied a balance law formulation to a Cosserat surface to recover the dynamical equations obtained by Naghdi, [♯] provided in Eqs. (6) and (7). Waxman also realized that by proposing constitutive relations between the in-plane stresses and in-plane rate of strain, for example, one could incorporate Scriven's fluid film results [‖] into Naghdi's description. However, Waxman failed to recognize that the elastic contributions to the in-plane stresses $N^{\alpha\beta}$ and the out-of-plane shear forces S^{α} arise from a single thermodynamic potential. This inconsistency, in violation of the second law of thermodynamics, was pointed out by D. Hu, P. Zhang, and W. E in 2007; [∀] the authors extended Waxman's result by properly accounted for the energetics of a Cosserat surface using variational techniques. This result marks the first correct presentation of the fully nonlinear equations governing the dynamics of an arbitrarily curved and deforming single-component lipid membrane. In our notation, the in-plane stresses and shear forces can be expressed as $N^{\alpha\beta} = N_b^{\alpha\beta} + N_{fl}^{\alpha\beta}$ and $S^{\alpha} = S_b^{\alpha}$, where the bending contributions $N_b^{\alpha\beta}$ and S_b^{α} are both obtained from the bending terms in the Helfrich energy (9), and the fluid film contributions were introduced previously. We feel the work by Hu, Zhang, and E [∀] deserves special attention as it is relatively unknown within the membrane biophysics community. Deriving the constitutive forms of $N^{\alpha\beta}$ and S^{α} will be a major focus of Chapter V.

In an independent effort, D.J. Steigmann [◇] clarified the relationship between a Kirchhoff–

[‡] E.A. Evans. "Bending resistance and chemically induced moments in membrane bilayers". *Biophys. J.* **14** (1974), 923–931.

[†] E.A. Evans and R.M. Hochmuth. "Mechanochemical Properties of Membranes". *Membrane Properties: Mechanical Aspects, Receptors, Energetics and Calcium-Dependence of Transport.* Ed. by F. Bronner and A. Kleinzeller. Vol. 10. Current Topics in Membranes and Transport. Academic Press, 1978, pp. 1–64.

[*] Zhong-can and Helfrich, "Bending energy of vesicle membranes: General expressions for the first, second, and third variation of the shape energy and applications to spheres and cylinders".

[§] Waxman, "Dynamics of a couple-stress fluid membrane".

[♯] Naghdi, "The Theory of Shells and Plates".

[‖] Scriven, "Dynamics of a fluid interface: Equation of motion for Newtonian surface fluids".

[∀] D. Hu, P. Zhang, and W. E. "Continuum theory of a moving membrane". *Phys. Rev. E* **75** (2007), 041605

[◇] D.J. Steigmann. "On the relationship between the Cosserat and Kirchhoff–Love theories of elastic shells".

Love shell and a Cosserat surface whose director field is constrained to lie normal to the surface, within Naghdi's framework. Steigmann then applied this understanding to obtain the equilibrium equations governing such an elastic material, with additional insights regarding possible boundary conditions if one were to consider only a patch of material, as well as how to enforce areal incompressibility via a Lagrange multiplier field. [‡] By then recognizing that the membrane energy must be invariant under Galilean transformations, Steigmann obtained the general, fully nonlinear equilibrium equations for a fluid film with an elastic bending energy depending only on the mean curvature H and Gaussian curvature K—from which the out-of-plane equilibrium equation of Helfrich could easily be obtained. Importantly, in enforcing areal incompressibility with a Lagrange multiplier field, Steigmann also found the in-plane equilibrium equations governing such a material, namely Eq. $(4)_1$. Just over a decade later, Steigmann and his collaborators incorporated the in-plane fluid stresses first obtained by Scriven to obtain a dynamical description of lipid membrane behavior, [†] which—though the authors were unaware of it at the time—was identical to that of Hu, Zhang, and E when inertial forces were negligible.

The final major theoretical contribution we wish to highlight is that of M. Arroyo and A. DeSimone, [*] who used variational methods to determine the elastic contributions to membrane dynamics, combined with the so-called Rayleigh dissipation potential to determine the viscous forces. In the limit of negligible inertial forces, the resultant equations of motion agree with the earlier work of Hu, Zhang, and E, as well as the later of work of Steigmann and his colleagues. Importantly, at the end of 2012, there were three different theoretical approaches to obtain the dynamical equations of motion governing a single-component lipid membrane.

(c). Our theoretical contributions

While the aforementioned theoretical developments used different frameworks to obtain the dynamical membrane equations, each study used what are now standard methods to determine the elastic stresses and forces, and generally included the in-plane viscous stresses in an ad-hoc fashion. While such developments are theoretically sound, they cannot easily be extended to model more complicated membrane systems—such as those with in-plane phase transitions, or with proteins binding to and diffusing on the membrane surface. In particular, multi-component lipid membranes undergoing chemical reactions have complicated in-plane and out-of-plane couplings between both reversible and irreversible phenomena, and it is not straightforward to posit the form of various stresses and forces. Thus, at the time when we developed our membrane theory, [§] there was no comprehensive framework to include all the biologically relevant processes mentioned thus far, and it was unclear how such phenomena

Math. Mech. Solids **4** (1998), 275–288.

[‡]D.J. Steigmann. "Fluid films with curvature elasticity". *Arch. Ration. Mech. Anal.* **150** (1999), 127–152.

[†]P. Rangamani et al. "Interaction between surface shape and intra-surface viscous flow on lipid membranes". *Biomech. Model. Mechan.* **12** (2012), 833–845.

[*]M. Arroyo and A. DeSimone. "Relaxation dynamics of fluid membranes". *Phys. Rev. E* **79** (2009), 31915–31931.

[§]Sahu et al., "Irreversible thermodynamics of curved lipid membranes".

would be coupled to in-plane viscous flows and elastic out-of-plane shape deformations in arbitrary geometries.

In the following chapter, we develop the general theory of irreversible thermodynamics for arbitrarily curved and deforming lipid membranes, and provide a formalism to determine the equations governing membrane dynamics. While single-component lipid membranes are the focus of this thesis, we previously demonstrated how the theory can be extended to describe multi-component systems with in-plane phase transitions and chemical reactions. [‡] Our work is inspired by the seminal developments of irreversible thermodynamics by Prigogine [†] as well as de Groot and Mazur. [*] While these classical developments are for systems modeled using Cartesian coordinate systems, we carry out all of our analysis within a differential geometric framework. We first obtain the local form of the balance of mass, linear momentum, angular momentum, energy, and entropy, as well as the second law of thermodynamics. We then determine the internal entropy production, from which we posit linear relationships between the thermodynamic fluxes and forces. In going so, we find the in-plane stresses $N^{\alpha\beta}$ and shear forces S^{α} in three cases: (i) a compressible, inviscid membrane, (ii) a compressible, viscous membrane, and (iii) an incompressible, viscous membrane. We close by presenting the governing equations and admissible boundary conditions in each scenario.

References

[1] R. Aris. *Vectors, Tensors, and the Basic Equations of Fluid Mechanics*. New York: Dover, 1989

[2] M. Arroyo and A. DeSimone. "Relaxation dynamics of fluid membranes". *Phys. Rev. E* **79** (2009), 31915–31931

[3] J. Boussinesq. "Sur l'existence d'une viscosité superficielle, dans la mince couche de transition séparant un liquide d'un autre fluide contigu". *Ann. Chim. Phys.* **29** (1913), 349–357

[4] P.B. Canham. "The minimum energy of bending as a possible explanation of the biconcave shape of the human red blood cell". *J. Theor. Biol.* **26** (1970), 61–81

[5] E. Cosserat and F. Cosserat. *Théorie des Corps Déformables*. Paris: A. Hermann et Fils, 1909

[6] S.R. de Groot and P. Mazur. *Non-Equilibrium Thermodynamics*. New York: Dover, 1984

[7] D.A. Edwards, H. Brenner, and D.T. Wasan. *Interfacial Transport Processes and Rheology*. Butterworth Heinemann Series in Chemical Engineering. Boston: Butterworth-Heinemann, 1991

[8] J.L. Ericksen and C. Truesdell. "Exact theory of stress and strain in rods and shells". *Arch. Ration. Mech. Anal.* **1** (1958), 295–323

[‡] Sahu et al., "Irreversible thermodynamics of curved lipid membranes".

[†] I. Prigogine. *Introduction to Thermodynamics of Irreversible Processes*. 3rd ed. New York: Interscience Publishers, 1967.

[*] S.R. de Groot and P. Mazur. *Non-Equilibrium Thermodynamics*. New York: Dover, 1984.

[9] E.A. Evans. "Bending resistance and chemically induced moments in membrane bilayers". *Biophys. J.* **14** (1974), 923–931

[10] E.A. Evans and R.M. Hochmuth. "Mechanochemical Properties of Membranes". *Membrane Properties: Mechanical Aspects, Receptors, Energetics and Calcium-Dependence of Transport*. Ed. by F. Bronner and A. Kleinzeller. Vol. 10. Current Topics in Membranes and Transport. Academic Press, 1978, pp. 1–64

[11] A.E. Green, P.M. Naghdi, and W.L. Wainwright. "A general theory of a Cosserat surface". *Arch. Ration. Mech. Anal.* **20** (1965), 287–308

[12] W. Helfrich. "Elastic properties of lipid bilayers: Theory and possible experiments". *Z. Naturforsch. C* **28** (1973), 693–699

[13] D. Hu, P. Zhang, and W. E. "Continuum theory of a moving membrane". *Phys. Rev. E* **75** (2007), 041605

[14] G. Kirchhoff. "Über das Gleichgewicht und die Bewegung einer elastischen Schiebe". *Crelles J.* **40** (1850), 51–88

[15] P.S. Laplace. *Traité Mécanique Céleste*. Vol. 4. Supplément au Livre X. Paris: Gauthier-Villars, 1805

[16] A.E.H. Love. *A Treatise on the Mathematical Theory of Elasticity*. 4th ed. New York: Dover, 1944

[17] A.E.H. Love. "The small free vibrations and deformation of a thin elastic shell". *Phil. Trans. R. Soc. London* **179** (1888), 491–546

[18] C. Marangoni. "Ueber die Ausbreitung der Tropfen einer Flüssigkeit auf der Oberfläche einer anderen". *Ann. Phys. Chem.* **219** (1871), 337–354

[19] J.C. Maxwell. "Remarks on the mathematical classification of physical quantities". *Proc. London Math. Soc.* **1** (1871), 224–233

[20] P.M. Naghdi. "The Theory of Shells and Plates". *Linear Theories of Elasticity and Thermoelasticity: Linear and Nonlinear Theories of Rods, Plates, and Shells*. Ed. by C. Truesdell. Berlin, Heidelberg: Springer, 1973, pp. 425–640

[21] I. Prigogine. *Introduction to Thermodynamics of Irreversible Processes*. 3rd ed. New York: Interscience Publishers, 1967

[22] P. Rangamani et al. "Interaction between surface shape and intra-surface viscous flow on lipid membranes". *Biomech. Model. Mechan.* **12** (2012), 833–845

[23] A. Sahu et al. "Irreversible thermodynamics of curved lipid membranes". *Phys. Rev. E* **96** (2017), 042409. arXiv: 1701.06495

[24] L.E. Scriven. "Dynamics of a fluid interface: Equation of motion for Newtonian surface fluids". *Chem. Eng. Sci.* **12** (1960), 98–108

[25] D.J. Steigmann. "Fluid films with curvature elasticity". *Arch. Ration. Mech. Anal.* **150** (1999), 127–152

[26] D.J. Steigmann. "On the relationship between the Cosserat and Kirchhoff–Love theories of elastic shells". *Math. Mech. Solids* **4** (1998), 275–288

[27] C.V. Sternling and L.E. Scriven. "Interfacial turbulence: Hydrodynamic instability and the Marangoni effect". *A.I.Ch.E. J.* **5** (1959), 514–523

[28] H.A. Stone. "Interfaces: in fluid mechanics and across disciplines". *J. Fluid Mech.* **645** (2010), 1–25

[29] J. Thomson. "On certain curious motions observable at the surfaces of wine and other alcoholic liquors". *Philos. Mag.* **10** (1855), 330–333

[30] C. Truesdell and R. Toupin. "The classical field theories". *Principles of Classical Mechanics and Field Theory*. Ed. by S. Flügge. Berlin, Heidelberg: Springer, 1960, pp. 226–858

[31] A.M. Waxman. "Dynamics of a couple-stress fluid membrane". *Studies Appl. Math.* **70** (1984), 63–86

[32] T. Young. "III. An essay on the cohesion of fluids". *Philos. Trans. R. Soc.* **95** (1805), 65–87

[33] O.-Y. Zhong-can and W. Helfrich. "Bending energy of vesicle membranes: General expressions for the first, second, and third variation of the shape energy and applications to spheres and cylinders". *Phys. Rev. A* **39** (1989), 5280–5288

Chapter V

Single-Component Lipid Membranes

> *The notion of a model for an idealized body, a system or even a universe permeates the structure of classical physics; and is, in fact, the cornerstone of all field theories ... To elaborate, we recall that since the field equations of the classical continuum mechanics hold for every medium, it is only the constitutive equations which differ from one medium to another. Now constitutive equations (even those which embrace considerable generality) are always developed with a view towards a particular model ... We have come to accept the point of view describing the behavior of different materials through different sets of continuum equations which, in turn, represent characterization of a particular model we have in mind.*
>
> —Paul M. Naghdi, 1973 [‡]

In this chapter, we develop a comprehensive description of a single-component lipid membrane, in which lipids flow in-plane as a two-dimensional viscous fluid while the membrane bends out-of-plane as an elastic shell. We follow the same general structure as in our analysis of bulk materials in Chapter III: the kinematics of an arbitrarily curved and deforming surface are presented in §1, the balance laws are provided in §2, membrane thermodynamics are described in §3, and the equations governing lipid membranes with different constitutive behaviors are obtained in §4, §5, and §6. Much of the contents of this chapter are contained in Secs. II and III of our previous theoretical development. [†]

1. The kinematics of a deforming surface

Throughout this work, the phospholipid bilayer is modeled as a single differentiable manifold about the membrane mid-plane, for which it is implicitly assumed there is no slip between the two bilayer leaflets. The geometry of the membrane surface is characterized in Chapter II; we now describe the kinematics of how such a surface evolves in time. Although we were not

[‡]P.M. Naghdi. "The Theory of Shells and Plates". *Linear Theories of Elasticity and Thermoelasticity: Linear and Nonlinear Theories of Rods, Plates, and Shells*. Ed. by C. Truesdell. Berlin, Heidelberg: Springer, 1973, pp. 425–640.

[†]A. Sahu et al. "Irreversible thermodynamics of curved lipid membranes". *Phys. Rev. E* **96** (2017), 042409. arXiv: 1701.06495.

aware of it until recently, the discussion by Waxman [‡] provides an excellent account of surface kinematics, and resolves several important discrepancies in established works. Unfortunately, many more recent studies—including our aforementioned theoretical contribution—do not include Waxman's corrections. Luckily, however, the resultant errors tend to arise in the inertial terms of the equations of motion—which, as will be shown in Part C, contribute negligibly to membrane dynamics in biologically relevant situations.

(a). The current configuration and surface-fixed coordinates

Consider an abstract body $\mathscr{B}$ as a collection of points belonging to a material surface. At any time t, the configuration of the body is defined to be the surface $\mathcal{S}$ occupied by $\mathscr{B}$, of which we consider an arbitrary patch $\mathcal{P} \subset \mathcal{S}$. Moreover, the patch $\mathcal{P}$ is parametrized by the two variables θ^α, as introduced in Chapter II. The position of any point $\tilde{\boldsymbol{x}} \in \mathcal{P}$ on the membrane patch, at time t, is given by

$$\tilde{\boldsymbol{x}} = \boldsymbol{x}\big(\theta^\alpha, t\big) , \qquad \text{or equivalently} \qquad \tilde{\boldsymbol{x}} = x^i(\theta^\alpha, t)\, \boldsymbol{e}_i , \tag{1}$$

for a time-independent choice of orthonormal basis $\{\boldsymbol{e}_i\}$. The configuration of the membrane patch at time t, denoted $\mathcal{P}(t)$, is referred to as the *current configuration*. As the membrane surface evolves in time, the position corresponding to a particular choice of coordinates θ^α will in general evolve as well—expressed mathematically as $[\partial \boldsymbol{x}/\partial t]|_{\theta^\alpha} \neq \boldsymbol{0}$. In our developments, we choose for a point $\boldsymbol{x}$ of constant θ^α to move only in the direction normal to the surface, for which $\boldsymbol{a}_\beta \cdot [\partial \boldsymbol{x}/\partial t]|_{\theta^\alpha} = 0$, as discussed further below. The coordinates θ^α are hereafter referred to as surface-fixed coordinates, as a point of constant θ^α does not change its position when there are no out-of-plane deformations and only in-plane flows (see Fig. 1).

(b). The reference configuration and convected coordinates

Consider the configuration of the body $\mathscr{B}$ at an arbitrary reference time t_0, which we label the *reference configuration* of the membrane and denote as $\mathcal{P}_0 := \mathcal{P}(t_0)$. The coordinates $\xi^{\hat{\alpha}}$, which we define to be the value of θ^α at time t_0, parametrize the reference configuration. At any later time $t > t_0$, the membrane patch can be mapped back to its reference configuration, such that a membrane element of constant $\xi^{\hat{\alpha}}$ is a material element (see Fig. 1). The coordinates $\xi^{\hat{\alpha}}$ are thus convected along with the material, and are referred to as convected coordinates. At any time t, a mapping exists between the surface-fixed and convected coordinates, expressed as

$$\theta^\alpha = \theta^\alpha(\xi^{\hat{\alpha}}, t) \qquad \text{and} \qquad \xi^{\hat{\alpha}} = \xi^{\hat{\alpha}}(\theta^\alpha, t) . \tag{2}$$

Moreover, given that θ^α and $\xi^{\hat{\alpha}}$ coincide at time t_0 by construction, the reference position $\hat{\boldsymbol{X}}$ satisfies

$$\hat{\boldsymbol{X}}(\xi^{\hat{\alpha}}) = \boldsymbol{x}(\theta^\alpha(\xi^{\hat{\alpha}}, t_0), t_0) . \tag{3}$$

[‡] A.M. Waxman. "Dynamics of a couple-stress fluid membrane". *Studies Appl. Math.* **70** (1984), 63–86.

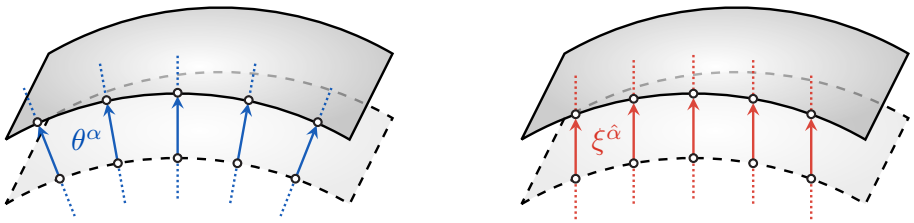

(a) surface-fixed (b) convected

Figure 1: Schematic showing the different surface parametrizations as the membrane undergoes a rigid body translation. (a) The surface-fixed coordinates θ^α move only normal to the surface—in this case spreading out as the surface moves upward. The surface-fixed parametrization is particularly useful in describing surfaces with in-plane fluidity, as a point of constant θ^α is not convected by in-plane flows. (b) The coordinates $\xi^{\hat\alpha}$, on the other hand, are attached to material points, and so maintain the same distance from one another during the translation. If there are in-plane shear flows, two material points initially close to one another can flow arbitrarily far apart.

With a notion of a reference configuration, we describe the change in the differential area of a membrane element over time. First consider the parametric area element $\mathrm{d}\theta^1\,\mathrm{d}\theta^2$. The corresponding area element in physical space is a parallelogram with sides of length $\boldsymbol{a}_1\,\mathrm{d}\theta^1$ and $\boldsymbol{a}_2\,\mathrm{d}\theta^2$, whose area $\mathrm{d}a$ is given by

$$\mathrm{d}a \;=\; \big|\,\boldsymbol{a}_1\,\mathrm{d}\theta^1 \times \boldsymbol{a}_2\,\mathrm{d}\theta^2\,\big| \;=\; \big|\,\boldsymbol{a}_1 \times \boldsymbol{a}_2\,\big|\,\mathrm{d}\theta^1\,\mathrm{d}\theta^2 \;=\; \sqrt{\det a_{\alpha\beta}}\;\mathrm{d}\theta^1\,\mathrm{d}\theta^2\;, \tag{4}$$

where we used the relation $\boldsymbol{a}_1 \times \boldsymbol{a}_2 = \sqrt{\det a_{\alpha\beta}}\;\boldsymbol{n}$ [Chapter II, Eq. (33)]. The reference area $\mathrm{d}A$ is similarly

$$\mathrm{d}A = \sqrt{\det A_{\hat\alpha\hat\beta}}\;\mathrm{d}\xi^{\hat1}\,\mathrm{d}\xi^{\hat2}\;, \tag{5}$$

where $A_{\hat\alpha\hat\beta} := \hat{\boldsymbol{X}}_{,\hat\alpha} \cdot \hat{\boldsymbol{X}}_{,\hat\beta}$ is the metric tensor of the reference patch. As we are tracking a material element, $\mathrm{d}\theta^1\,\mathrm{d}\theta^2 = \mathrm{d}\xi^{\hat1}\,\mathrm{d}\xi^{\hat2}$, in which case the Jacobian determinant of the motion is given by

$$J \;:=\; \frac{\mathrm{d}a}{\mathrm{d}A} \;=\; \left(\frac{\det a_{\alpha\beta}}{\det A_{\hat\alpha\hat\beta}}\right)^{1/2}\;. \tag{6}$$

In obtaining Eq. (6), we considered a current configuration parametrized by θ^α and a reference configuration parametrized by $\xi^{\hat\alpha}$. It is important to note, however, that the convected coordinates can also be used to parametrize the current configuration—for which the position is written as

$$\tilde{\boldsymbol{x}} \;=\; \hat{\boldsymbol{x}}(\xi^{\hat\alpha}, t)\;. \tag{7}$$

With Eq. (7), we can construct another set of in-plane basis vectors $\boldsymbol{a}_{\hat\alpha} := \partial\hat{\boldsymbol{x}}/\partial\xi^{\hat\alpha}$, metric tensor $a_{\hat\alpha\hat\beta} := \boldsymbol{a}_{\hat\alpha} \cdot \boldsymbol{a}_{\hat\beta}$, and all other geometric quantities discussed in Chapter II. Moreover, as both parametrizations describe the same physical surface, Eqs. (1), (2), and (7) require

$$\tilde{\boldsymbol{x}} \;=\; \boldsymbol{x}(\theta^\alpha, t) \;=\; \boldsymbol{x}(\theta^\alpha(\xi^{\hat\alpha}, t),\, t) \;=\; \hat{\boldsymbol{x}}(\xi^{\hat\alpha}, t)\;. \tag{8}$$

We can similarly decompose any vector $\tilde{\boldsymbol{v}} \in \mathbb{R}^3$ in terms of either set of basis vectors, as given by

$$\begin{aligned} \tilde{\boldsymbol{v}} \;&=\; \boldsymbol{v}(\theta^\alpha, t) \;=\; v^\alpha \boldsymbol{a}_\alpha \,+\, v\boldsymbol{n} \;=\; v_\alpha \boldsymbol{a}^\alpha \,+\, v\boldsymbol{n} \\ &=\; \hat{\boldsymbol{v}}(\xi^{\hat{\alpha}}, t) \;=\; v^{\hat{\alpha}} \boldsymbol{a}_{\hat{\alpha}} \,+\, \hat{v}\hat{\boldsymbol{n}} \;=\; v_{\hat{\alpha}} \boldsymbol{a}^{\hat{\alpha}} \,+\, \hat{v}\hat{\boldsymbol{n}} \;. \end{aligned} \tag{9}$$

Note that when a quantity is a function of the convected coordinates and contains a Greek index, we place the 'hat' accent only on the index, while for scalar quantities we place the accent over the quantity itself: for example, $\hat{\boldsymbol{n}} = \hat{\boldsymbol{n}}(\xi^{\hat{\alpha}}, t)$, and $v^{\hat{\alpha}} = v^{\hat{\alpha}}(\xi^{\hat{\beta}}, t)$. The usual tensor transformation laws relate quantities parametrized by θ^α and $\xi^{\hat{\alpha}}$, for example [cf. Chapter II, Eq. (21)]

$$v^\alpha \;=\; \frac{\partial \theta^\alpha}{\partial \xi^{\hat{\alpha}}}\, v^{\hat{\alpha}} \;, \qquad \boldsymbol{a}_\alpha \;=\; \frac{\partial \xi^{\hat{\alpha}}}{\partial \theta^\alpha}\, \boldsymbol{a}_{\hat{\alpha}} \;, \qquad \text{and} \qquad a_{\alpha\beta} \;=\; \frac{\partial \xi^{\hat{\alpha}}}{\partial \theta^\alpha} \frac{\partial \xi^{\hat{\beta}}}{\partial \theta^\beta}\, a_{\hat{\alpha}\hat{\beta}} \;. \tag{10}$$

Note the mapping between surface-fixed and convected coordinates (2) can be used to express any quantity in terms of either parametrization, as for a general quantity $\tilde{f}$

$$\tilde{f} \;=\; f(\theta^\alpha, t) \;=\; f(\theta^\alpha(\xi^{\hat{\alpha}}, t),\, t) = \hat{f}(\xi^{\hat{\alpha}}, t) \;. \tag{11}$$

(c). The time evolution of kinematic quantities

We end our discussion of surface kinematics by calculating the time derivatives of various quantities. The membrane velocity $\tilde{\boldsymbol{v}}$ is defined as the rate of change of position of a material point, and is calculated according to

$$\tilde{\boldsymbol{v}} \;=\; \hat{\boldsymbol{v}}(\xi^{\hat{\alpha}}, t) \;:=\; \frac{\partial}{\partial t}\Big(\hat{\boldsymbol{x}}(\xi^{\hat{\alpha}}, t)\Big) \;. \tag{12}$$

To express the velocity in terms of the surface-fixed coordinates, Eq. (8) is substituted into Eq. (12) to yield

$$\boldsymbol{v} \;=\; \frac{\partial}{\partial t}\Big(\boldsymbol{x}(\theta^\alpha, t)\Big)\Big|_{\xi^{\hat{\alpha}}} \;=\; \frac{\partial}{\partial t}\Big(\boldsymbol{x}(\theta^\alpha, t)\Big) \,+\, \frac{\partial \theta^\alpha}{\partial t}\bigg|_{\xi^{\hat{\alpha}}} \frac{\partial}{\partial \theta^\alpha}\Big(\boldsymbol{x}(\theta^\alpha, t)\Big) \;=\; \frac{\partial \boldsymbol{x}}{\partial t} \,+\, \frac{\partial \theta^\alpha}{\partial t}\bigg|_{\xi^{\hat{\alpha}}} \boldsymbol{a}_\alpha \;. \tag{13}$$

At this point, we introduce the shorthand $(\,\cdot\,)_{,t} := [\partial(\,\cdot\,)/\partial t]|_{\theta^\alpha}$. As discussed previously, the surface-fixed coordinates θ^α are *chosen* such that a point of constant θ^α moves only normal to the surface—for which $\boldsymbol{x}_{,t} \cdot \boldsymbol{a}^\alpha = 0$. Contracting the result of Eq. (13) with $\boldsymbol{a}^\beta$ and $\boldsymbol{n}$, and recognizing $v = \boldsymbol{v} \cdot \boldsymbol{n}$ and $v^\alpha = \boldsymbol{v} \cdot \boldsymbol{a}^\alpha$, then reveals

$$v \;=\; \boldsymbol{x}_{,t} \cdot \boldsymbol{n} \qquad \text{and} \qquad v^\alpha \;=\; \frac{\partial \theta^\alpha}{\partial t}\bigg|_{\xi^{\hat{\alpha}}} \;. \tag{14}$$

As the membrane surface deforms over time, the in-plane velocity components v^α will vary, such that $\theta^\alpha = \theta^\alpha(\xi^{\hat{\alpha}}, t)$ is some nontrivial function. Consequently, care must be taken when obtaining the time derivative of tensorial components. Consider, for example, the

usual tensor transformation law relating components expressed in convected and surface-fixed coordinates—written as [cf. Chapter II, Eq. (21)]

$$\frac{\partial\theta^{\alpha}}{\partial\xi^{\hat{\alpha}}}\,T^{\hat{\alpha}}{}_{\hat{\beta}} \;=\; \frac{\partial\theta^{\beta}}{\partial\xi^{\hat{\beta}}}\,T^{\alpha}{}_{\beta}\;. \tag{15}$$

Importantly, as noticed by J.G. Oldroyd [‡] in his study of bulk materials, $\partial\theta^{\alpha}/\partial\xi^{\hat{\alpha}}$ are time-dependent quantities. Thus, taking the time derivative of both sides of Eq. (15) at fixed $\xi^{\hat{\mu}}$ yields

$$\frac{\partial}{\partial t}\left(\frac{\partial\theta^{\alpha}}{\partial\xi^{\hat{\alpha}}}\right)\bigg|_{\xi^{\hat{\mu}}} T^{\hat{\alpha}}{}_{\hat{\beta}} + \frac{\partial\theta^{\alpha}}{\partial\xi^{\hat{\alpha}}}\,\frac{\partial T^{\hat{\alpha}}{}_{\hat{\beta}}}{\partial t}\bigg|_{\xi^{\hat{\mu}}} = \frac{\partial}{\partial t}\left(\frac{\partial\theta^{\beta}}{\partial\xi^{\hat{\beta}}}\right)\bigg|_{\xi^{\hat{\mu}}} T^{\alpha}{}_{\beta} + \frac{\partial\theta^{\beta}}{\partial\xi^{\hat{\beta}}}\,\frac{\partial T^{\alpha}{}_{\beta}}{\partial t}\bigg|_{\xi^{\hat{\mu}}}\;. \tag{16}$$

By recognizing partial derivatives with respect to time and the convected coordinates commute, such that

$$\frac{\partial}{\partial t}\left(\frac{\partial\theta^{\alpha}}{\partial\xi^{\hat{\alpha}}}\right)\bigg|_{\xi^{\hat{\mu}}} = \frac{\partial}{\partial\xi^{\hat{\alpha}}}\left(\frac{\partial\theta^{\alpha}}{\partial t}\bigg|_{\xi^{\hat{\mu}}}\right) = \frac{\partial v^{\alpha}}{\partial\xi^{\hat{\alpha}}} = v^{\alpha}_{,\hat{\alpha}}\;, \tag{17}$$

and applying the chain rule to obtain

$$\frac{\partial T^{\alpha}{}_{\beta}}{\partial t}\bigg|_{\xi^{\hat{\mu}}} = \frac{\partial T^{\alpha}{}_{\beta}}{\partial t}\bigg|_{\theta^{\mu}} + \frac{\partial\theta^{\mu}}{\partial t}\bigg|_{\xi^{\hat{\mu}}}\frac{\partial T^{\alpha}{}_{\beta}}{\partial\theta^{\mu}} = T^{\alpha}{}_{\beta,t} + v^{\mu}\,T^{\alpha}{}_{\beta,\mu}\;, \tag{18}$$

we find Eq. (16) can be written as

$$\frac{\partial T^{\hat{\alpha}}{}_{\hat{\beta}}}{\partial t}\bigg|_{\xi^{\hat{\mu}}} = \frac{\partial\xi^{\hat{\alpha}}}{\partial\theta^{\alpha}}\,\frac{\partial\theta^{\beta}}{\partial\xi^{\hat{\beta}}}\left[T^{\alpha}{}_{\beta,t} + v^{\mu}T^{\alpha}{}_{\beta,\mu} - v^{\alpha}_{,\mu}T^{\mu}{}_{\beta} + v^{\mu}_{,\beta}T^{\alpha}{}_{\mu}\right]. \tag{19}$$

Equation (19) has the usual structure of a tensor transformation law, from which we *define* the material time derivative of $T^{\alpha}{}_{\beta}$, denoted $\dot{T}^{\alpha}_{\beta}$, to be given by

$$\dot{T}^{\alpha}_{\beta} \;:=\; \frac{\partial\theta^{\alpha}}{\partial\xi^{\hat{\alpha}}}\,\frac{\partial\xi^{\hat{\beta}}}{\partial\theta^{\beta}}\left(\frac{\partial T^{\hat{\alpha}}{}_{\hat{\beta}}}{\partial t}\bigg|_{\xi^{\hat{\mu}}}\right) = T^{\alpha}{}_{\beta,t} + v^{\mu}\,T^{\alpha}{}_{\beta,\mu} - v^{\alpha}_{,\mu}T^{\mu}{}_{\beta} + v^{\mu}_{,\beta}T^{\alpha}{}_{\mu}\;. \tag{20}$$

By applying Eq. (20) to a general scalar quantity f and the vector components h^{α} and h_{α} of a general vector $\boldsymbol{h}$, we find

$$\dot{f} \;=\; f_{,t} + v^{\alpha}f_{,\alpha}\;, \tag{21}$$

$$\dot{h}^{\alpha} \;=\; h^{\alpha}_{,t} + v^{\beta}h^{\alpha}_{,\beta} - v^{\alpha}_{,\beta}h^{\beta}\;, \tag{22}$$

and

$$\dot{h}_{\alpha} \;=\; h_{\alpha,t} + v^{\beta}h_{\alpha,\beta} + v^{\beta}_{,\alpha}h_{\beta}\;. \tag{23}$$

[‡] J.G. Oldroyd. "On the formulation of rheological equations of state". *P. Roy. Soc. Lond. A Mat.* **200** (1950), 523–541.

Equations (20)–(23) are collectively referred to as *Oldroyd's Theorem*, a terminology introduced by Waxman. ‡

From the general form of Oldroyd's Theorem (20), we find partial derivatives with respect to θ^α commute with partial time derivatives at fixed $\xi^{\hat\gamma}$—for example,

$$\dot{\boldsymbol{a}}_\alpha \;=\; \frac{\partial \xi^{\hat\alpha}}{\partial \theta^\alpha}\,\frac{\partial \boldsymbol{a}_{\hat\alpha}}{\partial t}\bigg|_{\xi^{\hat\gamma}} \;=\; \frac{\partial \xi^{\hat\alpha}}{\partial \theta^\alpha}\,\frac{\partial}{\partial t}\left(\frac{\partial \hat{\boldsymbol{x}}}{\partial \xi^{\hat\alpha}}\right)\bigg|_{\xi^{\hat\gamma}} \;=\; \frac{\partial \xi^{\hat\alpha}}{\partial \theta^\alpha}\,\frac{\partial}{\partial \xi^{\hat\alpha}}\left(\frac{\partial \hat{\boldsymbol{x}}}{\partial t}\bigg|_{\xi^{\hat\gamma}}\right) \;=\; \frac{\partial \xi^{\hat\alpha}}{\partial \theta^\alpha}\,\frac{\partial \hat{\boldsymbol{v}}}{\partial \xi^{\hat\alpha}} \;=\; \boldsymbol{v}_{,\alpha}\;. \tag{24}$$

The expression for $\boldsymbol{v}_{,\alpha}$ was obtained in Chapter II, Eq. (64), for which

$$\dot{\boldsymbol{a}}_\alpha \;=\; \boldsymbol{v}_{,\alpha} \;=\; \big(v^\beta_{;\alpha} \,-\, v b^\beta_\alpha\big)\boldsymbol{a}_\beta \,+\, \big(v_{,\alpha} \,+\, v^\beta b_{\alpha\beta}\big)\boldsymbol{n}\;. \tag{25}$$

With Eq. (25), we calculate the material time derivative of several geometric quantities. By taking the material derivative of the identities $\boldsymbol{n}\cdot\boldsymbol{n} = 1$ and $\boldsymbol{n}\cdot\boldsymbol{a}_\alpha = 0$, we find

$$\dot{\boldsymbol{n}}\cdot\boldsymbol{n} \;=\; 0 \qquad \text{and} \qquad \dot{\boldsymbol{n}}\cdot\boldsymbol{a}_\alpha \;=\; -\boldsymbol{n}\cdot\dot{\boldsymbol{a}}_\alpha \;=\; -\big(v_{,\alpha} \,+\, v^\beta b_{\alpha\beta}\big)\;. \tag{26}$$

By further recognizing $\dot{\boldsymbol{n}} = \mathbf{1}\dot{\boldsymbol{n}} = \boldsymbol{n}\,(\boldsymbol{n}\cdot\dot{\boldsymbol{n}}) + \boldsymbol{a}^\alpha(\boldsymbol{a}_\alpha\cdot\dot{\boldsymbol{n}})$, where $\mathbf{1}$ is the three-dimensional identity tensor, we obtain

$$\dot{\boldsymbol{n}} \;=\; -\big(\boldsymbol{a}^\alpha\otimes\boldsymbol{n}\big)\,\dot{\boldsymbol{a}}_\alpha \;=\; -\big(a^{\alpha\beta}v_{,\beta} \,+\, v^\beta b^\alpha_\beta\big)\,\boldsymbol{a}_\alpha\;. \tag{27}$$

The material derivative of the metric tensor is calculated from the relation $a_{\alpha\beta} = \boldsymbol{a}_\alpha\cdot\boldsymbol{a}_\beta$, and is given by

$$\dot a_{\alpha\beta} \;=\; \dot{\overline{\boldsymbol{a}_\alpha\cdot\boldsymbol{a}_\beta}} \;=\; \dot{\boldsymbol{a}}_\alpha\cdot\boldsymbol{a}_\beta \,+\, \boldsymbol{a}_\alpha\cdot\dot{\boldsymbol{a}}_\beta \;=\; v_{\alpha;\beta} \,+\, v_{\beta;\alpha} \,-\, 2v b_{\alpha\beta}\;. \tag{28}$$

As the metric and contravariant metric are related by $a^{\alpha\beta} = a_{\mu\nu}a^{\alpha\mu}a^{\beta\nu}$, we obtain

$$\begin{aligned}\dot a^{\alpha\beta} \;&=\; \dot a_{\mu\nu}\,a^{\alpha\mu}\,a^{\beta\nu} \,+\, a_{\mu\nu}\,\dot a^{\alpha\mu}\,a^{\beta\nu} \,+\, a_{\mu\nu}\,a^{\alpha\mu}\,\dot a^{\beta\nu}\\ &=\; \dot a_{\mu\nu}\,a^{\alpha\mu}\,a^{\beta\nu} \,+\, \dot a^{\alpha\beta} \,+\, \dot a^{\beta\alpha}\;,\end{aligned} \tag{29}$$

where the product rule was used in the first line and the identity $a_{\mu\nu}a^{\beta\nu} = \delta^\beta_\mu$ was used in the second line. As $a^{\alpha\beta}$ is symmetric, $\dot a^{\alpha\beta}$ is symmetric as well. Rearranging terms in Eq. (29) then reveals

$$\dot a^{\alpha\beta} \;=\; -\dot a_{\mu\nu}\,a^{\alpha\mu}\,a^{\beta\nu}\;. \tag{30}$$

The material derivative of $\boldsymbol{a}^\alpha$ is calculated by first recognizing $\boldsymbol{a}^\alpha\cdot\boldsymbol{n} = 0$ and $\boldsymbol{a}^\alpha\cdot\boldsymbol{a}_\beta = \delta^\alpha_\beta$, such that $\dot{\boldsymbol{a}}^\alpha\cdot\boldsymbol{n} = -\boldsymbol{a}^\alpha\cdot\dot{\boldsymbol{n}}$ and $\dot{\boldsymbol{a}}^\alpha\cdot\boldsymbol{a}_\beta = -\boldsymbol{a}^\alpha\cdot\dot{\boldsymbol{a}}_\beta$. As $\dot{\boldsymbol{a}}^\alpha = \mathbf{1}\,\dot{\boldsymbol{a}} = \boldsymbol{a}^\beta(\boldsymbol{a}_\beta\cdot\dot{\boldsymbol{a}}^\alpha) + \boldsymbol{n}(\boldsymbol{n}\cdot\dot{\boldsymbol{a}}^\alpha)$, we find

$$\dot{\boldsymbol{a}}^\alpha \;=\; \Big(a^{\alpha\beta}\boldsymbol{n}\otimes\boldsymbol{n} \,-\, \boldsymbol{a}^\beta\otimes\boldsymbol{a}^\alpha\Big)\,\dot{\boldsymbol{a}}_\beta \;=\; -\big(v^\alpha_{;\beta} \,-\, b^\alpha_\beta\big)\,\boldsymbol{a}^\beta \,+\, \big(a^{\alpha\beta}v_{,\beta} \,+\, v^\beta b^\alpha_\beta\big)\,\boldsymbol{n}\;. \tag{31}$$

Since the metric tensor of the reference configuration $A_{\hat\alpha\hat\beta}$ does not change in time, the material derivative of the Jacobian determinant (6) is calculated as

$$\dot J \;=\; \frac{1}{(\det A_{\hat\alpha\hat\beta})^{1/2}}\;\frac{1}{2\,(\det a_{\alpha\beta})^{1/2}}\;\dot{\overline{\det a_{\alpha\beta}}}\;. \tag{32}$$

‡Waxman, "Dynamics of a couple-stress fluid membrane".

By recognizing $a^{\alpha\beta}$ is the matrix inverse of $a_{\alpha\beta}$, such that $a^{11} = a_{22}/(\det a_{\alpha\beta})$, $a^{22} = a_{11}/(\det a_{\alpha\beta})$, and $a^{12} = a^{21} = -a_{12}/(\det a_{\alpha\beta})$, we can express

$$a^{\alpha\beta}\,\dot{a}_{\alpha\beta} \;=\; \frac{1}{\det a_{\alpha\beta}}\,\overline{\dot{\det a_{\alpha\beta}}}\;. \tag{33}$$

Upon substituting Eq. (33) into Eq. (32) and applying Eq. (28), we obtain

$$\frac{\dot{J}}{J} \;=\; \frac{1}{2}\,a^{\alpha\beta}\,\dot{a}_{\alpha\beta} \;=\; v^{\alpha}_{;\alpha} \;-\; 2vH\;. \tag{34}$$

In three-dimensional Cartesian systems, $\dot{J}/J = \operatorname{div}\boldsymbol{v}$; Eq. (34) indicates the two-dimensional analog for the divergence of the velocity field is the surface divergence $v^{\alpha}_{;\alpha} - 2vH$.

To calculate the material derivative of the curvature components, we once again take advantage of the material time derivative commuting with spatial derivatives in the convected coordinates. Taking the material time derivative of the equation $b_{\alpha\beta} = \boldsymbol{n}\cdot\boldsymbol{x}_{;\alpha\beta}$ yields

$$\dot{b}_{\alpha\beta} \;=\; \dot{\boldsymbol{n}}\cdot\boldsymbol{x}_{;\alpha\beta} \;+\; \boldsymbol{n}\cdot\overline{\dot{\boldsymbol{x}}_{;\alpha\beta}}\;, \tag{35}$$

where the first term on the right-hand side simplifies to $\dot{\boldsymbol{n}}\cdot b_{\alpha\beta}\boldsymbol{n} = 0$. The last term in Eq. (35) can be expanded as

$$\boldsymbol{n}\cdot\overline{\dot{\boldsymbol{x}}_{;\alpha\beta}} \;=\; \boldsymbol{n}\cdot\overline{\dot{(\boldsymbol{x}_{,\alpha\beta} \;-\; \boldsymbol{a}_{\mu}\Gamma^{\mu}_{\alpha\beta})}} \;=\; \boldsymbol{n}\cdot\overline{\dot{\boldsymbol{x}}_{,\alpha\beta}} \;-\; \overbrace{\boldsymbol{n}\cdot\boldsymbol{a}_{\mu}}^{=0}\,\dot{\Gamma}^{\mu}_{\alpha\beta} \;-\; \boldsymbol{n}\cdot\dot{\boldsymbol{a}}_{\mu}\,\Gamma^{\mu}_{\alpha\beta}\;. \tag{36}$$

At this point, we recognize $\boldsymbol{n}\cdot\boldsymbol{a}_{\mu} = 0$ by definition, $\dot{\boldsymbol{a}}_{\mu} = \boldsymbol{v}_{,\mu}$ (25), and through Oldroyd's Theorem $\overline{\dot{\boldsymbol{x}}_{,\alpha\beta}} = \boldsymbol{v}_{,\alpha\beta}$—for which

$$\dot{b}_{\alpha\beta} \;=\; \boldsymbol{n}\cdot\overline{\dot{\boldsymbol{x}}_{;\alpha\beta}} \;=\; \boldsymbol{n}\cdot\boldsymbol{v}_{,\alpha\beta} \;-\; \boldsymbol{n}\cdot\boldsymbol{v}_{,\mu}\,\Gamma^{\mu}_{\alpha\beta} \;=\; \boldsymbol{n}\cdot\big(\boldsymbol{v}_{,\alpha\beta} \;-\; \boldsymbol{v}_{,\mu}\,\Gamma^{\mu}_{\alpha\beta}\big) \;=\; \boldsymbol{n}\cdot\boldsymbol{v}_{;\alpha\beta}\;. \tag{37}$$

By recognizing $\boldsymbol{v}_{;\alpha} = \boldsymbol{v}_{,\alpha}$ and substituting the expression for $\boldsymbol{v}_{,\alpha}$ (25) into Eq. (37), we obtain

$$\begin{aligned}
\boldsymbol{n}\cdot\boldsymbol{v}_{;\alpha\beta} \;&=\; \boldsymbol{n}\cdot\big(\boldsymbol{v}_{;\alpha}\big)_{;\beta} \qquad (38)\\
&=\; \boldsymbol{n}\cdot\Big[\big(v^{\mu}_{;\alpha} \;-\; vb^{\mu}_{\alpha}\big)\boldsymbol{a}_{\mu} \;+\; \big(v_{,\alpha} \;+\; v^{\mu}b_{\alpha\mu}\big)\boldsymbol{n}\Big]_{;\beta}\\
&=\; \boldsymbol{n}\cdot\Big[\big(v^{\mu}_{;\alpha} \;-\; vb^{\mu}_{\alpha}\big)_{;\beta}\,\boldsymbol{a}_{\mu} \;+\; \big(v^{\mu}_{;\alpha} \;-\; vb^{\mu}_{\alpha}\big)\underbrace{\boldsymbol{a}_{\mu;\beta}}_{b_{\beta\mu}\boldsymbol{n}} + \big(v_{,\alpha} \;+\; v^{\mu}b_{\alpha\mu}\big)_{;\beta}\boldsymbol{n} \;+\; \big(v_{,\alpha} \;+\; v^{\mu}b_{\alpha\mu}\big)\underbrace{\boldsymbol{n}_{;\beta}}_{-b^{\nu}_{\beta}\,\boldsymbol{a}_{\nu}}\Big]\;.
\end{aligned}$$

With the identities $\boldsymbol{n}\cdot\boldsymbol{n} = 1$ and $\boldsymbol{n}\cdot\boldsymbol{a}_{\alpha} = 0$, we find the material time derivative of the curvature tensor to be given by

$$\dot{b}_{\alpha\beta} \;=\; \big(v^{\mu}_{;\alpha} \;-\; vb^{\mu}_{\alpha}\big)\,b_{\beta\mu} \;+\; \big(v_{,\alpha} \;+\; v^{\mu}b_{\alpha\mu}\big)_{;\beta}\;. \tag{39}$$

We end our discussion of the surface kinematics by determining the acceleration $\boldsymbol{c} = c^{\alpha}\boldsymbol{a}_{\alpha} + c\boldsymbol{n}$. By definition, the acceleration is the material time derivative of the velocity, for which

$$\boldsymbol{c} \;=\; \dot{\boldsymbol{v}} \;=\; \overline{\dot{v^{\alpha}\boldsymbol{a}_{\alpha} \;+\; v\boldsymbol{n}}} \;=\; \dot{v}^{\alpha}\boldsymbol{a}_{\alpha} \;+\; v^{\alpha}\dot{\boldsymbol{a}}_{\alpha} \;+\; \dot{v}\boldsymbol{n} \;+\; v\dot{\boldsymbol{n}}\;. \tag{40}$$

The material time derivatives of the in-plane and out-of-plane velocity components are found to be [see Eqs. (21) and (22)]

$$\dot{v}^\alpha = v^\alpha_{,t} \qquad \text{and} \qquad \dot{v} = v_{,t} + v^\alpha v_{,\alpha} \,. \tag{41}$$

Substituting Eqs. (25), (27), and (41) into Eq. (40) reveals the components of the acceleration are given by

$$c^\alpha = v^\alpha_{,t} + v^\beta v^\alpha_{;\beta} - 2vv^\beta b^\alpha_\beta - v v_{,\beta} a^{\alpha\beta} \tag{42}$$

and

$$c = v_{,t} + 2v^\alpha v_{,\alpha} + v^\alpha v^\beta b_{\alpha\beta} \,. \tag{43}$$

Though Eqs. (42) and (43) were first given by Waxman [‡] in 1984 and incorporated into the membrane literature by Hu, Zhang, and E [†] in 2007, recent work by both ourselves [*] and others [§] had incorrect expressions for the components of the material acceleration.

Example 1: Vortex Acceleration

Consider a two-dimensional fluid on a planar surface, flowing with a constant angular velocity ω about the origin, as shown to the right. The surface is parametrized by the distance from the origin r and azimuthal angle θ, for which the surface-fixed coordinates are $\theta^1 = r$ and $\theta^2 = \theta$. The position is given by

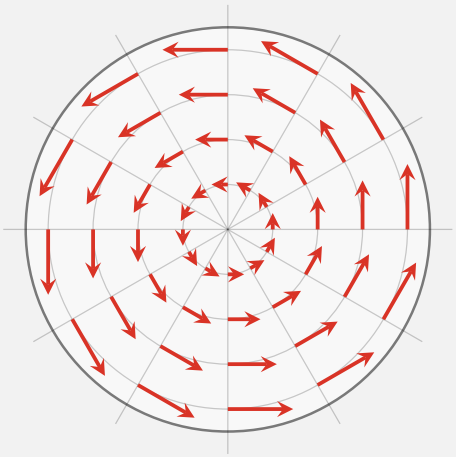

$$\boldsymbol{x} = r\,\boldsymbol{e}_r(\theta) \,,$$

with the basis vectors given by

$$\boldsymbol{a}_1 = \boldsymbol{e}_r \,, \quad \boldsymbol{a}_2 = r\,\boldsymbol{e}_\theta \,, \quad \text{and} \quad \boldsymbol{n} = \boldsymbol{e}_z \,.$$

In order to calculate the components of the acceleration, we require the curvature tensor $b_{\alpha\beta}$ the Christoffel symbols $\Gamma^\alpha_{\beta\mu}$. It is left as an exercise to the reader to calculate

$$b_{\alpha\beta} = 0 \,, \qquad \Gamma^2_{12} = r^{-1} \,, \qquad \text{and} \qquad \Gamma^1_{22} = -r \,,$$

with all other Christoffel symbols being zero. Finally, we express the velocity $\boldsymbol{v}$ in

[‡] Waxman, "Dynamics of a couple-stress fluid membrane".

[†] D. Hu, P. Zhang, and W. E. "Continuum theory of a moving membrane". *Phys. Rev. E* **75** (2007), 041605.

[*] Sahu et al., "Irreversible thermodynamics of curved lipid membranes".

[§] M. Arroyo and A. DeSimone. "Relaxation dynamics of fluid membranes". *Phys. Rev. E* **79** (2009), 31915–31931.

terms of the basis vectors as

$$\boldsymbol{v} = \omega r \boldsymbol{e}_\theta = \omega \boldsymbol{a}_2 ,$$

for which

$$v^1 = 0 , \qquad v^2 = \omega , \qquad \text{and} \qquad v = 0 .$$

Through Eqs. (42) and (43), we calculate

$$c^1 = \underbrace{v^1_{,t}}_{=0} + v^\beta v^1_{;\beta} - \underbrace{2 v v^\beta b^1_\beta}_{=0} - \underbrace{v v_{,\beta} a^{1\beta}}_{=0} = v^2 \Gamma^1_{22} v^2 = -r\omega^2 ,$$

$$c^2 = \underbrace{v^2_{,t}}_{=0} + v^\beta v^2_{;\beta} - \underbrace{2 v v^\beta b^2_\beta}_{=0} - \underbrace{v v_{,\beta} a^{2\beta}}_{=0} = v^2 \left(\Gamma^2_{21} v^1 + \Gamma^2_{22} v^2 \right) = 0 ,$$

and

$$c = v_{,t} + 2 v^\alpha v_{,\alpha} + v^\alpha v^\beta b_{\alpha\beta} = 0 .$$

In vector form, the acceleration is expressed as

$$\boldsymbol{c} = c^\alpha \boldsymbol{a}_\alpha + c \boldsymbol{n} = -r\omega^2 \boldsymbol{e}_r ,$$

which is the well-known centripetal acceleration of uniform circular motion.

2. The balance laws

With the mathematical machinery to describe the membrane geometry and kinematics, we now derive the fundamental balance laws. Our general procedure is to start with a global form of the balance law for an arbitrary membrane patch $\mathcal{P}$, convert each term to an integral over the membrane surface, and invoke the arbitrariness of $\mathcal{P}$ to determine the local form of the balance law. To convert terms in the global balance laws to integrals over the membrane patch, we employ three results with bulk analogs: the Reynolds transport theorem, the surface divergence theorem, and the localization theorem.

The Jacobian determinant (6) relates the area of differential elements in the current and reference configurations. Consequently, the integral of a general quantity $\tilde{f}$ over the membrane area can be equivalently written as

$$\int_{\mathcal{P}} f(\theta^\alpha, t) \, \mathrm{d}a = \int_{\mathcal{P}_0} \hat{f}(\xi^{\hat{\alpha}}, t) \, \hat{J}(\xi^{\hat{\alpha}}, t) \, \mathrm{d}A , \tag{44}$$

where f and $\hat{f}$ are related by Eq. (11). Taking the material time derivative of Eq. (44) and

recognizing the reference patch does not change in time yields [cf. Chapter III, Eq. (17)]

$$\begin{aligned}\frac{\mathrm{d}}{\mathrm{d}t}\Big(\int_{\mathcal{P}} f(\theta^\alpha,t)\,\mathrm{d}a\Big) &= \frac{\mathrm{d}}{\mathrm{d}t}\Big(\int_{\mathcal{P}_0} \hat{f}(\xi^{\hat\alpha},t)\,\hat{J}(\xi^{\hat\alpha},t)\,\mathrm{d}A\Big)\\ &= \int_{\mathcal{P}_0}\Big[\frac{\partial}{\partial t}\Big(\hat{f}(\xi^{\hat\alpha},t)\Big)\,\hat{J}(\xi^{\hat\alpha},t) + \hat{f}(\xi^{\hat\alpha},t)\,\frac{\partial}{\partial t}\Big(\hat{J}(\xi^{\hat\alpha},t)\Big)\Big]\,\mathrm{d}A\\ &= \int_{\mathcal{P}_0}\Big(\frac{\mathrm{d}\hat{f}}{\mathrm{d}t}\,\hat{J} + \hat{f}\,\frac{\mathrm{d}\hat{J}}{\mathrm{d}t}\Big)\,\mathrm{d}A\\ &= \int_{\mathcal{P}}\Big(\dot{f} + f\,\frac{\dot{J}}{J}\Big)\,\mathrm{d}a\,.\end{aligned} \tag{45}$$

By substituting Eq. (34) into the result of Eq. (45), we obtain the Reynolds transport theorem—given by

$$\frac{\mathrm{d}}{\mathrm{d}t}\Big(\int_{\mathcal{P}} f(\theta^\alpha,t)\,\mathrm{d}a\Big) = \int_{\mathcal{P}}\Big(\dot{f} + f\big(v^\alpha_{;\alpha} - 2vH\big)\Big)\,\mathrm{d}a\,. \tag{46}$$

The surface divergence theorem is provided here without proof, and is written as

$$\int_{\partial\mathcal{P}} h^\alpha \nu_\alpha\,\mathrm{d}s = \int_{\mathcal{P}} h^\alpha_{;\alpha}\,\mathrm{d}a\,. \tag{47}$$

In Eq. (47), $\boldsymbol{h} = h^\alpha \boldsymbol{a}_\alpha + h\boldsymbol{n}$ is a general vector, $h^\alpha\nu_\alpha = \boldsymbol{h}\cdot\boldsymbol{\nu}$, $\mathrm{d}s$ is an infinitesimal line element on the membrane boundary, and $\boldsymbol{\nu}$ is the in-plane unit normal [see Chapter II, Eq. (50)]. The localization theorem is similarly presented without proof, and states

$$\int_{\mathcal{P}} f\,\mathrm{d}a = 0 \qquad \forall\ \mathcal{P}\subset\mathcal{S} \qquad \text{if and only if} \qquad f = 0 \quad \text{in } \mathcal{S}\,. \tag{48}$$

For readers seeking more details regarding the surface divergence and localization theorems, we refer to the detailed treatment by Naghdi. [‡]

(a). The balance of mass

Consider a membrane patch $\mathcal{P}(t)$ which tracks the same material points over time. We denote the mass per unit area of the patch as $\rho(\theta^\alpha,t)$. The total mass of the membrane patch is conserved, and the global form of the conservation of mass can be written as

$$\frac{\mathrm{d}}{\mathrm{d}t}\Big(\int_{\mathcal{P}} \rho\,\mathrm{d}a\Big) = 0\,. \tag{49}$$

Applying the Reynolds transport theorem (46) to the global mass balance (49) brings the time derivative inside the integral, and we obtain

$$\int_{\mathcal{P}}\Big(\dot{\rho} + \rho\big(v^\alpha_{;\alpha} - 2vH\big)\Big)\,\mathrm{d}a = 0\,. \tag{50}$$

[‡]Naghdi, "The Theory of Shells and Plates".

Since Eq. (50) holds for all $\mathcal{P} \in \mathcal{S}$, application of the localization theorem (48) yields the local form of the conservation of mass, given by

$$\dot{\rho} + \rho\big(v^{\alpha}_{;\alpha} - 2vH\big) = 0 \,. \tag{51}$$

Lipid membranes are nearly area-incompressible, and stretch only 2–3 % before tearing. [‡] It is often useful to model lipid membranes as area-incompressible materials, in which case the density ρ is constant, $\dot{\rho} = 0$, and Eq. (51) simplifies to

$$v^{\alpha}_{;\alpha} - 2vH = 0 \,. \tag{52}$$

Equations (51) and (52) are often referred to as the continuity equation for compressible and incompressible membranes, respectively.

For both compressible and incompressible membranes, several useful relations can be obtained. The total mass of the membrane patch is conserved, and the mass at any time t is equal to the mass at time t_0. Introducing $\hat{\rho}_0(\xi^{\hat{\alpha}}) = \hat{\rho}(\xi^{\hat{\alpha}}, t_0)$ as the areal mass density of the reference patch at time t_0, conservation of mass requires

$$\int_{\mathcal{P}} \rho(\theta, t)\, \mathrm{d}a = \int_{\mathcal{P}_0} \hat{\rho}_0(\xi^{\hat{\alpha}})\, \mathrm{d}A \,. \tag{53}$$

Applying Eq. (44) to the left hand side of Eq. (53) yields

$$\int_{\mathcal{P}_0} \hat{\rho}(\xi^{\hat{\alpha}}, t)\, \hat{J}(\xi^{\hat{\alpha}}, t)\, \mathrm{d}A = \int_{\mathcal{P}_0} \hat{\rho}_0(\xi^{\hat{\alpha}})\, \mathrm{d}A \,. \tag{54}$$

As the membrane patch $\mathcal{P}$ is arbitrary, the reference patch $\mathcal{P}_0$ is arbitrary as well. With the localization theorem (48), Eq. (54) implies the Jacobian determinant $\tilde{J}$ is given by

$$\tilde{J} = \hat{J}(\xi^{\hat{\alpha}}, t) = \frac{\hat{\rho}_0(\xi^{\hat{\alpha}})}{\hat{\rho}(\xi^{\hat{\alpha}}, t)} \,, \tag{55}$$

in addition to the form provided in Eq. (6). Additionally, by substituting $f = \rho u$ into the Reynolds transport theorem (46) for an arbitrary quantity per unit mass u, and then substituting the local form of the balance of mass (51), we obtain

$$\frac{\mathrm{d}}{\mathrm{d}t}\bigg(\int_{\mathcal{P}} \rho u\, \mathrm{d}a\bigg) = \int_{\mathcal{P}} \Big(\rho \dot{u} + u\,\big[\underbrace{\dot{\rho} + \rho\big(v^{\alpha}_{;\alpha} - 2vH\big)}_{=0}\big]\Big)\, \mathrm{d}a = \int_{\mathcal{P}} \rho \dot{u}\, \mathrm{d}a \,. \tag{56}$$

Equation (56) is a modified Reynolds transport theorem and will be used often in our later developments.

[‡] E.A. Evans and R. Skalak. *Mechanics and Thermodynamics of Biomembranes*. Boca Raton: CRC Press, 1980.

(b). The balance of linear momentum

It is well-known from Newtonian and continuum mechanics that the rate of change of momentum of a body is equal to the sum of the external forces acting on it. Lipid membranes may be acted upon by two types of forces: body forces on the membrane patch $\mathcal{P}$ and tractions on the membrane boundary $\partial\mathcal{P}$. The body force per unit area of the patch is denoted $\boldsymbol{f}(\theta^\alpha, t)$. At a point $\boldsymbol{x}_\mathrm{b} = \boldsymbol{x}(\theta^\alpha_\mathrm{b}, t)$ on the membrane boundary $\partial\mathcal{P}$ with in-plane unit normal $\boldsymbol{\nu}$, the boundary traction is the force per unit length acting on the membrane boundary—denoted $\boldsymbol{T}(\theta^\alpha_\mathrm{b}, t; \boldsymbol{\nu})$. The global form of the balance of linear momentum is then given by

$$\frac{\mathrm{d}}{\mathrm{d}t}\left(\int_{\mathcal{P}} \rho \boldsymbol{v} \, \mathrm{d}a \right) \;=\; \int_{\mathcal{P}} \boldsymbol{f} \, \mathrm{d}a \;+\; \int_{\partial\mathcal{P}} \boldsymbol{T} \, \mathrm{d}s \;, \tag{57}$$

where the left hand side is the time derivative of the total linear momentum of the membrane patch and the right hand side is the sum of the external forces acting on the body.

For three-dimensional systems in Cartesian coordinates, one may use Cauchy's tetrahedron arguments to decompose the boundary tractions and define the Cauchy stress tensor, which specifies the total state of stress at any location. [‡] Naghdi performed an analogous procedure on a curvilinear triangle, as a subset of an arbitrary surface, to show boundary tractions may be expressed as a linear combination of the stress vectors $\boldsymbol{T}^\alpha$ according to [†]

$$\boldsymbol{T}(\theta^\alpha_\mathrm{b}, t; \boldsymbol{\nu}) = \boldsymbol{T}^\alpha(\theta^\alpha_\mathrm{b}, t)\, \nu_\alpha \;. \tag{58}$$

The stress vectors $\boldsymbol{T}^\alpha$ describe the tractions along curves of constant θ^α and are independent of the in-plane boundary unit normal $\boldsymbol{\nu}$. Substituting the traction decomposition (58) into the global linear momentum balance (57), applying the surface divergence theorem (47) on the traction term, and applying the Reynolds transport theorem (56) on the left hand side, we obtain

$$\int_{\mathcal{P}} \rho \boldsymbol{c} \, \mathrm{d}a \;=\; \int_{\mathcal{P}} \boldsymbol{f} \, \mathrm{d}a \;+\; \int_{\mathcal{P}} \boldsymbol{T}^\alpha_{;\alpha} \, \mathrm{d}a \;, \tag{59}$$

where the acceleration $\boldsymbol{c} = \dot{\boldsymbol{v}}$ is given by Eq. (40). Since the patch $\mathcal{P}$ is arbitrary, applying the localization theorem (48) to Eq. (59) yields the local form of the linear momentum balance as

$$\rho \boldsymbol{c} \;=\; \boldsymbol{f} \;+\; \boldsymbol{T}^\alpha_{;\alpha} \;. \tag{60}$$

To recast the traction decomposition (58) into a more familiar form involving the Cauchy stress tensor, we express the stress vectors $\boldsymbol{T}^\alpha$ in the $\{\boldsymbol{a}_\beta, \boldsymbol{n}\}$ basis without loss of generality as

$$\boldsymbol{T}^\alpha \;=\; N^{\alpha\beta}\boldsymbol{a}_\beta \;+\; S^\alpha \boldsymbol{n} \;, \tag{61}$$

where the physical interpretation of $N^{\alpha\beta}$ and S^α is shown in Fig. 2. Substituting the form of the stress vectors $\boldsymbol{T}^\alpha$ (61) into the traction decomposition (58) allows us to write

$$\boldsymbol{T} \;=\; \boldsymbol{\sigma}^{\mathrm{T}} \boldsymbol{\nu} \;, \tag{62}$$

[‡] P. Chadwick. *Continuum Mechanics: Concise Theory and Problems*. 2nd ed. Mineola: Dover, 1999.
[†] Naghdi, "The Theory of Shells and Plates".

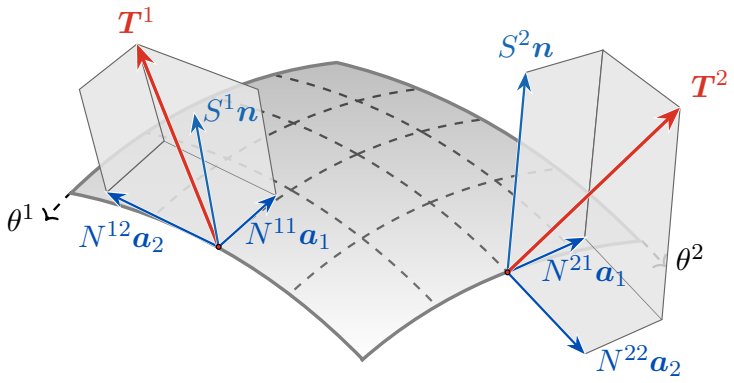

Figure 2: Schematic showing the decomposition of the stress vectors $\boldsymbol{T}^\alpha$ in the $\{\boldsymbol{a}_\beta, \boldsymbol{n}\}$ basis, according to Eq. (61). The four components N^{11}, N^{12}, N^{21}, and N^{22}, collectively denoted $N^{\alpha\beta}$, are the in-plane stress components. On the other hand, the two components S^1 and S^2—referred to as S^α—are the out-of-plane stress components, and are sometimes called the out-of-plane shears. Together, the six quantities are the components of the Cauchy stress tensor $\boldsymbol{\sigma}$ [see Eq. (63)].

where $\boldsymbol{\sigma}$ is the Cauchy stress tensor given by

$$\boldsymbol{\sigma} \;=\; N^{\alpha\beta}\boldsymbol{a}_\alpha \otimes \boldsymbol{a}_\beta \;+\; S^\alpha \boldsymbol{a}_\alpha \otimes \boldsymbol{n}\;. \tag{63}$$

Consequently, $N^{\alpha\beta}$ and S^α can be interpreted as the in-plane and out-of-plane components of the stress tensor $\boldsymbol{\sigma}$. In specifying $N^{\alpha\beta}$ and S^α, we will have completely determined the total state of stress at any location on the membrane.

When solving for and analyzing the dynamical equations of motion, it is often useful to consider the linear momentum balance (60) in component form. In what follows, we decompose the equations of motion in the directions normal and tangential to the surface. To this end, the body force $\boldsymbol{f}$ is decomposed as

$$\boldsymbol{f} \;=\; f^\alpha \boldsymbol{a}_\alpha \;+\; f\boldsymbol{n}\;. \tag{64}$$

We note that f is the net force per area acting normal to the membrane, often attributed to a pressure drop across the membrane surface. Here, f^α are the in-plane contravariant components of the body force per unit area—arising, for example, when the surrounding fluid exerts shear forces on the membrane. To express $\boldsymbol{T}^\alpha_{;\alpha}$ in component form, we apply the Gauss (63) and Weingarten (60) equations to the stress vector decomposition (61) and obtain

$$\begin{aligned}
\boldsymbol{T}^\alpha_{;\alpha} \;&=\; \Big(N^{\alpha\beta}\boldsymbol{a}_\beta \;+\; S^\alpha \boldsymbol{n}\Big)_{;\alpha} \\
&=\; N^{\alpha\beta}_{;\alpha}\boldsymbol{a}_\beta \;+\; N^{\alpha\beta}\underbrace{\boldsymbol{a}_{\beta;\alpha}}_{b_{\alpha\beta}\boldsymbol{n}} \;+\; S^\alpha_{;\alpha}\boldsymbol{n} \;+\; S^\alpha \underbrace{\boldsymbol{n}_{,\alpha}}_{-b^\beta_\alpha \boldsymbol{a}_\beta} \\
&=\; \Big(N^{\beta\alpha}_{;\beta} \;-\; S^\beta b^\alpha_\beta\Big)\boldsymbol{a}_\alpha \;+\; \Big(N^{\alpha\beta}b_{\alpha\beta} \;+\; S^\alpha_{;\alpha}\Big)\boldsymbol{n}\;,
\end{aligned} \tag{65}$$

where in the last line we swapped the dummy indices 'α' and 'β'. Substituting the body force decomposition (64) and divergence of the stress vectors (65) into the local form of the

linear momentum balance (60), we find the tangential and normal momentum equations are respectively given by

$$\rho c^\alpha = f^\alpha + N^{\beta\alpha}_{;\beta} - S^\beta b^\alpha_\beta \tag{66}$$

and

$$\rho c = f + N^{\alpha\beta} b_{\alpha\beta} + S^\alpha_{;\alpha} . \tag{67}$$

The normal component of the linear momentum balance (67) is often referred to as the shape equation. [‡] Although we do not yet know the form of the stresses $N^{\alpha\beta}$ and S^α, Eqs. (66) and (67) already reveal coupling between in-plane and out-of-plane membrane behavior. In particular, the in-plane stresses $N^{\alpha\beta}$ and the out-of-plane shears S^α appear in both the tangential equations (66) and the shape equation (67). Thus, we expect in-plane flows to influence and be influenced by out-of-plane shape changes. Such couplings lead to a rich variety of nonlinear membrane behaviors, as will be detailed subsequently.

At this point, local forms of the mass and linear momentum balances are obtained, and are collectively referred to as the *governing equations*. To solve these equations, however, we must first determine the forms of $N^{\alpha\beta}$ and S^α. In what follows, we systematically determine the in-plane and shear stresses in the membrane before returning to the equations of motion, in a similar fashion to our bulk analysis in Chapter III.

(c). The balance of angular momentum

Thus far, the global forms of the membrane balance laws were similar to their bulk counterparts. When analyzing the balance of angular momentum, however, care must be taken in treating a lipid membrane as an infinitely thin, two-dimensional surface. We account for the membrane's five nanometer thickness within our theory by endowing the surface with a director field $\boldsymbol{d}(\theta, t)$: a dimensionless vector field capturing rotations and stretches of the material that are independent from the deformation of the overall surface. [†] For example, if the director field $\boldsymbol{d}$ is not aligned with the unit normal $\boldsymbol{n}$, i.e. when $\boldsymbol{d} \times \boldsymbol{n} \neq \boldsymbol{0}$, then the phospholipids are tilted relative to the orientation of the surface (see Fig. 3). Importantly, at a point $\boldsymbol{x}_\mathrm{b} = \boldsymbol{x}(\theta^\alpha_\mathrm{b}, t)$ on the membrane patch boundary $\partial\mathcal{P}$, so-called *director tractions* $\boldsymbol{M}(\theta^\alpha_\mathrm{b}, t)$ can exert equal and opposite forces on the director—thus inducing a couple per length $\boldsymbol{m} = \boldsymbol{d} \times \boldsymbol{M}$ which either twists or bends the membrane (see Fig. 4). Such couples play a crucial role in the mechanics and dynamics of lipid membranes, and are in fact necessary to sustain the out-of-plane shear stresses S^α introduced in Eq. (61).

To properly account for a director field as a new kinematic quantity, it would be necessary to include the director velocity $\dot{\boldsymbol{d}}$ in an additional balance law for the director momentum, as described by Naghdi [*] and the references cited therein. Including the director as an additional unknown would enable us to examine small length scale phenomena, for example transmembrane proteins causing phospholipids to tilt—which would induce local inhomogeneities in

[‡]The term "shape equation" was originally used by O.-Y. Zhong-can and W. Helfrich. "Instability and deformation of a spherical vesicle by pressure". *Phys. Rev. Lett.* **59** (1987), 2486–2488.

[†]As discussed in our historical introduction to the membrane theory (Chapter IV, §2), a surface endowed with a director field is known as a Cosserat surface [E. Cosserat and F. Cosserat. *Théorie des Corps Déformables*. Paris: A. Hermann et Fils, 1909].

[*]Naghdi, "The Theory of Shells and Plates".

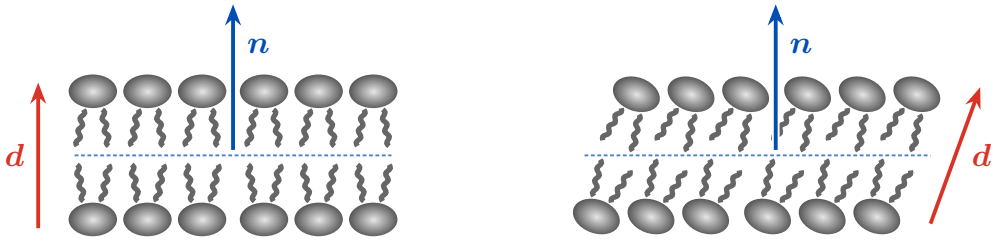

(a) $\boldsymbol{d} \times \boldsymbol{n} = \boldsymbol{0}$ (b) $\boldsymbol{d} \times \boldsymbol{n} \neq \boldsymbol{0}$

Figure 3: Close-up schematics of a lipid bilayer, in which phospholipid molecules are either (a) not tilted or (b) tilted relative to the unit normal to the surface $\boldsymbol{n}$. In both situations, our two-dimensional continuum description models the lipid bilayer as a flat sheet, represented by a dashed horizontal line. The surface is endowed with a director field $\boldsymbol{d}$ to capture small length scale effects of the lipid orientation, and differentiate the two situations.

the director field. In this work, however, we choose not to study such phenomena. In this case, the director is prescribed to be equal to the normal at every point on the membrane surface, written as

$$\boldsymbol{d}(\theta^\alpha, t) \;=\; \boldsymbol{n}(\theta^\alpha, t) \;. \tag{68}$$

Equation (68) is equivalent to the Kirchhoff–Love assumption discussed in §2 of Chapter IV. With the simplification in Eq. (68), the moment per unit length acting on the patch boundary, $\boldsymbol{m}$, is given by

$$\boldsymbol{m} \;=\; \boldsymbol{n} \times \boldsymbol{M} \;. \tag{69}$$

Importantly, Eq. (69) is necessary to write the global form of the angular momentum balance, which states that the rate of change of the total angular momentum of the membrane patch is equal to the sum of the external torques and couples acting on it—expressed as

$$\frac{\mathrm{d}}{\mathrm{d}t}\left(\int_{\mathcal{P}} \boldsymbol{x} \times \rho \boldsymbol{v} \; \mathrm{d}a \right) \;=\; \int_{\mathcal{P}} \boldsymbol{x} \times \boldsymbol{f} \; \mathrm{d}a \;+\; \int_{\partial\mathcal{P}} \Big(\boldsymbol{x} \times \boldsymbol{T} \;+\; \boldsymbol{n} \times \boldsymbol{M} \Big) \; \mathrm{d}s \;. \tag{70}$$

In Eq. (70), $\boldsymbol{x} \times \rho \boldsymbol{v}$ is the angular momentum density at the point $\boldsymbol{x}$, and $\boldsymbol{x} \times \boldsymbol{f}$ and $\boldsymbol{x} \times \boldsymbol{T}$ are the torque densities due to body forces and tractions, respectively.

While the director traction $\boldsymbol{M}$ may in general have normal and tangential components, the component in the normal direction has no effect on the resulting couple $\boldsymbol{m}$, as can be seen from Eq. (69). We thus restrict $\boldsymbol{M}$ to be in the plane of the membrane. Once again using the elementary curvilinear triangle arguments described by Naghdi, the director traction $\boldsymbol{M}$ can be written as

$$\boldsymbol{M}(\theta^\alpha_{\mathrm{b}}, t; \boldsymbol{\nu}) \;=\; \boldsymbol{M}^\alpha(\theta^\alpha_{\mathrm{b}}, t) \, \nu_\alpha \;. \tag{71}$$

The couple-stress vectors $\boldsymbol{M}^\alpha$ in Eq. (71) must be in the plane of the membrane due to our imposed restriction, and can be written without loss of generality as

$$\boldsymbol{M}^\alpha \;=\; -M^{\alpha\beta} \boldsymbol{a}_\beta \;. \tag{72}$$

Substituting the couple-stress decomposition (72) into the director traction decomposition (71) allows us to express the director traction as

$$\boldsymbol{M} \;=\; \boldsymbol{\mu}^{\mathrm{T}} \, \boldsymbol{\nu} \;, \tag{73}$$

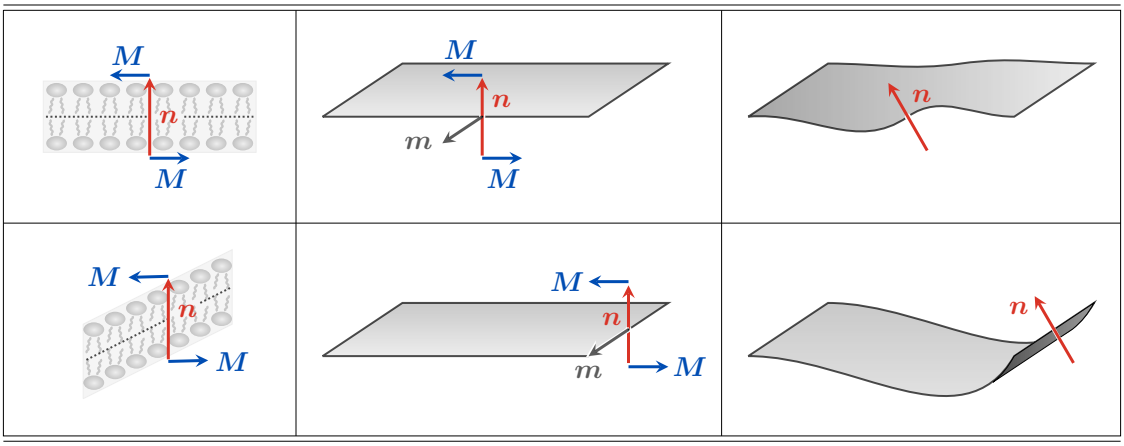

Figure 4: A director traction $\boldsymbol{M}$ acting on the unit normal $\boldsymbol{n}$ at the membrane boundary results in edge twisting (top) and bending (bottom). The director traction, which has units of couple per length, acts in the manner of a force on the dimensionless normal vector to produce a moment per length $\boldsymbol{m}$. The left column gives a microscopic perspective of how the director tractions act on the membrane, the center column shows the corresponding continuum picture, and the right column depicts the resultant membrane configuration. In general, the couple per length $\boldsymbol{m}$ acting on the membrane is a superposition of that shown in the top and bottom rows, and lies in the tangent plane.

where $\boldsymbol{\mu}$ is the couple-stress tensor—given by

$$\boldsymbol{\mu} \;=\; -M^{\alpha\beta}\boldsymbol{a}_\alpha \otimes \boldsymbol{a}_\beta \;. \tag{74}$$

As we require director tractions to not lie in the normal direction, the couple-stress tensor $\boldsymbol{\mu}$ in Eq. (74) does not have any $\boldsymbol{a}_\alpha \otimes \boldsymbol{n}$ component.

Returning to the global form of the angular momentum balance (70), we substitute the director traction decomposition (71) and stress vector decomposition (58) to obtain

$$\frac{\mathrm{d}}{\mathrm{d}t}\left(\int_{\mathcal{P}} \boldsymbol{x}\times\rho\boldsymbol{v}\;\mathrm{d}a\right) \;=\; \int_{\mathcal{P}} \boldsymbol{x}\times\boldsymbol{f}\;\mathrm{d}a \;+\; \int_{\partial\mathcal{P}}\left(\boldsymbol{x}\times\boldsymbol{T}^\alpha + \boldsymbol{n}\times\boldsymbol{M}^\alpha\right)\nu_\alpha\;\mathrm{d}s \;. \tag{75}$$

Using the Reynolds transport theorem (56) and the surface divergence theorem (47), and recalling $\dot{\boldsymbol{x}} = \boldsymbol{v}$ and $\boldsymbol{v}\times\boldsymbol{v} = \boldsymbol{0}$, Eq. (75) simplifies to

$$\int_{\mathcal{P}} \boldsymbol{x}\times\rho\boldsymbol{c}\;\mathrm{d}a \;=\; \int_{\mathcal{P}}\left[\boldsymbol{x}\times\boldsymbol{f} \;+\; \left(\boldsymbol{x}\times\boldsymbol{T}^\alpha\right)_{;\alpha} \;+\; \left(\boldsymbol{n}\times\boldsymbol{M}^\alpha\right)_{;\alpha}\right]\mathrm{d}a \;. \tag{76}$$

Since the membrane patch $\mathcal{P}$ is arbitrary, application of the localization theorem (48) to Eq. (76) yields the local form of the angular momentum balance, given by

$$\boldsymbol{x}\times\rho\boldsymbol{c} \;=\; \boldsymbol{x}\times\boldsymbol{f} \;+\; \boldsymbol{a}_\alpha\times\boldsymbol{T}^\alpha \;+\; \boldsymbol{x}\times\boldsymbol{T}^\alpha_{;\alpha} \;-\; b^\beta_\alpha\boldsymbol{a}_\beta\times\boldsymbol{M}^\alpha \;+\; \boldsymbol{n}\times\boldsymbol{M}^\alpha_{;\alpha} \;. \tag{77}$$

In obtaining Eq. (77), we distributed the covariant derivatives and used the Weingarten equation [Chapter II, Eq. (60)].

It is useful to know what constraints the local form of the angular momentum balance (77) imposes in addition to what was known from the linear momentum balance (60). Taking the cross product of $\boldsymbol{x}$ with Eq. (60) and subtracting the result from Eq. (77) yields

$$\boldsymbol{a}_\alpha \times \boldsymbol{T}^\alpha \,-\, b^\beta_\alpha\, \boldsymbol{a}_\beta \times \boldsymbol{M}^\alpha \,+\, \boldsymbol{n} \times \boldsymbol{M}^\alpha_{;\alpha} \,=\, \boldsymbol{0}\,. \tag{78}$$

Next, by substituting the couple-stress decomposition (72) and traction decomposition (58) into Eq. (78) and then applying the Gauss equation [Chapter II, Eq. (63)], we obtain

$$\boldsymbol{a}_\alpha \times \left[\left(N^{\alpha\beta} \,-\, b^\beta_\mu\, M^{\mu\alpha}\right)\boldsymbol{a}_\beta \,+\, \left(S^\alpha \,+\, M^{\beta\alpha}_{;\beta}\right)\boldsymbol{n}\right] \,=\, \boldsymbol{0}\,. \tag{79}$$

Equation (79) indicates that in order for both the linear momentum balance and the angular momentum balance to be locally satisfied,

$$\sigma^{\alpha\beta} \,:=\, \left(N^{\alpha\beta} \,-\, b^\beta_\mu M^{\mu\alpha}\right) \quad \text{is symmetric} \tag{80}$$

and

$$S^\alpha \,=\, -M^{\beta\alpha}_{;\beta}\,. \tag{81}$$

In Eq. (80), we introduced the tensor $\sigma^{\alpha\beta}$, which captures the moment-free components of the in-plane stresses $N^{\alpha\beta}$. Equations (80) and (81) reveal the combination of linear and angular momentum balances impose restrictions between the in-plane stress components $N^{\alpha\beta}$, out-of-plane shear stress components S^α, and the couple-stress components $M^{\alpha\beta}$. Moreover, as the boundary moment per length $\boldsymbol{m}$ is related to the components of $M^{\alpha\beta}$, Eq. (81) reveals how out-of-plane shear stresses and boundary moments are related. If director tractions had not been included in the global form of the balance of angular momentum, there would consequently be no out-of-plane shears at any point on the membrane surface.

We close our discussion by noting that it will later be useful to express the boundary moment per length, $\boldsymbol{m}$, in terms of the in-plane boundary tangent $\boldsymbol{\tau}$ and boundary normal $\boldsymbol{\nu}$ as

$$\boldsymbol{m} \,=\, m_\nu \boldsymbol{\nu} \,+\, m_\tau \boldsymbol{\tau}\,. \tag{82}$$

Recognizing

$$\boldsymbol{a}_\beta \times \boldsymbol{n} \,=\, (\tau_\beta \boldsymbol{\tau} \,+\, \nu_\beta \boldsymbol{\nu}) \times \boldsymbol{n} \,=\, \tau_\beta(\boldsymbol{\tau} \times \boldsymbol{n}) \,+\, \nu_\beta(\boldsymbol{\nu} \times \boldsymbol{n}) \,=\, \tau_\beta \boldsymbol{\nu} \,-\, \nu_\beta \boldsymbol{\tau}\,, \tag{83}$$

we can combine Eqs. (69), (71) and (72) to obtain

$$\boldsymbol{m} \,=\, M^{\alpha\beta}\nu_\alpha \boldsymbol{a}_\beta \times \boldsymbol{n} \,=\, M^{\alpha\beta}\nu_\alpha\tau_\beta\, \boldsymbol{\nu} \,-\, M^{\alpha\beta}\nu_\alpha\nu_\beta\, \boldsymbol{\tau}\,, \tag{84}$$

from which we find the components of the boundary moment per length $\boldsymbol{m}$ to be given by

$$m_\nu \,=\, M^{\alpha\beta}\nu_\alpha\tau_\beta \qquad \text{and} \qquad m_\tau \,=\, -M^{\alpha\beta}\nu_\alpha\nu_\beta\,. \tag{85}$$

With Eqs. (71), (72), and (85), as well as the decomposition $\boldsymbol{a}_\beta = \nu_\beta \boldsymbol{\nu} + \tau_\beta \boldsymbol{\tau}$, the director traction $\boldsymbol{M}$ can be expressed as

$$\boldsymbol{M} \,=\, m_\tau \boldsymbol{\nu} \,-\, m_\nu \boldsymbol{\tau}\,. \tag{86}$$

We will return to Eqs. (85) and (86) when considering possible boundary conditions for the membrane equations.

(d). The balance of mechanical power

While a mechanical power balance does not impose any new constraints on membrane dynamics, it expresses the relationship between the kinetic energy, internal forces, and external forces—which is useful in our thermodynamic considerations in subsequent sections. We begin by taking the dot product of the local momentum balance (60) with the velocity $\boldsymbol{v}$ and integrating over the membrane patch $\mathcal{P}$ to obtain

$$\int_{\mathcal{P}} \boldsymbol{v} \cdot \rho \boldsymbol{c} \, \mathrm{d}a \;=\; \int_{\mathcal{P}} \boldsymbol{v} \cdot \boldsymbol{f} \, \mathrm{d}a \;+\; \int_{\mathcal{P}} \boldsymbol{v} \cdot \boldsymbol{T}^{\alpha}_{;\alpha} \, \mathrm{d}a \; . \tag{87}$$

At this point, Eq. (87) is expressed in a more useful form. We first recognize the left-hand side of Eq. (87) is the material derivative of the total kinetic energy, as an application of the Reynolds transport theorem (56) shows

$$\frac{\mathrm{d}}{\mathrm{d}t}\left(\int_{\mathcal{P}} \frac{\rho \boldsymbol{v} \cdot \boldsymbol{v}}{2} \, \mathrm{d}a \right) \;=\; \int_{\mathcal{P}} \rho \boldsymbol{v} \cdot \boldsymbol{c} \, \mathrm{d}a \; . \tag{88}$$

Next, the second term on the right-hand side of Eq. (87) is expanded as

$$\begin{aligned} \int_{\mathcal{P}} \boldsymbol{v} \cdot \boldsymbol{T}^{\alpha}_{;\alpha} \, \mathrm{d}a \;&=\; \int_{\mathcal{P}} \left[\left(\boldsymbol{v} \cdot \boldsymbol{T}^{\alpha} \right)_{;\alpha} \;-\; \boldsymbol{v}_{,\alpha} \cdot \boldsymbol{T}^{\alpha} \right] \mathrm{d}a \\ &=\; \int_{\partial \mathcal{P}} \left(\boldsymbol{v} \cdot \boldsymbol{T}^{\alpha} \right) \nu_{\alpha} \, \mathrm{d}s \;-\; \int_{\mathcal{P}} \boldsymbol{v}_{,\alpha} \cdot \boldsymbol{T}^{\alpha} \, \mathrm{d}a \\ &=\; \int_{\partial \mathcal{P}} \boldsymbol{v} \cdot \boldsymbol{T} \, \mathrm{d}s \;-\; \int_{\mathcal{P}} \boldsymbol{v}_{,\alpha} \cdot \boldsymbol{T}^{\alpha} \, \mathrm{d}a \; , \end{aligned} \tag{89}$$

where the second equality is obtained by invoking the surface divergence theorem (47) and the third equality from the boundary traction decomposition (58). With Eqs. (61), (80), and (81), the stress vectors can be written as

$$\boldsymbol{T}^{\alpha} \;=\; \left(\sigma^{\alpha\beta} \;+\; b^{\beta}_{\mu} M^{\mu\alpha} \right) \boldsymbol{a}_{\beta} \;-\; M^{\beta\alpha}_{;\beta} \, \boldsymbol{n} \;=\; \sigma^{\alpha\beta} \boldsymbol{a}_{\beta} \;-\; \left(M^{\beta\alpha} \boldsymbol{n} \right)_{;\beta} \; , \tag{90}$$

where in the second equality we employed the Weingarten equation [Chapter II, Eq. (60)] and swapped dummy indices. Substituting Eq. (90) into the last term in Eq. (89) then yields

$$\int_{\mathcal{P}} \boldsymbol{v}_{,\alpha} \cdot \boldsymbol{T}^{\alpha} \, \mathrm{d}a \;=\; \int_{\mathcal{P}} \boldsymbol{v}_{,\alpha} \cdot \sigma^{\alpha\beta} \boldsymbol{a}_{\beta} \, \mathrm{d}a \;-\; \int_{\mathcal{P}} \boldsymbol{v}_{,\alpha} \cdot \left(M^{\beta\alpha} \boldsymbol{n} \right)_{;\beta} \, \mathrm{d}a \; . \tag{91}$$

Additionally, the last term in Eq. (91) is rearranged as

$$\begin{aligned} -\int_{\mathcal{P}} \boldsymbol{v}_{,\alpha} \cdot \left(M^{\beta\alpha} \boldsymbol{n} \right)_{;\beta} \, \mathrm{d}a \;&=\; -\int_{\mathcal{P}} \left(\boldsymbol{v}_{,\alpha} \cdot M^{\beta\alpha} \boldsymbol{n} \right)_{;\beta} \, \mathrm{d}a \;+\; \int_{\mathcal{P}} \boldsymbol{v}_{;\alpha\beta} \cdot M^{\beta\alpha} \boldsymbol{n} \, \mathrm{d}a \\ &=\; -\int_{\partial \mathcal{P}} \boldsymbol{v}_{,\alpha} \cdot M^{\beta\alpha} \nu_{\beta} \, \boldsymbol{n} \, \mathrm{d}s \;+\; \int_{\mathcal{P}} \boldsymbol{v}_{;\alpha\beta} \cdot M^{\beta\alpha} \boldsymbol{n} \, \mathrm{d}a \; , \end{aligned} \tag{92}$$

where the product rule and surface divergence theorem were used in the first and second lines, respectively. By recalling that $\boldsymbol{a}^{\mu} \cdot \boldsymbol{a}_{\alpha} = \delta^{\mu}_{\alpha}$ is an identity for the Kronecker delta, $\dot{\boldsymbol{n}}$

is provided in Eq. (27), and $\boldsymbol{M} = -M^{\beta\alpha}\nu_\beta\,\boldsymbol{a}_\alpha$ is the director traction, the integrand of the first term in the last line of Eq. (92) is expressed as

$$\begin{aligned}\boldsymbol{v}_{,\alpha}\cdot M^{\beta\alpha}\nu_\beta\,\boldsymbol{n} &= \left(\boldsymbol{v}_{,\mu}\,\delta^\mu_\alpha\right)\cdot M^{\beta\alpha}\nu_\beta\,\boldsymbol{n}\\ &= \left(\boldsymbol{v}_{,\mu}\cdot\boldsymbol{n}\right)\underbrace{M^{\beta\alpha}\nu_\beta\left(\boldsymbol{a}_\alpha\cdot\boldsymbol{a}^\mu\right)}_{=\boldsymbol{M}} = \underbrace{-\left(\boldsymbol{v}_{,\mu}\cdot\boldsymbol{n}\right)\boldsymbol{a}^\mu}_{=\dot{\boldsymbol{n}}}\cdot\boldsymbol{M} = \dot{\boldsymbol{n}}\cdot\boldsymbol{M}\,.\end{aligned} \tag{93}$$

Substituting Eqs. (88)–(93) into Eq. (87) yields

$$\begin{aligned}\frac{\mathrm{d}}{\mathrm{d}t}\left(\int_{\mathcal{P}}\frac{\rho\boldsymbol{v}\cdot\boldsymbol{v}}{2}\,\mathrm{d}a\right) + \int_{\mathcal{P}}\boldsymbol{v}_{,\alpha}\cdot\sigma^{\alpha\beta}\,\boldsymbol{a}_\beta\,\mathrm{d}a + \int_{\mathcal{P}}\boldsymbol{v}_{;\alpha\beta}\cdot M^{\alpha\beta}\,\boldsymbol{n}\,\mathrm{d}a\\ = \int_{\mathcal{P}}\boldsymbol{v}\cdot\boldsymbol{f}\,\mathrm{d}a + \int_{\partial\mathcal{P}}\left(\boldsymbol{v}\cdot\boldsymbol{T} + \dot{\boldsymbol{n}}\cdot\boldsymbol{M}\right)\mathrm{d}s\,.\end{aligned} \tag{94}$$

Finally, with the symmetry of $\sigma^{\alpha\beta}$ (80) and the kinematic results $\dot{a}_{\alpha\beta} = \boldsymbol{v}_{,\alpha}\cdot\boldsymbol{a}_\beta + \boldsymbol{a}_\alpha\cdot\boldsymbol{v}_{,\beta}$ and $\dot{b}_{\alpha\beta} = \boldsymbol{n}\cdot\boldsymbol{v}_{;\alpha\beta}$ from §1, we find

$$\boldsymbol{v}_{,\alpha}\cdot\sigma^{\alpha\beta}\boldsymbol{a}_\beta = \frac{1}{2}\left(\boldsymbol{v}_{,\alpha}\cdot\sigma^{\alpha\beta}\boldsymbol{a}_\beta + \boldsymbol{v}_{,\beta}\cdot\sigma^{\alpha\beta}\boldsymbol{a}_\alpha\right) = \frac{1}{2}\,\sigma^{\alpha\beta}\left(\boldsymbol{v}_{,\alpha}\cdot\boldsymbol{a}_\beta + \boldsymbol{v}_{,\beta}\cdot\boldsymbol{a}_\alpha\right) = \frac{1}{2}\,\sigma^{\alpha\beta}\,\dot{a}_{\alpha\beta} \tag{95}$$

and

$$\boldsymbol{v}_{;\alpha\beta}\cdot M^{\alpha\beta}\,\boldsymbol{n} = M^{\alpha\beta}\,\dot{b}_{\alpha\beta}\,. \tag{96}$$

By substituting Eqs. (95) and (96) into Eq. (94), we obtain the global form of the balance of mechanical power, written as

$$\frac{\mathrm{d}}{\mathrm{d}t}\left(\int_{\mathcal{P}}\frac{\rho\boldsymbol{v}\cdot\boldsymbol{v}}{2}\,\mathrm{d}a\right) + \int_{\mathcal{P}}\left(\frac{1}{2}\,\sigma^{\alpha\beta}\,\dot{a}_{\alpha\beta} + M^{\alpha\beta}\,\dot{b}_{\alpha\beta}\right)\mathrm{d}a = \int_{\mathcal{P}}\boldsymbol{v}\cdot\boldsymbol{f}\,\mathrm{d}a + \int_{\partial\mathcal{P}}\left(\boldsymbol{v}\cdot\boldsymbol{T} + \dot{\boldsymbol{n}}\cdot\boldsymbol{M}\right)\mathrm{d}s\,. \tag{97}$$

The left-hand side of Eq. (97) contains the material derivative of the kinetic energy (88), as well as a term capturing internal changes involving the shape and stresses of the membrane—which describe the membrane's internal power. The terms on the right-hand side of the mechanical power balance (97) describe the power due to external forces and moments acting on the membrane patch.

3. A thermodynamic description of a material surface

At this stage, the equations governing single-component lipid membrane dynamics are completely specified by the couple-free in-plane stress tensor $\sigma^{\alpha\beta}$ and the couple-stress tensor $M^{\alpha\beta}$. With these quantities, one calculates the in-plane stresses $N^{\alpha\beta}$ and the out-of-plane shear stresses S^α from the results of the angular momentum balance [Eqs. (80) and (81)], and then substitutes them into the in-plane and out-of-plane equations of motion [Eqs. (66) and (67)]. All previous works modeling the dissipative in-plane flows of lipids used either variational methods or balance law formulations, and proposed constitutive forms of the in-plane viscous stresses in an ad-hoc manner. While such approaches are theoretically

sound, they cannot easily be extended to more complicated systems—for example, multi-component membranes with chemical reactions. In the present work, however, we develop the irreversible thermodynamic framework required to understand general couplings between reversible and irreversible membrane phenomena. Within the setting of differential geometry, we formulate local forms of the first and second laws of thermodynamics, as well as the balance of entropy. We then follow the approach developed by Mandadapu, [‡] in which the Helmholtz free energy plays a central role and connects the balances of energy and entropy. Next, we choose the fundamental thermodynamic variables for the free energy, and determine the contributions to the entropy flux, external entropy supply, and internal entropy production. Single-component lipid membranes with different constitutive behaviors are analyzed subsequently. Importantly, the irreversible thermodynamic framework—based on entropy production—is naturally extendable to multi-component systems and systems with chemical reactions, as we previously demonstrated. [†]

(a). The first law: The balance of energy

According to the first law of thermodynamics, the total energy of the membrane patch changes due to work being done on the membrane or heat flowing into the membrane. The mechanical power balance (97) describes the rate of work being done on the membrane due to external tractions, moments, and forces. Furthermore, heat may enter or exit the membrane patch in one of two ways: from the surrounding bulk material, as a flux of heat in the normal direction, or in the plane of the membrane across the patch boundary. We denote the heat source per unit mass as $r(\theta^\alpha, t)$, and the in-plane heat flux as $\boldsymbol{J}_\mathrm{q} = J_\mathrm{q}^\alpha \boldsymbol{a}_\alpha$, to respectively account for these two terms. [*] By convention, the heat flux $\boldsymbol{J}_\mathrm{q}$ is positive when heat flows out of the system. Defining $e(\theta^\alpha, t)$ to be the total energy per unit mass of the membrane, the global form of the first law of thermodynamics is written as

$$\frac{\mathrm{d}}{\mathrm{d}t}\left(\int_{\mathcal{P}} \rho e \,\mathrm{d}a\right) = \int_{\mathcal{P}} \rho r \,\mathrm{d}a - \int_{\partial\mathcal{P}} \boldsymbol{J}_\mathrm{q}\cdot\boldsymbol{\nu}\,\mathrm{d}s + \int_{\mathcal{P}} \boldsymbol{v}\cdot\boldsymbol{f}\,\mathrm{d}a + \int_{\partial\mathcal{P}}\left(\boldsymbol{v}\cdot\boldsymbol{T} + \dot{\boldsymbol{n}}\cdot\boldsymbol{M}\right)\mathrm{d}s\,. \tag{98}$$

The total energy per unit mass e, by definition, consists of the internal energy per unit mass u and the kinetic energy per unit mass $\frac{1}{2}\boldsymbol{v}\cdot\boldsymbol{v}$—written as [§]

$$\rho e := \rho u + \frac{\rho \boldsymbol{v}\cdot\boldsymbol{v}}{2}\,. \tag{99}$$

By substituting Eq. (99) into Eq. (98), applying the Reynolds transport theorem (56), and recognizing $\boldsymbol{J}_\mathrm{q}\cdot\boldsymbol{\nu} = J_\mathrm{q}^\alpha \nu_\alpha$, we obtain

$$\int_{\mathcal{P}}\left(\rho\dot{u} + \rho\boldsymbol{v}\cdot\dot{\boldsymbol{v}}\right)\mathrm{d}a = \int_{\mathcal{P}} \rho r\,\mathrm{d}a - \int_{\partial\mathcal{P}} J_\mathrm{q}^\alpha \nu_\alpha\,\mathrm{d}s + \int_{\mathcal{P}} \boldsymbol{v}\cdot\boldsymbol{f}\,\mathrm{d}a + \int_{\partial\mathcal{P}}\left(\boldsymbol{v}\cdot\boldsymbol{T} + \dot{\boldsymbol{n}}\cdot\boldsymbol{M}\right)\mathrm{d}s\,. \tag{100}$$

[‡] K.K. Mandadapu. "Homogeneous Non-Equilibrium Molecular Dynamics Methods for Calculating the Heat Transport Coefficient of Solids and Mixtures". PhD thesis. University of California, Berkeley, 2011.

[†] Sahu et al., "Irreversible thermodynamics of curved lipid membranes".

[*] The heat source per unit area, ρr, is equivalently the heat flux from the surrounding bulk to the membrane in the normal direction. If $\boldsymbol{J}_\mathrm{q}^+$ is the heat flux in the fluid above the membrane and $\boldsymbol{J}_\mathrm{q}^-$ that in the fluid below the membrane, then $\rho r = -(\boldsymbol{J}_\mathrm{q}^+ - \boldsymbol{J}_\mathrm{q}^-)\cdot\boldsymbol{n}$.

[§] As in the bulk analysis in Chapter III, we do not consider potential energy contributions for simplicity.

Equation (100) shares several terms with the mechanical power balance (97). By subtracting the latter from the former, the balance of internal energy is obtained as

$$\begin{aligned}\int_{\mathcal{P}} \rho \dot{u} \, \mathrm{d}a \;&=\; \int_{\mathcal{P}} \rho r \, \mathrm{d}a \;-\; \int_{\partial\mathcal{P}} J^{\alpha}_{\mathrm{q}} \nu_{\alpha} \, \mathrm{d}s \;+\; \int_{\mathcal{P}} \left(\frac{1}{2} \sigma^{\alpha\beta} \dot{a}_{\alpha\beta} \;+\; M^{\alpha\beta} \dot{b}_{\alpha\beta} \right) \mathrm{d}a \\ &=\; \int_{\mathcal{P}} \left(\rho r \;-\; J^{\alpha}_{\mathrm{q};\alpha} \;+\; \frac{1}{2} \sigma^{\alpha\beta} \dot{a}_{\alpha\beta} \;+\; M^{\alpha\beta} \dot{b}_{\alpha\beta} \right) \mathrm{d}a \;,\end{aligned} \tag{101}$$

where the second equality is obtained by using the surface divergence theorem (47) on the boundary term. Since the membrane patch $\mathcal{P}$ is arbitrary, we apply the localization theorem (48) to Eq. (101) and find the local form of the internal energy balance to be given by

$$\rho \dot{u} \;=\; \rho r \;-\; J^{\alpha}_{\mathrm{q};\alpha} \;+\; \frac{1}{2} \sigma^{\alpha\beta} \dot{a}_{\alpha\beta} \;+\; M^{\alpha\beta} \dot{b}_{\alpha\beta} \;. \tag{102}$$

The first two terms on the right hand side of Eq. (102) describe the rate of heat flow into the system, and the last two terms describe the rate of internal energy change due to internal work being done on the system.

(b). The second law and the balance of entropy

As discussed in our bulk analysis [Chapter III, §3 (b)], our irreversible thermodynamic formulation requires a local description of the second law of thermodynamics. To this end, we introduce the entropy per unit mass $\tilde{s} = s(\theta^{\alpha}, t)$, for which the entropy of the patch is given by $\int_{\mathcal{P}} \rho s \, \mathrm{d}a$. Moreover, we posit that the entropy of the patch can change in one of three ways, as described by de Groot and Mazur. [‡] First, entropy can flow in the plane of the membrane across the patch boundary—captured by the in-plane entropy flux $\boldsymbol{J}_{\mathrm{s}}(\theta^{\alpha}, t) = J^{\alpha}_{\mathrm{s}} \boldsymbol{a}_{\alpha}$. Second, entropy can be supplied to the membrane as a flux from the surrounding material. We accordingly define $\eta_{\mathrm{e}}(\theta^{\alpha}, t)$ to be the rate of external entropy supply per unit mass. Importantly, the first two mechanisms describe a flow of entropy that has already been created. The third mechanism, however, captures new entropy that is produced—for which we define $\eta_{\mathrm{i}}(\theta^{\alpha}, t)$ to be the rate of internal entropy production per unit mass. Given how entropy changes to the membrane are accounted for, the global form of the second law of thermodynamics is given by

$$\int_{\mathcal{P}} \rho \eta_{\mathrm{i}} \, \mathrm{d}a \;\geq\; 0 \;. \tag{103}$$

Since the membrane patch in Eq. (103) is arbitrary, application of the localization theorem (48) reveals

$$\rho \eta_{\mathrm{i}} \;\geq\; 0 \;. \tag{104}$$

Equation (104) is the local form of the second law of thermodynamics, with the equality holding only when all processes are reversible.

With the definitions for the in-plane entropy flux, rate of external entropy supply, and rate of internal entropy production, the global form of the balance of entropy is given by

$$\frac{\mathrm{d}}{\mathrm{d}t} \left(\int_{\mathcal{P}} \rho s \, \mathrm{d}a \right) \;=\; -\int_{\partial\mathcal{P}} \boldsymbol{J}_{\mathrm{s}} \cdot \boldsymbol{\nu} \, \mathrm{d}s \;+\; \int_{\mathcal{P}} \rho \eta_{\mathrm{e}} \, \mathrm{d}a \;+\; \int_{\mathcal{P}} \rho \eta_{\mathrm{i}} \, \mathrm{d}a \;, \tag{105}$$

[‡] S.R. de Groot and P. Mazur. *Non-Equilibrium Thermodynamics*. New York: Dover, 1984.

where by definition $\boldsymbol{J}_{\mathrm{s}} \cdot \boldsymbol{\nu} = J_{\mathrm{s}}^{\alpha} \nu_{\alpha}$ is positive when entropy flows out of the system. By applying Eq. (56) to the left-hand side of Eq. (105) and the surface divergence theorem (47) to the boundary term, we obtain

$$\int_{\mathcal{P}} \rho \dot{s} \, \mathrm{d}a \; = \; \int_{\mathcal{P}} \Big(- J^{\alpha}_{\mathrm{s};\alpha} \, + \, \rho \eta_{\mathrm{e}} \, + \, \rho \eta_{\mathrm{i}} \Big) \, \mathrm{d}a \; . \tag{106}$$

Again, owing to the arbitrariness of the membrane patch $\mathcal{P}$, application of the localization theorem (48) to Eq. (106) yields the local form of the balance of entropy, written as

$$\rho \dot{s} \; = \; - J^{\alpha}_{\mathrm{s};\alpha} \, + \, \rho \eta_{\mathrm{e}} \, + \, \rho \eta_{\mathrm{i}} \; . \tag{107}$$

(c). The choice of thermodynamic potential

The internal entropy production is central to our irreversible thermodynamic framework. Thus far, however, $\rho \eta_{\mathrm{i}}$ only appears in Eqs. (104) and (107). To obtain the form of the internal entropy production, we follow Mandadapu [‡] and recognize the natural thermodynamic potential describing the membrane patch is the Helmholtz free energy. Accordingly, we introduce the Helmholtz free energy per unit mass $\tilde{\psi} = \psi(\theta^{\alpha}, t)$, which satisfies

$$\psi \; = \; u \, - \, T s \; . \tag{108}$$

In Eq. (108), $\tilde{T} = T(\theta^{\alpha}, t)$ is the local temperature field of the membrane. By taking the material derivative of Eq. (108) and multiplying the result by the mass density ρ, we find

$$\rho \dot{\psi} \; = \; \rho \dot{u} \, - \, \rho \dot{T} s \, - \, \rho T \dot{s} \; . \tag{109}$$

Equation (109) relates the local forms of the balances of internal energy (102) and entropy (107) through the terms $\rho \dot{u}$ and $\rho \dot{s}$; combining the three equations leads to

$$\rho \dot{s} \; = \; - J^{\alpha}_{\mathrm{s};\alpha} \, + \, \rho \eta_{\mathrm{e}} \, + \, \rho \eta_{\mathrm{i}} \; = \; \frac{1}{T} \left(\rho r \, - \, J^{\alpha}_{\mathrm{q};\alpha} \, + \, \frac{1}{2} \sigma^{\alpha\beta} \dot{a}_{\alpha\beta} \, + \, M^{\alpha\beta} \dot{b}_{\alpha\beta} \, - \, \rho \dot{T} s \, - \, \rho \dot{\psi} \right) \; . \tag{110}$$

Equation (110) is important to our irreversible thermodynamic developments, as it relates thermodynamic quantities, the membrane stresses and couple-stresses, and heat flows. We now show how a choice of the fundamental thermodynamic variables for the Helmholtz free energy allows us to determine the in-plane entropy flux, rate of external entropy supply, and internal entropy production.

(d). The internal entropy production

Thus far, we considered only a general Helmholtz free energy density ψ. As a thermodynamic state function, ψ captures all reversible (or elastic) behavior. For the two-dimensional membrane under consideration, the fundamental thermodynamic variables are the metric

[‡] Mandadapu, "Homogeneous Non-Equilibrium Molecular Dynamics Methods for Calculating the Heat Transport Coefficient of Solids and Mixtures".

tensor $a_{\alpha\beta}$, the curvature tensor $b_{\alpha\beta}$, and the temperature T.[‡] The simplest form of the Helmholtz free energy density is written as

$$\psi \;=\; \psi(a_{\alpha\beta}, b_{\alpha\beta}, T)\;. \tag{111}$$

As the metric and curvature tensors are symmetric, the material time derivative of ψ is given by

$$\dot{\psi} \;=\; \frac{1}{2}\left(\frac{\partial\psi}{\partial a_{\alpha\beta}} + \frac{\partial\psi}{\partial a_{\beta\alpha}}\right)\dot{a}_{\alpha\beta} + \frac{1}{2}\left(\frac{\partial\psi}{\partial b_{\alpha\beta}} + \frac{\partial\psi}{\partial b_{\beta\alpha}}\right)\dot{b}_{\alpha\beta} + \frac{\partial\psi}{\partial T}\dot{T}\;. \tag{112}$$

By multiplying Eq. (112) by ρ, substituting the result into Eq. (110), and rearranging terms, we obtain

$$\begin{aligned}\rho\dot{s} \;&=\; -J^{\alpha}_{\mathrm{s};\alpha} + \rho\eta_{\mathrm{e}} + \rho\eta_{\mathrm{i}} \qquad (113)\\ &=\; \frac{1}{T}\left\{\rho r - J^{\alpha}_{\mathrm{q};\alpha} - \rho\dot{T}\left(s + \frac{\partial\psi}{\partial T}\right)\right.\\ &\qquad \left. + \frac{1}{2}\left[\sigma^{\alpha\beta} - \rho\left(\frac{\partial\psi}{\partial a_{\alpha\beta}} + \frac{\partial\psi}{\partial a_{\beta\alpha}}\right)\right]\dot{a}_{\alpha\beta} + \left[M^{\alpha\beta} - \frac{\rho}{2}\left(\frac{\partial\psi}{\partial b_{\alpha\beta}} + \frac{\partial\psi}{\partial b_{\beta\alpha}}\right)\right]\dot{b}_{\alpha\beta}\right\}.\end{aligned}$$

At this point, we make several simplifications. First, for notational convenience, we define

$$\pi^{\alpha\beta} \;:=\; \sigma^{\alpha\beta} - \rho\left(\frac{\partial\psi}{\partial a_{\alpha\beta}} + \frac{\partial\psi}{\partial a_{\beta\alpha}}\right) \tag{114}$$

and

$$\omega^{\alpha\beta} \;:=\; M^{\alpha\beta} - \frac{\rho}{2}\left(\frac{\partial\psi}{\partial b_{\alpha\beta}} + \frac{\partial\psi}{\partial b_{\beta\alpha}}\right)\;. \tag{115}$$

As we will see in §5 and §6, $\pi^{\alpha\beta}$ and $\omega^{\alpha\beta}$ capture irreversible stresses and couple-stresses, respectively, as the membrane deforms. Next, we recognize that while the entire membrane system is in general out of thermodynamic equilibrium, a continuum point $\boldsymbol{x}$ on the membrane surface captures many phospholipid molecules in its local neighborhood. Thus, assuming length and time scale separation between the microscopic and continuum dynamics, we posit that the usual thermodynamic relations hold locally in our continuum description.[†] Given this local equilibrium assumption, the entropy density can be obtained from the Helmholtz free energy density as

$$s \;=\; -\left(\frac{\partial\psi}{\partial T}\right)_{a_{\alpha\beta}, b_{\alpha\beta}}\;, \tag{116}$$

where the partial derivative is taken at constant $a_{\alpha\beta}$ and $b_{\alpha\beta}$. Our final simplification is to rewrite the heat flux term in Eq. (113) as

$$-\frac{J^{\alpha}_{\mathrm{q};\alpha}}{T} \;=\; -\left(\frac{J^{\alpha}_{\mathrm{q}}}{T}\right)_{;\alpha} - \frac{J^{\alpha}_{\mathrm{q}}\,T_{,\alpha}}{T^2}\;. \tag{117}$$

[‡]D.J. Steigmann. "Fluid films with curvature elasticity". *Arch. Ration. Mech. Anal.* **150** (1999), 127–152.

[†]de Groot and Mazur, *Non-Equilibrium Thermodynamics*.

By substituting Eqs. (114)–(117) into Eq. (113), we obtain

$$\begin{aligned}\rho\dot{s} &= -J^{\alpha}_{\mathrm{s};\alpha} + \rho\eta_{\mathrm{e}} + \rho\eta_{\mathrm{i}} \\ &= -\left(\frac{J^{\alpha}_{\mathrm{q}}}{T}\right)_{;\alpha} + \frac{\rho r}{T} - \frac{J^{\alpha}_{\mathrm{q}}\,T_{,\alpha}}{T^2} + \frac{1}{T}\left\{\frac{1}{2}\,\pi^{\alpha\beta}\,\dot{a}_{\alpha\beta} + \omega^{\alpha\beta}\,\dot{b}_{\alpha\beta}\right\}.\end{aligned} \tag{118}$$

Equation (118) arose from our choice of the fundamental thermodynamic variables (111) and the local equilibrium assumption (116), and is used to determine the in-plane entropy flux, rate of external entropy supply, and rate of internal entropy production. From dimensional arguments, equating the surface divergence terms in the first and second lines of Eq. (118) reveals

$$J^{\alpha}_{\mathrm{s}} = \frac{J^{\alpha}_{\mathrm{q}}}{T}\,, \qquad \text{or equivalently} \qquad \boldsymbol{J}_{\mathrm{s}} = \frac{\boldsymbol{J}_{\mathrm{q}}}{T}\,. \tag{119}$$

Next, the rate of external entropy supply $\rho\eta_{\mathrm{e}}$ captures entropy being absorbed or emitted from the surrounding material. The only term on the second line of Eq. (118) describing such a change involves the heat supply r, for which

$$\rho\eta_{\mathrm{e}} = \frac{\rho r}{T}\,. \tag{120}$$

Equations (119) and (120) capture a familiar result: heat flow into or out of the system is accompanied by an entropy change. The remaining terms on the second line of Eq. (118) all contribute to the internal entropy production, written as

$$\rho\eta_{\mathrm{i}} = -\frac{J^{\alpha}_{\mathrm{q}}\,T_{,\alpha}}{T^2} + \frac{1}{T}\left\{\frac{1}{2}\,\pi^{\alpha\beta}\,\dot{a}_{\alpha\beta} + \omega^{\alpha\beta}\,\dot{b}_{\alpha\beta}\right\} \geq 0\,. \tag{121}$$

The inequality in Eq. (121) arises from the local form of the second law of thermodynamics (104). Now that we have obtained the internal entropy production (121), irreversible thermodynamics provides a framework to determine $\pi^{\alpha\beta}$ and $\omega^{\alpha\beta}$, from which $\sigma^{\alpha\beta}$ and $M^{\alpha\beta}$ are calculated [see Eqs. (114) and (115)] and the dynamical membrane equations are fully specified. In the following sections, we systematically consider three situations of increasing complexity: (*i*) a compressible, inviscid membrane in §4, (*ii*) a compressible, viscous membrane in §5, and (*iii*) an incompressible, viscous membrane in §6. In all cases, the membrane is assumed to bend elastically out-of-plane.

4. The case of a compressible, inviscid membrane

In this section, we consider an inviscid lipid membrane, in which membrane deformations are reversible and do not produce any entropy. Such a situation is not biologically relevant, as lipids flow in-plane as a two-dimensional viscous fluid. However, our analysis highlights several important features that will be useful in subsequent sections. In the limiting case of no dissipation in the system, we begin by obtaining the membrane stresses and couple-stresses. Next, we present the Gibbs equation, which relates infinitesimal changes in thermodynamic state functions of the membrane. We then demonstrate how the functional form of the

Helmholtz free energy ψ is restricted by the requirements of Galilean invariance and material symmetries. When changing to the restricted set of thermodynamic variables, the membrane stresses and couple-stresses obtain a new form. We close by substituting the stresses and couple-stresses into the equations of motion, and specializing our results to a particular, well-known choice of the Helmholtz free energy: the Helfrich free energy.

(a). The Gibbs equation

When membrane deformations are reversible, the form of the internal entropy production (121) requires $\pi^{\alpha\beta} = 0$ and $\omega^{\alpha\beta} = 0$.[‡] From Eqs. (114) and (115), we find

$$\sigma_{\text{el}}^{\alpha\beta} = \rho\left(\frac{\partial\psi}{\partial a_{\alpha\beta}} + \frac{\partial\psi}{\partial a_{\beta\alpha}}\right) \qquad \text{and} \qquad M_{\text{el}}^{\alpha\beta} = \frac{\rho}{2}\left(\frac{\partial\psi}{\partial b_{\alpha\beta}} + \frac{\partial\psi}{\partial b_{\beta\alpha}}\right), \tag{122}$$

where the subscript 'el' indicates that only the elastic membrane behavior is captured. At this stage, we derive the Gibbs equation for a single-component membrane system. By multiplying Eq. (112) by the mass density ρ and substituting Eqs. (116) and (122), we obtain

$$\rho\dot{\psi} = \frac{1}{2}\,\sigma_{\text{el}}^{\alpha\beta}\,\dot{a}_{\alpha\beta} + M_{\text{el}}^{\alpha\beta}\,\dot{b}_{\alpha\beta} - \rho\dot{T}s\,. \tag{123}$$

Next, by substituting Eq. (123) into Eq. (109) and rearranging terms, we obtain

$$\rho T\dot{s} = \rho\dot{u} - \frac{1}{2}\,\sigma_{\text{el}}^{\alpha\beta}\,\dot{a}_{\alpha\beta} - M_{\text{el}}^{\alpha\beta}\,\dot{b}_{\alpha\beta}\,. \tag{124}$$

Finally, by considering the changes to the thermodynamic quantities in Eq. (124) over a time interval $\mathrm{d}t$, we obtain the Gibbs equation for a two-dimensional single-component lipid membrane—given by

$$\rho T\,\mathrm{d}s = \rho\,\mathrm{d}u - \frac{1}{2}\,\sigma_{\text{el}}^{\alpha\beta}\,\mathrm{d}a_{\alpha\beta} - M_{\text{el}}^{\alpha\beta}\,\mathrm{d}b_{\alpha\beta}\,. \tag{125}$$

Equation (125) is the Gibbs equation for a two-dimensional membrane surface with out-of-plane elastic bending and in-plane elastic compression and stretching.

We wish to highlight here that, in general, it is technically difficult to write the Gibbs equation for a system whose energetics depend on tensorial quantities. For this reason, we began by choosing an appropriate form of the Helmholtz free energy, and naturally obtained the Gibbs equation after the internal entropy production was determined. Our sequence of developments thus contains an important difference from that of de Groot and Mazur,[†] who instead *begin* with the local equilibrium assumption and Gibbs equation—from which they arrive at the internal entropy production.

(b). The change of thermodynamic variables

We have so far developed general equations of how the elastic membrane stresses and couple-stresses depend on the Helmholtz free energy density ψ [see Eq. (122)], which in turn depends

[‡]This requirement will be shown explicitly in the following section.

[†]de Groot and Mazur, *Non-Equilibrium Thermodynamics*.

on the metric tensor $a_{\alpha\beta}$, the curvature tensor $b_{\alpha\beta}$, and the temperature T (111). However, as the Helmholtz free energy ψ is an absolute scalar field, it must be invariant to Galilean transformations. For materials with in-plane fluidity, Steigmann [‡] showed Galilean invariance requires ψ to depend on the surface configuration only through the areal mass density ρ and the invariants of the curvature tensor $\boldsymbol{b} = b_{\alpha\beta}\boldsymbol{a}^{\alpha} \otimes \boldsymbol{a}^{\beta}$—which are the mean curvature $H = \frac{1}{2}\mathrm{tr}(\boldsymbol{b})$ and Gaussian curvature $K = \det(\boldsymbol{b})$ [see Chapter II, §2 (e)]. Accordingly, the Helmholtz free energy density can be written as

$$\psi(a_{\alpha\beta}, b_{\alpha\beta}, T) \;=\; \bar{\psi}(\rho, H, K, T) \;. \tag{126}$$

We note that Eq. (126) can also be shown using material symmetry arguments. [†]

Our task now is to express $\sigma_{\mathrm{el}}^{\alpha\beta}$ and $M_{\mathrm{el}}^{\alpha\beta}$ (122) in terms of $\bar{\psi}$ rather than ψ. To this end, we recognize that when substituting Eq. (126) into Eq. (122) and applying the chain rule, we encounter the terms

$$\frac{\partial\bar{\psi}}{\partial a_{\alpha\beta}} \;=\; \frac{\partial\bar{\psi}}{\partial\rho}\frac{\partial\rho}{\partial a_{\alpha\beta}} + \frac{\partial\bar{\psi}}{\partial H}\frac{\partial H}{\partial a_{\alpha\beta}} + \frac{\partial\bar{\psi}}{\partial K}\frac{\partial K}{\partial a_{\alpha\beta}} \tag{127}$$

and

$$\frac{\partial\bar{\psi}}{\partial b_{\alpha\beta}} \;=\; \frac{\partial\bar{\psi}}{\partial\rho}\frac{\partial\rho}{\partial b_{\alpha\beta}} + \frac{\partial\bar{\psi}}{\partial H}\frac{\partial H}{\partial b_{\alpha\beta}} + \frac{\partial\bar{\psi}}{\partial K}\frac{\partial K}{\partial b_{\alpha\beta}} \;, \tag{128}$$

as well as their transposes. In what follows, we calculate the partial derivatives of ρ, H, and K with respect to $a_{\alpha\beta}$ and $b_{\alpha\beta}$. Our results are summarized in Table 1.

Useful relations

We begin by calculating the partial derivatives of various quantities with respect to one another, which will be useful both here and in later developments. First, as $a_{\alpha\beta}$ and $b_{\alpha\beta}$ are symmetric, we have

$$\frac{\partial a_{\mu\nu}}{\partial a_{\alpha\beta}} \;=\; \frac{\partial b_{\mu\nu}}{\partial b_{\alpha\beta}} \;=\; \frac{1}{2}\left(\delta_{\mu}^{\alpha}\delta_{\nu}^{\beta} \,+\, \delta_{\nu}^{\alpha}\delta_{\mu}^{\beta}\right) \;. \tag{129}$$

Next, as the quantities $a_{\alpha\beta}$ and $b_{\alpha\beta}$ are independent,

$$\frac{\partial a_{\mu\nu}}{\partial b_{\alpha\beta}} \;=\; 0 \qquad \text{and} \qquad \frac{\partial b_{\mu\nu}}{\partial a_{\alpha\beta}} \;=\; 0 \;. \tag{130}$$

To calculate the partial derivative of the contravariant metric tensor with respect to the covariant metric tensor, we recognize $a^{\mu\nu} = a_{\gamma\lambda}\,a^{\mu\gamma}\,a^{\nu\lambda}$, such that

$$\frac{\partial a^{\mu\nu}}{\partial a_{\alpha\beta}} \;=\; \frac{\partial}{\partial a_{\alpha\beta}}\left(a_{\gamma\lambda}\,a^{\mu\gamma}\,a^{\nu\lambda}\right) \;=\; \frac{\partial a_{\gamma\lambda}}{\partial a_{\alpha\beta}}\,a^{\mu\gamma}\,a^{\nu\lambda} \;+\; \frac{\partial a^{\mu\gamma}}{\partial a_{\alpha\beta}}\underbrace{a_{\gamma\lambda}\,a^{\nu\lambda}}_{=\delta_{\gamma}^{\nu}} + \frac{\partial a^{\nu\lambda}}{\partial a_{\alpha\beta}}\underbrace{a_{\gamma\lambda}\,a^{\mu\gamma}}_{=\delta_{\lambda}^{\mu}} \;. \tag{131}$$

[‡]Steigmann, "Fluid films with curvature elasticity".

[†]J.T. Jenkins. "The equations of mechanical equilibrium of a model membrane". *SIAM J. Appl. Math.* **32** (1977), 755–764.

Table 1: Partial derivatives of the areal mass density ρ, mean curvature H, and Gaussian curvature K with respect to the metric tensor $a_{\alpha\beta}$ and curvature tensor $b_{\alpha\beta}$.

$\dfrac{\partial \rho}{\partial a_{\alpha\beta}} = -\dfrac{1}{2}\,\rho\, a^{\alpha\beta}$	$\dfrac{\partial H}{\partial a_{\alpha\beta}} = -\dfrac{1}{2}\, b^{\alpha\beta}$	$\dfrac{\partial K}{\partial a_{\alpha\beta}} = -K\, a^{\alpha\beta}$
$\dfrac{\partial \rho}{\partial b_{\alpha\beta}} = 0$	$\dfrac{\partial H}{\partial b_{\alpha\beta}} = \dfrac{1}{2}\, a^{\alpha\beta}$	$\dfrac{\partial K}{\partial b_{\alpha\beta}} = \bar{b}^{\alpha\beta}$

By recognizing the right-most term in Eq. (131) is $\partial a^{\mu\nu}/\partial a_{\alpha\beta}$, which is also the left-most term, and substituting Eq. (129), we obtain

$$\frac{\partial a^{\mu\nu}}{\partial a_{\alpha\beta}} = -\frac{1}{2}\left(a^{\mu\alpha}a^{\nu\beta} + a^{\mu\beta}a^{\nu\alpha}\right) . \tag{132}$$

Our next two results rely on the relation $b^{\mu\nu} = b_{\gamma\lambda}a^{\mu\gamma}a^{\nu\lambda}$. First, we calculate the partial derivative with respect to $b_{\alpha\beta}$:

$$\frac{\partial b^{\mu\nu}}{\partial b_{\alpha\beta}} = \frac{\partial}{\partial b_{\alpha\beta}}\left(b_{\gamma\lambda}\, a^{\mu\gamma}\, a^{\nu\lambda}\right) = \frac{\partial b_{\gamma\lambda}}{\partial b_{\alpha\beta}}\, a^{\mu\gamma}\, a^{\nu\lambda} = \frac{1}{2}\left(a^{\mu\alpha}a^{\nu\beta} + a^{\mu\beta}a^{\nu\alpha}\right) . \tag{133}$$

In the third equality in Eq. (133), we substituted Eq. (129); note also that $\partial a^{\mu\nu}/\partial a_{\alpha\beta} = -\partial b^{\mu\nu}/\partial b_{\alpha\beta}$. Second, we find

$$\begin{aligned}
\frac{\partial b^{\mu\nu}}{\partial a_{\alpha\beta}} &= \frac{\partial}{\partial a_{\alpha\beta}}\left(b_{\gamma\lambda}\, a^{\mu\gamma}\, a^{\nu\lambda}\right) = \frac{\partial a^{\mu\gamma}}{\partial a_{\alpha\beta}}\overbrace{b_{\gamma\lambda}\, a^{\nu\lambda}}^{=b^{\nu}_{\gamma}} + \frac{\partial a^{\nu\lambda}}{\partial a_{\alpha\beta}}\overbrace{b_{\gamma\lambda}\, a^{\mu\gamma}}^{=b^{\mu}_{\lambda}} \\
&= -\frac{1}{2}\left(v^{\nu}_{\gamma}\left(a^{\mu\alpha}a^{\gamma\beta} + a^{\mu\beta}a^{\gamma\alpha}\right) + b^{\mu}_{\lambda}\left(a^{\nu\alpha}a^{\lambda\beta} + a^{\nu\beta}a^{\lambda\alpha}\right)\right) \\
&= -\frac{1}{2}\left(b^{\nu\beta}a^{\mu\alpha} + b^{\nu\alpha}a^{\mu\beta} + b^{\mu\beta}a^{\nu\alpha} + v^{\mu\alpha}a^{\nu\beta}\right) .
\end{aligned} \tag{134}$$

Finally, we calculate the partial derivatives of the determinant of the metric tensor. Recalling that $\det(a_{\alpha\beta}) = a_{11}a_{22} - a_{12}a_{21}$, we immediately note Eq. (130) implies

$$\frac{\partial \det(a_{\mu\nu})}{\partial b_{\alpha\beta}} = 0 . \tag{135}$$

At this point, we recognize that from the properties of symmetric 2×2 matrices,

$$a_{22} = \det(a_{\mu\nu})\, a^{11} , \qquad a_{11} = \det(a_{\mu\nu})\, a^{22} , \qquad \text{and} \qquad a_{12} = a_{21} = -\det(a_{\mu\nu})\, a^{12} . \tag{136}$$

With Eqs. (129), (136), and the expression for the determinant, we calculate

$$\begin{aligned}\frac{\partial \det(a_{\mu\nu})}{\partial a_{\alpha\beta}} &= \frac{\partial}{\partial a_{\alpha\beta}}\Big(a_{11}a_{22} - (a_{12})^2\Big) = a_{22}\frac{\partial a_{11}}{\partial a_{\alpha\beta}} + a_{11}\frac{\partial a_{22}}{\partial a_{\alpha\beta}} - 2a_{12}\frac{\partial a_{12}}{\partial a_{\alpha\beta}} \\ &= \det(a_{\mu\nu})\Big(\delta_1^\alpha\,\delta_1^\beta\,a^{11} + \delta_2^\alpha\,\delta_2^\beta\,a^{22} + \delta_1^\alpha\,\delta_2^\beta\,a^{12} + \delta_2^\alpha\,\delta_1^\beta\,a^{21}\Big) \\ &= a^{\alpha\beta}\det(a_{\mu\nu})\ .\end{aligned} \tag{137}$$

As it turns out, we do not explicitly require the partial derivatives of the determinant of the curvature tensor in our calculations.

Partial derivatives of the density

According to Eqs. (6) and (55), the areal mass density ρ can be expressed in terms of the determinant of the metric tensor as

$$\rho = \rho_0\left(\det A_{\alpha\beta}\right)^{1/2}\left(\det a_{\alpha\beta}\right)^{-1/2}\ , \tag{138}$$

where ρ_0 and $A_{\alpha\beta}$ do not vary as the membrane deforms. We thus calculate

$$\begin{aligned}\frac{\partial\rho}{\partial a_{\alpha\beta}} &= -\frac{1}{2}\rho_0\left(\det A_{\mu\nu}\right)^{1/2}\left(\det a_{\mu\nu}\right)^{-3/2}\frac{\partial\det(a_{\mu\nu})}{\partial a_{\alpha\beta}} \\ &= -\frac{1}{2}\underbrace{\rho_0\left(\det A_{\mu\nu}\right)^{1/2}\left(\det a_{\mu\nu}\right)^{-1/2}}_{=\rho}a^{\alpha\beta} \\ &= -\frac{1}{2}\rho\,a^{\alpha\beta}\ .\end{aligned} \tag{139}$$

In the first equality of Eq. (139) we applied the chain rule, in the second equality we substituted Eq. (137), and in the third equality we recognized the form of ρ (138). Additionally, with Eq. (135), we find

$$\frac{\partial\rho}{\partial b_{\alpha\beta}} = 0\ . \tag{140}$$

Equations (139) and (140) constitute the left column of Table 1.

Partial derivatives of the mean curvature

We next consider the mean curvature H, which is conveniently expressed as $H = \frac{1}{2}a^{\alpha\beta}b_{\alpha\beta}$ [Chapter II, Eq. (41)]. With Eqs. (132) and (133), as well as the symmetry of the metric and curvature tensors, we calculate

$$\frac{\partial H}{\partial a_{\alpha\beta}} = \frac{1}{2}\frac{\partial a^{\mu\nu}}{\partial a_{\alpha\beta}} = -\frac{1}{4}\Big(a^{\mu\alpha}a^{\nu\beta} + a^{\mu\beta}a^{\nu\alpha}\Big)b_{\mu\nu} = -\frac{1}{2}b^{\alpha\beta} \tag{141}$$

and

$$\frac{\partial H}{\partial b_{\alpha\beta}} = \frac{1}{2}a^{\mu\nu}\frac{\partial b_{\mu\nu}}{\partial b_{\alpha\beta}} = \frac{1}{4}a^{\mu\nu}\Big(\delta_\mu^\alpha\,\delta_\nu^\beta + \delta_\nu^\alpha\,\delta_\mu^\beta\Big) = \frac{1}{2}a^{\alpha\beta}\ . \tag{142}$$

Equations (141) and (142) are given in the middle column of Table 1.

Partial derivatives of the Gaussian curvature

In Eq. (42) of Chapter II, we presented two equivalent expressions for the Gaussian curvature: $K = \frac{1}{2}\varepsilon^{\alpha\beta}\varepsilon^{\mu\nu}b_{\alpha\mu}b_{\beta\nu} = \det(b_{\alpha\beta})/\det(a_{\alpha\beta})$, where $\varepsilon^{\alpha\beta}$ is the Levi–Civita tensor. We use both expressions to calculate the partial derivatives of the Gaussian curvature. First, we find

$$\frac{\partial K}{\partial a_{\alpha\beta}} = \frac{\partial}{\partial a_{\alpha\beta}}\left(\frac{\det(b_{\mu\nu})}{\det(a_{\mu\nu})}\right) = -\frac{\det(b_{\mu\nu})}{[\det(a_{\mu\nu})]^2}\frac{\partial \det(a_{\mu\nu})}{\partial a_{\alpha\beta}} = -\frac{\det(b_{\mu\nu})}{\det(a_{\mu\nu})}a^{\alpha\beta} = -K\,a^{\alpha\beta}\,, \tag{143}$$

where in the second equality we used the chain rule, and in the third equality we substituted Eq. (137). Next, we calculate

$$\begin{aligned}\frac{\partial K}{\partial b_{\alpha\beta}} &= \frac{\partial}{\partial b_{\alpha\beta}}\left(\frac{1}{2}\,\varepsilon^{\gamma\lambda}\,\varepsilon^{\mu\nu}\,b_{\gamma\mu}\,b_{\lambda\nu}\right) = \frac{1}{2}\,\varepsilon^{\gamma\lambda}\,\varepsilon^{\mu\nu}\left(\frac{\partial b_{\gamma\mu}}{\partial b_{\alpha\beta}}\,b_{\lambda\nu} + \frac{\partial b_{\lambda\nu}}{\partial b_{\alpha\beta}}\,b_{\gamma\mu}\right)\\ &= \frac{1}{4}\,\varepsilon^{\gamma\lambda}\,\varepsilon^{\mu\nu}\left(b_{\lambda\nu}\left(\delta^{\alpha}_{\gamma}\,\delta^{\beta}_{\mu} + \delta^{\alpha}_{\mu}\,\delta^{\beta}_{\gamma}\right) + b_{\gamma\mu}\left(\delta^{\alpha}_{\lambda}\,\delta^{\beta}_{\nu} + \delta^{\alpha}_{\nu}\,\delta^{\beta}_{\lambda}\right)\right)\\ &= \frac{1}{4}\left(\varepsilon^{\alpha\lambda}\,\varepsilon^{\beta\nu}\,b_{\lambda\nu} + \varepsilon^{\beta\lambda}\,\varepsilon^{\alpha\nu}\,b_{\lambda\nu} + \varepsilon^{\gamma\alpha}\,\varepsilon^{\mu\beta}\,b_{\gamma\mu} + \varepsilon^{\gamma\beta}\,\varepsilon^{\mu\alpha}\,b_{\gamma\mu}\right)\\ &= \varepsilon^{\alpha\lambda}\,\varepsilon^{\beta\nu}\,b_{\lambda\nu} = \bar{b}^{\alpha\beta}\,.\end{aligned} \tag{144}$$

In Eq. (144), we used the product rule in the first line, substituted Eq. (129) in the second line, expanded terms in the third line, and simplified terms in the fourth line. In the last line of Eq. (144), we substituted the form of the cofactor of curvature provided in Eq. (43) of Chapter II. Equations (143) and (144) are presented in the right column of Table 1.

Modified form of the stresses and couple-stresses

With the results of our partial derivative calculations presented in Table 1, we express the tensors $\sigma^{\alpha\beta}_{\text{el}}$ and $M^{\alpha\beta}_{\text{el}}$ in terms of the energy density $\bar{\psi}$. To this end, Eqs. (127) and (128) are rewritten as

$$\begin{aligned}\frac{\partial\bar{\psi}}{\partial a_{\alpha\beta}} &= -\frac{1}{2}\,\rho\,a^{\alpha\beta}\,\frac{\partial\bar{\psi}}{\partial\rho} - \frac{1}{2}\,b^{\alpha\beta}\,\frac{\partial\bar{\psi}}{\partial H} - K a^{\alpha\beta}\,\frac{\partial\bar{\psi}}{\partial K}\\ &= a^{\alpha\beta}\left(-\frac{\rho}{2}\,\frac{\partial\bar{\psi}}{\partial\rho} - H\,\frac{\partial\bar{\psi}}{\partial H} - K\,\frac{\partial\bar{\psi}}{\partial K}\right) + \frac{1}{2}\,\bar{b}^{\alpha\beta}\,\frac{\partial\bar{\psi}}{\partial H}\end{aligned} \tag{145}$$

and

$$\frac{\partial\bar{\psi}}{\partial b_{\alpha\beta}} = \frac{1}{2}\,a^{\alpha\beta}\,\frac{\partial\bar{\psi}}{\partial H} + \bar{b}^{\alpha\beta}\,\frac{\partial\bar{\psi}}{\partial K}\,. \tag{146}$$

In Eqs. (145) and (146), we choose to include only the contravariant metric tensor $a^{\alpha\beta}$ and cofactor of curvature $\bar{b}^{\alpha\beta}$, as doing so simplifies our later calculations. Substituting Eqs. (145) and (146) into Eq. (122) yields

$$\sigma^{\alpha\beta}_{\text{el}} = -\rho\,a^{\alpha\beta}\left(\rho\,\frac{\partial\bar{\psi}}{\partial\rho} + 2H\,\frac{\partial\bar{\psi}}{\partial H} + 2K\,\frac{\partial\bar{\psi}}{\partial K}\right) + \rho\,\bar{b}^{\alpha\beta}\,\frac{\partial\bar{\psi}}{\partial H} \tag{147}$$

Table 2: Elastic stresses and couple-stresses in a single-component lipid membrane with Helmholtz free energy density of the general form in Eq. (126). This table is provided for visual convenience: the same results are provided in Eqs. (147)–(150).

$\sigma_{\rm el}^{\alpha\beta} = -\rho\, a^{\alpha\beta}\left(\rho\dfrac{\partial\bar{\psi}}{\partial\rho} + 2H\dfrac{\partial\bar{\psi}}{\partial H} + 2K\dfrac{\partial\bar{\psi}}{\partial K}\right) + \rho\,\bar{b}^{\alpha\beta}\dfrac{\partial\bar{\psi}}{\partial H}$
$M_{\rm el}^{\alpha\beta} = \dfrac{\rho}{2}\,a^{\alpha\beta}\dfrac{\partial\bar{\psi}}{\partial H} + \rho\,\bar{b}^{\alpha\beta}\dfrac{\partial\bar{\psi}}{\partial K}$
$N_{\rm el}^{\alpha\beta} = -\rho\, a^{\alpha\beta}\left(\rho\dfrac{\partial\bar{\psi}}{\partial\rho} + H\dfrac{\partial\bar{\psi}}{\partial H} + K\dfrac{\partial\bar{\psi}}{\partial K}\right) + \dfrac{\rho}{2}\,\bar{b}^{\alpha\beta}\dfrac{\partial\bar{\psi}}{\partial H}$
$S_{\rm el}^{\alpha} = -a^{\alpha\beta}\left(\dfrac{\rho}{2}\dfrac{\partial\bar{\psi}}{\partial H}\right)_{;\beta} - \bar{b}^{\alpha\beta}\left(\rho\dfrac{\partial\bar{\psi}}{\partial K}\right)_{;\beta}$

and

$$M_{\rm el}^{\alpha\beta} = \frac{\rho}{2}\,a^{\alpha\beta}\frac{\partial\bar{\psi}}{\partial H} + \rho\,\bar{b}^{\alpha\beta}\frac{\partial\bar{\psi}}{\partial K}\,. \tag{148}$$

At this point, we also calculate the elastic in-plane stresses $N_{\rm el}^{\alpha\beta}$ and out-of-plane shears $S_{\rm el}^{\alpha}$, which enter the equations of motion. By substituting Eqs. (147) and (148) into Eq. (80), rearranging terms, and applying the relations $\bar{b}^{\alpha\beta} = 2H\,a^{\alpha\beta} - b^{\alpha\beta}$ and $b_{\mu}^{\beta}\,\bar{b}^{\mu\alpha} = K\,a^{\alpha\beta}$ from Chapter II, §2 (e), we obtain

$$N_{\rm el}^{\alpha\beta} = -\rho\, a^{\alpha\beta}\left(\rho\frac{\partial\bar{\psi}}{\partial\rho} + H\frac{\partial\bar{\psi}}{\partial H} + K\frac{\partial\bar{\psi}}{\partial K}\right) + \frac{\rho}{2}\,\bar{b}^{\alpha\beta}\frac{\partial\bar{\psi}}{\partial H}\,. \tag{149}$$

Finally, by substituting Eq. (148) into Eq. (81) and recognizing $a_{;\alpha}^{\alpha\beta} = 0$ and $\bar{b}_{;\alpha}^{\alpha\beta} = 0$, we calculate the elastic out-of-plane shear stresses to be given by

$$S_{\rm el}^{\alpha} = -a^{\alpha\beta}\left(\frac{\rho}{2}\frac{\partial\bar{\psi}}{\partial H}\right)_{;\beta} - \bar{b}^{\alpha\beta}\left(\rho\frac{\partial\bar{\psi}}{\partial K}\right)_{;\beta}\,. \tag{150}$$

Equations (147)–(150) are collected in Table 2 for visual convenience, and capture the elastic stresses and couple-stresses in a single-component lipid membrane. We note that Eqs. (147)–(150) are identical to the results of a prior study using variational methods; [‡] the two techniques agree as there is no dissipation in the system.

[‡]Steigmann, "Fluid films with curvature elasticity".

(c). The equations of motion

With the results presented in Table 2, we have completely determined the thermodynamically consistent elastic stresses and couple-stresses in a single-component lipid membrane. To obtain the equations of motion, we simply substitute the results of Table 2 into Eqs. (66) and (67). We note, however, that there are four fundamental unknowns describing the behavior of a compressible lipid membrane: the three components of the velocity $\boldsymbol{v}$, as well as the mass density ρ. As such, the compressible continuity equation (51) is required to close the problem; we refer to these four equations as the governing equations. After much algebra, we find the governing equations to be given by [‡]

$$\rho_{,t} + v^\alpha \rho_{,\alpha} + \rho\big(v^\alpha_{;\alpha} - 2vH\big) = 0 \,, \tag{151}$$

$$\rho\Big(v^\alpha_{,t} + v^\beta v^\alpha_{;\beta} - 2vv^\beta b^\alpha_\beta - v v_{,\beta} a^{\alpha\beta}\Big) = f^\alpha - \rho\, a^{\alpha\beta}\left(\bar{\psi} + \rho\frac{\partial\bar{\psi}}{\partial\rho}\right)_{,\beta} \,, \tag{152}$$

and

$$\begin{aligned}&\rho\Big(v_{,t} + 2v^\alpha v_{,\alpha} + v^\alpha v^\beta b_{\alpha\beta}\Big) \\ &= f - \rho\Big(2H^2 - K\Big)\frac{\partial\bar{\psi}}{\partial H} - 2\rho H\left(\rho\frac{\partial\bar{\psi}}{\partial\rho} + K\frac{\partial\bar{\psi}}{\partial K}\right) - \Delta_{\mathrm{s}}\left(\frac{\rho}{2}\frac{\partial\bar{\psi}}{\partial H}\right) - \bar{b}^{\alpha\beta}\left(\rho\frac{\partial\bar{\psi}}{\partial K}\right)_{;\beta\alpha} \,,\end{aligned} \tag{153}$$

where the surface Laplacian operator Δ_{s} is defined in Eq. (30) of Chapter II. In Eqs. (151)–(153), we expanded the material time derivative of the density and substituted the components of the acceleration from Eqs. (42) and (43). In doing so, we highlight that ρ and $\boldsymbol{v}$ are the fundamental unknowns. Note the membrane position $\boldsymbol{x}$ can be calculated from the *initial position* $\boldsymbol{x}_0(\theta^\alpha) := \boldsymbol{x}(\theta^\alpha, t = t_0)$ at a known time t_0 by recognizing $\boldsymbol{x}_{,t} = v\boldsymbol{n}$, for which

$$\boldsymbol{x}(\theta^\alpha, t) = \boldsymbol{x}_0(\theta^\alpha) + \int_{t_0}^{t} v(\theta^\alpha, t)\, \boldsymbol{n}(\theta^\alpha, t)\, \mathrm{d}t \,. \tag{154}$$

Accordingly, all geometric quantities can be calculated with knowledge of the initial position and the membrane velocity over time.

Equations (151)–(153) describe an elastic lipid membrane with no in-plane viscosity. As such a system is unphysical, we delay our discussion of appropriate boundary conditions until our analysis of a membrane with in-plane viscosity in §5. Instead, in what follows, we specialize the governing equations to a specific, well-known choice of the Helmholtz free energy.

(d). The Helfrich free energy

Our analysis thus far assumed a general form of the Helmholtz free energy per unit mass, as a function of the areal mass density ρ, mean curvature H, Gaussian curvature K, and

[‡]Equations (152) and (153), in the absence of inertial forces, are presented by Steigmann, "Fluid films with curvature elasticity".

temperature T. To predict the geometry and dynamics of lipid membranes, however, a specific form of the free energy must be chosen. We apply simple energetic arguments to arrive at an expression for the free energy, which is similar to the celebrated results of Canham [‡] and Helfrich [†] (see Chapter IV, §3 (a) for historical notes). We then calculate the membrane stresses and couple-stresses, and obtain the governing equations.

To begin, it is convenient to consider the entire Helmholtz free energy of the patch, as well as the free energy per unit area—respectively denoted W and w. Given that $\bar{\psi}$ is the Helmholtz free energy per unit mass, W, w, and $\bar{\psi}$ are related by

$$w = \rho\bar{\psi} \qquad \text{and} \qquad W = \int_{\mathcal{P}} w \, \mathrm{d}a = \int_{\mathcal{P}} \rho\bar{\psi} \, \mathrm{d}a \, . \tag{155}$$

Next, we consider the energetic contributions from two categories of deformations: (i) membrane bending, which leads to changes in curvatures, and (ii) membrane stretching and compressing, which changes the areal mass density. The total free energy can then be decomposed as

$$W = W_{\mathrm{H}} + W_{\mathrm{c}} \, , \qquad \text{with} \qquad W_{\mathrm{H}} = \int_{\mathcal{P}} w_{\mathrm{H}} \, \mathrm{d}a \qquad \text{and} \qquad W_{\mathrm{c}} = \int_{\mathcal{P}} w_{\mathrm{c}} \, \mathrm{d}a \, . \tag{156}$$

In Eq. (156), the subscript 'H' refers to the Helfrich free energy, given by [*]

$$w_{\mathrm{H}} = k_{\mathrm{b}} H^2 + k_{\mathrm{g}} K \, , \tag{157}$$

where k_{b} is the mean bending modulus and k_{g} is the Gaussian bending modulus. We note that Eq. (157) can be understood as an expansion of the free energy to lowest order in the membrane curvature, [§] with both mean and Gaussian curvatures being penalized. The subscript 'c' in Eq. (157) refers to compression (or stretching) of the membrane relative to some reference configuration. To energetically penalize dilation or compression with respect to the reference configuration, we posit a total energy cost of the form

$$W_{\mathrm{c}} = \int_{\mathcal{P}_0} \frac{1}{2} k_{\mathrm{c}} \left(\hat{J} - 1\right)^2 \mathrm{d}A \, , \tag{158}$$

where k_{c} is the compressibility modulus and $J = \rho_0/\rho$ measures the change in area relative to the reference configuration. By recalling $W_{\mathrm{c}} = \int_{\mathcal{P}} w_{\mathrm{c}} \, \mathrm{d}a = \int_{\mathcal{P}_0} \hat{w}_{\mathrm{c}} \hat{J} \, \mathrm{d}A$, we express w_{c} as

$$w_{\mathrm{c}} = \frac{1}{2} \frac{k_{\mathrm{c}}}{J} \left(J - 1\right)^2 \, . \tag{159}$$

[‡] P.B. Canham. "The minimum energy of bending as a possible explanation of the biconcave shape of the human red blood cell". *J. Theor. Biol.* **26** (1970), 61–81.

[†] W. Helfrich. "Elastic properties of lipid bilayers: Theory and possible experiments". *Z. Naturforsch. C* **28** (1973), 693–699.

[*] Here, we assume the monolayer leaflets are symmetric, such that there is no spontaneous curvature (as considered by Helfrich).

[§] R. Capovilla, J. Guven, and J.A. Santiago. "Deformations of the geometry of lipid vesicles". *J. Phys. A: Math. Gen.* **36** (2003), 6281–6295. arXiv: cond-mat/0212118.

Finally, Eqs. (156)–(159) can be combined to yield the Helmholtz free energy density of a compressible, single-component membrane—written as

$$w = \rho\bar{\psi} = w_{\mathrm{H}} + w_{\mathrm{c}} = k_{\mathrm{b}}H^2 + k_{\mathrm{g}}K + \frac{1}{2}\frac{k_{\mathrm{c}}}{J}\big(J-1\big)^2 \,. \tag{160}$$

Importantly, as the free energy by definition only captures reversible behavior, Eq. (160) also describes the energetics of a compressible lipid membrane with viscous in-plane flows.

With a form of the Helmholtz free energy, we simply substitute Eq. (160) into the results of §4 (b) and §4 (c) to arrive at the membrane stresses and governing equations. We first calculate the partial derivatives

$$\frac{\partial\bar{\psi}}{\partial\rho} = -\frac{1}{\rho^2}\Big(k_{\mathrm{b}}H^2 + k_{\mathrm{g}}K + k_{\mathrm{c}}\big(J-1\big)\Big) \,, \qquad \frac{\partial\bar{\psi}}{\partial H} = \frac{2k_{\mathrm{b}}H}{\rho} \,, \qquad \frac{\partial\bar{\psi}}{\partial K} = \frac{k_{\mathrm{g}}}{\rho} \,. \tag{161}$$

Substituting Eq. (161) into the results of Table 2 show the elastic membrane stresses and couple-stresses are given by

$$\sigma_{\mathrm{el}}^{\alpha\beta} = a^{\alpha\beta}\Big(-3k_{\mathrm{b}}H^2 - k_{\mathrm{g}}K + k_{\mathrm{c}}(J-1)\Big) + 2k_{\mathrm{b}}H\bar{b}^{\alpha\beta} \,, \tag{162}$$

$$M_{\mathrm{el}}^{\alpha\beta} = k_{\mathrm{b}}H\,a^{\alpha\beta} + k_{\mathrm{g}}\bar{b}^{\alpha\beta} \,, \tag{163}$$

$$N_{\mathrm{el}}^{\alpha\beta} = a^{\alpha\beta}\Big(-k_{\mathrm{b}}H^2 + k_{\mathrm{c}}(J-1)\Big) + k_{\mathrm{b}}H\bar{b}^{\alpha\beta} \,, \tag{164}$$

and

$$S_{\mathrm{el}}^{\alpha} = -k_{\mathrm{b}}\,a^{\alpha\beta}H_{,\beta} \,. \tag{165}$$

Here we notice that the out-of-plane shears S_{el}^{α} contain a derivative of the mean curvature H—which itself contains two derivatives of the position. Such a result is well-known from the study of beam bending. We also calculate the isotropic portion of the in-plane stresses as $\frac{1}{2}N^{\alpha\beta}a_{\alpha\beta} = k_{\mathrm{c}}(J-1)$—revealing that areal compression or dilation leads to an in-plane tension. By substituting Eq. (161) into the equations of motion (151)–(153), we arrive at the governing equations:

$$\rho_{,t} + v^{\alpha}\rho_{,\alpha} + \rho\big(v^{\alpha}_{;\alpha} - 2vH\big) = 0 \,, \tag{166}$$

$$\rho\Big(v^{\alpha}_{,t} + v^{\beta}v^{\alpha}_{;\beta} - 2vv^{\beta}b^{\alpha}_{\beta} - vv_{,\beta}a^{\alpha\beta}\Big) = f^{\alpha} - k_{\mathrm{c}}\frac{\rho_0}{\rho^2}\,a^{\alpha\beta}\rho_{,\beta} \,, \tag{167}$$

and

$$\rho\Big(v_{,t} + 2v^{\alpha}v_{,\alpha} + v^{\alpha}v^{\beta}b_{\alpha\beta}\Big) = f + 2k_{\mathrm{c}}H\big(J-1\big) - 2k_{\mathrm{b}}H\big(H^2-K\big) - k_{\mathrm{b}}\Delta_{\mathrm{s}}H \,. \tag{168}$$

Equations (166)–(168) are respectively the continuity, in-plane, and shape equations. As no dissipative terms were included by construction, these are the Euler–Lagrange equations corresponding to the Helmholtz free energy density in Eq. (160). The right-hand side of Eq. (167) contains the gradient of the in-plane tension $k_{\mathrm{c}}(J-1)$; these Marangoni forces drive an in-plane flow of lipids. The first two terms on the right-hand side of the shape equation (168) are those found in the Young–Laplace equation if f arises due to a pressure drop across the membrane surface. The remaining terms are bending forces, and are expected to arise when the membrane is curved.

5. The case of a compressible, viscous membrane

Thus far, we have calculated only specific forms of the elastic membrane stresses and couple-stresses, in which no entropy is produced as the material deforms. However, the main advantage of our irreversible thermodynamic framework is the ability to naturally capture dissipative behavior. In this section, we consider the biologically relevant situation of a compressible lipid membrane in which lipids flow in-plane as a viscous fluid. We begin with the internal entropy production, from which we determine the thermodynamic forces and fluxes in the system. By proposing linear relationships between the forces and fluxes in the linear irreversible regime, we arrive at forms for the membrane stresses and couple-stresses which account for the viscous in-plane flow of lipids. We end by obtaining the governing equations, both for generic energy densities and the specific case of the Helfrich free energy density, and providing possible boundary conditions.

(a). The internal entropy production

Recall the general form of the internal entropy production in Eq. (121). As discussed in §4 (a) of Chapter III, the internal entropy production can be expressed as a product of thermodynamic forces and thermodynamic fluxes: the former can be *imposed* on the system, while the latter are the system's *driven response.* We denote the set of thermodynamic forces as $\{X_k\}$ and the set of corresponding fluxes as $\{J^k\}$, such that Eq. (121) is equivalently written as

$$\rho\eta_{\mathrm{i}} = \sum_k J^k \cdot X_k \geq 0 \,. \tag{169}$$

In Eq. (169), the indices k are used as a label; X_k and J^k may be scalars, vectors, or tensors. As described by Prigogine [‡] as well as de Groot and Mazur, [†] we posit that we are in the *linear irreversible regime,* where the system is close to thermodynamic equilibrium. In this case, there is a linear relationship between thermodynamic fluxes and forces, given by

$$J^j = \sum_k L^{jk} X_k \,, \tag{170}$$

where L^{jk} are the phenomenological coefficients. Substituting Eq. (170) into Eq. (169) reveals

$$\rho\eta_{\mathrm{i}} = \sum_{j,k} L^{jk} X_j \, X_k \geq 0 \,, \tag{171}$$

implying the matrix representation of the phenomenological coefficients is positive semi-definite. As shown by Onsager, [*, §] when microscopic dynamics are time-reversal symmetric, the phenomenological coefficients are symmetric as well.

[‡] I. Prigogine. *Introduction to Thermodynamics of Irreversible Processes.* 3rd ed. New York: Interscience Publishers, 1967.

[†] de Groot and Mazur, *Non-Equilibrium Thermodynamics.*

[*] L. Onsager. "Reciprocal relations in irreversible processes. I.". *Phys. Rev.* **37** (1931), 405–426.

[§] L. Onsager. "Reciprocal relations in irreversible processes. II.". *Phys. Rev.* **38** (1931), 2265–2279.

Our first task is to determine the thermodynamic fluxes and forces in Eq. (121). As the temperature T is always positive, we treat

$$-T_{,\alpha} \ , \qquad \dot{a}_{\alpha\beta} \ , \qquad \text{and} \qquad \dot{b}_{\alpha\beta} \tag{172}$$

as the thermodynamic forces, with

$$J_{\rm q}^{\alpha} \ , \qquad \pi^{\alpha\beta} \ , \qquad \text{and} \qquad \omega^{\alpha\beta} \tag{173}$$

being the corresponding thermodynamic fluxes. According to Eq. (170), and with the symmetry of the phenomenological coefficients, we express the linear relationships between the forces and fluxes as

$$J_{\rm q}^{\alpha} \ = \ \kappa^{\alpha\beta}(-T_{,\beta}) + \ P^{\alpha\mu\nu}\dot{a}_{\mu\nu} + \ Q^{\alpha\mu\nu}\dot{b}_{\mu\nu} \ , \tag{174}$$

$$\pi^{\alpha\beta} \ = \ P^{\alpha\beta\mu}(-T_{,\mu}) + R^{\alpha\beta\mu\nu}\dot{a}_{\mu\nu} + S^{\alpha\beta\mu\nu}\dot{b}_{\mu\nu} \ , \tag{175}$$

and

$$\omega^{\alpha\beta} \ = \ Q^{\alpha\beta\mu}(-T_{,\mu}) + S^{\alpha\beta\mu\nu}\dot{a}_{\mu\nu} + T^{\alpha\beta\mu\nu}\dot{b}_{\mu\nu} \ . \tag{176}$$

Now, assuming the membrane is isotropic in-plane, all the tensorial phenomenological coefficients are isotropic as well. For two-dimensional surfaces, the contravariant components of any isotropic tensor can be expressed as a combination of the contravariant metric $a^{\alpha\beta}$ and the contravariant Levi–Civita tensor $\varepsilon^{\alpha\beta}$ [defined in Chapter II, §2 (e)]. [‡]. Accordingly, there are no isotropic third-order tensors in two dimension, implying $P^{\alpha\mu\nu} = 0$ and $Q^{\alpha\mu\nu} = 0$. Accordingly, Eq. (176) simplifies to

$$J_{\rm q}^{\alpha} \ = \ -\kappa^{\alpha\beta}T_{,\beta} \ , \tag{177}$$

and we recognize $\kappa^{\alpha\beta}$ as the thermal conductivity tensor. The symmetry of the phenomenological coefficients implies $\kappa^{\alpha\beta} = \kappa^{\beta\alpha}$, and thus for $\kappa^{\alpha\beta}$ being isotropic we have $\kappa^{\alpha\beta} = \kappa a^{\alpha\beta}$, where the constant κ is the scalar thermal conductivity. In this case, equation (177) simplifies to

$$J_{\rm q}^{\alpha} \ = \ -\kappa\, a^{\alpha\beta}T_{,\beta} \ . \tag{178}$$

Equation (178) is the two-dimensional version of Fourier's first law. Note that in the case of lipid bilayers, there are usually no temperature gradients and Eq. (178) does not play a major role in describing irreversible phenomena.

With the understanding that there are no third-order isotropic tensors on two-dimensional surfaces, Eqs. (175) and (176) simplify to

$$\pi^{\alpha\beta} \ = \ R^{\alpha\beta\mu\nu}\dot{a}_{\mu\nu} + S^{\alpha\beta\mu\nu}\dot{b}_{\mu\nu} \tag{179}$$

and

$$\omega^{\alpha\beta} \ = \ S^{\alpha\beta\mu\nu}\dot{a}_{\mu\nu} + T^{\alpha\beta\mu\nu}\dot{b}_{\mu\nu} \ . \tag{180}$$

[‡]Here, we generalize to curved surface the result of J.M. Epstein and K.K. Mandadapu. "Time-reversal symmetry breaking in two dimensional nonequilibrium viscous fluids". *Phys. Rev. E* **101** (2020), 052614. arXiv: 1907.10041

where the fourth-order contravariant tensors $R^{\alpha\beta\mu\nu}$, $S^{\alpha\beta\mu\nu}$, and $T^{\alpha\beta\mu\nu}$ are general phenomenological viscous coefficients. Note the quantity $S^{\alpha\beta\mu\nu}$ describes *interference* or *cross-coupling* between two irreversible processes driven by $\dot{a}_{\alpha\beta}$ and $\dot{b}_{\alpha\beta}$, which we assume to be zero for the case of lipid bilayers. Equations (179) and (180) then reduce to

$$\pi^{\alpha\beta} \;=\; R^{\alpha\beta\mu\nu}\dot{a}_{\mu\nu} \tag{181}$$

and

$$\omega^{\alpha\beta} \;=\; T^{\alpha\beta\mu\nu}\dot{b}_{\mu\nu}\;. \tag{182}$$

Given the form of the internal entropy production (121), Eqs. (181) and (182) indicate $\pi^{\alpha\beta}$ captures the dissipation due to in-plane flows and $\omega^{\alpha\beta}$ captures the dissipation due to out-of-plane bending. In general, $T^{\alpha\beta\mu\nu}$ need not be equal to zero and bending can be a mechanism by which the membrane dissipates energy. However, in this work we assume out-of-plane-bending is not a dissipative process, and so $T^{\alpha\beta\mu\nu} = 0$. Consequently,

$$\omega^{\alpha\beta} \;=\; 0\;. \tag{183}$$

For a membrane in which lipids flow in-plane as a two-dimensional viscous fluid, entropy is produced as lipids flow and $\pi^{\alpha\beta}$ is nonzero. We thus seek the form of $R^{\alpha\beta\mu\nu}$, which is a fourth-order isotropic tensor. As detailed by J.M. Epstein and K.K. Mandadapu,[‡] in two spatial dimensions the space of such tensors is six-dimensional. However, we assume the flow does not have any chiral nature—equivalently expresses as the dynamics being invariant to exchanging the basis vectors $\boldsymbol{a}_1$ and $\boldsymbol{a}_2$, for which $\boldsymbol{n} \mapsto -\boldsymbol{n}$. With this parity requirement, the space of such tensors reduces from six to three, and we can represent $R^{\alpha\beta\mu\nu}$ as

$$R^{\alpha\beta\gamma\mu} \;=\; \frac{1}{2}\,\zeta\left(a^{\alpha\mu}a^{\beta\nu} \;+\; a^{\alpha\nu}a^{\beta\mu}\right) \;+\; \frac{1}{2}\,\xi\, a^{\alpha\beta}a^{\mu\nu} \;+\; \frac{1}{2}\,\Omega\,\varepsilon^{\alpha\beta}\varepsilon^{\mu\nu}\;. \tag{184}$$

In Eq. (184), ζ, ξ, and Ω are constants,[†] with the factors of $\frac{1}{2}$ included for notational simplicity later on. By substituting Eq. (184) into Eq. (181), we obtain

$$\pi^{\alpha\beta} \;=\; \frac{1}{2}\,\zeta\left(a^{\alpha\mu}a^{\beta\nu} \;+\; a^{\alpha\nu}a^{\beta\mu}\right)\dot{a}_{\mu\nu} \;+\; \frac{1}{2}\,\xi\, a^{\alpha\beta}\underbrace{a^{\mu\nu}\dot{a}_{\mu\nu}}_{2(v^{\mu}_{;\mu}-2vH)} \;+\; \frac{1}{2}\,\Omega\,\varepsilon^{\alpha\beta}\underbrace{\varepsilon^{\mu\nu}\dot{a}_{\mu\nu}}_{=0}\;. \tag{185}$$

In Eq. (185), we recognized (i) $\dot{a}_{\mu\nu}$ is symmetric, (ii) $a^{\mu\nu}\dot{a}_{\mu\nu} = 2(v^{\mu}_{;\mu} - 2vH)$ [see Eq. (34)], and (iii) $\varepsilon^{\mu\nu}$ is antisymmetric. Accordingly, the terms in parenthesis in Eq. (185) both give the same contribution to $\pi^{\alpha\beta}$, and the last term is zero. The form of the dissipative in-plane stresses can then be written as

$$\pi^{\alpha\beta} \;=\; \zeta\, a^{\alpha\mu}a^{\beta\nu}\dot{a}_{\mu\nu} \;+\; \xi\, a^{\alpha\beta}\left(v^{\mu}_{;\mu} - 2vH\right)\;. \tag{186}$$

At this point, similar to our bulk developments in §4 (b) of Chapter III, we partition $\dot{a}_{\alpha\beta}$ into deviatioric [superscript '(d)'] and isotropic [superscript '(i)'] components as

$$\dot{a}_{\alpha\beta} \;=\; \dot{a}^{(\mathrm{d})}_{\alpha\beta} \;+\; \dot{a}^{(\mathrm{i})}_{\alpha\beta}\;, \qquad \text{where by construction} \qquad a^{\alpha\beta}\,\dot{a}^{(\mathrm{d})}_{\alpha\beta} \;=\; 0\;. \tag{187}$$

[‡]Epstein and Mandadapu, "Time-reversal symmetry breaking in two dimensional nonequilibrium viscous fluids".

[†]In this section only, ξ denotes a viscous coefficient rather than the twist at the boundary.

By once again recognizing $a^{\alpha\beta}\dot{a}_{\alpha\beta} = 2(v^{\mu}_{;\mu} - 2vH)$ [see Eq. (34)], we find the deviatoric and isotropic components of $\dot{a}_{\alpha\beta}$ to be given by

$$\dot{a}^{(\mathrm{d})}_{\alpha\beta} \;=\; \dot{a}_{\alpha\beta} \;-\; \big(v^{\mu}_{;\mu} - 2vH\big)\, a_{\alpha\beta} \qquad \text{and} \qquad \dot{a}^{(\mathrm{i})}_{\alpha\beta} \;=\; \big(v^{\mu}_{;\mu} - 2vH\big)\, a_{\alpha\beta}\;. \tag{188}$$

Given the partition of $\dot{a}_{\alpha\beta}$ in Eqs. (187) and (188), the in-plane stresses can be written as

$$\pi^{\alpha\beta} \;=\; \zeta\, a^{\alpha\mu} a^{\beta\nu} \dot{a}^{(\mathrm{d})}_{\mu\nu} \;+\; \eta\, a^{\alpha\beta}\big(v^{\mu}_{;\mu} - 2vH\big)\;, \tag{189}$$

where we define

$$\eta \;:=\; \zeta \;+\; \xi\;. \tag{190}$$

We now substitute Eqs. (178), (183), and (189) into Eq. (121), and recall $a^{\alpha\mu}a^{\beta\nu}\,\dot{a}^{(\mathrm{i})}_{\alpha\beta}\,\dot{a}^{(\mathrm{i})}_{\mu\nu} = 2(v^{\mu}_{;\mu} - 2vH)^2$, to obtain the internal entropy production as

$$\rho\eta_{\mathrm{i}} \;=\; \frac{\kappa\, a^{\alpha\beta} T_{,\alpha}\, T_{,\beta}}{T^2} \;+\; \frac{1}{2T}\left\{\zeta\, a^{\alpha\mu} a^{\beta\nu}\, \dot{a}^{(\mathrm{d})}_{\alpha\beta}\, \dot{a}^{(\mathrm{d})}_{\mu\nu} \;+\; \eta\, a^{\alpha\mu} a^{\beta\nu}\, \dot{a}^{(\mathrm{i})}_{\alpha\beta}\, \dot{a}^{(\mathrm{i})}_{\mu\nu}\right\} \;\geq\; 0\;. \tag{191}$$

From Eq. (191), we recognize ζ as the two-dimensional intramembrane shear viscosity and η as the two-dimensional dilational viscosity, with κ noted earlier to be the scalar thermal conductivity. Since we can construct processes in which $T_{,\alpha}$, $\dot{a}^{(\mathrm{d})}_{\alpha\beta}$, and $\dot{a}^{(\mathrm{i})}_{\alpha\beta}$ are specified independently, Eq. (191) reveals $\kappa > 0$, $\zeta > 0$, and $\eta > 0$.

While the forms of the in-plane viscous stresses $\pi^{\alpha\beta}$ in Eqs. (186) and (189) are theoretically sound, they are not amenable for obtaining the relevant equations of motion and boundary conditions. For ease in our later calculations, we express $\pi^{\alpha\beta}$ as

$$\begin{aligned}
\pi^{\alpha\beta} \;&=\; \zeta\, a^{\alpha\mu} a^{\beta\nu} \dot{a}_{\mu\nu} \;+\; \big(\eta - \zeta\big)\, a^{\alpha\beta}\big(v^{\mu}_{;\mu} - 2vH\big) \\
&=\; \zeta\left(v^{\beta}_{;\mu}\, a^{\alpha\mu} \;+\; v^{\alpha}_{;\nu}\, a^{\beta\nu} \;-\; 2v b^{\alpha\beta}\right) \;+\; \big(\eta - \zeta\big)\, a^{\alpha\beta}\Big(v^{\mu}_{;\mu} \;-\; 2vH\Big) \\
&=\; \zeta\left(v^{\beta}_{;\mu}\, a^{\alpha\mu} \;+\; v^{\alpha}_{;\nu}\, a^{\beta\nu} \;+\; 2v\bar{b}^{\alpha\beta} \;-\; 4vH a^{\alpha\beta}\right) \;+\; \big(\eta - \zeta\big)\, a^{\alpha\beta}\Big(v^{\mu}_{;\mu} \;-\; 2vH\Big)\;.
\end{aligned} \tag{192}$$

In Eq. (192), we substituted the expression for $\dot{a}_{\mu\nu}$ in the second line, and then the expression for $\bar{b}^{\alpha\beta}$ in the third line.

(b). The membrane stresses and couple-stresses

With our calculation of $\omega^{\alpha\beta}$ and $\pi^{\alpha\beta}$, the membrane stresses and couple-stresses are completely determined. Equations (115) and (183) reveal the constitutive form of the couple-stress tensor $M^{\alpha\beta}$ is given by $M^{\alpha\beta} = M^{\alpha\beta}_{\mathrm{el}}$, for which the out-of-plane shear stresses S^{α} are given by $S^{\alpha} = S^{\alpha}_{\mathrm{el}}$. Moreover, with our determination of the viscous stresses $\pi^{\alpha\beta}$ in Eq. (186), the couple-free in-plane stresses are written as $\sigma^{\alpha\beta} = \sigma^{\alpha\beta}_{\mathrm{el}} + \pi^{\alpha\beta}$, and the corresponding in-plane stresses are given by $N^{\alpha\beta} = N^{\alpha\beta}_{\mathrm{el}} + \pi^{\alpha\beta}$. In terms of a general Helmholtz free energy density $\bar{\psi}$ (126), the membrane stress and couple-stresses are listed in Table 3; those corresponding to our choice of Helfrich and compression energies (160) are given in Table 4.

Table 3: Stresses and couple-stresses in a single-component lipid membrane with Helmholtz free energy density of the general form in Eq. (126), and an in-plane viscous flow of lipids. Here, $\pi^{\alpha\beta}$ is given by Eq. (192).

$\sigma^{\alpha\beta} \;=\; -\rho\, a^{\alpha\beta}\left(\rho\,\dfrac{\partial\bar{\psi}}{\partial\rho} \;+\; 2H\,\dfrac{\partial\bar{\psi}}{\partial H} \;+\; 2K\,\dfrac{\partial\bar{\psi}}{\partial K}\right) \;+\; \rho\,\bar{b}^{\alpha\beta}\,\dfrac{\partial\bar{\psi}}{\partial H} \;+\; \pi^{\alpha\beta}$
$M^{\alpha\beta} \;=\; \dfrac{\rho}{2}\,a^{\alpha\beta}\,\dfrac{\partial\bar{\psi}}{\partial H} \;+\; \rho\,\bar{b}^{\alpha\beta}\,\dfrac{\partial\bar{\psi}}{\partial K}$
$N^{\alpha\beta} \;=\; -\rho\, a^{\alpha\beta}\left(\rho\,\dfrac{\partial\bar{\psi}}{\partial\rho} \;+\; H\,\dfrac{\partial\bar{\psi}}{\partial H} \;+\; K\,\dfrac{\partial\bar{\psi}}{\partial K}\right) \;+\; \dfrac{\rho}{2}\,\bar{b}^{\alpha\beta}\,\dfrac{\partial\bar{\psi}}{\partial H} \;+\; \pi^{\alpha\beta}$
$S^{\alpha} \;=\; -a^{\alpha\beta}\left(\dfrac{\rho}{2}\,\dfrac{\partial\bar{\psi}}{\partial H}\right)_{;\beta} \;-\; \bar{b}^{\alpha\beta}\left(\rho\,\dfrac{\partial\bar{\psi}}{\partial K}\right)_{;\beta}$

Table 4: Stresses and couple-stresses in a single-component lipid membrane with a Helmholtz free energy containing Helfrich and compressible contributions (160), where lipids flow in-plane as a viscous fluid and $\pi^{\alpha\beta}$ is given by Eq. (192).

$\sigma^{\alpha\beta} \;=\; a^{\alpha\beta}\Big(-3k_{\mathrm{b}}H^2 \;-\; k_{\mathrm{g}}K \;+\; k_{\mathrm{c}}(J-1)\Big) \;+\; 2k_{\mathrm{b}}H\bar{b}^{\alpha\beta} \;+\; \pi^{\alpha\beta}$
$M^{\alpha\beta} \;=\; k_{\mathrm{b}}H\,a^{\alpha\beta} \;+\; k_{\mathrm{g}}\bar{b}^{\alpha\beta}$
$N^{\alpha\beta} \;=\; a^{\alpha\beta}\Big(-k_{\mathrm{b}}H^2 \;+\; k_{\mathrm{c}}(J-1)\Big) \;+\; k_{\mathrm{b}}H\bar{b}^{\alpha\beta} \;+\; \pi^{\alpha\beta}$
$S^{\alpha} \;=\; -k_{\mathrm{b}}\,a^{\alpha\beta}H_{,\beta}$

(c). The equations of motion

Let us compare the membrane stresses and couple-stresses in two different cases: when the in-plane flow of lipids is inviscid (Table 2), and when viscous dissipation arises from lipid flow (Table 3). The only difference is the presence of the in-plane viscous stresses $\pi^{\alpha\beta}$ in $\sigma^{\alpha\beta}$, and consequently $N^{\alpha\beta}$, in the latter case. Thus, in order to determine the governing equations for a lipid membrane with viscous in-plane flows, we need only to add the quantity $\pi^{\beta\alpha}_{;\beta}$ to the in-plane equations (152) and $\pi^{\alpha\beta}b_{\alpha\beta}$ to the shape equation (153) [cf. Eqs. (66) and (67)]. To this end, we calculate

$$\begin{aligned}
\pi^{\beta\alpha}_{;\beta} &= \zeta\left(v^{\alpha}_{;\mu}\,a^{\beta\mu} + v^{\beta}_{;\nu}\,a^{\alpha\nu} + 2v\bar{b}^{\alpha\beta} - 4vHa^{\alpha\beta}\right)_{;\beta} + \left(\eta-\zeta\right)a^{\alpha\beta}\left(v^{\mu}_{;\mu} - 2vH\right)_{;\beta} \\
&= \zeta\Big(\underbrace{v^{\alpha}_{;\mu\beta}\,a^{\beta\mu}}_{\Delta_{\mathrm{s}}v^{\alpha}} + \underbrace{v^{\beta}_{;\nu\beta}\,a^{\alpha\nu}}_{v^{\beta}_{;\beta\nu}\,a^{\alpha\nu}+Kv^{\alpha}} + 2v_{,\beta}\bar{b}^{\alpha\beta} - 4(vH)_{,\beta}a^{\alpha\beta}\Big) + \left(\eta-\zeta\right)a^{\alpha\beta}\left(v^{\mu}_{;\mu} - 2vH\right)_{;\beta} \\
&= \zeta\Big(\Delta_{\mathrm{s}}v^{\alpha} + Kv^{\alpha} + \underbrace{v^{\beta}_{;\beta\nu}\,a^{\alpha\nu} - 2(vH)_{,\beta}a^{\alpha\beta}}_{a^{\alpha\beta}(v^{\mu}_{;\mu}-2vH)_{;\beta}} + 2v_{,\beta}\bar{b}^{\alpha\beta} - 2(vH)_{,\beta}a^{\alpha\beta}\Big) \\
&\qquad + \left(\eta-\zeta\right)a^{\alpha\beta}\left(v^{\mu}_{;\mu} - 2vH\right)_{;\beta},
\end{aligned} \tag{193}$$

where in the second line we distributed the covariant derivative, and in the third line we substituted Eqs. (30) and (47) from Chapter II. After some rearrangement, the result of Eq. (193) can be written as

$$\pi^{\beta\alpha}_{;\beta} = \zeta\left(\Delta_{\mathrm{s}}v^{\alpha} + Kv^{\alpha} + 2v_{,\beta}Ha^{\alpha\beta} - 2v_{,\beta}b^{\alpha\beta} - 2vH_{,\beta}a^{\alpha\beta}\right) + \eta\,a^{\alpha\beta}\left(v^{\mu}_{;\mu} - 2vH\right)_{;\beta}. \tag{194}$$

We also use the identities $a^{\alpha\beta}b_{\alpha\beta} = 2H$ and $\bar{b}^{\alpha\beta}b_{\alpha\beta} = 2K$ to find

$$\pi^{\alpha\beta}b_{\alpha\beta} = 2\zeta\left(v^{\alpha}_{;\beta}\,b^{\beta}_{\alpha} - 2v\left(2H^2-K\right) - H\left(v^{\alpha}_{;\alpha} - 2vH\right)\right) + 2\eta H\left(v^{\alpha}_{;\alpha} - 2vH\right). \tag{195}$$

In the case where the membrane energetics are captured by the Helfrich and compression energies (160), the governing equations are given by [cf. Eqs. (166)–(168)]

$$\rho_{,t} + v^{\alpha}\rho_{,\alpha} + \rho\left(v^{\alpha}_{;\alpha} - 2vH\right) = 0\,, \tag{196}$$

$$\begin{aligned}
\rho\left(v^{\alpha}_{,t} + v^{\beta}v^{\alpha}_{;\beta} - 2vv^{\beta}b^{\alpha}_{\beta} - vv_{,\beta}a^{\alpha\beta}\right) &= f^{\alpha} - k_{\mathrm{c}}\frac{\rho_0}{\rho^2}\,a^{\alpha\beta}\rho_{,\beta} + \eta\,a^{\alpha\beta}\left(v^{\mu}_{;\mu} - 2vH\right)_{;\beta} \\
&\quad + \zeta\left(\Delta_{\mathrm{s}}v^{\alpha} + Kv^{\alpha} + 2v_{,\beta}Ha^{\alpha\beta} - 2v_{,\beta}b^{\alpha\beta} - 2vH_{,\beta}a^{\alpha\beta}\right),
\end{aligned} \tag{197}$$

and

$$\begin{aligned}
\rho\left(v_{,t} + 2v^{\alpha}v_{,\alpha} + v^{\alpha}v^{\beta}b_{\alpha\beta}\right) &= f + 2k_{\mathrm{c}}H\left(J-1\right) - 2k_{\mathrm{b}}H\left(H^2-K\right) - k_{\mathrm{b}}\Delta_{\mathrm{s}}H \\
&\quad + 2\zeta\left(v^{\alpha}_{;\beta}\,b^{\beta}_{\alpha} - 2v\left(2H^2-K\right) - H\left(v^{\alpha}_{;\alpha} - 2vH\right)\right) + 2\eta H\left(v^{\alpha}_{;\alpha} - 2vH\right).
\end{aligned} \tag{198}$$

Equations (196)–(198) are the continuity, in-plane, and shape equations, which respectively govern the areal mass density ρ, the in-plane velocity components v^α, and the out-of-plane velocity v.

At this point, it is useful to discuss the nature of the governing equations. We first note that the membrane position $\boldsymbol{x}$ is calculated from the velocity $\boldsymbol{v}$ according to Eq. (154). Thus, all geometric quantities in the governing equations—including the mean and Gaussian curvatures and the Christoffel symbols—can be thought of as functions of the out-of-plane velocity v. With this perspective, the in-plane equations (197) contain two derivatives of the in-plane velocities v^α through the surface Laplacian term, as is often found in fluid equations. The shape equation, on the other hand, contains two derivatives of the mean curvature H in the surface Laplacian, and the mean curvature itself contains two derivatives of the position through the curvature tensor. Thus, the shape equation (198) is a fourth-order equation for the out-of-plane velocity v; the four spatial derivatives are reminiscent of classic beam bending problems. We also note that when viscous terms are included, all governing equations (196)–(198) involve the density ρ and three components of the velocity $\boldsymbol{v}$, such that membrane dynamics are highly coupled. We address this coupling in more detail in later chapters.

(d). The boundary conditions

The decomposition of the equations of motion into in-plane and out-of-plane components gives us an intuition of the types of allowed boundary conditions. The in-plane equations are in fact identical to those of a two-dimensional viscous fluid film, such that we expect to prescribe either the in-plane velocities v^α or the in-plane forces at the membrane patch boundary. The shape equation contains four spatial derivatives of the membrane shape; in drawing analogy to the study of elastic plates and shells we expect to specify two of the following boundary conditions at each point on the patch boundary: the position, slope, moment, and out-of-plane force. In what follows, we systematically determine a well-posed set of boundary conditions by drawing on techniques from variational calculus, as motivated by standard practices in finite element analysis.

We begin by contracted the vector form of the linear momentum balance (60) with an *arbitrary velocity variation* $\delta\boldsymbol{v}$, and integrating over the membrane patch to obtain

$$\int_{\mathcal{P}} \delta\boldsymbol{v}\cdot\rho\dot{\boldsymbol{v}}\,\mathrm{d}a \;=\; \int_{\mathcal{P}} \delta\boldsymbol{v}\cdot\boldsymbol{f}\,\mathrm{d}a \;+\; \int_{\mathcal{P}} \delta\boldsymbol{v}\cdot\boldsymbol{T}^{\alpha}_{;\alpha}\,\mathrm{d}a\;. \tag{199}$$

Equation (199) is similar to the starting point of the mechanical power balance (87); by following an analogous set of manipulations, we find it can be expressed as [cf. Eq. (94)]

$$\begin{aligned}\int_{\mathcal{P}} \delta\boldsymbol{v}\cdot\rho\dot{\boldsymbol{v}}\,\mathrm{d}a \;+\; \int_{\mathcal{P}} (\delta\boldsymbol{v})_{,\alpha}\cdot\sigma^{\alpha\beta}\,\boldsymbol{a}_\beta\,\mathrm{d}a \;+\; \int_{\mathcal{P}} (\delta\boldsymbol{v})_{;\alpha\beta}\cdot M^{\alpha\beta}\,\boldsymbol{n}\,\mathrm{d}a \\ -\int_{\mathcal{P}} \delta\boldsymbol{v}\cdot\boldsymbol{f}\,\mathrm{d}a \;-\; \int_{\partial\mathcal{P}} \Big(\delta\boldsymbol{v}\cdot\boldsymbol{T} \;+\; \delta\dot{\boldsymbol{n}}\cdot\boldsymbol{M}\Big)\,\mathrm{d}s \;=\; 0\;,\end{aligned} \tag{200}$$

where $\delta\dot{\boldsymbol{n}} = -(\boldsymbol{a}^\alpha\otimes\boldsymbol{n})(\delta\boldsymbol{v})_{,\alpha}$ in analogy to Eq. (27). Generally, with a boundary term like that of Eq. (200), we would conclude that either $\boldsymbol{v}$ or $\boldsymbol{T}$ is specified on the boundary, and

similarly either $\dot{\boldsymbol{n}}$ or $\boldsymbol{M}$ is specified there as well. In this case, however, $\delta\boldsymbol{v}$ and $\delta\dot{\boldsymbol{n}}$ are not independent, [‡, †] and such a conclusion cannot be drawn. The boundary term in Eq. (200) is rewritten by first decomposing $\delta\dot{\boldsymbol{n}}$ in the $\{\boldsymbol{\nu}, \boldsymbol{\tau}\}$ basis, [*] for which

$$\delta\dot{\boldsymbol{n}} \cdot \boldsymbol{\nu} \;=\; -\boldsymbol{n} \cdot \nu^{\alpha} (\delta\boldsymbol{v})_{,\alpha} \;=\; -\boldsymbol{n} \cdot \frac{\partial(\delta\boldsymbol{v})}{\partial \nu} \tag{201}$$

and

$$\delta\dot{\boldsymbol{n}} \cdot \boldsymbol{\tau} \;=\; -\boldsymbol{n} \cdot \tau^{\alpha} (\delta\boldsymbol{v})_{,\alpha} \;=\; -\boldsymbol{n} \cdot \frac{\partial(\delta\boldsymbol{v})}{\partial s} \;. \tag{202}$$

In Eqs. (201) and (202), we introduced the notation

$$\frac{\partial(\,\cdot\,)}{\partial \nu} \;:=\; \nu^{\alpha} (\,\cdot\,)_{,\alpha} \qquad \text{and} \qquad \frac{\partial(\,\cdot\,)}{\partial s} \;:=\; \tau^{\alpha} (\,\cdot\,)_{,\alpha} \;, \tag{203}$$

as the partial derivatives along the $\boldsymbol{\nu}$ and $\boldsymbol{\tau}$ directions, respectively. With Eqs. (201) and (202), as well as the representation of the director traction $\boldsymbol{M}$ as $\boldsymbol{M} = m_{\tau}\boldsymbol{\nu} - m_{\nu}\boldsymbol{\tau}$ provided in Eq. (86), we find

$$\begin{aligned} \delta\dot{\boldsymbol{n}} \cdot \boldsymbol{M} \;&=\; \delta\dot{\boldsymbol{n}} \cdot \big(m_{\tau}\boldsymbol{\nu} \,-\, m_{\nu}\boldsymbol{\tau}\big) \;=\; -m_{\tau}\, \boldsymbol{n} \cdot \frac{\partial(\delta\boldsymbol{v})}{\partial \nu} \,+\, m_{\nu}\, \boldsymbol{n} \cdot \frac{\partial(\delta\boldsymbol{v})}{\partial s} \;, \\ &=\; -m_{\tau}\, \boldsymbol{n} \cdot \frac{\partial(\delta\boldsymbol{v})}{\partial \nu} \,+\, \frac{\partial}{\partial s}\big(m_{\nu}\, \delta\boldsymbol{v} \cdot \boldsymbol{n}\big) \,-\, \delta\boldsymbol{v} \cdot \frac{\partial}{\partial s}\big(m_{\nu}\, \boldsymbol{n}\big) \;, \end{aligned} \tag{204}$$

where the product rule was used in the second line. Next, substituting Eq. (204) into the boundary term in Eq. (200) yields

$$\begin{aligned} &\int_{\mathcal{P}} \Big(\delta\boldsymbol{v} \cdot \boldsymbol{T} \,+\, \delta\dot{\boldsymbol{n}} \cdot \boldsymbol{M}\Big)\, \mathrm{d}a \\ &\qquad =\; \int_{\partial\mathcal{P}} \left(\delta\boldsymbol{v} \cdot \Big[\boldsymbol{T} \,-\, \frac{\partial}{\partial s}\big(m_{\nu}\, \boldsymbol{n}\big)\Big] \,-\, \frac{\partial(\delta\boldsymbol{v})}{\partial \nu} \cdot m_{\tau}\, \boldsymbol{n} \,+\, \frac{\partial}{\partial s}\big(\delta\boldsymbol{v} \cdot m_{\nu}\, \boldsymbol{n}\big) \right) \mathrm{d}s \;. \end{aligned} \tag{205}$$

By recognizing we are integrating around a closed curve, namely the patch boundary, the last term in Eq. (205) only contributes to the integral at the corners of the domain—where $\boldsymbol{\tau}$ is discontinuous. Denoting N_{c} as the number of corners on the patch boundary, and $[\![\,\cdot\,]\!]_i$ as the jump in $(\,\cdot\,)$ when traversing the i^{th} corner, Eq. (205) simplifies to

$$\begin{aligned} &\int_{\mathcal{P}} \Big(\delta\boldsymbol{v} \cdot \boldsymbol{T} \,+\, \delta\dot{\boldsymbol{n}} \cdot \boldsymbol{M}\Big)\, \mathrm{d}a \\ &\qquad =\; \int_{\partial\mathcal{P}} \left(\delta\boldsymbol{v} \cdot \Big[\boldsymbol{T} \,-\, \frac{\partial}{\partial s}\big(m_{\nu}\, \boldsymbol{n}\big)\Big] \,-\, \frac{\partial}{\partial \nu}\big(\delta\boldsymbol{v}\big) \cdot m_{\tau}\boldsymbol{n} \right) \mathrm{d}s \;+\; \sum_{i=1}^{N_{\mathrm{c}}} \delta\boldsymbol{v} \cdot [\![m_{\nu}\, \boldsymbol{n}]\!]_i \;. \end{aligned} \tag{206}$$

[‡] A.E. Green and P.M. Naghdi. "The Cosserat Surface". *Mechanics of Generalized Continua.* Ed. by E. Kröner. Berlin, Heidelberg: Springer, 1968, pp. 36–48.

[†] D.J. Steigmann. "On the relationship between the Cosserat and Kirchhoff–Love theories of elastic shells". *Math. Mech. Solids* **4** (1998), 275–288.

[*] We note that $\delta\dot{\boldsymbol{n}}$ has no component in the normal direction, as $\delta\dot{\boldsymbol{n}} \cdot \boldsymbol{n} = -(\boldsymbol{n} \cdot \boldsymbol{a}^{\alpha})[\boldsymbol{n} \cdot (\delta\boldsymbol{v})_{,\alpha}] = 0$.

Importantly, $\delta\boldsymbol{v}$ and $\partial(\delta\boldsymbol{v})/\partial\nu$ are independent quantities, and are respectively conjugate to the force and moment on the boundary.[‡, †] Thus, we define the force on the boundary $\boldsymbol{F}$, moment on the boundary M, and force on the i^{th} corner of the boundary $\boldsymbol{F}_i$ as

$$\boldsymbol{F} := \boldsymbol{T} - \frac{\partial}{\partial s}\big(m_\nu\,\boldsymbol{n}\big)\,, \qquad M := -m_\tau\,, \qquad \text{and} \qquad \boldsymbol{F}_i := [\![m_\nu\,\boldsymbol{n}]\!]_i\,. \tag{207}$$

With the result of Eq. (206) and the shorthand introduced in Eq. (207), Eq. (200) is equivalently given by

$$\begin{aligned}\int_{\mathcal{P}} \delta\boldsymbol{v}\cdot\rho\dot{\boldsymbol{v}}\;\mathrm{d}a \;+\; \int_{\mathcal{P}} (\delta\boldsymbol{v})_{,\alpha}\cdot\sigma^{\alpha\beta}\,\boldsymbol{a}_\beta\;\mathrm{d}a \;+\; \int_{\mathcal{P}} (\delta\boldsymbol{v})_{;\alpha\beta}\cdot M^{\alpha\beta}\,\boldsymbol{n}\;\mathrm{d}a \\ -\int_{\mathcal{P}} \delta\boldsymbol{v}\cdot\boldsymbol{f}\;\mathrm{d}a \;-\; \int_{\partial\mathcal{P}}\left(\delta\boldsymbol{v}\cdot\boldsymbol{F} + \frac{\partial(\delta\boldsymbol{v})}{\partial\nu}\cdot M\boldsymbol{n}\right)\mathrm{d}s \;-\; \sum_{i=1}^{N_c}\delta\boldsymbol{v}\cdot\boldsymbol{F}_i \;=\; 0\,.\end{aligned} \tag{208}$$

The boundary integral in Eq. (208) implies we can specify either $\boldsymbol{v} = v^\alpha\boldsymbol{a}_\alpha + v\boldsymbol{n}$ or $\boldsymbol{F} = F_\nu\boldsymbol{\nu} + F_\tau\boldsymbol{\tau} + F_n\boldsymbol{n}$ on the membrane boundary, and similarly either $\boldsymbol{n}\cdot(\partial\boldsymbol{v}/\partial\nu)$ or M; note that specifying $\boldsymbol{n}\cdot(\partial\boldsymbol{v}/\partial\nu)$ is essentially specifying the slope of the patch boundary. In component form, we recognize the in-plane equations (197) are well-posed if we specify

$$\Big\{\, v^1 = \bar{v}^1 \quad\text{and}\quad v^2 = \bar{v}^2 \,\Big\} \qquad \text{or} \qquad \Big\{\, F_\nu = \bar{F}_\nu \quad\text{and}\quad F_\tau = \bar{F}_\tau \,\Big\} \tag{209}$$

on the membrane boundary, where $\bar{v}^1$, $\bar{v}^2$, $\bar{F}_\nu$, and $\bar{F}_\tau$ are known entities. The former set of conditions are known as *Dirichlet boundary conditions,* while the latter are called *Neumann boundary conditions.* Equation (209) confirms our intuition that the in-plane fluid equations are well-posed if we specify either the in-plane velocities or in-plane tractions. Next, we consider the boundary conditions in the normal direction, which correspond to the shape equation. Here, we are required to specify either

$$v = \bar{v} \qquad \text{or} \qquad F_n = \bar{F}_n \tag{210}$$

on the boundary, as well as either

$$\boldsymbol{n}\cdot\frac{\partial\boldsymbol{v}}{\partial\nu} = \bar{v}_\nu \qquad \text{or} \qquad M = \bar{M}\,, \tag{211}$$

where $\bar{v}$, $\bar{F}_n$, $\bar{v}_\nu$, and $\bar{M}$ are prescribed quantities. Here, we again see that our intuition was correct: the shape equation contains four spatial derivatives, and we consequently specify two boundary conditions—either the change in position or the force, and either the change in slope or the moment.

Our final task is to determine the functional form of the boundary force $\boldsymbol{F}$ and moment M, such that they can be prescribed as required. We begin by writing the force $\boldsymbol{F}$ in Eq. $(207)_1$ as

$$\boldsymbol{F} = N^{\alpha\beta}\nu_\alpha\big(\nu_\beta\boldsymbol{\nu} + \tau_\beta\boldsymbol{\tau}\big) + S^\alpha\nu_\alpha\boldsymbol{n} - \frac{\partial m_\nu}{\partial s}\,\boldsymbol{n} - m_\nu\,\frac{\partial\boldsymbol{n}}{\partial s}\,, \tag{212}$$

[‡]Green and Naghdi, "The Cosserat Surface".

[†]Steigmann, "On the relationship between the Cosserat and Kirchhoff–Love theories of elastic shells".

where we substituted the traction decomposition (58), stress vector decomposition (61), and expanded the partial derivative. Next, we calculate

$$\frac{\partial \boldsymbol{n}}{\partial s} = \boldsymbol{n}_{,\alpha}\frac{\partial \theta^\alpha}{\partial s} = \boldsymbol{n}_{,\alpha}\tau^\alpha = -b^\beta_\alpha \boldsymbol{a}_\beta \tau^\alpha = -b^{\alpha\beta}\tau_\alpha \nu_\beta \boldsymbol{\nu} - b^{\alpha\beta}\tau_\alpha\tau_\beta \boldsymbol{\tau} , \tag{213}$$

where we applied the chain rule, definition of $\boldsymbol{\tau}$, the Weingarten equation, and the decomposition of $\boldsymbol{a}_\beta$ provided in Chapter II. By substituting Eq. (213) into Eq. (212) and rearranging terms, we obtain

$$\boldsymbol{F} = \left(N^{\alpha\beta}\nu_\alpha\nu_\beta + m_\nu b^{\alpha\beta}\tau_\alpha\nu_\beta\right)\boldsymbol{\nu} + \left(N^{\alpha\beta}\nu_\alpha\tau_\beta + m_\nu b^{\alpha\beta}\tau_\alpha\tau_\beta\right)\boldsymbol{\tau} + \left(S^\alpha\nu_\alpha - \frac{\partial m_\nu}{\partial s}\right)\boldsymbol{n} , \tag{214}$$

for which the components of the boundary force are given by

$$F_\nu = N^{\alpha\beta}\nu_\alpha\nu_\beta + m_\nu b^{\alpha\beta}\tau_\alpha\nu_\beta , \tag{215}$$

$$F_\tau = N^{\alpha\beta}\nu_\alpha\tau_\beta + m_\nu b^{\alpha\beta}\tau_\alpha\tau_\beta , \tag{216}$$

and

$$F_n = S^\alpha\nu_\alpha - \frac{\partial m_\nu}{\partial s} . \tag{217}$$

For completeness, we reiterate the expression for boundary moment M provided in Eq. (85) as

$$M = -m_\tau = M^{\alpha\beta}\nu_\alpha\nu_\beta . \tag{218}$$

The three components of the boundary force, provided in Eqs. (215)–(217), and the boundary moment M (218) are the general forms of the forces and moments on the membrane boundary.

We close by providing the boundary forces and moments for the membrane systems considered thus far, expressed in terms of the boundary curvatures. To this end, recall the definitions of the normal curvatures κ_ν and κ_τ in the $\boldsymbol{\nu}$ and $\boldsymbol{\tau}$ directions, the twist ξ, and their relation to the mean and Gaussian curvatures [see Chapter II, §2 (f)]. For a general Helmholtz free energy per unit mass $\bar{\psi}$, the membrane stresses are given in Table 3; substituting these results into Eqs. (215)–(218) and rearranging terms yields

$$F_\nu = -\rho^2\frac{\partial\bar{\psi}}{\partial\rho} - \frac{\rho\,\kappa_\nu}{2}\frac{\partial\bar{\psi}}{\partial H} - \rho\,\kappa_\nu\,\kappa_\tau\frac{\partial\bar{\psi}}{\partial K} + \pi^{\alpha\beta}\nu_\alpha\nu_\beta , \tag{219}$$

$$F_\tau = -\frac{\rho\,\xi}{2}\frac{\partial\bar{\psi}}{\partial H} - \rho\,\kappa_\tau\,\xi\frac{\partial\bar{\psi}}{\partial K} + \pi^{\alpha\beta}\tau_\alpha\nu_\beta , \tag{220}$$

$$F_n = -\frac{1}{2}\frac{\partial}{\partial\nu}\left(\rho\frac{\partial\bar{\psi}}{\partial H}\right) - \bar{b}^{\alpha\beta}\nu_\alpha\left(\rho\frac{\partial\bar{\psi}}{\partial K}\right)_{,\beta} + \frac{\partial}{\partial s}\left(\rho\,\xi\frac{\partial\bar{\psi}}{\partial K}\right) , \tag{221}$$

and

$$M = \frac{\rho}{2}\frac{\partial\bar{\psi}}{\partial H} + \rho\,\kappa_\tau\frac{\partial\bar{\psi}}{\partial K} . \tag{222}$$

For the specific case of the Helfrich and compression energies (160), we substitute the results of Eq. (161) into the above equations to obtain

$$F_\nu = \frac{k_\mathrm{b}}{4}\left(\kappa_\tau^2 - \kappa_\nu^2\right) - k_\mathrm{g}\,\xi^2 + k_\mathrm{c}\left(J-1\right) + \pi^{\alpha\beta}\nu_\alpha\nu_\beta \,, \tag{223}$$

$$F_\tau = -\frac{k_\mathrm{b}\,\xi}{2}\left(\kappa_\nu + \kappa_\tau\right) - k_\mathrm{g}\,\xi\,\kappa_\tau + \pi^{\alpha\beta}\tau_\alpha\nu_\beta \,, \tag{224}$$

$$F_n = -\frac{k_\mathrm{b}}{2}\left(\frac{\partial\kappa_\nu}{\partial\nu} + \frac{\partial\kappa_\tau}{\partial\nu}\right) + k_\mathrm{g}\frac{\partial\xi}{\partial s} \,, \tag{225}$$

and

$$M = \frac{k_\mathrm{b}}{2}\left(\kappa_\nu + \kappa_\tau\right) + k_\mathrm{g}\kappa_\tau \,. \tag{226}$$

We have now provided the governing equations, with possible boundary conditions, for both the in-plane and shape equations. As such, our problem is mathematically well-posed. This concludes the theoretical development of a single-component, area-compressible lipid membrane with elastic out-of-plane bending and viscous in-plane lipid flow.

6. The case of an incompressible, viscous membrane

In biologically relevant systems, lipid membranes can only stretch 2–3% before they tear, [‡] and are thus practically area-incompressible. In this section, we obtain the equations governing a perfectly incompressible membrane, for which the areal mass density ρ is constant and the Jacobian determinant $J = 1$. The continuity equation simplifies to the incompressibility constraint provided in Eq. (52), which is enforced at each point on the membrane surface with the Lagrange multiplier field $\tilde{\lambda} = \lambda(\theta^\alpha, t)$. Physically, we recognize λ as the surface tension, in analogous fashion to the pressure p enforcing bulk incompressibility in a three-dimensional fluid [see Chapter III, §4 (b)].

(a). The Helmholtz free energy

As was the case for a compressible membrane, we begin by considering the Helmholtz free energy W of the entire patch, and the free energy per area w (155). In this case, the total free energy is decomposed as [cf. Eqs. (156) and (157)]

$$W = W_\mathrm{H} + W_\mathrm{i} \,, \qquad \text{with} \qquad W_\mathrm{H} = \int_\mathcal{P} w_\mathrm{H}\,\mathrm{d}a \qquad \text{and} \qquad W_\mathrm{i} = \int_\mathcal{P} w_\mathrm{i}\,\mathrm{d}a \,. \tag{227}$$

Here, W_H is again the Helfrich free energy, while W_i is the portion of the free energy arising from the incompressibility constraint $J = 1$. We enforce the constraint in the reference configuration, about which area dilations and compressions are measured, for which

$$W_\mathrm{i} = \int_{\mathcal{P}_0} \hat{\lambda}\left(\hat{J}-1\right)\mathrm{d}A = \int_\mathcal{P} \frac{\lambda}{J}\left(J-1\right)\mathrm{d}a \,. \tag{228}$$

[‡] Evans and Skalak, *Mechanics and Thermodynamics of Biomembranes*.

Recalling $J = \rho_0/\rho$ (55) and $J\,\mathrm{d}A = \mathrm{d}a$ (6), from Eqs. $(227)_3$ and (228) we recognize

$$w_{\mathrm{i}} \;=\; \frac{\lambda}{J}\left(J-1\right) \qquad \text{and} \qquad \bar{\psi}_{\mathrm{i}} \;=\; \lambda\left(\frac{1}{\rho}\,-\,\frac{1}{\rho_0}\right). \tag{229}$$

Thus, the total Helmholtz free energy per unit area and per unit mass are respectively given by

$$w \;=\; k_{\mathrm{b}}H^2 \,+\, k_{\mathrm{g}}K \,+\, \frac{\lambda}{J}\left(J-1\right) \qquad \text{and} \qquad \bar{\psi} \;=\; \frac{1}{\rho}\left(k_{\mathrm{b}}H^2 \,+\, k_{\mathrm{g}}K\right) \,+\, \lambda\left(\frac{1}{\rho}\,-\,\frac{1}{\rho_0}\right). \tag{230}$$

(b). The internal entropy production

With a form for the Helmholtz free energy we can calculate the elastic components of the stresses and couple-stresses, and our irreversible thermodynamic framework naturally allows us to determine the irreversible components as well. The internal entropy production is again given by Eq. (121), with the definitions of $\pi^{\alpha\beta}$ and $\omega^{\alpha\beta}$ unchanged from Eqs. (114) and (115). We then follow the same procedure as in §5 (a) to determine the thermodynamic fluxes and forces, with the assumption that out-of-plane bending is reversible while in-plane flows are dissipative. In this case, the irreversible couple-stresses are given by

$$\omega^{\alpha\beta} \;=\; 0 \tag{231}$$

as in Eq. (183), and the expression for $\pi^{\alpha\beta}$ can be simplified with the incompressibility constraint $v^{\alpha}_{;\alpha} - 2vH = 0$ [see Eq. (52)]—for which Eq. (186) simplifies to

$$\pi^{\alpha\beta} \;=\; \zeta\, a^{\alpha\mu}a^{\beta\nu}\dot{a}_{\mu\nu}\,. \tag{232}$$

Equation (232) indicates there is no longer a two-dimensional dilational viscosity, as expected. With the in-plane heat flux unchanged from Eq. (178), the internal entropy production is given by

$$\rho\eta_{\mathrm{i}} \;=\; \frac{\kappa\, a^{\alpha\beta}T_{,\alpha}\,T_{,\beta}}{T^2} \,+\, \frac{1}{2T}\,\zeta\, a^{\alpha\mu}a^{\beta\nu}\dot{a}_{\alpha\beta}\dot{a}_{\mu\nu} \;\geq\; 0\,. \tag{233}$$

According to Eq. (233), the scalar thermal conductivity κ and the two-dimensional membrane shear viscosity ζ are both positive.

(c). The membrane stresses and couple-stresses

At this point, we have determined both the elastic and irreversible contributions to the membrane stresses and couple-stresses. We begin by rewriting the form of $\pi^{\alpha\beta}$ in Eq. (232) as

$$\pi^{\alpha\beta} \;=\; \zeta\left(v^{\beta}_{;\mu}\,a^{\alpha\mu} \,+\, v^{\alpha}_{;\nu}\,a^{\beta\nu} \,+\, 2v\bar{b}^{\alpha\beta} \,-\, 4vH a^{\alpha\beta}\right). \tag{234}$$

With the expression in Eq. (234), the general results of Table 3 once again hold for an area-incompressible membrane. By substituting Eq. (229) into the results of Table 3, we obtain the stresses and couple-stresses for an area-incompressible membrane with in-plane viscous

Table 5: Stresses and couple-stresses in a single-component, incompressible lipid membrane with viscous in-plane flows. The Helmholtz free energy contains Helfrich and incompressible contributions (230), and the in-plane viscous stresses $\pi^{\alpha\beta}$ are given by Eq. (234).

$\sigma^{\alpha\beta} \;=\; a^{\alpha\beta}\Big(-3k_{\rm b}H^2 \,-\, k_{\rm g}K \,+\, \lambda\Big) \,+\, 2k_{\rm b}H\bar{b}^{\alpha\beta} \,+\, \pi^{\alpha\beta}$
$M^{\alpha\beta} \;=\; k_{\rm b}H\,a^{\alpha\beta} \,+\, k_{\rm g}\bar{b}^{\alpha\beta}$
$N^{\alpha\beta} \;=\; a^{\alpha\beta}\Big(-k_{\rm b}H^2 \,+\, \lambda\Big) \,+\, k_{\rm b}H\bar{b}^{\alpha\beta} \,+\, \pi^{\alpha\beta}$
$S^{\alpha} \;=\; -k_{\rm b}\,a^{\alpha\beta}H_{,\beta}$

flows given in Table 5. All the bending components are identical to those in Table 4, and the quantity $k_{\rm c}\,a^{\alpha\beta}(J-1)$ is replaced by $\lambda\,a^{\alpha\beta}$ in both $\sigma^{\alpha\beta}$ and $N^{\alpha\beta}$. We can thus associate $k_{\rm c}(J-1)$ as the surface tension of a compressible membrane, as noted previously, and λ as the surface tension of an incompressible membrane.

(d). The equations of motion

The equations of motion are determined by substituting the result of Table 5 into the equations of motion [Eqs. (66) and (67)]. However, in comparing the compressible stresses in Table 4 to the incompressible stresses, we note all the bending terms are identical. Thus, we expect only a few differences from the governing equations of a compressible membrane (196)–(198): (*i*) the continuity equation simplifies to the incompressibility constraint, (*ii*) there is no longer a dilational viscosity, and (*iii*) terms involving the compressibility modulus $k_{\rm c}$ are replaced by terms involving the surface tension λ. Indeed, by substituting the results of Table 5 into the equations of motion, we find the governing equations are given by

$$v^{\alpha}_{;\alpha} \,-\, 2vH \;=\; 0\;, \tag{235}$$

$$\begin{aligned}&\rho\Big(v^{\alpha}_{,t} \,+\, v^{\beta}v^{\alpha}_{;\beta} \,-\, 2vv^{\beta}b^{\alpha}_{\beta} \,-\, vv_{,\beta}a^{\alpha\beta}\Big)\\ &\qquad= f^{\alpha} \,+\, a^{\alpha\beta}\lambda_{,\beta} \,+\, \zeta\Big(\Delta_{\rm s}v^{\alpha} \,+\, Kv^{\alpha} \,+\, 2v_{,\beta}Ha^{\alpha\beta} \,-\, 2v_{,\beta}b^{\alpha\beta} \,-\, 2vH_{,\beta}a^{\alpha\beta}\Big)\;,\end{aligned} \tag{236}$$

and

$$\begin{aligned}&\rho\Big(v_{,t} \,+\, 2v^{\alpha}v_{,\alpha} \,+\, v^{\alpha}v^{\beta}b_{\alpha\beta}\Big)\\ &\qquad= f \,+\, 2\lambda H \,-\, 2k_{\rm b}H\Big(H^2-K\Big) \,-\, k_{\rm b}\Delta_{\rm s}H \,+\, 2\zeta\Big(v^{\alpha}_{;\beta}\,b^{\beta}_{\alpha} \,-\, 2v(2H^2-K)\Big)\;.\end{aligned} \tag{237}$$

We note that Eq. (235) was used to simplify Eqs. (236) and (237). Notice that the in-plane equations (236) contain a surface tension gradient, just as the three-dimensional Navier–Stokes equations [Chapter III, Eq. (98)] contain a negative gradient in pressure. Additionally, in the limit where inertial forces, viscous forces, and bending forces are negligible, the shape equation simplifies to $f + 2\lambda H = 0$—which, when $f = [\![p]\!]$ is the pressure drop across the membrane, is the celebrated Young–Laplace equation.

(e). The boundary conditions

Our discussion of relevant boundary conditions for membrane dynamics in §5 (d) was completely general, and only specialized to the case of a compressible membrane when we calculated the components of the boundary force $\boldsymbol{F}$ and moment M in Eqs. (223)–(226). Moreover, as all the bending stresses and forces are identical for compressible and incompressible membranes, we need only to calculate how the surface tension contribution is different. We easily obtain [cf. Eqs. (223)–(226)]

$$F_\nu = \frac{k_\mathrm{b}}{4}\left(\kappa_\tau^2 - \kappa_\nu^2\right) - k_\mathrm{g}\,\xi^2 + \lambda + \pi^{\alpha\beta}\nu_\alpha\nu_\beta \,, \tag{238}$$

$$F_\tau = -\frac{k_\mathrm{b}\,\xi}{2}\left(\kappa_\nu + \kappa_\tau\right) - k_\mathrm{g}\,\xi\,\kappa_\tau + \pi^{\alpha\beta}\tau_\alpha\nu_\beta \,, \tag{239}$$

$$F_n = -\frac{k_\mathrm{b}}{2}\left(\frac{\partial\kappa_\nu}{\partial\nu} + \frac{\partial\kappa_\tau}{\partial\nu}\right) + k_\mathrm{g}\,\frac{\partial\xi}{\partial s} \,, \tag{240}$$

and

$$M = \frac{k_\mathrm{b}}{2}\left(\kappa_\nu + \kappa_\tau\right) + k_\mathrm{g}\kappa_\tau \,, \tag{241}$$

where $\pi^{\alpha\beta}$ is now given by Eq. (234). The Lagrange multiplier λ only enters the boundary force in the direction of the in-plane unit normal $\boldsymbol{\nu}$, thus reinforcing the idea that λ is the membrane surface tension. With Eqs. (235)–(241), and the general result of §5 (d), we determined the governing equations and possible boundary conditions for a single-component, area-incompressible lipid membrane; this concludes our development of the theory. We see that the general equations governing membrane dynamics are highly nonlinear, with in-plane flows and out-of-plane deformations coupled by the continuity equation and curvature of the surface. We probe this coupling in Part C via approximate analytical methods.

References

[1] M. Arroyo and A. DeSimone. "Relaxation dynamics of fluid membranes". *Phys. Rev. E* **79** (2009), 31915–31931

[2] P.B. Canham. "The minimum energy of bending as a possible explanation of the biconcave shape of the human red blood cell". *J. Theor. Biol.* **26** (1970), 61–81

[3] R. Capovilla, J. Guven, and J.A. Santiago. "Deformations of the geometry of lipid vesicles". *J. Phys. A: Math. Gen.* **36** (2003), 6281–6295. arXiv: cond-mat/0212118

[4] P. Chadwick. *Continuum Mechanics: Concise Theory and Problems*. 2nd ed. Mineola: Dover, 1999

[5] E. Cosserat and F. Cosserat. *Théorie des Corps Déformables*. Paris: A. Hermann et Fils, 1909

[6] S.R. de Groot and P. Mazur. *Non-Equilibrium Thermodynamics*. New York: Dover, 1984

[7] J.M. Epstein and K.K. Mandadapu. "Time-reversal symmetry breaking in two dimensional nonequilibrium viscous fluids". *Phys. Rev. E* **101** (2020), 052614. arXiv: 1907.10041

[8] E.A. Evans and R. Skalak. *Mechanics and Thermodynamics of Biomembranes*. Boca Raton: CRC Press, 1980

[9] A.E. Green and P.M. Naghdi. "The Cosserat Surface". *Mechanics of Generalized Continua*. Ed. by E. Kröner. Berlin, Heidelberg: Springer, 1968, pp. 36–48

[10] W. Helfrich. "Elastic properties of lipid bilayers: Theory and possible experiments". *Z. Naturforsch. C* **28** (1973), 693–699

[11] D. Hu, P. Zhang, and W. E. "Continuum theory of a moving membrane". *Phys. Rev. E* **75** (2007), 041605

[12] J.T. Jenkins. "The equations of mechanical equilibrium of a model membrane". *SIAM J. Appl. Math.* **32** (1977), 755–764

[13] K.K. Mandadapu. "Homogeneous Non-Equilibrium Molecular Dynamics Methods for Calculating the Heat Transport Coefficient of Solids and Mixtures". PhD thesis. University of California, Berkeley, 2011

[14] P.M. Naghdi. "The Theory of Shells and Plates". *Linear Theories of Elasticity and Thermoelasticity: Linear and Nonlinear Theories of Rods, Plates, and Shells*. Ed. by C. Truesdell. Berlin, Heidelberg: Springer, 1973, pp. 425–640

[15] J.G. Oldroyd. "On the formulation of rheological equations of state". *P. Roy. Soc. Lond. A Mat.* **200** (1950), 523–541

[16] L. Onsager. "Reciprocal relations in irreversible processes. I.". *Phys. Rev.* **37** (1931), 405–426

[17] L. Onsager. "Reciprocal relations in irreversible processes. II.". *Phys. Rev.* **38** (1931), 2265–2279

[18] I. Prigogine. *Introduction to Thermodynamics of Irreversible Processes*. 3rd ed. New York: Interscience Publishers, 1967

[19] A. Sahu et al. "Irreversible thermodynamics of curved lipid membranes". *Phys. Rev. E* **96** (2017), 042409. arXiv: 1701.06495

[20] D.J. Steigmann. "Fluid films with curvature elasticity". *Arch. Ration. Mech. Anal.* **150** (1999), 127–152

[21] D.J. Steigmann. "On the relationship between the Cosserat and Kirchhoff–Love theories of elastic shells". *Math. Mech. Solids* **4** (1998), 275–288

[22] A.M. Waxman. "Dynamics of a couple-stress fluid membrane". *Studies Appl. Math.* **70** (1984), 63–86

[23] O.-Y. Zhong-can and W. Helfrich. "Instability and deformation of a spherical vesicle by pressure". *Phys. Rev. Lett.* **59** (1987), 2486–2488

Part C

Hydrodynamic Stability

List of important symbols

$A_{(0)}$	generic, base state fundamental unknown
$\tilde{A}$	generic, perturbed fundamental unknown
$\hat{A}_{\boldsymbol{q}}$	normal mode of $\tilde{A}$ corresponding to $\boldsymbol{q}$
ϵ	small parameter used in linearization
$\mathit{\Gamma}$	Föppl–von Kármán number: $\mathit{\Lambda} L^2/k_\mathrm{b}$
ℓ	in-plane length scale arising if $\boldsymbol{v}_{(0)} \neq \boldsymbol{0}$
L	characteristic length scale
$\mathit{\Lambda}$	characteristic surface tension scale
ω	normal mode frequency, assumed complex
$\boldsymbol{q}$	generic normal mode wavevector
Re	membrane Reynolds number: $\rho V L/\zeta$
SL	Scriven–Love number: $\zeta V L/k_\mathrm{b}$
τ	characteristic time scale
V	characteristic velocity scale
$(\cdot)^*$	dimensionless form of the quantity $(\cdot)$
$(\cdot)'$	quantity $(\cdot)$ non-dimensionalized by ℓ

Flat Patches

$\tilde{h}$	perturbed membrane height
q_x, q_y	wavevector components in x and y

Spherical Vesicles

$\dot{\gamma}$	shear rate, often in vesicle experiments
$\mathit{\Omega}$	characteristic angular velocity
φ	azimuthal angle, in spherical coordinates
$\tilde{r}$	perturbed membrane radius
θ	polar angle, in spherical coordinates
$Y_{\ell m}$	scalar spherical harmonics
$\mathbf{Y}_{\ell m}$	vector spherical harmonic (generic)

Cylindrical Tubes

δ	ratio of angular to axial length scales
f_pull	pull force on a cylindrical tether
m	angular wavenumber
ω_0	absolute wavenumber of the saddle point
q	axial wavenumber
q_ms	marginally stable wavenumber
q_0	absolute wavenumber of the saddle point
θ	azimuthal angle, in cylindrical coordinates
SL_ac	absolute-to-convective value of SL
SL_f	dimensionless speed of propagating front

Chapter VI

Introduction and Overview

> *In considering the stability of such a system we essentially seek to determine the reaction of the system to small disturbances. Specifically, we ask: if the system is disturbed, will the disturbance gradually die down, or will the disturbance grow in amplitude in such a way that the system progressively departs from the initial state and never reverts to it? In the former case, we say the system is* stable *with respect to the particular disturbance; and in the latter case, we say that it is* unstable.
>
> —Subrahmanyan Chandrasekhar, 1961 [‡]

In Part B of the present work, we obtained the general equations governing the dynamics of lipid membranes, as well as appropriate boundary conditions. With these results, we now analyze the behavior of lipid membranes in various biologically relevant situations. It is important to reiterate that the governing membrane equations are intricately coupled, highly nonlinear partial differential equations written on a surface which is itself arbitrarily curved and deforming over time. Thus, the dynamical evolution of lipid membranes cannot in general be solved for analytically. Consequently, the present portion of this thesis uses approximate analytical methods to understand the dynamical evolution of biological membranes. Here, our analytical techniques take advantage of an experimental observation: in biological systems, lipid membranes are predominantly observed in one of three geometries, namely flat patches, spheres, and cylinders. For example, at the neuronal synapse, spherical lipid membrane vesicles rapidly develop from planar membrane sheets to recycle lipids and proteins during ultrafast endocytosis. [†] It is also known that spherical white blood cells rapidly rotate as they travel through the blood stream, [*] and additionally that thin membrane tubes can shoot suddenly from the endoplasmic reticulum into the cell cytoplasm [§,♯]—often fusing with

[‡] S. Chandrasekhar. *Hydrodynamic and Hydromagnetic Stability*. New York: Dover, 1981.

[†] S. Watanabe et al. "Ultrafast endocytosis at mouse hippocampal synapses". *Nature* **504** (2013), 242–247.

[*] E. Kolaczkowska and P. Kubes. "Neutrophil recruitment and function in health and inflammation". *Nat. Rev. Immunol.* **13** (2013), 159–175.

[§] M. Terasaki, L.B. Chen, and K. Fujiwara. "Microtubules and the endoplasmic reticulum are highly interdependent structures". *J. Cell Biol.* **103** (1986), 1557–1568.

[♯] J. Nixon-Abell et al. "Increased spatiotemporal resolution reveals highly dynamic dense tubular matrices in the peripheral ER". *Science* **354** (2016), aaf3928.

one another when they cross. Importantly, the general equations governing membrane behavior in the aforementioned situations show in-plane and out-of-plane membrane dynamics are nontrivially coupled through the continuity and curvature of the material [see Chapter V, §6 (d)]. Consequently, the equations governing a flat sheet at the neuronal synapse are different from those describing spherical lipid membrane vesicles carrying chemical cargo in a shear flow, which are again different from the equations governing cylindrical tubes shooting from the endoplasmic reticulum. Moreover, though the general single-component governing equations were first provided in 2007, [‡] there were no additional efforts to methodically analyze membrane dynamics in biologically relevant settings and geometries. As a result, despite much experimental evidence for the dynamic behavior of lipid membranes in biological systems, the physical mechanisms governing membrane motion—and their coupling to membrane geometry—remained poorly understood.

In what follows, we employ the concepts of *non-dimensionalization, scaling* and *hydrodynamic stability* to systematically study how lipid membrane geometry and dynamics are coupled. To this end, we begin by choosing the geometry of the system we would like to consider, and seek to determine a biologically relevant *stationary state*—in which the membrane behavior is not changing in time. For the systems under investigation, a stationary state consists of the membrane position $\boldsymbol{x}_{(0)}(\theta^\alpha)$, velocity $\boldsymbol{v}_{(0)}(\theta^\alpha)$, and surface tension $\lambda_{(0)}(\theta^\alpha)$. Here and from now on, a subscript or superscript '(0)' signifies that a quantity corresponds to the stationary state, which by construction does not vary in time. For any such state, we follow S. Chandrasekhar [†] in asking a fundamental question: How does the membrane respond to an infinitesimal perturbation, and what are the relevant parameters governing the response? This question is systematically addressed for planar, spherical, and cylindrical geometries in Chapters VII, VIII, and IX, respectively. The general procedure we employ is outlined below.

Consider a membrane of a particular geometry, with position $\boldsymbol{x}_{(0)}(\theta^\alpha)$. Now, suppose we begin with a valid stationary state, in which the surface tension and velocity fields (i) satisfy the governing membrane equations and (ii) are consistent with a stationary membrane solution. In practice, a necessary condition for the latter requirement is $v_{(0)} := \boldsymbol{v}_{(0)} \cdot \boldsymbol{n}_{(0)} = 0$. An infinitesimal disturbance is then applied to the system, such that the perturbed state can be represented as

$$\boldsymbol{x}(\theta^\alpha, t) = \boldsymbol{x}_{(0)}(\theta^\alpha) + \epsilon \tilde{\boldsymbol{x}}(\theta^\alpha, t) \,, \tag{1}$$

$$\boldsymbol{v}(\theta^\alpha, t) = \boldsymbol{v}_{(0)}(\theta^\alpha) + \epsilon \tilde{\boldsymbol{v}}(\theta^\alpha, t) \,, \tag{2}$$

and

$$\lambda(\theta^\alpha, t) = \lambda_{(0)}(\theta^\alpha) + \epsilon \tilde{\lambda}(\theta^\alpha, t) \,. \tag{3}$$

In Eqs. (1)–(3) and from now on, ϵ is an infinitesimal dimensionless parameter and a 'tilde' accent denotes a perturbed, time-dependent quantity. We substitute Eqs. (1)–(3) into the general equations governing membrane dynamics, and separate the resultant terms based on the number of factors of ϵ they contain. The terms which only involve unperturbed quantities,

[‡] D. Hu, P. Zhang, and W. E. "Continuum theory of a moving membrane". *Phys. Rev. E* **75** (2007), 041605.

[†] Chandrasekhar, *Hydrodynamic and Hydromagnetic Stability*.

i.e. those with no factors of ϵ, correspond to the stationary state. As such terms already satisfy the governing equations, they do not contribute to the dynamics of the perturbed system. Next, since the parameter ϵ is assumed to be infinitesimal, all terms containing two or more powers of ϵ can be neglected relative to those terms which are linear in the perturbed variables. The resultant *linearized equations* govern the temporal evolution of a membrane of a particular geometry, subject to small disturbances. The following sections discuss how we study such equations: a convenient form of the governing equations is provided in §1, non-dimensionalization and scaling are discussed in §2, and the general procedure to assess the stability of the system is presented in §3.

1. The general governing equations

The general equations governing single-component, area-incompressible lipid membranes are provided in Chapter V, Eqs. (235)–(237). [‡] However, these equations are presented in a compact form, where we understand covariant derivatives are to be expanded using the Christoffel symbols. As small disturbances to the membrane shape will correspondingly alter the Christoffel symbols, it is convenient to expand all covariant derivatives and provide the governing equations in a form more amenable to linearization. To this end, we begin with the continuity equation [Chapter V, Eq. (235)], which involves the covariant derivative $v^\alpha_{;\alpha}$ and is easily expanded to yield

$$v^\alpha_{,\alpha} + \Gamma^\alpha_{\alpha\beta} v^\beta - 2vH = 0 \,. \tag{4}$$

We next consider the in-plane equations, which are presented as Eq. (236) in Chapter V. Here, the inertial terms involve the covariant derivative $v^\alpha_{;\beta}$, which is equivalently expressed as $v^\alpha_{,\beta} + \Gamma^\alpha_{\beta\mu} v^\mu$. However, the in-plane viscous stresses now involve the surface Laplacian of the in-plane velocity components, $\Delta_{\mathrm{s}} v^\alpha = v^\alpha_{;\beta\mu} a^{\beta\mu}$. Some care is required when expanding the two covariant derivatives, and we find

$$v^\alpha_{;\beta\mu} = v^\alpha_{,\beta\mu} + \Gamma^\alpha_{\beta\nu,\mu} v^\nu + \Gamma^\alpha_{\beta\nu} v^\nu_{,\mu} + \Gamma^\alpha_{\mu\nu} v^\nu_{,\beta} + \Gamma^\alpha_{\mu\nu}\Gamma^\nu_{\beta\gamma} v^\gamma - \Gamma^\nu_{\beta\mu} v^\alpha_{,\nu} - \Gamma^\nu_{\beta\mu}\Gamma^\alpha_{\nu\gamma} v^\gamma \,.$$

The in-plane equations, without body forces, are then given by [cf. Chapter V, Eq. (236)]

$$\begin{aligned} &\rho\left(v^\alpha_{,t} - v v_{,\beta} a^{\alpha\beta} - 2v v^\beta b^\alpha_\beta + v^\beta\left(v^\alpha_{,\beta} + \Gamma^\alpha_{\lambda\beta} v^\lambda\right)\right) \\ &\quad = \zeta\Big[2\left(v_{,\beta} H - v H_{,\beta}\right) a^{\alpha\beta} + K v^\alpha + \Big(v^\alpha_{,\beta\mu} + \Gamma^\alpha_{\beta\nu,\mu} v^\nu + \Gamma^\alpha_{\beta\nu} v^\nu_{,\mu} \\ &\qquad + \Gamma^\alpha_{\mu\nu} v^\nu_{,\beta} + \Gamma^\alpha_{\mu\nu}\Gamma^\nu_{\beta\gamma} v^\gamma - \Gamma^\nu_{\beta\mu} v^\alpha_{,\nu} - \Gamma^\nu_{\beta\mu}\Gamma^\alpha_{\nu\gamma} v^\gamma\Big) a^{\beta\mu} - 2 v_{,\mu} b^{\mu\alpha}\Big] + a^{\alpha\beta}\lambda_{,\beta} \,. \end{aligned} \tag{5}$$

We finally examine the shape equation [Chapter V, Eq. (237)], which contains two terms with covariant derivatives: $v^\alpha_{;\beta}$ and $\Delta_{\mathrm{s}} H$. The former is easily expanded, and we also recall that $H_{;\alpha} = H_{,\alpha}$ is a vector component. Thus, the surface Laplacian of the mean curvature

[‡] For the remainder of this thesis, we consider only area-incompressible lipid membranes for simplicity.

is given by $\Delta_{\mathrm{s}} H = (H_{,\alpha\beta} - \Gamma^{\mu}_{\alpha\beta} H_{,\mu}) a^{\alpha\beta}$, and the shape equation is equivalently written as

$$\begin{aligned} \rho \left(v_{,t} + 2 v^{\alpha} v_{,\alpha} + v^{\alpha} v^{\beta} b_{\alpha\beta} \right) & \\ = \llbracket p \rrbracket + 2\lambda H - 2 k_{\mathrm{b}} \left(H^3 - H K \right) - k_{\mathrm{b}} \left(H_{,\alpha\beta} - \Gamma^{\mu}_{\alpha\beta} H_{,\mu} \right) a^{\alpha\beta} & \\ + \zeta \left(2 b^{\beta}_{\alpha} \left(v^{\alpha}_{,\beta} + \Gamma^{\alpha}_{\beta\mu} v^{\mu} \right) - 4 v \left(2H^2 - K \right) \right) . & \end{aligned} \tag{6}$$

In Eq. (6) and from now on, we use the symbol $\llbracket p \rrbracket$ to denote the jump in normal stress across the membrane surface—which is usually attributed to the jump in hydrodynamic pressure in the surrounding fluid. Equations (4)–(6) are respectively the continuity, in-plane, and shape equations governing an area-incompressible, single-component lipid membrane, and are identical to Eqs. (235)–(237) in Chapter V.

2. The Scriven–Love and Föppl–von Kármán numbers

With the linearized equations, our first task is to determine how many independent parameters govern the dynamics of the membrane. To this end, we non-dimensionalize the governing equations via a scaling analysis. When the dynamics of the surrounding medium are neglected, three dimensionless numbers govern membrane dynamics, only two of which are relevant. [‡] To see how the first of these numbers emerges, we reproduce the in-plane equations, without body forces, as [cf. Chapter V, Eqs. (66) and (236)]

$$\underbrace{\rho c^{\alpha}}_{O(\rho V^2/L)} = \underbrace{a^{\alpha\beta} \lambda_{,\beta}}_{O(\Lambda/L)} + \underbrace{\pi^{\beta\alpha}_{;\beta}}_{O(\zeta V/L^2)} . \tag{7}$$

In Eq. (7), each term is annotated with its order of magnitude. Here, L is a typical length in the system, V is a typical velocity scale, and Λ is the scale of the surface tension; the dimension of all quantities is provided in Table 1. By taking the ratio of inertial to viscous forces, we obtain the well-known Reynolds number Re, given by

$$Re := \frac{\rho V L}{\zeta} . \tag{8}$$

As is generally the case in cellular and sub-cellular systems, [†] the Reynolds number is exceedingly small in the situations we consider. Inertial forces can then, to an excellent approximation, be entirely neglected in the study of membrane dynamics. It is useful to note the right-hand side of Eq. (7) can be written as $(\lambda a^{\alpha\beta} + \pi^{\beta\alpha})_{;\beta}$, i.e. the surface divergence of the in-plane fluid stresses $\lambda a^{\alpha\beta} + \pi^{\alpha\beta}$.

[‡] If we consider a membrane surrounded by a Newtonian fluid, and include the dynamics of the fluid as the membrane deforms, then an additional dimensionless parameter emerges. The Boussinesq number $Bo := \zeta/(\mu L)$ compares the dissipative mechanisms of in-plane lipid flow and the flow of the surrounding fluid; here μ is the fluid shear viscosity and L is a characteristic length scale. In the systems of interest, $Bo \gg 1$, and dissipation is primarily driven by the intramembrane viscosity. Consequently, the dynamics of the surrounding fluid are not considered in this work.

[†] E.M. Purcell. "Life at low Reynolds number". *Am. J. Phys.* **45** (1977), 3–11.

Table 1: Dimension and units of various membrane quantities.

Sym.	Parameter	Dimension	Units
ρ	mass density	mass/length^2	pg/nm^2
V	velocity	length/time	nm/μsec
L	typical length	length	nm
Λ	surface tension	force/length	pN/nm
ζ	membrane viscosity	force·time/length	pN · μsec/nm
k_b	bending modulus	force·length	pN · nm

We now consider the membrane shape equation, which in the absence of body forces can be written as [cf. Chapter V, Eqs. (67) and (237)]

$$\underbrace{\rho c}_{O(\rho V^2/L)} = \underbrace{\lambda a^{\alpha\beta} b_{\alpha\beta}}_{O(\Lambda/L)} + \underbrace{\pi^{\alpha\beta} b_{\alpha\beta}}_{O(\zeta V/L^2)} + \underbrace{k_\mathrm{b}\big[-2H\big(H^2-K\big) - \Delta_\mathrm{s} H\big]}_{O(k_\mathrm{b}/L^3)} . \tag{9}$$

Before discussing the order of magnitude of the various terms in Eq. (9), it is useful to discuss their origin. The inertial term ρc is expected, as it accounts for the out-of-plane acceleration of the surface. Terms involving the bending modulus k_b are also not surprising, as lipid membranes are known to bend in the out-of-plane direction. The two remaining terms in Eq. (9), $(\lambda a^{\alpha\beta} + \pi^{\alpha\beta}) b_{\alpha\beta}$, couple the in-plane fluid stresses to membrane curvature and lead to both tensile and viscous forces in the normal direction. Interestingly, the viscous forces arise despite the membrane deforming elastically, or reversibly, in the out-of-plane direction [see Chapter V, §5 (a)]. To understand how in-plane stresses lead to out-of-plane forces, first consider the surface tension term in Eq. (9). The stress associated with the surface tension, $\lambda a^{\alpha\beta}$, is in-plane and isotropic—yet when the membrane is curved and $H = \frac{1}{2} a^{\alpha\beta} b_{\alpha\beta} \neq 0$, the surface tension acts in different directions at different locations (see Fig. 1a). These contributions sum to give the well-known $\lambda a^{\alpha\beta} b_{\alpha\beta} = 2\lambda H$ term in the shape equation, often called the Laplace pressure. Now consider the shear stresses arising from a planar extensional flow, for which streamlines and boundary tractions are shown on the left-hand side of Fig. 1b as solid and dotted arrows, respectively. Just as in the case of the surface tension, when the membrane is curved, the viscous stresses act in different directions at different locations on the surface and give rise to the $\pi^{\alpha\beta} b_{\alpha\beta}$ force in the normal direction (Fig. 1b).

With an understanding of the origin of all the terms in the shape equation (9), we return to our original question regarding the different parameters governing membrane dynamics. A comparison of the out-of-plane tension forces to bending forces yields the Föppl–von Kármán number,[‡] denoted Γ and defined as

$$\Gamma := \frac{\Lambda L^2}{k_\mathrm{b}} . \tag{10}$$

[‡]J. Lidmar, L. Mirny, and D.R. Nelson. "Virus shapes and buckling transitions in spherical shells". *Phys. Rev. E* **68** (2003), 051910.

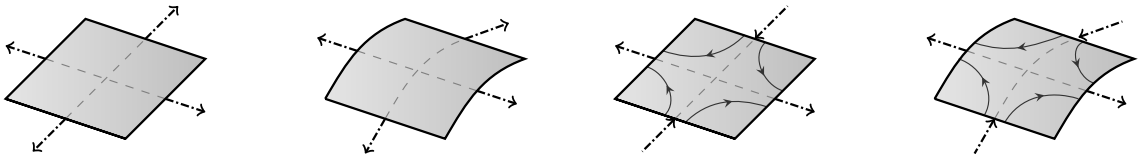

(a) tension forces: $\lambda a^{\alpha\beta} b_{\alpha\beta} = 2\lambda H$ (b) viscous forces: $\pi^{\alpha\beta} b_{\alpha\beta}$

Figure 1: A schematic showing how surface tension and viscous forces arise in the normal direction, with dashed arrows depicting boundary tractions. (a) The surface tension λ pulls the membrane at each edge, such that when the shape is perturbed a normal force $2\lambda H$ arises. (b) In an extensional flow, the velocity field is given by $\boldsymbol{v} = \dot{\gamma}\,(x\boldsymbol{e}_x - y\boldsymbol{e}_y)$ for strain rate $\dot{\gamma}$, as depicted by the solid arrows. The tractions push and pull the fluid, as shown with the dashed arrows. When the membrane is perturbed, a viscous force $\pi^{\alpha\beta} b_{\alpha\beta}$ arises in the normal direction.

Tension forces in the out-of-plane direction are well-understood from the study of soap bubbles and the Young–Laplace equation. Accordingly, tensile forces are generally properly accounted for in membrane studies, where the Föppl–von Kármán number naturally emerges—though it is sometimes referred to as the dimensionless surface tension.

While the Laplace pressure is expected in the shape equation from the study of bubbles and droplets, the connection between in-plane viscous stresses and membrane curvature was not well-established prior to our own efforts. [‡] By comparing the magnitude of out-of-plane viscous forces and bending forces, we found a new dimensionless number—named the Scriven–Love number, denoted $\mathcal{SL}$ and given by

$$\mathcal{SL} := \frac{\zeta V L}{k_{\mathrm{b}}} \,. \tag{11}$$

The Scriven–Love number was named in honor of the seminal works on the surface flows of arbitrarily curved two-dimensional fluids by Scriven [†] and on the elasticity of two-dimensional shells by Love. [*] However, because the out-of-plane viscous forces were previously not well-understood, they were often omitted from prior investigations. [§, ♯, ‖, ∀, ◇, $]

[‡] A. Sahu et al. "Geometry and dynamics of lipid membranes: The Scriven–Love number". *Phys. Rev. E* **101** (2020), 052401. arXiv: 1910.10693.

[†] L.E. Scriven. "Dynamics of a fluid interface: Equation of motion for Newtonian surface fluids". *Chem. Eng. Sci.* **12** (1960), 98–108.

[*] A.E.H. Love. *A Treatise on the Mathematical Theory of Elasticity*. 4th ed. New York: Dover, 1944.

[§] T.R. Powers, G. Huber, and R.E. Goldstein. "Fluid-membrane tethers: Minimal surfaces and elastic boundary layers". *Phys. Rev. E* **65** (2002), 041901. arXiv: cond-mat/0201290.

[♯] J. Guven. "Membrane geometry with auxiliary variables and quadratic constraints". *J. Phys. A: Math. Gen.* **37** (2004), L313–L319.

[‖] A. Agrawal and D.J. Steigmann. "Boundary-value problems in the theory of lipid membranes". *Continuum Mech. Therm.* **21** (2009), 57–82.

[∀] H. Zhao and E.S.G. Shaqfeh. "The dynamics of a vesicle in simple shear flow". *J. Fluid Mech.* **674** (2011), 578–604.

[◇] A. Maitra et al. "Activating membranes". *Phys. Rev. Lett.* **112** (2014), 258101.

[$] S.C. Al-Izzi et al. "Hydro-osmotic instabilities in active membrane tubes". *Phys. Rev. Lett.* **120** (2018), 138102. arXiv: 1709.02703.

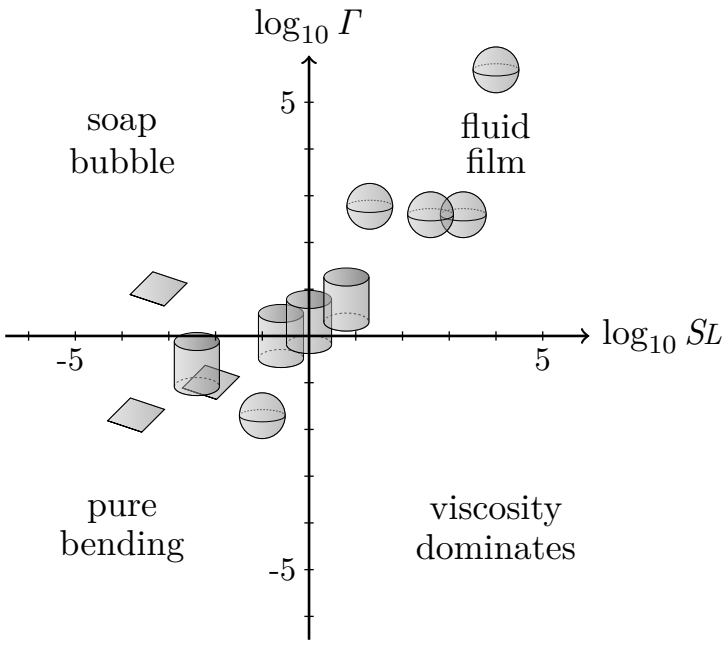

Figure 2: Plot of the Scriven–Love number $\mathcal{SL}$ (11) and Föppl–von Kármán number Γ (10) in past experiments involving planar, spherical, and cylindrical geometries. The magnitude of these two parameters governs the constitutive behavior of the membrane. For example, in the lower left quadrant the out-of-plane bending forces dominates, while in the upper right quadrant these forces are negligible. The experimental details for membranes with planar, spherical, and cylindrical morphologies are respectively provided in Chapters VII, VIII, and IX.

Though the Scriven–Love number was implicitly set to zero in the many studies which ignore viscous in-plane flows, we seek to determine its relevance—as well as the importance of tensile forces—in governing the dynamics of biological systems. To this end, we analyze the linearized dynamics of planar, spherical, and cylindrical membranes in subsequent chapters, and determine the relevant length, velocity, and surface tension scales. We then examine past experimental results, and calculate $\mathcal{SL}$ and Γ when sufficient data is reported for us to do so. Figure 2 summarizes the findings from this analysis, and also shows how the values of $\mathcal{SL}$ and Γ dictate the approximate constitutive behavior of a biological membrane. For example, if $\mathcal{SL} \ll 1$ and $\Gamma \ll 1$, then bending forces dominate the membrane shape. If instead $\mathcal{SL} \ll 1$ while $\Gamma \gg 1$, then tension forces dominate bending and viscous forces—for which the membrane behaves constitutively like a soap bubble. As mentioned previously, the scenarios where $\mathcal{SL} \ll 1$ were generally properly accounted for in prior studies, as viscous forces do not significantly affect membrane shape. However, all experiments in which $\mathcal{SL} \geq 1$ have non-negligible viscous forces in the normal direction. Figure 2 shows $\mathcal{SL} \gg 1$ and $\Gamma \gg 1$ in several experiments involving spherical vesicles and cylindrical tubes, such that the membrane behaves constitutively more like a fluid film than an elastic shell. In such cases, the out-of-plane forces are highly coupled to in-plane flows. Consequently, it is generally necessary to incorporate all hydrodynamic couplings between in-plane and out-of-plane behavior when analyzing membrane dynamics.

3. The analysis in terms of normal modes

Our earlier discussion details how, for a given geometry, the linearized equations governing infinitesimal disturbances are obtained and expressed in dimensionless form. The task now at hand is to investigate the dynamical response of the stationary state to small perturbations. Moreover, since our scaling analysis revealed Γ and $\mathcal{SL}$ to be the relevant parameters characterizing the system's response, we investigate how the membrane responds over biologically relevant ranges of these two dimensionless numbers.

As is common in a *linear stability analysis* of a dynamical system, we seek to characterize how membranes of a particular geometry respond to any arbitrary perturbation. If, for even a single disturbance, the system does not return to the stationary state but rather departs to another state, then the system is said to be *unstable*. Conversely, if the system always returns to its starting state, then it is referred to as *stable*. In order to represent the entire range of permissible disturbances, it is natural to decompose the arbitrary disturbance into a complete set of normal modes. Symbolically, such a decomposition is written as

$$\tilde{A}(\theta^\alpha, t) \;=\; \sum_{\boldsymbol{q}} \hat{A}_{\boldsymbol{q}}(\theta^\alpha)\, \mathrm{e}^{-i\omega t}\;, \tag{12}$$

where $\tilde{A}$ represents any perturbed membrane unknown and $\boldsymbol{q}$ represents the various independent modes pertaining to a specific geometry. By substituting Eq. (12) into the linearized equations and recognizing the different modes are independent, we can solve for the frequency $\omega = \omega(\boldsymbol{q})$, which captures the temporal evolution of each mode and is often referred to as the *dispersion relation*. The time evolution of the system also depends on the Föppl–von Kármán and Scriven–Love numbers; this dependence is sometimes explicitly written as $\omega = \omega(\boldsymbol{q}; \Gamma, \mathcal{SL})$.

In the normal mode analysis, the frequency ω is in general complex, here represented as $\omega = \omega^{(r)} + i\omega^{(i)}$. The decomposition in Eq. (12) can then be rewritten as

$$\tilde{A}(\theta^\alpha, t) \;=\; \sum_{\boldsymbol{q}} \hat{A}_{\boldsymbol{q}}(\theta^\alpha)\, \mathrm{e}^{-i\omega^{(r)}t}\, \mathrm{e}^{\omega^{(i)}t}\;. \tag{13}$$

From Eq. (13), it is immediately clear that the imaginary part of the complex frequency informs us as to whether the system is stable or unstable. If $\omega^{(i)}(\boldsymbol{q}; \Gamma, \mathcal{SL}) < 0$ for all $\boldsymbol{q}$, and over all biologically relevant values of the parameters Γ and $\mathcal{SL}$, then the system is stable. On the other hand, if there exists even a single mode $\boldsymbol{q}$, and choice of Γ and $\mathcal{SL}$, for which $\omega^{(i)} > 0$, then the system is unstable. For an unstable mode, the real part of the frequency dictates the nature of the temporal response. In particular, if $\omega^{(r)} = 0$ then the instability will grow monotonically, while if $\omega^{(r)} \neq 0$ then we expect an oscillatory response as the instability grows.

The above discussion outlines the general procedure with which we investigate the stability of a stationary state, i.e. a stationary solution of the governing equations. In the following chapters, we apply these techniques to three commonly observed membrane geometries in biological systems: flat patches (Chapter VII), spherical vesicles (Chapter VIII), and cylindrical tubes (Chapter IX).

References

[1] A. Agrawal and D.J. Steigmann. "Boundary-value problems in the theory of lipid membranes". *Continuum Mech. Therm.* **21** (2009), 57–82

[2] S. Chandrasekhar. *Hydrodynamic and Hydromagnetic Stability*. New York: Dover, 1981

[3] J. Guven. "Membrane geometry with auxiliary variables and quadratic constraints". *J. Phys. A: Math. Gen.* **37** (2004), L313–L319

[4] D. Hu, P. Zhang, and W. E. "Continuum theory of a moving membrane". *Phys. Rev. E* **75** (2007), 041605

[5] S.C. Al-Izzi et al. "Hydro-osmotic instabilities in active membrane tubes". *Phys. Rev. Lett.* **120** (2018), 138102. arXiv: 1709.02703

[6] E. Kolaczkowska and P. Kubes. "Neutrophil recruitment and function in health and inflammation". *Nat. Rev. Immunol.* **13** (2013), 159–175

[7] J. Lidmar, L. Mirny, and D.R. Nelson. "Virus shapes and buckling transitions in spherical shells". *Phys. Rev. E* **68** (2003), 051910

[8] A.E.H. Love. *A Treatise on the Mathematical Theory of Elasticity*. 4th ed. New York: Dover, 1944

[9] A. Maitra et al. "Activating membranes". *Phys. Rev. Lett.* **112** (2014), 258101

[10] J. Nixon-Abell et al. "Increased spatiotemporal resolution reveals highly dynamic dense tubular matrices in the peripheral ER". *Science* **354** (2016), aaf3928

[11] T.R. Powers, G. Huber, and R.E. Goldstein. "Fluid-membrane tethers: Minimal surfaces and elastic boundary layers". *Phys. Rev. E* **65** (2002), 041901. arXiv: cond-mat/0201290

[12] E.M. Purcell. "Life at low Reynolds number". *Am. J. Phys.* **45** (1977), 3–11

[13] A. Sahu et al. "Geometry and dynamics of lipid membranes: The Scriven–Love number". *Phys. Rev. E* **101** (2020), 052401. arXiv: 1910.10693

[14] L.E. Scriven. "Dynamics of a fluid interface: Equation of motion for Newtonian surface fluids". *Chem. Eng. Sci.* **12** (1960), 98–108

[15] M. Terasaki, L.B. Chen, and K. Fujiwara. "Microtubules and the endoplasmic reticulum are highly interdependent structures". *J. Cell Biol.* **103** (1986), 1557–1568

[16] S. Watanabe et al. "Ultrafast endocytosis at mouse hippocampal synapses". *Nature* **504** (2013), 242–247

[17] H. Zhao and E.S.G. Shaqfeh. "The dynamics of a vesicle in simple shear flow". *J. Fluid Mech.* **674** (2011), 578–604

Chapter VII

Flat Membrane Patches

> *Let us imagine ourselves inhabitants of a surface. Like the Lines and Polygons who populate Abbott's* Flatland [‡] *we are not aware of a third dimension except as an abstract mathematical notion. Unlike the inhabitants of* Flatland *we find that our surface may at times have curvature—curvature which changes with time. As hydrodynamicists and engineers we seek to describe mathematically the motion of material in our world . . .*
>
> —Laurence E. Scriven, 1960 [†]

We begin our hydrodynamic stability analysis by studying nearly planar lipid membranes. Following the procedure outline in Chapter VI, we first obtain the unperturbed equations describing an undeformed flat membrane. We then select two stationary states: one without a flow of lipids, and one with an in-plane flow of lipids. In each case, an infinitesimal disturbance is applied to the system. The linearized equations are then obtained and subsequently non-dimensionalized. Regardless of whether or not there is a base flow, the Föppl–von Kármán number Γ determines the relative importance of surface tension and bending forces in governing the membrane's dynamical response to a shape perturbation. Interestingly, however, the Scriven–Love number $\mathcal{SL}$ arises only in the stationary state with a base flow—in which case it quantifies the relative importance of out-of-plane viscous forces to bending forces. An investigation of past experimental data reveals that even in biologically relevant systems with an in-plane flow of lipids, $\mathcal{SL} \ll 1$. Accordingly, membrane shape changes about planar geometries are governed by surface tension and bending forces—irrespective of whether lipids are flowing in the stationary state.

Once the linearized governing equations are obtained and non-dimensionalized, a natural next step is to investigate the stability of the aforementioned stationary states by following the procedure outlined in Chapter VI, §3. However, when the hydrodynamics of the surrounding fluid are neglected, we find the linearized equations admit only the trivial solution in which all perturbed quantities are zero. These seemingly unphysical results can be remedied by including the fluid flows in the surrounding medium, which are induced when the membrane shape is disturbed, or by considering the second-order governing equations—

[‡] E.A. Abbott. *Flatland: A Romance of Many Dimensions*. 6th ed. New York: Dover, 1952.

[†] L.E. Scriven. "Dynamics of a fluid interface: Equation of motion for Newtonian surface fluids". *Chem. Eng. Sci.* **12** (1960), 98–108.

where each term is $\mathcal{O}(\epsilon^2)$. However, both of these analyses are outside the scope of this thesis: the hydrodynamics of the surrounding medium are not incorporated here, and we also do not consider higher-order effects.

1. The unperturbed equations

Consider a perfectly flat lipid membrane patch with a characteristic size L, as shown in Fig. 1a. The surface is parametrized by the canonical Cartesian coordinates

$$\theta^1 := x \in [0, L] \qquad \text{and} \qquad \theta^2 := y \in [0, L] \,. \tag{1}$$

In this case, the unperturbed position is written as

$$\boldsymbol{x}_{(0)}(x, y) = x\boldsymbol{e}_1 + y\boldsymbol{e}_2 \,, \tag{2}$$

where $\boldsymbol{e}_1$ and $\boldsymbol{e}_2$ are the usual Cartesian unit vectors. With a parametrization of the surface, all geometric quantities described in Chapter II, §2 can be calculated. We find

$$\begin{aligned} &\boldsymbol{a}^{(0)}_\alpha = \boldsymbol{e}_\alpha \,, \qquad a^{(0)}_{\alpha\beta} = \delta_{\alpha\beta} \,, \qquad a^{\alpha\beta}_{(0)} = \delta^{\alpha\beta} \,, \qquad \boldsymbol{n}_{(0)} = \boldsymbol{e}_3 \,, \\ &b^{(0)}_{\alpha\beta} = 0 \,, \qquad H_{(0)} = 0 \,, \qquad K_{(0)} = 0 \,, \qquad \Gamma^{\alpha\,(0)}_{\lambda\mu} = 0 \,, \end{aligned} \tag{3}$$

where $\delta_{\alpha\beta}$ and $\delta^{\alpha\beta}$ denote the Kronecker delta.

Next, we consider the kinematics of a planar stationary state. For a perfectly flat membrane, the surface by construction does not deform in time. The normal velocity $v_{(0)}$ then satisfies $v_{(0)} := \boldsymbol{v}_{(0)} \cdot \boldsymbol{n}_{(0)} = 0$. Accordingly, the velocity $\boldsymbol{v}_{(0)}$ lies entirely in the plane of the membrane, and is expressed as

$$\boldsymbol{v}_{(0)} = v^1_{(0)}\,\boldsymbol{e}_1 + v^2_{(0)}\,\boldsymbol{e}_2 \,. \tag{4}$$

As the stationary state corresponding to any fixed geometry has zero out-of-plane velocity by definition, we will find the unperturbed velocity always lies in the tangent plane to the undisturbed surface—irrespective of the starting geometry.

Finally, by substituting Eqs. (3) and (4) into the general continuity, in-plane, and shape equations [see Chapter VI, Eqs. (4)–(6)], we respectively obtain

$$v^\alpha_{(0),\alpha} = 0 \,, \tag{5}$$

$$\rho\, v^\beta_{(0)}\, v^\alpha_{(0),\beta} = \delta^{\alpha\beta}\lambda_{(0),\beta} + \zeta\left(v^\alpha_{(0),xx} + v^\alpha_{(0),yy}\right) \,, \tag{6}$$

and

$$[\![p]\!] = 0 \,. \tag{7}$$

The continuity equation (5) and in-plane equations (6) are identical to the continuity and Navier–Stokes equations of an incompressible two-dimensional Newtonian fluid, in which the pressure is replaced with the negative surface tension [cf. Chapter III, Eq. (98)] and $v^\alpha_{(0),t} = 0$ in the stationary state. The shape equation (7) indicates that for a perfectly flat membrane, there are no out-of-plane forces arising from viscous–curvature coupling, surface tension, or the bending energy.

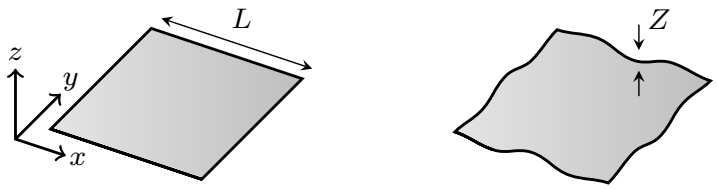

(a) unperturbed: $\boldsymbol{x}_{(0)}(x,y)$ (b) perturbed: $\boldsymbol{x}(x,y,t)$

Figure 1: Schematic of the unperturbed (a) and perturbed (b) flat plane geometries. The membrane patch has a characteristic length L, and perturbations are of a characteristic height Z, with $\epsilon := Z/L \ll 1$.

2. The perturbed equations

We now introduce a height disturbance in the normal direction, such that the perturbed membrane position is given by

$$\boldsymbol{x}(x,y,t) \;=\; \underbrace{x\boldsymbol{e}_1 \,+\, y\boldsymbol{e}_2}_{\boldsymbol{x}_{(0)}(x,y)} \,+\, \epsilon\,\tilde{h}(x,y,t)\,\boldsymbol{e}_3 \;. \tag{8}$$

In Eq. (8), the total height perturbation $\epsilon\,\tilde{h}(\theta^\alpha,t)$ is assumed to be $O(Z)$, where $Z \ll L$ by construction. In this case, $\epsilon := Z/L$ is a small parameter and $\tilde{h}$ is $O(L)$, as depicted in Fig. 1b. The surface parametrization in Eq. (8) is commonly used in the study of nearly planar surfaces, and is called the Monge parametrization. [‡] The height disturbance modifies the geometry of the surface, and to first order in ϵ we employ the results of Chapter II, §2 to find

$$\begin{gathered}
\boldsymbol{a}_\alpha \;=\; \boldsymbol{e}_\alpha + \epsilon\tilde{h}_{,\alpha}\boldsymbol{e}_3 \;, \qquad a_{\alpha\beta} \;=\; \delta_{\alpha\beta} \;, \qquad a^{\alpha\beta} \;=\; \delta^{\alpha\beta} \;, \qquad \boldsymbol{n} \;=\; \boldsymbol{e}_3 - \epsilon\tilde{h}_{,1}\boldsymbol{e}_1 - \epsilon\tilde{h}_{,2}\boldsymbol{e}_2 \;, \\
b_{\alpha\beta} \;=\; \epsilon\,\tilde{h}_{,\alpha\beta} \;, \qquad \Gamma^{\mu}_{\alpha\beta} \;=\; 0 \;, \qquad H \;=\; \frac{1}{2}\,\epsilon\,\Delta_{\mathrm{s}}\tilde{h} \;, \qquad \text{and} \qquad K \;=\; 0 \;.
\end{gathered} \tag{9}$$

In Eq. (9), Δ_{s} denotes the surface Laplacian [see Chapter II, Eq. (30)]. For scalar quantities on a nearly planar membrane, the surface Laplacian is given by

$$\Delta_{\mathrm{s}}\,(\,\cdot\,) \;:=\; (\,\cdot\,)_{,xx} \,+\, (\,\cdot\,)_{,yy} \;, \tag{10}$$

and is identical to the two-dimensional Cartesian Laplacian.

Just as we applied a shape disturbance in Eq. (8), the membrane velocity components and surface tension are similarly expanded as

$$\begin{gathered}
v^1 \;=\; v^1_{(0)} \,+\, \epsilon\,\tilde{v}^1 \;, \qquad\qquad v^2 \;=\; v^2_{(0)} \,+\, \epsilon\,\tilde{v}^2 \;, \\
v \;=\; \epsilon\,\tilde{h}_{,t} \;, \qquad\qquad \text{and} \qquad\qquad \lambda \;=\; \lambda_{(0)} \,+\, \epsilon\,\tilde{\lambda} \;,
\end{gathered} \tag{11}$$

[‡] G. Monge. *Application de l'analyse à la géométrie*. Paris: Bernard, 1807.

where the parameter ϵ captures the smallness of the perturbations to the velocity components and surface tension. In Eq. (11), quantities with a 'tilde' accent are assumed to be of the same order as their unperturbed counterparts. For example, $v^\alpha_{(0)}$ and $\tilde{v}^\alpha$ are both the same order, and the smallness of the velocity perturbation is contained in ϵ. The normal velocity component v in Eq. $(11)_3$ is calculated from the definition [see Chapter V, §1 (c)]

$$\begin{aligned} v &= \boldsymbol{x}_{,t} \cdot \boldsymbol{n} \\ &= \epsilon\, \tilde{h}_{,t}\, \boldsymbol{e}_3 \cdot \left(\boldsymbol{e}_3 - \epsilon\, \tilde{h}_{,x}\, \boldsymbol{e}_1 - \epsilon\, \tilde{h}_{,y}\, \boldsymbol{e}_2 \right) \\ &= \epsilon\, \tilde{h}_{,t} \ . \end{aligned} \tag{12}$$

Substituting Eqs. (9) and (11) into the general governing equations in Chapter VI, §1 and keeping terms to first order in ϵ, the linearized perturbed equations are obtained as [‡]

$$\tilde{v}^\alpha_{,\alpha} = 0 \ , \tag{13}$$

$$\rho\left(\tilde{v}^\alpha_{,t} + \tilde{v}^\beta\, v^\alpha_{(0),\beta} + v^\beta_{(0)}\, \tilde{v}^\alpha_{,\beta} \right) = \delta^{\alpha\beta}\, \tilde{\lambda}_{,\beta} + \zeta \left(\tilde{v}^\alpha_{,xx} + \tilde{v}^\alpha_{,yy} \right) \ , \tag{14}$$

and

$$\rho\left(\tilde{h}_{,tt} + 2 v^\alpha_{(0)}\, \tilde{h}_{,t\alpha} + v^\alpha_{(0)}\, v^\beta_{(0)}\, \tilde{h}_{,\alpha\beta} \right) = 2\zeta\, \tilde{h}_{,\alpha\lambda}\, \delta^{\lambda\beta}\, v^\alpha_{(0),\beta} - \frac{1}{2}\, k_\mathrm{b}\, \Delta_\mathrm{s}^2\, \tilde{h} + \lambda_{(0)}\, \Delta_\mathrm{s} \tilde{h} \ . \tag{15}$$

Equation (15) indicates that velocity gradients in the base state ($v^\alpha_{(0),\beta} \neq 0$) lead to viscous forces in the normal direction, and bring about the Scriven–Love number. In the following sections, the unperturbed (5)–(7) and perturbed (13)–(15) governing equations are non-dimensionalized for two cases: (i) an initially static membrane, and (ii) a membrane with an initial base flow.

3. The dynamics about an initially static patch

We first non-dimensionalize the unperturbed and perturbed governing equations in the case of an initially flat, static lipid membrane, for which $\boldsymbol{v}_{(0)} = \boldsymbol{0}$. According to Eqs. (5)–(7), $\lambda_{(0)}$ is a constant, which we denote λ_0 and assume to be known from how the membrane patch is constrained at its boundary. The unperturbed solution is then written as

$$v^\alpha_{(0)} = 0 \ , \qquad v_{(0)} = 0 \ , \qquad \text{and} \qquad \lambda_{(0)} = \lambda_0 \ . \tag{16}$$

We introduce the surface tension scale $\mathit{\Lambda}$ as

$$\mathit{\Lambda} := \lambda_0 \ , \tag{17}$$

[‡]As discussed in Chapter V, §1 (c), the form of the acceleration in our prior works contained an error. Here, the factor of 2 appearing in the left-hand side of Eq. (15) was not present in the Supplemental Material of A. Sahu et al. "Geometry and dynamics of lipid membranes: The Scriven–Love number". *Phys. Rev. E* **101** (2020), 052401. arXiv: 1910.10693. The same correction will be made throughout our analysis of different membrane geometries in Chapters VII, VIII, and IX.

and assume the size of the patch L sets the characteristic length over which perturbed quantities vary. However, the stationary state does not set a characteristic time or velocity scale, which are instead determined by non-dimensionalizing the linearized equations.

Substituting the unperturbed solution (16) into the first-order perturbed equations (13)–(15) yields

$$\tilde{v}^{\alpha}_{,\alpha} = 0 \,, \tag{18}$$

$$\rho\, \tilde{v}^{\alpha}_{,t} = \delta^{\alpha\beta}\, \tilde{\lambda}_{,\beta} + \zeta \left(\tilde{v}^{\alpha}_{,xx} + \tilde{v}^{\alpha}_{,yy} \right) , \tag{19}$$

and

$$\rho\, \tilde{h}_{,tt} = -\frac{1}{2}\, k_{\mathrm{b}}\, \Delta_{\mathrm{s}}^2\, \tilde{h} + \lambda_0\, \Delta_{\mathrm{s}} \tilde{h} \,. \tag{20}$$

Note that in a flat geometry with no initial flow, viscous forces do not arise in the shape equation (20) and so the Scriven–Love number will not appear when the equations are non-dimensionalized.

At this point, we determine the appropriate dimensionless variables. The perturbation in the normal direction, $\epsilon\tilde{h}$, is prescribed to be of a length scale Z such that $\epsilon\tilde{h}/Z$ is $O(1)$, where $\epsilon := Z/L \ll 1$ is a small parameter and $\tilde{h}$ is $O(L)$. An initial perturbation is assumed to relax over a time scale τ, such that $\tilde{h}_{,t}$ is $O(L/\tau)$. Moreover, the out-of-plane perturbation induces in-plane flows of a characteristic velocity, denoted V, which vary in-plane over the length scale L, such that $\tilde{v}^{\alpha}$ is $O(V)$ and $\tilde{v}^{\alpha}_{,\beta}$ is $O(V/L)$. Finally, $\tilde{\lambda}$ is assumed to be $O(\Lambda)$, where Λ is known [see Eq. (17)]. Corresponding dimensionless quantities are then defined as

$$\begin{aligned} \theta^{\alpha *} &:= \frac{\theta^{\alpha}}{L} \,, & \tilde{h}^{*} &:= \frac{\tilde{h}}{L} \,, & \tilde{v}^{\alpha *} &:= \frac{\tilde{v}^{\alpha}}{V} \,, \\ \tilde{\lambda}^{*} &:= \frac{\tilde{\lambda}}{\Lambda} \,, & & \text{and} & t^{*} &:= \frac{t}{\tau} \,, \end{aligned} \tag{21}$$

and are all assumed to be $O(1)$. We now seek to determine the velocity scale V and the time scale τ from a scaling analysis of the perturbed equations.

Upon substituting Eq. (21) into Eq. (18), the dimensionless perturbed continuity equation is obtained as

$$\frac{V}{L}\, \tilde{v}^{\alpha *}_{,\alpha^*} = 0 \qquad \text{or equivalently} \qquad \tilde{v}^{\alpha *}_{,\alpha^*} = 0 \,. \tag{22}$$

Although Eq. (22) does not contain the out-of-plane velocity v, the general continuity equation [Chapter VI, Eq. (4)] requires lipids to flow in-plane to accommodate out-of-plane shape changes. We thus assume the time scale τ and velocity scale V are related by

$$\tau = \frac{L}{V} \,. \tag{23}$$

Equation (23) implies that in-plane velocities and out-of-plane velocities take on the same characteristic values, with the latter also being given by L/τ.

Next, the in-plane equations (19) are considered. Substituting Eq. (21) into Eq. (19) yields

$$\frac{\rho V}{\tau}\, \tilde{v}^{\alpha *}_{,t^*} = \frac{\Lambda}{L}\, \delta^{\alpha^*\beta^*}\, \tilde{\lambda}^{*}_{,\beta^*} + \frac{\zeta\, V}{L^2} \left(\tilde{v}^{\alpha *}_{,x^* x^*} + \tilde{v}^{\alpha *}_{,y^* y^*} \right) , \tag{24}$$

which consists of inertial, tensile, and viscous forces, respectively. At this point, the time scale τ (23) is substituted into Eq. (24), and terms are rearranged to yield

$$Re\, \tilde{v}^{\alpha*}_{,t^*} = \frac{\Lambda L}{\zeta V}\, \delta^{\alpha^*\beta^*}\, \tilde{\lambda}^*_{,\beta^*} + \tilde{v}^{\alpha*}_{,x^*x^*} + \tilde{v}^{\alpha*}_{,y^*y^*} \ . \tag{25}$$

In Eq. (25), the Reynolds number Re compares the magnitude of inertial to viscous forces, and is defined as

$$Re := \frac{\rho V L}{\zeta} \ , \tag{26}$$

where the dimensions of the various entities are provided in Chapter VI, Table 1. For biological lipid membranes, inertial terms are generally negligible ($Re \ll 1$), as will be justified shortly. The surface tension and velocity terms in Eq. (24) are then assumed to balance, such that [cf. Eq. (23)]

$$V = \frac{L\Lambda}{\zeta} \qquad \text{and} \qquad \tau = \frac{\zeta}{\Lambda} \ . \tag{27}$$

Given the scaling in Eq. (27), we now check to see if inertial terms are negligible, as was assumed. Characteristic values of the various dimensional parameters are provided in Table 1. With these values, we find the Reynolds number (26) ranges from $Re \sim 10^{-10}$–10^{-5}, such that inertial terms are indeed negligible. The in-plane equations (25) then simplify to

$$\tilde{v}^{\alpha*}_{,x^*x^*} + \tilde{v}^{\alpha*}_{,y^*y^*} + \delta^{\alpha^*\beta^*}\, \tilde{\lambda}^*_{,\beta^*} = 0 \ , \tag{28}$$

and are identical to the two-dimensional Stokes equation—in which the negative pressure is replaced by the surface tension.

Combined with the continuity equation (22), we observe that the perturbed system behaves as a two-dimensional fluid film. Moreover, the in-plane dynamics are not affected by the shape disturbance, as $\tilde{h}^*$ does not appear in Eqs. (22) or (28). Rather, the continuity and in-plane equations constitute three equations for the unknowns $\tilde{v}^\alpha$ and $\tilde{\lambda}$, which we can solve for using standard hydrodynamic techniques. The general procedure to do so was described in Chapter VI, §3—though in this case we can determine the in-plane solution with several algebraic manipulations. In particular, by taking the partial derivative of Eq. (28) with respect to $\theta^{\alpha*}$ and substituting the continuity equation (22), we find

$$\Delta^*_{\mathrm{s}}\, \tilde{\lambda}^* = 0 \ . \tag{29}$$

Assuming there is no surface tension perturbation at the edge of the domain, we find $\tilde{\lambda}^* = 0$. The in-plane equations (28) then simplify to

$$\tilde{v}^{\alpha*}_{,x^*x^*} + \tilde{v}^{\alpha*}_{,y^*y^*} = 0 \ , \tag{30}$$

which—now assuming no perturbed velocity at the domain edge—yields $\tilde{v}^{\alpha*} = 0$. Thus, the linearized in-plane equations admit only the trivial solution where all perturbed quantities are identically zero. [‡]

[‡]Nontrivial solutions are possible if $\tilde{\lambda}$ or $\tilde{v}^\alpha$ are nonzero at the membrane boundary. However, it is generally assumed that the base state satisfies all boundary conditions, for which perturbed quantities are zero on the domain boundary.

Table 1: Characteristic membrane material parameters. The surface tension can span a wide range of values to prevent significant areal dilation; characteristic low and high values are provided.

Sym.	Parameter	Value	Ref.
k_b	bending modulus	10^2 pN $\cdot$ nm	‡
Λ	surface tension	10^{-4}–10^{-1} pN/nm	‡, †
ζ	membrane viscosity	10 pN $\cdot$ μsec/nm	*, §
ρ	mass density	10^{-8} pg/nm^2	♯
L	patch size	10^2–10^3 nm	–

Finally, the perturbed shape equation is analyzed. Substituting Eq. (21) into Eq. (20) yields

$$\frac{\rho L}{\tau^2}\,\tilde{h}^*_{,t^*t^*} \;=\; -\frac{1}{2}\,\frac{k_\mathrm{b}}{L^3}\,(\Delta^*_\mathrm{s})^2\,\tilde{h}^* \;+\; \frac{\Lambda}{L}\,\Delta^*_\mathrm{s}\,\tilde{h}^*\;, \tag{31}$$

which consists of inertial, bending, and tension terms, respectively. In Eq. (31),

$$\Delta^*_\mathrm{s}(\,\cdot\,) \;:=\; L^2\,\Delta_\mathrm{s}(\,\cdot\,) \tag{32}$$

is the dimensionless surface Laplacian. We define the Föppl–von Kármán number Γ to be the ratio of tension to bending terms, given by

$$\Gamma \;:=\; \frac{\Lambda L^2}{k_\mathrm{b}}\;. \tag{33}$$

With Eq. (33) and the definition of the Reynolds number (26), Eq. (31) can be rewritten as

$$Re\,\Gamma\;\tilde{h}^*_{,t^*t^*} \;=\; -\frac{1}{2}\,(\Delta^*_\mathrm{s})^2\,\tilde{h}^* \;+\; \Gamma\,\Delta^*_\mathrm{s}\,\tilde{h}^*\;. \tag{34}$$

With the values of various quantities provided in Table 1, we calculate $\Gamma \sim 10^{-2}$–10^3. We now seek to determine if the magnitude of the inertial forces, $Re\,\Gamma$, is negligible in the biological systems of interest. To this end, we recognize that with the choice of velocity scale in Eq. $(27)_1$, the magnitude of the left-hand side of Eq. (34) can be expressed as $Re\,\Gamma = \Gamma^2\rho k_\mathrm{b}/\zeta^2$, where the dimensionless parameter $\rho k_\mathrm{b}/\zeta^2 \sim 10^{-8}$. Thus, when $\Gamma \leq 1$, then $Re\,\Gamma \ll \Gamma$

‡J. Pécréaux et al. "Refined contour analysis of giant unilamellar vesicles". *Eur. Phys. J. E* **13** (2004), 277–290

†J. Dai et al. "Membrane tension in swelling and shrinking molluscan neurons". *J. Neurosci.* **18** (1998), 6681–6692

*P. Cicuta, S.L. Keller, and S.L. Veatch. "Diffusion of liquid domains in lipid bilayer membranes". *J. Phys. Chem. B* **111** (2007), 3328–3331. arXiv: `cond-mat/0611492`

§A.R. Honerkamp-Smith et al. "Membrane viscosity determined from shear-driven flow in giant vesicles". *Phys. Rev. Lett.* **111** (2013), 038103. arXiv: `1308.6440`

♯P. Parkkila et al. "Biophysical characterization of supported lipid bilayers using parallel dual-wavelength surface plasmon resonance and quartz crystal microbalance measurements". *Langmuir* **34** (2018), 8081–8091

and inertial terms are negligible relative to both surface tension and bending forces. On the other hand, when Γ is large, we compare $Re\Gamma$ to the $O(1)$ bending terms. For even the largest values of the Föppl–von Kármán number ($\Gamma \sim 10^3$), $Re\,\Gamma \sim 10^{-2} \ll 1$, and inertial terms can again be neglected. Thus, inertial terms are negligible over the entire range of biologically relevant Föppl–von Kármán numbers, and Eq. (34) simplifies to

$$\Gamma\,\Delta_s^*\,\tilde{h}^* - \frac{1}{2}\,(\Delta_s^*)^2\,\tilde{h}^* = 0\,. \tag{35}$$

Table 1 provides characteristic values of various membrane parameters. Note that the surface tension scale Λ is set in the base state, and can be arbitrarily small or large as required by the membrane's areal incompressibility constraint—up to values as large as ∼1–10 pN/nm, at which point the membrane tears. [‡,†] We additionally recognize that in the dimensionless governing equations [Eqs. (22), (28), and (35)], the Föppl–von Kármán number Γ is the only relevant dimensionless number. At low tensions of $\Lambda \sim 10^{-4}$ pN/nm with $L \sim 100$ nm, $\Gamma \sim 10^{-2} \ll 1$ and bending dominates the shape equation (35)—which simplifies to $(\Delta_s^*)^2\,\tilde{h}^* = 0$, i.e. the well-known biharmonic equation that often arises in the study of beam bending. At high tensions of $\Lambda \sim 10^{-1}$ pN/nm with $L \sim 10^3$ nm, $\Gamma \sim 10^3 \gg 1$ and the shape equation $\Delta_s^*\,\tilde{h}^* = 0$ is tension-dominated as for a fluid film or soap bubble. Finally, at moderate tensions of $\Lambda \sim 10^{-2}$ pN/nm and length scales $L \sim 100$ nm, $\Gamma \sim 1$ and the surface tension and bending terms balance in governing the membrane shape. In all three cases, intramembrane viscous forces play no role in determining the membrane shape.

In the above analysis of the shape equation (35), inertia was neglected due to scaling arguments. However, the inertial term is the only time-dependent quantity in Eq. (34), and its removal in Eq. (35) leads to a singular perturbation problem. [*] We recognize that while inertial forces are small on the membrane timescale $\tau = \zeta/\Lambda$ $(27)_2$, they are significant on smaller timescales. Suppose, for example, that $\Gamma < 1$—in which case we define $t' := t^*/\sqrt{Re\Gamma}$ and express Eq. (34) as

$$\tilde{h}^*_{,t't'} = \Gamma\Delta_s^*\tilde{h}^* - \frac{1}{2}\,\Delta_s^{*2}\,\tilde{h}^*\,. \tag{36}$$

If $\Gamma \geq 1$ on the other hand, we define $\bar{t} := t^*/\sqrt{Re}$ and write the shape equation (34) as

$$\tilde{h}^*_{,\bar{t}\,\bar{t}} = \Delta_s^*\tilde{h}^* - \frac{1}{2\Gamma}\,\Delta_s^{*2}\,\tilde{h}^*. \tag{37}$$

In both cases, however, an additional complexity arises because the fluid surrounding the membrane provides a dissipative mechanism that causes the height deviation to relax to zero over time. The analysis of how the surrounding fluid exerts forces on the membrane is outside the scope of this thesis, though in planar geometries it is well-known how to include such effects. [§]

[‡]E.A. Evans and R. Skalak. *Mechanics and Thermodynamics of Biomembranes*. Boca Raton: CRC Press, 1980.

[†]J.A. Nichol and O.F. Hutter. "Tensile strength and dilatational elasticity of giant sarcolemmal vesicles shed from rabbit muscle". *J. Physiol.* **493** (1996), 187–198.

[*]When solving Eq. (35) with appropriate boundary conditions, we find the trivial solution $\tilde{h}^* = 0$.

[§]See §3.1 of H. Turlier and T. Betz. "Fluctuations in Active Membranes". *Physics of Biological Membranes*. Ed. by P. Bassereau and P. Sens. Cham: Springer Nature Switzerland, 2018, pp. 581–619.

4. The dynamics about a patch with a base flow

We next consider a planar membrane with some initial nontrivial in-plane flow satisfying the unperturbed equations (5)–(7), for which $v^\alpha_{(0),\beta} \neq 0$. As in the case with no base flow, the base state sets the characteristic surface tension scale Λ. In this case, however, the base in-plane flow $v^\alpha_{(0)}$ sets the characteristic velocity scale V, where in-plane speeds vary from zero to V over the patch size L. The specification of the velocity scale from the base flow leads to an additional complexity: we are no longer free to choose a velocity scale such that in-plane surface tension and viscous forces balance in the perturbed dynamics. Thus, if were to assume that all perturbed unknowns—$\tilde{v}^1$, $\tilde{v}^2$, $\tilde{h}$, and $\tilde{\lambda}$—varied over the length L, we arrive at an unphysical result in the in-plane dynamics. Conversely, if we assume the aforementioned quantities all vary over a new length scale ℓ, then tension and viscous forces can be balanced in the in-plane equations with an appropriate choice of ℓ. Unfortunately, under this assumption, the shape equation becomes unphysical. We thus arrive at a nontrivial result: when the base state involves a flow of lipids, different perturbed unknowns vary over different length scales. Namely, the in-plane quantities $\tilde{v}^1$, $\tilde{v}^2$, and $\tilde{\lambda}$ vary over a to-be-determined length scale ℓ, while membrane deformations $\tilde{h}$ vary over the patch size L. Despite this complexity, we find that when the perturbed shape equation is non-dimensionalized, the competition between viscous forces and bending forces gives rise to the Scriven–Love number SL—as defined in Eq. (11) of Chapter VI. We then go on to analyze past experimental data, in which planar membranes have a base lipid flow. In all biologically relevant situations, $\mathit{SL} \ll 1$ and out-of-plane bending forces are negligible. Accordingly, the Föppl–von Kármán number Γ is the only relevant parameter governing membrane dynamics about planar geometries.

(a). The unperturbed equations

We begin by assuming a known stationary state, in which the membrane velocity and surface tension are expressed as [cf. Eqs. (2), (4)]

$$v^\alpha_{(0)} = v^\alpha_{(0)}(\theta^\beta) \,, \qquad v_{(0)} = 0 \,, \qquad \text{and} \qquad \lambda_{(0)} = \lambda_{(0)}(\theta^\alpha) \,. \tag{38}$$

Here, $v^\alpha_{(0)}$ and $\lambda_{(0)}$ dictate the velocity scale V and surface tension scale Λ, for which we define

$$v^{\alpha *}_{(0)} := \frac{v^\alpha_{(0)}}{V} \qquad \text{and} \qquad \lambda^*_{(0)} := \frac{\lambda_{(0)}}{\Lambda} \,. \tag{39}$$

The unperturbed governing equations (5)–(7) can then be recast in dimensionless form as

$$v^{\alpha *}_{(0),\alpha^*} = 0 \,, \tag{40}$$

$$\mathit{Re}\, v^{\beta *}_{(0)}\, v^{\alpha *}_{(0),\beta^*} = \frac{\Lambda L}{\zeta V}\, \delta^{\alpha^*\beta^*} \lambda^*_{(0),\beta^*} + v^{\alpha *}_{(0),x^*x^*} + v^{\alpha *}_{(0),y^*y^*} \,, \tag{41}$$

and

$$[\![p^*]\!] = 0 \,, \tag{42}$$

where in Eq. (41) the Reynolds number Re is again given by Eq. (26).

At this point, we characterize the order of magnitude of the various terms in the in-plane equations (41). To this end, we investigate three prior experimental efforts with lipids flowing in planar geometries, as discussed in §4 (c). We find the base velocity scale V ranges from 10^{-6}–10^{-3} nm/μsec (equivalently 10^{-3}–1 μm/sec); all other parameters are provided in Table 1. For these characteristic values, the Reynolds number Re (26) ranges from 10^{-13} to 10^{-9} and $\zeta V/(\Lambda L)$ ranges from 10^{-7} to 1. Accordingly, inertial terms are neglected in Eq. (41), which simplifies to

$$\frac{\zeta V}{\Lambda L}\left(v^{\alpha *}_{(0),x^*x^*} + v^{\alpha *}_{(0),y^*y^*}\right) + \delta^{\alpha^*\beta^*}\lambda^*_{(0),\beta^*} = 0\,. \tag{43}$$

Equation (43) consists of the two in-plane equations describing a stationary state with a base flow, and is equivalent to the two-dimensional Stokes equation. Thus, we can easily choose the well-known Stokes flow solutions to be the membrane base state. For example, we previously investigated the dynamics of a membrane with a simple shear flow in the stationary state. [‡]

(b). The perturbed equations

We now consider the linearized dynamics of a perturbed membrane patch with a base flow. As before, all perturbed quantities are assumed to be the same order as their unperturbed counterparts, with ϵ capturing the smallness of the perturbation [see discussion below Eq. (11)]. All perturbed quantities are non-dimensionalized as in Eq. (21), where in this case the velocity scale V is set by the base state. We then seek to determine the order of magnitude of the various membrane forces, with one important condition: in the limit where the velocity scale V goes to zero, we expect to recover the results of §3—in which the membrane had no flow in the base state. As we will see, this requirement brings about a new length scale over which only $\tilde{v}^1$, $\tilde{v}^2$, and $\tilde{\lambda}$ vary, while $\tilde{h}$ continues to vary over the patch size L. To demonstrate how such a nontrivial scaling arises, we first attempt two more straightforward scaling choices, with inertial terms neglected for simplicity. We show how each attempt breaks down, and then provide the correct scaling solution.

Scaling Attempt #1: Variations over patch size L (incorrect)

We begin by assuming all membrane unknowns vary over the patch size L, such that every spatial derivative introduces a factor of $1/L$ in our scaling analysis. By substituting Eq. (21) into the perturbed continuity (13) and in-plane (14) equations and neglecting inertial terms for simplicity, we obtain

$$\tilde{v}^{\alpha *}_{,\alpha^*} = 0 \tag{44}$$

and

$$\delta^{\alpha^*\beta^*}\,\tilde{\lambda}^*_{,\beta^*} + \frac{\zeta V}{\Lambda L}\left(\tilde{v}^{\alpha *}_{,x^*x^*} + \tilde{v}^{\alpha *}_{,y^*y^*}\right) = 0\,. \tag{45}$$

In the limit where $\zeta V/(\Lambda L) \ll 1$, as is the case when the velocity scale is small, the in-plane equations (45) simplify to $\tilde{\lambda}^*_{,\beta^*} = 0$. In this case, $\tilde{\lambda}^*$ is constant and surface tension gradients

[‡]Sahu et al., "Geometry and dynamics of lipid membranes: The Scriven–Love number".

no longer balance in-plane viscous forces. However, as described above, we expect to recover the perturbed in-plane equations governing the dynamics of an initially static patch (28) in the limit where the base velocity scale V tends to zero. As this is not the case, the solution of $\tilde{\lambda}^*$ being constant in the limit of small V is unphysical, and our assumption that all quantities vary over a length scale L is incorrect.

Scaling Attempt #2: Variations over new length scale ℓ (incorrect)

Since our first attempt led to an unphysical scaling, we next assume all perturbed quantities vary over some unknown length scale ℓ, which is to be determined via a scaling analysis. In this case, we define

$$x' := \frac{x}{\ell} \,, \qquad y' := \frac{y}{\ell} \qquad \text{and} \qquad \Delta_{\mathrm{s}}'(\,\cdot\,) := \ell^2\, \Delta_{\mathrm{s}}(\,\cdot\,) \,, \tag{46}$$

such that the dimensionless continuity (13) and in-plane (14) equations are given by

$$\tilde{v}^{\alpha *}_{,\alpha'} = 0 \tag{47}$$

and

$$\delta^{\alpha^*\beta'}\, \tilde{\lambda}^*_{,\beta'} + \frac{\zeta V}{\Lambda \ell} \left(\tilde{v}^{\alpha *}_{,x'x'} + \tilde{v}^{\alpha *}_{,y'y'} \right) = 0 \,. \tag{48}$$

Again, for the sake of argument, we ignore inertial terms for simplicity. Given Eq. (48), we choose the length scale ℓ to be given by

$$\ell := \frac{\zeta V}{\Lambda} \,, \tag{49}$$

such that viscous and tension forces balance. The in-plane equations then have the same structure as their initially static counterparts (28) for any base state velocity scale V, as required by our analysis.

With the determination of a new length scale ℓ, the perturbed shape equation (15) is non-dimensionalized with Eqs. (21), (39), and (46)—yielding

$$2\, \frac{\zeta V}{\ell^2}\, \tilde{h}^*_{,\alpha'\lambda'}\, \delta^{\lambda'\beta^*}\, v^{\alpha *}_{(0),\beta^*} - \frac{1}{2}\, \frac{k_{\mathrm{b}} L}{\ell^4}\, \Delta_{\mathrm{s}}'^2\, \tilde{h}^* + \frac{\Lambda L}{\ell^2}\, \lambda^*_{(0)}\, \Delta_{\mathrm{s}}'\, \tilde{h}^* = 0 \,. \tag{50}$$

Substituting Eq. (49) into Eq. (50), rearranging terms, and defining

$$\ell^* := \frac{\ell}{L} = \frac{\zeta V}{\Lambda L} \tag{51}$$

for notational convenience, we obtain

$$\frac{\zeta^2 V^2}{k_{\mathrm{b}} \Lambda} \left(2\ell^*\, \tilde{h}^*_{,\alpha'\lambda'}\, \delta^{\lambda'\beta^*}\, v^{\alpha *}_{(0),\beta^*} + \lambda^*_{(0)}\, \Delta_{\mathrm{s}}'\, \tilde{h}^* \right) - \frac{1}{2}\, \Delta_{\mathrm{s}}'^2\, \tilde{h}^* = 0 \,. \tag{52}$$

However, in the limit of vanishing base state velocity (i.e. when V goes to zero), Eq. (52) simplifies to $\Delta_{\mathrm{s}}'^2\, \tilde{h}^* = 0$, and the initially static solution (35) is not recovered. Consequently, the assumption that all perturbed quantities vary over the length scale ℓ is also incorrect.

Scaling Attempt #3: Variations over multiple length scales (correct)

At this point, neither of our scaling attempts were valid. However, our two incorrect attempts reveal (*i*) the problem requires an additional length scale ℓ over which $\tilde{v}^\alpha$ and $\tilde{\lambda}$ vary, and (*ii*) the out-of-plane shape disturbance $\tilde{h}$ cannot vary over that same length scale. We therefore posit that $\tilde{h}$ varies over the patch size L, while $\tilde{v}^\alpha$ and $\tilde{\lambda}$ vary over the length scale ℓ obtained in Eq. (49). The first-order continuity equation (13) is then non-dimensionalized as

$$\tilde{v}^{\alpha*}_{,\alpha'} = 0 \, . \tag{53}$$

The in-plane equations are non-dimensionalized by substituting Eqs. (21) and (46) into Eq. (14), yielding

$$\frac{\rho V^2}{\ell}\left(\frac{\ell}{V\tau}\,\tilde{v}^{\alpha*}_{,t^*} + \frac{\ell}{L}\,\tilde{v}^{\beta*}\,v^{\alpha*}_{(0),\beta^*} + v^{\beta*}_{(0)}\,\tilde{v}^{\alpha*}_{,\beta'}\right) = \frac{\Lambda}{\ell}\,\delta^{\alpha'\beta'}\,\tilde{\lambda}^*_{,\beta'} + \frac{\zeta V}{\ell^2}\left(\tilde{v}^{\alpha*}_{,x'x'} + \tilde{v}^{\alpha*}_{,y'y'}\right) . \tag{54}$$

In considering the inertial terms in Eq. (54), we first recognize $\ell/L = \zeta V/(\Lambda L)$, which was found in §4 (a) to range from 10^{-7} to 1 over the experiments of interest. Accordingly, we choose the time scale τ to be given by

$$\tau = \frac{\ell}{V} = \frac{\zeta}{\Lambda} \, , \tag{55}$$

such that the first and third terms on the left-hand side of Eq. (54) are balanced. By substituting Eqs. (26), (49), (51), and (55) into Eq. (54) and rearranging terms, we obtain

$$Re\,\ell^*\left(\tilde{v}^{\alpha*}_{,t^*} + \ell^*\,\tilde{v}^{\beta*}\,v^{\alpha*}_{(0),\beta^*} + v^{\beta*}_{(0)}\,\tilde{v}^{\alpha*}_{,\beta'}\right) = \delta^{\alpha'\beta'}\,\tilde{\lambda}^*_{,\beta'} + \tilde{v}^{\alpha*}_{,x'x'} + \tilde{v}^{\alpha*}_{,y'y'} \, . \tag{56}$$

As $Re \ll 1$ for the experimental systems under consideration [see §4 (a)] and $\ell^* \leq 1$, inertial terms are negligible in Eq. (56). The dimensionless perturbed in-plane equations are given by

$$\tilde{v}^{\alpha*}_{,x'x'} + \tilde{v}^{\alpha*}_{,y'y'} + \delta^{\alpha'\beta'}\,\tilde{\lambda}^*_{,\beta'} = 0 \, , \tag{57}$$

and are nearly identical to their analogs about a stationary state with no base flow (28). The only difference between the two equations is the length scale over which in-plane quantities vary.

Thus far, the in-plane and continuity equations are identical to those of our second scaling attempt. However, we now analyze the perturbed shape equation with the assumption that the perturbed membrane height $\tilde{h}$ varies over the patch size L—as was the case in our first scaling attempt. To this end, we substitute Eqs. (21), (39), and (46) into Eq. (15) and obtain

$$\begin{aligned}\rho\left(\frac{L}{\tau^2}\,\tilde{h}^*_{,t^*t^*} + \frac{V^2}{L}\,v^{\alpha*}_{(0)}v^{\beta*}_{(0)}\tilde{h}^*_{,\alpha^*\beta^*} + \frac{V}{\tau}\,v^{\alpha*}_{(0)}\tilde{h}^*_{,t^*\alpha^*}\right) \\ = 2\,\frac{\zeta\,V}{L^2}\,\tilde{h}^*_{,\alpha^*\lambda^*}\,\delta^{\lambda^*\beta^*}\,v^{\alpha*}_{(0),\beta^*} - \frac{1}{2}\,\frac{k_\mathrm{b}}{L^3}(\Delta^*_\mathrm{s})^2\,\tilde{h}^* + \frac{\Lambda}{L}\,\lambda^*_{(0)}\Delta^*_\mathrm{s}\,\tilde{h}^* \, .\end{aligned} \tag{58}$$

Note that in Eq. (58), all spatial derivatives of the perturbed shape are taken with respect to the length L, denoted by $(\,\cdot\,)_{,\alpha^*}$. With Eqs. (26), (33), (49), (51), and (55), Eq. (58) can

be rewritten as

$$\frac{Re\Gamma}{\ell^*}\left(\tilde{h}^*_{,t^*t^*} + (\ell^*)^2\, v^{\alpha*}_{(0)}\, v^{\beta*}_{(0)}\, \tilde{h}^*_{,\alpha^*\beta^*} + \ell^*\, v^{\alpha*}_{(0)}\, \tilde{h}^*_{,t^*\alpha^*}\right) = 2\,\frac{\zeta VL}{k_\mathrm{b}}\,\tilde{h}^*_{,\alpha^*\lambda^*}\,\delta^{\lambda^*\beta^*}\, v^{\alpha*}_{(0),\beta^*} + \Gamma\,\lambda^*_{(0)}\,\Delta^*_\mathrm{s}\,\tilde{h}^* - \frac{1}{2}\,(\Delta^*_\mathrm{s})^2\,\tilde{h}^*\,. \tag{59}$$

The coefficient $Re\Gamma/\ell^*$ on the left-hand side of Eq. (59) can be expressed as $\rho L^4 \Lambda^2/(k_\mathrm{b}\zeta^2)$, which ranges from 10^{-12} to 10^{-2} over the experiments considered. Accordingly, inertial terms are negligible in the shape equation (59), which simplifies to

$$2\,\frac{\zeta VL}{k_\mathrm{b}}\,\tilde{h}^*_{,\alpha^*\lambda^*}\,\delta^{\lambda^*\beta^*}\, v^{\alpha*}_{(0),\beta^*} + \Gamma\,\lambda^*_{(0)}\,\Delta^*_\mathrm{s}\,\tilde{h}^* - \frac{1}{2}\,(\Delta^*_\mathrm{s})^2\,\tilde{h}^* = 0\,. \tag{60}$$

In Eq. (60), the coefficient of the first term is the ratio of viscous forces to bending forces in the out-of-plane direction. We thus define the Scriven–Love number to be given by

$$\mathit{SL} := \frac{\zeta VL}{k_\mathrm{b}}\,, \tag{61}$$

such that the dimensionless perturbed shape equation is found to be

$$2\,\mathit{SL}\,\tilde{h}^*_{,\alpha^*\lambda^*}\,\delta^{\lambda^*\beta^*}\, v^{\alpha*}_{(0),\beta^*} + \Gamma\,\lambda^*_{(0)}\,\Delta^*_\mathrm{s}\,\tilde{h}^* - \frac{1}{2}\,(\Delta^*_\mathrm{s})^2\,\tilde{h}^* = 0\,. \tag{62}$$

As quantified in §4 (c), $\mathit{SL} \ll 1$ in all biologically relevant planar systems with a base flow. Accordingly, Eq. (62) simplifies to

$$\Gamma\,\lambda^*_{(0)}\,\Delta^*_\mathrm{s}\,\tilde{h}^* - \frac{1}{2}\,(\Delta^*_\mathrm{s})^2\,\tilde{h}^* = 0\,, \tag{63}$$

which—when $\lambda_{(0)}$ is constant—is identical to the initially static result (35). As before, our decision to not include the dynamics of the surrounding fluid prevents us from investigating the stability of such systems.

(c). The analysis of past experimental data

We now present the experimental data used to calculate the Scriven–Love and Föppl–von Kármán numbers in planar systems with a base flow, and reiterate that the Scriven–Love number does not appear in initially static planar systems. The results of the three past experiments are summarized in Fig. 2, and detailed in Tables 2–4. In all cases, we assume $k_\mathrm{b} = 100$ pN·nm, $\Lambda = 10^{-3}$ pN/nm, and $\zeta = 10$ pN·μsec/nm,[‡, †] as these values were not provided in the experimental studies.

The three situations considered in Tables 2–4 involve vesicles being released from an initially planar membrane during endocytosis. To estimate the velocity scale of in-plane flows

[‡]P. Cicuta, S.L. Keller, and S.L. Veatch. "Diffusion of liquid domains in lipid bilayer membranes". *J. Phys. Chem. B* **111** (2007), 3328–3331. arXiv: cond-mat/0611492.

[†]A.R. Honerkamp-Smith et al. "Membrane viscosity determined from shear-driven flow in giant vesicles". *Phys. Rev. Lett.* **111** (2013), 038103. arXiv: 1308.6440.

Experiment #1: Ultrafast endocytosis

Table 2: Calculations from S. Watanabe et al. "Ultrafast endocytosis at *Caenorhabditis elegans* neuromuscular junctions". *eLife* **2** (2013), e00723.

Quantity	Value	Calculation
V	$8 \cdot 10^{-4}$ nm/μsec	Eq. (64); $R_v \sim 20$ nm, $\Delta t \sim 50$ ms (Fig. 2)
L	$1 \cdot 10^{2}$ nm	Estimated from Figs. 2(e) and 2(f)
SL	$8 \cdot 10^{-3}$	Eq. (61)
Γ	$1 \cdot 10^{-1}$	Eq. (33)

Experiment #2: Ultrafast endocytosis

Table 3: Calculations from S. Watanabe et al. "Ultrafast endocytosis at *Caenorhabditis elegans* neuromuscular junctions". *eLife* **2** (2013), e00723.

Quantity	Value	Calculation
V	$3 \cdot 10^{-5}$ nm/μsec	Eq. (64); $R_v \sim 40$ nm, $\Delta t \sim 3$ s (Fig. 6)
L	$5 \cdot 10^{1}$ nm	Estimated from Fig. 6(g)
SL	$2 \cdot 10^{-4}$	Eq. (61)
Γ	$2 \cdot 10^{-2}$	Eq. (33)

Experiment #3

Table 4: Calculations from E. Cocucci et al. "The first five seconds in the life of a Clathrin-coated pit". *Cell* **150** (2012), 495–507.

Quantity	Value	Calculation
V	$6 \cdot 10^{-6}$ nm/μsec	Eq. (64); $R_v \sim 100$ nm, $\Delta t \sim 30$ s [Figs. 3(a), 5(a)]
L	$1 \cdot 10^{3}$ nm	Estimated from Fig. 5(a)
SL	$6 \cdot 10^{-4}$	Eq. (61)
Γ	$1 \cdot 10^{1}$	Eq. (33)

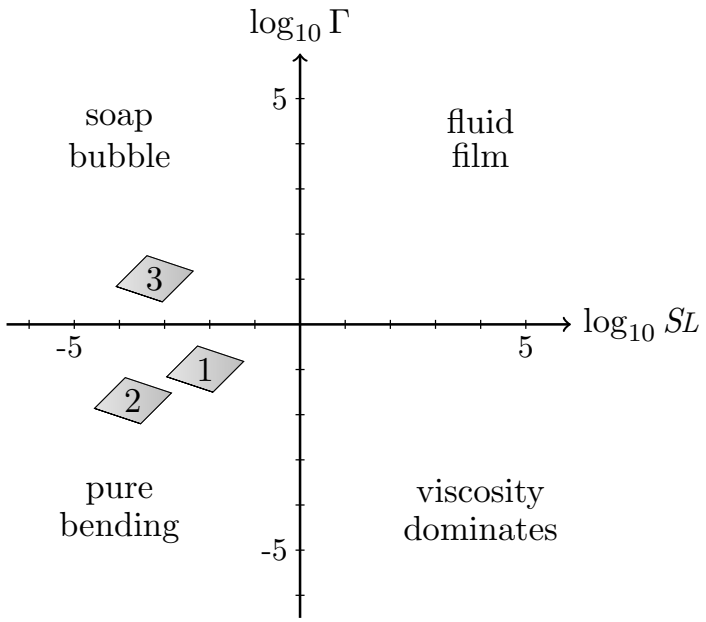

Figure 2: Plot of the Scriven–Love number SL and Föppl–von Kármán number Γ in three past experiments involving planar geometries [cf. Chapter VI, Fig. 2]. Each numbered figure corresponds to a single experiment, which is described in Tables 2–4. Experiment #1 and #2 are bending-dominated, while Experiment #3 is tension-dominated. In all cases, viscous forces do not significantly affect membrane shape.

on the planar membrane, we approximate the distance moved by lipids near the endocytic site, over the time Δt of the event. Consider an initially flat circular patch of lipids, with radius R_f, that eventually forms a vesicle of radius R_v. The continuity of the material requires $\pi R_\mathrm{f}^2 = 4\pi R_\mathrm{v}^2$, such that the in-plane velocity scale $V \sim R_\mathrm{f}/\Delta t$ can be approximated as

$$V \sim \frac{2R_\mathrm{v}}{\Delta t} \,. \tag{64}$$

In the experiments under consideration, R_v and Δt are reported and Eq. (64) is used to approximate the velocity scale V.

(d). Concluding remarks

In comparing the dimensionless perturbed equations for an initially flat membrane patch with a base flow [Eqs. (53), (57), and (63)] to their counterparts without a base flow [Eqs. (22), (28), and (35)], we make several observations. First, the continuity and in-plane equations now involve spatial derivatives over the length scale ℓ, rather than the patch length L. As a result, in-plane viscous and tension forces are both $O(\Lambda^2/(\zeta V))$, a scaling which is difficult to predict from a simple non-dimensionalization of the governing equations. Second, the length scale ℓ satisfies the relation $\ell = L\,\Gamma^{-1} SL$, such that the relative distance over which perturbed in-plane and out-of-plane quantities vary is set by the ratio of the Scriven–Love and Föppl–von Kármán numbers. In the limit of V going to zero, both SL and ℓ tend to zero and there is no longer a new length scale over which perturbed in-plane quantities vary. The

Scriven–Love number emerges in Eq. (62) due to the perturbed $\pi^{\alpha\beta}b_{\alpha\beta}$ term, which contains the coupling between in-plane shear stresses and membrane curvature (see Chapter VI, §1). Linearizing $\pi^{\alpha\beta}b_{\alpha\beta}$ in planar geometries yields $\pi^{\alpha\beta}_{(0)}\tilde{h}_{,\alpha\beta}$, and thus shear stresses must exist in the stationary state in order for the Scriven–Love number to emerge.

At this point, we conclude our calculations for an initially flat membrane patch. We note the Föppl–von Kármán number enters the shape equation both when the membrane is initially static (35) and has a base flow (63). The Scriven–Love number appears only in the latter case. Though we find viscous forces in the out-of-plane direction to be negligible in all experimental systems considered, as shown in §4 (c), the tension forces can be significant—and in some instances dominate bending forces in governing the perturbed membrane's dynamical response.

References

[1] E.A. Abbott. *Flatland: A Romance of Many Dimensions*. 6th ed. New York: Dover, 1952

[2] P. Cicuta, S.L. Keller, and S.L. Veatch. "Diffusion of liquid domains in lipid bilayer membranes". *J. Phys. Chem. B* **111** (2007), 3328–3331. arXiv: cond-mat/0611492

[3] E. Cocucci et al. "The first five seconds in the life of a Clathrin-coated pit". *Cell* **150** (2012), 495–507

[4] J. Dai et al. "Membrane tension in swelling and shrinking molluscan neurons". *J. Neurosci.* **18** (1998), 6681–6692

[5] E.A. Evans and R. Skalak. *Mechanics and Thermodynamics of Biomembranes*. Boca Raton: CRC Press, 1980

[6] A.R. Honerkamp-Smith et al. "Membrane viscosity determined from shear-driven flow in giant vesicles". *Phys. Rev. Lett.* **111** (2013), 038103. arXiv: 1308.6440

[7] G. Monge. *Application de l'analyse à la géométrie*. Paris: Bernard, 1807

[8] J.A. Nichol and O.F. Hutter. "Tensile strength and dilatational elasticity of giant sarcolemmal vesicles shed from rabbit muscle". *J. Physiol.* **493** (1996), 187–198

[9] P. Parkkila et al. "Biophysical characterization of supported lipid bilayers using parallel dual-wavelength surface plasmon resonance and quartz crystal microbalance measurements". *Langmuir* **34** (2018), 8081–8091

[10] J. Pécréaux et al. "Refined contour analysis of giant unilamellar vesicles". *Eur. Phys. J. E* **13** (2004), 277–290

[11] A. Sahu et al. "Geometry and dynamics of lipid membranes: The Scriven–Love number". *Phys. Rev. E* **101** (2020), 052401. arXiv: 1910.10693

[12] L.E. Scriven. "Dynamics of a fluid interface: Equation of motion for Newtonian surface fluids". *Chem. Eng. Sci.* **12** (1960), 98–108

[13] H. Turlier and T. Betz. "Fluctuations in Active Membranes". *Physics of Biological Membranes*. Ed. by P. Bassereau and P. Sens. Cham: Springer Nature Switzerland, 2018, pp. 581–619

[14] S. Watanabe et al. "Ultrafast endocytosis at *Caenorhabditis elegans* neuromuscular junctions". *eLife* **2** (2013), e00723

Chapter VIII

Spherical Membrane Vesicles

> *We wish to obtain equations of motion and boundary-conditions in terms of the displacements of a point on the middle-surface of the shell . . . As the geometrical theory of the deformation of extensible surfaces appears not to have been hitherto made out, it was necessary to give the elements of such a theory for small deformations.*
>
> —Augustus E.H. Love, 1888 [‡]

We next consider spherical lipid membrane vesicles, which are found throughout the cell: vesicles are involved in endocytosis [†] and exocytosis [*] as material is transported across the cell membrane, lysosomes fuse with food vacuoles to break down chemical compounds during phagocytosis, [§] and transport vesicles shuttle proteins and lipids between the endoplasmic reticulum and Golgi complex. [♯] Moreover, spherical GUVs are a canonical tool of *in vitro* studies. GUVs are often used to probe static membrane properties, such as the bending modulus k_b and base state surface tension λ_0, [‖,∀] as well as dynamic properties—such as the membrane's response to a shear flow. [♢,$,&,¶]

[‡]A.E.H. Love. "The small free vibrations and deformation of a thin elastic shell". *Phil. Trans. R. Soc. London* **179** (1888), 491–546.

[†]M.K. Higgins and H.T. McMahon. "Snap-shots of clathrin-mediated endocytosis". *Trends Biochem. Sci.* **27** (2002), 257–263.

[*]Z. Zhang and M.B. Jackson. "Membrane bending energy and fusion pore kinetics in Ca^{2+}-triggered exocytosis". *Biophys. J.* **98** (2010), 2524–2534.

[§]L.-A.H. Allen and A. Aderem. "Mechanisms of phagocytosis". *Curr. Opin. Immunol.* **8** (1996), 36–40.

[♯]C. Lee and L.-B. Chen. "Dynamic behavior of endoplasmic reticulum in living cells". *Cell* **54** (1988), 37–46.

[‖]J. Pécréaux et al. "Refined contour analysis of giant unilamellar vesicles". *Eur. Phys. J. E* **13** (2004), 277–290.

[∀]J.B. Dahl et al. "Experimental observation of the asymmetric instability of intermediate-reduced-volume vesicles in extensional flow". *Soft Matter* **12** (2016), 3787–3796.

[♢]K.H. de Haas et al. "Deformation of giant lipid bilayer vesicles in shear flow". *Phys. Rev. E* **56** (1997), 7132–7137.

[$]V. Kantsler and V. Steinberg. "Orientation and dynamics of a vesicle in tank-treading motion in shear flow". *Phys. Rev. Lett.* **95** (2005), 258101.

[&]M. Abkarian and A. Viallat. "Vesicles and red blood cells in shear flow". *Soft Matter* **4** (2008), 653–657.

[¶]J. Deschamps, V. Kantsler, and V. Steinberg. "Phase diagram of single vesicle dynamical states in shear flow". *Phys. Rev. Lett.* **102** (2009), 118105.

To study the dynamics of spherical membrane vesicles, we follow the general procedure described in Chapter VI and employed when characterizing planar membranes in Chapter VII. We first obtain the unperturbed governing equations, from which we select two stationary states to analyze: (i) a static spherical vesicle and (ii) a spherical vesicle rotating with constant angular velocity about an axis. [‡] We then investigate how each system responds to an infinitesimal perturbation. In both cases, the Föppl–von Kármán number $\mathit{\Gamma}$ quantifies the relative importance of surface tension and bending forces in the dynamics of the perturbed system. Just as in the planar geometry, the Scriven–Love number Sl does not appear in the initially static case—a surprising result, since we generally expect both when the membrane is curved [see Chapter VI, Eq. (6)]. However, when a rotating spherical vesicle is perturbed, the Scriven–Love number emerges and characterizes the relative importance of viscous and bending forces in the membrane's dynamical response. We analyze past experiments in which vesicles have such a base flow, and find both the Föppl–von Kármán and Scriven–Love numbers span a wide range of values. Our analysis reveals that in many biologically relevant situations involving rotating spherical vesicles, the membrane can behave as either a fluid film or an elastic shell—or some nontrivial combination of the two.

With the dimensionless perturbed equations, we proceed to examine the linear stability of lipid membrane vesicles. To this end, we decompose the membrane unknowns into normal modes, and then solve for the dispersion relation governing the temporal evolution of each mode. However, unlike the planar case, some care must be taken when choosing the normal mode decomposition. As we will see, one cannot simply expand each membrane velocity component in terms of the well-known scalar spherical harmonics. Rather, the perturbed membrane velocity $\tilde{\boldsymbol{v}}$ is expanded in terms of the *vector spherical harmonics*, which necessitates a reformulation of the governing equations. Our analysis reveals the natural relaxation frequency of each mode due only to internal membrane forces, and also shows that the base surface tension λ_0—through the Föppl–von Kármán number—completely specifies the stability of the system. In particular, when a spherical vesicles is under tension and $\mathit{\Gamma} > 0$, the vesicle is stable. On the other hand, when the vesicle is under compression ($\mathit{\Gamma} < 0$), long-wavelength undulations become unstable. Since the base surface tension $\lambda_{(0)}$ is specified by the hydrodynamic pressure difference between the interior and exterior of the vesicle, our analysis leads to quantitative predictions of the time evolution of spherical membrane systems.

1. The unperturbed equations

An unperturbed spherical lipid membrane vesicle of radius R is parametrized by the polar angle θ and azimuthal angle φ, as shown in Fig. 1a. In terms of our differential geometric formulation, we define

$$\theta^1 := \theta \in [0, \pi] \qquad \text{and} \qquad \theta^2 := \varphi \in [0, 2\pi) \tag{1}$$

[‡]One could in principle investigate systems with more complicated lipid flows in the stationary state. However, the algebra required to describe such systems is cumbersome. In an effort to extract the most significant physical insights from our analysis, we consider only the simplest stationary states in the present work.

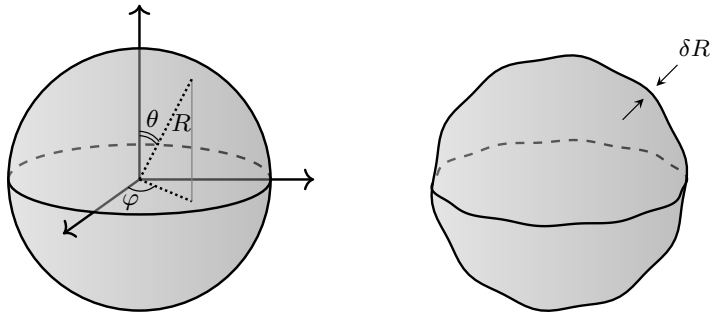

(a) unperturbed: $\boldsymbol{x}_{(0)}(\theta,\varphi)$ (b) perturbed: $\boldsymbol{x}(\theta,\varphi,t)$

Figure 1: Schematic of the unperturbed (a) and perturbed (b) spherical geometries. The sphere has radius R and is characterized by the polar angle θ and azimuthal angle φ. Membrane perturbations are of characteristic size δR, with $\epsilon := \delta R/R \ll 1$.

to be the generalized coordinates. The unperturbed membrane position is given by

$$\boldsymbol{x}_{(0)}(\theta,\varphi) \;=\; R\,\boldsymbol{e}_r(\theta,\varphi)\;, \tag{2}$$

where $\boldsymbol{e}_r$ is the usual unit vector in the radial direction. With the machinery described in Chapter II, we determine the geometric quantities

$$\begin{aligned}
&\boldsymbol{a}_1^{(0)} = R\,\boldsymbol{e}_\theta\;, && \boldsymbol{a}_2^{(0)} = R\,\sin\theta\,\boldsymbol{e}_\varphi\;, && \boldsymbol{n}_{(0)} = \boldsymbol{e}_r\;,\\
&a_{\alpha\beta}^{(0)} = R^2\,\mathrm{diag}\,(1,\sin^2\theta)\;, && H_{(0)} = -R^{-1}\;, && K_{(0)} = R^{-2}\;,\\
&a_{(0)}^{\alpha\beta} = R^{-2}\,\mathrm{diag}\,(1,\csc^2\theta)\;, && && \Gamma_{21}^{2(0)} = \Gamma_{12}^{2(0)} = \cot\theta\;,\\
&b_{\alpha\beta}^{(0)} = -R\,\mathrm{diag}\,(1,\sin^2\theta)\;, && \text{and} && \Gamma_{22}^{1(0)} = -\sin\theta\,\cos\theta\;,
\end{aligned} \tag{3}$$

where only the nonzero Christoffel symbols are provided. As the stationary state by definition has no out-of-plane velocity, $v_{(0)} := \boldsymbol{v}_{(0)}\cdot\boldsymbol{n}_{(0)} = 0$ and the unperturbed membrane velocity $\boldsymbol{v}_{(0)}$ is expressed as

$$\boldsymbol{v}_{(0)}(\theta,\varphi) \;=\; v_{(0)}^\alpha\,\boldsymbol{a}_\alpha \;=\; v_{(0)}^1 R\,\boldsymbol{e}_\theta \;+\; v_{(0)}^2 R\sin\theta\,\boldsymbol{e}_\varphi\;. \tag{4}$$

From Eq. (4), we see that $v_{(0)}^1$ and $v_{(0)}^2$ have units of inverse time. It is important to note the difference between the velocity components v^1 and v^2 in our differential geometric formulation, and the more common decomposition in spherical coordinates:

$$\boldsymbol{v}_{(0)}(\theta,\varphi) \;=\; v_\theta^{(0)}\,\boldsymbol{e}_\theta \;+\; v_\varphi^{(0)}\,\boldsymbol{e}_\varphi\;. \tag{5}$$

In comparing Eqs. (4) and (5), we recognize

$$v_\theta^{(0)} \;=\; v_{(0)}^1 R \qquad \text{and} \qquad v_\varphi^{(0)} \;=\; v_{(0)}^2 R\sin\theta\;, \tag{6}$$

with $v_\theta^{(0)}$ and $v_\varphi^{(0)}$ having units of length per time.

With our geometric and kinematic description of the unperturbed system, we substitute Eqs. (3) and (4) into the general governing equations [Chapter VI, Eqs. (4)–(6)]. The unperturbed continuity equation is expressed as

$$v^1_{(0),\theta} + v^2_{(0),\varphi} + \cot\theta\, v^1_{(0)} = 0 \,, \tag{7}$$

and relates the spatial derivatives of the two velocity components. The in-plane θ and in-plane φ equations are respectively given by

$$\begin{aligned} &\rho R^2\Big(v^1_{(0),t} + v^1_{(0)}\, v^1_{(0),\theta} + v^2_{(0)}\, v^1_{(0),\varphi} - \sin\theta\cos\theta\,(v^2_{(0)})^2\Big) \\ &\qquad = \zeta\Big(v^1_{(0)} + v^1_{(0),\theta\theta} + \csc^2\theta\, v^1_{(0),\varphi\varphi} - \cot\theta\, v^2_{(0),\varphi} + 2\cot\theta\, v^1_{(0),\theta}\Big) + \lambda_{(0),\theta} \,, \end{aligned} \tag{8}$$

and

$$\begin{aligned} &\rho R^2\Big(v^2_{(0),t} + v^1_{(0)}\, v^2_{(0),\theta} + v^2_{(0)}\, v^2_{(0),\varphi} + 2\cot\theta\, v^1_{(0)}\, v^2_{(0)}\Big) \\ &\qquad = \zeta\Big(v^2_{(0),\theta\theta} + \csc^2\theta\, v^2_{,(0)\varphi\varphi} + 2\cot\theta\,\csc^2\theta\, v^1_{(0),\varphi} + 3\cot\theta\, v^2_{(0),\theta}\Big) + \csc^2\theta\,\lambda_{(0),\varphi} \,, \end{aligned} \tag{9}$$

and have a similar structure to their planar counterparts [Chapter VII, Eq. (6)]. In particular, they involve inertial, viscous, and tensile forces—and are identical to the equations governing a two-dimensional Newtonian fluid. Finally, the unperturbed shape equation is found to be

$$-\rho R^2\Big[(v^1_{(0)})^2 + (v^2_{(0)})^2\sin^2\theta\Big] = [\![p]\!]R - 2\lambda_{(0)} \,. \tag{10}$$

Unlike in the planar system [Chapter VII, Eq. (7)], here Eq. (10) involves a balance of inertial, external, and tensile forces. In the limit where inertial forces are negligible, the shape equation simplifies to the Young–Laplace equation $[\![p]\!] = 2\lambda_{(0)}/R$, which (assuming a constant pressure drop $[\![p]\!]$) defines the surface tension scale

$$\Lambda := \lambda_{(0)} = \frac{[\![p]\!]R}{2} \,. \tag{11}$$

In principle, one could choose any base state satisfying Eqs. (7)–(10), and then consider the linearized dynamics when such a system is perturbed. However, doing so involves much algebra—yet does not yield many additional insights. Thus, from now on, we consider only systems with base velocity given by

$$v^1_{(0)} = 0 \,, \qquad v^2_{(0)} = \Omega \,, \qquad \text{and} \qquad v_{(0)} = 0 \,, \tag{12}$$

where Ω is a constant that we select. When $\Omega = 0$, the base state is static, while if $\Omega \neq 0$ then the sphere is rotating at a constant angular velocity about the z-axis prior to being perturbed. In either case, Eq. (10) requires the base surface tension be given by

$$\lambda_{(0)} = \frac{[\![p]\!]R}{2} + \frac{\rho R^2\Omega^2}{2}\sin^2\theta \,. \tag{13}$$

2. The perturbed equations

At this point, we introduce a radial shape perturbation, such that the membrane position is given by

$$\boldsymbol{x}(\theta,\varphi,t) \;=\; \underbrace{R\,\boldsymbol{e}_r(\theta,\varphi)}_{\boldsymbol{x}_{(0)}(\theta,\varphi)} + \epsilon\,\tilde{r}(\theta,\varphi,t)\,\boldsymbol{e}_r(\theta,\varphi) \;=\; \Big[R \,+\, \epsilon\,\tilde{r}(\theta,\varphi,t)\Big]\,\boldsymbol{e}_r(\theta,\varphi)\;. \tag{14}$$

In Eq. (14), the total radial perturbation $\epsilon\tilde{r}$ is of characteristic size $\delta R \ll R$, with $\mathcal{O}(\tilde{r}) = R$ and $\epsilon := \delta R/R \ll 1$ being the small parameter (see Fig. 1b). With the perturbed membrane shape, we find the following geometric quantities to first order in ϵ:

$$\begin{aligned}
&\boldsymbol{a}_1 \;=\; \big(R+\epsilon\,\tilde{r}\big)\,\boldsymbol{e}_\theta \,+\, \epsilon\,\tilde{r}_{,\theta}\,\boldsymbol{e}_r\;, && \boldsymbol{a}_2 \;=\; \big(R+\epsilon\,\tilde{r}\big)\,\sin\theta\,\boldsymbol{e}_\varphi \,+\, \epsilon\,\tilde{r}_{,\varphi}\,\boldsymbol{e}_r\;,\\
&\boldsymbol{n} \;=\; \boldsymbol{e}_r \,-\, \frac{\epsilon\,\tilde{r}_{,\theta}}{R}\,\boldsymbol{e}_\theta \,-\, \frac{\epsilon\,\tilde{r}_{,\varphi}}{R}\,\csc\theta\,\boldsymbol{e}_\varphi\;, && a_{\alpha\beta} \;=\; \big(R^2 + 2\,\epsilon\,\tilde{r}\,R\big)\,\mathrm{diag}\,(1,\,\sin^2\theta)\;,\\
&H \;=\; -\frac{1}{R} \,+\, \frac{\epsilon}{2R^2}\,\big(2\tilde{r} \,+\, R^2\,\Delta_{\mathrm{s}}\tilde{r}\big)\;, && K \;=\; \frac{1}{R^2} \,-\, \frac{\epsilon}{R^3}\,\big(2\tilde{r} \,+\, R^2\,\Delta_{\mathrm{s}}\tilde{r}\big)\;,\\
&\Gamma^1_{22} \;=\; -\sin\theta\,\cos\theta \,-\, \frac{\epsilon\,\tilde{r}_{,\theta}}{R}\,\sin^2\theta\;, && \Gamma^2_{21} \;=\; \Gamma^2_{12} \;=\; \cot\theta \,+\, \frac{\epsilon\,\tilde{r}_{,\theta}}{R}\;,\\
&\Gamma^1_{12} \;=\; \Gamma^1_{21} \;=\; \frac{\epsilon\,\tilde{r}_{,\varphi}}{R}\;, && \Gamma^2_{11} \;=\; -\,\frac{\epsilon\,\tilde{r}_{,\varphi}}{R}\,\csc^2\theta\;,\\
&\Gamma^1_{11} \;=\; \frac{\epsilon\,\tilde{r}_{,\theta}}{R}\;, && \Gamma^2_{22} \;=\; \frac{\epsilon\,\tilde{r}_{,\varphi}}{R}\;,
\end{aligned} \tag{15}$$

and

$$b_{\alpha\beta} \;=\; \begin{bmatrix} -\,R \,-\, \epsilon\,\tilde{r} \,+\, \epsilon\,\tilde{r}_{,\theta\theta} & \epsilon\,\tilde{r}_{,\theta\varphi} \,-\, \epsilon\,\tilde{r}_{,\varphi}\,\cot\theta \\[2ex] \epsilon\,\tilde{r}_{,\theta\varphi} \,-\, \epsilon\,\tilde{r}_{,\varphi}\,\cot\theta & -\,R\sin^2\theta \,+\, \epsilon\,\big(\tilde{r}_{,\varphi\varphi} \,-\, \tilde{r}\sin^2\theta \,+\, \tilde{r}_{,\theta}\,\sin\theta\,\cos\theta\big) \end{bmatrix}\;.$$

On a nearly spherical surface, the surface Laplacian Δ_{s} of a scalar quantity is given by

$$\Delta_{\mathrm{s}}(\,\cdot\,) \;:=\; \frac{1}{R^2}\,\Big[(\,\cdot\,)_{,\theta\theta} \,+\, (\,\cdot\,)_{,\theta}\,\cot\theta \,+\, (\,\cdot\,)_{,\varphi\varphi}\,\csc^2\theta\Big]\;. \tag{16}$$

Finally, the fundamental membrane unknowns are expanded to first order in the small parameter ϵ as [cf. Eqs. (12) and (13)]

$$\begin{aligned}
&v^1 \;=\; \epsilon\,\tilde{v}^1\;, && v^2 \;=\; \Omega \,+\, \epsilon\,\tilde{v}^2\;,\\
&v \;=\; \epsilon\,\tilde{r}_{,t}\;, \qquad \text{and} && \lambda \;=\; \lambda_{(0)} \,+\, \epsilon\,\tilde{\lambda}\;,
\end{aligned} \tag{17}$$

where in the case of an initially static membrane $\Omega = 0$. In Eq. (17), the normal velocity v is calculated according to $v = \boldsymbol{x}_{,t} \cdot \boldsymbol{n}$.

As in the unperturbed case, we relate the membrane velocity components in the differential geometric and spherical coordinate systems. The membrane velocity $\boldsymbol{v}$ is expanded as

$$\begin{aligned} \boldsymbol{v} &= v^\alpha \boldsymbol{a}_\alpha + v\boldsymbol{n} \\ &= v_r \boldsymbol{e}_r + v_\theta \boldsymbol{e}_\theta + v_\varphi \boldsymbol{e}_\varphi \ , \end{aligned} \tag{18}$$

which upon substitution of Eqs. (15) and (17) and comparison with Eqs. (4) and (6) yields

$$\begin{aligned} v_r &= \epsilon \left(\tilde{r}_{,t} + \tilde{r}_{,\varphi}\, \Omega \right) \ , \qquad\qquad v_\theta = \epsilon\, \tilde{v}^1 R \ , \\ \text{and} \qquad v_\varphi &= \Omega R \sin\theta + \epsilon \left(\tilde{v}^2 R \sin\theta + \tilde{r}\, \Omega \sin\theta \right) \ . \end{aligned} \tag{19}$$

While Eq. (19) will not be used in our scaling analysis of the dynamics of a spherical membrane, it will be relevant when we subsequently analyze the stability of such systems.

We now substitute the geometric quantities in Eq. (15) and the membrane unknowns in Eq. (17) into the general governing equations (Chapter VI, §1), and keep only terms involving a single power of ϵ to obtain the first-order perturbed equations. The continuity equation is expressed as

$$R \left(\tilde{v}^1_{,\theta} + \tilde{v}^2_{,\varphi} + \tilde{v}^1 \cot\theta \right) + 2 \left(\tilde{r}_{,t} + \tilde{r}_{,\varphi}\, \Omega \right) = 0 \ , \tag{20}$$

and involves the perturbed in-plane velocities $\tilde{v}^1$ and $\tilde{v}^2$, the base velocity Ω, and variations of the vesicle shape in both time and space. Next, the perturbed polar and azimuthal in-plane equations are given by

$$\begin{aligned} &\rho R^2 \Big(\tilde{v}^1_{,t} + \tilde{v}^1_{,\varphi} \Omega - 2\tilde{v}^2 \Omega \sin\theta \cos\theta - \frac{\tilde{r}_{,\theta}}{R} \Omega^2 \sin^2\theta \Big) \\ &\quad = \zeta \Big(\tilde{v}^1 + \tilde{v}^1_{,\theta\theta} + \tilde{v}^1_{,\varphi\varphi} \csc^2\theta + \tilde{v}^1_{,\theta} \cot\theta - 2\tilde{v}^2_{,\varphi} \cot\theta - \tilde{v}^1 \cot^2\theta \Big) + \tilde{\lambda}_{,\theta} \ , \end{aligned} \tag{21}$$

and

$$\begin{aligned} &\rho R^2 \Big(\tilde{v}^2_{,t} + \frac{2\tilde{r}_{,t}\, \Omega}{R} + \tilde{v}^\varphi_{,\varphi} \Omega + 2\tilde{v}^1 \Omega \cot\theta + \frac{\tilde{r}_{,\varphi}}{R} \Omega^2 \Big) \\ &\quad = \zeta \Big(\tilde{v}^2_{,\theta\theta} + \tilde{v}^2_{,\varphi\varphi} \csc^2\theta + 2\tilde{v}^1_{,\varphi} \cot\theta \csc^2\theta + 3\tilde{v}^2_{,\theta} \cot\theta \Big) + \tilde{\lambda}_{,\varphi} \csc^2\theta \ , \end{aligned} \tag{22}$$

respectively. Equations (21) and (22) are both comprised of inertial, viscous, and tensile forces. Finally, the perturbed shape equation is written as

$$\begin{aligned} &\rho R^2 \Big(\tilde{r}_{,tt} - 2\tilde{v}^\varphi \Omega R \sin^2\theta + \Omega^2 \left[\tilde{r}_{,\theta} \sin\theta \cos\theta + \tilde{r}_{,\varphi\varphi} - \tilde{r} \sin^2\theta \right] + \tilde{r}_{,t\varphi}\, \Omega \Big) \\ &\quad = -2R\tilde{\lambda} + \lambda_{(0)} \Big(2\tilde{r} + R^2 \Delta_{\mathrm{s}} \tilde{r} \Big) - \frac{k_{\mathrm{b}}}{2} \Big(R^2 \Delta_{\mathrm{s}}^2\, \tilde{r} + 2\Delta_{\mathrm{s}} \tilde{r} \Big) \\ &\qquad + 2\zeta\, \Omega \Big(\tilde{r}_{,\theta\varphi} \cos\theta \big[\csc\theta - \sin\theta \big] - \tilde{r}_{,\varphi} \cos^2\theta \cot^2\theta \Big) \ . \end{aligned} \tag{23}$$

We now non-dimensionalize both the unperturbed (7)–(10) and perturbed (20)–(23) governing equations for the initially static and rotating base states.

3. The dynamics about an initially static vesicle

For a spherical vesicle initially at rest, $\Omega = 0$ in Eq. (12). In this case, the unperturbed continuity equation (7) is automatically satisfied, and the equations of motion (8)–(10) simplify to

$$\lambda_{(0),\theta} = 0 \,, \qquad \lambda_{(0),\varphi} = 0 \,, \qquad \text{and} \qquad \lambda_{(0)} = \frac{[\![p]\!]R}{2} \,. \tag{24}$$

The unperturbed solution is then given by

$$v^1_{(0)} = 0 \,, \qquad v^2_{(0)} = 0 \,, \qquad v_{(0)} = 0 \,, \qquad \text{and} \qquad \lambda_{(0)} = \lambda_0 := \frac{[\![p]\!]R}{2} \,. \tag{25}$$

The base state sets the length scale R, as well as the surface tension scale $\mathit{\Lambda}$, with the latter provided in Eq. (11). We now seek to determine the velocity and time scales via non-dimensionalization of the perturbed equations, as these quantities are not set in the base state.

Substituting the unperturbed solution (25) into the perturbed equations (20)–(23) yields

$$\tilde{v}^1_{,\theta} + \tilde{v}^2_{,\varphi} + \cot\theta\,\tilde{v}^1 + \frac{2}{R}\,\tilde{r}_{,t} = 0 \,, \tag{26}$$

$$\rho R^2\,\tilde{v}^1_{,t} = \zeta\left(\tilde{v}^1 + \tilde{v}^1_{,\theta\theta} + \csc^2\theta\,\tilde{v}^1_{,\varphi\varphi} + \cot\theta\,\tilde{v}^1_{,\theta} - 2\cot\theta\,\tilde{v}^2_{,\varphi} - \cot^2\theta\,\tilde{v}^1\right) + \tilde{\lambda}_{,\theta} \,, \tag{27}$$

$$\rho R^2\,\tilde{v}^2_{,t} = \zeta\left(\tilde{v}^2_{,\theta\theta} + \csc^2\theta\,\tilde{v}^2_{,\varphi\varphi} + 2\cot\theta\,\csc^2\theta\,\tilde{v}^1_{,\varphi} + 3\cot\theta\,\tilde{v}^2_{,\theta}\right) + \csc^2\theta\,\tilde{\lambda}_{,\varphi} \,, \tag{28}$$

and

$$\rho R^2\,\tilde{r}_{,tt} = -2R\tilde{\lambda} + \lambda_0\left(2\tilde{r} + R^2\Delta_{\mathrm{s}}\tilde{r}\right) - \frac{k_{\mathrm{b}}}{2}\left(R^2\Delta_{\mathrm{s}}^2\tilde{r} + 2\Delta_{\mathrm{s}}\tilde{r}\right) . \tag{29}$$

As in the flat case, viscous terms do not appear in the perturbed shape equation of an initially static spherical vesicle (29). Therefore, in this case, we will not obtain the Scriven–Love number SL upon non-dimensionalization.

At this point, we provide characteristic scales for all unknown quantities. We assume the perturbed velocities $\tilde{v}^1$ and $\tilde{v}^2$ are of the same order, which we denote $\mathit{\Omega}$. Recalling that ϵ captures the smallness of all perturbed quantities, we recognize that the perturbed surface tension $\tilde{\lambda}$ is of order $\mathit{\Lambda}$, as defined in Eq. (11). Finally, we assume the radial shape perturbations $\tilde{r}$, which are of characteristic size R, vary over a time scale τ. This leads to the following dimensionless quantities:

$$\begin{gathered} \theta^* := \theta \,, \qquad \varphi^* := \varphi \,, \qquad \tilde{r}^* := \frac{\tilde{r}}{R} \,, \qquad \tilde{v}^{1*} := \frac{\tilde{v}^1}{\mathit{\Omega}} \,, \\ \tilde{v}^{2*} := \frac{\tilde{v}^2}{\mathit{\Omega}} \,, \qquad \tilde{\lambda}^* := \frac{\tilde{\lambda}}{\mathit{\Lambda}} \,, \qquad \text{and} \qquad t^* := \frac{t}{\tau} \,, \end{gathered} \tag{30}$$

which are all $\mathcal{O}(1)$ by construction. Substituting Eq. (30) into the perturbed continuity equation (26), we obtain

$$\tilde{v}^{1*}_{,\theta^*} + \tilde{v}^{2*}_{,\varphi^*} + \cot\theta^*\,\tilde{v}^{1*} + \frac{2}{\tau\mathit{\Omega}}\,\tilde{r}^*_{,t^*} = 0 \,. \tag{31}$$

As in-plane flows are required to balance shape changes to the membrane, we find the angular velocity scale Ω is given by

$$\Omega \;=\; \frac{1}{\tau}\;. \tag{32}$$

Next, the in-plane equations are considered. Substituting Eqs. (30) and (32) into the perturbed in-plane equations (27, 28) and rearranging terms yields

$$Re\,\tilde{v}^{1*}_{,t^*} \;=\; \tilde{v}^{1*} \;+\; \tilde{v}^{1*}_{,\theta^*\theta^*} \;+\; \csc^2\theta^*\,\tilde{v}^{1*}_{,\varphi^*\varphi^*} \;+\; \cot\theta^*\,\tilde{v}^{1*}_{,\theta^*} \;-\; 2\cot\theta^*\,\tilde{v}^{2*}_{,\varphi^*} \;-\; \cot^2\theta^*\,\tilde{v}^{1*} \;+\; \frac{\Lambda}{\zeta\Omega}\,\tilde{\lambda}^*_{,\theta^*} \tag{33}$$

and

$$Re\,\tilde{v}^{2*}_{,t^*} \;=\; \tilde{v}^{2*}_{,\theta^*\theta^*} \;+\; \csc^2\theta^*\,\tilde{v}^{2*}_{,\varphi^*\varphi^*} \;+\; 2\cot\theta^*\csc^2\theta^*\,\tilde{v}^{1*}_{,\varphi^*} \;+\; 3\cot\theta^*\,\tilde{v}^{2*}_{,\theta^*} \;+\; \frac{\Lambda}{\zeta\Omega}\csc^2\theta^*\,\tilde{\lambda}^*_{,\varphi^*}\;, \tag{34}$$

where for spherical vesicles the Reynolds number Re is given by

$$Re \;:=\; \frac{\rho\Omega R^2}{\zeta}\;. \tag{35}$$

Assuming viscous forces are of the same order as surface tension forces in the perturbed in-plane equations, one obtains

$$\Omega \;=\; \frac{\Lambda}{\zeta}\;, \qquad \text{with} \qquad \tau \;=\; \frac{\zeta}{\Lambda}\;, \tag{36}$$

such that the base state surface tension sets the scale of angular velocities and also the time scale over which radial perturbations change. In this case, over the range of experiments considered in this work, $\mathcal{O}(Re) \leq 10^{-4}$ and inertial terms are indeed negligible.

Finally, substituting Eqs. (30), (32), and (36) into the perturbed shape equation (29), we obtain

$$Re\,\Gamma\,\tilde{r}^*_{,t^*t^*} \;=\; \Gamma\Big(2\tilde{r}^* + \Delta^*_{\mathrm{s}}\tilde{r}^* - 2\tilde{\lambda}^*\Big) \;-\; \frac{1}{2}\Big(\Delta^{*2}_{\mathrm{s}}\tilde{r}^* \;+\; 2\Delta^*_{\mathrm{s}}\tilde{r}^*\Big)\;, \tag{37}$$

where the Föppl–von Kármán number Γ is defined as

$$\Gamma \;:=\; \frac{\Lambda R^2}{k_{\mathrm{b}}} \tag{38}$$

and the dimensionless surface Laplacian is given by $\Delta^*_{\mathrm{s}}(\,\cdot\,) := R^2\Delta_{\mathrm{s}}(\,\cdot\,)$ [cf. Eq. (16)]. As the inertial terms on the left-hand side of Eq. (37) contains a factor of $Re\,\Gamma$ and $Re \ll 1$, inertial terms are always negligible compared to surface tension terms. However, we note that in cases where Γ is large, inertial terms can be comparable to bending terms. Regardless of the value of Γ, inertial forces do not significantly affect the out-of-plane membrane dynamics. The dimensionless perturbed equations governing initially static spherical vesicles are then given by

$$\tilde{v}^{1*}_{,\theta^*} \;+\; \tilde{v}^{2*}_{,\varphi^*} \;+\; \cot\theta^*\,\tilde{v}^{1*} \;+\; 2\tilde{r}^*_{,t^*} \;=\; 0\;, \tag{39}$$

$$\tilde{v}^{1*} + \tilde{v}^{1*}_{,\theta^*\theta^*} + \csc^2\theta^*\,\tilde{v}^{1*}_{,\varphi^*\varphi^*} + \cot\theta^*\,\tilde{v}^{1*}_{,\theta^*} - 2\cot\theta^*\,\tilde{v}^{2*}_{,\varphi^*} - \cot^2\theta^*\,\tilde{v}^{1*} + \tilde{\lambda}^*_{,\theta^*} = 0\,, \tag{40}$$

$$\tilde{v}^{2*}_{,\theta^*\theta^*} + \csc^2\theta^*\,\tilde{v}^{\varphi*}_{,\varphi^*\varphi^*} + 2\cot\theta^*\csc^2\theta^*\,\tilde{v}^{1*}_{,\varphi^*} + 3\cot\theta^*\,\tilde{v}^{2*}_{,\theta^*} + \csc^2\theta^*\,\tilde{\lambda}^*_{,\varphi^*} = 0\,, \tag{41}$$

and

$$\mathit{\Gamma}\left(2\tilde{r}^* + \Delta^*_{\mathrm{s}}\tilde{r}^* - 2\tilde{\lambda}^*\right) - \frac{1}{2}\left(\Delta^{*2}_{\mathrm{s}}\tilde{r}^* + 2\Delta^*_{\mathrm{s}}\tilde{r}^*\right) = 0\,. \tag{42}$$

While Eqs. (39)–(42) contain more terms than their flat counterparts [Chapter VII, Eqs. (22), (28), and (35)], their fundamental structure is similar. The continuity equation (39) connects in-plane flows with out-of-plane shape deformations, while Eqs. (40) and (41) relate angular velocities and their derivatives to surface tension gradients. Interestingly, no viscous forces appear in the perturbed shape equation of an initially static vesicle (42), as was the case for an initially static flat patch [Chapter VII, Eq. (35)]—despite the geometries being different. The first term in parenthesis in Eq. (42) arises from the out-of-plane surface tension force $2\lambda H$, sometimes referred to as the Laplace pressure, while the second term arises from the bending-induced forces $-2k_{\mathrm{b}}H(H^2 - K) - k_{\mathrm{b}}\Delta_{\mathrm{s}}H$. We once again see the Föppl–von Kármán number capturing the relative importance of bending and tension terms in governing the membrane's dynamical response to a perturbation. For example, in GUVs we have characteristic values $\mathit{\Lambda} \sim 10^{-4}$ pN/nm and $R \sim 10$ μm [‡], while in small membrane vesicles surrounding retrovirus particles $R \sim 50$ nm [†]. Assuming $\mathit{\Lambda} \sim 10^{-3}$ pN/nm in the latter, $\mathit{\Gamma}$ ranges from 10^{-2} to 10^{2}—such that the dynamical response of large vesicles is tension-dominated while that of small vesicles is bending-dominated. However, as discussed previously, the base state surface tension can span a wide range of values at any radius to enforce areal incompressibility, and $\mathit{\Gamma}$ can span an even wider range of values than those presented here.

4. The dynamics about an initially rotating vesicle

When a spherical lipid membrane is placed in a bulk shear flow, the velocity gradient in the surrounding fluid imparts a torque on the membrane and can cause it to rotate about a fixed axis with a nonzero angular velocity $v^2_{(0)} = \mathit{\Omega} \neq 0$. In experimental systems, when the inner and outer fluids have the same viscosity, rotating GUVs are observed in shear flows with shear rates $\dot{\gamma}$ up to 10^{-4} μs^{-1}. [*, §, ♯, ‖] Moreover, in large blood vessels in the human body, shear rates can be as high as $\dot{\gamma} \sim 10^{-3}$ μs^{-1}. [∀] For a spherical lipid membrane vesicle

[‡] Pécréaux et al., "Refined contour analysis of giant unilamellar vesicles".

[†] F. Förster et al. "Retrovirus envelope protein complex structure in situ studied by cryo-electron tomography". *Proc. Natl. Acad. Sci. U.S.A.* **102** (2005), 4729–4734.

[*] Haas et al., "Deformation of giant lipid bilayer vesicles in shear flow".

[§] Kantsler and Steinberg, "Orientation and dynamics of a vesicle in tank-treading motion in shear flow".

[♯] Deschamps, Kantsler, and Steinberg, "Phase diagram of single vesicle dynamical states in shear flow".

[‖] S. Ota, S. Yoshizawa, and S. Takeuchi. "Microfluidic formation of monodisperse, cell-sized, and unilamellar vesicles". *Angew. Chem. Int. Edit.* **48** (2009), 6533–6537.

[∀] H.H. Lipowsky, S. Usami, and S. Chien. "In vivo measurements of "apparent viscosity" and microvessel hematocrit in the mesentery of the cat". *Microvasc. Res.* **19** (1980), 297–319.

in a shear flow, we assume the angular velocity

$$\Omega = \dot{\gamma} \tag{43}$$

in the base state, and in our non-dimensionalization set the scale of $\tilde{v}^1$ and $\tilde{v}^2$ to be Ω. We are thus in a similar situation to the case of a planar membrane with a base flow: here, the base state sets the length scale R, surface tension scale Λ [cf. Eq. (11)], and angular velocity scale Ω—for which viscous forces and tension forces may not balance in the perturbed in-plane equations. Consequently, the introduction of a flow of lipids in the base state leads to a new length scale over which in-plane quantities vary, while the perturbed membrane shape $\tilde{r}$ continues to vary over a length R. The emergence of a new length scale in the perturbed equations implies care must be taken when predicting the magnitude of perturbed in-plane and out-of-plane forces.

(a). The unperturbed equations

We begin by revisiting the unperturbed equations, where we now suppose a base flow velocity $\boldsymbol{v}_{(0)}$ given by [cf. Eq. (4)]

$$\boldsymbol{v}_{(0)} = \Omega R \sin\theta \boldsymbol{e}_\varphi \,, \qquad \text{for which} \qquad v^1_{(0)} = 0 \quad \text{and} \quad v^2_{(0)} = \Omega \,. \tag{44}$$

Substituting Eq. (44) into the unperturbed equations (7)–(10) reveals the continuity equations is automatically satisfied; the remaining equations simplify to

$$\lambda_{(0),\theta} = \rho R^2 \Omega^2 \sin\theta \cos\theta \,, \tag{45}$$

$$\lambda_{(0),\varphi} = 0 \,, \tag{46}$$

and

$$\lambda_{(0)} = \frac{1}{2}\left([\![p]\!] R + \rho R^2 \Omega^2 \sin^2\theta \right) . \tag{47}$$

For a constant pressure drop $[\![p]\!]$ across the membrane surface, the base tension $\lambda_{(0)}$ obtained in Eq. (47) satisfies the in-plane equations. The state of the unperturbed vesicle is then fully characterized by the in-plane velocity components in Eq. (44) and surface tension in Eq. (47).

At this point, we recognize that for the spherical vesicles under consideration [see §4 (c)], $\rho \sim 10^{-8}$ pg/nm^2, $R \sim 10^2$–10^4 nm, $\Omega \leq 10^{-3}$ μsec^{-1}, and $\lambda_{(0)} \sim 10^{-4}$–$10^{-1}$ pN/nm. In this case, $O(\rho R^2 \Omega^2) \sim 10^{-12}$–$10^{-6}$ pN/nm, and inertial forces are negligible relative to their tensile counterparts. Equations (45)–(47) then simplify to

$$\lambda_{(0),\theta} = 0 \,, \qquad \lambda_{(0),\varphi} = 0 \,, \qquad \text{and} \qquad \lambda_{(0)} = \frac{[\![p]\!] R}{2} \,, \tag{48}$$

such that the unperturbed solution is given by

$$v^1_{(0)} = 0 \,, \qquad v^2_{(0)} = \Omega \,, \qquad v_{(0)} = 0 \,, \qquad \text{and} \qquad \lambda_{(0)} = \Lambda := \frac{[\![p]\!] R}{2} \,. \tag{49}$$

In this case, the characteristic scales

$$\Omega := \dot{\gamma} \qquad \text{and} \qquad \Lambda = \frac{[\![p]\!]R}{2} \tag{50}$$

are set by the base state—which, as we will now show, leads to the fundamental membrane unknowns varying over different length scales in the perturbed dynamics.

(b). The perturbed equations

In the base state, quantities are expected to vary over $\mathcal{O}(1)$ changes in the angles θ and φ, or equivalently over $\mathcal{O}(R)$ lengths on the membrane surface. As in the planar case, the introduction of an angular velocity scale Ω in the base state allows for the possibility of a new length scale ℓ—or equivalently, a new angular scale $\Phi = \ell/R$—over which quantities can vary in the perturbed system. As the governing equations are written in terms of angular derivatives, we will predominantly use the new angular scale Φ in our analysis here. Following the developments in the planar case, we first demonstrate why a new angular scale is needed, as we expect to recover the static vesicle results in the limit where Ω goes to zero. We then show why all quantities cannot vary over the new angular scale, and determine which quantities vary over Φ. Note that due to the geometry of the system, $\Phi \leq 1$.

Scaling Attempt #1: Variations over radius R (incorrect)

First, assume all perturbed quantities vary over $\mathcal{O}(1)$ changes in θ and φ, such that $\theta^* = \theta$ and $\varphi^* = \varphi$. In this case, all perturbed quantities are scaled according to Eq. (30), where the angular velocity scale Ω and surface tension scale Λ are set by the base state (50). The perturbed continuity equation (20) is non-dimensionalized as

$$\tilde{v}^{1*}_{,\theta^*} + \tilde{v}^{2*}_{,\varphi^*} + \cot\theta^*\,\tilde{v}^{1*} + 2\tilde{r}^*_{,\varphi^*} + \frac{2}{\tau\,\Omega}\,\tilde{r}^*_{,t^*} = 0\,, \tag{51}$$

for which we choose the time scale τ to given by $\tau = 1/\Omega$ such that in-plane and out-of-plane quantities are of the same order. Equation (51) then simplifies to

$$\tilde{v}^{1*}_{,\theta^*} + \tilde{v}^{2*}_{,\varphi^*} + \cot\theta^*\,\tilde{v}^{1*} + 2\,\tilde{r}^*_{,\varphi^*} + 2\,\tilde{r}^*_{,t^*} = 0\,. \tag{52}$$

Next, Eq. (30) is substituted into the in-plane equations (21, 22). Neglecting inertial terms for the simplicity of our argument, we obtain

$$\tilde{v}^{1*} + \tilde{v}^{1*}_{,\theta^*\theta^*} + \csc^2\theta^*\,\tilde{v}^{1*}_{,\varphi^*\varphi^*} + \cot\theta^*\,\tilde{v}^{1*}_{,\theta^*} - 2\cot\theta^*\,\tilde{v}^{2*}_{,\varphi^*} - \cot^2\theta^*\,\tilde{v}^{1*} + \frac{\Lambda}{\zeta\,\Omega}\,\tilde{\lambda}^*_{,\theta^*} = 0 \tag{53}$$

and

$$\tilde{v}^{2*}_{,\theta^*\theta^*} + \csc^2\theta^*\,\tilde{v}^{2*}_{,\varphi^*\varphi^*} + 2\cot\theta^*\,\csc^2\theta^*\,\tilde{v}^{1*}_{,\varphi^*} + 3\cot\theta^*\,\tilde{v}^{2*}_{,\theta^*} + \frac{\Lambda}{\zeta\,\Omega}\,\csc^2\theta^*\,\tilde{\lambda}^*_{,\varphi^*} = 0\,. \tag{54}$$

Recalling that Ω and Λ are set by the base state (50), we find that in the limit of vanishing Ω, i.e. when Ω tends to zero, the in-plane equations (53, 54) imply $\tilde{\lambda}^* = \text{constant}$. However, in the limit of vanishing base velocity, we expect to recover the initially static shape equation (42), in which the perturbed surface tension varies over the patch in reaction to the perturbed membrane shape. This is not the case, and thus our assumption that all quantities vary over $\mathcal{O}(1)$ changes in θ and φ is unphysical.

Scaling Attempt #2: Variations over new length scale (incorrect)

Next, we attempt to find a consistent scaling result by introducing a new angular scale Φ over which all perturbed quantities vary. In this case, we define the new quantities

$$\theta' := \frac{\theta}{\Phi} , \qquad \varphi' := \frac{\varphi}{\Phi} \qquad \text{and} \qquad \Delta_{\mathrm{s}}'(\,\cdot\,) := \Phi^2 R^2 \Delta_{\mathrm{s}}(\,\cdot\,) , \tag{55}$$

such that all angular derivatives are non-dimensionalized with θ' and φ' rather than θ^* and φ^*. All other perturbed quantities are non-dimensionalized as in Eq. (30). The dimensionless continuity equation is obtained by substituting Eqs. (30) and (55) into Eq. (20), and is found to be

$$\tilde{v}^{1*}_{,\theta'} + \tilde{v}^{2*}_{,\varphi'} + \Phi \cot\theta^* \, \tilde{v}^{1*} + 2\tilde{r}^*_{,\varphi'} + \frac{2\Phi}{\tau\Omega} \tilde{r}^*_{,t^*} = 0 . \tag{56}$$

As $\Phi \leq 1$ due to geometric constraints, and it is possible that $\Phi \ll 1$, Eq. (56) requires the time scale τ to be given by

$$\tau = \frac{\Phi}{\Omega} \tag{57}$$

such that in-plane and out-of-plane motions are of the same order. Accordingly, Eq. (56) simplifies to

$$\tilde{v}^{1*}_{,\theta'} + \tilde{v}^{2*}_{,\varphi'} + \Phi \cot\theta^* \, \tilde{v}^{1*} + 2\tilde{r}^*_{,\varphi'} + 2\tilde{r}^*_{,t^*} = 0 . \tag{58}$$

Neglecting inertial terms to simplify our argument, we express the in-plane θ and φ equations, respectively, as [cf. Eqs. (21) and (22)]

$$\Phi^2 \tilde{v}^{1*} + \tilde{v}^{1*}_{,\theta'\theta'} + \csc^2\theta' \, \tilde{v}^{1*}_{,\varphi'\varphi'} + \Phi \cot\theta^* \, \tilde{v}^{1*}_{,\theta'} - 2\Phi \cot\theta^* \, \tilde{v}^{2*}_{,\varphi'} - \Phi^2 \cot^2\theta^* \, \tilde{v}^{1*} + \frac{\Lambda\Phi}{\zeta\Omega} \tilde{\lambda}^*_{,\theta'} = 0 \tag{59}$$

and

$$\tilde{v}^{2*}_{,\theta'\theta'} + \csc^2\theta^* \, \tilde{v}^{2*}_{,\varphi'\varphi'} + 2\Phi \cot\theta^* \csc^2\theta^* \, \tilde{v}^{1*}_{,\varphi'} + 3\Phi \cot\theta^* \, \tilde{v}^{2*}_{,\theta'} + \frac{\Lambda\Phi}{\zeta\Omega} \csc^2\theta^* \, \tilde{\lambda}^*_{,\varphi'} = 0 . \tag{60}$$

To ensure surface tension gradients are of the same order as in-plane viscous forces, even in the limit of small Ω, we must have

$$\Phi = \frac{\zeta\Omega}{\Lambda} \qquad \text{and} \qquad \tau = \frac{\zeta}{\Lambda} , \tag{61}$$

with the latter satisfying Eq. (57). Finally, the shape equation (23) is non-dimensionalized with Eqs. (30) and (55), and is given by

$$\begin{aligned} \Phi^2\Lambda \left(2\Phi^2 \tilde{r}^* + \Delta_{\mathrm{s}}' \, \tilde{r}^* - 2\Phi^2 \tilde{\lambda}^* \right) - \frac{k_{\mathrm{b}}}{2R^2} \left(\Delta_{\mathrm{s}}'^2 \, \tilde{r}^* + 2\Phi^2 \Delta_{\mathrm{s}}' \, \tilde{r}^* \right) \\ + 2\zeta\Omega\Phi^2 \left(\cos\theta^* \big[\csc\theta^* - \sin\theta^* \big] \, \tilde{r}^*_{,\theta'\varphi'} - \Phi \cos^2\theta^* \cot^2\theta^* \, \tilde{r}^*_{,\varphi'} \right) = 0 . \end{aligned} \tag{62}$$

Thus, in the limit where Ω tends to zero, for which [see Eq. (61)] Φ tends to zero as well, Eq. (62) simplifies to

$$\Delta_{\mathrm{s}}'^2 \, \tilde{r}^* = 0 . \tag{63}$$

However, one must recover the initially static shape equation (42) when Ω goes to zero. As this is not the case, our choice of scaling here is again incorrect.

Scaling Attempt #3: Variations over multiple length scales (correct)

At this point, we recognize that $\tilde{v}^1$, $\tilde{v}^2$, and $\tilde{\lambda}$ must vary over $\mathcal{O}(\Phi)$ changes in θ and φ, or equivalently an $\mathcal{O}(\ell)$ length scale, while $\tilde{r}$ does not. We assume $\tilde{r}$ varies over $\mathcal{O}(1)$ changes in θ and φ, as in the initially static scenario. With this choice, the first-order continuity equation (20) is non-dimensionalized as

$$\tilde{v}^{1*}_{,\theta'} + \tilde{v}^{\varphi*}_{,\varphi'} + \Phi\left(\cot\theta^*\,\tilde{v}^{1*} + 2\tilde{r}^*_{,\varphi^*}\right) + \frac{2\Phi}{\tau\,\Omega}\,\tilde{r}^*_{,t^*} = 0\,, \tag{64}$$

which once more requires the time and angular velocity scales to be given by Eq. (61). In Eq. (64), and throughout the rest of this section, spatial derivatives of the perturbed velocities and surface tensions are with respect to θ' and φ', while those of the perturbed radius are with respect to θ^* and φ^*. Upon substitution of Eq. (61) into Eq. (64), we obtain the appropriate scaled continuity equation

$$\tilde{v}^{1*}_{,\theta'} + \tilde{v}^{2*}_{,\varphi'} + \Phi\left(\cot\theta^*\,\tilde{v}^{1*} + 2\,\tilde{r}^*_{,\varphi^*}\right) + 2\,\tilde{r}^*_{,t^*} = 0\,. \tag{65}$$

The perturbed in-plane equations are non-dimensionalized in the same manner, for which

$$\begin{aligned} &Re\,\Phi\left(\tilde{v}^{1*}_{,t^*} + \tilde{v}^{1*}_{,\varphi'} - 2\,\Phi\sin\theta^*\cos\theta^*\,\tilde{v}^{2*} - \Phi\sin^2\theta^*\,\tilde{r}^*_{,\theta^*}\right) \\ &\quad = \tilde{v}^{1*}_{,\theta'\theta'} + \csc^2\theta^*\,\tilde{v}^{1*}_{,\varphi'\varphi'} + \Phi\cot\theta^*\left(\tilde{v}^{1*}_{,\theta'} - 2\,\tilde{v}^{2*}_{,\varphi'}\right) + \Phi^2\,\tilde{v}^{1*}\left(1-\cot^2\theta^*\right) + \tilde{\lambda}^*_{,\theta'} \end{aligned} \tag{66}$$

and

$$\begin{aligned} &Re\,\Phi\left(\tilde{v}^{2*}_{,t^*} + 2\,\tilde{r}^*_{,t^*} + \tilde{v}^{2*}_{,\varphi'} + 2\,\Phi\cot\theta^*\,\tilde{v}^{1*} + \Phi\,\tilde{r}^*_{,\varphi^*}\right) \\ &\quad = \tilde{v}^{2*}_{,\theta'\theta'} + \csc^2\theta^*\,\tilde{v}^{2*}_{,\varphi'\varphi'} + \Phi\cot\theta^*\left(2\csc^2\theta^*\,\tilde{v}^{1*}_{,\varphi'} + 3\,\tilde{v}^{2*}_{,\theta'}\right) + \csc^2\theta^*\,\tilde{\lambda}^*_{,\varphi'}\,. \end{aligned} \tag{67}$$

In Eqs. (66) and (67), the Reynolds number Re is defined in Eq. (35) and the choice of Φ in Eq. (61) ensures viscous forces and tension forces are the same order. As $Re \ll 1$ (to be shown subsequently) and $\Phi \leq 1$ by definition, Eqs. (66) and (67) simplify to

$$\tilde{v}^{1*}_{,\theta'\theta'} + \csc^2\theta^*\,\tilde{v}^{1*}_{,\varphi'\varphi'} + \Phi\cot\theta^*\left(\tilde{v}^{1*}_{,\theta'} - 2\,\tilde{v}^{2*}_{,\varphi'}\right) + \Phi^2\,\tilde{v}^{1*}\left(1-\cot^2\theta^*\right) + \tilde{\lambda}^*_{,\theta'} = 0 \tag{68}$$

and

$$\tilde{v}^{2*}_{,\theta'\theta'} + \csc^2\theta^*\,\tilde{v}^{2*}_{,\varphi'\varphi'} + \Phi\cot\theta^*\left(2\csc^2\theta^*\,\tilde{v}^{1*}_{,\varphi'} + 3\,\tilde{v}^{2*}_{,\theta'}\right) + \csc^2\theta^*\,\tilde{\lambda}^*_{,\varphi'} = 0\,, \tag{69}$$

which are the properly scaled perturbed in-plane equations governing an initially rotating vesicle. Finally, the perturbed shape equation (23) is considered. Upon substitution of Eqs. (55) and (61) into the shape equation and rearranging terms, we obtain

$$\begin{aligned} &\frac{Re\Gamma}{\Phi}\left(\tilde{r}^*_{,t^*t^*} + \Phi\,\tilde{r}^*_{,t^*\varphi^*} + \Phi^2\Big[-2\sin^2\theta^*\,\tilde{v}^{2*} - \sin\theta^*\,\tilde{r}^* + \sin\theta^*\cos\theta^*\,\tilde{r}^*_{,\theta^*} + \tilde{r}^*_{,\varphi^*\varphi^*}\Big]\right) \\ &\quad = 2\,\frac{\zeta\Omega R^2}{k_{\mathrm{b}}}\left(\cos\theta^*\left[\csc\theta^* - \sin\theta^*\right]\tilde{r}^*_{,\theta^*\varphi^*} - \cos^2\theta^*\cot^2\theta^*\,\tilde{r}^*_{,\varphi^*}\right) \\ &\qquad + \Gamma\left(2\tilde{r}^* + \Delta^*_{\mathrm{s}}\,\tilde{r}^* - 2\tilde{\lambda}^*\right) - \frac{1}{2}\left(\Delta^{*2}_{\mathrm{s}}\,\tilde{r}^* + 2\Delta^*_{\mathrm{s}}\,\tilde{r}^*\right). \end{aligned} \tag{70}$$

As we will see in §4 (c), for the systems under consideration, $Re/\Phi \leq 10^{-3} \ll 1$—such that inertial forces are always negligible relative to tension forces. Equation (70) shows the ratio of out-of-plane viscous forces to bending forces gives rise to the Scriven–Love number, here defined as

$$\mathcal{SL} := \frac{\zeta \Omega R^2}{k_\mathrm{b}} \,. \tag{71}$$

Substituting Eq. (71) into Eq. (70) and neglecting inertial terms leads to the final form of the perturbed shape equation, given by

$$\begin{aligned} &2\,\mathcal{SL}\left(\cos\theta^*\left[\csc\theta^* - \sin\theta^*\right]\tilde{r}^*_{,\theta^*\varphi^*} - \cos^2\theta^*\cot^2\theta^*\,\tilde{r}^*_{,\varphi^*}\right) \\ &\quad + \Gamma\left(2\tilde{r}^* + \Delta^*_\mathrm{s}\,\tilde{r}^* - 2\tilde{\lambda}^*\right) - \frac{1}{2}\left(\Delta^{*2}_\mathrm{s}\,\tilde{r}^* + 2\Delta^*_\mathrm{s}\,\tilde{r}^*\right) = 0 \,. \end{aligned} \tag{72}$$

The first line in Eq. (72) consists of the out-of-plane viscous forces arising from the rotational base flow, which were not present in the perturbed shape equation of an initially static spherical vesicle (29). The second line in Eq. (72) contains the surface tension and bending forces, which are identical to those found in the static vesicle [cf. Eq. (72)]. We note that with Eq. (71), the angular scale Φ can be expressed as $\Phi = \Gamma^{-1}\mathcal{SL}$, such that the ratio of the Scriven–Love and Föppl–von Kármán numbers dictates the relative size of various terms in the continuity (65) and in-plane (68, 69) equations as well. We also observe that in the limit where Ω goes to zero, $\mathcal{SL}$ goes to zero as well (71) and the shape equation (72) simplifies to its initially static counterpart, namely Eq. (42).

(c). The analysis of past experimental data

We now present our calculation of the Scriven–Love and Föppl–von Kármán numbers, for initially rotating spherical vesicles, as the Scriven–Love number does not arise for initially static spheres. The results of five prior experiments are summarized in Fig. 2, and detailed in Tables 1–5 below. When values of the bending modulus k_b and surface tension scale Λ are not provided, we assume $k_\mathrm{b} = 100$ pN $\cdot$ nm and $\Lambda = 10^{-3}$ pN/nm. In all cases, we use $\zeta = 10$ pN $\cdot$ μsec/nm. [‡, †] Furthermore, in all experiments considered, the shear rate $\dot{\gamma}$ is provided; we choose $\Omega = \dot{\gamma}$ and calculate the velocity scale V as

$$V = \dot{\gamma} R \,. \tag{73}$$

(d). The findings of our scaling analysis

For spherical membranes with a base flow, we find three experimentally relevant regimes; in each case, we provide the relevant data in Fig. 2 and Tables 1–5. The bending-dominated regime is characteristic of small membrane vesicles, as in the case of 100 nm vesicles surrounding retrovirus particles, [*] for which $\mathcal{SL} \ll 1$ and $\Gamma \ll 1$. In this case, the shape equation

[‡] P. Cicuta, S.L. Keller, and S.L. Veatch. "Diffusion of liquid domains in lipid bilayer membranes". *J. Phys. Chem. B* **111** (2007), 3328–3331. arXiv: cond-mat/0611492.

[†] A.R. Honerkamp-Smith et al. "Membrane viscosity determined from shear-driven flow in giant vesicles". *Phys. Rev. Lett.* **111** (2013), 038103. arXiv: 1308.6440.

[*] Förster et al., "Retrovirus envelope protein complex structure in situ studied by cryo-electron tomography".

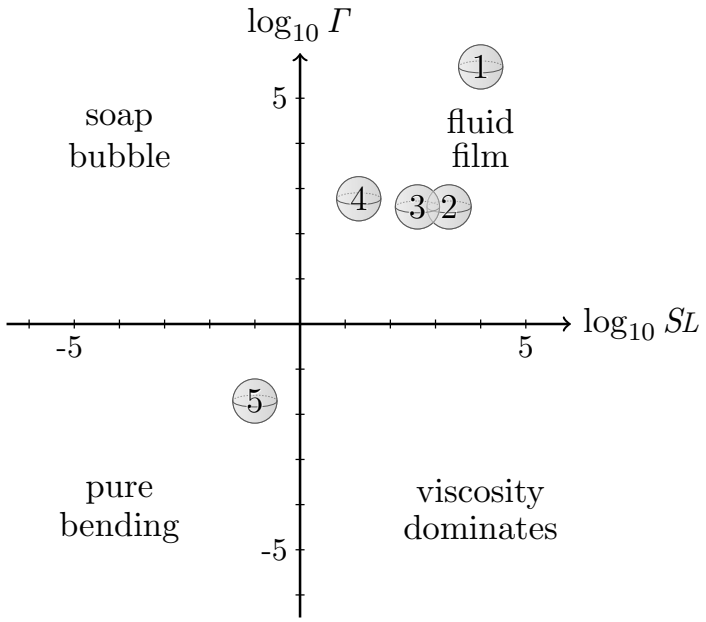

Figure 2: Plot of the Scriven–Love number SL and Föppl–von Kármán number Γ in five past experiments involving spherical geometries [cf. Chapter VI, Fig. 2]. Each numbered figure corresponds to a single experiment, which is described in Tables 1–5. Experiments #1 through #4 have large tensile and viscous forces in the out-of-plane direction, and thus behave constitutively like a fluid film. Experiment #5, on the other hand, is bending-dominated.

Experiment #1: GUVs in shear flow

Table 1: Calculations from Figs. 2, 4, and 6 of K.H. de Haas et al. "Deformation of giant lipid bilayer vesicles in shear flow". *Phys. Rev. E* **56** (1997), 7132–7137. Note the bending modulus k_c in this study is related to k_b in the present work according to $k_b = 2k_c$.

Quantity	Value	Calculation
V	$6 \cdot 10^{-1}$ nm/μsec	Eq. (73), with $\dot{\gamma} \sim 10^{-5}$ μsec^{-1} (Fig. 2)
R	$6 \cdot 10^{4}$ nm	Fig. 4
k_b	30 pN·nm	Fig. 4, text on page 7136
Λ	$4 \cdot 10^{-3}$ pN/nm	Fig. 6
SL	$1 \cdot 10^{4}$	Eq. (71)
Γ	$5 \cdot 10^{5}$	Eq. (38)

Experiment #2: White blood cells in blood vessel

Table 2: Calculations from Table 1 of H.H. Lipowsky, S. Usami, and S. Chien. "In vivo measurements of "apparent viscosity" and microvessel hematocrit in the mesentery of the cat". *Microvasc. Res.* **19** (1980), 297–319, as well as Fig. 1 of E. Kolaczkowska and P. Kubes. "Neutrophil recruitment and function in health and inflammation". *Nat. Rev. Immunol.* **13** (2013), 159–175. Both studies investigate white blood cells in a shear flow within a blood vessel. To calculate the shear rate $\dot{\gamma}$ in a blood vessel, we used the result $\dot{\gamma} \sim Q/R_{\mathrm{t}}^3$ for laminar flow in a tube of radius R_{t}, with flow rate Q.

Quantity	Value	Calculation
V	3 nm/μsec	Eq. (73), with $\dot{\gamma} \sim 5 \cdot 10^{-4}$ μsec^{-1} (Lipowsky et al.)
R	$6 \cdot 10^3$ nm	Estimated from Fig. 1 of Kolaczkowska et al.
SL	$2 \cdot 10^3$	Eq. (71)
Γ	$4 \cdot 10^2$	Eq. (38)

Experiment #3: GUVs in shear flow

Table 3: Considerations for experimental data of GUVs in a shear flow, from Fig. 2 and Video 1 of S. Ota, S. Yoshizawa, and S. Takeuchi. "Microfluidic formation of monodisperse, cell-sized, and unilamellar vesicles". *Angew. Chem. Int. Edit.* **48** (2009), 6533–6537. We approximated the shear rate as $\dot{\gamma} \sim V_{\mathrm{s}}/10$ μm, where V_{s} is the free streaming velocity and 10 μm is the height of the post about which the vesicle is formed. From Video 1 of the Supporting information, we calculate $V_{\mathrm{s}} \sim 1$ nm/μsec, such that $\dot{\gamma} \sim 10^{-4}$ μsec^{-1}.

Quantity	Value	Calculation
V	$6 \cdot 10^{-1}$ nm/μsec	Eq. (73), with $\dot{\gamma} \sim 10^{-4}$ μsec^{-1} (Fig. 2(a), Video 1)
R	$6 \cdot 10^3$ nm	Fig. 2(d)
SL	$4 \cdot 10^2$	Eq. (71)
Γ	$4 \cdot 10^2$	Eq. (38)

Experiment #4: GUVs in shear flow

Table 4: Investigations of experimental data for GUVs in a shear flow, from line 18 in Table 1 of M.-A. Mader et al. "Dynamics of viscous vesicles in shear flow". *Eur. Phys. J. E* **19** (2006), 389–397. Note the bending modulus κ_c in this study is related to k_b in the present work according to $k_b = 2\kappa_c$.

Quantity	Value	Calculation
V	$3 \cdot 10^{-2}$ nm/μsec	Eq. (73), with $\dot{\gamma} \sim 2 \cdot 10^{-6}$ μsec^{-1} (Table 1, line 18)
R	$1 \cdot 10^{4}$ nm	Table 1, line 18
k_b	170 pN·nm	Page 394, below Eq. (9)
SL	$2 \cdot 10^{1}$	Eq. (71)
Γ	$6 \cdot 10^{2}$	Eq. (38)

Experiment #5: Retrovirus in blood vessel

Table 5: Calculations involving experimental measurements of retrovirus particles in a shear flow, within a blood vessel. The data on retrovirus particles is obtained from Fig. 1 of F. Förster et al. "Retrovirus envelope protein complex structure in situ studied by cryo-electron tomography". *Proc. Natl. Acad. Sci. U.S.A.* **102** (2005), 4729–4734. The data describing blood flow is once again obtained from Table 1 of H.H. Lipowsky, S. Usami, and S. Chien. "In vivo measurements of "apparent viscosity" and microvessel hematocrit in the mesentery of the cat". *Microvasc. Res.* **19** (1980), 297–319. The shear rate calculation is identical to that of Experiment #2 (see Table 2).

Quantity	Value	Calculation
V	$3 \cdot 10^{-3}$ nm/μsec	Eq. (73), with $\dot{\gamma} \sim 5 \cdot 10^{-4}$ μsec^{-1} (Lipowsky et al.)
R	$5 \cdot 10^{1}$ nm	Estimated from Fig. 1 of Förster et al.
SL	$1 \cdot 10^{-1}$	Eq. (71)
Γ	$2 \cdot 10^{-2}$	Eq. (38)

(72) simplifies to contain only the bending terms, and is given by

$$\Delta_s^{*2}\,\tilde{r}^* + 2\,\Delta_s^*\,\tilde{r}^* = 0\,. \tag{74}$$

Next, in large GUVs at low shear rates, [‡, †] we find $\Gamma \gg SL$ and $\Gamma \gg 1$, such that the shape equation is tension-dominated and simplifies to

$$2\,\tilde{r}^* + \Delta_s^*\,\tilde{r}^* - 2\,\tilde{\lambda}^* = 0\,. \tag{75}$$

On the other hand, for white blood cells [*] or GUVs [§] in flows with high shear rates, $SL \sim \Gamma \gg 1$ and both viscous and tension forces dominate bending forces. In this case, the shape equation is given by

$$2SL\left(\cos\theta^*\left[\csc\theta^* - \sin\theta^*\right]\tilde{r}^*_{,\theta^*\varphi^*} - \cos^2\theta^*\cot^2\theta^*\,\tilde{r}^*_{,\varphi^*}\right) + \Gamma\left(2\tilde{r}^* + \Delta_s^*\,\tilde{r}^* - 2\tilde{\lambda}^*\right) = 0\,. \tag{76}$$

We refer to systems for which Eq. (76) governs the perturbed out-of-plane dynamics as the 'fluid film' regime, as in the absence of bending forces the membrane equations are identical to those governing a two-dimensional Newtonian fluid film. [♯] In such cases, the dynamical response of an initially spherical, rotating lipid membrane vesicle can be significantly affected by the viscous forces arising from the intramembrane fluidity. In particular, out-of-plane viscous forces could lead to non-trivial corrections in many of the theoretical and numerical studies of membrane-bound vesicles immersed in shearing bulk fluids. [‖, ∀, ◇, $, &, ¶, ‡‡, ††, **, §§] We reiterate that our analysis does not include effects from the bulk fluid besides the pressure drop in the base state, and so a comprehensive study involving both the bulk fluid and full membrane equations is necessary to understand vesicle behavior in such situations.

[‡]Haas et al., "Deformation of giant lipid bilayer vesicles in shear flow".

[†]M.-A. Mader et al. "Dynamics of viscous vesicles in shear flow". *Eur. Phys. J. E* **19** (2006), 389–397.

[*]E. Kolaczkowska and P. Kubes. "Neutrophil recruitment and function in health and inflammation". *Nat. Rev. Immunol.* **13** (2013), 159–175.

[§]Ota, Yoshizawa, and Takeuchi, "Microfluidic formation of monodisperse, cell-sized, and unilamellar vesicles".

[♯]L.E. Scriven. "Dynamics of a fluid interface: Equation of motion for Newtonian surface fluids". *Chem. Eng. Sci.* **12** (1960), 98–108.

[‖]S.R. Keller and R. Skalak. "Motion of a tank-treading ellipsoidal particle in a shear flow". *J. Fluid Mech.* **120** (1982), 27–47.

[∀]M. Kraus et al. "Fluid vesicles in shear flow". *Phys. Rev. Lett.* **77** (1996), 3685–3688.

[◇]U. Seifert. "Fluid membranes in hydrodynamic flow fields: Formalism and an application to fluctuating quasispherical vesicles in shear flow". *Eur. Phys. J. B* **8** (1999), 405–415.

[$]J. Beaucourt et al. "Steady to unsteady dynamics of a vesicle in a flow". *Phys. Rev. E* **69** (2004), 011906.

[&]V.V. Lebedev, K.S. Turitsyn, and S.S. Vergeles. "Dynamics of nearly spherical vesicles in an external flow". *Phys. Rev. Lett.* **99** (2007), 218101.

[¶]H. Noguchi and G. Gompper. "Swinging and tumbling of fluid vesicles in shear flow". *Phys. Rev. Lett.* **98** (2007), 128103.

[‡‡]P.M. Vlahovska and R.S. Gracia. "Dynamics of a viscous vesicle in linear flows". *Phys. Rev. E* **75** (2007), 016313.

[††]S. Messlinger et al. "Dynamical regimes and hydrodynamic lift of viscous vesicles under shear". *Phys. Rev. E* **80** (2009), 011901.

[**]H. Zhao and E.S.G. Shaqfeh. "The dynamics of a vesicle in simple shear flow". *J. Fluid Mech.* **674** (2011), 578–604.

[§§]H. Zhao, A.P. Spann, and E.S.G. Shaqfeh. "The dynamics of a vesicle in a wall-bound shear flow". *Phys. Fluids* **23** (2011), 121901.

5. The temporal stability of a static vesicle

Following the general procedure outlined in Chapter VI, §1, we now investigate the stability of spherical membrane systems. In order to employ a linear stability analysis, we first decompose all membrane unknowns into normal modes. A complication arises, however, because the individual components of the perturbed membrane velocity—namely $\tilde{v}^1$, $\tilde{v}^2$, and $\tilde{v}$—cannot be decomposed using the well-known scalar spherical harmonics. Rather, the entire membrane velocity $\tilde{\boldsymbol{v}}$ is decomposed in terms of the vector spherical harmonics, which we review below. We limit our analysis to situations with no base flow, as we are unable to express the perturbed equations with a base flow in terms of independent normal modes—even with the more general decomposition of $\tilde{\boldsymbol{v}}$. [‡]

With an appropriate normal mode decomposition, we express the governing equations in terms of the normal mode coefficients, and then determine how each mode evolves in time according to the linear theory. If the base surface tension is positive and the Föppl–von Kármán number $\Gamma > 0$, then all modes are stable. When $\Gamma < 0$, on the other hand, short-wavelength modes remain stable while long-wavelength modes become unstable. The cutoff between stable and unstable wavelengths is a function of only the Föppl–von Kármán number, which additionally determines the growth rate of the unstable modes. We note the results in this section are provided for completeness, as they are not new: the stability requirements were previously obtained from energetic arguments, [†, *] and the time evolution of the normal modes—including the dynamics of both the membrane and the surrounding fluid—was also determined in a prior effort. [§]

(a). Mathematical preliminaries

The study of systems with spherical symmetry has a rich history in many disciplines, including (for example) fluid mechanics and electrodynamics. Here, we review the well-known *scalar* spherical harmonics, which are eigenfunctions of the scalar surface Laplacian on the unit sphere. We then motivate why the membrane velocity components cannot easily be decomposed using the scalar spherical harmonics, and proceed to introduce a less well-known set of functions—namely, the *vector* spherical harmonics—which are more suitable for our analysis.

The scalar spherical harmonics

In our study of perturbed spherical membrane vesicles, we will often need to expand quantities in terms of normal modes. For scalar functions, the natural basis for doing so are the *scalar spherical harmonics,* which are the eigenfunctions of the scalar Laplacian operator in

[‡]This difficulty was noted previously. [§]

[†]Seifert, "Fluid membranes in hydrodynamic flow fields: Formalism and an application to fluctuating quasispherical vesicles in shear flow".

[*]L. Miao, M.A. Lomholt, and J. Kleis. "Dynamics of shape fluctuations of quasi-spherical vesicles revisited". *Eur. Phys. J. E* **9** (2002), 143–160.

[§]P.M. Vlahovska. "Dynamics of Membrane-Bound Particles: Capsules and Vesicles". *Fluid–Structure Interactions in Low-Reynolds-Number Flows.* Ed. by C. Duprat and H.A. Stone. RSC Soft Matter Series. The Royal Society of Chemistry, 2016, pp. 313–346

spherical coordinates. The properties of these functions are well-known and can be found in many texts; here, we follow the presentation by J.D. Jackson. [‡]

Consider some scalar function $Y(\theta,\varphi)$ defined on a sphere of radius R, which satisfies the eigenvalue equation $R^2\Delta_{\rm s}Y = -\ell(\ell+1)Y$, explicitly written as

$$Y_{,\theta\theta} \,+\, Y_{,\theta}\cot\theta \,+\, Y_{,\varphi\varphi}\csc^2\theta \;=\; -\,\ell(\ell+1)\,Y \;. \tag{77}$$

In Eq. (77), $\ell(\ell+1)$ is an unknown constant that is to be solved for. Following the usual method of separation of variables, we assume the function $Y(\theta,\varphi)$ can be decomposed into polar and azimuthal components as [†]

$$Y(\theta,\varphi) \;=\; \Theta(\theta)\,\Phi(\varphi) \;. \tag{78}$$

Upon substituting Eq. (78) into Eq. (77), multiplying by $\sin^2\theta$, and rearranging terms, we obtain

$$\underbrace{\ell(\ell+1)\sin^2\theta \,+\, \frac{\sin\theta}{\Theta}\,\frac{\mathrm{d}}{\mathrm{d}\theta}\left(\sin\theta\,\frac{\mathrm{d}\Theta}{\mathrm{d}\theta}\right)}_{=m^2} \,+\, \underbrace{\frac{1}{\Phi}\,\frac{\mathrm{d}^2\Phi}{\mathrm{d}\varphi^2}}_{=-m^2} \;=\; 0 \;. \tag{79}$$

In Eq. (79), the first two terms are only a function of θ, while the second terms is only a function of φ. Accordingly, both terms must be a constant; the last term is chosen to be equal to $-m^2$. We easily solve for the azimuthal function Φ, as

$$\frac{\mathrm{d}^2\Phi}{\mathrm{d}\varphi^2} \;=\; -m^2\,\Phi \;, \qquad \text{for which} \qquad \Phi \;=\; \mathrm{e}^{\pm im\varphi} \;. \tag{80}$$

In order for $\Phi(\varphi)$ to be periodic on the sphere and satisfy $\Phi(\varphi+2\pi)=\Phi(\varphi)$, we require $m\in\mathbb{Z}$.

Let us now consider the equation for $\Theta(\theta)$. By making the change of variables $x\equiv\cos\theta$, we obtain the *generalized Legendre equation*

$$\frac{\mathrm{d}}{\mathrm{d}x}\left[\left(1-x^2\right)\frac{\mathrm{d}\Theta}{\mathrm{d}x}\right] \,+\, \left[\ell(\ell+1) \,-\, \frac{m^2}{1-x^2}\right]\Theta \;=\; 0 \;, \tag{81}$$

whose solutions are the *associated Legendre functions*. Note that when there is azimuthal symmetry and $m=0$ (equivalently $\Phi=1$), the above equation simplifies to the Legendre equation, whose solutions are the Legendre polynomials $P_\ell(x)$ which satisfy Rodrigues' formula

$$P_\ell(x) \;=\; \frac{1}{2^\ell\,\ell!}\,\frac{\mathrm{d}^\ell}{\mathrm{d}x^\ell}\left[\left(x^2-1\right)^\ell\right] \;. \tag{82}$$

The Legendre polynomials form a complete set of orthogonal functions on the domain $x\in[-1,1]$, and satisfy the orthogonality relation

$$\int_{-1}^{+1} P_{\ell'}(x)\,P_\ell(x)\;\mathrm{d}x \;=\; \frac{2}{2\ell+1}\,\delta_{\ell',\ell} \;. \tag{83}$$

[‡] J.D. Jackson. *Classical Electrodynamics*. 3rd ed. New York: Wiley, 1999.

[†] The azimuthal component $\Phi(\varphi)$ is distinct from the angular scale Φ introduced in §4 (b).

At this point, we recognize that in order for the function $Y(\theta, \varphi)$ to be finite in the polar angle domain $\theta \in [0, \pi]$, or equivalently $x \in [-1, 1]$, ℓ must be zero or a positive integer, and m is restricted to the range $-\ell$, $-(\ell - 1)$, $\ldots$ 0, $\ldots$ $(\ell - 1)$, ℓ. The corresponding solutions to the general equation for $\Theta(x)$ are the associated Legendre functions, denoted $P_\ell^m(x)$ and given—for both positive and negative m—by

$$P_{\ell m}(x) \;:=\; \frac{(-1)^m}{2^\ell \ell!} \left(1 - x^2\right)^{m/2} \frac{\mathrm{d}^{\ell+m}}{\mathrm{d}x^{\ell+m}} \left[\left(x^2 - 1\right)^\ell \right] . \tag{84}$$

Moreover, the associated Legendre functions with negative m are related to those of positive m by

$$P_{\ell,-m}(x) \;=\; (-1)^m \frac{(\ell - m)!}{(\ell + m)!} P_{\ell m}(x) \;, \tag{85}$$

and we have the orthogonality relation

$$\int_{-1}^{1} P_{\ell' m}(x) \, P_{\ell m}(x) \, \mathrm{d}x \;=\; \frac{2}{2\ell + 1} \frac{(\ell + m)!}{(\ell - m)!} \, \delta_{\ell',\ell} \;. \tag{86}$$

Finally, we recognize that we can form a complete orthonormal set of functions defined on the unit sphere by combining the functions Θ and Φ. These scalar spherical harmonics are denoted $Y_{\ell m}(\theta, \varphi)$, and are given by

$$Y_{\ell m}(\theta, \varphi) \;=\; \sqrt{\frac{(2\ell + 1)}{4\pi} \frac{(\ell - m)!}{(\ell + m)!}} \; P_\ell^m(\cos\theta) \, \mathrm{e}^{im\varphi} \;. \tag{87}$$

Additionally, the harmonic functions with a negative value of m are related to those with a positive value of m by

$$Y_{\ell,-m}(\theta, \varphi) \;=\; (-1)^m \, Y_{\ell m}^\dagger(\theta, \varphi) \;, \tag{88}$$

where in this chapter the '†' accent denotes complex conjugation. The spherical harmonics satisfy the orthogonality relation

$$\int_0^\pi \sin\theta \, \mathrm{d}\theta \int_0^{2\pi} \mathrm{d}\varphi \left[Y_{\ell m}(\theta, \varphi) \, Y_{\ell' m'}^\dagger(\theta, \varphi) \right] \;=\; \delta_{\ell',\ell} \, \delta_{m',m} \;, \tag{89}$$

where the integral is over the unit sphere.

With the form of the scalar spherical harmonics, we can now understand why these functions are unsuitable for the decomposition of the membrane velocity components. Consider, for example, the in-plane equations (21, 22)—which contain partial derivatives of the velocity components with respect to θ and φ. From Eq. (87), we find

$$Y_{\ell m,\theta} \;=\; m \cot\theta \, Y_{\ell m} \;+\; \sqrt{(\ell - m)(\ell + m + 1)} \, \mathrm{e}^{-i\varphi} \, Y_{\ell,m+1} \tag{90}$$

and

$$Y_{\ell m,\varphi} \;=\; im \, Y_{\ell m} \;, \tag{91}$$

where a derivative in the polar angle θ couples the modes $Y_{\ell m}$ and $Y_{\ell,m+1}$. Such mode coupling leads to difficulties when seeking the dynamics of a single mode, and motivates our use of the vector spherical harmonics.

The vector spherical harmonics

In listing the properties of the scalar spherical harmonics, we recognized that $Y_{\ell m}$ is not an eigenfunction of the operator $\partial/\partial\theta$, implying that care must be taken when decomposing our fundamental variables into normal modes. As we will see, it is useful to generate a set of three linearly independent vectorial quantities from each scalar spherical harmonic, with which to decompose vector quantities. These vector spherical harmonics are given by

$$\mathbf{Y}^{\mathrm{s}}_{\ell m}(\theta,\varphi) \;=\; Y_{\ell m}(\theta,\varphi)\,\boldsymbol{e}_r \;, \tag{92}$$

$$\mathbf{Y}^{\mathrm{e}}_{\ell m}(\theta,\varphi) \;=\; \frac{R\boldsymbol{\nabla}_{\mathrm{s}}Y_{\ell m}(\theta,\varphi)}{\sqrt{\ell(\ell+1)}} \;=\; \frac{1}{\sqrt{\ell(\ell+1)}}\Big(\,Y_{\ell m,\theta}\,\boldsymbol{e}_\theta \;+\; Y_{\ell m,\varphi}\csc\theta\,\boldsymbol{e}_\varphi\Big)\;, \tag{93}$$

and

$$\mathbf{Y}^{\mathrm{m}}_{\ell m}(\theta,\varphi) \;=\; \frac{\boldsymbol{e}_r\times R\boldsymbol{\nabla}_{\mathrm{s}}Y_{\ell m}(\theta,\varphi)}{\sqrt{\ell(\ell+1)}} \;=\; \frac{1}{\sqrt{\ell(\ell+1)}}\Big(\,-\,Y_{\ell m,\varphi}\csc\theta\,\boldsymbol{e}_\theta \;+\; Y_{\ell m,\theta}\,\boldsymbol{e}_\varphi\Big)\;, \tag{94}$$

where $\boldsymbol{\nabla}_{\mathrm{s}}$ is the surface gradient operator, for which $R\boldsymbol{\nabla}_{\mathrm{s}}(\,\cdot\,) = \boldsymbol{e}_\theta\,(\,\cdot\,)_{,\theta} + \boldsymbol{e}_\varphi\csc\theta\,(\,\cdot\,)_{,\varphi}$. In Eqs. (92)–(94), the superscripts 's,' 'e,' and 'm' stand for 'scalar,' 'electric,' and 'magnetic,' respectively—originating from the use of such functions in quantum electrodynamics. The vector spherical harmonics have a number of useful properties, of which the most relevant are provided here. First, just as was the case for the scalar spherical harmonics, the vector spherical harmonics of negative m are related to those of positive m by

$$\mathbf{Y}^{\mathrm{s}}_{\ell,-m} \;=\; (-1)^m\,\mathbf{Y}^{\mathrm{s}\,\dagger}_{\ell m}\;, \qquad \mathbf{Y}^{\mathrm{e}}_{\ell,-m} \;=\; (-1)^m\,\mathbf{Y}^{\mathrm{e}\,\dagger}_{\ell m}\;, \qquad \text{and} \qquad \mathbf{Y}^{\mathrm{m}}_{\ell,-m} \;=\; (-1)^m\,\mathbf{Y}^{\mathrm{m}\,\dagger}_{\ell m}\;. \tag{95}$$

Next, the vector spherical harmonics are orthogonal at a single point in space $\boldsymbol{r}$:

$$\mathbf{Y}^{\mathrm{s}}_{\ell m}(\boldsymbol{r})\cdot\mathbf{Y}^{\mathrm{e}}_{\ell m}(\boldsymbol{r}) \;=\; 0\;, \qquad \mathbf{Y}^{\mathrm{e}}_{\ell m}(\boldsymbol{r})\cdot\mathbf{Y}^{\mathrm{m}}_{\ell m}(\boldsymbol{r}) \;=\; 0\;, \qquad \text{and} \qquad \mathbf{Y}^{\mathrm{m}}_{\ell m}(\boldsymbol{r})\cdot\mathbf{Y}^{\mathrm{s}}_{\ell m}(\boldsymbol{r}) \;=\; 0\;. \tag{96}$$

Finally, denoting $\mathrm{d}\Omega := \mathrm{d}\varphi\sin\theta\mathrm{d}\theta$ as the differential area element on the unit sphere, we express the orthonormality of the vector spherical harmonics over the sphere as

$$\int \mathbf{Y}^{\mathrm{s}}_{\ell m}(\theta,\varphi)\cdot\mathbf{Y}^{\mathrm{s}\,\dagger}_{\ell' m'}(\theta,\varphi)\;\mathrm{d}\Omega \;=\; \delta_{\ell'\ell}\,\delta_{m'm}\;, \tag{97}$$

$$\int \mathbf{Y}^{\mathrm{e}}_{\ell m}(\theta,\varphi)\cdot\mathbf{Y}^{\mathrm{e}\,\dagger}_{\ell' m'}(\theta,\varphi)\;\mathrm{d}\Omega \;=\; \delta_{\ell'\ell}\,\delta_{m'm}\;, \tag{98}$$

$$\int \mathbf{Y}^{\mathrm{m}}_{\ell m}(\theta,\varphi)\cdot\mathbf{Y}^{\mathrm{m}\,\dagger}_{\ell' m'}(\theta,\varphi)\;\mathrm{d}\Omega \;=\; \delta_{\ell'\ell}\,\delta_{m'm}\;, \tag{99}$$

$$\int \mathbf{Y}^{\mathrm{s}}_{\ell m}(\theta,\varphi)\cdot\mathbf{Y}^{\mathrm{e}\,\dagger}_{\ell' m'}(\theta,\varphi)\;\mathrm{d}\Omega \;=\; 0\;, \tag{100}$$

$$\int \mathbf{Y}^{\mathrm{e}}_{\ell m}(\theta,\varphi)\cdot\mathbf{Y}^{\mathrm{m}\,\dagger}_{\ell' m'}(\theta,\varphi)\;\mathrm{d}\Omega \;=\; 0\;, \tag{101}$$

and

$$\int \mathbf{Y}^{\mathrm{m}}_{\ell m}(\theta,\varphi)\cdot\mathbf{Y}^{\mathrm{s}\,\dagger}_{\ell' m'}(\theta,\varphi)\;\mathrm{d}\Omega \;=\; 0\;. \tag{102}$$

(b). The governing equations

The dimensionless equations governing an initially static vesicle were obtained in §3, and presented in terms of our differential geometric description of the membrane surface. In order to study the stability of such systems, however, it is convenient to express quantities in terms of the standard orthonormal spherical basis $\{\boldsymbol{e}_r, \boldsymbol{e}_\theta, \boldsymbol{e}_\varphi\}$. To this end, we decompose the perturbed membrane velocity as

$$\begin{aligned}\tilde{\boldsymbol{v}} &= \tilde{v}^1 \boldsymbol{a}_1^{(0)} + \tilde{v}^2 \boldsymbol{a}_2^{(0)} + \tilde{v}\, \boldsymbol{n}_{(0)} \\ &= \tilde{v}^1 R\, \boldsymbol{e}_\theta + \tilde{v}^2 R \sin\theta\, \boldsymbol{e}_\theta + \tilde{v} \boldsymbol{e}_r \\ &= \tilde{v}_\theta \boldsymbol{e}_\theta + \tilde{v}_\varphi \boldsymbol{e}_\varphi + \tilde{v}_r \boldsymbol{e}_r \ ,\end{aligned} \tag{103}$$

from which we immediately obtain the following relationships between velocity components:

$$\tilde{v}_\theta = \tilde{v}^1 R \ , \qquad \tilde{v}_\varphi = \tilde{v}^2 R \sin\theta \ , \qquad \text{and} \qquad \tilde{v}_r = \tilde{v} = \tilde{r}_{,t} \ . \tag{104}$$

In this case, we define the dimensionless velocity in terms of the length scale R and time scale τ (36) as

$$\tilde{\boldsymbol{v}}^* = \frac{\tau \tilde{\boldsymbol{v}}}{R} = \frac{\zeta \tilde{\boldsymbol{v}}}{\Lambda R} \ , \tag{105}$$

and express the dimensionless continuity equation (39) as

$$\tilde{v}^*_{\theta,\theta} + \tilde{v}^*_{\varphi,\varphi} \csc\theta + \tilde{v}^*_\theta \cot\theta + 2\tilde{v}^*_r = 0 \ . \tag{106}$$

The three components of the linear momentum balance (40)–(42) are similarly expressed as the single vector equation

$$\begin{aligned}\mathbf{0} &= \left\{ \tilde{v}^*_{\theta,\theta\theta} + \tilde{v}^*_{\theta,\theta} \cot\theta + \tilde{v}^*_{\theta,\varphi\varphi} - 2\tilde{v}^*_{\varphi,\varphi} \cot\theta \csc\theta + \tilde{v}^*_\theta \left(1 - \cot^2\theta\right) + \tilde{\lambda}^*_{,\theta} \right\} \boldsymbol{e}_\theta \\ &+ \left\{ \tilde{v}^*_{\varphi,\theta\theta} + \tilde{v}^*_{\varphi,\theta} \cot\theta + \tilde{v}^*_{\varphi,\varphi\varphi} \csc^2\theta + 2\tilde{v}^*_{\theta,\varphi} \cot\theta \csc\theta + \tilde{v}^*_\varphi \left(1 - \cot^2\theta\right) + \tilde{\lambda}^*_{,\varphi} \csc\theta \right\} \boldsymbol{e}_\varphi \\ &+ \left\{ \Gamma \left(2\tilde{r}^* + \Delta^*_{\mathrm{s}} \tilde{r}^* - 2\tilde{\lambda}^* \right) - \frac{1}{2} \left(\Delta^{*2}_{\mathrm{s}} \tilde{r}^* + 2\Delta^*_{\mathrm{s}} \tilde{r}^* \right) \right\} \boldsymbol{e}_r \ ,\end{aligned} \tag{107}$$

which is more amenable for analysis with the vector spherical harmonics.

(c). The decomposition into normal modes

At this point, we decompose all membrane unknowns into normal modes. The perturbed surface tension $\tilde{\lambda}^*$ and out-of-plane displacement $\tilde{r}^*$ are decomposed with the scalar spherical harmonics as

$$\tilde{\lambda}^*(\theta, \varphi, t^*) = \sum_{\ell=0}^{\infty} \sum_{m=-\ell}^{+\ell} \lambda_{\ell m}(t^*)\, Y_{\ell m}(\theta, \varphi) \tag{108}$$

and

$$\tilde{r}^*(\theta,\varphi,t^*) \;=\; \sum_{\ell=0}^{\infty}\sum_{m=-\ell}^{+\ell} r_{\ell m}(t^*)\, Y_{\ell m}(\theta,\varphi)\;, \tag{109}$$

where we have not yet assumed a time dependence of our fundamental unknowns. The perturbed membrane velocity $\tilde{\boldsymbol{v}}$ is similarly expanded in terms of the vector spherical harmonics as

$$\tilde{\boldsymbol{v}}^*(\theta,\varphi,t^*) \;=\; \sum_{\ell=0}^{\infty}\sum_{m=-\ell}^{+\ell}\Big[\, v^{\mathrm{s}}_{\ell m}(t^*)\,\mathbf{Y}^{\mathrm{s}}_{\ell m}(\theta,\varphi) \;+\; v^{\mathrm{e}}_{\ell m}(t^*)\,\mathbf{Y}^{\mathrm{e}}_{\ell m}(\theta,\varphi) \;+\; v^{\mathrm{m}}_{\ell m}(t^*)\,\mathbf{Y}^{\mathrm{m}}_{\ell m}(\theta,\varphi)\Big]\;. \tag{110}$$

By substituting the expansion of the vector spherical harmonics (92)–(94) into Eq. (110) and rearranging terms, we find the components of the velocity can be expressed as

$$\tilde{v}^*_r(\theta,\varphi,t^*) \;=\; \sum_{\ell=0}^{\infty}\sum_{m=-\ell}^{+\ell} v^{\mathrm{s}}_{\ell m}\, Y_{\ell m}\;, \tag{111}$$

$$\tilde{v}^*_\theta(\theta,\varphi,t^*) \;=\; \sum_{\ell=0}^{\infty}\sum_{m=-\ell}^{+\ell} \frac{1}{\sqrt{\ell(\ell+1)}}\Big(v^{\mathrm{e}}_{\ell m}\, Y_{\ell m,\theta} \;-\; v^{\mathrm{m}}_{\ell m}\, Y_{\ell m,\varphi}\csc\theta\Big)\;, \tag{112}$$

and

$$\tilde{v}^*_\varphi(\theta,\varphi,t^*) \;=\; \sum_{\ell=0}^{\infty}\sum_{m=-\ell}^{+\ell} \frac{1}{\sqrt{\ell(\ell+1)}}\Big(v^{\mathrm{e}}_{\ell m}\, Y_{\ell m,\varphi}\csc\theta \;+\; v^{\mathrm{m}}_{\ell m}\, Y_{\ell m,\theta}\Big)\;. \tag{113}$$

Additionally, we recognize our kinematic requirement $\tilde{v}^*_r = \tilde{r}^*_{,t^*}$ [see Eq. $(104)_3$] dictates

$$v^{\mathrm{s}}_{\ell m} \;=\; \frac{\mathrm{d}r_{\ell m}}{\mathrm{d}t^*}\;. \tag{114}$$

With the decomposition of all membrane unknowns into normal modes, we now seek to expand the governing equations in terms of the coefficients $\lambda_{\ell m}$, $r_{\ell m}$, $v^{\mathrm{s}}_{\ell m}$, $v^{\mathrm{e}}_{\ell m}$, and $v^{\mathrm{m}}_{\ell m}$. To this end, we begin by substituting Eqs. (111)–(113) into the continuity equation (106) and multiplying by $\sqrt{\ell(\ell+1)}$ to obtain

$$\begin{aligned}\Big(v^{\mathrm{e}}_{\ell m}\, Y_{\ell m,\theta} \;-\; v^{\mathrm{m}}_{\ell m}\, Y_{\ell m,\varphi}\csc\theta\Big)_{,\theta} \;+\; \Big(v^{\mathrm{e}}_{\ell m}\, Y_{\ell m,\varphi}\csc\theta \;+\; v^{\mathrm{m}}_{\ell m}\, Y_{\ell m,\theta}\Big)_{,\varphi}\csc\theta \\ +\; \Big(v^{\mathrm{e}}_{\ell m}\, Y_{\ell m,\theta} \;-\; v^{\mathrm{m}}_{\ell m}\, Y_{\ell m,\varphi}\csc\theta\Big)\cot\theta \;+\; 2\sqrt{\ell(\ell+1)}\, v^{\mathrm{s}}_{\ell m}\, Y_{\ell m} \;=\; 0\;.\end{aligned} \tag{115}$$

Upon distributing the partial derivatives and rearranging quantities, we find all terms involving $v^{\mathrm{m}}_{\ell m}$ in Eq. (115) sum to zero—an unsurprising result, since $\boldsymbol{\nabla}_{\mathrm{s}}\cdot\mathbf{Y}^{\mathrm{m}}_{\ell m} = 0$. Equation (115) then simplifies to

$$2\sqrt{\ell(\ell+1)}\, v^{\mathrm{s}}_{\ell m}\, Y_{\ell m} \;+\; v^{\mathrm{e}}_{\ell m}\Big(Y_{\ell m,\theta\theta} \;+\; Y_{\ell m,\theta}\cot\theta \;+\; Y_{\ell m,\varphi\varphi}\csc^2\theta\Big) \;=\; 0\;. \tag{116}$$

We recognize the quantity in parenthesis in Eq. (116) is the dimensionless surface Laplacian of $Y_{\ell m}$, for which $\Delta_{\rm s}^* Y_{\ell m} = -\ell(\ell+1) Y_{\ell m}$ [see Eq. (77)]. Moreover, since $Y_{\ell m} \neq 0$, the membrane velocity coefficients satisfy

$$2 v^{\rm s}_{\ell m} - \sqrt{\ell(\ell+1)}\, v^{\rm e}_{\ell m} = 0 \,, \tag{117}$$

which is the continuity equation expressed in terms of normal modes.

In a similar manner, we substitute the normal mode decomposition (111)–(113) into the vector form of the linear momentum balance (107). After much algebra, we find the latter can be written as

$$\begin{aligned} \mathbf{0} = &\left\{ -2\Gamma\, \lambda_{\ell m} - (\ell-1)(\ell+2)\left(\Gamma + \frac{\ell(\ell+1)}{2}\right) r_{\ell m} \right\} \mathbf{Y}^{\rm s}_{\ell m} \\ &+ \left\{ -(\ell-1)(\ell+2)\, v^{\rm e}_{\ell m} + \sqrt{\ell(\ell+1)}\, \Gamma\, \lambda_{\ell m} \right\} \mathbf{Y}^{\rm e}_{\ell m} + \left\{ -(\ell-1)(\ell+2)\, v^{\rm m}_{\ell m} \right\} \mathbf{Y}^{\rm m}_{\ell m} \,. \end{aligned} \tag{118}$$

As the vector spherical harmonics form an orthonormal basis, each quantity in curly braces in Eq. (118) is zero. With the contunity equation (117), kinematic constraint (114), and linear momentum balance (118), we express the four equations governing the four unknown quantities $r_{\ell m}$, $\lambda_{\ell m}$, $v^{\rm e}_{\ell m}$, and $v^{\rm m}_{\ell m}$ as

$$2\frac{{\rm d}r_{\ell m}}{{\rm d}t^*} - \sqrt{\ell(\ell+1)}\, v^{\rm e}_{\ell m} = 0 \,, \tag{119}$$

$$-(\ell-1)(\ell+2)\, v^{\rm m}_{\ell m} = 0 \,, \tag{120}$$

$$-(\ell-1)(\ell+2)\, v^{\rm e}_{\ell m} + \sqrt{\ell(\ell+1)}\, \Gamma\, \lambda_{\ell m} = 0 \,, \tag{121}$$

and

$$-2\Gamma\, \lambda_{\ell m} - (\ell-1)(\ell+2)\left(\Gamma + \frac{\ell(\ell+1)}{2}\right) r_{\ell m} = 0 \,. \tag{122}$$

(d). The dispersion relation

The dynamical equations governing a perturbed vesicle have now been simplified to a set of coupled algebraic equations, which include only a single time derivative: ${\rm d}r_{\ell m}/{\rm d}t^*$. We now seek to describe how the perturbed membrane shape evolves in time. However, recall that ℓ is a non-negative integer, for which equations (119)–(122) have different solutions depending on whether $\ell = 0$, $\ell = 1$, or $\ell \geq 2$. In what follows, we discuss these three cases.

Table 6: Scalar and vector spherical harmonics when $\ell = 0$ and $m = 0$.

$Y_{00} = \dfrac{1}{\sqrt{4\pi}}$	$\mathbf{Y}^{\rm s}_{00} = \dfrac{1}{\sqrt{4\pi}}\, \boldsymbol{e}_r$	$\mathbf{Y}^{\rm e}_{00} = \mathbf{0}$	$\mathbf{Y}^{\rm m}_{00} = \mathbf{0}$

The solution when $\ell = 0$

When $\ell = 0$, the only allowed azimuthal index is $m = 0$. The corresponding scalar and vector spherical harmonics are provided in Table 6. In this case, the in-plane components of the linear momentum balance are automatically satisfied. The continuity equation simplifies to

$$\frac{\mathrm{d}r_{00}}{\mathrm{d}t^*} = 0 \,, \qquad \text{for which} \qquad r_{00} = \text{const.} \tag{123}$$

Additionally, the shape equation can be written as

$$-2\lambda_{00} + 2r_{00} = 0 \,, \qquad \text{implying} \qquad \lambda_{00}(t) = r_{00}(t) \,. \tag{124}$$

As expected, we find that a uniform change in the vesicle radius is accompanied by a constant change in surface tension. As we are considering fluctuations of a membrane vesicle with a known average radius, we have

$$r_{00} = 0 \qquad \text{and} \qquad \lambda_{00} = 0 \,. \tag{125}$$

Moreover, as we are considering a membrane vesicle with zero base flow, we assume

$$v^{\mathrm{e}}_{00} = 0 \qquad \text{and} \qquad v^{\mathrm{m}}_{00} = 0 \tag{126}$$

as well.

The solution when $\ell = 1$

In the case where $\ell = 1$, the allowed values of m are -1, 0, and $+1$. The corresponding scalar and vector spherical harmonics are given in Table 7. As the vector spherical harmonics are all nonzero, the governing equations simplify to

$$\sqrt{2}\,\frac{\mathrm{d}r_{1m}}{\mathrm{d}t^*} = \sqrt{2}\,v^{\mathrm{s}}_{1m} = v^{\mathrm{e}}_{1m} \qquad \text{and} \qquad \lambda_{1m} = 0 \,, \tag{127}$$

Table 7: Scalar and vector spherical harmonics when $\ell = 1$ and $m = -1$, 0, and $+1$.

$Y_{1,-1} = \sqrt{\frac{3}{8\pi}}\,\sin\theta\,\mathrm{e}^{-i\varphi}$	$Y_{10} = \sqrt{\frac{3}{4\pi}}\,\cos\theta$	$Y_{11} = -\sqrt{\frac{3}{8\pi}}\,\sin\theta\,\mathrm{e}^{i\varphi}$
$\mathbf{Y}^{\mathrm{s}}_{1,-1} = \sqrt{\frac{3}{8\pi}}\,\sin\theta\,\mathrm{e}^{-i\varphi}\,\boldsymbol{e}_r$	$\mathbf{Y}^{\mathrm{s}}_{10} = \sqrt{\frac{3}{4\pi}}\,\cos\theta\,\boldsymbol{e}_r$	$\mathbf{Y}^{\mathrm{s}}_{11} = -\sqrt{\frac{3}{8\pi}}\,\sin\theta\,\mathrm{e}^{i\varphi}\,\boldsymbol{e}_r$
$\mathbf{Y}^{\mathrm{e}}_{1,-1} = \sqrt{\frac{3}{16\pi}}\left(\cos\theta\,\boldsymbol{e}_\theta - i\boldsymbol{e}_\varphi\right)\mathrm{e}^{-i\varphi}$	$\mathbf{Y}^{\mathrm{e}}_{10} = -\sqrt{\frac{3}{8\pi}}\,\sin\theta\,\boldsymbol{e}_\theta$	$\mathbf{Y}^{\mathrm{e}}_{11} = -\sqrt{\frac{3}{16\pi}}\left(\cos\theta\,\boldsymbol{e}_\theta + i\boldsymbol{e}_\varphi\right)\mathrm{e}^{i\varphi}$
$\mathbf{Y}^{\mathrm{m}}_{1,-1} = \sqrt{\frac{3}{16\pi}}\left(i\boldsymbol{e}_\theta + \cos\theta\,\boldsymbol{e}_\varphi\right)\mathrm{e}^{-i\varphi}$	$\mathbf{Y}^{\mathrm{m}}_{10} = \sqrt{\frac{3}{8\pi}}\,\sin\theta\,\boldsymbol{e}_\varphi$	$\mathbf{Y}^{\mathrm{m}}_{11} = -\sqrt{\frac{3}{16\pi}}\left(-i\boldsymbol{e}_\theta + \cos\theta\,\boldsymbol{e}_\varphi\right)\mathrm{e}^{i\varphi}$

with v^{m}_{1m} being free to take any value. We note the $\ell = 1$ vector spherical harmonics can be combined to yield the Cartesian orthonormal basis vectors as

$$\frac{1}{2}\sqrt{\frac{8\pi}{3}}\left(\mathbf{Y}^{\mathrm{s}}_{1,-1} - \mathbf{Y}^{\mathrm{s}}_{11} + \sqrt{2}\left(\mathbf{Y}^{\mathrm{e}}_{1,-1} - \mathbf{Y}^{\mathrm{e}}_{11}\right)\right) = \boldsymbol{e}_x \ , \tag{128}$$

$$\frac{i}{2}\sqrt{\frac{8\pi}{3}}\left(\mathbf{Y}^{\mathrm{s}}_{1,-1} + \mathbf{Y}^{\mathrm{s}}_{11} + \sqrt{2}\left(\mathbf{Y}^{\mathrm{e}}_{1,-1} + \mathbf{Y}^{\mathrm{e}}_{11}\right)\right) = \boldsymbol{e}_y \ , \tag{129}$$

and

$$\sqrt{\frac{4\pi}{3}}\left(\mathbf{Y}^{\mathrm{s}}_{10} + \sqrt{2}\,\mathbf{Y}^{\mathrm{e}}_{10}\right) = \boldsymbol{e}_z \ . \tag{130}$$

Thus, with some algebraic manipulations, we can express the membrane velocity $\boldsymbol{v}_{\ell=1}$ resulting from only the $\ell = 1$ modes as

$$\boldsymbol{v}_{\ell=1} = \sqrt{\frac{3}{4\pi}}\left\{\frac{(v^{\mathrm{s}}_{1,-1} - v^{\mathrm{s}}_{11})}{2\sqrt{2}}\,\boldsymbol{e}_x - \frac{i(v^{\mathrm{s}}_{1,-1} + v^{\mathrm{s}}_{11})}{2\sqrt{2}}\,\boldsymbol{e}_y + v^{\mathrm{s}}_{10}\,\boldsymbol{e}_z\right\} + \sum_{m=-1}^{+1} v^{\mathrm{m}}_{1m}\,\mathbf{Y}^{\mathrm{m}}_{1m} \ . \tag{131}$$

Accordingly, we find the longitudinal and electric components of the membrane velocity are rigid translations of the membrane center of mass, and the $\ell = 1$ modes are ignored in our subsequent analysis.

The solution when $\ell \geq 2$

In cases where $\ell \geq 2$, all the vector spherical harmonics are nonzero and all coefficients in the governing equations are nonzero as well. We begin by considering the magnetic component of the linear momentum balance (120), which reveals

$$v^{\mathrm{m}}_{\ell m} = 0 \ . \tag{132}$$

Accordingly,the magnetic component of the membrane velocity is identically zero. With some algebraic manipulation, Eqs. (119), (121), and (122) can be combined to yield a single equation for the membrane shape, written as

$$\frac{\mathrm{d}r_{\ell m}}{\mathrm{d}t^*} = -\frac{\ell(\ell+1)}{4}\left(\Gamma + \frac{\ell(\ell+1)}{2}\right) r_{\ell m} \ . \tag{133}$$

At this point, we propose that all fundamental unknowns have a temporal character captured by $\mathrm{e}^{-i\omega^* t^*}$, where $\omega^* \in \mathbb{C}$ is the dimensionless, complex angular frequency. In this case, the radial shape deviation is expressed as

$$r_{\ell m}(t^*) = \hat{r}_{\ell m}\mathrm{e}^{-i\omega^* t^*} \ , \tag{134}$$

which upon substitution into Eq. (133) yields the dispersion relation

$$\omega^* = -\,i\,\frac{\ell(\ell+1)}{4}\left(\Gamma + \frac{\ell(\ell+1)}{2}\right) . \tag{135}$$

From Eqs. (133) and (135), we make several observations. First, the stability of the system depends only on the normal mode degree, ℓ, and Föppl–von Kármán number—and is independent of the normal mode order, m, and Scriven–Love number. Moreover, if the base tension is positive ($\Gamma > 0$), then the system is stable. On the other hand, if the base surface tension is negative ($\Gamma < 0$), then the $\ell \geq 2$ modes satisfying $\Gamma < -\ell(\ell+1)/2$ are unstable. We thus easily determine the Föppl–von Kármán number at which any radial mode becomes unstable. For example, the $\ell = 2$ modes are unstable when $\Gamma < -3$, the $\ell = 3$ modes are unstable when $\Gamma < -6$, and the $\ell = 4$ modes are unstable when $\Gamma < -10$. Moreover, for any unstable Γ, the long-wavelength (small ℓ) modes are unstable, while the short-wavelength (large ℓ) modes are stable. We leave the investigation of the long-time morphologies of unstable vesicles to a future study, and thus conclude our investigation of spherical membrane geometries.

References

[1] M. Abkarian and A. Viallat. "Vesicles and red blood cells in shear flow". *Soft Matter* **4** (2008), 653–657

[2] L.-A.H. Allen and A. Aderem. "Mechanisms of phagocytosis". *Curr. Opin. Immunol.* **8** (1996), 36–40

[3] J. Beaucourt et al. "Steady to unsteady dynamics of a vesicle in a flow". *Phys. Rev. E* **69** (2004), 011906

[4] P. Cicuta, S.L. Keller, and S.L. Veatch. "Diffusion of liquid domains in lipid bilayer membranes". *J. Phys. Chem. B* **111** (2007), 3328–3331. arXiv: `cond-mat/0611492`

[5] J.B. Dahl et al. "Experimental observation of the asymmetric instability of intermediate-reduced-volume vesicles in extensional flow". *Soft Matter* **12** (2016), 3787–3796

[6] J. Deschamps, V. Kantsler, and V. Steinberg. "Phase diagram of single vesicle dynamical states in shear flow". *Phys. Rev. Lett.* **102** (2009), 118105

[7] F. Förster et al. "Retrovirus envelope protein complex structure in situ studied by cryo-electron tomography". *Proc. Natl. Acad. Sci. U.S.A.* **102** (2005), 4729–4734

[8] K.H. de Haas et al. "Deformation of giant lipid bilayer vesicles in shear flow". *Phys. Rev. E* **56** (1997), 7132–7137

[9] M.K. Higgins and H.T. McMahon. "Snap-shots of clathrin-mediated endocytosis". *Trends Biochem. Sci.* **27** (2002), 257–263

[10] A.R. Honerkamp-Smith et al. "Membrane viscosity determined from shear-driven flow in giant vesicles". *Phys. Rev. Lett.* **111** (2013), 038103. arXiv: `1308.6440`

[11] J.D. Jackson. *Classical Electrodynamics*. 3rd ed. New York: Wiley, 1999

[12] V. Kantsler and V. Steinberg. "Orientation and dynamics of a vesicle in tank-treading motion in shear flow". *Phys. Rev. Lett.* **95** (2005), 258101

[13] S.R. Keller and R. Skalak. "Motion of a tank-treading ellipsoidal particle in a shear flow". *J. Fluid Mech.* **120** (1982), 27–47

[14] E. Kolaczkowska and P. Kubes. "Neutrophil recruitment and function in health and inflammation". *Nat. Rev. Immunol.* **13** (2013), 159–175

[15] M. Kraus et al. "Fluid vesicles in shear flow". *Phys. Rev. Lett.* **77** (1996), 3685–3688

[16] V.V. Lebedev, K.S. Turitsyn, and S.S. Vergeles. "Dynamics of nearly spherical vesicles in an external flow". *Phys. Rev. Lett.* **99** (2007), 218101

[17] C. Lee and L.-B. Chen. "Dynamic behavior of endoplasmic reticulum in living cells". *Cell* **54** (1988), 37–46

[18] H.H. Lipowsky, S. Usami, and S. Chien. "In vivo measurements of "apparent viscosity" and microvessel hematocrit in the mesentery of the cat". *Microvasc. Res.* **19** (1980), 297–319

[19] A.E.H. Love. "The small free vibrations and deformation of a thin elastic shell". *Phil. Trans. R. Soc. London* **179** (1888), 491–546

[20] M.-A. Mader et al. "Dynamics of viscous vesicles in shear flow". *Eur. Phys. J. E* **19** (2006), 389–397

[21] S. Messlinger et al. "Dynamical regimes and hydrodynamic lift of viscous vesicles under shear". *Phys. Rev. E* **80** (2009), 011901

[22] L. Miao, M.A. Lomholt, and J. Kleis. "Dynamics of shape fluctuations of quasi-spherical vesicles revisited". *Eur. Phys. J. E* **9** (2002), 143–160

[23] H. Noguchi and G. Gompper. "Swinging and tumbling of fluid vesicles in shear flow". *Phys. Rev. Lett.* **98** (2007), 128103

[24] S. Ota, S. Yoshizawa, and S. Takeuchi. "Microfluidic formation of monodisperse, cell-sized, and unilamellar vesicles". *Angew. Chem. Int. Edit.* **48** (2009), 6533–6537

[25] J. Pécréaux et al. "Refined contour analysis of giant unilamellar vesicles". *Eur. Phys. J. E* **13** (2004), 277–290

[26] L.E. Scriven. "Dynamics of a fluid interface: Equation of motion for Newtonian surface fluids". *Chem. Eng. Sci.* **12** (1960), 98–108

[27] U. Seifert. "Fluid membranes in hydrodynamic flow fields: Formalism and an application to fluctuating quasispherical vesicles in shear flow". *Eur. Phys. J. B* **8** (1999), 405–415

[28] P.M. Vlahovska. "Dynamics of Membrane-Bound Particles: Capsules and Vesicles". *Fluid–Structure Interactions in Low-Reynolds-Number Flows*. Ed. by C. Duprat and H.A. Stone. RSC Soft Matter Series. The Royal Society of Chemistry, 2016, pp. 313–346

[29] P.M. Vlahovska and R.S. Gracia. "Dynamics of a viscous vesicle in linear flows". *Phys. Rev. E* **75** (2007), 016313

[30] Z. Zhang and M.B. Jackson. "Membrane bending energy and fusion pore kinetics in Ca^{2+}-triggered exocytosis". *Biophys. J.* **98** (2010), 2524–2534

[31] H. Zhao and E.S.G. Shaqfeh. "The dynamics of a vesicle in simple shear flow". *J. Fluid Mech.* **674** (2011), 578–604

[32] H. Zhao, A.P. Spann, and E.S.G. Shaqfeh. "The dynamics of a vesicle in a wall-bound shear flow". *Phys. Fluids* **23** (2011), 121901

Chapter IX

Cylindrical Membrane Tubes

> *There is one more thing I should like to explain, and that is why I am going to show experiments at all. You will at once answer, because it would be so dreadfully dull if I didn't. Perhaps it would. But that is not the only reason. I would remind you then that when we want to find out anything that we do not know, there are two ways of proceeding. We may either ask somebody else who does know, or read what the most learned people have written about it, which is a very good plan if anybody happens to be able to answer our question; or else we may adopt the other plan, and by arranging an experiment, find out for ourselves. An experiment is a question which we ask of Nature, who is always ready to give a correct answer, provided we ask properly, that is, provided we arrange a proper experiment. An experiment is not a conjuring trick, something simply to make you wonder, nor is it simply shown because it is beautiful, or because it serves to relieve the monotony of a lecture; if any of the experiments I show are beautiful, or do serve to make these lectures a little less dull, so much the better; but their chief object is to enable you to see for yourselves what the true answers are to the questions that I shall ask.*
>
> —Charles V. Boys, 1890 [‡]

We close our hydrodynamic stability analysis by considering lipid membrane tubes, which are ubiquitous in both *in vitro* and biological systems. Cylindrical membrane tethers are often pulled from synthetic vesicles [†] and cells [*] to measure the bending rigidity k_b and the resting membrane tension λ_0, with several prior investigations also extracting dissipative parameters by changing the tether length over time. [§] From an experimental perspective, membrane tubes are used in part because they can be formed in different ways, including

[‡]C.V. Boys. *Soap Bubbles: Their Colors and the Forces Which Mold Them.* New York: Dover, 1959.

[†]E.A. Evans and A. Yeung. "Hidden dynamics in rapid changes of bilayer shape". *Chem. Phys. Lipids* **73** (1994), 39–56.

[*]Z. Shi et al. "Cell membranes resist flow". *Cell* **175** (2018), 1769–1779.

[§]J.-B. Fournier et al. "Chemically triggered ejection of membrane tubules controlled by intermonolayer friction". *Phys. Rev. Lett.* **102** (2009), 018102.

with optical tweezers, [‡] osmotic mismatches, [†] and molecular motors traveling along microtubules. [*] In biological systems, membrane tubes play an important role in many cellular processes—including the transport of material between the Golgi complex and endoplasmic reticulum, [§] as well as intracellular communication. [♯] Neurons also exhibit cylindrical geometries, as both axons and dendrites can often be approximated as tubes. It is important to note that a cylindrical membrane geometry can sustain a uniform axial flow of lipids, as observed in growing axons [‖,∀] and *in vitro* cylindrical tethers. [◇]

Here we investigate the dynamics of lipid membrane tubes using the general procedure outlined in Chapter VI. First, the equations governing a membrane tube of fixed radius are obtained. Two base states are considered: one with no movement of lipids, and one with an axial base lipid flow—as motivated by the aforementioned biological and *in vitro* scenarios. In both cases, we determine the linearized equations governing an infinitesimal disturbance to the system, and subsequently non-dimensionalize these equations. Compared to the planar and spherical cases, the cylindrical geometry presents a new complexity in that the base surface tension scale can be set by either bending forces or the jump in the normal stress across the membrane surface. Moreover, a tube can have an axial length scale which is much longer than the tube radius, such that quantities can vary over different distances in the axial and angular directions. The governing equations contain significant differences in the aforementioned scenarios, and are presented systematically in §3 and §4. In all cases, the Föppl–von Kármán number Γ captures the relative magnitude of surface tension and bending forces in governing the perturbed membrane shape. The Scriven–Love number $\mathcal{SL}$ also emerges in all situations, irrespective of whether or not the membrane tube has a base flow. In contrast, the planar and spherical dynamics only contained the Scriven–Love number in situations with a base flow of lipids. Such qualitative differences highlight the important role of geometry in the dynamics of lipid membranes.

Once the linearized dynamical equations are obtained and non-dimensionalized, we proceed to study the stability of cylindrical membranes. To this end, all membrane unknowns are decomposed into normal modes, and the dispersion relation is obtained in §6. Interestingly, the Scriven–Love number captures the frequency of temporal oscillations in the membrane's response, while the Föppl–von Kármán number completely determines the stability of the system. As we will see, tubes are unstable at sufficiently large *and* sufficiently small (increas-

[‡]D. Cuvelier et al. "Coalescence of membrane tethers: Experiments, theory, and applications". *Biophys. J.* **88** (2005), 2714–2726.

[†]Fournier et al., "Chemically triggered ejection of membrane tubules controlled by intermonolayer friction".

[*]A. Roux et al. "A minimal system allowing tubulation with molecular motors pulling on giant liposomes". *Proc. Natl. Acad. Sci. U.S.A.* **99**.8 (2002), 5394–5399.

[§]C. Lee and L.-B. Chen. "Dynamic behavior of endoplasmic reticulum in living cells". *Cell* **54** (1988), 37–46.

[♯]A. Rustom et al. "Nanotubular highways for intercellular organelle transport". *Science* **303** (2004), 1007–1010.

[‖]J. Dai and M.P. Sheetz. "Mechanical properties of neuronal growth cone membranes studied by tether formation with laser optical tweezers". *Biophys. J.* **68** (1995), 988–996.

[∀]J. Dai and M.P. Sheetz. "Axon membrane flows from the growth cone to the cell body". *Cell* **83** (1995), 693–701.

[◇]P.G. Dommersnes et al. "Marangoni transport in lipid nanotubes". *Europhys. Lett.* **70** (2005), 271–277.

ingly negative) values of the Föppl–von Kármán number—the former leads to axisymmetric pearling, while the latter yields non-axisymmetric buckling modes reminiscent of those in a spherical vesicle. Moreover, the structure of the dispersion relation motivates us to consider the response of an unstable membrane tube to local, rather than global, perturbations. To do so, we introduce the concept of a *spatiotemporal* stability analysis in §7. We then demonstrate how local perturbations to unstable membrane tubes yield propagating fronts, with the Föppl–von Kármán number selecting the pattern in the wake of the front and the Scriven–Love number capturing the long-time response as seen by a stationary observer.

1. The unperturbed equations

The position of an unperturbed cylindrical membrane tube of radius R and length $2Z$ is given by

$$\boldsymbol{x}_{(0)}(\theta, z) \;=\; R\boldsymbol{e}_r(\theta) \;+\; z\boldsymbol{e}_z \;, \tag{1}$$

where in terms of our differential geometric formulation

$$\theta^1 \;:=\; \theta \;\in\; [0, 2\pi) \qquad \text{and} \qquad \theta^2 \;:=\; z \;\in\; [-Z, Z] \tag{2}$$

are respectively the polar angle and axial position of a standard cylindrical coordinate system (see Fig. 1b). Relevant geometric quantities are calculated as

$$\begin{aligned}
\boldsymbol{a}_1^{(0)} \;&=\; R\boldsymbol{e}_\theta \;, \qquad & \boldsymbol{a}_2^{(0)} \;&=\; \boldsymbol{e}_z \;, \qquad & \boldsymbol{n}_{(0)} \;&=\; \boldsymbol{e}_r \;, \\
a_{\alpha\beta}^{(0)} \;&=\; \mathrm{diag}\,(R^2, 1) \;, \qquad & a_{(0)}^{\alpha\beta} \;&=\; \mathrm{diag}\,(R^{-2}, 1) \;, \\
b_{\alpha\beta}^{(0)} \;&=\; \mathrm{diag}\,(-R, 0) \;, \qquad & H_{(0)} \;&=\; -1/(2R) \;, \\
K_{(0)} \;&=\; 0 \;, \qquad \text{and} \qquad & \Gamma_{\lambda\mu}^{\alpha\,(0)} \;&=\; 0 \;.
\end{aligned} \tag{3}$$

Furthermore, an unperturbed membrane tube has no velocity component in the normal direction, so $v_{(0)} := \boldsymbol{v}_{(0)} \cdot \boldsymbol{n}_{(0)} = 0$ and the membrane velocity $\boldsymbol{v}_{(0)}$ is given by

$$\boldsymbol{v}_{(0)} \;=\; v_{(0)}^\alpha \boldsymbol{a}_\alpha^{(0)} \;=\; v_{(0)}^1 R\boldsymbol{e}_\theta \;+\; v_{(0)}^2 \boldsymbol{e}_z \;. \tag{4}$$

From Eq. (4), we observe that $v_{(0)}^1$ is an angular velocity with dimensions of inverse time, while $v_{(0)}^2$ is a velocity with dimensions of length per time. In contrast, the velocity can also be decomposed in the usual cylindrical coordinate basis as

$$\boldsymbol{v}_{(0)} \;=\; v_\theta^{(0)} \boldsymbol{e}_\theta \;+\; v_z^{(0)} \boldsymbol{e}_z \;, \tag{5}$$

where $v_\theta^{(0)}$ and $v_z^{(0)}$ have dimensions of length per time. In comparing Eqs. (4) and (5), we find the velocity components are related by

$$v_\theta^{(0)} \;=\; v_{(0)}^1 R \qquad \text{and} \qquad v_z^{(0)} \;=\; v_{(0)}^2 \;, \tag{6}$$

which confirms $v_{(0)}^1$ as the angular velocity and $v_{(0)}^2$ as the axial velocity.

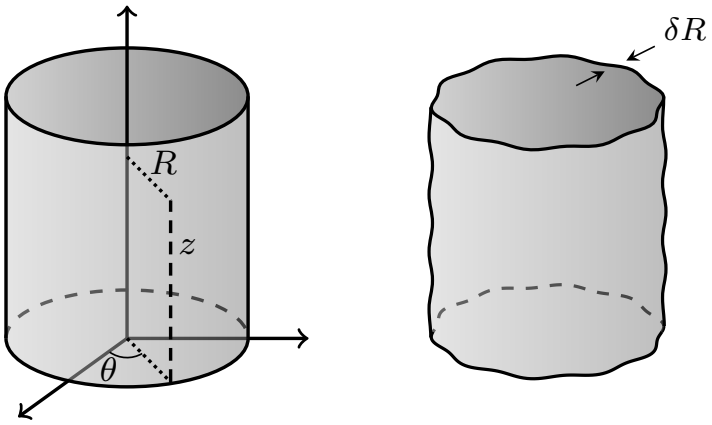

(a) unperturbed: $\boldsymbol{x}_{(0)}(\theta, z)$ (b) perturbed: $\boldsymbol{x}(\theta, z, t)$

Figure 1: Schematic of unperturbed (a) and perturbed (b) cylindrical geometries. The cylinder has radius R and is characterized by the polar angle θ and axial distance z. Membrane perturbations are of characteristic size δR, with $\epsilon := \delta R/R \ll 1$.

Given the geometric quantities in Eq. (3) and the general governing equations in Chapter VI, §1, we find the unperturbed continuity, in-plane θ, in-plane z, and shape equations are respectively given by

$$v^1_{(0),\theta} + v^2_{(0),z} = 0 \,, \tag{7}$$

$$\rho R^2 \left(v^1_{(0)}\, v^1_{(0),\theta} + v^2_{(0)}\, v^1_{(0),z} \right) = \zeta \left(v^1_{(0),\theta\theta} + R^2 v^1_{(0),zz} \right) + \lambda_{(0),\theta} \,, \tag{8}$$

$$\rho R \left(v^1_{(0)}\, v^2_{(0),\theta} + v^2_{(0)}\, v^2_{(0),z} \right) = \frac{\zeta}{R} \left(v^2_{(0),\theta\theta} + R^2 v^2_{(0),zz} \right) + R\lambda_{(0),z} \,, \tag{9}$$

and

$$-\rho R^2 \left(v^1_{(0)} \right)^2 = [\![p]\!] R - \lambda_{(0)} + \frac{k_\mathrm{b}}{4R^2} + 2\zeta v^2_{(0),z} \,. \tag{10}$$

As before, in Eq. (10) $[\![p]\!] = p_\mathrm{in} - p_\mathrm{out}$ is the jump in normal traction across the membrane surface, which is generally attributed to the pressure drop. While the continuity (7) and in-plane (8, 9) equations are similar in structure to those of a flat plane [Chapter VII, Eqs. (5) and (6)], the cylindrical shape equation (10) differs from its flat and spherical counterparts in that it balances forces arising from inertia, pressure drops, surface tension, and the intramembrane viscosity [cf. Chapter VII, Eq. (7) and Chapter VIII, Eq. (10)].

In the subsequent analysis, one could in principle consider base states with an arbitrary in-plane flow of lipids and spatially varying surface tensions which satisfy Eqs. (7)–(10). However, we are unaware of such stationary states in biological settings, and instead focus on a membrane tube with a constant axial flow of lipids. In this case, the components of the unperturbed velocity are given by

$$v^1_{(0)} = 0 \qquad \text{and} \qquad v^2_{(0)} = V \,, \qquad\qquad \text{for which} \qquad \boldsymbol{v}_{(0)} = V \boldsymbol{e}_z \,. \tag{11}$$

The choice of base flow (11) satisfies the continuity equation (7). By substituting Eq. (11) into the in-plane equations (8, 9), we find $\lambda_{(0),\theta} = 0$ and $\lambda_{(0),z} = 0$, for which the base surface

tension $\lambda_{(0)}$ is uniform along the tube. The shape equation (10) can then be solved for the base tension, which also sets the surface tension scale Λ—given by

$$\Lambda := \lambda_{(0)} = [\![p]\!] R + \frac{k_\mathrm{b}}{4R^2} \,. \tag{12}$$

In Eq. (12), $[\![p]\!]$ is assumed to be a known constant.

(a). The pull force on a stationary tether

Before proceeding, we would like to comment on the mechanical properties of cylindrical tethers, which are often pulled from artificial vesicles [‡] and live cells [†] to probe the membrane tension. In such experiments, the pull force f_pull on the tether is measured—often via optical tweezers manipulating a bead attached to the membrane (see Fig. 2). Moreover, the bending modulus k_b is often assumed or measured beforehand using a different assay, and so the pull force is thought to identify the base surface tension $\lambda_{(0)}$. An implicit assumption in the many studies reporting membrane tension in this manner is that the pressure drop $[\![p]\!] = 0$, which is often not the case—leading to many incorrect reports of the surface tension. In what follows, we determine the general expression for the pull force in two different ways, and comment on its simplified form when $[\![p]\!] = 0$, which is ubiquitous in the membrane biophysics literature.

The determination via membrane stresses

In many experiments, a micron-sized bead is adhered to a portion of the membrane, and pulled away with an optical tweezer until a tether forms—shown schematically in Fig. 2. As the interaction between the bead and the tether involves complicated adhesion energies, we imagine cutting the tether slightly away from the bead, such that our system consists of the bead and a small portion of the end of the tether (see Fig. 2d). In order for the system to remain stationary, a force balance requires

$$f_\mathrm{pull} + \pi R^2 [\![p]\!] = 2\pi R\, F_\nu \,. \tag{13}$$

In Eq. (13), f_pull is the magnitude of the force exerted by the optical trap on the bead, $\pi R^2 [\![p]\!]$ accounts for the internal pressure pushing the bead to the left while the net external pressure pushes the bead to the right, and F_ν is the force per length on the cut edge due to internal membrane tractions. The general form of F_ν for an incompressible, viscous membrane was provided in Eq. (238) of Chapter V, and is reproduced here as

$$F_\nu = \frac{k_\mathrm{b}}{4}\left(\kappa_\tau^2 - \kappa_\nu^2\right) - k_\mathrm{g}\,\xi^2 + \lambda + \pi^{\alpha\beta}\nu_\alpha\nu_\beta \,. \tag{14}$$

In our unperturbed cylindrical system, the in-plane surface tangent $\boldsymbol{\tau} = \tau^\alpha \boldsymbol{a}_\alpha = \boldsymbol{e}_\theta$ and the in-plane surface normal $\boldsymbol{\nu} = \nu^\alpha \boldsymbol{a}_\alpha = \boldsymbol{e}_z$, for which [cf. Eq. (3)]

$$\tau^1 = \frac{1}{R} \,, \qquad \tau^2 = 0 \,, \qquad \nu^1 = 0 \,, \qquad \text{and} \qquad \nu^2 = 1 \,. \tag{15}$$

[‡] G. Koster et al. "Membrane tube formation from giant vesicles by dynamic association of motor proteins". *Proc. Natl. Acad. Sci. U.S.A.* **100** (2003), 15583–15588.

[†] A. Datar et al. "Dynamics of membrane tethers reveal novel aspects of cytoskeleton–membrane interactions in axons". *Biophys. J.* **108** (2015), 489–497.

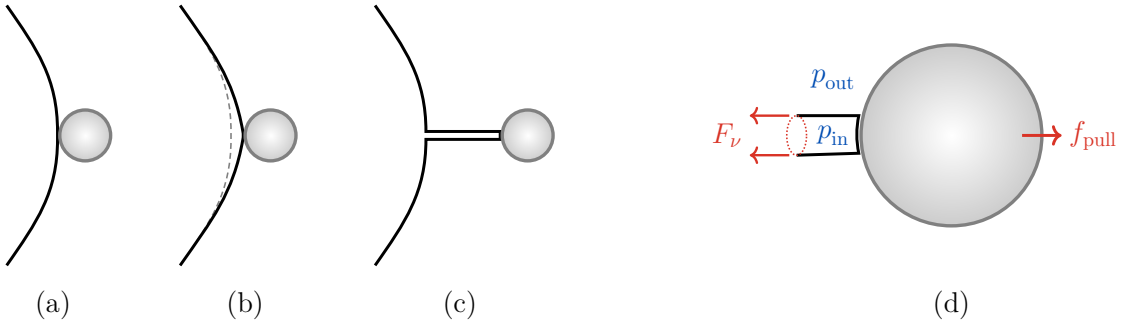

Figure 2: Schematic of tether pulling experiments via an optical trap. (a)–(c) Sequence of events as an inert bead (gray) is (a) brought in contact with the membrane, and then (b) pulled to the right until (c) a long tether forms, and is held stationary. (d) A virtual cut of the membrane tether, which shows the different forces acting on the system. The optical trap exerts a force f_{pull} to the right. The difference in internal and external pressures also leads to a net force $(p_{\text{in}} - p_{\text{out}})\pi R^2$ to the right. The internal membrane tractions exert a force per length F_ν, so the total internal membrane force is $2\pi R F_\nu$ to the left. At mechanical equilibrium, all the forces sum to zero, giving rise to Eq. (13).

With Eq. (15) and the curvature tensor $b_{\alpha\beta}$ (3), we calculate the curvatures κ_τ and κ_ν as well as the twist ξ—which were introduced in §2 (f) of Chapter II—as

$$\kappa_\tau = b_{\alpha\beta}\tau^\alpha\tau^\beta = -\frac{1}{R}\,, \qquad \kappa_\nu = b_{\alpha\beta}\nu^\alpha\nu^\beta = 0\,, \qquad \text{and} \qquad \xi = b_{\alpha\beta}\nu^\alpha\tau^\beta = 0\,. \tag{16}$$

Moreover, assuming no in-plane viscous stresses as the tether is stationary, we find

$$F_\nu = \frac{k_{\text{b}}}{4R^2} + \lambda_{(0)}\,. \tag{17}$$

By substituting Eq. (17) into Eq. (13), we determine the general expression for the pull force as

$$f_{\text{pull}} = \frac{\pi k_{\text{b}}}{2R} + 2\pi R\lambda_{(0)} - \pi R^2[\![p]\!]\,. \tag{18}$$

The unperturbed, static shape equation (12) is then substituted into Eq. (18) to yield three equivalent expressions for the pull force—written as

$$\begin{aligned} f_{\text{pull}} &= \frac{\pi k_{\text{b}}}{R} + \pi R^2[\![p]\!] \\ &= 4\pi R\,\lambda_{(0)} - 3\pi R^2[\![p]\!] \\ &= \pi R\,\lambda_{(0)} + \frac{3\pi k_{\text{b}}}{4R}\,. \end{aligned} \tag{19}$$

In the case where there is no pressure drop, the shape equation (12) simplifies to $\lambda_{(0)} = k_{\text{b}}/(4R^2)$ and the pull force is given by

$$f_{\text{pull}}^{(p=0)} = \frac{\pi k_{\text{b}}}{R} = 2\pi\sqrt{k_{\text{b}}\lambda_{(0)}}\,. \tag{20}$$

Thus, if k_b is known then one can determine both $\lambda_{(0)} = [f_\mathrm{pull}/(2\pi)]^2/k_\mathrm{b}$ and $R = \pi k_\mathrm{b}/f_\mathrm{pull}$ from a single measurement of the pull force. Unfortunately, in experiments the hydrodynamic pressure jump is not in one's control, and in almost all instances sufficient data is not reported to determine whether or not $[\![p]\!] = 0$. Accordingly, we often cannot determine whether the provided values of $\lambda_{(0)}$ are accurate.

The determination via membrane energetics

Here, we provide an alternate derivation of the pull force based on the energy of the entire tether and bead system. Though this calculation was presented over a decade ago, [‡] the general relation between f_pull, $\lambda_{(0)}$, k_b, and R remains largely unappreciated in the membrane biophysics community—which is why we reproduce it here. The total free energy of the system, for a tether of length L_t, is given by

$$W \;=\; 2\pi R L_\mathrm{t}\left(\frac{k_\mathrm{b}}{4R^2} \,+\, \lambda_{(0)}\right) \,-\, \pi R^2 L_\mathrm{t}[\![p]\!] \,-\, f_\mathrm{pull}\, L_\mathrm{t}\ , \tag{21}$$

which consists of three terms. The first term is the product of the tether surface area and the membrane energy per unit area, which contains bending and surface tension contributions. Recall that for a cylinder, the Helfrich energy density $w_\mathrm{H} = k_\mathrm{b}H^2 + k_\mathrm{g}K = k_\mathrm{b}/(4R^2)$ [cf. Chapter V, §4 (d), Eq. (157)]. The second term in Eq. (21) captures the pressure–volume work associated with changing the tube length, and the last term is the work done by the optical tweezer on the bead. At mechanical equilibrium, we require $\delta W/\delta R = 0$ and $\delta W/\delta L_\mathrm{t} = 0$, for which

$$\lambda_{(0)} \;=\; \frac{k_\mathrm{b}}{4R^2} \,+\, [\![p]\!]R \qquad \text{and} \qquad f_\mathrm{pull} \;=\; 2\pi R\left(\frac{k_\mathrm{b}}{4R^2} \,+\, \lambda_{(0)}\right) \,-\, \pi R^2[\![p]\!]\ , \tag{22}$$

respectively. The first relation in Eq. (22) is the shape equation of a static tube (12), while the second relation is the general expression of the pull force (18).

2. The perturbed equations

With the base state described by Eqs. (11) and (12), we introduce a height perturbation in the normal direction and seek to describe how the systems evolves in time. To this end, the membrane position is now expressed as

$$\boldsymbol{x}(\theta, z, t) \;=\; \Big[R \,+\, \epsilon\,\tilde{r}(\theta, z, t)\Big]\boldsymbol{e}_r(\theta) \,+\, z\boldsymbol{e}_z\ . \tag{23}$$

In this case, the small parameter ϵ is defined as

$$\epsilon \;:=\; \frac{\delta R}{R} \;\ll\; 1\ , \tag{24}$$

[‡] S. Monnier et al. "Long-range protein coupling mediated by critical low-energy modes of tubular lipid membranes". *Phys. Rev. Lett.* **105** (2010), 028102.

where as in the spherical scenario δR is the characteristic size of the radial perturbation and $\tilde{r}$ is $\mathcal{O}(R)$, as shown in Fig. 1b. To first order in ϵ, the perturbed geometric quantities are given by

$$\begin{aligned}
\Gamma^1_{11} &= \frac{\epsilon\tilde{r}_{,\theta}}{R}\,, & \boldsymbol{a}_1 &= \left(R + \epsilon\,\tilde{r}\right)\boldsymbol{e}_\theta + \epsilon\,\tilde{r}_{,\theta}\,\boldsymbol{e}_r\,,\\
\Gamma^2_{11} &= -\epsilon R\,\tilde{r}_{,z}\,, & \boldsymbol{a}_2 &= \boldsymbol{e}_z + \epsilon\,\tilde{r}_{,z}\,\boldsymbol{e}_r\,,\\
\Gamma^1_{12} &= \frac{\epsilon\tilde{r}_{,z}}{R}\,, & \boldsymbol{n} &= \boldsymbol{e}_r - \frac{\epsilon\tilde{r}_{,\theta}}{R}\,\boldsymbol{e}_\theta - \epsilon\tilde{r}_{,z}\,\boldsymbol{e}_z\,,\\
\Gamma^1_{21} &= \frac{\epsilon\tilde{r}_{,z}}{R}\,, & a_{\alpha\beta} &= \operatorname{diag}\left(R^2 + 2\epsilon\tilde{r}\,R,\ 1\right)\,,\\
K &= -\frac{\epsilon\tilde{r}_{,zz}}{R}\,, & b_{\alpha\beta} &= -\operatorname{diag}\left(R + \epsilon\,\tilde{r},\ 0\right) - \epsilon\,\tilde{r}_{,\alpha\beta}\,,\\
\text{and}\qquad & & H &= -\frac{1}{2R^2}\left(R - \epsilon\,\tilde{r} - \epsilon\,R^2\,\Delta_{\mathrm{s}}\,\tilde{r}\right)\,.
\end{aligned} \tag{25}$$

In Eq. (25) we introduce the surface Laplacian operator, Δ_{s}, which is given by

$$\Delta_{\mathrm{s}}\left(\,\cdot\,\right) = \frac{1}{R^2}\left(\,\cdot\,\right)_{,\theta\theta} + \left(\,\cdot\,\right)_{,zz} \tag{26}$$

when operating on a scalar quantity. The fundamental unknowns are similarly expanded to first order as

$$v^1 = \epsilon\,\tilde{v}^1\,, \qquad v^2 = V + \epsilon\,\tilde{v}^2\,, \qquad v = \epsilon\,\tilde{r}_{,t}\,, \qquad \text{and} \qquad \lambda = \lambda_{(0)} + \epsilon\,\tilde{\lambda}\,, \tag{27}$$

where as before quantities with a 'tilde' are assumed to be the same order as their unperturbed counterparts. By substituting Eqs. (25) and (27) into the general continuity, in-plane, and shape equations provided in Chapter VI, §1 and then keeping only first-order terms, we find the first-order perturbed governing equations as

$$R\,\tilde{v}^1_{,\theta} + R\,\tilde{v}^2_{,z} + V\,\tilde{r}_{,z} + \tilde{r}_{,t} = 0\,, \tag{28}$$

$$\rho R^2\left(\tilde{v}^1_{,t} + V\,\tilde{v}^1_{,z}\right) = \frac{\zeta}{R}\left(\tilde{r}_{,t\theta} + R\,\tilde{v}^1_{,\theta\theta} + R^3\,\tilde{v}^1_{,zz} + V\,\tilde{r}_{,\theta z}\right) + \tilde{\lambda}_{,\theta}\,, \tag{29}$$

$$\rho R\left(\tilde{v}^2_{,t} + V\,\tilde{v}^2_{,z}\right) = \zeta\left(-\tilde{r}_{,tz} + \frac{1}{R}\,\tilde{v}^2_{,\theta\theta} + R\,\tilde{v}^2_{,zz} - V\tilde{r}_{,zz}\right) + R\,\tilde{\lambda}_{,z}\,, \tag{30}$$

and

$$\begin{aligned}
&\rho R\Big(\tilde{r}_{,tt} + 2V\tilde{r}_{,tz} - V^2\,\tilde{r}_{,zz}\Big)\\
&\quad = 2\zeta\,\tilde{v}^2_{,z} - \tilde{\lambda} + \frac{\lambda_{(0)}}{R}\left(\tilde{r} + R^2\,\Delta_{\mathrm{s}}\tilde{r}\right) - \frac{k_{\mathrm{b}}}{4R^3}\Big(3\tilde{r} + 4\tilde{r}_{,\theta\theta} + R^2\,\Delta_{\mathrm{s}}\,\tilde{r} + 2R^4\,\Delta_{\mathrm{s}}^2\,\tilde{r}\Big)\,.
\end{aligned} \tag{31}$$

In what follows, we non-dimensionalize Eqs. (28)–(31), which describe tubes which are either static or have a flow in their base state. We already see from the shape equation (31) that viscous forces arise in scenarios with and without a base flow. The presence of viscous, tensile, and bending forces in Eq. (31) lead to the emergence of the Scriven–Love and Föppl–von Kármán numbers in all the situations we consider.

3. The dynamics about a static tube

For an initially static tube, the base state is given by [cf. Eqs. (11) and (12)]

$$v^1_{(0)} = 0 \,, \qquad v^2_{(0)} = 0 \,, \qquad v_{(0)} = 0 \,, \qquad \text{and} \qquad \lambda_{(0)} = \Lambda = [\![p]\!]R + \frac{k_\mathrm{b}}{4R^2} \,. \tag{32}$$

When $[\![p]\!] \gg k_\mathrm{b}/(4R^3)$, then $\Lambda \approx [\![p]\!]R$, while if $|p_\mathrm{in} - p_\mathrm{out}| \ll k_\mathrm{b}/(4R^3)$ then $\Lambda \approx k_\mathrm{b}/(4R^2)$. We refer to these two limits as the pressure-dominated and bending-dominated regimes, respectively. Note that in this work, we only consider cases where $[\![p]\!] \geq 0$, and defer the analysis of lipid membrane tubes under compression to a future study.

At this point, we introduce the relevant dimensionless quantities. The small parameter ϵ is defined in Eq. (24), such that $\tilde{r}$ is $\mathcal{O}(R)$. We additionally assume a shape perturbation causes angular gradients over $\mathcal{O}(1)$ changes in θ. In a tubular lipid membrane, however, the distance L over which quantities vary in the axial direction may be much larger than the cylinder radius R. We therefore define the dimensionless parameter

$$\delta := \frac{R}{L} \tag{33}$$

to characterize the length scale over which quantities vary in the axial direction, relative to the cylinder radius. We emphasize that δ is not the aspect ratio of the tube: L is the length scale over which quantities are expected to vary in the axial direction, and two tubes with the same aspect ratio can have different values of δ depending on the membrane perturbation and the phenomena of interest (see Fig. 3). We also denote the currently unknown characteristic angular velocity scale as Ω and axial velocity scale as V. Finally, we introduce the unknown time scale τ over which radial perturbations vary, and define the dimensionless quantities

$$\begin{gathered} \theta^* := \theta \,, \qquad z^* := \frac{z}{L} \,, \qquad \tilde{r}^* := \frac{\tilde{r}}{R} \,, \qquad \tilde{v}^{1*} := \frac{\tilde{v}^1}{\Omega} \,, \\ \tilde{v}^{2*} := \frac{\tilde{v}^2}{V} \,, \qquad \tilde{\lambda}^* := \frac{\tilde{\lambda}}{\Lambda} \,, \qquad \text{and} \qquad t^* := \frac{t}{\tau} \,. \end{gathered} \tag{34}$$

We now consider separately the case where $\delta \sim 1$, which is referred to as a thick tube, and the case where $\delta \ll 1$, from now on referred to as a thin tube. With Λ and L known, we seek to determine Ω, V, and τ through appropriate non-dimensionalization of the perturbed governing equations (28)–(31) for thick and thin tubes. In both cases, viscous forces enter the perturbed equations and the Scriven–Love number emerges—unlike the initially static flat and spherical geometries. We thus find that when membranes with different morphologies are perturbed, different forces arise in their response—illustrating the connection between membrane geometry and dynamics.

(a) $\delta \sim 1$ (b) $\delta \ll 1$

Figure 3: Schematic showing cylinders of the same aspect ratio, with different values of δ. (a) When $\delta \sim 1$, out-of-plane quantities vary over a length scale $L \sim R$. (b) When $\delta \ll 1$, out-of-plane quantities vary over a length scale $L \gg R$. The choice of δ depends on the membrane behavior under consideration.

(a). The case of a thick tube ($L \sim R$)

For thick tubes, the axial length scale over which gradients are expected is equal to the tube radius, written as $L = R$, for which $\delta = 1$. We substitute Eq. (34) into the perturbed continuity equation (28) to obtain

$$\Omega\, \tilde{v}^{1*}_{,\theta^*} + \frac{V}{R}\, \tilde{v}^{2*}_{,z^*} + \frac{1}{\tau}\, \tilde{r}^{*}_{,t^*} = 0\,. \tag{35}$$

Assuming both axial and angular in-plane velocity gradients account for the changes in membrane shape, we require

$$\Omega = \frac{V}{R} = \frac{1}{\tau}\,, \tag{36}$$

such that Eq. (35) simplifies to

$$\tilde{v}^{1*}_{,\theta^*} + \tilde{v}^{2*}_{,z^*} + \tilde{r}^{*}_{,t^*} = 0\,. \tag{37}$$

The continuity equation (37) connects out-of-plane deformations and in-plane flows, and along with Eq. (36) indicates that the time scale τ over which height perturbations vary is equal to the time scales $1/\Omega$ and R/V of angular and axial in-plane flows, respectively.

We next substitute Eqs. (34) and (36) into the perturbed in-plane equations (29, 30) and rearrange terms to obtain

$$Re\, \tilde{v}^{1*}_{,t^*} = \tilde{r}^{*}_{,t^*\theta^*} + \tilde{v}^{1*}_{,\theta^*\theta^*} + \tilde{v}^{1*}_{,z^*z^*} + \frac{\Lambda R}{\zeta V}\, \tilde{\lambda}^{*}_{,\theta^*} \tag{38}$$

and

$$Re\, \tilde{v}^{2*}_{,t^*} = -\tilde{r}^{*}_{,t^*z^*} + \tilde{v}^{2*}_{,\theta^*\theta^*} + \tilde{v}^{2*}_{,z^*z^*} + \frac{\Lambda R}{\zeta V}\, \tilde{\lambda}^{*}_{,z^*}\,, \tag{39}$$

where for cylindrical tubes the Reynolds number Re is defined as

$$Re := \frac{\rho V R}{\zeta}\,. \tag{40}$$

We choose for the axial velocity scale V to satisfy $\zeta V = \Lambda R$, such that surface tension and viscous forces balance in the in-plane equations (38, 39). As a result, the time and velocity scales are found to be

$$\tau = \frac{\zeta}{\Lambda}\,, \qquad \Omega = \frac{\Lambda}{\zeta}\,, \qquad \text{and} \qquad V = \frac{\Lambda R}{\zeta}\,. \tag{41}$$

Equation (41) reveals that the base surface tension sets the time scale, as well as the scale of in-plane axial and angular velocities. For a lipid membrane tube with a given geometry, those with larger jumps in the normal stress $[\![p]\!]$ have a larger base state tension (12), and consequently faster perturbed in-plane flows and more rapid out-of-plane shape rearrangements as well. With Eq. (41), the Reynolds number (40) can be written as $Re = \rho \Lambda R^2/\zeta^2$, which ranges from 10^{-12} to 10^{-7} over the experiments considered—as described and quantified in §5. Since $Re \ll 1$ in all cases, Eqs. (38) and (39) simplify to

$$\tilde{r}^*_{,t^*\theta^*} + \tilde{v}^{1*}_{,\theta^*\theta^*} + \tilde{v}^{1*}_{,z^*z^*} + \tilde{\lambda}^*_{,\theta^*} = 0 \tag{42}$$

and

$$-\tilde{r}^*_{,t^*z^*} + \tilde{v}^{2*}_{,\theta^*\theta^*} + \tilde{v}^{2*}_{,z^*z^*} + \tilde{\lambda}^*_{,z^*} = 0\,, \tag{43}$$

which contain only viscous and tensile forces. Equations (42) and (43) are the dimensionless in-plane equations governing perturbations to a thick, initially static tube.

Finally, we non-dimensionalize the shape equation (31). By substituting Eqs. (34), (36), and (41) into Eq. (31) and rearranging terms, we obtain

$$\frac{\rho \Lambda^2 R^4}{\zeta^2 k_\mathrm{b}}\,\tilde{r}^*_{,t^*t^*} = 2\,\frac{\zeta V R}{k_\mathrm{b}}\,\tilde{v}^{2*}_{,z^*} + \frac{\Lambda R^2}{k_\mathrm{b}}\Big(\tilde{r}^* + \Delta^*_\mathrm{s}\,\tilde{r}^* - \tilde{\lambda}^*\Big) - \frac{1}{4}\Big(3\tilde{r}^* + 4\tilde{r}^*_{,\theta^*\theta^*} + \Delta^*_\mathrm{s}\,\tilde{r}^* + 2\Delta^{*2}_\mathrm{s}\,\tilde{r}^*\Big)\,, \tag{44}$$

where for thick tubes $\Delta^*_\mathrm{s}(\,\cdot\,) = R^2\Delta_\mathrm{s}(\,\cdot\,)$. In Eq. (44), the coefficient $\zeta V R/k_\mathrm{b}$ compares viscous and bending forces while the coefficient $\Lambda R^2/k_\mathrm{b}$ compares tension and viscous forces. We accordingly define the Scriven–Love and Föppl–von Kármán numbers as

$$\mathit{SL} = \frac{\zeta V R}{k_\mathrm{b}} \qquad \text{and} \qquad \mathit{\Gamma} = \frac{\Lambda R^2}{k_\mathrm{b}}\,, \tag{45}$$

for which Eq. (44) can be written as

$$Re\,\mathit{\Gamma}\,\tilde{r}^*_{,t^*t^*} = 2\,\mathit{SL}\,\tilde{v}^{2*}_{,z^*} + \mathit{\Gamma}\Big(\tilde{r}^* + \Delta^*_\mathrm{s}\,\tilde{r}^* - \tilde{\lambda}^*\Big) - \frac{1}{4}\Big(3\tilde{r}^* + 4\tilde{r}^*_{,\theta^*\theta^*} + \Delta^*_\mathrm{s}\,\tilde{r}^* + 2\Delta^{*2}_\mathrm{s}\,\tilde{r}^*\Big)\,. \tag{46}$$

Note that given the relations in Eq. (41), in this scenario $\mathit{SL} = \mathit{\Gamma}$. Moreover, as we found $Re \ll 1$ in the biological systems considered, inertial forces are always negligible relative to tension forces. The shape equation governing an initially static, thick tube is accordingly found to be

$$2\,\mathit{SL}\,\tilde{v}^{2*}_{,z^*} + \mathit{\Gamma}\Big(\tilde{r}^* + \Delta^*_\mathrm{s}\,\tilde{r}^* - \tilde{\lambda}^*\Big) - \frac{1}{4}\Big(3\tilde{r}^* + 4\tilde{r}^*_{,\theta^*\theta^*} + \Delta^*_\mathrm{s}\,\tilde{r}^* + 2\Delta^{*2}_\mathrm{s}\,\tilde{r}^*\Big) = 0\,. \tag{47}$$

We now consider the form of the shape equation in the bending-dominated and pressure-dominated regimes.

When $[\![p]\!] \ll k_\mathrm{b}/(4R^3)$ in the bending-dominated regime, the unperturbed shape equation (12) indicates $\Lambda \approx k_\mathrm{b}/(4R^2)$. Consequently, $\mathit{SL} = \mathit{\Gamma} = \frac{1}{4}$ and surface tension, bending, and viscous forces are all balanced in the perturbed shape equation (47)—which simplifies to

$$2\,\tilde{v}^{2*}_{,z^*} - 2\tilde{r}^* - \tilde{\lambda}^* - 4\,\tilde{r}^*_{,\theta^*\theta^*} - 2\,\Delta^{*2}_\mathrm{s}\,\tilde{r}^* = 0\,. \tag{48}$$

In §5, we discuss several experimental scenarios in this regime.

When $[\![p]\!] \gg k_\mathrm{b}/(4R^3)$ in the pressure-dominated regime, on the other hand, Eq. (12) shows the surface tension scales as $\Lambda \approx [\![p]\!]R \gg k_\mathrm{b}/(4R^2)$, such that $\mathit{SL} = \Gamma \gg 1$. The viscous and tension terms then dominate the bending forces in Eq. (47), for which the rightmost quantity in parenthesis is negligible and the shape equation simplifies to

$$2\,\tilde{v}^{2*}_{,z^*} + \tilde{r}^* + \Delta^*_\mathrm{s}\,\tilde{r}^* - \tilde{\lambda}^* = 0\,. \tag{49}$$

Experimentally, we found one study in this regime, where $\mathit{SL} = \Gamma \sim 7$ and bending forces are small relative to tension and viscous forces (see §5, Experiment #1). In such situations, the equations governing the dynamics of a membrane tube (37, 42, 43, 49) are identical to those describing a cylindrical, two-dimensional viscous fluid film—for example, a soap bubble. Such films, with no bending modulus, are known to undergo a pearling-like instability mediated by in-plane flows when their length exceeds their circumference. [‡] Therefore, Eqs. (37), (42), (43), and (49) indicate lipid membrane tubes with a large normal stress jump across their surface, for which $\Gamma \gg 1$ [see Eq. (12)], are unstable. This conclusion will be expanded on in our subsequent analysis of the stability of lipid membrane tubes in §6 and §7.

(b). The case of a thin tube ($L \gg R$)

When the length scale L over which axial gradients are expected to occur is much larger than the tube radius R, then $\delta \ll 1$, as portrayed in Fig. 3b. Such tubes can be found, for example, in the endoplasmic reticulum. [†, *] To analyze such systems, we begin by substituting the dimensionless definitions in Eq. (34) into the perturbed continuity equation (28), which yields

$$\Omega\,\tilde{v}^{1*}_{,\theta^*} + \frac{V}{L}\,\tilde{v}^{2*}_{,z^*} + \frac{1}{\tau}\,\tilde{r}^*_{,t^*} = 0\,. \tag{50}$$

Again assuming both axial and angular in-plane velocity gradients account for the changing membrane shape, we find

$$\Omega = \frac{V}{L} = \frac{1}{\tau}\,, \tag{51}$$

such that Eq. (50) simplifies to

$$\tilde{v}^{1*}_{,\theta^*} + \tilde{v}^{2*}_{,z^*} + \tilde{r}^*_{,t^*} = 0\,. \tag{52}$$

Equation (52) is identical to the dimensionless continuity equation for a thick tube (37).

Next, the in-plane equations are non-dimensionalized. Substituting Eqs. (33), (34), and (51) into the in-plane equations (29, 30) and rearranging terms yields

$$\mathit{Re}\,\delta\,\tilde{v}^{1*}_{,t^*} = \tilde{r}^*_{,t^*\theta^*} + \tilde{v}^{1*}_{,\theta^*\theta^*} + \delta^2\,\tilde{v}^{1*}_{,z^*z^*} + \frac{\Lambda L}{\zeta V}\,\tilde{\lambda}^*_{,\theta^*} \tag{53}$$

[‡] A. Sahu et al. "Arbitrary Lagrangian–Eulerian finite element formulation for curved and deforming surfaces. I. General theory and application to fluid interfaces". *J. Comp. Phys.* **407** (2020), 109253. arXiv: 1812.05086.

[†] M. Terasaki, L.B. Chen, and K. Fujiwara. "Microtubules and the endoplasmic reticulum are highly interdependent structures". *J. Cell Biol.* **103** (1986), 1557–1568.

[*] J. Nixon-Abell et al. "Increased spatiotemporal resolution reveals highly dynamic dense tubular matrices in the peripheral ER". *Science* **354** (2016), aaf3928.

and

$$Re\,\delta\,\tilde{v}^{2*}_{,t^*} \;=\; -\delta^2\,\tilde{r}^{*}_{,t^*z^*} \;+\; \tilde{v}^{2*}_{,\theta^*\theta^*} \;+\; \delta^2\,\tilde{v}^{2*}_{,z^*z^*} \;+\; \delta^2\,\frac{\Lambda L}{\zeta V}\,\tilde{\lambda}^{*}_{,z^*}\;, \tag{54}$$

with the Reynolds number $Re = \rho V R/\zeta$ as defined in Eq. (40). Given Eqs. (53) and (54), there are now two choices for the velocity scale V: we could choose (i) $V = \delta^2\Lambda L/\zeta$, such that viscous forces and tension gradients balance in the z-direction (54), or (ii) $V = \Lambda L/\zeta$, such that viscous and tensile forces balance in the θ-direction (53). We consider both scaling relations below, ignoring inertial terms as necessary for the clarity of our argument.

Scaling Attempt #1: Balance axial forces (incorrect)

In our first attempt, we balance in-plane axial shear and surface tension forces by choosing

$$V \;=\; \frac{\delta^2\Lambda L}{\zeta}\;, \tag{55}$$

in which case the in-plane angular and axial equations can respectively be expressed as

$$\delta^2\,\tilde{r}^{*}_{,t^*\theta^*} \;+\; \delta^2\,\tilde{v}^{1*}_{,\theta^*\theta^*} \;+\; \delta^4\,\tilde{v}^{1*}_{,z^*z^*} \;+\; \tilde{\lambda}^{*}_{,\theta^*} \;=\; 0 \tag{56}$$

and

$$-\delta^2\,\tilde{r}^{*}_{,t^*z^*} \;+\; \tilde{v}^{2*}_{,\theta^*\theta^*} \;+\; \delta^2\,\tilde{v}^{2*}_{,z^*z^*} \;+\; \tilde{\lambda}^{*}_{,z^*} \;=\; 0\;. \tag{57}$$

Under the assumption that $\delta \ll 1$, we find all viscous forces are negligible in Eq. (56), which simplifies to $\tilde{\lambda}^{*}_{,\theta^*} = 0$—implying $\tilde{\lambda}^{*}$ is independent of θ^*. In the in-plane z-equation (57), on the other hand, the leading order viscous term balances the surface tension gradient, and we obtain

$$\tilde{v}^{2*}_{,\theta^*\theta^*} \;+\; \tilde{\lambda}_{,z^*} \;=\; 0\;. \tag{58}$$

As $\tilde{\lambda}^{*}$ is independent of θ^*, $\tilde{v}^{2*}_{,\theta^*\theta^*}$ is independent of θ^* as well, and $\tilde{v}^{2*}$ is at most quadratic in the angle θ^*. However, due to the cylindrical geometry $\tilde{v}^{2*}$ must be periodic in θ^*, which implies $\tilde{v}^{2*}$ is not a function of θ^*. As a result, the z-equation simplifies to $\tilde{\lambda}^{*}_{,z^*} = 0$. We thus find $\tilde{\lambda}^{*}$ is independent of both θ^* and z^*, regardless of how local a perturbation we apply. As such a result is unphysical, this choice of velocity scaling is incorrect, and we turn to the second option.

Scaling Attempt #2: Balance angular forces (correct)

In our second attempt, we balance in-plane angular shear and surface tension forces with the choice

$$V \;=\; \frac{\Lambda L}{\zeta}\;. \tag{59}$$

The in-plane θ-equation then simplifies to

$$Re\,\delta\,\tilde{v}^{1*}_{,t^*} \;=\; \tilde{r}^{*}_{,t^*\theta^*} \;+\; \tilde{v}^{1*}_{,\theta^*\theta^*} \;+\; \tilde{\lambda}^{*}_{,\theta^*}\;. \tag{60}$$

However, the product of the Reynolds number and length scale ratio is given by $Re\,\delta = \rho\Lambda R^2/\zeta^2$, which was previously shown to be much less than unity in the biological systems

of interest. Accordingly, inertial terms can be neglected, and the in-plane θ-equation can be written as

$$\tilde{r}^*_{,t^*\theta^*} + \tilde{v}^{1*}_{,\theta^*\theta^*} + \tilde{\lambda}^*_{,\theta^*} = 0 \,. \tag{61}$$

Given the choice of scaling in Eq. (59), the in-plane z-equation simplifies to

$$\tilde{v}^{2*}_{,\theta^*\theta^*} = 0 \tag{62}$$

at leading order. However, since all quantities must be periodic in θ^*, we find $\tilde{v}^{2*}$ is independent of θ^* and thus has the functional form $\tilde{v}^{2*} = \tilde{v}^{2*}(z^*, t^*)$. In this case, taking the partial derivative of the continuity equation (52) with respect to θ^* yields $\tilde{v}^{1*}_{,\theta^*\theta^*} + \tilde{r}^*_{,t^*\theta^*} = 0$; upon substitution of this result into Eq. (61) we find

$$\tilde{\lambda}^*_{,\theta^*} = 0 \,. \tag{63}$$

Since $\tilde{\lambda}^*$ is independent of θ^*, the surface tension also has the functional form $\tilde{\lambda}^* = \tilde{\lambda}^*(z^*, t^*)$. Thus, we find that for a thin tube, the choice of velocity scale in Eq. (59) results in both the axial velocity $\tilde{v}^{2*}$ and the surface tension $\tilde{\lambda}^*$ being axisymmetric—a physically reasonable result for such a system.

Consequences of the Velocity Scaling

With the choice of velocity scale in Eq. (59) and the scaling results in Eq. (51), we find the time scale τ and angular velocity scale Ω are given by

$$\tau = \frac{\zeta}{\Lambda} \qquad \text{and} \qquad \Omega = \frac{\Lambda}{\zeta} \,. \tag{64}$$

The shape equation (31) is then non-dimensionalized as

$$\Gamma Re\, \delta\, \tilde{r}^*_{,t^*t^*} = 2\mathit{SL}\, \delta\, \tilde{v}^{2*}_{,z^*} + \Gamma \left(\tilde{r}^* + \tilde{r}^*_{,\theta^*\theta^*} - \tilde{\lambda}^* \right) - \frac{1}{4} \left(3\tilde{r}^* + 5\tilde{r}^*_{,\theta^*\theta^*} + 2\tilde{r}^*_{,\theta^*\theta^*\theta^*\theta^*} \right) , \tag{65}$$

where the Scriven–Love and Föppl–von Kármán numbers are identical to those provided in the case of a thick tube [see Eq. (45)]. To compare the magnitude of the different terms in Eq. (65), we first recognize that $\mathit{SL}\, \delta = \Gamma$ given our choice of velocity scale (59). Thus, even for $\delta \ll 1$ the viscous terms and tension terms in Eq. (65) are the same order. Next, we observe that $Re\, \delta = \rho \Lambda R^2 / \zeta \ll 1$, such that inertial forces are always negligible relative to tension and viscous forces. Accordingly, the shape equation governing a thin, static tube can be written as

$$2\mathit{SL}\delta\, \tilde{v}^{2*}_{,z^*} + \Gamma \left(\tilde{r}^* + \tilde{r}^*_{,\theta^*\theta^*} - \tilde{\lambda}^* \right) - \frac{1}{4} \left(3\tilde{r}^* + 5\tilde{r}^*_{,\theta^*\theta^*} + 2\tilde{r}^*_{,\theta^*\theta^*\theta^*\theta^*} \right) = 0 \,. \tag{66}$$

Equations (52), (61), (62), and (66) are respectively the continuity, in-plane θ, in-plane z, and shape equations governing a thin, static lipid membrane tube. Interestingly, in Eq. (66) and its thick tube analog, Eq. (47), we see the emergence of the Scriven–Love number SL in perturbed, initially static tubes. As the Scriven–Love number did not appear in the equations governing initially static flat patches or spherical vesicles, the cylindrical equations demonstrate how geometry plays an important role in the dynamics of lipid membranes.

We now briefly consider how the shape equation differs in the pressure-dominated and bending-dominated cases. When $[\![p]\!] \ll k_\mathrm{b}/(4R^3)$ and $\Lambda \approx k_\mathrm{b}/(4R^2)$ in the bending-dominated limit [cf. Eq. (12)], $\mathcal{SL}\,\delta = \Gamma = \frac{1}{4}$ and the shape equation (66) simplifies to

$$2\,\tilde{v}^{2*}_{,z^*} - 2\,\tilde{r}^* - 4\,\tilde{r}^*_{,\theta^*\theta^*} - \tilde{\lambda}^* - 2\,\tilde{r}^*_{,\theta^*\theta^*\theta^*\theta^*} = 0\,. \tag{67}$$

On the other hand, in the pressure-dominated limit where $[\![p]\!] \gg k_\mathrm{b}/(4R^3)$ and $\Lambda \approx [\![p]\!]R$, we find $\mathcal{SL}\,\delta = \Gamma \gg 1$—for which the shape equation (66) simplifies to

$$2\,\tilde{v}^{2*}_{,z^*} + \tilde{r}^* + \tilde{r}^*_{,\theta^*\theta^*} - \tilde{\lambda}^* = 0\,. \tag{68}$$

Thus, for both thick and thin initially static tubes, viscous and tension forces always play an important role in the membrane's dynamical response to perturbations.

In comparing the thick and thin tube equations, for the same base state surface tension, we note several important differences. First, the thin tube axial velocity scale is larger than its thick tube counterpart by a factor of δ^{-1}, despite the angular velocity and time scales being identical. Second, thin tubes have axisymmetric axial velocities and surface tensions, while thick tubes in general do not. Despite these differences, however, thick and thin tubes have identical continuity equations and similar shape equations. Thus, in both cases radial shape changes lead to axial and in-plane flows, and viscous forces enter the shape equation, leading to the emergence of the Scriven–Love number.

4. The dynamics about a tube with a base flow

In biological and *in vitro* systems, lipid membrane tubes often have a base axial flow of lipids—for example, when tubes shoot suddenly from the endoplasmic reticulum into the cytoplasm of the cell, [‡] in neuronal flows along the length of the axon, [†, *] and in tube pulling experiments with GUVs [§, ♯] or live cells. [‖] In biological systems, velocities of up to 10 μm/sec (10^{-2} nm/μsec) are observed, [*, ∀] while velocities of ≤ 1 μm/sec (10^{-3} nm/μsec) are more common. [♢, $] In such situations, we assume the velocity field in the base state is given by $\boldsymbol{v}_{(0)} = V\boldsymbol{e}_z$, which introduces the velocity scale V [cf. Eq. (11)]. The unperturbed shape

[‡] Terasaki, Chen, and Fujiwara, "Microtubules and the endoplasmic reticulum are highly interdependent structures".

[†] Dai and Sheetz, "Mechanical properties of neuronal growth cone membranes studied by tether formation with laser optical tweezers".

[*] Dai and Sheetz, "Axon membrane flows from the growth cone to the cell body"

[§] Roux et al., "A minimal system allowing tubulation with molecular motors pulling on giant liposomes".

[♯] Dommersnes et al., "Marangoni transport in lipid nanotubes".

[‖] A. Upadhyaya and M.P. Sheetz. "Tension in tubulovesicular networks of Golgi and endoplasmic reticulum membranes". *Biophys. J.* **86** (2004), 2923–2928.

[∀] C. Kaether, P. Skehel, and C.G. Dotti. "Axonal membrane proteins are transported in distinct carriers: A two-color video microscopy study in cultured hippocampal neurons". *Mol. Biol. Cell* **11** (2000), 1213–1224.

[♢] C. Leduc et al. "Cooperative extraction of membrane nanotubes by molecular motors". *Proc. Natl. Acad. Sci. U.S.A.* **101** (2004), 17096–17101.

[$] Shi et al., "Cell membranes resist flow".

equation is again given by Eq. (12), and we express the base state as

$$v^1_{(0)} = 0\,, \qquad v^2_{(0)} = V\,, \qquad v_{(0)} = 0\,, \qquad \text{and} \qquad \lambda_{(0)} = \Lambda = [\![p]\!]\,R + \frac{k_\mathrm{b}}{4R^2}\,. \tag{69}$$

In addition to considering both the bending-dominated and pressure-dominated regimes, we now also seek to understand how a base flow of lipids affects the magnitude of the different in-plane and out-of-plane forces that arise when the membrane tube is perturbed. As was the case for planar and spherical membranes, a nontrivial scaling analysis is required to non-dimensionalize the first-order perturbed equations governing cylindrical systems. In what follows, we employ a similar procedure to demonstrate the need for a new length scale ℓ over which some quantities vary, and then non-dimensionalize the governing equations. Cylindrical membrane tubes exhibit an additional complexity relative to their planar and spherical counterparts in that there are now three length scales to consider: the cylinder radius R, the length scale L governing whether the tube is thick or thin, and the emergent length scale ℓ caused by the base flow.

Scaling Attempt #1: Variations over length L (incorrect)

When considering the first-order perturbed governing equations, we begin by assuming all quantities vary over the known length scale L in the axial direction. As before, $L = R$ for thick tubes and $L \gg R$ for thin tubes. By substituting the dimensionless quantities in Eq. (34) into the perturbed continuity equation (28) and rearranging terms, we find

$$\Omega\,\tilde{v}^{1*}_{,\theta^*} + \frac{V}{L}\,\tilde{v}^{2*}_{,z^*} + \frac{V}{L}\,\tilde{r}^*_{,z^*} + \frac{1}{\tau}\,\tilde{r}^*_{,t^*} = 0\,. \tag{70}$$

Given the structure of Eq. (70), we choose $\Omega = 1/\tau = V/L$, where here V and L are known quantities. Next, we non-dimensionalize the in-plane equations (29, 30), and neglect inertial terms for the sake of argument. With Eq. (34), we express the in-plane equations as

$$\tilde{r}^*_{,t^*\theta^*} + \tilde{v}^{1*}_{,\theta^*\theta^*} + \delta^2\,\tilde{v}^{1*}_{,z^*z^*} + \tilde{r}^*_{,\theta^*z^*} + \frac{\Lambda L}{\zeta V}\,\tilde{\lambda}^*_{,\theta^*} = 0 \tag{71}$$

and

$$-\,\delta^2\,\tilde{r}^*_{,t^*z^*} + \tilde{v}^{2*}_{,\theta^*\theta^*} + \delta^2\,\tilde{v}^{2*}_{,z^*z^*} - \delta^2\,\tilde{r}^*_{,z^*z^*} + \delta^2\,\frac{\Lambda L}{\zeta V}\,\tilde{\lambda}^*_{,z^*} = 0\,. \tag{72}$$

Due to the base lipid flow setting the velocity scale V, the quantity $\Lambda L/(\zeta V)$ appearing in Eqs. (71) and (72) is set by the base state. Importantly, as V tends to zero, Eq. (71) requires $\tilde{\lambda}^*_{,\theta^*} = 0$, for which $\tilde{\lambda}^* = \tilde{\lambda}^*(z^*, t^*)$. Thus, our choice of scaling predicts that the perturbed surface tension is axisymmetric, regardless of whether the tube is thick or thin. However, in the case where V tends to zero, we expect the surface tension to behave as in the initially static case—for which it responds to shape perturbations according to Eqs. (42) and (61) in thick and thin tubes, respectively. Accordingly, our assumption that all quantities vary over the known length scale L is incorrect.

Scaling Attempt #2: Variations over new length scale (incorrect)

Next, we assume all quantities vary over some unknown length scale ℓ in the axial direction. As the base flow is only in the z-direction, we assume angular gradients are unchanged, i.e. quantities still vary over $\mathcal{O}(1)$ changes in the angle θ. The dimensionless form of the continuity equation (28) is now written as

$$\Omega\, \tilde{v}^{1*}_{,\theta^*} + \frac{V}{\ell}\, \tilde{v}^{2*}_{,z'} + \frac{V}{\ell}\, \tilde{r}^{*}_{,z'} + \frac{1}{\tau}\, \tilde{r}^{*}_{,t^*} = 0 \,, \tag{73}$$

where ℓ is a yet-to-be-determined characteristic length scale. We follow the notation of Chapters VII and VIII by denoting

$$z' := \frac{z}{\ell} \tag{74}$$

as a new dimensionless length, and observe Eq. (73) implies $\Omega = V/\ell = 1/\tau$.

With our choice that all axial derivatives vary over the length scale ℓ, we proceed to non-dimensionalize the in-plane equations (29, 30). With some algebraic manipulations, and again neglecting inertial terms for simplicity, the dimensionless in-plane equations are expressed as

$$\tilde{r}^{*}_{,t^*\theta^*} + \tilde{v}^{1*}_{,\theta^*\theta^*} + \frac{R^2}{\ell^2}\, \tilde{v}^{1*}_{,z'z'} + \tilde{r}^{*}_{,\theta^*z'} + \frac{\Lambda\ell}{\zeta V}\, \tilde{\lambda}^{*}_{,\theta^*} = 0 \tag{75}$$

and

$$-\frac{R^2}{\ell^2}\, \tilde{r}^{*}_{,t^*z'} + \tilde{v}^{2*}_{,\theta^*\theta^*} + \frac{R^2}{\ell^2}\, \tilde{v}^{2*}_{,z'z'} - \frac{R^2}{\ell^2}\, \tilde{r}^{*}_{,z'z'} + \frac{R^2}{\ell^2}\, \frac{\Lambda\ell}{\zeta V}\, \tilde{\lambda}^{*}_{,z'} = 0 \,. \tag{76}$$

Equations (75) and (76) indicate there are several choices for the length scale ℓ, depending on which terms are to balance one another. For example, suppose $\Lambda\ell/(\zeta V) = 1$, for which $\ell = \zeta V/\Lambda$. In this case, ℓ is proportional to V, as was also true in the planar and spherical situations. In the limit where V tends to zero, R/ℓ diverges and the surface Laplacian operator simplifies to $\Delta_{\mathrm{s}}(\,\cdot\,) = (\,\cdot\,)_{,z'z'}$. The shape equation (31) can then be expressed as $\tilde{r}^{*}_{,z'z'z'z'} = 0$—which disagrees with the corresponding result for an initially static tube. Thus, our choice of $\ell = \zeta V/\Lambda$ is incorrect.

Another choice for the length scale ℓ is motivated by the in-plane z-equation (76), where $R^2\Lambda/(\zeta\ell V) = 1$ or equivalently $\ell = R^2\Lambda/(\zeta V)$. In this case, ℓ diverges as V tends to zero, for which the time scale $\tau = \ell/V = R^2\Lambda/(\zeta V^2)$ diverges as well. Such a result is again unphysical, and we find there is no choice of ℓ over which both in-plane and out-of-plane quantities vary.

Scaling Attempt #3: Variations over multiple length scales (correct)

As in the planar and spherical geometries, we obtain a proper scaling for membrane tubes with a base flow by positing that different quantities vary over different axial distances. In particular, the in-plane quantities $\tilde{v}^1$, $\tilde{v}^2$, and $\tilde{\lambda}$ are assumed to vary over $\mathcal{O}(\ell)$ changes in the axial position, with our earlier analysis motivating the choice

$$\ell = \frac{\zeta V}{\Lambda} \,. \tag{77}$$

The radial out-of-plane shape changes $\tilde{r}$, on the other hand, are assumed to vary over $\mathcal{O}(L)$ distances in the axial direction, with $L = R$ for thick tubes and $L \gg R$ for thin tubes. Given our choice of scaling, we have (for example) $\mathcal{O}(\tilde{v}^2_{,z}) = V/\ell$ while $\mathcal{O}(\tilde{r}_{,z}) = R/L$. Moreover, we assume that all quantities vary over $\mathcal{O}(1)$ changes in the polar angle θ—an assumption that would be reexamined in biological situations with a base angular flow of lipids.

With the aforementioned scaling of in-plane and out-of-plane quantities, we non-dimensionalize the first-order governing equations. The continuity equation (28) is expressed as

$$\Omega\, \tilde{v}^{1*}_{,\theta^*} + \frac{V}{\ell}\, \tilde{v}^{2*}_{,z'} + \frac{V}{L}\, \tilde{r}^*_{,z^*} + \frac{1}{\tau}\, \tilde{r}^*_{,t^*} = 0\,, \tag{78}$$

where we now see that the second and third terms have different magnitudes when $\ell \neq L$. Next, the in-plane θ-equation (29) and z-equation (30) are respectively given by

$$\frac{\rho R^2 \Omega}{\zeta}\left(\frac{1}{\tau}\, \tilde{v}^{1*}_{,t^*} + \frac{V}{\ell}\, \tilde{v}^{1*}_{,z'}\right) = \frac{1}{\tau}\, \tilde{r}^*_{,t^*\theta^*} + \Omega\, \tilde{v}^{1*}_{,\theta^*\theta^*} + \frac{\Omega R^2}{\ell^2}\, \tilde{v}^{1*}_{,z'z'} + \frac{V}{L}\, \tilde{r}^*_{,\theta^* z^*} + \frac{\Lambda}{\zeta}\, \tilde{\lambda}^*_{,\theta^*} \tag{79}$$

and

$$\frac{\rho V R}{\zeta}\left(\frac{1}{\tau}\, \tilde{v}^{2*}_{,t^*} + \frac{V}{\ell}\, \tilde{v}^{2*}_{,z'}\right) = -\frac{R}{\tau L}\, \tilde{r}^*_{,t^* z^*} + \frac{V}{R}\, \tilde{v}^{2*}_{,\theta^*\theta^*} + \frac{VR}{\ell^2}\, \tilde{v}^{2*}_{,z'z'} - \frac{VR}{L^2}\, \tilde{r}^*_{,z^* z^*} + \frac{\Lambda R}{\zeta \ell}\, \tilde{\lambda}^*_{,z'}\,, \tag{80}$$

where in this case we do not yet know the relationship between τ, ℓ, L, and V. Finally, the shape equation (31) is written as

$$\begin{aligned} &\rho R^2 \left(\frac{1}{\tau^2}\, \tilde{r}^*_{,t^*t^*} + \frac{2V}{\tau L}\, \tilde{r}^*_{,t^* z^*} - \frac{V^2}{L^2}\, \tilde{r}^*_{,z^* z^*}\right) \\ &\quad = \frac{2\zeta V}{\ell}\, \tilde{v}^{2*}_{,z'} + \Lambda\left(\tilde{r}^* + \Delta^*_{\mathrm{s}} \tilde{r}^* - \tilde{\lambda}^*\right) - \frac{k_{\mathrm{b}}}{4R^2}\left(3\tilde{r}^* + 4\tilde{r}^*_{,\theta^*\theta^*} + \Delta^*_{\mathrm{s}} \tilde{r}^* + 2\Delta^{*2}_{\mathrm{s}}\, \tilde{r}^*\right). \end{aligned} \tag{81}$$

At this point, we recognize there are three length scales in the problem: (i) the in-plane axial length scale ℓ, (ii) the cylinder radius R, and (iii) the out-of-plane axial length scale L. When non-dimensionalizing Eqs. (78)–(81), we require the relative sizes of ℓ, R, and L. To this end, we define the dimensionless quantity

$$\ell^* := \frac{\ell}{R} = \frac{\zeta V}{\Lambda R} \tag{82}$$

comparing the sizes of ℓ and R, and note that the ratio R/L is captured by δ [see Eq. (33)]. In what follows, we simplify Eqs. (78)–(81) for different values of ℓ^* and δ. As depicted in Fig. 4, the values of the parameters δ and ℓ^* lead to four regimes with different governing equations, which are considered separately in the subsequent sections. However, before discussing each regime individually, we first highlight their commonalities. We note that ℓ^* can be thought of as a dimensionless velocity, as for a fixed tube radius and normal stress jump, changing V changes ℓ^*. We frequently refer to regimes of different ℓ^* by corresponding values of the velocity from here on.

The first commonality across the four regimes is that in all cases, the Scriven–Love and Föppl–von Kármán numbers are given by Eq. (45), which sets the dimensionless parameter

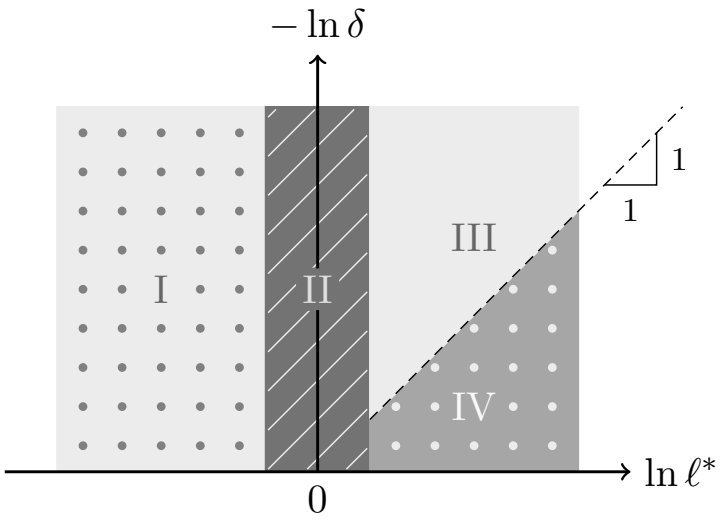

Figure 4: Schematic of the cylindrical regimes, which are defined by δ, the ratio of the radius to the axial length scale (33), and the parameter ℓ^* (82), which captures the dimensionless base flow velocity. Note the logarithmic scale on both axes. Regimes I and II correspond to small ($\ell^* \ll 1$) and moderate ($\ell^* \sim 1$) velocities, respectively. For large velocities ($\ell^* \gg 1$), the governing equations differ for thin tubes ($\delta \ll 1$, Regime III) and thick tubes ($\delta \sim 1$, Regime IV).

ℓ^* according to $\ell^* = \Gamma^{-1} Sl$. Furthermore, in all regimes the linearized perturbed shape equation is given by

$$2\,\frac{Sl}{\ell^*}\,\tilde{v}^{2*}_{,z'} + \Gamma\left(\tilde{r}^* + \Delta^*_{\mathrm{s}}\tilde{r}^* - \tilde{\lambda}^*\right) - \frac{1}{4}\left(3\,\tilde{r}^* + 4\,\tilde{r}^*_{,\theta^*\theta^*} + \Delta^*_{\mathrm{s}}\tilde{r}^* + 2\,\Delta^{*2}_{\mathrm{s}}\,\tilde{r}^*\right) = 0\,, \tag{83}$$

where although $Sl/\ell^* = \Gamma$, we include both numbers to delineate viscous and tension forces. As before, we consider only cases where the jump in the normal stress $[\![p]\!] \geq 0$, for which $\Gamma \geq \frac{1}{4}$ and $Sl/\ell^* \geq \frac{1}{4}$—indicating viscous forces in the normal direction are always significant, irrespective of the speed of the base flow. Additionally, in the pressure-dominated regime where $[\![p]\!] \gg k_{\mathrm{b}}/(4R^3)$ [cf. Eq. (69)], the surface tension scales as $\Lambda \approx [\![p]\!]R \gg k_{\mathrm{b}}/(4R^2)$, such that $Sl/\ell^* = \Gamma \gg 1$ and bending forces are negligible compared to viscous forces and tension forces in the normal direction. In the limit of a large normal stress jump in the base state, the shape equation (83) again reduces to that of a two-dimensional fluid film with a base flow. We previously found such films could admit time-oscillating solutions, unlike their initially static counterparts, and also undergo a pearling instability. [‡] The characterization of the instabilities of lipid membrane tubes, with and without a base flow, is the subject of §6 and §7. Now that we have discussed the common features of membrane tubes across the four regimes, we non-dimensionalize the governing equations in each case.

[‡]Sahu et al., "Arbitrary Lagrangian–Eulerian finite element formulation for curved and deforming surfaces. I. General theory and application to fluid interfaces".

(a). The case where ℓ is less than L

We first consider situations where $\ell \leq L$, for which $\ell^* \leq \delta^{-1}$. The continuity equation (78) then implies

$$\Omega \;=\; \frac{V}{\ell} \;=\; \frac{\Lambda}{\zeta} \;=\; \frac{1}{\tau}\;, \tag{84}$$

and the governing equations (78)–(81) simplify to

$$\tilde{v}^{1*}_{,\theta^*} + \tilde{v}^{2*}_{,z'} + \ell^*\delta\,\tilde{r}^*_{,z^*} + \tilde{r}^*_{,t^*} \;=\; 0\;, \tag{85}$$

$$\frac{Re}{\ell^*}\left(\tilde{v}^{1*}_{,t^*} + \tilde{v}^{1*}_{,z'}\right) \;=\; \tilde{r}^*_{,t^*\theta^*} + \tilde{v}^{1*}_{,\theta^*\theta^*} + \frac{1}{(\ell^*)^2}\,\tilde{v}^{1*}_{,z'z'} + \ell^*\delta\,\tilde{r}^*_{,\theta^*z^*} + \tilde{\lambda}^*_{,\theta^*}\;, \tag{86}$$

$$Re\,\ell^*\left(\tilde{v}^{2*}_{,t^*} + \tilde{v}^{2*}_{,z'}\right) \;=\; -\ell^*\delta\,\tilde{r}^*_{,t^*z^*} + (\ell^*)^2\,\tilde{v}^{2*}_{,\theta^*\theta^*} + \tilde{v}^{2*}_{,z'z'} - (\ell^*\delta)^2\,\tilde{r}^*_{,z^*z^*} + \tilde{\lambda}^*_{,z'}\;, \tag{87}$$

and

$$\begin{aligned}\frac{Re\,\Gamma}{\ell^*}\Big(\tilde{r}^*_{,t^*t^*} + \ell^*\delta\,\tilde{r}^*_{,t^*z^*} + (\ell^*\delta)^2\,\tilde{r}^*_{,z^*z^*}\Big) \\ = 2\,\frac{SL}{\ell^*}\,\tilde{v}^{2*}_{,z'} + \Gamma\Big(\tilde{r}^* + \Delta^*_{\rm s}\tilde{r}^* - \tilde{\lambda}^*\Big) - \frac{1}{4}\Big(3\tilde{r}^* + 4\tilde{r}^*_{,\theta^*\theta^*} + \Delta^*_{\rm s}\tilde{r}^* + 2\Delta^{*2}_{\rm s}\,\tilde{r}^*\Big)\;,\end{aligned} \tag{88}$$

where $SL/\ell^* = \Gamma$. The governing equations are now analyzed in three different regimes: small velocities, where $\ell^* \ll 1$, moderate velocities, where $\ell^* \sim 1$, and large velocities with a thin tube, where $1 \ll \ell^* \ll \delta^{-1}$. The case of large velocities with a thick tube, i.e. when $1 \leq \delta^{-1} \ll \ell$, are analyzed subsequently in §4 (b).

Regime I: The equations when the base flow is slow.

In the first regime, the base velocity V is small relative to the intrinsic velocity scale $R\Lambda/\zeta$ such that $\ell^* \ll 1$. Such would be the case, for example, with the following biologically motivated choices of characteristic values in tether pulling experiments: $\Lambda \sim 10^{-2}$ pN/nm, $R \sim 100$ nm, and $V \sim 10^{-4}$ nm/μsec, for which $\ell^* \sim 2\cdot 10^{-3}$. As $\ell^* \ll 1$ and $\delta \leq 1$ by construction, $\ell^*\delta \ll 1$ as well, and Eqs. (85)–(87) simplify to

$$\tilde{v}^{1*}_{,\theta^*} + \tilde{v}^{2*}_{,z'} + \tilde{r}^*_{,t^*} \;=\; 0\;, \tag{89}$$

$$\tilde{v}^{1*}_{,z'z'} \;=\; 0\;, \tag{90}$$

and

$$\tilde{v}^{2*}_{,z'z'} + \tilde{\lambda}^*_{,z'} \;=\; 0\;. \tag{91}$$

The angular velocities are at most linear in z' (90), and axial surface tension changes are balanced by two axial derivatives of the z-velocity (91). To simplify the shape equation (88), we recognize $Re/\ell^* = \rho\Lambda R^2/\zeta^2$, which is independent of the velocity scale V and is negligible. Thus, in this regime, the shape equation is given by Eq. (83).

Regime II: The equations when the base flow is moderate.

When the base velocity scale V is comparable to the intrinsic velocity scale $R\Lambda/\zeta$, the length scale ℓ is comparable to the radius R. In this regime, $\ell^* \sim 1$, and the tube could be either thick or thin. A thick tube would satisfy the criterion when, for example, $V \sim 10^{-3}$ nm/μsec, $\Lambda \sim 10^{-4}$ pN/nm, and $R = L \sim 100$ nm; corresponding values for a thin tube are $V \sim 10^{-3}$ nm/μsec, $\Lambda \sim 10^{-3}$ pN/nm, $R \sim 10$ nm, and $L \sim 10^3$ nm. In either case, the governing equations are easily obtained by substituting $\ell^* \sim 1$ into Eqs. (85)–(88). The continuity and in-plane equations are found to be

$$\tilde{v}^{1*}_{,\theta^*} + \tilde{v}^{2*}_{,z'} + \delta\,\tilde{r}^*_{,z^*} + \tilde{r}^*_{,t^*} = 0\,, \tag{92}$$

$$\tilde{r}^*_{,t^*\theta^*} + \tilde{v}^{1*}_{,\theta^*\theta^*} + \tilde{v}^{1*}_{,z'z'} + \delta\,\tilde{r}^*_{,\theta^*z^*} + \tilde{\lambda}^*_{,\theta^*} = 0\,, \tag{93}$$

and

$$-\delta\,\tilde{r}^*_{,t^*z^*} + \tilde{v}^{2*}_{,\theta^*\theta^*} + \tilde{v}^{2*}_{,z'z'} - \delta^2\,\tilde{r}^*_{,z^*z^*} + \tilde{\lambda}^*_{,z'} = 0\,, \tag{94}$$

where for long, thin tubes ($\delta \ll 1$) all terms containing factors of δ are negligible. The shape equation is once again found to be given by Eq. (83).

Regime III: The equations when the base flow is fast and the tube is thin.

In the third regime, $V \gg \Lambda R/\zeta$ and $\delta \ll 1$, such that $1 \ll \ell^* \ll \delta^{-1}$. This could be the case, for example, if $V \sim 10^{-2}$ nm/μsec, $\Lambda \sim 10^{-3}$ pN/nm, $R \sim 10$ nm, and $L \sim 10^3$ nm, i.e. if the thin tube example from Regime II had an order of magnitude larger velocity. In this case, Eqs. (85)–(87) simplify to

$$\tilde{v}^{1*}_{,\theta^*} + \tilde{v}^{2*}_{,z'} + \tilde{r}^*_{,t^*} = 0\,, \tag{95}$$

$$\tilde{r}^*_{,t^*\theta^*} + \tilde{v}^{1*}_{,\theta^*\theta^*} + \tilde{\lambda}^*_{,\theta^*} = 0\,, \tag{96}$$

and

$$\tilde{v}^{2*}_{,\theta^*\theta^*} = 0\,. \tag{97}$$

In this regime, the shape equation is given by Eq. (83). However, following an analogous procedure to the case of a thin, initially static tube, we can show $\tilde{v}^{2*}$ is axisymmetric, thus implying

$$\tilde{\lambda}^*_{,\theta^*} = 0\,, \tag{98}$$

such that $\tilde{\lambda}^*$ is also axisymmetric. Comparing Eqs. (95)–(97) to their counterparts for an initially static thin tube (52, 61–63), the only difference is the $\tilde{v}^{z*}_{,z'}$ term in Eq. (95) replaces $\tilde{v}^{z*}_{,z^*}$ in Eq. (52).

(b). The case where ℓ is much greater than L

We end by considering thick tubes with a large base flow, for which the emergent length scale ℓ can become longer than the axial length scale L. As L is at least as large as the tube radius R, in this regime $\ell \gg L \geq R$, or equivalently $\ell^* \gg \delta^{-1} \geq 1$. Such a case can arise, for example, when $V \sim 10^{-2}$ nm/μsec $= 10$ μm/sec, $\Lambda \sim 10^{-4}$ pN/nm, and

$R = L \sim 100$ nm. The continuity equation (78) indicates that for out-of-plane shape changes to be accommodated by in-plane angular and axial flows,

$$\Omega = \frac{V}{L} = \frac{1}{\tau} \, . \tag{99}$$

The governing equations (78)–(81) can then be written as

$$\tilde{v}^{1*}_{,\theta^*} + \frac{L}{\ell} \, \tilde{v}^{2*}_{,z'} + \tilde{r}^{*}_{,z^*} + \tilde{r}^{*}_{,t^*} = 0 \, , \tag{100}$$

$$Re \, \delta \left(\tilde{v}^{1*}_{,t^*} + \frac{L}{\ell} \, \tilde{v}^{1*}_{,z'} \right) = \tilde{r}^{*}_{,t^*\theta^*} + \tilde{v}^{1*}_{,\theta^*\theta^*} + \frac{1}{(\ell^*)^2} \, \tilde{v}^{1*}_{,z'z'} + \tilde{r}^{*}_{,\theta^* z^*} + \frac{L}{\ell} \, \tilde{\lambda}^{*}_{,\theta^*} \, , \tag{101}$$

$$\frac{Re}{\delta} \left(\tilde{v}^{2*}_{,t^*} + \frac{L}{\ell} \, \tilde{v}^{2*}_{,z'} \right) = -\tilde{r}^{*}_{,t^* z^*} + \frac{L^2}{R^2} \, \tilde{v}^{2*}_{,\theta^*\theta^*} + \frac{L^2}{\ell^2} \, \tilde{v}^{2*}_{,z'z'} - \tilde{r}^{*}_{,z^* z^*} + \frac{L^2}{\ell^2} \, \tilde{\lambda}^{*}_{,z'} \, , \tag{102}$$

and

$$\begin{aligned} Re \, \Gamma \, \delta^2 \ell^* \left(\tilde{r}^{*}_{,t^* t^*} + \tilde{r}^{*}_{,t^* z^*} + \tilde{r}^{*}_{,z^* z^*} \right) & \\ = 2 \, \frac{SL}{\ell^*} \, \tilde{v}^{z*}_{,z'} + \Gamma \left(\tilde{r}^* + \Delta_s^* \tilde{r}^* - \tilde{\lambda}^* \right) - \frac{1}{4} \left(3\tilde{r}^* + 4\tilde{r}^{*}_{,\theta^*\theta^*} + \Delta_s^* \tilde{r}^* + 2\Delta_s^{*2} \, \tilde{r}^* \right) \, , & \end{aligned} \tag{103}$$

where the Scriven–Love and Föppl–von Kármán numbers are given by Eq. (45), and the Reynolds number (40) is at most 10^{-8} in all cases considered. As $Re \ll 1$ and $L/\ell \ll 1$ in this scenario, Eqs. (100)–(102) can be simplified to

$$\tilde{v}^{1*}_{,\theta^*} + \tilde{r}^{*}_{,z^*} + \tilde{r}^{*}_{,t^*} = 0 \, , \tag{104}$$

$$-\tilde{v}^{2*}_{,z'\theta^*} + \tilde{\lambda}^{*}_{,\theta^*} = 0 \, , \tag{105}$$

and

$$-\tilde{r}^{*}_{,t^* z^*} + \frac{1}{\delta^2} \, \tilde{v}^{2*}_{,\theta^*\theta^*} - \tilde{r}^{*}_{,z^* z^*} = 0 \, , \tag{106}$$

where to obtain the θ-equation (105) we take the partial derivative of Eq. (100) with respect to θ^*, substitute the result into Eq. (101), and simplify. When $\delta \ll 1$, Eq. (106) simplifies to $\tilde{v}^{2*}_{,\theta^*\theta^*} = 0$, again implying $\tilde{v}^{2*} = \tilde{v}^{2*}(z', t^*)$ and $\tilde{\lambda}^* = \tilde{\lambda}^*(z', t^*)$. Despite the differences in scaling in this regime, the shape equation (103) is once again given by Eq. (83). We refer to the present case, where $\ell \gg L$, as Regime IV [cf. Fig. 4].

With the governing equations in each of the four regimes, we recognize the importance of a scaling analysis in elucidating the relative magnitude of various in-plane and out-of-plane forces. Our discussion in this section closes our scaling analysis of lipid membrane tubes, with and without a base flow. We highlight that in all cases considered, the Scriven–Love and Föppl–von Kármán numbers are given by Eq. (45). Moreover, in every situation, viscous and tension forces are found to be significant in describing the dynamics of a perturbed lipid membrane tube, as also shown in Fig. 5.

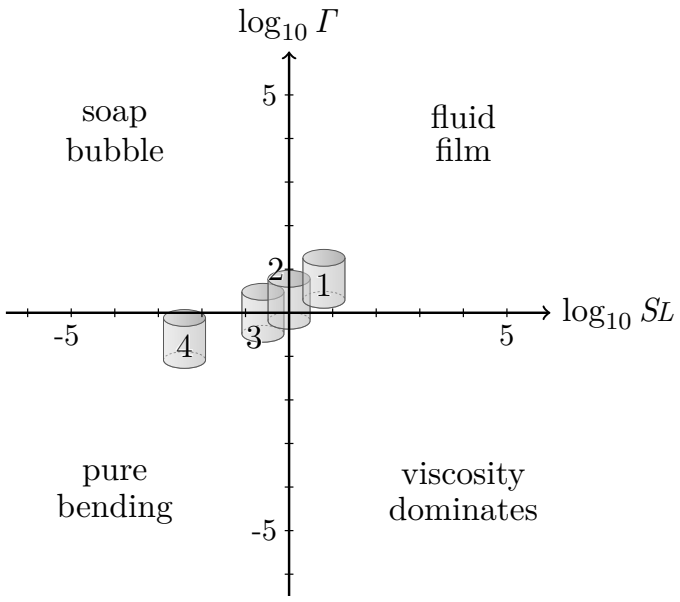

Figure 5: Plot of the Scriven–Love number SL and Föppl–von Kármán number Γ in four past experiments involving cylindrical geometries [cf. Chapter VI, Fig. 2]. Each numbered figure corresponds to a single experiment, which is described in Tables 1–4. Experiments #1 through #3 involve thick tubes with no base flow, with $SL = \Gamma \geq \frac{1}{4}$. On the other hand, in Experiment #4, a membrane tube is pulled at a constant velocity.

5. The analysis of past experimental data

At this point, we provide the calculation of the Scriven–Love and Föppl–von Kármán numbers in four experiments involving membrane tubes, with and without a base flow of lipids. All four experiments are taken from the study by Z. Shi et al., [‡] which—as mentioned previously—was the only study we found that provided sufficient data to compute both the tube radius and base surface tension. The first three experiments are concerned with a static tube. As we will see, for two of these experiments, $\Gamma > \frac{3}{4}$. We will determine subsequently that such systems are expected to undergo a pearling instability, which involves shape changes over an axial length scale $L = R$. We therefore use the results of our scaling analysis for thick tubes in §3 (a) to quantify the aforementioned experiments.

The fourth experiment considers a tube pulled at a constant rate, such that the base axial velocity V is constant. In this instance, we determine the Scriven–Love and Föppl–von Kármán numbers based on the scaling analysis in §4. As we are neglecting hydrodynamic effects from the surrounding fluid, the pull force is once again given by Eq. (19), which simplifies to Eq. (20) when there is no pressure drop $[\![p]\!]$ across the membrane. We note that in all cases, the value of the intramembrane viscosity ζ is not provided; we assume a value of $\zeta = 10$ pN $\cdot$ μsec/nm [†, *] as in the planar and spherical geometries. In addition, the

[‡] Shi et al., "Cell membranes resist flow".

[†] P. Cicuta, S.L. Keller, and S.L. Veatch. "Diffusion of liquid domains in lipid bilayer membranes". *J. Phys. Chem. B* **111** (2007), 3328–3331. arXiv: cond-mat/0611492.

[*] A.R. Honerkamp-Smith et al. "Membrane viscosity determined from shear-driven flow in giant vesicles". *Phys. Rev. Lett.* **111** (2013), 038103. arXiv: 1308.6440.

Experiment #1: Tether subject to osmotic forces

Table 1: Data of a membrane tube pulled from a cell bleb and held stationary. A pipette injecting pure water is brought towards and away from the tether to vary the osmotic pressure drop across the membrane. To calculate Λ, we note $[\![p]\!]$ and f_{pull} increase as the pipette moves towards the tether—in accordance with Eq. (19). Assuming $[\![p]\!] = 0$ when the pipette is furthest from the tether, we find $f_{\text{pull}} = 11$ pN $= \pi k_{\text{b}}/R$; for the reported value of k_{b}, $R = 110$ nm. Next, we consider where the membrane tears. Assuming R does not change, $f_{\text{pull}} = 79\,\text{pN} = \pi k_{\text{b}}/R + [\![p]\!]\pi R^2$. Thus, $[\![p]\!]\pi R^2 = 68$ pN, and $[\![p]\!] = 1.8 \cdot 10^{-3}$ pN/nm^2. With R and $[\![p]\!]$ known, we calculate Λ as $\Lambda \approx 0.2$ pN/nm (19). Finally, V, SL, and Γ are calculated with R and Λ known.

Quantity	Value	Calculation
V	2 nm/μsec	Eq. $(41)_3$
R	$1 \cdot 10^2$ nm	Eq. (20) at max pipette distance
k_{b}	380 pN $\cdot$ nm	Fig. S2 caption
Λ	$2 \cdot 10^{-1}$ pN/nm	Fig. S2(e), Eq. (19)
SL	7	Eq. $(45)_1$
Γ	7	Eq. $(45)_2$

Experiment #2: Static tether relaxing after being pulled

Table 2: Data of a membrane tether pulled from a cell bleb, and then held stationary as f_{pull} relaxes. The tube is pulled from $t \approx 18$ seconds to $t \approx 22$ seconds, and then kept at a fixed length while f_{pull} decreases over time. The tube radius R is constant during this relaxation (Fig. S2(c), blue curve); according to Eq. $(19)_1$ the pressure drop $[\![p]\!]$ also decreases during the relaxation. We assume $[\![p]\!] \approx 0$ at $t \approx 45$ seconds when f_{pull} has relaxed, and seek to calculate $[\![p]\!]$ at $t \approx 22$ seconds when the tube is initially held still. We recognize $f_{\text{pull}} = 30$ pN at $t \approx 45$ seconds, and approximate $f_{\text{pull}} = 60$ pN at $t \approx 22$ seconds. Following the same calculations as in Experiment #1, we find $[\![p]\!] \approx 6 \cdot 10^{-3}$ pN/nm^2 and $\Lambda \sim 0.3$ pN/nm, and then calculate all other values.

Quantity	Value	Calculation
V	1 nm/μsec	Eq. $(41)_3$
R	$4 \cdot 10^1$ nm	Eq. (20) at $t = 45$ seconds
k_{b}	380 pN $\cdot$ nm	Fig. S2 caption
Λ	$3 \cdot 10^{-1}$ pN/nm	Fig. S2(c), Eq. (19)
SL	1	Eq. $(45)_1$
Γ	1	Eq. $(45)_2$

Experiment #3: Tether pulled from GUV, subject to pipette aspiration

Table 3: Experimental data in which a lipid membrane tube is pulled from a GUV, and the membrane tension is altered via pipette aspiration. The data in Fig. S1(d) shows $f_{\text{pull}} \sim \sqrt{\lambda_{(0)}}$, which indicates the pressure drop is negligible and for which Eq. (20) holds. The slope of the curve in Fig. S1(d) indicates $k_{\text{b}} = 250$ pN$\cdot$nm. In Fig. S1(b), at $t = 100$ sec, $\Lambda \approx 0.15$ pN/nm and $f_{\text{pull}} \approx 33$ pN, for which $R = 20$ nm (20).

Quantity	Value	Calculation
V	$4 \cdot 10^{-1}$ nm/μsec	Eq. $(41)_3$
R	$2 \cdot 10^{1}$ nm	Eq. (20)
k_{b}	250 pN$\cdot$nm	Slope of Fig. S1(d), with Eq. (20)
Λ	$2 \cdot 10^{-1}$ pN/nm	Fig. S1(b)
SL	$\frac{1}{4}$	Eq. $(45)_1$
Γ	$\frac{1}{4}$	Eq. $(45)_2$

Experiment #4: Tether pulled from cell bleb

Table 4: The same experimental data as was analyzed in Experiment #2, in which a lipid membrane tether is pulled from a cell bleb, and then held stationary while the pull force relaxes. In this case, however, we consider the data when the tether is being pulled. As was the case in Experiment #2, we assume $[\![p]\!] \approx 0$ at time $t \approx 45$ seconds, for which $R \sim 40$ nm. The velocity scale V can be calculated from Fig. S2(c) as $V \sim 4 \cdot 10^{-3}$ nm/μsec $= 4$ μm/sec, and k_{b} is reported to be 380 pN$\cdot$nm. To approximate the surface tension scale at $t \approx 18$ seconds when the tether pulling starts, we estimate $f_{\text{pull}} \approx 100$ pN at that time. In this case, Eq. (19) indicates $[\![p]\!] \sim 1 \cdot 10^{-2}$ pN/nm^2 and $\Lambda \sim 0.6$ pN/nm.

Quantity	Value	Calculation
V	$4 \cdot 10^{-3}$ nm/μsec	Fig. S2(c)
R	$4 \cdot 10^{1}$ nm	Fig. S2(c), Experiment #2
k_{b}	380 pN$\cdot$nm	Fig. S2 caption
Λ	$6 \cdot 10^{-1}$ pN/nm	Fig. S2(e), Eq. (19)
SL	$4 \cdot 10^{-3}$	Eq. $(45)_1$
Γ	2	Eq. $(45)_2$

bending modulus κ in the study under consideration is related to k_b in the present work according to $k_\mathrm{b} = 2\kappa$.

6. The temporal stability of a membrane tube

With the linearized equations governing perturbations to lipid membrane tubes, as well as an understanding of the magnitudes of the various forces, we are prepared to investigate the stability of such systems in response to perturbations along the length of the cylinder—hereafter referred to as *global perturbations*. We begin by presenting a different non-dimensionalization of the governing equations, which can be used in cases both with and without a base flow. The fundamental membrane unknowns are then decomposed into normal modes, and the algebraic equations governing the normal mode coefficients are obtained. The dispersion relation is subsequently calculated, and we close by presenting stability criteria. We find that axisymmetric perturbations are unstable when $\Gamma > \frac{3}{4}$ and the membrane is under tension, for which the tube undergoes a pearling instability reminiscent of the well-known Rayleigh–Plateau instability in fluid columns. [‡, †] Experimentally, pearled membrane configurations are observed irrespective of how the system is perturbed—whether it be via spontaneous thermal fluctuations, [*] an applied extensional flow, [§, ♯] or osmotic shocks. [‖, ∀, ♢] Non-axisymmetric disturbances, on the other hand, are unstable when $\Gamma < -\frac{3}{4}$ and the membrane tube is under compression. In such cases, the system undergoes a buckling instability, with the angular dependence and growth rate of the most unstable mode set entirely by the Föppl–von Kármán number.

We note that none of the stability criteria presented in this section are new. In fact, many prior investigations considered the energetics of a membrane tube subjected to small perturbations. If the free energy is expanded to quadratic order in terms of the normal modes, then the system becomes unstable when at least one of the quadratic coefficients transitions from positive to negative. In this manner, the axisymmetric stability criterion was determined nearly three decades ago, [$] and since that time many works considered the

[‡] S. Tomotika. "On the instability of a cylindrical thread of a viscous liquid surrounded by another viscous fluid". *Proc. R. Soc. Lond. A* **150** (1935), 322–337.

[†] S. Chandrasekhar. *Hydrodynamic and Hydromagnetic Stability*. New York: Dover, 1981.

[*] R. Bar-Ziv, T. Tlusty, and E. Moses. "Critical dynamics in the pearling instability of membranes". *Phys. Rev. Lett.* **79** (1997), 1158–1161.

[§] V. Kantsler, E. Segre, and V. Steinberg. "Critical dynamics of vesicle stretching transition in elongational flow". *Phys. Rev. Lett.* **101** (2008), 048101.

[♯] J.B. Dahl et al. "Experimental observation of the asymmetric instability of intermediate-reduced-volume vesicles in extensional flow". *Soft Matter* **12** (2016), 3787–3796.

[‖] P.A. Pullarkat et al. "Osmotically driven shape transformations in axons". *Phys. Rev. Lett.* **96** (2006), 048104.

[∀] M. Yanagisawa, M. Imai, and T. Taniguchi. "Shape deformation of ternary vesicles coupled with phase separation". *Phys. Rev. Lett.* **100** (2008), 148102.

[♢] J. Sanborn et al. "Transient pearling and vesiculation of membrane tubes under osmotic gradients". *Faraday Discuss.* **161** (2013), 167–176.

[$] R. Bar-Ziv and E. Moses. "Instability and "pearling" states produced in tubular membranes by competition of curvature and tension". *Phys. Rev. Lett.* **73** (1994), 1392–1395.

dynamics of the pearling instability. [‡, †, *, §, ♯] The study of non-axisymmetric disturbances to membrane tubes is less well-established, though was clearly laid out in a recent effort that incorporated the membrane and fluid viscosities in a description of the membrane dynamics. [‖] Despite the multitude of studies concerned with the energetics and dynamics of lipid membrane tubes, our analysis incorporates one often overlooked feature: the base axial flow of lipids. As we will see, the effect of a base flow on the dynamics of unstable systems motivates further analysis in §7, where we consider perturbations that are localized in both space and time.

(a). The governing equations

In our earlier scaling analysis of membrane tubes in §3 and §4, we recognized that different quantities could have different characteristic values, depending on the physical situation under consideration. For example, we obtained different results depending on whether or not there was a base flow of lipids, and depending on the axial length scale over which disturbances were expected to vary. In the present analysis, however, we seek a non-dimensionalization which is valid in all cases, such that by varying dimensionless parameters we can investigate the different regimes of cylindrical membrane dynamics. To this end, we define the timescale

$$\tau := \frac{\zeta R^2}{k_\mathrm{b}} \tag{107}$$

and introduce the dimensionless quantities

$$\begin{gathered} \theta^* := \theta\,, \qquad z^* := \frac{z}{R}\,, \qquad \tilde{r}^* := \frac{\tilde{r}}{R}\,, \qquad \tilde{v}^{1*} := \tau\tilde{v}^1\,, \\ \tilde{v}^{2*} := \frac{\tau\tilde{v}^2}{R}\,, \qquad \tilde{\lambda}^* := \frac{\tilde{\lambda}}{\lambda_{(0)}}\,, \qquad \text{and} \qquad t^* := \frac{t}{\tau}\,. \end{gathered} \tag{108}$$

Importantly, Eqs. (107) and (108) provide a non-dimensionalization independent of the speed of the base flow: $\tilde{v}^{2*}$ is defined for both $V = 0$ and $V \neq 0$, unlike that of our earlier analysis [cf. §3, §4]. We next define the Föppl–von Kármán number Γ and Scriven–Love number SL as

$$\Gamma = \frac{\Lambda R^2}{k_\mathrm{b}} \qquad \text{and} \qquad \mathit{SL} = \frac{\zeta V R}{k_\mathrm{b}}\,, \tag{109}$$

[‡] P. Nelson, T. Powers, and U. Seifert. "Dynamical theory of the pearling instability in cylindrical vesicles". *Phys. Rev. Lett.* **74** (1995), 3384–3387.

[†] R. Granek and Z. Olami. "Dynamics of Rayleigh-like instability induced by laser tweezers in tubular vesicles of self-assembled membranes". *J. Phys. II* **5** (1995), 1349–1370.

[*] K.L. Gurin, V.V. Lebedev, and A.R. Muratov. "Dynamic instability of a membrane tube". *J. Expl. Theor. Phys.* **83** (1996), 321–326.

[§] G. Boedec, M. Jaeger, and M. Leonetti. "Pearling instability of a cylindrical vesicle". *J. Fluid Mech.* **743** (2014), 262–279.

[♯] S.C. Al-Izzi et al. "Hydro-osmotic instabilities in active membrane tubes". *Phys. Rev. Lett.* **120** (2018), 138102. arXiv: 1709.02703.

[‖] V. Narsimhan, A.P. Spann, and E.S.G. Shaqfeh. "Pearling, wrinkling, and buckling of vesicles in elongational flows". *J. Fluid Mech.* **777** (2015), 1–26.

where now $SL = 0$ in cases without a base flow ($V = 0$). Given our modified choice of non-dimensionalization, it is useful to imagine a membrane tube of a given radius R and bending modulus k_b. Equation (109) then implies that Γ and SL can be understood as the dimensionless base surface tension and axial base flow speed, respectively.

By substituting Eqs. (107)–(109) into Eqs. (28)–(31), recognizing inertial forces are negligible in all scenarios of interest, and rearranging terms, we obtain the dimensionless perturbed governing equations as

$$\tilde{v}^{1*}_{,\theta^*} + \tilde{v}^{2*}_{,z^*} + \tilde{r}^*_{,t^*} + SL\,\tilde{r}^*_{,z^*} = 0 \,, \tag{110}$$

$$\tilde{v}^{1*}_{,\theta^*\theta^*} + \tilde{v}^{1*}_{,z^*z^*} + \tilde{r}^*_{,t^*\theta^*} + SL\,\tilde{r}^*_{,\theta^*z^*} + \Gamma\,\tilde{\lambda}^*_{,\theta} = 0 \,, \tag{111}$$

$$\tilde{v}^{2*}_{,\theta^*\theta^*} + \tilde{v}^{2*}_{,z^*z^*} - \tilde{r}^*_{,t^*z^*} - SL\,\tilde{r}^*_{,z^*z^*} + \Gamma\,\tilde{\lambda}^*_{,z^*} = 0 \,, \tag{112}$$

and

$$\Gamma\left(\tilde{r}^* + \Delta^*_\mathrm{s}\tilde{r}^* - \tilde{\lambda}^*\right) - \frac{1}{4}\left(3\tilde{r}^* + 4\tilde{r}^*_{,\theta^*\theta^*} + \Delta^*_\mathrm{s}\,\tilde{r}^* + 2\Delta^{*2}_\mathrm{s}\,\tilde{r}^*\right) + 2\tilde{v}^{2*}_{,z^*} = 0 \,. \tag{113}$$

We reiterate here that the above governing equations (110)–(113) differ from the scaling results of §3 and §4 because we now apply a single non-dimensionalization to all base states. The present approach has the advantage that the governing equations are applicable in all scenarios, with the dynamics of a membrane tube completely specified by the values of Γ and SL. On the other hand, the magnitudes of the various terms in Eqs. (110)–(113) are not immediately obvious, as a scaling analysis was not employed.

Before proceeding, it is useful to highlight the relationship between the normal stress jump $[\![p]\!]$ and the Föppl–von Kármán number. In particular, for the base state described by Eqs. (11) and (12), the shape equation can be written in dimensionless form as

$$\Gamma = \frac{[\![p]\!]R^3}{k_\mathrm{b}} + \frac{1}{4} \,. \tag{114}$$

Thus, for a tube with a given bending modulus k_b and initial radius R, the jump in the normal stress $[\![p]\!]$ determines the value of Γ. We define the value

$$\Gamma_0 := \frac{1}{4} \tag{115}$$

to be the Föppl–von Kármán number when $p = 0$. With this definition, if $\Gamma > \Gamma_0$ then the surrounding fluid provides a net force that is radially outwards. If $\Gamma < \Gamma_0$, on the other hand, then the net force from the surrounding fluid is radially inwards and the tube is compressed by its surroundings. In what follows, we are primarily concerned with membrane tubes for which $\Gamma \geq \Gamma_0$.

The axisymmetric evolution equation

Lipid membrane tubes which deform axisymmetrically will be relevant in our later investigations. In the case where the tube is axisymmetric, such that $\tilde{v}^1 = 0$ and no quantities depend on θ, the four governing equations (110)–(113) can be condensed into a single equation for

the perturbed membrane shape, $\tilde{r}^*$. To this end, we first integrate Eq.(112) with respect to z^*, thereby obtaining

$$-\tilde{r}^*_{,t^*} - \mathit{SL}\,\tilde{r}^*_{,z^*} + \tilde{v}^{2*}_{,z^*} + \mathit{\Gamma}\,\tilde{\lambda}^* = 0\,, \tag{116}$$

where we set the integration constant to zero such that an unperturbed cylinder ($\tilde{r}^* = 0$) has a constant, unperturbed tension ($\tilde{\lambda}^* = 0$). Next, we substitute Eq. (116) into the linearized shape equation (113) and obtain

$$-3\big(\tilde{r}^*_{,t^*} + \mathit{SL}\,\tilde{r}^*_{,z^*}\big) + \tilde{v}^{2*}_{,z^*} + \big(\mathit{\Gamma} - \tfrac{3}{4}\big)\,\tilde{r}^* + \big(\mathit{\Gamma} - \mathit{\Gamma}_0\big)\,\tilde{r}^*_{,z^*z^*} - \frac{1}{2}\,\tilde{r}_{,z^*z^*z^*z^*} = 0\,. \tag{117}$$

The only term in Eq. (117) not involving the perturbed radius is the axial velocity gradient $\tilde{v}^{2*}_{,z^*}$. However, we notice from the continuity equation (110) that $\tilde{v}^{2*}_{,z^*} = -\tilde{r}^*_{,t^*} - \mathit{SL}\tilde{r}^*_{,z^*}$. Substituting this result into Eq. (117) yields

$$\tilde{r}^*_{,t^*} + \mathit{SL}\,\tilde{r}^*_{,z^*} = \left(\frac{\mathit{\Gamma} - \frac{3}{4}}{4}\right)\tilde{r}^* + \left(\frac{\mathit{\Gamma} - \mathit{\Gamma}_0}{4}\right)\tilde{r}^*_{,z^*z^*} - \frac{1}{8}\,\tilde{r}^*_{,z^*z^*z^*z^*}\,. \tag{118}$$

Equation (118) is a single, linearized evolution equation for lipid membrane tubes involving only the dimensionless perturbed membrane shape $\tilde{r}^*$.

(b). The analysis in terms of normal modes

The perturbed governing equations (110)–(113) contain four fundamental unknowns, namely the dimensionless perturbed quantities $\tilde{r}^*$, $\tilde{v}^{1*}$, $\tilde{v}^{2*}$, and $\tilde{\lambda}^*$. We use the shorthand $\tilde{A}^*$ to denote any of these four unknowns, which are decomposed into normal modes according to [cf. Chapter VI, Eq. (12)]

$$\tilde{A}^*(\theta^*, z^*, t^*) = \sum_{m,q^*} \hat{A}\,\exp\big[i\big(m\theta^* + q^*z^* - \omega^*t^*\big)\big]\,, \tag{119}$$

with the coefficient $\hat{A} = \hat{A}_{m,q^*}$ depending on both m and q^*. In Eq. (119), the angular wavenumber $m \in \mathbb{Z}$, the dimensionless axial wavenumber $q^* \in \mathbb{R}$, and the dimensionless frequency $\omega^* = \omega^{(r)}_* + i\omega^{(i)}_* \in \mathbb{C}$. Here q^* and ω^* are related to their dimensional counterparts by $q^* = qR$ and $\omega^* = \omega\tau$, with the timescale τ defined in Eq. (107). We note that here and from now on, the '$*$' accent denoting a dimensionless quantity is placed as either a subscript or a superscript, as is notationally convenient. For the fundamental unknowns with the functional dependence given in Eq. (119), we have

$$\begin{gathered}\partial_{\theta^*} = im\,, \qquad \partial_{z^*} = iq^*\,, \qquad \partial_{t^*} = -i\omega^*\,, \qquad \partial_{\theta^*\theta^*} = -m^2\,,\\ \partial_{z^*z^*} = -q_*^2\,, \qquad \text{and} \qquad \Delta^*_{\mathrm{s}} = -\big(m^2 + q_*^2\big)\,.\end{gathered} \tag{120}$$

Substituting Eqs. (119) and (120) into Eqs. (110)–(113) and recognizing all normal modes are independent, we obtain the equations governing the normal mode coefficients as

$$m\hat{v}^1 + q^*\hat{v}^2 + \big(\mathit{SL}\,q^* - \omega^*\big)\,\hat{r} = 0\,, \tag{121}$$

$$-\big(m^2 + q_*^2\big)\,\hat{v}^1 + \big(\omega^*m - \mathit{SL}\,q^*m\big)\,\hat{r} + im\mathit{\Gamma}\,\hat{\lambda} = 0\,, \tag{122}$$

$$-\big(m^2 + q_*^2\big)\,\hat{v}^2 + \big(\mathit{SL}\,q_*^2 - \omega^*q^*\big)\,\hat{r} + iq^*\mathit{\Gamma}\,\hat{\lambda} = 0\,, \tag{123}$$

and

$$\alpha \hat{r} \, - \, \Gamma \hat{\lambda} \, + \, 2iq \, \hat{v}^2 \, = \, 0 \, , \tag{124}$$

where we briefly introduce the following notation for convenience:

$$\alpha \, := \, \Gamma \Big(1 \, - \, m^2 \, - \, q_*^2 \Big) \, - \, \frac{1}{4} \Big[3 \, - \, 5m^2 \, - \, q_*^2 \, + \, 2 \big(m^2 \, + \, q_*^2 \big)^2 \Big] \, . \tag{125}$$

(c). The calculation of the dispersion relation

Equations (121)–(124) consists of four linear, algebraic equations in the four unknowns $\hat{r}$, $\hat{v}^1$, $\hat{v}^2$, and $\hat{\lambda}$. Various techniques can be used to calculate the dispersion relation $\omega^* = \omega^*(q^*)$; here we use a series of algebraic manipulations. We first recognize the in-plane z-equation (123) and the shape equation (124) do not involve $\hat{v}^1$, and seek to combine the other two governing equations (121,122) to eliminate $\hat{v}^1$. To this end, we multiply the continuity equation (121) by $(m^2 + q_*^2)$, multiply the in-plane θ-equation by m, and add the two to obtain

$$- \, q_*^2 \big(\omega^* \, - \, \mathit{SL} \, q^* \big) \hat{r} \, + \, q^* \big(m^2 \, + \, q_*^2 \big) \hat{v}^2 \, + \, i \Gamma m^2 \, \hat{\lambda} \, = \, 0 \, . \tag{126}$$

We next seek to remove the $\hat{v}^2$ dependence from the system of equations. By multiplying the shape equation (124) by $(m^2 + q_*^2)$, multiplying Eq. (126) by $-2i$, and combining the results, we find

$$\Big[\alpha \big(m^2 \, + \, q_*^2 \big) \, + \, 2iq_*^2 \big(\omega^* \, - \, \mathit{SL} \, q^* \big) \Big] \hat{r} \, + \, \Gamma \big(m^2 \, - \, q_*^2 \big) \hat{\lambda} \, = \, 0 \, , \tag{127}$$

with α defined in Eq. (125). Similarly, multiplying the in-plane z-equation (123) by q^* and adding Eq. (126) yields

$$- \, 2q_*^2 \big(\omega^* \, - \, \mathit{SL} \, q^* \big) \hat{r} \, + \, i \Gamma \big(m^2 \, + \, q_*^2 \big) \hat{\lambda} \, = \, 0 \, . \tag{128}$$

With Eqs. (127) and (128), we simplified our initial set of equations into a system of two equations and two unknowns.

We now combine Eqs. (127) and (128) to obtain a single equation for the perturbed shape coefficient $\hat{r}$. By multiplying Eq. (127) by $i(m^2 + q_*^2)$, multiplying Eq. (128) by $(q_*^2 - m^2)$, and summing the two results, we obtain

$$\Big[\alpha i \big(m^2 \, + q_*^2 \big)^2 \, - \, 4q_*^4 \big(\omega^* \, - \, \mathit{SL} \, q^* \big) \Big] \hat{r} \, = \, 0 \, . \tag{129}$$

To obtain a nontrivial solution, i.e. one for which $\hat{r} \neq 0$, we require

$$\alpha i \big(m^2 \, + q_*^2 \big)^2 \, - \, 4q_*^4 \big(\omega^* \, - \, \mathit{SL} \, q^* \big) \, = \, 0 \, . \tag{130}$$

Solving Eq. (130) for ω^* and inserting the expression for α (125) yields the dispersion relation

$$\omega^* \, = \, \mathit{SL} \, q^* + i \, \frac{(m^2 \, + \, q_*^2)^2}{4q_*^4} \left(\Gamma \big(1 - m^2 - q_*^2 \big) \, - \, \frac{1}{4} \Big[3 \, - \, 5m^2 \, - \, q_*^2 \, + \, 2 \big(m^2 + q_*^2 \big)^2 \Big] \right) \, . \tag{131}$$

Given our normal mode decomposition $\sim \mathrm{e}^{-i\omega^* t^*} = \mathrm{e}^{\omega_*^{(i)} t^*} \mathrm{e}^{-i\omega_*^{(r)} t^*}$ in Eq. (119), Eq. (131) indicates that a nonzero base flow ($\mathit{SL} \neq 0$) leads to temporally oscillating solutions while the base tension (captured by Γ) dictates the growth rate of the perturbation envelope. Importantly, our choice of non-dimensionalization in Eqs. (107)–(109) allows for the two dimensionless numbers SL and Γ to be decoupled in the dispersion relation (131).

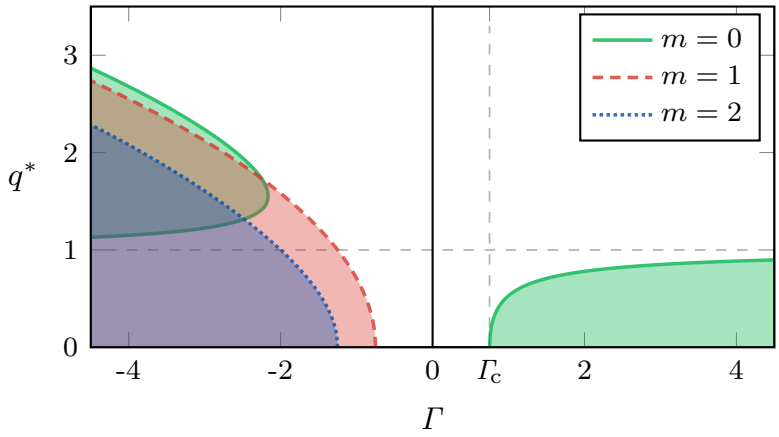

Figure 6: Stable and unstable regimes for angular wavenumbers $m = 0$ (green, solid), $m = 1$ (red, dashed), and $m = 2$ (blue, dotted), with the unstable regimes being shaded. Only long wavelength axisymmetric $m = 0$ modes are unstable when $\Gamma > \Gamma_0 = \frac{1}{4}$, with the solid green line being the marginally stable wavenumber q^*_{ms} calculated in Eq. (137). Short wavelength axisymmetric modes are also unstable when the tube is under compression, and $\Gamma < \Gamma_0$. Non-axisymmetric modes are only unstable when the tube is under compression. The vertical dashed line at $\Gamma = \Gamma_c = \frac{3}{4}$ marks the critical value of the Föppl–von Kármán number above which membrane tubes can undergo a pearling instability [see Eq. (135)].

(d). The linear stability analysis

With the decomposition into normal modes established in Eq. (119), our system is unstable when $\omega^{(i)}_* > 0$. The dispersion relation (131) then indicates a lipid membrane tube is unstable when

$$\Gamma\big(1 - m^2 - q_*^2\big) - \frac{1}{4}\Big[3 - 5m^2 - q_*^2 + 2\big(m^2 + q_*^2\big)^2\Big] > 0\,. \tag{132}$$

As the angular wavenumber $m \in \mathbb{Z}$ is discrete, for each value of m we use Eq. (132) to determine which points in the (Γ, q^*) plane are unstable. The unstable regions for $m = 0$, $m = 1$, and $m = 2$ are plotted as shaded regions in Fig. 6, from which we immediately make two observations. First, the amplitude of modes with $m \geq 1$ can only grow in time when the tube is under compression, for which $\Gamma < \Gamma_0$. Second, for tubes under tension, only axisymmetric $m = 0$ modes are unstable. As the present study is concerned with tubes under tension, only axisymmetric perturbations are considered from this point onwards.

When $m = 0$ and all membrane unknowns are axisymmetric, the dispersion relation (131) simplifies to

$$\omega^* = \mathit{SL}\, q^* + \frac{i}{4}\left(\Gamma\big(1 - q_*^2\big) - \frac{1}{4}\Big[3 - q_*^2 + 2q_*^4\Big]\right). \tag{133}$$

Moreover, the instability criterion (132) simplifies to

$$\Gamma\big(1 - q_*^2\big) - \frac{1}{4}\Big[3 - q_*^2 + 2q_*^4\Big] > 0\,. \tag{134}$$

Note that Eqs. (133) and (134) can also be obtained directly by substituting the normal mode decomposition for $\tilde{r}$ (119) into the linearized evolution equation for the perturbed membrane

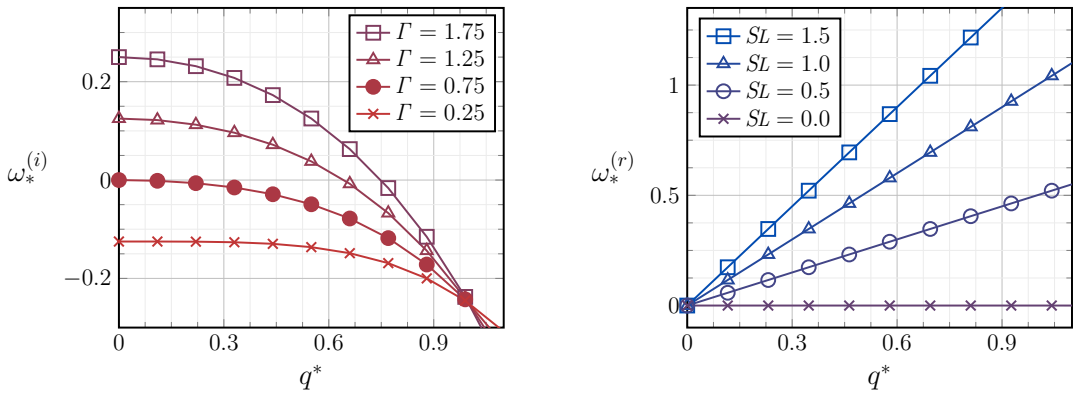

(a) growth rate $\omega_*^{(i)}$ (b) oscillation frequency $\omega_*^{(r)}$

Figure 7: Plots of (a) the growth rate $\omega_*^{(i)}$ and (b) the oscillation frequency $\omega_*^{(r)}$ of a perturbed axisymmetric membrane tube, for different values of the Föppl–von Kármán number Γ and the Scriven–Love number SL. Note that the growth rate only depends on Γ, while the oscillation frequency only depends on SL. (a) The growth rate is negative and the tube is stable when $\Gamma < \Gamma_c = \frac{3}{4}$. When $\Gamma > \Gamma_c$, the growth rate is positive for modes $q^* \in (0, q^*_{ms})$, with the marginally stable wavenumber calculated in Eq. (137). For unstable tubes, $q^* = 0$ is the fastest growing mode. (b) The oscillation frequency is linear in the wavenumber, with the proportionality constant being the Scriven–Love number SL.

shape (118). The real and imaginary parts of the axisymmetric dispersion relation (133) are plotted in Fig. 7, from which we make several additional observations. First, a necessary condition for a membrane tube to be unstable is

$$\Gamma > \Gamma_c \,, \qquad \text{where} \qquad \Gamma_c := \frac{3}{4} \tag{135}$$

is the critical value of the Föppl–von Kármán number at which a lipid membrane tube first becomes unstable. The condition in Eq. (135) is consistent with the $m = 0$ curve in Fig. 6, with the vertical dashed line located at $\Gamma = \Gamma_c$. Second, given a membrane tube with $\Gamma > \Gamma_c$, $q^* = 0$ is the fastest growing mode. [‡] The corresponding growth rate $\omega^{*(i)}_{max}$ is given by

$$\omega^{*(i)}_{max} = \frac{\Gamma - \Gamma_c}{4} \,, \tag{136}$$

and is a function of only the Föppl–von Kármán number. We additionally find that when $\Gamma > \Gamma_c$, unstable perturbations are limited to a finite range of wavenumbers $q^* \in [0, q^*_{ms}]$, where q^*_{ms} is the marginally stable wavenumber for which $\omega_*^{(i)} = 0$. Applying the definition of q^*_{ms} to Eq. (133), we obtain

$$\begin{aligned} q^*_{ms} &= \sqrt{-(\Gamma - \Gamma_0) + \sqrt{(\Gamma - \Gamma_0)^2 + 2(\Gamma - \Gamma_c)}} \\ &= \sqrt{-\Gamma + \tfrac{1}{4} + \sqrt{\Gamma^2 + \tfrac{3}{2}\Gamma - \tfrac{23}{16}}} \,. \end{aligned} \tag{137}$$

[‡]The fastest growing mode has a nonzero, finite wavenumber when the dynamics of the surrounding fluid are included, as described by Narsimhan, Spann, and Shaqfeh, "Pearling, wrinkling, and buckling of vesicles in elongational flows".

The marginally stable wavenumber q^*_{ms} for axisymmetric $m = 0$ modes is plotted as the solid green line in Fig. 6 when $\Gamma > \Gamma_0$, and also predicts the point where $\omega^{(i)}_*$ crosses zero in Fig. 7a. Moreover, in the limit of $\Gamma \to \Gamma_{\mathrm{c}}^+$, we find $q^*_{\mathrm{ms}} \sim (\Gamma - \Gamma_{\mathrm{c}})^{1/2} \to 0$ such that only infinitely long axial perturbations are unstable. Finally, we observe that the Scriven–Love number $\mathcal{SL}$ does not affect the growth rate of the perturbed system, but rather provides an oscillation frequency to the temporal evolution of axisymmetric modes (see Fig. 7b).

7. The spatiotemporal stability of a membrane tube

In the stability analysis presented thus far, we were primarily concerned with how an axisymmetric membrane tube under tension responds to a global disturbance of the form $\sim \mathrm{e}^{iq^*z^*}$ at time $t^* = 0$. While tube stability is governed by the Föppl–von Kármán number, the real part of the dispersion relation (133) indicates a nonzero base flow ($\mathcal{SL} \neq 0$) leads to temporal oscillations in the membrane response. By construction, we considered global disturbances along the entire tube, for which the solution to the linearized dynamics about an unstable tube is a traveling wave whose amplitude grows in time. However, if we examine the dimensional form of the left-hand side of the axisymmetric evolution equation (118), the quantity $\partial\tilde{r}/\partial t + V\,\partial\tilde{r}/\partial z$ looks like a material time derivative—despite us neglecting all inertial terms in our analysis. The presence of these terms motivates us to consider how the base flow of lipids could alter the long-time response of an unstable tube, particularly if the initial perturbation is localized to a small region. Indeed, various studies on other physical systems such as plasmas, [‡, †, *] geophysical flows, [§, ♯] open fluid flows such as wakes, jets and boundary layers, [‖, ∀] cylindrical fluid columns, [♢] and more recently thin films on substrates [$, &] have shown the effect of a base flow is best understood by addressing the following question: How does the unstable system respond to an initially *local*, rather than global, perturbation? In what follows, we address this question by extending the techniques presented thus far to perform a *spatiotemporal* stability analysis.

[‡] A. Bers and R.J. Briggs. "Criteria for determining absolute instability and distinguishing between amplifying and evanescent waves". *Bull. Am. Phys. Soc.* **9** (1963), 304.

[†] R.J. Briggs. *Electron-Stream Interactions with Plasmas*. MIT Press, 1964.

[*] F. Moser. "Convective and absolute instability of the positive column with longitudinal magnetic field". *Plasma Physics* **17** (1975), 821–840.

[§] L.-O. Merkine. "Convective and absolute instability of baroclinic eddies". *Geophys. Astro. Fluid* **9** (1977), 129–157.

[♯] R.T. Pierrehumbert. "Local and global baroclinic instability of zonally varying flow". *J. Atmos. Sci.* **41** (1984), 2141.

[‖] P. Huerre and P.A. Monkewitz. "Local and global instabilities in spatially developing flows". *Annu. Rev. Fluid Mech.* **22** (1990), 473–537.

[∀] P. Huerre and M. Rossi. "Hydrodynamic instabilities in open flows". *Hydrodynamics and Nonlinear Instabilities*. Ed. by C. Godrèche and P. Manneville. New York: Cambridge University Press, 1998, pp. 81–294.

[♢] T.R. Powers et al. "Propagation of a topological transition: The Rayleigh instability". *Phys. Fluids* **10** (1998), 1052–1057. arXiv: cond-mat/9708169.

[$] C. Duprat et al. "Absolute and convective instabilities of a viscous film flowing down a vertical fiber". *Phys. Rev. Lett.* **98** (2007), 244502.

[&] B. Scheid, N. Kofman, and W. Rohlfs. "Critical inclination for absolute/convective instability transition in inverted falling films". *Phys. Fluids* **28** (2016), 044107.

Before starting our calculations, we would like to provide additional motivation for the question posed above. In particular, the justification thus far focused on the form of the evolution equation, and then highlighted results from other disciplines. It is important to note, however, that there are many prior experimental efforts involving local perturbations to membrane tubes. When such tubes are under high tension, an infinitesimal local perturbation grows and invades the undisturbed region via propagating fronts. For example, drug treatments disrupting the internal structure of axons show fronts propagate from the neuron's growth cone to its soma, in the direction of lipid flow. [‡] In contrast, when a laser is aimed at a point on an axon, two fronts propagate outward in different directions. [‡] An additional complexity is that different patterns can be selected in the front wakes, leading to distinct morphologies at long times. For example, identical laser ablation experiments on axons result in a thin, atrophied tube—whose connection to the unperturbed regions appears pearled in some experiments and monotonic in others. [‡] Despite many experimental findings, however, the physical mechanisms governing these behaviors, namely (i) the pattern selection in the membrane region connecting thin atrophied tubes to moving fronts and (ii) the direction of instability propagation, remain poorly understood.

For the remainder of this chapter, we shed light on the aforementioned mechanisms by applying more sophisticated techniques to the axisymmetric cylindrical membrane equations. Our presentation largely mirrors that of one of our earlier studies. [†] We first invoke the hydrodynamic concept of *absolute* and *convective* instabilities [*, §] to understand the long-time behavior of lipid membrane tubes subjected to initially localized perturbations. We next investigate the dynamics of how the fronts ensuing from a local perturbation invade the unperturbed membrane tube. We employ the so-called marginal stability criterion, [♯, ‖] and corroborate our analytical results with direct numerical simulations and a weakly nonlinear analysis of the shape evolution of an unstable tube. Importantly, we find both atrophied and pearled morphologies can result from a local perturbation, with the selected pattern depending only on the Föppl–von Kármán number Γ.

(a). The complex wavenumber and frequency

We begin by considering a membrane tube with a base flow that is perturbed at one location—for example, an axon subject to laser ablation or the local administration of specific drugs. [‡] For any unstable tube with $\Gamma > \Gamma_c$, the Föppl–von Kármán number dictates the initial growth rate of the disturbance. However, the base flow speed, as captured by the Scriven–Love number, determines how initially localized perturbations spatially invade the system over time. For a fixed observer at a local station along the tube, the fate of

[‡] A. Datar et al. "The roles of microtubules and membrane tension in axonal beading, retraction, and atrophy". *Biophys. J.* **117** (2019), 880–891

[†] J. Tchoufag, A. Sahu, and K.K. Mandadapu. "Absolute vs convective instabilities and front propagation in lipid membrane tubes". *Phys. Rev. Lett.* **128** (2022), 068101. arXiv: 2008.13780.

[*] Bers and Briggs, "Criteria for determining absolute instability and distinguishing between amplifying and evanescent waves".

[§] Huerre and Rossi, "Hydrodynamic instabilities in open flows".

[♯] G.T. Dee and J.S. Langer. "Propagating pattern selection". *Phys. Rev. Lett.* **50** (1983), 383–386.

[‖] W. van Saarloos. "Front propagation into unstable states. II. Linear versus nonlinear marginal stability and rate of convergence". *Phys. Rev. A* **39** (1989), 6367–6390.

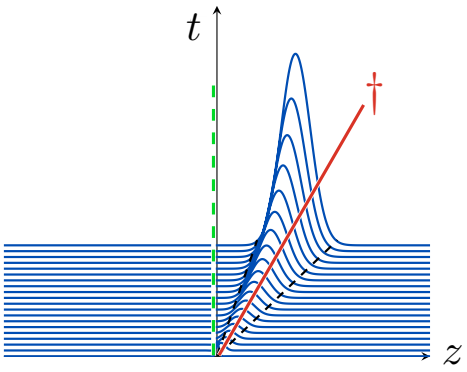

Figure 8: Space–time plots showing the response of a membrane tube with a base flow to a localized disturbance at $z = 0$ and $t = 0$. Successive snapshots show how the perturbation grows, and is also convected downstream. Such a situation is referred to as convectively unstable. A stationary observer (dashed green line) sees a stable system at long times, with $\omega^{(i)} < 0$. A moving observer (solid red line, †), on the other hand, sees the disturbance growing in time—for which $\omega^{\dagger(i)} > 0$. To capture the different growth rates, both the wavenumber q and frequency ω are chosen to be complex: $q \in \mathbb{C}$ and $\omega \in \mathbb{C}$, as justified in the text. The generation of such space–time plots is discussed in §7 (e).

the observed local disturbances will depend on the competition between the amplification of the instability, characterized by Γ, and its advection downstream, captured by Sl. In particular, for a specific choice of the growth rate (e.g. for a choice of Γ), larger values of the Scriven–Love number more quickly advect the growing perturbations downstream. Eventually the Scriven–Love number Sl will become so large that the instability is advected along the tube faster than it grows, and the instability undergoes a so-called *absolute-to-convective* transition. In the case of an *absolutely unstable* system, the initially localized perturbation will eventually invade the entire domain. In contrast, for a *convectively unstable* system, any stationary observer will eventually see an unperturbed tube at long times—despite the perturbation continuing to grow over time. For the remainder of this section, we use a spatiotemporal stability analysis to determine under what conditions a lipid membrane tube is absolutely or convectively unstable.

In searching for the absolute-to-convective transition, we recognize that observers moving at different speeds will in general see different growth rates, since the initial perturbation is localized in space. This possibility in fact requires both the wavenumber q and frequency ω to be complex variables. [‡] To understand why, see Fig. 8, which presents space–time plots of the perturbed membrane radius, which is evolving according to Eq. (118). We notice that the base flow is large enough to convect the shape disturbance downstream, such that a stationary observer situated at the dashed green line sees a decay at long times—for which $\omega^{(i)} < 0$. On the other hand, if we imagine a moving observer (†) traveling along the solid red line with speed u, then the axial positions and frequencies of the two observers are related by $z^\dagger = z - ut$ and $\omega^\dagger = \omega - uq$. Moreover, the moving observer sees the disturbance growing in time, and thus $\omega^{\dagger(i)} = \omega^{(i)} - uq^{(i)} > 0$. Since $\omega^{(i)} < 0$ and $\omega^{(i)} - uq^{(i)} > 0$, we recognize $q^{(i)} \neq 0$ in order for different observers to see different growth rates—for which the

[‡] J. Eggers and E. Villermaux. "Physics of liquid jets". *Rep. Prog. Phys.* **71** (2008), 036601.

wavenumber is complex. In general, a spatiotemporal stability analysis requires both $q \in \mathbb{C}$ and $\omega \in \mathbb{C}$. For the remainder of this section, we follow well-established procedures [‡, †, *] to investigate how membrane tubes with a nonzero base flow respond to an initially localized shape perturbation.

(b). The saddle points of the dispersion relation

Imagine an unstable membrane tube, with $\Gamma > \Gamma_c$, subject to a spatially localized disturbance at one instant in time. As the perturbation grows, we search for the particular disturbances seen at long times in the laboratory frame—namely, perturbations with zero group velocity. The so-called *absolute wavenumber* q_0^* and *absolute frequency* ω_0^* corresponding to zero group velocity disturbances are determined according to

$$\left.\frac{\mathrm{d}\omega^*}{\mathrm{d}q^*}\right|_{q_0^*} = 0 \qquad \text{and} \qquad \omega_0^* = \omega^*(q_0^*) \,. \tag{138}$$

It is important to reiterate that here and henceforth, ω^* and q^* are complex variables. In addition, the pair (q_0^*, ω_0^*) is referred to as a saddle point due to the nature of $\omega_*^{(r)}$ when it is plotted as a function of $q_*^{(r)}$ and $q_*^{(i)}$.

By applying the two saddle point criteria (138) to the dispersion relation (133), we respectively obtain the conditions

$$SL - \frac{i}{2}\left\{\left(\Gamma - \Gamma_0\right) q_0^* + \left(q_0^*\right)^3\right\} = 0 \tag{139}$$

and

$$\omega_0^* = SL\, q_0^* + \frac{i}{8}\left\{2\left(\Gamma - \Gamma_c\right) - 2\left(\Gamma - \Gamma_0\right)\left(q_0^*\right)^2 - \left(q_0^*\right)^4\right\} . \tag{140}$$

Next, the relations $q_0^* = q_0^{*(r)} + i q_0^{*(i)}$ and $\omega_0^* = \omega_0^{*(r)} + i\omega_0^{*(i)}$ are substituted into Eqs. (139) and (140), and the resulting equations are split into real and imaginary components to yield four conditions, respectively given by

$$2\,SL + \left(\Gamma - \Gamma_0\right) q_0^{*(i)} + 3\left(q_0^{*(r)}\right)^2 q_0^{*(i)} - \left(q_0^{*(i)}\right)^3 = 0 \,, \tag{141}$$

$$q_0^{*(r)}\left[\left(\Gamma - \Gamma_0\right) + \left(q_0^{*(r)}\right)^2 - 3\left(q_0^{*(i)}\right)^2\right] = 0 \,, \tag{142}$$

$$\omega_0^{*(r)} = q_0^{*(r)}\left\{SL + \frac{1}{2} q_0^{*(i)}\left[\left(\Gamma - \Gamma_0\right) + \left(q_0^{*(r)}\right)^2 - \left(q_0^{*(i)}\right)^2\right]\right\} , \tag{143}$$

and

$$\begin{aligned}\omega_0^{*(i)} = SL\, q_0^{*(i)} + \frac{1}{8}\Big\{&2\left(\Gamma - \Gamma_c\right) + 2\left(\Gamma - \Gamma_0\right)\left[\left(q_0^{*(i)}\right)^2 - \left(q_0^{*(r)}\right)^2\right] \\ &- \left(q_0^{*(r)}\right)^4 + 6\left(q_0^{*(r)}\right)^2\left(q_0^{*(i)}\right)^2 - \left(q_0^{*(i)}\right)^4\Big\} .\end{aligned} \tag{144}$$

[‡] Huerre and Rossi, "Hydrodynamic instabilities in open flows".
[†] Huerre and Monkewitz, "Local and global instabilities in spatially developing flows".
[*] F. Charru. *Hydrodynamic Instabilities*. New York: Cambridge University Press, 2011.

We now have four equations (141)–(144) corresponding to the four unknowns $q_0^{*(r)}$, $q_0^{*(i)}$, $\omega_0^{*(r)}$, and $\omega_0^{*(i)}$, for any values of the parameters SL and Γ.

At this point, we seek to determine the boundary between absolutely and convectively unstable regimes. We recognize that a stationary observer will see a positive growth rate, for which $\omega_0^{*(i)} > 0$, when the tube is absolutely unstable, and a negative growth rate, with $\omega_0^{*(i)} < 0$, when the tube is convectively unstable. A necessary condition for the absolute-to-convective transition is thus given by

$$\omega_0^{*(i)} = 0 \,. \tag{145}$$

With Eq. (145), we now have an additional equation relating SL and Γ. In what follows, for every unstable tube with $\Gamma > \Gamma_c$ we calculate the saddle point (q_0^*, ω_0^*) and the critical Scriven–Love number $SL_{ac}(\Gamma)$ corresponding to the absolute-to-convective transition, for which Eqs. (141)–(145) are satisfied. Due to Eq. (142), this calculation is split into two cases, as either

$$q_0^{*(r)} = 0 \qquad \text{or} \qquad \left(q_0^{*(r)}\right)^2 = 3\left(q_0^{*(i)}\right)^2 - \left(\Gamma - \Gamma_0\right) \,. \tag{146}$$

We note that Eq. (145) is a necessary but not sufficient condition for the absolute-to-convective transition—implying our calculation of the saddle point and critical base flow velocity may not be physical. Consequently, in §7 (c) we investigate whether the calculated values of q_0^*, ω_0^*, and SL_{ac} are physical or spurious.

The case with a purely imaginary absolute wavenumber

When $q_0^{*(r)} = 0$, Eqs. (141)–(145) simplify to

$$2\,SL_{ac} + \left(\Gamma - \Gamma_0\right) q_0^{*(i)} - \left(q_0^{*(i)}\right)^3 = 0 \,, \tag{147}$$

$$SL_{ac}\, q_0^{*(i)} + \frac{1}{8}\left\{2\left(\Gamma - \Gamma_c\right) + 2\left(\Gamma - \Gamma_0\right)\left(q_0^{*(i)}\right)^2 - \left(q_0^{*(i)}\right)^4\right\} = 0 \,, \tag{148}$$

and

$$\omega_0^{*(r)} = 0 \,. \tag{149}$$

If $q_0^{*(i)} = 0$ as well, Eqs. (147) and (148) reduce to $\Gamma = \Gamma_c$ and $SL_{ac} = 0$. Since we are interested in obtaining SL_{ac} for all Γ, we assume $q_0^{*(i)} \neq 0$. This allows us to multiply Eq. (147) by $-q_0^{*(i)}$ and add the result to twice Eq. (148), which after some rearrangement yields the following equation for $q_0^{*(i)}$:

$$3\left(q_0^{*(i)}\right)^4 - 2\left(\Gamma - \Gamma_0\right)\left(q_0^{*(i)}\right)^2 + 2\left(\Gamma - \Gamma_c\right) = 0 \,. \tag{150}$$

As $q_0^{*(i)} \in \mathbb{R}$, we find Eq. (150) has only real roots when

$$\Gamma \in \Omega_A := [\Gamma_c, \Gamma_1] \cup [\Gamma_2, \infty) \,, \tag{151}$$

where Γ_1 and Γ_2 are defined as

$$\Gamma_1 := \frac{13}{4} - \sqrt{6} \approx 0.801 \qquad \text{and} \qquad \Gamma_2 := \frac{13}{4} + \sqrt{6} \approx 5.699 \,. \tag{152}$$

Thus, the four solutions of Eq. (150) for $q_0^{*(i)}$ are given by

$$q_0^{*(i)} = \pm\frac{1}{\sqrt{3}}\sqrt{\left(\Gamma-\Gamma_0\right) \pm \sqrt{\left(\Gamma-\Gamma_0\right)^2 - 6\left(\Gamma-\Gamma_c\right)}}\ , \qquad \text{with} \qquad \Gamma \in \Omega_A\ . \tag{153}$$

At this point, we note that of the four solutions in Eq. (153), two are positive and two are negative. However, our spatial ansatz $\sim \exp(i\,q^*z^*) = \exp(-q_*^{(i)}z^*)\exp(i\,q_*^{(r)}z^*)$ and the base flow is in the positive z-direction. As we are interested in the absolute-to-convective transition, for which a perturbation initially at the origin ($z^* = 0$) grows downstream ($z^* > 0$), we choose only the negative solutions of $q_0^{*(i)}$ in Eq. (153) such that our spatial ansatz grows downstream, and find

$$\begin{aligned} q_0^{*(i)\pm} &= \frac{-1}{\sqrt{3}}\sqrt{\left(\Gamma-\Gamma_0\right) \pm \sqrt{\left(\Gamma-\Gamma_0\right)^2 - 6\left(\Gamma-\Gamma_c\right)}} \\ &= \frac{-1}{2\sqrt{3}}\sqrt{4\Gamma - 1 \pm \sqrt{16\Gamma^2 - 104\Gamma + 73}}\ , \qquad \text{with} \qquad \Gamma \in \Omega_A\ . \end{aligned} \tag{154}$$

Substituting Eq. (154) into Eq. (147) yields two solutions for SL_{ac} as

$$SL_{ac}^{\pm} = \frac{-1}{48\sqrt{3}}\sqrt{4\Gamma - 1 \pm \sqrt{16\Gamma^2-104\Gamma+73}}\left(-8\Gamma + 2 \pm \sqrt{16\Gamma^2-104\Gamma+73}\right), \tag{155}$$

with $\Gamma \in \Omega_A$. However, we will show subsequently that only one of these absolute-to-convective Scriven–Love numbers, namely SL_{ac}^{-}, is physically meaningful. Before doing so, we next consider the other possible case from Eq. (146), where $q_0^{*(r)} \neq 0$.

The case with nonzero real wavenumber

When $q_0^{*(r)} \neq 0$, Eq. (142) requires the real and imaginary parts of the absolute wavenumber to be related by [see also Eq. $(146)_2$]

$$\left(q_0^{*(r)}\right)^2 = 3\left(q_0^{*(i)}\right)^2 - \left(\Gamma-\Gamma_0\right)\ . \tag{156}$$

By substituting Eq. (156) into Eqs. (141) and (144), making use of Eq. (145), and rearranging terms, we obtain two equations for $q_0^{*(i)}(\Gamma)$ and $SL_{ac}(\Gamma)$—given by

$$SL_{ac} + q_0^{*(i)}\left[4\left(q_0^{*(i)}\right)^2 - \left(\Gamma-\Gamma_0\right)\right] = 0 \tag{157}$$

and

$$SL_{ac}\,q_0^{*(i)} + \left(q_0^{*(i)}\right)^4 - \frac{\Gamma-\Gamma_0}{2}\left(q_0^{*(i)}\right)^2 + \frac{1}{8}\left(\Gamma-\Gamma_0\right)^2 + \frac{1}{4}\left(\Gamma-\Gamma_c\right) = 0\ . \tag{158}$$

If we assume $q_0^{*(i)} = 0$, then Eqs. (157) and (158) require $SL_{ac} = 0$ and $\Gamma < \Gamma_c$: an unphysical result, since the absolute-to-convective transition is only physically meaningful for unstable tubes, in which $\Gamma > \Gamma_c$. Thus $q_0^{*(i)} \neq 0$, allowing us to multiply Eq. (157) by $-q_0^{*(i)}$ and add the result to Eq. (158) to obtain

$$24\left(q_0^{*(i)}\right)^4 - 4\left(\Gamma-\Gamma_0\right)\left(q_0^{*(i)}\right)^2 - \left(\Gamma-\Gamma_0\right)^2 - 2\left(\Gamma-\Gamma_c\right) = 0\ . \tag{159}$$

Solving Eq. (159) for $q_0^{*(i)}$, with the requirements that (i) $q_0^{*(i)} \in \mathbb{R}$ and (ii) $q_0^{*(i)} < 0$ such that the mode grows spatially downstream ($z > 0$), we find

$$q_0^{*(i)} = -\frac{1}{4\sqrt{3}}\sqrt{4\Gamma - 1 + \sqrt{112\Gamma^2 + 136\Gamma - 137}}\ , \tag{160}$$

for all $\Gamma > \Gamma_c$. By substituting Eq. (160) into Eq. (156), we obtain the real part of the absolute wavenumber as

$$q_0^{*(r)\pm} = \pm\frac{1}{4}\sqrt{-12\Gamma + 3 + \sqrt{112\Gamma^2 + 136\Gamma - 137}}\ . \tag{161}$$

However, as $q_0^{*(r)} \in \mathbb{R}$, Eq. (161) is only meaningful when $-12\Gamma+3+\sqrt{112\Gamma^2 + 136\Gamma - 137} > 0$, which requires

$$\Gamma \in \Omega_B := (\Gamma_1, \Gamma_2)\ , \tag{162}$$

where Γ_1 and Γ_2 were defined in Eq. (152). Interestingly, Ω_B is complementary to Ω_A, such that $\Omega_A \cap \Omega_B = \varnothing$ and $\overline{\Omega_A \cup \Omega_B} = [\Gamma_c, \infty)$, the latter being the entire range of Föppl–von Kármán numbers corresponding to unstable tubes. For $\Gamma \in \Omega_B$, we determine the absolute-to-convective Scriven–Love number SL_{ac}^- via Eq. (157) as

$$SL_{ac}^- = \frac{1}{48\sqrt{3}}\sqrt{4\Gamma - 1 + \sqrt{112\Gamma^2 + 136\Gamma - 137}}\left(-8\Gamma + 2 + \sqrt{112\Gamma^2 + 136\Gamma - 137}\right). \tag{163}$$

Note that when $\Gamma \in \Omega_B$, there is only a single value of SL_{ac} (163), while for $\Gamma \in \Omega_A$ we obtained two values of SL_{ac} (155). Finally, we calculate the real part of the absolute frequency, $\omega_0^{*(r)}$, using Eq. (143), and find

$$\omega_0^{*(r)\pm} = \frac{\mp 1}{128\sqrt{3}}\sqrt{16\Gamma^2 + 40\Gamma - 35 - \tfrac{1}{2}(4\Gamma - 1)\sqrt{112\Gamma^2 + 136\Gamma - 137}} \times \ldots \\ \ldots \times \left(12\Gamma - 3 - \sqrt{112\Gamma^2 + 136\Gamma - 137}\right). \tag{164}$$

(c). The absolute-to-convective transition

At this point, we found analytical expressions for the saddle point (q_0^*, ω_0^*) and the absolute-to-convective Scriven–Love number SL_{ac} by solving the saddle point and growth rate conditions in Eqs. (141)–(145) simultaneously; all quantities have different expressions depending on whether $\Gamma \in \Omega_A$ or $\Gamma \in \Omega_B$. However, as mentioned earlier, the condition $\omega_0^{*(i)} = 0$ (145) is necessary but not sufficient to determine SL_{ac}. In this section, we evaluate whether the previously calculated values of SL_{ac} do in fact describe where our cylindrical membrane system transitions from being absolutely unstable to being convectively unstable. We follow the approach detailed by A. Bers and R.J. Briggs, [‡, †] and subsequently other authors, [*, §]

[‡] Bers and Briggs, "Criteria for determining absolute instability and distinguishing between amplifying and evanescent waves".

[†] Briggs, *Electron-Stream Interactions with Plasmas*.

[*] K. Kupfer, A. Bers, and A.K. Ram. "The cusp map in the complex-frequency plane for absolute instabilities". *Phys. Fluids* **30** (1987), 3075–3082.

[§] Huerre and Monkewitz, "Local and global instabilities in spatially developing flows".

in which a geometric criterion was found to determine if a saddle point is associated with a transition from an absolute to a convective instability. A rigorous explanation of this criterion is outside the scope of our work, and requires long-time asymptotics and an analysis of pole singularities in the complex plane. ‡ However, in what follows, we describe several major themes of the criterion and then provide the procedure used to determine if the saddle points are physical or spurious in nature. The description is drawn almost entirely from the analysis by P. HUERRE and M. ROSSI, ‡ who analyze the absolute-to-convective transition of the well-known Ginzburg–Landau equation. We highly recommend this work to interested readers, and as a result highlight its relevant sections in the following presentation.

The geometric criterion obtained by Bers and Briggs is largely concerned with the nature of solutions to the dispersion relation $\omega^* = \omega^*(q^*)$ in the vicinity of the saddle point. By Taylor expanding the dispersion relation about the saddle point and recalling $\omega_*'(q_0^*) = 0$ from Eq. $(138)_1$, where here a 'prime' denotes differentiation with respect to q^*, one obtains

$$\omega^* - \omega_0^* \approx \frac{\omega_*''(q_0^*)}{2}\,(q^* - q_0^*)^2 \,, \tag{165}$$

or equivalently

$$q^* - q_0^* \approx \pm \left(\frac{2}{\omega_*''(q_0^*)}\right)^{1/2} (\omega^* - \omega_0^*)^{1/2} \,. \tag{166}$$

Note that our dispersion relation (133) is a fourth-order polynomial in q^*, and solving it for a particular choice of $\omega^* \in \mathbb{C}$ yields four solutions for $q^* \in \mathbb{C}$. Similarly, a contour in the complex frequency plane $(\omega_*^{(r)}, \omega_*^{(i)})$ corresponds to four contours in the complex wavenumber plane $(q_*^{(r)}, q_*^{(i)})$, with the latter being referred to as *generalized spatial branches*. For our purposes, we choose frequency contours with constant $\omega_*^{(i)}$; such contours are denoted L_ω as in Sec. 3.2.2 of Huerre and Rossi. ‡

For an arbitrary choice of L_ω, the spatial branches will in general not intersect one another. However, when L_ω passes through ω_0^*, two spatial branches will pinch, implying the long-time dynamics are influenced by the behavior of both of those branches. To see how the branches pinch, we note that along this particular choice of L_ω, $\omega^* - \omega_0^* = \omega_*^{(r)} - \omega_0^{*(r)}$. By additionally defining $\alpha + i\beta := (2/\omega_*''(q_0^*))^{1/2}$ for notational convenience, with α and β being real constants, Eq. (166) simplifies to $q^* - q_0^* \approx \pm(\alpha + i\beta)(\omega_*^{(r)} - \omega_0^{*(r)})^{1/2}$, for which

$$\frac{q_*^{(i)} - q_0^{*(i)}}{q_*^{(r)} - q_0^{*(r)}} = \begin{cases} \pm\dfrac{\beta}{\alpha} & \text{when} \quad \omega^{(r)} - \omega_0^{*(r)} > 0 \\ \mp\dfrac{\alpha}{\beta} & \text{when} \quad \omega^{(r)} - \omega_0^{*(r)} < 0 \,. \end{cases} \tag{167}$$

Accordingly, $q_*^{(i)} - q_0^{*(i)} \propto \pm(q_*^{(r)} - q_0^{*(r)})$ in the vicinity of the saddle point, implying two spatial branches pinch at the saddle point. We therefore seek to characterize the long-time dynamics of the two spatial branches that pinch at the saddle point. To this end, we apply the following procedure, as detailed in Sec. 3.2.2 of Huerre and Rossi; ‡ relevant steps are illustrated in Fig. 9.

‡Huerre and Rossi, "Hydrodynamic instabilities in open flows"

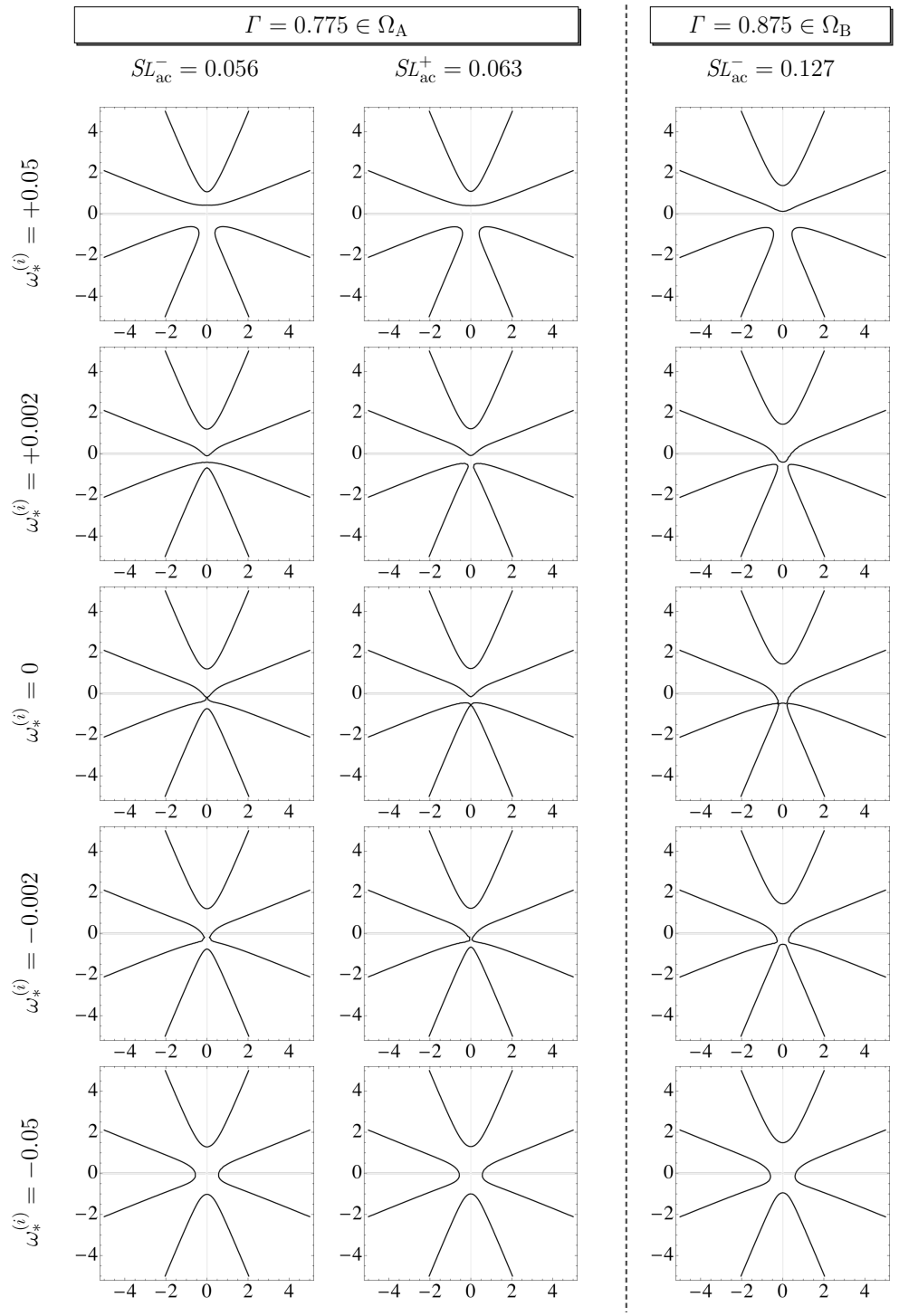

Figure 9: Solution branches in the complex wavenumber plane $(q_*^{(r)}, q_*^{(i)})$, for different values of $\omega_*^{(i)}$. When $\Gamma \in \Omega_A$, two values of SL_{ac} are calculated in Eq. (155), corresponding to the left and center columns. As $\omega_*^{(i)}$ is decreased, pinching between spatial branches originating from upper and lower half-planes occurs when $SL = SL_{ac}^{-}$ (left column), but not when $SL = SL_{ac}^{+}$ (center column). Accordingly, when $\Gamma \in \Omega_A$, only SL_{ac}^{-} corresponds to a true absolute-to-convective transition. As shown in the right column, when $\Gamma \in \Omega_B$, the value of SL_{ac}^{-} in Eq. (163) satisfies the pinching criterion.

1. Choose a value $\mathit{\Gamma}_{\text{test}}$ of the Föppl–von Kármán number, with $\mathit{\Gamma}_{\text{test}} > \mathit{\Gamma}_{\text{c}}$, to ensure a temporal instability. In Fig. 9, we chose $\mathit{\Gamma}_{\text{test}} = 0.775 \in \Omega_{\text{A}}$ (left and center columns) and $\mathit{\Gamma}_{\text{test}} = 0.875 \in \Omega_{\text{B}}$ (right column).

2. Calculate the value of $\mathit{SL}_{\text{ac}}(\mathit{\Gamma}_{\text{test}})$ with Eq. (155) if $\mathit{\Gamma}_{\text{test}} \in \Omega_{\text{A}}$ or Eq. (163) if $\mathit{\Gamma}_{\text{test}} \in \Omega_{\text{B}}$. In Fig. 9, the left and center columns correspond to the two values of SL_{ac} when $\mathit{\Gamma}_{\text{test}} = 0.775 \in \Omega_{\text{A}}$, namely $\mathit{SL}_{\text{ac}}^{-} = 0.056$ and $\mathit{SL}_{\text{ac}}^{+} = 0.063$, while the right column corresponds to $\mathit{SL}_{\text{ac}}^{-}$ when $\mathit{\Gamma}_{\text{test}} = 0.875 \in \Omega_{\text{B}}$.

3. Choose a value of $\omega_*^{(i)} > \omega_{\text{max}}^{*(i)}$, such that $\omega_*^{(i)}$ is greater than the largest temporal growth rate (136). In Fig. 9, we chose $\omega_*^{(i)} = 0.05$ in all cases (top row).

4. For the choice of $\omega_*^{(i)}$, introduce the contour $L_\omega = \omega_*^{(r)} + \omega_*^{(i)}$, where $\omega_*^{(r)}$ varies over $\mathbb{R}$. Solve Eq. (144) for the spatial branches $(q_*^{(r)}, q_*^{(i)})$ in the complex wavenumber plane. Due to the choice of $\omega_*^{(i)}$ in Step 3, no spatial branches can cross the $q_*^{(r)}$ axis, as doing so would indicate there exists a mode with real q^* that grows faster than the largest possible growth rate—a contradiction. Thus, the spatial branches lie entirely above or below the $q_*^{(r)}$ axis. Since $q_*^{(i)} \neq 0$, the normal modes can be written as

$$\exp\left[\, i\left(q^* z^* - \omega^* t^*\right)\right] = \underbrace{\exp\left[-q_*^{(i)}\left(z^* - \frac{\omega_*^{(i)}}{q_*^{(i)}}\, t^*\right)\right]}_{\mathcal{F}(z^* - c^* t^*)} \exp\left[\, i\left(q_*^{(r)} z^* - \omega_*^{(r)} t^*\right)\right]. \quad (168)$$

   As $\omega^{(i)} > 0$, the sign of $q_*^{(i)}$ determines the sign of $c^* = \omega_*^{(i)}/q_*^{(i)}$ and thus dictates the traveling direction of the spatial branch modes: when $q_*^{(i)} > 0$, the mode moves to the right, while if $q_*^{(i)} < 0$ the mode moves to the left. The top row in Fig. 9 shows that in all cases, two modes are right-moving and two modes are left-moving.

5. Continuously select new contours L_ω as the value of $\omega_*^{(i)}$ is steadily decreased, until $\omega_*^{(i)} < 0$; for each L_ω, solve for the four spatial branches $(q_*^{(r)}, q_*^{(i)})$ in the complex wavenumber plane. Figure 9 shows how the spatial branches evolve as $\omega_*^{(i)}$ is lowered from $+0.05$ (top row) to -0.05 (bottom row).

6. Monitor how the four spatial branches evolve as L_ω is lowered in Step 5, paying special attention to the two branches that pinch at $\omega_*^{(i)} = 0$. As we solved for SL_{ac} with the requirement that $\omega_0^{*(i)} = 0$, the branch pinching reveals which spatial branches contribute to the long-time dynamics of the saddle point (q_0^*, ω_0^*). If the pinching branches belonged to different half-planes $q_0^{*(i)} > 0$ and $q_0^{*(i)} < 0$ for higher $\omega_*^{(i)}$ (such as in Step 3), then the corresponding modes are moving in different directions and the system is on the verge of losing its sense of directionality—characteristic of an absolute instability. In this case, our calculation of $\mathit{SL}_{\text{ac}}(\mathit{\Gamma}_{\text{test}})$ indeed corresponds to an absolute-to-convective transition. Otherwise, both modes are traveling in the same direction, and the system is not on the verge of losing its sense of directionality; the saddle point does not represent an absolute-to-convective transition and is thus unphysical.

As we show in Fig. 9, when $\Gamma \in \Omega_{\mathrm{A}}$, only the saddle point of absolute wavenumber $q_0^* = iq_0^{*(i)-}$ (154) satisfies the pinching criterion. Therefore, the absolute-to-convective transition speed is given by $\mathcal{SL}_{\mathrm{ac}}^{-}$ (155). When $\Gamma \in \Omega_{\mathrm{B}}$, the two saddle points of wavenumber $q_0^* = q_0^{*(r)\pm} + iq_0^{*(i)}$ (160) simultaneously satisfy the pinching criterion. In this case, the absolute-to-convective transition speed is given by Eq. (163), and plotted in Fig. 10. Although the analytical expressions for $\mathcal{SL}_{\mathrm{ac}}(\Gamma)$ differ depending on whether $\Gamma \in \Omega_{\mathrm{A}}$ or $\Gamma \in \Omega_{\mathrm{B}}$, Fig. 10 reveals that the absolute-to-convective transition speed is a smoothly varying function of the Föppl–von Kármán number. In contrast, the saddle point (q_0^*, ω_0^*) undergoes two bifurcations as Γ is varied: one at $\Gamma = \Gamma_1$ and another at $\Gamma = \Gamma_2$, as shown in Fig. 11. We discuss how the saddle point bifurcations affect the long-time response of a perturbed lipid membrane tube when we analyze front propagation in §7 (f), and we comment on the nature of Γ_1 and Γ_2 in §7 (g). Our calculation of the physically meaningful saddle point and critical Scriven–Love number, for all $\Gamma > \Gamma_{\mathrm{c}}$, is also summarized in Table 5.

(d). The limiting behavior of $\mathcal{SL}_{\mathrm{ac}}$

With the calculated values of the Scriven–Love number corresponding to the absolute-to-convective transition plotted in Fig. 10, we recognize that for every $\Gamma > \Gamma_{\mathrm{c}}$ the tube is absolutely unstable when $\mathcal{SL} = 0$. As the Scriven–Love number is increased, the nature of the instability eventually transitions from absolute to convective when $\mathcal{SL} = \mathcal{SL}_{\mathrm{ac}}(\Gamma)$, such that the system is convectively unstable when $\mathcal{SL} > \mathcal{SL}_{\mathrm{ac}}$. We now comment on the limiting behavior of the absolute-to-convective Scriven–Love number, $\mathcal{SL}_{\mathrm{ac}}$, in two cases: $\Gamma \to \infty$ and $\Gamma \to \Gamma_{\mathrm{c}}^{+}$.

The limiting behavior when Γ is large

An infinite Föppl–von Kármán number corresponds to the limiting case of a two-dimensional fluid film, in which the bending modulus is negligible. For such systems, we take the limit of the expression for $\mathcal{SL}_{\mathrm{ac}}$ provided in Table 5, when $\Gamma \in \Omega_{\mathrm{A}}$, and find

$$\lim_{\Gamma \to \infty} \mathcal{SL}_{\mathrm{ac}}(\Gamma) = \frac{\Gamma}{2} \, . \tag{169}$$

Interestingly, although Eq. (169) is only valid asymptotically, the result $\mathcal{SL}_{\mathrm{ac}} \sim \Gamma/2$ is a reasonable approximation for all $\Gamma > \Gamma_1 \approx 0.801$, as shown in Fig. 10. However, as Γ approaches the instability threshold value of Γ_{c}, the approximation breaks down.

The limiting behavior when Γ approaches Γ_{c}

As the Föppl–von Kármán number Γ approaches Γ_{c}, the absolute-to-convective Scriven–Love number can be expanded as the Puiseux series [‡]

$$\mathcal{SL}_{\mathrm{ac}} = \frac{\sqrt{2}}{4}\left(\Gamma - \Gamma_{\mathrm{c}}\right)^{1/2} - \frac{\sqrt{2}}{2}\left(\Gamma - \Gamma_{\mathrm{c}}\right)^{5/2} - 4\sqrt{2}\left(\Gamma - \Gamma_{\mathrm{c}}\right)^{7/2} + \ldots \, . \tag{170}$$

[‡]This series expansion was obtained using `Mathematica`.

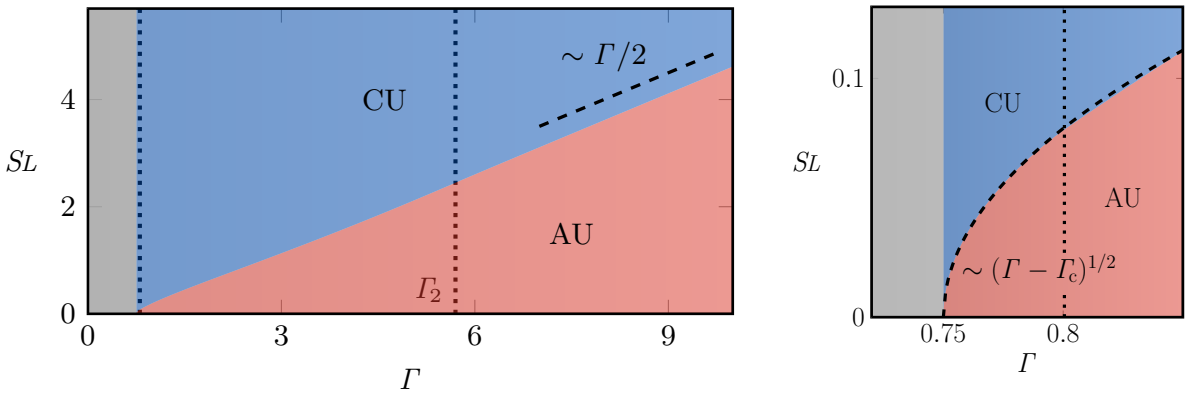

Figure 10: Stability diagram of lipid membrane tubes in the space of Γ and $\mathcal{SL}$, showing stable (gray, $\Gamma < \Gamma_c = \frac{3}{4}$), absolutely unstable (AU, red), and convectively unstable (CU, blue) regimes. The critical velocity of the absolute-to-convective transition scales as $\mathcal{SL}_{ac} \sim \Gamma/2$ at large Γ, but as $\mathcal{SL}_{ac} \sim (\Gamma - \Gamma_c)^{1/2}$ for $\Gamma \to \Gamma_c^+$—as highlighted in the plot on the right. The vertical dotted lines mark the interval (Γ_1, Γ_2) where fronts invading the undeformed tube are oscillatory. For unstable tubes with a Föppl–von Kármán number outside this range, front propagation is monotonic, with no oscillations at the leading edge.

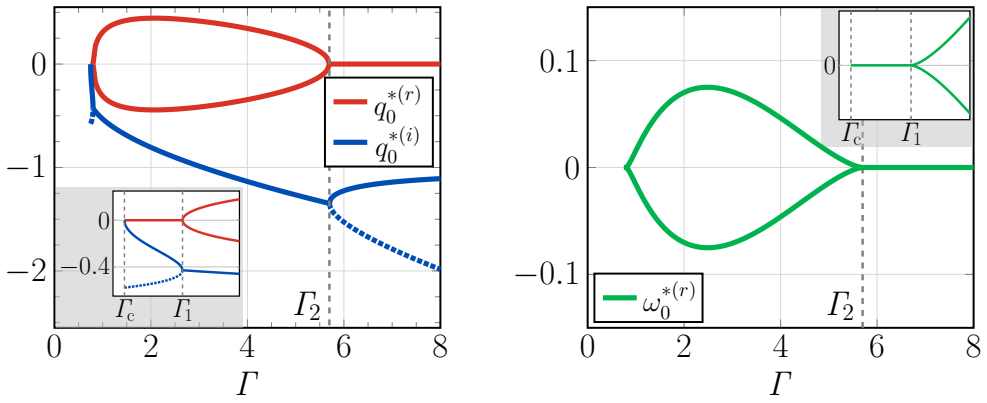

Figure 11: Real and imaginary components of the absolute wavenumber q_0^* (left) and real part of the absolute frequency ω_0^* (right), with $\omega_0^{*(i)} = 0$. The solid (respectively dashed) lines correspond to the relevant (respectively spurious) saddle points obtained when searching for the boundary between absolutely unstable and convectively unstable membrane tubes. As the Föppl–von Kármán number is increased, the bifurcation at Γ_1 signals a transition from steady to oscillatory spatiotemporal dynamics, with the reverse being true at Γ_2.

Table 5: Calculated values of the saddle point (q_0^*, ω_0^*) and absolute-to-convective Scriven–Love number $SL_{\rm ac}$, for all $\Gamma > \Gamma_{\rm c}$. When $\Gamma \in \Omega_{\rm A}$, only one of the previously calculated solutions is physically meaningful (see Fig. 9).

$\Gamma \in \Omega_{\rm A}$	$g(\Gamma) := -\sqrt{16\Gamma^2 - 104\Gamma + 73}$ $q_0^{*(r)} = 0$ $q_0^{*(i)} = \dfrac{-1}{2\sqrt{3}}\sqrt{4\Gamma - 1 + g(\Gamma)}$ $\omega_0^{*(r)} = 0$ $\omega_0^{*(i)} = 0$ $SL_{\rm ac} = \dfrac{8\Gamma - 2 - g(\Gamma)}{48\sqrt{3}}\sqrt{4\Gamma - 1 + g(\Gamma)}$
$\Gamma \in \Omega_{\rm B}$	$g(\Gamma) := \sqrt{112\Gamma^2 + 136\Gamma - 137}$ $q_0^{*(r)\pm} = \pm\dfrac{1}{4}\sqrt{-12\Gamma + 3 + g(\Gamma)}$ $q_0^{*(i)} = -\dfrac{1}{4\sqrt{3}}\sqrt{4\Gamma - 1 + g(\Gamma)}$ $\omega_0^{*(r)\pm} = \mp\dfrac{12\Gamma - 3 - g(\Gamma)}{48\sqrt{3}}\sqrt{16\Gamma^2 + 40\Gamma - 35 - \frac{1}{2}(4\Gamma - 1)\, g(\Gamma)}$ $\omega_0^{*(i)} = 0$ $SL_{\rm ac} = \dfrac{-8\Gamma + 2 + g(\Gamma)}{48\sqrt{3}}\sqrt{4\Gamma - 1 + g(\Gamma)}$

Thus, close to the instability threshold, one may approximate $SL_{\rm ac}$ as

$$SL_{\rm ac} \approx \frac{\sqrt{2}}{4}\left(\Gamma - \Gamma_{\rm c}\right)^{1/2} \qquad \text{for} \qquad \Gamma \to \Gamma_{\rm c}^{+} \,. \tag{171}$$

As shown in Fig. 10, Eq. (171) is a reasonable approximation for Γ between $\Gamma_{\rm c}$ and Γ_1. Over this range, $\Gamma \in \Omega_{\rm A}$, such that q_0^* is purely imaginary and ω_0^* is identically zero at the absolute-to-convective transition (see Table 5).

The square root dependence seen in Eq. (171), as well as the relations $q_0^{*(r)} = 0$ and $\omega_0^{*(r)} = 0$, are reminiscent of the well-studied Ginzburg–Landau equation. For a general scalar field $\phi \in \mathbb{R}$ and constant real control parameters u and κ, the linearized Ginzburg–Landau equation is given by

$$\phi_{,t} + u\,\phi_{,x} = \kappa\,\phi + \phi_{,xx} \,. \tag{172}$$

It is well-known that Eq. (172) is unstable when $\kappa > 0$, and undergoes an absolute-to-convective transition for $u_{\rm ac} = 2\kappa^{1/2}$.[‡] At this point, we recall the linearized evolution equation for the perturbed membrane radius $\tilde{r}^*$ (118)—which is similar in structure to the linearized Ginzburg–Landau equation (172). The important difference is the $\tilde{r}^*_{,z^*z^*z^*z^*}$ term arising from the $-k_{\rm b}\Delta_{\rm s}H$ term in the shape equation (31). As such, Eq. (118) belongs to the family of so-called extended Fisher–Kolmogorov equations.[†, *, §] Nonetheless, the similarities between membrane dynamics for $\Gamma \to \Gamma_{\rm c}^+$ and the solution of the Ginzburg–Landau equation (172) motivate us to determine if the fourth-order term in Eq. (118) is indeed negligible in the limit $\Gamma \to \Gamma_{\rm c}^+$—in which case the rich set of behaviors predicted by the Ginzburg–Landau equation would also be relevant in understanding the dynamics of lipid membrane tubes.

We start by noting the fourth-order term is not the only bending term in Eq. (118): both $-(\Gamma_{\rm c}/4)\,\tilde{r}^*$ and $-(\Gamma_0/4)\,\tilde{r}^*_{,z^*z^*}$ originate from bending forces as well. While $\tilde{r}^*_{,z^*z^*z^*z^*}$ is negligible when $\Gamma \to \infty$, in this limit the other bending terms are also unimportant, thus yielding $\mathit{SL}_{\rm ac} \sim \Gamma/2$, as discussed previously. In the limit where $\Gamma \to \Gamma_{\rm c}$, however, the crucial insight is that the marginally stable wavenumber goes to zero as $q^*_{\rm ms} \sim (\Gamma - \Gamma_{\rm c})^{1/2}$ [see Eq. (137)], such that only long wavelength perturbations are unstable. Since the dominant wavenumbers are those for which $q^* < q^*_{\rm ms}$, the various contributions on the right hand side of Eq. (118) scale at most as

$$\left(\frac{\Gamma - \Gamma_{\rm c}}{4}\right)\tilde{r}^* \sim \left(\Gamma - \Gamma_{\rm c}\right), \tag{173}$$

$$\left(\frac{\Gamma - \Gamma_0}{4}\right)\tilde{r}^*_{,z^*z^*} \sim \left(\Gamma_{\rm c} - \Gamma_0\right)\left(\Gamma - \Gamma_{\rm c}\right), \tag{174}$$

and

$$-\frac{1}{8}\,\tilde{r}^*_{,z^*z^*z^*z^*} \sim \left(\Gamma - \Gamma_{\rm c}\right)^2 \tag{175}$$

as Γ approaches $\Gamma_{\rm c}$. In this limit, the $\tilde{r}^*_{,z^*z^*z^*z^*}$ term is negligible relative to the other terms, and Eq. (118) simplifies to

$$\tilde{r}^*_{,t^*} + \mathit{SL}\,\tilde{r}^*_{,z^*} = \left(\frac{\Gamma - \Gamma_{\rm c}}{4}\right)\tilde{r}^* + \left(\frac{\Gamma - \Gamma_0}{4}\right)\tilde{r}^*_{,z^*z^*} \qquad \text{as} \qquad \Gamma \to \Gamma_{\rm c}^+ . \tag{176}$$

Equation (176) can be recast in a similar form to the linearized Ginzburg–Landau equation (172) with the change of variables $x^* = 2z^*(\Gamma - \Gamma_0)^{-1/2}$, for which Eq. (176) becomes

$$\tilde{r}^*_{,t^*} + \left(\frac{2\,\mathit{SL}}{\sqrt{\Gamma - \Gamma_0}}\right)\tilde{r}^*_{,x^*} = \left(\frac{\Gamma - \Gamma_{\rm c}}{4}\right)\tilde{r}^* + \tilde{r}^*_{,x^*x^*} \qquad \text{as} \qquad \Gamma \to \Gamma_{\rm c}^+ . \tag{177}$$

In the limit of $\Gamma \to \Gamma_{\rm c}$, our parameters can be related to those in the linearized Ginzburg–Landau equation (172) by $u = 2\mathit{SL}(\Gamma - \Gamma_0)^{-1/2}$ and $\kappa = (\Gamma - \Gamma_{\rm c})/4$. As the Ginzburg–Landau

[‡]Huerre and Rossi, "Hydrodynamic instabilities in open flows".

[†]P. Coullet, C. Elphick, and D. Repaux. "Nature of spatial chaos". *Phys. Rev. Lett.* **58** (1987), 431–434.

[*]G.T. Dee and W. van Saarloos. "Bistable systems with propagating fronts leading to pattern formation". *Phys. Rev. Lett.* **60** (1988), 2641–2644.

[§]V. Rottschäfer and A. Doelman. "On the transition from the Ginzburg–Landau equation to the extended Fisher–Kolmogorov equation". *Physica D* **118** (1998), 261–292.

equation is unstable when $\kappa > 0$ and undergoes an absolute-to-convective transition when $u_{\mathrm{ac}} = 2\kappa^{1/2}$, we expect our membrane system to be unstable when $\Gamma > \Gamma_{\mathrm{c}}$ and undergo an absolute-to-convective transition when $SL_{\mathrm{ac}} = \frac{1}{2}(\Gamma - \Gamma_0)^{1/2}(\Gamma - \Gamma_{\mathrm{c}})^{1/2} \approx \frac{\sqrt{2}}{4}(\Gamma - \Gamma_{\mathrm{c}})^{1/2}$ as $\Gamma \to \Gamma_{\mathrm{c}}$. The latter condition agrees with the prediction of the series expansion in Eq. (170).

(e). The numerical solution of the linearized dynamics

We conclude our linear analysis of unstable lipid membrane tubes by presenting results from numerical simulations, which confirm our theoretical predictions of the absolute-to-convective transition. We first describe our numerical method to solve for the evolving membrane shape over time, as predicted by the linear theory, and then show the space–time evolution of an unstable, axisymmetric tube which is locally perturbed. One such result from our simulations was already shown in Fig. 8.

An axisymmetric lipid membrane tube is described by three fundamental unknowns, namely the perturbed shape $\tilde{r}^*(z^*, t^*)$, surface tension $\tilde{\lambda}^*(z^*, t^*)$, and in-plane axial velocity $\tilde{v}^{2*}(z^*, t^*)$. The three corresponding governing equations can be combined into a single evolution equation for $\tilde{r}^*$, as presented in Eq. (118). Thus, to solve for the membrane shape over time according to the linearized dynamics, we need only to solve Eq. (118) numerically. To this end, we observe that as Γ increases, $SL_{\mathrm{ac}}(\Gamma)$ increases as well. Accordingly, when the Föppl–von Kármán number is large, we are required to simulate systems with a large base flow to observe the absolute-to-convective transition. In this case, to ensure the disturbance does not flow past the edge of our computational domain, a large spatial domain is required. To avoid this numerical inconvenience, we introduce the rescaled variables

$$T = \left(\frac{\Gamma - \Gamma_{\mathrm{c}}}{4}\right) t^* \qquad \text{and} \qquad Z = \left(\frac{\Gamma - \Gamma_{\mathrm{c}}}{\Gamma - \Gamma_0}\right)^{1/2} z^* \,, \tag{178}$$

which are only physically meaningful when $\Gamma > \Gamma_{\mathrm{c}}$; note that rescaling time by $(\Gamma - \Gamma_{\mathrm{c}})$ and space by $(\Gamma - \Gamma_{\mathrm{c}})^{1/2}$ is a common technique when studying universality properties of the Ginzburg–Landau equation.[‡] By substituting Eq. (178) into the linearized evolution equation (118) and recognizing the Scriven–Love number is correspondingly rescaled as

$$\overline{SL} = \frac{4SL}{(\Gamma - \Gamma_{\mathrm{c}})^{1/2}\,(\Gamma - \Gamma_0)^{1/2}} \,, \tag{179}$$

we obtain

$$\tilde{r}^*_{,T} + \overline{SL}\,\tilde{r}^*_{,Z} = \tilde{r}^* + \tilde{r}^*_{,ZZ} - \frac{1}{2}\frac{(\Gamma - \Gamma_{\mathrm{c}})}{(\Gamma - \Gamma_0)^2}\,\tilde{r}^*_{,ZZZZ} \,. \tag{180}$$

Importantly, in the absence of spatial variations, Eq. (180) simplifies to $\tilde{r}^*_{,T} = \tilde{r}^*$, such that the growth rate is independent of the Föppl–von Kármán number. Moreover, the rescaled absolute-to-convective Scriven–Love number $\overline{SL}_{\mathrm{ac}}$ is of order unity for all unstable Föppl–von Kármán numbers Γ. Consequently, we may now use the same spatial and temporal domains for all simulations.

[‡]M. Cross and H. Greenside. *Pattern Formation and Dynamics in Nonequilibrium Systems*. New York: Cambridge University Press, 2009.

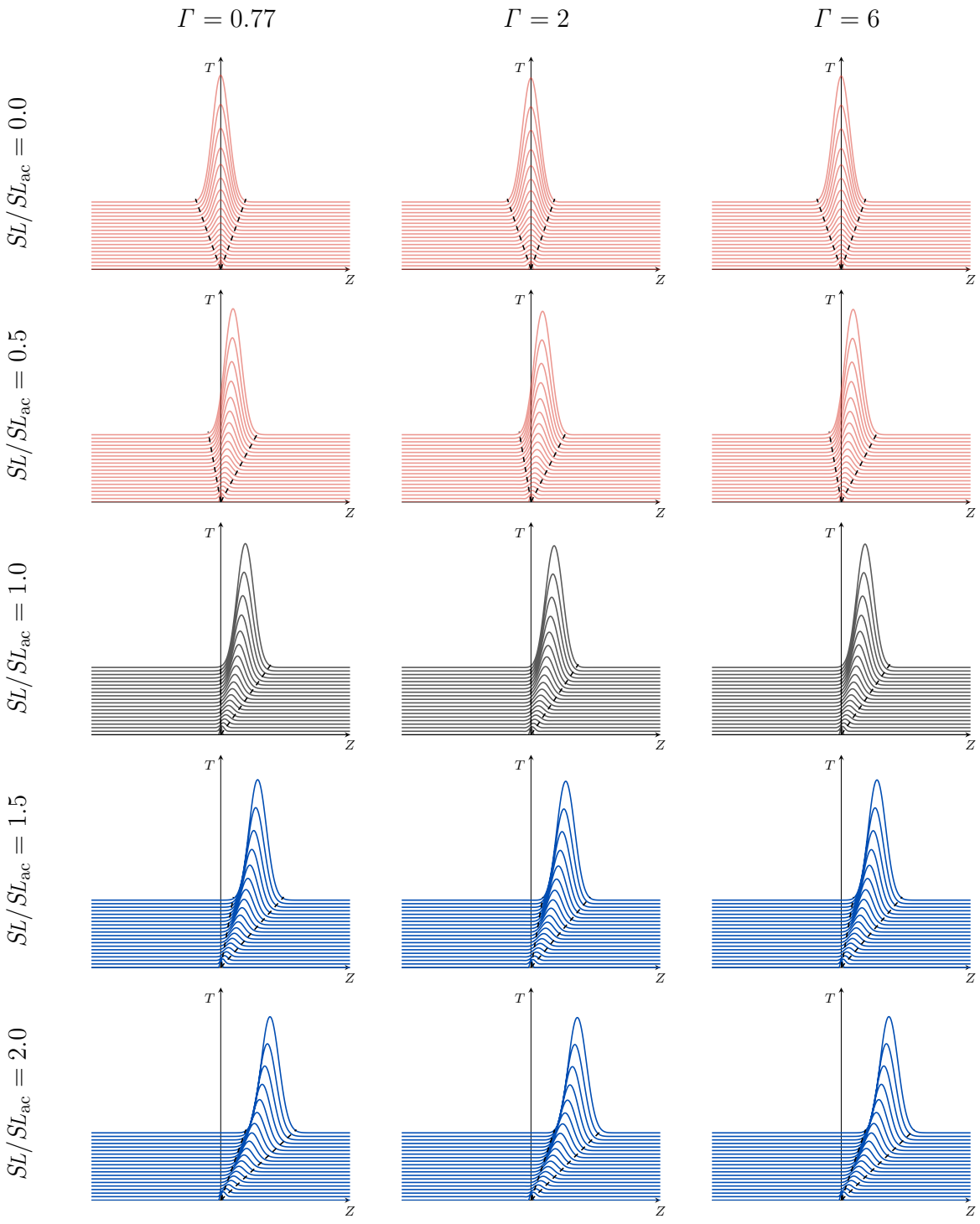

Figure 12: Space–time plots showing snapshots of the perturbed membrane tube radius at different instants and for different values of the control parameters. From left to right, $\Gamma = 0.77$, 2, and 6; from top to bottom, $SL/SL_{ac} = 0$, 0.5, 1, 1.5, and 2. The dashed black lines show the edges of the growing wavepacket and were obtained by determining the propagation speed of a front invading an unstable tube [see Eq. (187)].

The results of our numerical simulations, in terms of the rescaled variables Z and T, are shown in Fig. 12. All simulations were run on the fixed domain $Z \in [-50, 50]$ and with the initial condition $\tilde{r}^*(Z, 0) = 0.1 \exp(-10Z^2)$. We chose three different Föppl–von Kármán numbers: $\Gamma = 0.77 \in [\Gamma_c, \Gamma_1]$, $\Gamma = 2 \in (\Gamma_1, \Gamma_2)$, and $\Gamma = 6 > \Gamma_2$. For each choice of Γ, simulations were carried out at five values of the Scriven–Love number: $\overline{SL}/\overline{SL}_{ac} = SL/SL_{ac} =$ 0, 0.5, 1, 1.5, and 2, which were chosen such that we sampled (i) absolutely unstable systems, (ii) convectively unstable systems, and (iii) systems at the transition between the two. As shown in Fig. 12, our numerical results confirm our theoretical calculation of SL_{ac}. In particular, when $SL < SL_{ac}$, the instability grows to invade the entire domain, while if $SL > SL_{ac}$ then a stationary observer downstream will see a transient growth followed by a decay at long times. Moreover, our simulations show that as an initial perturbation grows, its edges propagate outward and invade the unstable tube at a constant velocity (see the dashed lines in Fig. 12). In all cases, the velocity of the leading edge is positive; however the velocity of the trailing edge is negative when $SL < SL_{ac}$, zero when $SL = SL_{ac}$, and positive when $SL > SL_{ac}$. In the following section, we investigate the dynamics of the moving fronts via linear methods.

(f). The marginal stability criterion and propagating front speed

To determine the speed at which an initially local perturbation invades the neighboring unperturbed tube, we apply the classical marginal stability criterion [‡, †, *]—one of the many well-established techniques for studying front propagation. Consider an initially localized wavepacket consisting of perturbations of the form $\sim \exp[i(q^* z^* - \omega^* t^*)]$, which is growing and spreading in an unstable system. If an observer is moving at a speed slightly greater than the front velocity V_f, they will see an unperturbed tube as they remain ahead of the growing wavepacket. If, on the other hand, an observer moves slightly slower than the front velocity, they will then see the tube changing shape: either growing or decaying, based on the sign of the growth rate in the traveling frame. The marginal stability criterion is based on the hypothesis that an observer traveling at the front speed V_f would see the system in its marginal state, i.e. on the verge of being deformed. Thus, the marginal stability criterion states that in the reference frame of the front connecting the deformed and undeformed regions of the tube, an observer perceives perturbations of zero growth rate.

In terms of our dimensionless quantities, the front velocity V_f is captured by what we call the Scriven–Love number of the front, $SL_f := \zeta V_f R/k_b$. In the reference frame of the front, the Doppler-shifted axial position and frequency are denoted with a '†' accent, and are respectively given by

$$z_\dagger^* = z^* - SL_f\, t^* \qquad \text{and} \qquad \omega_\dagger^* = \omega^* - SL_f\, q^* \,. \tag{181}$$

[‡]Dee and Langer, "Propagating pattern selection".

[†]E. Ben-Jacob et al. "Pattern propagation in nonlinear dissipative systems". *Physica D* **14** (1985), 348–364.

[*]van Saarloos, "Front propagation into unstable states. II. Linear versus nonlinear marginal stability and rate of convergence".

A mode in our wave packet can then be expressed as [cf. Eq. (119)]

$$\begin{aligned}\exp\left\{i\left[q^*z^* - \omega^* t^*\right]\right\} &= \exp\left\{i\left[q^*\left(z^*_\dagger + SL_\mathrm{f}\, t^*\right) - \left(\omega^*_\dagger + SL_\mathrm{f}\, q^*\right)t^*\right]\right\} \\ &= \exp\left\{i\left[q^* z^*_\dagger - \omega^*_\dagger t^*\right]\right\}\,,\end{aligned} \tag{182}$$

for which the marginal stability criterion is expressed as

$$\omega^{*(i)}_\dagger = 0\,. \tag{183}$$

We additionally note that in the reference frame of the front, i.e. the frame in which the front is stationary, the edge of the wavepacket invading the unperturbed tube is traveling at zero group velocity—for which

$$\left.\frac{\mathrm{d}\omega^*_\dagger}{\mathrm{d}q^*}\right|_{q^*_\mathrm{f}} = 0\,, \qquad \text{thus requiring} \qquad \mathrm{Re}\left\{\left.\frac{\mathrm{d}\omega^*_\dagger}{\mathrm{d}q^*}\right|_{q^*_\mathrm{f}}\right\} = 0 \qquad \text{and} \qquad \mathrm{Im}\left\{\left.\frac{\mathrm{d}\omega^*_\dagger}{\mathrm{d}q^*}\right|_{q^*_\mathrm{f}}\right\} = 0\,. \tag{184}$$

In Eq. (184), q^*_f is the wavenumber associated with the front, which characterizes spatial oscillations at the point where the wavepacket invades the unperturbed tube.

With Eq. (183), the two conditions in Eq. (184), and the real and imaginary components of the dispersion relation $\omega^{*\dagger}_\mathrm{f} = \omega^*(q^*_\mathrm{f}) - SL_\mathrm{f}\, q^*_\mathrm{f}$ [see Eq. $(181)_2$], we have five equations which solve for the five unknowns $q^{*(r)}_\mathrm{f}$, $q^{*(i)}_\mathrm{f}$, $\omega^{*\dagger(r)}_\mathrm{f}$, $\omega^{*\dagger(i)}_\mathrm{f}$, and SL_f in terms of the Föppl–von Kármán number Γ. Note that when calculating $\omega^*(q^*_\mathrm{f})$ via the dispersion relation (133), the Scriven–Love number SL is in general not equal to the dimensionless front velocity SL_f. Interestingly, the system of equations under consideration is almost identical to those in the absolute versus convective analysis, in which the saddle point (q^*_0, ω^*_0) is replaced by $(q^*_\mathrm{f}, \omega^*_\mathrm{f})$—the one exception being that before, $\omega^*_0 = SL\, q^*_0 + i[\ldots]$ while now, $\omega^{*\dagger}_\mathrm{f} = (SL - SL_\mathrm{f})\, q^*_\mathrm{f} + i[\ldots]$ [cf. Eqs. (133), (181)]. In this case, the front wavenumber q^*_f is nearly identical to the absolute wavenumber q^*_0, with one important difference. In particular, as discussed below Eq. (153), we limited physically meaningful absolute wavenumbers to those with negative imaginary components, such that our spatial ansatz grew downstream, in the direction of the base flow. In this case, however, fronts can propagate in either direction (regardless of the base flow direction), so we place no restrictions on the sign of $q^{*(i)}_\mathrm{f}$. Accordingly, the real and imaginary components of the front wavenumber are given by (cf. Table 5)

$$\begin{cases} q^{*(r)}_\mathrm{f} = 0 \\ q^{*(i)}_\mathrm{f} = \dfrac{\pm 1}{2\sqrt{3}}\sqrt{4\Gamma - 1 + g(\Gamma)} \end{cases} \qquad \text{when} \qquad \Gamma \in \Omega_\mathrm{A} \tag{185}$$

and

$$\begin{cases} q^{*(r)}_\mathrm{f} = \pm\dfrac{1}{4}\sqrt{-12\Gamma + 3 + g(\Gamma)} \\ q^{*(i)}_\mathrm{f} = \dfrac{\pm 1}{4\sqrt{3}}\sqrt{4\Gamma - 1 + g(\Gamma)} \end{cases} \qquad \text{when} \qquad \Gamma \in \Omega_\mathrm{B}\,, \tag{186}$$

where $g(\Gamma)$ is defined in Table 5. As can be seen from Eq. (141) in the saddle point analysis, the '$\pm$' prefactor of $q^{*(i)}_\mathrm{f}$ in Eqs. (185) and (186) leads to the result $SL - SL_\mathrm{f} = \pm SL_\mathrm{ac}$. The

leading and trailing dimensionless front velocities, SL_f^+ and SL_f^-, are then respectively given by

$$SL_\mathrm{f}^+ = SL + SL_\mathrm{ac} \qquad \text{and} \qquad SL_\mathrm{f}^- = SL - SL_\mathrm{ac} \,, \tag{187}$$

where SL_ac is provided in Table 5 for all values of $\Gamma > \Gamma_\mathrm{c}$.

Equation (187) presents several useful predictions of the linear theory. First, Eq. (187) is consistent with our observations from Fig. 12: the velocity of the trailing front determines if the system is (i) absolutely unstable, with $SL_\mathrm{f}^- < 0$, (ii) convectively unstable, with $SL_\mathrm{f}^- > 0$, or (iii) at the absolute-to-convective transition, with $SL_\mathrm{f}^- = 0$. Next, Eq. (187) predicts that $SL_\mathrm{ac}(\Gamma)$ is the front propagation speed when there is no base flow, i.e. for which $SL = 0$. Additionally, Eqs. (185)–(187) confirm the connection [‡, †] between the marginal stability criterion and absolute-to-convective transition. In particular, the saddle point bifurcations in Fig. 11 also represent transitions in the dynamics of the propagating fronts. Specifically, when $\Gamma \in [\Gamma_\mathrm{c}, \Gamma_1] \cup [\Gamma_2, \infty)$, then $q_\mathrm{f}^{*(r)} = 0$, $\omega_\mathrm{f}^{*(r)} = 0$, and the front evolves as a steadily traveling envelope. In contrast, when $\Gamma \in (\Gamma_1, \Gamma_2)$, $q_\mathrm{f}^{*(r)} \neq 0$ and $\omega_\mathrm{f}^{*(r)} \neq 0$—for which the front oscillates in both time and space, and a pattern is selected in the wake of the front. We thus find the Föppl–von Kármán number governs whether or not a pattern is selected as the front propagates.

(g). The understanding of Γ_1 and Γ_2 as Lifshitz points

Results from our application of the marginal stability criterion to unstable membrane tubes are captured by Eqs. (185)–(187), which highlight the importance of the two particular values, Γ_1 and Γ_2, of the Föppl–von Kármán number. The predicted bifurcations in the wavenumber of the emerging state are reminiscent of the so-called Lifshitz points first introduced in the context of phase transitions, [*, §] at which the lowest-order gradient term in the free energy vanishes. Lifshitz points also arise in the study of extended Fisher–Kolmogorov equations—well-studied in the front propagation literature and known to possess several universal properties. For a scalar field $\phi \in \mathbb{R}$ and constant real parameter γ, one such equation can be written as

$$\phi_{,t} = \phi_{,xx} - \gamma\,\phi_{,xxxx} + \phi - \phi^3 \,. \tag{188}$$

Moreover, a field ϕ evolving according to Eq. (188) is known to undergo steady-to-oscillatory bifurcations in the front dynamics at the universal value of $\gamma = \gamma_\mathrm{c} = \frac{1}{12}$. [♯, ‖] This particular value of γ can be understood as a Lifshitz point, where the q^2 term in the dispersion relation

[‡] W. van Saarloos. "Front Propagation into Unstable States: Some Recent Developments and Surprises". *Nonlinear Evolution of Spatio-Temporal Structures in Dissipative Continuous Systems*. Ed. by F.H. Busse and L. Kramer. Boston: Springer US, 1990, pp. 499–508.

[†] J.-M. Chomaz and A. Couairon. "Propagating pattern selection and causality reconsidered". *Phys. Rev. Lett.* **84** (2000), 1910–1913.

[*] R.M. Hornreich, M. Luban, and S. Shtrikman. "Critical behavior at the onset of $\vec{k}$-instability on the λ-line". *Phys. Rev. Lett.* **35** (1975), 1678–1681.

[§] L. Kramer et al. "New results on the electrohydrodynamic instability in nematics". *Liq. Cryst.* **5** (1989), 699–715.

[♯] Dee and van Saarloos, "Bistable systems with propagating fronts leading to pattern formation".

[‖] M.C. Cross and P.C. Hohenberg. "Pattern formation outside of equilibrium". *Rev. Mod. Phys.* **65** (1993), 851–1112.

vanishes at the saddle point, [‡] and for which higher order gradients are required for an appropriate description of the system. [†]

In the case of lipid membrane tubes, we investigate the nature of $\mathit{\Gamma}_1$ and $\mathit{\Gamma}_2$ by first recalling that at long times, the dispersion relation in the reference frame of the front can be approximated by

$$\omega_\dagger^* \approx \omega_{\mathrm{f}}^{*\dagger} + \frac{1}{2}\frac{\mathrm{d}^2\omega_\dagger^*}{\mathrm{d}(q_{\mathrm{f}}^*)^2}\bigg|_{q_{\mathrm{f}}^*}\left(q^* - q_{\mathrm{f}}^*\right)^2 , \tag{189}$$

where $\omega_{\mathrm{f}}^{*\dagger} := \omega_\dagger^*(q_{\mathrm{f}}^*)$ and $(\mathrm{d}\omega_\dagger^*/\mathrm{d}q^*)|_{q_{\mathrm{f}}^*} = 0$ from Eq. (184). In what follows, we show that when $\mathit{\Gamma} = \mathit{\Gamma}_1$ and $\mathit{\Gamma} = \mathit{\Gamma}_2$, the right hand side of this approximation vanishes—which demonstrates that $\mathit{\Gamma}_1$ and $\mathit{\Gamma}_2$ are Lifshitz points. To this end, recall that by definition, $\omega_{\mathrm{f}}^{*\dagger} = \omega_{\mathrm{f}}^{*\dagger(r)}$ according to the marginal stability criterion (183), and thus

$$\omega_{\mathrm{f}}^{*\dagger}(\mathit{\Gamma}_1) = \omega_{\mathrm{f}}^{*\dagger}(\mathit{\Gamma}_2) = 0 . \tag{190}$$

Next, we recognize that Eq. $(181)_2$ implies $\mathrm{d}^2\omega_\dagger^*/\mathrm{d}q_*^2 = \mathrm{d}^2\omega^*/\mathrm{d}q_*^2$; by differentiating the dispersion relation Eq. (133) twice, we obtain

$$\frac{\mathrm{d}^2\omega_\dagger^*}{\mathrm{d}q_*^2}\bigg|_{q_{\mathrm{f}}^*} = -\frac{i}{8}\left(4\mathit{\Gamma} - 1 + 12(q_{\mathrm{f}}^*)^2\right) . \tag{191}$$

To calculate the front wavenumber q_{f}^*, we note that Ω_{A} and Ω_{B} coincide at $\mathit{\Gamma} = \mathit{\Gamma}_1$ and $\mathit{\Gamma} = \mathit{\Gamma}_2$, and the front wavenumber coincides at these values of the Föppl–von Kármán number as well. We find that in Ω_{A}, where $g(\mathit{\Gamma}) = -\sqrt{16\mathit{\Gamma}^2 - 104\mathit{\Gamma} + 73}$, $g(\mathit{\Gamma}_1) = g(\mathit{\Gamma}_2) = 0$; consequently, Eq. (185) simplifies to $q_{\mathrm{f}}^* = i\sqrt{(4\mathit{\Gamma} - 1)/12}$ at $\mathit{\Gamma}_1$ and $\mathit{\Gamma}_2$. Substituting this result into Eq. (191) yields

$$\frac{\mathrm{d}^2\omega_\dagger^*}{\mathrm{d}q_*^2}\bigg|_{q_{\mathrm{f}}^*} = -\frac{i}{8}\left(4\mathit{\Gamma} - 1 - 12\left(q_{\mathrm{f}}^{*(i)}\right)^2\right) = 0 \qquad \text{at} \quad \mathit{\Gamma} = \mathit{\Gamma}_1 \ \text{ and } \ \mathit{\Gamma} = \mathit{\Gamma}_2 . \tag{192}$$

With Eqs. (189), (190), and (192), we find that at $\mathit{\Gamma} = \mathit{\Gamma}_1$ and $\mathit{\Gamma} = \mathit{\Gamma}_2$, the usual long-time approximation of the dispersion relation is insufficient. Accordingly, $\mathit{\Gamma}_1$ and $\mathit{\Gamma}_2$ are identified as Lifshitz points, for which the expansion in Eq. (189) needs to be supplemented with higher order terms for a correct first approximation of the front dynamics. We thus find

$$\omega_\dagger^* \approx \frac{1}{6}\frac{\mathrm{d}^3\omega_\dagger^*}{\mathrm{d}q_{\mathrm{f}}^3}\bigg|_{q_{\mathrm{f}}^*}\left(q^* - q_{\mathrm{f}}^*\right)^3 = -\frac{i}{2}\,q_{\mathrm{f}}^*\left(q^* - q_{\mathrm{f}}^*\right)^3 \qquad \text{at} \quad \mathit{\Gamma} = \mathit{\Gamma}_1 \ \text{ and } \ \mathit{\Gamma} = \mathit{\Gamma}_2 . \tag{193}$$

Our finding that $\mathit{\Gamma}_1$ and $\mathit{\Gamma}_2$ are Lifshitz points is consistent with prior investigations of front propagation in the extended Fisher–Kolmogorov equation. In particular, we realize the rescaled membrane evolution equation (180) can be mapped to Eq. (188) by defining

$$\gamma(\mathit{\Gamma}) = \frac{\mathit{\Gamma} - \mathit{\Gamma}_{\mathrm{c}}}{(\mathit{\Gamma} - \mathit{\Gamma}_0)^2} , \tag{194}$$

[‡] W. Zimmermann. "Propagating fronts near a Lifshitz point". *Phys. Rev. Lett.* **66** (1991), 1546–1546.

[†] Hornreich, Luban, and Shtrikman, "Critical behavior at the onset of $\vec{k}$-instability on the λ-line".

for which $\gamma(\Gamma_1) = \gamma(\Gamma_2) = \frac{1}{12}$. Accordingly, both Γ_1 and Γ_2 correspond to the previously obtained critical value of $\gamma_c = \frac{1}{12}$.

To understand how two bifurcation points arise in the dynamics of unstable membrane tubes, such that fronts are oscillatory when $\Gamma \in (\Gamma_1, \Gamma_2)$ and monotonic otherwise, we investigate the linearized evolution equation in terms of rescaled variables (180). First, consider a tube with no base flow ($SL = 0$) and vanishing bending modulus—such that $k_b \to 0$, and $\Gamma \to \infty$. In this case, the fourth-order term in Eq. (180) is negligible. The resultant equation is known as the linearized Fisher–Kolmogorov equation, and has a dispersion relation of the form $\omega^* \sim i(1 - q_*^2)$ for the ansatz $\tilde{r}^* \sim \exp[i(q^* Z - \omega^* T)]$. If we decompose q^* into real and imaginary parts, then the ansatz can be expressed as $\tilde{r}^* \sim \exp(-q_*^{(i)} Z) \exp[i(q_*^{(r)} Z - \omega^* T)]$, for which $q_*^{(r)}$ captures spatial oscillations while $q_*^{(i)}$ describes an exponentially decaying envelope—for example, that at the leading edge of the front. The dispersion relation is then given by $\omega^* \sim i[1 + (q_*^{(i)})^2 - (q_*^{(r)})^2] + 2q_*^{(r)} q_*^{(i)}$, from which we see that $\omega_*^{(i)}$ is maximized if $q_*^{(r)} \to 0$. Accordingly, in the absence of bending terms, the growth rate is maximal when there is no spatial modulation, i.e. the front is monotonic.

Since we expect a monotonic front will dominate the long-time dynamics of the linearized Fisher–Kolmogorov equation when $\gamma(\Gamma) = 0$, the oscillations in the front dynamics of a membrane tube must arise from the fourth-order bending term in Eq. (180). One could in principle see this by once again examining the imaginary component of the frequency, but a more straightforward approach involves assuming the ansatz $\tilde{r}^* \sim \sin(q_*^{(r)} Z) \exp[-q_*^{(i)} Z - i\omega^* T]$—which once again involves an exponentially damped sinusoidal function in space, as we would expect at the leading edge of the front. If we also posit that $q_*^{(r)} = q_*^{(i)}$ for the simplicity of our argument, then $\partial^4 \tilde{r}^* / \partial Z^4 \sim -\tilde{r}^*$. The linearized evolution equation (180)

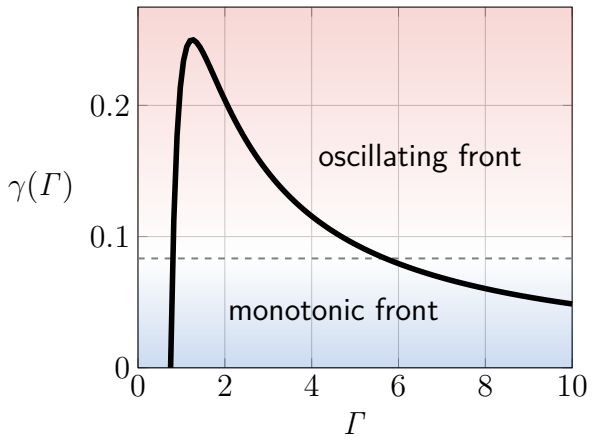

Figure 13: Plot of the coefficient γ, defined in Eq. (194), as a function of the Föppl–von Kármán number Γ. The rescaled evolution equation (180) shows γ captures the importance of the fourth-order bending forces. At large Γ, bending forces are dominated by tension forces, and γ is small. At intermediate Γ, bending forces are more relevant, and γ crosses the critical value of $\gamma_c = \frac{1}{12}$ (dashed gray line) above which fronts pearl. While bending forces continue to be more relevant as $\Gamma \to \Gamma_c^+$, only the longest wavelength modes are unstable; the bending forces of these unstable modes decreases. Accordingly, γ decreases as Γ approaches the instability threshold. Note γ intersects γ_c at $\Gamma = \Gamma_1$ and $\Gamma = \Gamma_2$.

can then be written as $\partial\tilde{r}^*/\partial T \sim (1+\gamma)\tilde{r}^* + \partial^2\tilde{r}^*/\partial Z^2$, from which we find the fourth-order derivative in fact tends to *favor* unstable oscillations in space. This result will be confirmed in our nonlinear analysis in §8, where spatial oscillations at the leading edge of the front eventually grow and saturate to yield a pearled morphology.

Returning to our original question of why two bifurcation points arise, let us begin with a membrane tube with $k_\mathrm{b} \approx 0$, $\Gamma \to \infty$, and $\gamma \approx 0$. In this case, the fourth-order term in the evolution equations is negligible, and the front is monotonic. If we imagine steadily increasing the bending modulus, however, then Γ will decrease and γ will increase (see Fig. 13). As we continue to increase k_b and decrease Γ, Γ_2 marks the first point where bending forces are large enough to favor an oscillating front. As the bending modulus is further increased and Γ approaches Γ_c, however, the marginally stable wavenumber q^*_ms diverges [see §7 (d)]. In this case, the modes that are unstable have progressively longer wavelengths, and the bending cost of such modes commensurately decreases. Thus, Γ_1 indicates where the fourth-order bending terms become negligible once again, and we find the competition between bending forces and long-wavelength oscillations is captured by $\gamma(\Gamma)$—as defined in Eq. (194) and shown in Fig. 13.

8. The nonlinear dynamics

Thus far, our temporal and spatiotemporal linear stability analysis focused entirely on the linearized governing equations. Within the linear theory, we found (*i*) initially localized perturbations to unstable tubes grow and invade the undeformed region via propagating fronts (see Fig. 12), (*ii*) the front speed is captured by the marginal stability criterion, and (*iii*) the value of the Föppl–von Kármán number dictates whether or not spatial oscillations are favored at the leading edge of the front. However, by definition, our linear analysis does not include nonlinear saturating effects—which, in experimental systems, would eventually dominate the unstable behavior.

In this section, we investigate the nonlinear dynamics of lipid membrane tubes via simulations under axisymmetric conditions. Furthermore, to better understand the physical mechanisms that arise when shape deformations become large and nonlinear effects dominate the dynamics, we develop a weakly nonlinear model for membrane tubes. In particular, we extend Eq. (180) by starting from the general governing equations, considering only axisymmetric deformations, and retaining some of the nonlinear terms. The resultant nonlinear evolution equation is useful in that it (*i*) provides a simplified physical understanding of nonlinearities in the system, and (*ii*) is straightforward to solve numerically. The robustness of our weakly nonlinear model is tested by comparing its predictions to results from fully nonlinear simulations. We find that both the fully and weakly nonlinear simulations predict the formation of a thin, atrophied tube once the shape change saturates, and both types of simulations exhibit an absolute-to-convective transition at the base flow speed $\mathcal{SL}_\mathrm{ac}(\Gamma)$ predicted by the linear theory. Unfortunately, the weakly nonlinear evolution equation is not able to capture the behavior of the oscillating fronts that arise when $\Gamma \in (\Gamma_1, \Gamma_2)$. The fully nonlinear simulations, on the other hand, reveal how a pearled morphology emerges to connect the atrophied and unperturbed cylindrical regions when $\Gamma \in (\Gamma_1, \Gamma_2)$—while no pearling occurs when Γ is outside this range.

(a). The nonlinear axisymmetric governing equations

We now return to the general governing equations presented in Chapter VI, §1. Though it is possible to develop general numerical methods to solve for the membrane dynamics, [‡, †] such implementations would be computationally expensive given that we are only interested in axisymmetric disturbances. In what follows, we represent the axisymmetric membrane surface as a curve in the r–z plane, and then provide two different surface parametrizations. As we will see subsequently, these surface representations allow us to implement nonlinear simulations and develop a nonlinear extension of the evolution equation.

The area parametrization

As shown in Fig. 14, we denote the z-axis to be the axis of rotational symmetry, and r to be the distance from the z-axis. Any axisymmetric surface can then be described as a curve in the r–z plane. Just as a curve can be parametrized by its arc length, here we parametrize an axisymmetric membrane surface by its area a—as motivated by prior investigations. [*, §] With rotational symmetry about the z-axis, we have

$$\mathrm{d}a \;=\; 2\pi r\sqrt{\mathrm{d}r^2 \,+\, \mathrm{d}z^2}\;, \tag{195}$$

such that we can define an angle φ satisfying

$$\frac{\mathrm{d}r}{\mathrm{d}a} \;=\; \frac{\cos\varphi}{2\pi r} \qquad \text{and} \qquad \frac{\mathrm{d}z}{\mathrm{d}a} \;=\; \frac{\sin\varphi}{2\pi r}\;, \tag{196}$$

as depicted in Fig. 14b. We parametrize the surface position as

$$\boldsymbol{x}(\theta, a, t) \;=\; r(a,t)\,\boldsymbol{e}_r(\theta) \,+\, z(a,t)\,\boldsymbol{e}_z\;, \tag{197}$$

and calculate the basis vectors to be given by

$$\boldsymbol{a}_1 \;=\; r\,\boldsymbol{e}_\theta\;, \qquad \boldsymbol{a}_2 \;=\; \frac{\cos\varphi}{2\pi r}\,\boldsymbol{e}_r \,+\, \frac{\sin\varphi}{2\pi r}\,\boldsymbol{e}_z\;, \qquad \text{and} \qquad \boldsymbol{n} \;=\; \sin\varphi\,\boldsymbol{e}_r \,-\, \cos\varphi\,\boldsymbol{e}_z\;, \tag{198}$$

where the basis vectors $\boldsymbol{a}_1$ and $\boldsymbol{a}_2$ were chosen such that the unit normal $\boldsymbol{n}$ points outwards. We next calculate the metric and curvature tensors as

$$a_{\alpha\beta} \;=\; \mathrm{diag}\Big(r^2,\, (2\pi r)^{-2}\Big) \qquad \text{and} \qquad b_{\alpha\beta} \;=\; -\,\mathrm{diag}\Big(r\sin\varphi,\, \varphi'/(2\pi r)\Big)\;. \tag{199}$$

In Eq. (199) and from now on, we use the notation $(\,\cdot\,)' := (\,\cdot\,)_{,a}$ to denote partial differentiation with respect to the area coordinate a; as we assume axisymmetry, the partial derivative

[‡] Sahu et al., "Arbitrary Lagrangian–Eulerian finite element formulation for curved and deforming surfaces. I. General theory and application to fluid interfaces".

[†] A. Torres-Sánchez, D. Millán, and M. Arroyo. "Modelling fluid deformable surfaces with an emphasis on biological interfaces". *J. Fluid Mech.* **872** (2019), 218–271. arXiv: 1812.02837.

[*] A. Agrawal and D.J. Steigmann. "Modeling protein-mediated morphology in biomembranes". *Biomech. Model. Mechan.* **8** (2009), 371–379.

[§] Y.A.D. Omar et al. "Non-axisymmetric shapes of biological membranes from locally induced curvature". *Biophys. J.* **119** (2020), 1065–1077.

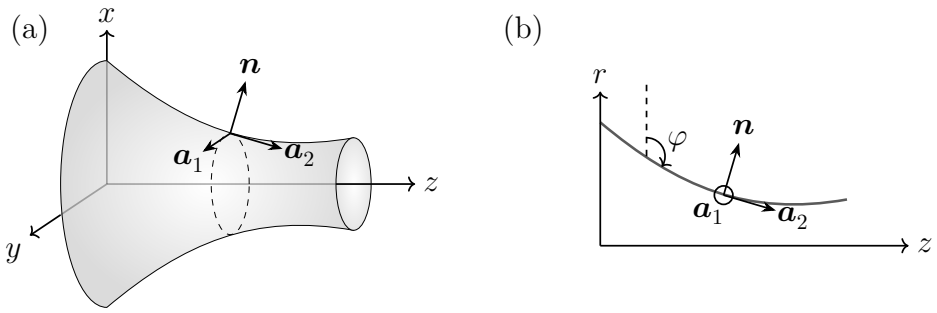

Figure 14: Schematic of an axisymmetric surface of revolution (a), and its representation as a curve in the r–z plane (b). In both cases, the basis vectors $\boldsymbol{a}_1$, $\boldsymbol{a}_2$, and $\boldsymbol{n}$ are shown. The angle φ depicted in (b) is introduced for notational and computational convenience.

of any quantity with respect to θ is zero. With the metric and curvature components, we calculate the mean and Gaussian curvature as

$$H \,=\, -\frac{1}{2}\left(2\pi r\,\varphi' \,+\, \frac{1}{r}\sin\varphi\right) \qquad \text{and} \qquad K \,=\, 2\pi\sin\varphi\,\varphi' \,. \tag{200}$$

Finally, the nonzero Christoffel symbols are found to be

$$\Gamma^2_{11} \,=\, -2\pi r^2\cos\varphi \,, \qquad \Gamma^1_{21} \,=\, \Gamma^1_{12} \,=\, \frac{\cos\varphi}{2\pi r^2} \,, \qquad \text{and} \qquad \Gamma^2_{22} \,=\, -\frac{\cos\varphi}{2\pi r^2} \,. \tag{201}$$

At this point, we substitute the geometric quantities obtained in Eqs. (195)–(201) into the general governing equations in Chapter VI, §1. We denote $u := \boldsymbol{v}\cdot\boldsymbol{a}^2 = v^2$ to be the in-plane velocity for notational convenience, and recognize the out-of-plane velocity $v = \boldsymbol{v}\cdot\boldsymbol{n}$ is given by

$$v \,=\, \sin\varphi\, r_{,t} \,-\, \cos\varphi\, z_{,t} \,. \tag{202}$$

The continuity, in-plane, and shape equations are then respectively given by

$$u' \,-\, 2vH \,=\, 0 \,, \tag{203}$$

$$\zeta\sin\varphi\left(\frac{\varphi' u}{\pi r^2} \,-\, \frac{2}{r}\,v'\right) \,+\, \lambda' \,=\, 0 \,, \tag{204}$$

and

$$\begin{aligned}[\![p]\!] \,+\, 2\lambda H \,-\, 2k_{\mathrm{b}}H\big(H^2-K\big) \,-\, k_{\mathrm{b}}\Big(4\pi\cos\varphi\,H' + 4\pi^2 r^2 H''\Big) \\ +\, 2\zeta\Big(-4\pi r v\varphi' H \,+\, \varphi'\, r^{-1}\, u\,\cos\varphi \,-\, \sin\varphi\cos\varphi\,(2\pi r^3)^{-1}\,u \,-\, 2v\big(2H^2-K\big)\Big) \,=\, 0 \,,\end{aligned} \tag{205}$$

where the continuity equation (203) was used to simplify both the in-plane (204) and shape (205) equations. By defining the quantity

$$\mathcal{L} \,:=\, k_{\mathrm{b}}\, 2\pi r^2\, H' \tag{206}$$

such that the fourth term in Eq. (205) can be written as $-2\pi\mathcal{L}'$, and also introducing an auxiliary variable for the in-plane velocity gradient

$$w \,:=\, u' \,, \tag{207}$$

the three governing equations (203)–(205) can be written as a system of eight first-order ordinary differential equations, given by [‡]

$$r' \;=\; \frac{\cos\varphi}{2\pi r}\;, \tag{208}$$

$$z' \;=\; \frac{\sin\varphi}{2\pi r}\;, \tag{209}$$

$$\varphi' \;=\; \frac{-1}{2\pi r}\Big(2H \;+\; \frac{1}{r}\,\sin\varphi\Big)\;, \tag{210}$$

$$H' \;=\; \frac{\mathcal{L}}{2\pi r^2\,k_\mathrm{b}}\;, \tag{211}$$

$$\mathcal{L}' \;=\; \frac{1}{2\pi}\Big([\![p]\!] \;+\; 2\lambda H \;-\; 2k_\mathrm{b}H\big(H^2-K\big) \;+\; \pi^{\alpha\beta}\,b_{\alpha\beta}\Big)\;, \tag{212}$$

$$\lambda' \;=\; \zeta\sin\varphi\left(\frac{2}{r}\,v' \;-\; \frac{\varphi' u}{\pi r^2}\right)\;, \tag{213}$$

$$u' \;=\; w\;, \tag{214}$$

and

$$w' \;=\; 2v'H \;+\; 2vH'\;, \tag{215}$$

where the $\pi^{\alpha\beta}b_{\alpha\beta}$ term in Eq. (212) is given by the second line of Eq. (205). We note that while the additional unknown w is not required to pose the governing equations as a system of first-order ordinary differential equations, it is useful when solving the system of equations numerically.

The axial distance parametrization

While the area parametrization can describe axisymmetric surfaces of arbitrary geometry, it is also useful to consider an axisymmetric parametrization specialized to nearly cylindrical surfaces, given by

$$\boldsymbol{x}(\theta,z,t) \;=\; r(z,t)\,\boldsymbol{e}_r(\theta) \;+\; z\,\boldsymbol{e}_z\;, \tag{216}$$

where $\boldsymbol{e}_r$ and $\boldsymbol{e}_z$ are the usual orthonormal basis vectors in a cylindrical coordinate system. The surface parametrization in Eq. (216) is capable of describing nonlinear deformations that do not break a one-to-one mapping with the base cylindrical shape, and will be useful in subsequent analysis when we develop a weakly nonlinear model. Following the differential geometric surface description provided in Chapter II, we calculate the basis vectors as

$$\boldsymbol{a}_1 \;=\; r\,\boldsymbol{e}_\theta\;, \qquad \boldsymbol{a}_2 \;=\; r_{,z}\,\boldsymbol{e}_r \;+\; \boldsymbol{e}_z\;, \qquad \text{and} \qquad \boldsymbol{n} \;=\; (a_{22})^{-1/2}\big(\boldsymbol{e}_r \;-\; r_{,z}\,\boldsymbol{e}_z\big)\;, \tag{217}$$

where $a_{22} = \boldsymbol{a}_2\cdot\boldsymbol{a}_2 = 1 + r_{,z}^2$ is the (z,z) component of the metric tensor, and is introduced for notational convenience. The metric and curvature tensors are given by

$$a_{\alpha\beta} \;=\; \mathrm{diag}\big(r^2,\; 1 \;+\; r_{,z}^2\big) \qquad \text{and} \qquad b_{\alpha\beta} \;=\; (a_{22})^{-1/2}\,\mathrm{diag}\big(-r\,,\; r_{,zz}\big)\;, \tag{218}$$

[‡]Omar et al., "Non-axisymmetric shapes of biological membranes from locally induced curvature".

with which we calculate the mean and Gaussian curvatures, respectively, as

$$H = \frac{-1}{2r\,(a_{22})^{1/2}}\left(1 - (a_{22})^{-1}\,r_{,zz}\,r\right) \qquad \text{and} \qquad K = \frac{-r_{,zz}}{r\,(a_{22})^2}\,. \tag{219}$$

Finally, the nonzero Christoffel symbols are found to be

$$\Gamma^1_{12} = \Gamma^1_{21} = \frac{r_{,z}}{r}\,, \qquad \Gamma^2_{11} = -(a_{22})^{-1}\,r_{,z}\,r\,, \qquad \text{and} \qquad \Gamma^2_{22} = (a_{22})^{-1}\,r_{,z}\,r_{,zz}\,. \tag{220}$$

By substituting Eqs. (217)–(220) into the general governing equations [Chapter VI, Eqs. (4)–(6)], and after much algebra, we obtain the continuity, in-plane z, and shape equations respectively as

$$v^2_{,z} + v^2\,r_{,z}\left(\frac{1}{r} + \frac{r_{,zz}}{1+r^2_{,z}}\right) + \frac{r_{,t}}{r\big(1+r^2_{,z}\big)}\left(1 - \frac{r_{,zz}\,r}{1+r^2_{,z}}\right) = 0\,, \tag{221}$$

$$\frac{2\zeta}{r}\left(\frac{r_{,t}\,r_{,z}\,r_{,zz}}{1+r^2_{,z}} - r_{,zz}\,v^2 - r_{,zt}\right) + \big(1 + r^2_{,z}\big)\,\lambda_{,z} = 0\,, \tag{222}$$

and

$$\begin{aligned}[\![p]\!] + 2\lambda H - 2k_{\mathrm{b}}H\big(H^2 - K\big) - \frac{k_{\mathrm{b}}}{r\,(1+r^2_{,z})^{1/2}}\cdot\frac{\partial}{\partial z}\left(\frac{r}{(1+r^2_{,z})^{1/2}}\,\frac{\partial H}{\partial z}\right) \\ - 2\zeta\left(\frac{r_{,t}}{r^2(1+r^2_{,z})^{3/2}} + \frac{r_{,t}\,r_{,zz}}{r(1+r^2_{,z})^{5/2}} - \frac{v^2 r_{,z}}{r^2(1+r^2_{,z})^{1/2}} + \frac{v^2 r_{,z} r_{,zz}}{r(1+r^2_{,z})^{3/2}}\right) = 0\,.\end{aligned} \tag{223}$$

We note that here, as before, the in-plane velocity component v^2 is defined as $v^2 = \boldsymbol{v}\cdot\boldsymbol{a}^2$, where in this case $\boldsymbol{a}^2 = (r_{,z}\,\boldsymbol{e}_r + \boldsymbol{e}_z)/(1+r^2_{,z})$ [cf. Eqs. (217) and (218)].

(b). The weakly nonlinear analysis

We are now prepared to begin our investigation of nonlinear effects in the dynamics of lipid membrane tubes. Here we derive a weakly nonlinear model by retaining some, but not all, nonlinearities of the general governing equations. In particular, we keep nonlinear terms that are algebraic in the perturbed radius, but neglect terms involving products of derivatives, as will be described in detail below. With this assumption, we first substitute the geometry and kinematics of the axisymmetric, axial distance parametrization into the general governing equations, and then condense the results into a single weakly nonlinear evolution equation for the membrane shape.

To begin, for an axisymmetric lipid membrane in one-to-one correspondence with an unperturbed cylinder and parametrized as in Eq. (216), membrane dynamics are governed by Eqs. (221)–(223). While the general equations are too complex to be treated analytically, we now seek a description which both maintains some of the nonlinearities and is also analytically tractable. To this end, we simplify the problem by assuming the perturbed shape

is weakly varying, such that derivatives of r are small. Defining $\partial_z^j r := \partial^j r/\partial z^j$, we express our assumption mathematically as

$$\partial_z^j r * \partial_z^k r \quad \text{is} \quad \begin{cases} \text{negligible if } j \geq 1 \text{ and } k \geq 1 \\ \text{non-negligible otherwise} \end{cases} . \tag{224}$$

We additionally assume that spatial gradients of the membrane shape are weakly coupled to its temporal evolution, for which

$$r_{,t} * \partial_z^j r \quad \text{is} \quad \begin{cases} \text{negligible if } j \geq 1 \\ \text{non-negligible otherwise} \end{cases} . \tag{225}$$

With Eq. (224), our previously calculated expression for $a_{22} = 1 + r_{,z}^2$ in Eq. (218) simplifies to unity. The mean curvature, Gaussian curvature, and nonzero Christoffel symbols are then given by [cf. Eqs. (219) and (220)]

$$\begin{aligned} H &= -\frac{1}{2r}\left(1 - r\, r_{,zz}\right) , & K &= -\frac{r_{,zz}}{r} , \\ \Gamma^1_{12} &= \Gamma^1_{21} = \frac{r_{,z}}{r} , \qquad \text{and} & \Gamma^2_{11} &= -r r_{,z} . \end{aligned} \tag{226}$$

By substituting Eq. (226) into Eqs. (221)–(223) and applying the weakly nonlinear assumptions in Eqs. (224) and (225), we obtain the governing equations

$$r v_{,z}^2 + r_{,z} v^2 + r_{,t} = 0 , \tag{227}$$

$$-2\zeta\left(r_{,zt} + v^2 r_{,zz}\right) + r\lambda_{,z} = 0 , \tag{228}$$

and

$$[\![p]\!] + \lambda\left(r_{,zz} - \frac{1}{r}\right) + 2\zeta\left(v_{,z}^2 r_{,zz} - \frac{v^2 r_{,z}}{r^2} - \frac{r_{,t}}{r^2}\right) - k_{\mathrm{b}}\left(\frac{-1}{4r^3} + \frac{r_{,zz}}{4r^2} + \frac{1}{2} r_{,zzzz}\right) = 0 , \tag{229}$$

where the continuity equation (227) was used to simplify the shape equation (229).

While Eqs. (227)–(229) constitute three equations for the three unknowns v^2, λ, and r, we have not yet commented on the magnitude of the in-plane velocity or surface tension. To this end, we expand both quantities as

$$v^2(z,t) = v_{(0)}^2 + v_{(1)}^2(z,t) \qquad \text{and} \qquad \lambda(z,t) = \lambda_{(0)} + \lambda_{(1)}(z,t) , \tag{230}$$

where $v_{(0)}^2$ and $\lambda_{(0)}$ are assumed to be constant quantities. In Eq. (230), we do not introduce the small parameter ϵ, and therefore employ a different notation from that in the linearized theory in §2. We now make the two additional assumptions that

$$v_{(1)}^2 * \partial_z^j r \qquad \text{and} \qquad \lambda_{(1)} * \partial_z^j r \quad \text{are} \quad \begin{cases} \text{negligible if } j \geq 1 \\ \text{non-negligible otherwise} , \end{cases} \tag{231}$$

in a manner consistent with our previous assumptions (224, 225). With Eqs. (230) and (231), the in-plane equation (228) becomes

$$-2\zeta\left(r_{,zt} + v_{(0)}^2\, r_{,zz}\right) + r\,\lambda_{(1),z} = 0\,. \tag{232}$$

We simplify the second term in Eq. (232) by recognizing

$$r\,\lambda_{(1),z} = \left(r\,\lambda_{(1)}\right)_{,z} - r_{,z}\,\lambda_{(1)} \approx \left(r\,\lambda_{(1)}\right)_{,z}\,, \tag{233}$$

where Eq. (231) was used in the last step. Equation (232) can then be integrated in z to yield

$$-2\zeta\left(r_{,t} + v_{(0)}^2\, r_{,z}\right) + r\,\lambda_{(1)} = c(t)\,, \tag{234}$$

for some integration constant $c(t)$. However, we assume perturbed quantities go to zero as $z \to \infty$, such that $c(t) = 0$, in which case the perturbed surface tension is given by

$$\lambda_{(1)} = \frac{2\zeta}{r}\left(r_{,t} + v_{(0)}^2\, r_{,z}\right)\,. \tag{235}$$

According to Eq. (235), the perturbed surface tension can be calculated from the evolution of the membrane shape over time.

To obtain the perturbed shape equation, we first recognize the membrane equations describing the base state (12) require $[\![p]\!] = \lambda_{(0)}/R - k_\mathrm{b}/(4R^3)$, where R is once again the unperturbed cylinder radius. By substituting this expression for the pressure drop, as well as Eq. (235), into Eq. (229), simplifying with our assumptions in Eqs. (224) and (231), and rearranging terms, we obtain

$$\begin{aligned}&\frac{\zeta R}{k_\mathrm{b}}\, r_{,t} + \frac{\zeta v_{(0)}^2 R}{k_\mathrm{b}}\, r_{,z} \\ &\qquad = \frac{R^2\,\lambda_{(0)}}{4k_\mathrm{b}}\left(\frac{r^2}{R^2} - \frac{r}{R} + \frac{r^2\, r_{,zz}}{R}\right) - \frac{1}{16}\left(\frac{r^2}{R^2} - \frac{R}{r} + R\, r_{,zz} + 2r^2 R\, r_{,zzzz}\right)\,.\end{aligned} \tag{236}$$

Equation (236) is a single equation for the membrane shape r, and can easily be nondimensionalized with Eqs. (107)–(109) and the additional definition $r^* := r/R$, with which we obtain

$$r^*_{,t^*} + \mathit{SL}\, r^*_{,z^*} = \frac{\Gamma}{4}\left(r_*^2 - r^* + r_*^2 r^*_{,z^*z^*}\right) - \frac{1}{16}\left(r_*^2 - \frac{1}{r^*} + r^*_{,z^*z^*} + 2r_*^2 r^*_{,z^*z^*z^*z^*}\right)\,. \tag{237}$$

At this point, we seek to express algebraic quantities in Eq. (237) in term of $(r^* - 1)$, namely the dimensionless deviation from the base radius. To this end, we substitute $r_*^2 - r^* = (r^* - 1) + (r^* - 1)^2$ and $r_*^2 - 1/r^* = 3(r^* - 1) + (r^* - 1)^2 - (r^* - 1)^2/r^*$ into Eq. (237) and rearrange terms to obtain

$$\begin{aligned}r^*_{,t^*} + \mathit{SL}\, r^*_{,z^*} = {}& \left(\frac{\Gamma - \Gamma_0}{4}\right) r^*_{,z^*z^*} - \frac{1}{8}\, r^*_{,z^*z^*z^*z^*} + \left(\frac{\Gamma - \Gamma_\mathrm{c}}{4}\right)(r^* - 1) + \left(\frac{\Gamma - \Gamma_0}{4}\right)(r^* - 1)^2 \\ &+ \frac{1}{16}\,\frac{(r^* - 1)^2}{r^*} + \left[(r^* - 1)^2 + 2(r^* - 1)\right]\left(\frac{\Gamma}{4}\, r^*_{,z^*z^*} - \frac{1}{8}\, r^*_{,z^*z^*z^*z^*}\right)\,.\end{aligned} \tag{238}$$

Finally, we once again assume the membrane shape is weakly varying, such that $(r^*-1)^j * \partial_{z^*}^k r^*$ is negligible relative to $(r^*-1)^j$ for $k \geq 1$. In this case, Eq. (238) simplifies to

$$r^*_{,t^*} + \mathit{SL}\, r^*_{,z^*} = \left(\frac{\mathit{\Gamma}-\mathit{\Gamma}_0}{4}\right) r^*_{,z^*z^*} - \frac{1}{8}\, r^*_{,z^*z^*z^*z^*} + \left(\frac{\mathit{\Gamma}-\mathit{\Gamma}_c}{4}\right)(r^*-1) + \left(\frac{\mathit{\Gamma}-\mathit{\Gamma}_0}{4}\right)(r^*-1)^2 + \frac{1}{16}\,\frac{(r^*-1)^2}{r^*}\,, \tag{239}$$

which is a single equation for the shape evolution of a perturbed membrane tube. As expected, Eq. (239) simplifies to Eq. (118) when we recognize $\epsilon\tilde{r}^* = r^*-1$ and neglect nonlinear terms.

While Eq. (239) is indeed a single nonlinear equation for the dynamics of a perturbed lipid membrane tube, solving the equation numerically presents the same difficulties as those from the linearized case [see discussion in §7 (e)]. We thus make the change of variables in Eqs. (178) and (179), for which Eq. (239) can be written as

$$r^*_{,T} + \overline{\mathit{SL}}\, r^*_{,Z} = r^*_{,ZZ} - \frac{1}{2}\,\frac{(\mathit{\Gamma}-\mathit{\Gamma}_c)}{(\mathit{\Gamma}-\mathit{\Gamma}_0)^2}\, r^*_{,ZZZZ} + f(r^*)\,, \tag{240}$$

where the forcing term $f(r^*)$ is given by

$$f(r^*) = (r^*-1) + \left(\frac{\mathit{\Gamma}-\mathit{\Gamma}_0}{\mathit{\Gamma}-\mathit{\Gamma}_c}\right)(r^*-1)^2 + \left(\frac{\mathit{\Gamma}_0}{\mathit{\Gamma}-\mathit{\Gamma}_c}\right)\frac{(r^*-1)^2}{r^*}\,. \tag{241}$$

Equation (240) has the structure of an extended Fisher–Kolmogorov equation, with the forcing term $f(r^*)$ plotted for three values of $\mathit{\Gamma}$ in Fig. 15. Note that in the absence of temporal variations ($r^*_{,T} = 0$) and spatial gradients ($r^*_{,Z} = 0$), the evolution equation (240) simplifies to $f(r^*) = 0$. As shown in Figs. 15a and 15b, the slope of $f(r^*)$ at $r^* = 1$ is positive, implying the base solution is unstable. However, in all cases there exists another solution of $f(r^*) = 0$, which we denote the 'homogeneous radius' r^*_h, that is found to be given by

$$r^*_h = 1 + \frac{1}{8\mathit{\Gamma}-2}\left(3 - 8\mathit{\Gamma} + \sqrt{16\mathit{\Gamma}-3}\right). \tag{242}$$

As $f'(r^*_h) < 0$, a tube of radius r^*_h is stable. Figure 15c plots the homogeneous radius as a function of the Föppl–von Kármán number, and shows $0 < r^*_h < 1$ for all $\mathit{\Gamma} > \mathit{\Gamma}_c$. The evolution equation thus predicts that when fronts are propagating along the z-axis away from an initially localized perturbation, the thin tube that develops behind the front is of radius r^*_h. Moreover, the homogeneous radius tends to zero in the limit $\mathit{\Gamma} \to \infty$, i.e. for a fluid film with no bending modulus: a result consistent with our previous findings.[‡] However, while the nonlinear extended Fisher–Kolmogorov equation (240) provides a simplified description of the dynamics of lipid membrane tubes, it includes only weak nonlinearities and is expected to be quantitatively predictive only in limited regimes of mild tube deformations. We now proceed to test the validity of Eq. (240) by comparing its shape predictions to results from simulations of the full nonlinear equations.

[‡]Sahu et al., "Arbitrary Lagrangian–Eulerian finite element formulation for curved and deforming surfaces. I. General theory and application to fluid interfaces".

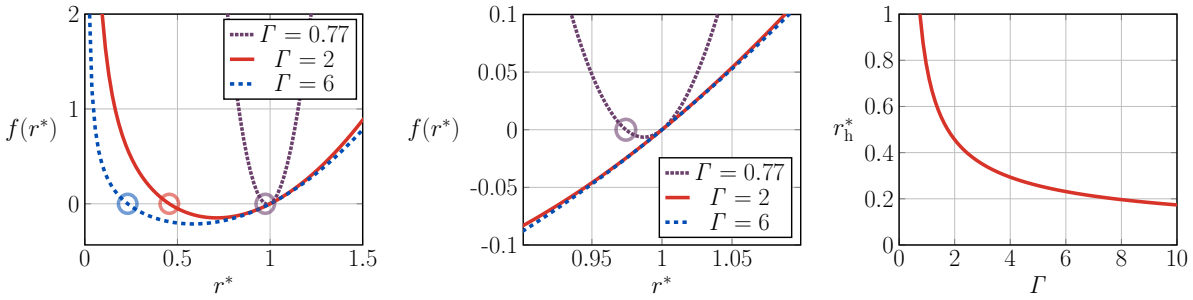

(a) forcing (b) forcing near $r^* = 1$ (c) homogeneous radius

Figure 15: (a),(b): Plots of the weakly nonlinear forcing term $f(r^*)$ in Eq. (241), at three different Föppl–von Kármán numbers: $\Gamma = 0.77$, $\Gamma = 2$, and $\Gamma = 6$. Open circles indicate stable solutions where $f(r^*) = 0$. Here, (b) shows a zoom of the forcing term near $r^* = 1$. (c) Plot of the homogeneous radius $r^*_{\rm h}$, as a function of the Föppl–von Kármán number, for all unstable $\Gamma > \Gamma_{\rm c}$.

(c). The comparison of weakly and fully nonlinear simulations

We now compare numerical simulations of the weakly nonlinear evolution equation (240) and the fully nonlinear axisymmetric equations (208)–(215). In all simulations, we choose for the physical dimensions to be set by the initial radius R, the bending modulus $k_{\rm b}$, and the intramembrane viscosity ζ; these fundamental parameters are set to unity in our numerical implementation. In this manner, the only remaining free parameters are the cylinder length L (expressed in units of R), the base surface tension Λ (expressed in units of $k_{\rm b}/R^2$), and the base flow velocity [expressed in units of $k_{\rm b}/(\zeta R)$]. Given our choice of fundamental parameters, there is no longer a distinction between dimensional and dimensionless quantities [cf. Eq. (108)]; we accordingly drop the '$*$' accent for the remainder of this section. Moreover, the base tension is identical to the Föppl–von Kármán number, and the base flow velocity is identical to the Scriven–Love number. Accordingly, each base state is completely specified by choosing the three parameters L, Γ, and $\mathcal{SL}$.

Once the base state is chosen, we apply an initial perturbation at time $t = 0$. For all of the results presented here, we apply an inward Gaussian disturbance, such that the initial radius is given by

$$r(z, t = 0) \;=\; R\left[\,1 \;-\; \epsilon\, \exp\left(\,-\,\frac{(z-\bar{\mu})^2}{2\sigma^2}\right)\right], \tag{243}$$

where the Gaussian is centered at $z = \bar{\mu}$ and has half-width $\sigma = 2R$. In Eq. (243) and from now on, $\epsilon = 10^{-3}$ is a small parameter. Additionally, we relate the axial and area parametrizations of an unperturbed tube via $z = a/(2\pi R)$, for which $a \in [0, 2\pi RL]$.

Fully nonlinear simulations: Tube with a base flow

The fully nonlinear equations (208)–(215) are solved with an in-house code similar to that described in our prior work,[‡] which employs the boundary-value problem solver `BVP5C` in

[‡]Omar et al., "Non-axisymmetric shapes of biological membranes from locally induced curvature".

MATLAB—suitable for a system of first-order ordinary differential equations. The eight corresponding boundary conditions for a tube with a base flow are given by

$$\begin{aligned} r(0) &= R\,, & z(0) &= 0\,, & \lambda(0) &= \Lambda\,, & H(0) &= H_0\,, \\ u(0) &= u_0\,, & w(0) &= 0\,, & \varphi(A) &= \varphi_0\,, & \mathcal{L}(A) &= 0\,, \end{aligned} \tag{244}$$

where for notational convenience we introduced the following quantities to correspond to an unperturbed tube:

$$H_0 := \frac{-1}{2R}\,, \qquad \varphi_0 := \frac{\pi}{2}\,, \qquad u_0 := 2\pi R\,Sl\,, \qquad \text{and} \qquad A := 2\pi RL\,. \tag{245}$$

We also centered the initial perturbation at $\bar{\mu} = L/4$, where L was chosen to be large enough that the simulation results were not affected by the finite size of the system.

The results of our nonlinear simulations, for a tube with $\Gamma = 6$ and $Sl/Sl_{\text{ac}} = 0.25$ and 2, are reported in Fig. 16; see also Movies M1–M3. We observe that a thin, atrophied tube develops in the wake of the propagating fronts. This tube is connected to the unperturbed regions via a monotonic shape transition, as predicted by the linear theory for $\Gamma > \Gamma_2$. In addition, Fig. 16 highlights the qualitative difference between absolutely and convectively unstable systems, when we inquire into the long-time response as seen by a stationary observer—for example, one stationed at the vertical dashed line. In the absolutely unstable case ($Sl = 0.25\,Sl_{\text{ac}}$, left column), our observer sees a deformed configuration, while in the convectively unstable case ($Sl = 2\,Sl_{\text{ac}}$, right column), the observer sees an undeformed configuration at long times, even as the disturbance grows while it is swept downstream.

In both cases, the leading and trailing front speeds are calculated numerically and compared to the linear prediction of Eq. (187), as shown in Fig. 17. It is well-known that a front can be either 'pulled' at the leading edge or 'pushed' by the growing nonlinearities behind the front, however one cannot in general anticipate which type of front will emerge from a local perturbation to invade a given nonlinear system. [‡, †] Our numerical simulations reveal the trailing edge is a pulled front, where the front speed agrees with the marginal stability criterion, while the leading edge is a pushed front traveling faster than what the marginal stability criterion predicts (Fig. 17). In the latter case, the front speed agrees with the linear theory at early times when perturbations are small (Fig. 17 insets).

Fully nonlinear simulations: Tube with no base flow

We now investigate the pattern selection mechanism in the wake of propagating fronts by simulating membrane tubes without a base flow, at different values of the Föppl–von Kármán number. Such a tube is symmetric about the center of our Gaussian perturbation (243), which we choose to be at $\bar{\mu} = 0$. Accordingly, only half the domain is simulated, for which the boundary conditions are given by

$$\begin{aligned} \varphi(0) &= \varphi_0\,, & z(0) &= 0\,, & u(0) &= 0\,, & \mathcal{L}(0) &= 0\,, \\ \varphi(A) &= \varphi_0\,, & \lambda(A) &= \Lambda\,, & w(A) &= 0\,, & \mathcal{L}(A) &= 0\,. \end{aligned} \tag{246}$$

[‡] van Saarloos, "Front propagation into unstable states. II. Linear versus nonlinear marginal stability and rate of convergence".

[†] W. van Saarloos. "Front propagation into unstable states". *Phys. Rep.* **386** (2003), 29–222. arXiv: cond-mat/0308540.

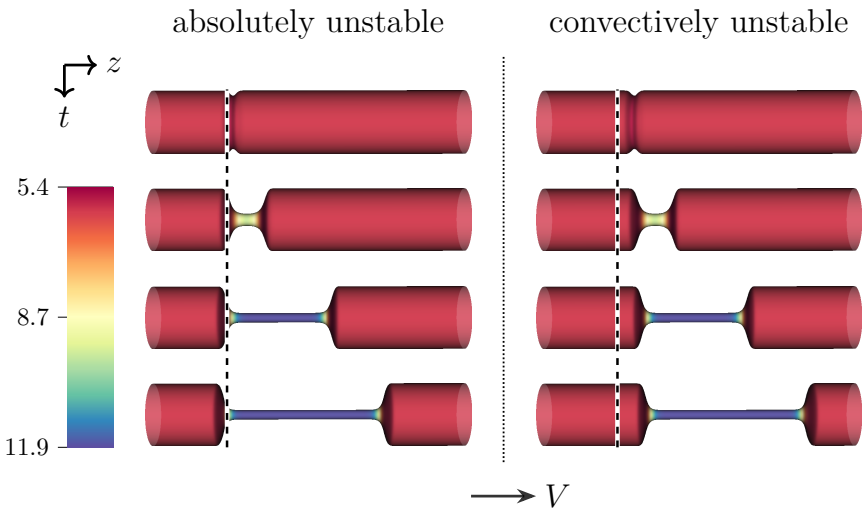

Figure 16: Successive snapshots from fully nonlinear simulations of an unstable membrane tube, with $\Gamma = 6$ (see also Movies M1–M3). An initial, local perturbation is applied at the vertical dashed line at a single instant in time. As the tube is unstable, the initial disturbance grows, saturates, and eventually forms two fronts that propagate outwards. In the left column, $SL = 0.25 SL_{\rm ac}$ and the tube is absolutely unstable, for which every stationary observer will see a perturbed system at late times. The tube on the right is convectively unstable, with $SL = 2SL_{\rm ac}$, such that any stationary observer sees and undeformed tube at long times. Here, flow is in the positive z-direction, the color bar indicates surface tension, and snapshots are scaled by a factor of 40 in the z-direction. The front velocities in these two cases are quantified in Fig. 17.

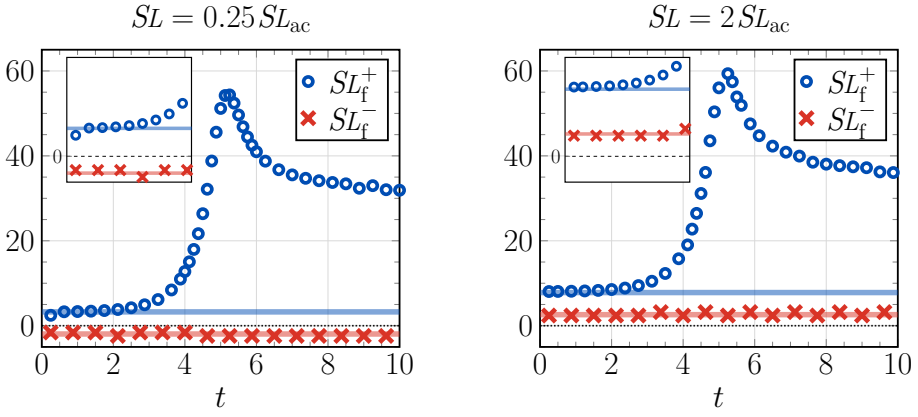

Figure 17: Plots of the leading (blue circles) and trailing (red crosses) front velocities over time, where $\Gamma = 6$ and $SL/SL_{\rm ac} = 0.25$ and 2 (cf. Fig. 16). Symbols correspond to simulations and lines are predictions from the marginal stability criterion (187). The insets show front speeds at early times, and confirm the trailing front moves to the left for $SL < SL_{\rm ac}$ and to the right for $SL > SL_{\rm ac}$; the leading front moves to the right in both cases. Additionally, the trailing front is a pulled front that travels at the speed predicted by the linear theory, while the leading front is a pushed front traveling faster than the linear prediction. However, at early times when deformations are small, both front speeds agree with the linear theory (see insets).

The results of our nonlinear simulations at three choices of the Föppl–von Kármán number, namely $\Gamma = 0.77 \in [\Gamma_c, \Gamma_1]$, $\Gamma = 2 \in (\Gamma_1, \Gamma_2)$, and $\Gamma = 6 > \Gamma_2$, are shown as solid lines in Fig. 18; see also Movies M4–M7. We once again see an agreement with the pattern predict by the marginal stability criterion: when $\Gamma \in [\Gamma_c, \Gamma_1] \cup [\Gamma_2, \infty)$, the front evolves with a steadily trailing envelope (Fig. 18a,c). On the other hand, if $\Gamma \in (\Gamma_1, \Gamma_2)$ then (i) the front has an oscillatory structure in both space and time, (ii) a pattern is selected in the wake of the front, and (iii) a pearled morphology develops to connect the thin and unperturbed cylindrical regions (Fig. 18b). We thus confirm that the value of the Föppl–von Kármán number governs whether or not a pattern is selected as a front propagates.

As it turns out, the oscillating fronts arising when $\Gamma \in (\Gamma_1, \Gamma_2)$ lead to numerical difficulties: the front sheds oscillatory modes, some of which reflect off the right boundary and contaminate the computational domain. To prevent such reflections, we follow past numerical developments in open flow systems [‡] and introduce a so-called sponge zone to dampen would-be reflected waves. In particular, when simulating a tube with area $A = 2\pi RL$, we extend our computational domain to have area $1.5A$; in the final third of the domain we also increase the numerical value of the intramembrane viscosity ζ to dampen reflected oscillatory modes. Denoting $\zeta_{\rm sim}$ as the value of the parameter used in numerical simulations, we have

$$\frac{\zeta_{\rm sim}}{\zeta} = \begin{cases} 1 & 0 \le a \le A \ , \\ 1 + 2\left[1 + \exp\left(\dfrac{\delta_{\rm r}}{a - A} - \dfrac{\delta_{\rm r}}{a + \delta_{\rm r} - A}\right)\right]^{-1} & A < a \le A + \delta_{\rm r} \\ 3 & a > A + \delta_{\rm r} \ , \end{cases} \tag{247}$$

where $\delta_{\rm r}$ is the length of the region over which the viscosity ramps up—here set to $0.25A$. We note that the size of the sponge zone, the ramp up length, and the maximum value of $\zeta_{\rm sim}$ were varied until oscillatory modes were no longer reflected into the domain, and are valid only for the specific problem at hand. As a validation test, we applied a sponge zone to simulations in which $\Gamma > \Gamma_2$ and no oscillations were expected; we found the numerical results were completely unchanged in this case.

Weakly nonlinear simulations

We end our presentation of numerical results by returning to the weakly nonlinear evolution equation (240). We solve Eq. (240) with the finite element solver `FreeFEM++`, [†] with the fourth-order spatial derivative necessitating the boundary conditions

$$r(-L) = 1 \ , \qquad r_{,z}(-L) = 0 \ , \qquad r(L) = 1 \ , \qquad \text{and} \qquad r_{,z}(L) = 0 \ . \tag{248}$$

We note that the boundary conditions in Eq. (248) are applied regardless of whether or not there is a base flow; in all cases, the entire domain is simulated. For ease in comparison with the fully nonlinear results, the weakly nonlinear shape profiles are plotted in terms of the unscaled axial position z and time t, rather than their scaled counterparts Z and T introduced in Eq. (178).

[‡] J.-M. Chomaz. "Fully nonlinear dynamics of parallel wakes". *J. Fluid Mech.* **495** (2003), 57–75.
[†] F. Hecht. "New development in FreeFem++". *J. Numer. Math.* **20** (2012), 251–265.

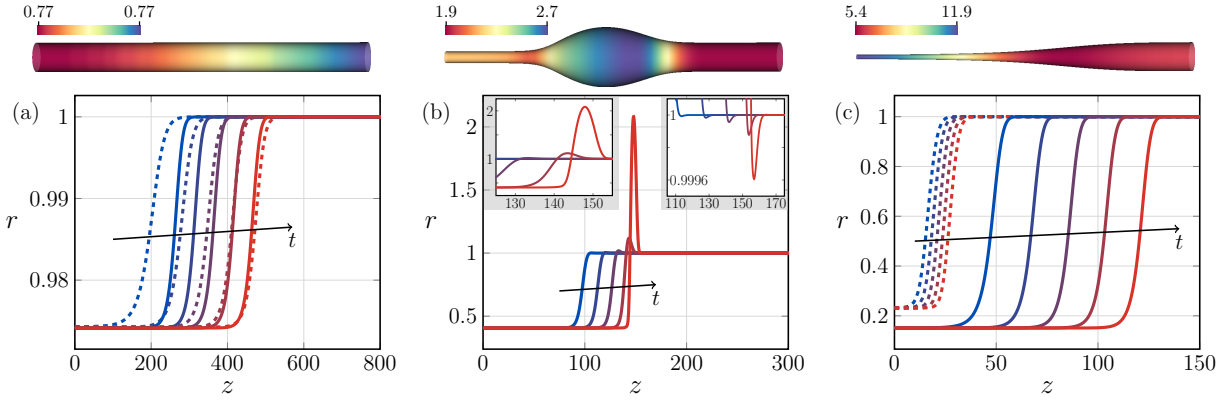

Figure 18: Plots of propagating fronts over time, with no base flow ($SL = 0$) and (a) $\Gamma = 0.77 \in [\Gamma_c, \Gamma_1]$, (b) $\Gamma = 2 \in (\Gamma_1, \Gamma_2)$, and (c) $\Gamma = 6 \in [\Gamma_2, \infty)$. Solid (respectively dashed) lines are results from nonlinear simulations (respectively the weakly nonlinear evolution equation). Snapshots are separated by (a) 1000τ, (b) 10τ, and (c) τ. A portion of the tube at the final snapshot is shown above each plot (color bars indicate surface tension); see also Movies M4–M7. When $\Gamma \in (\Gamma_1, \Gamma_2)$ as in (b), the front leaves pearls in its wake (left inset) and oscillates at the leading edge (right inset), in agreement with the linear theory. The outward bulges in this case cause the weakly nonlinear evolution equation (240) to fail.

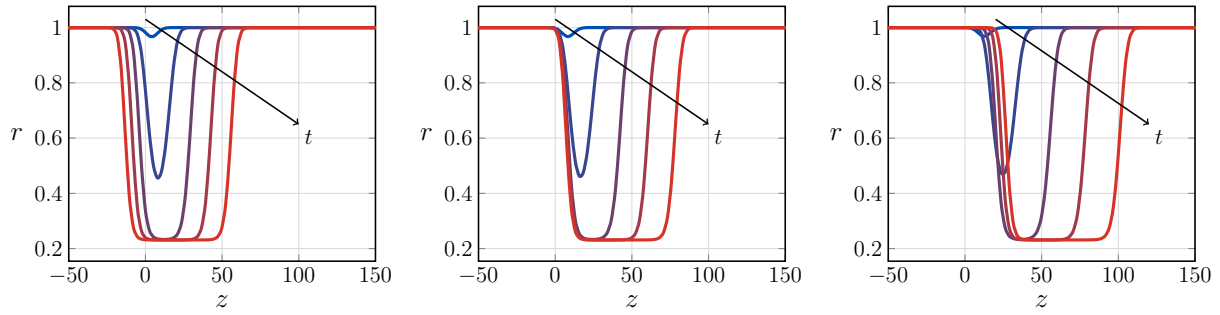

(a) $SL = 0.5\,SL_{ac}$ (b) $SL = SL_{ac}$ (c) $SL = 1.5\,SL_{ac}$

Figure 19: Snapshots from simulations of the weakly nonlinear evolution equation (240), at three different base flow speeds, with $\Gamma = 6$. In all cases, the initial perturbation is at $z = 0$, snapshots are separated by $\approx 3\tau$, and the perturbation saturates to form a thin tube with radius $r_h(\Gamma = 6) \approx 0.23$. The leading front travels to the right, while the trailing front (a) travels to the left when $SL < SL_{ac}$, (b) remains stationary when $SL = SL_{ac}$, and (c) travels to the right when $SL > SL_{ac}$. The simulations reveal the weakly nonlinear evolution equation gives rise to pulled fronts, which travel at the speed predicted by the linear theory.

Predictions from the weakly nonlinear model (248) and direct numerical simulations of the nonlinear equations are compared in Fig. 18, from which we make several observations. First, both sets of dynamics result in a thin, atrophied tube behind the front, with the weakly nonlinear atrophied radius given by Eq. (242). We also find that for $\Gamma \notin (\Gamma_1, \Gamma_2)$, the evolution equation serves as a good predictor of the front speed and final radius as $\Gamma \to \Gamma_c^+$ (Fig. 18a), while it only predicts r_h at large Γ (Fig. 18c). On the other hand, when $\Gamma \in (\Gamma_1, \Gamma_2)$, the front oscillates at the leading edge and the quadratic forcing terms in $f(r)$ amplify outward perturbations ($r > 1$), such that the weakly nonlinear model predicts an unphysical, diverging radius at finite times. [‡] Despite the quantitative shortcomings of the weakly nonlinear evolution equation (240), it still provides (*i*) a connection to previous studies of nonlinear dynamics and pattern formation, and (*ii*) a qualitative understanding of front propagation. In addition, simulation results for the weakly nonlinear equation, with and without a base flow, are reported in Figs. 18 and 19. We find a local disturbance gives rise to pulled fronts that travel at the speed predicted by the linear theory. Importantly, as the evolution equation (240) agrees with nonlinear simulations when $\Gamma \to \Gamma_c^+$, we expect the front velocity of an initially static tube to scale as $\mathcal{SL}_f \sim \mathcal{SL}_{ac} \sim (\Gamma - \Gamma_c)^{1/2}$ near the instability threshold [cf. Eqs. (171) and (187)].

(d). The analysis of local perturbations in experiments

With the results of the linear and nonlinear stability analysis, we now seek to determine if our predictions are observed in experiments. In particular, we would first like to see if the Föppl–von Kármán number indeed governs whether or not a pearled morphology develops in the wake of the moving fronts. Next, we seek to compare the front speeds observed in experiments to our calculated values—with the understanding that the pulled front speed determined by the marginal stability criterion is a lower bound for the speed of the nonlinear, pushed fronts exhibited by the full membrane equations. Finally, we search for biological systems with a base flow that are convectively unstable.

In what follows, we compare our results with experimental measurements from two prior studies: one involving *in vitro* tethers subject to a localized laser pulse, [†] and another applying various disturbances to stationary axons. [*] Although there are many other experimental investigations subjecting membrane tubes to localized disturbances, we limit our comparison to these two studies because all of our theoretical predictions require knowledge of the Föppl–von Kármán number—which often cannot be determined from experimental data due to incomplete measurements of the membrane tension [see discussion in §1 (a)]. Even in the aforementioned studies that we do consider, there are situations where sufficient data are not reported for us to test our theories. In such cases, however, we demonstrate that the data are consistent with our findings. We hope this agreement motivates future experimental investigations, so as to better test our theoretical understanding of membrane tubes.

[‡]Tchoufag, Sahu, and Mandadapu, "Absolute vs convective instabilities and front propagation in lipid membrane tubes".

[†]R. Bar-Ziv, E. Moses, and P. Nelson. "Dynamic excitations in membranes induced by optical tweezers". *Biophys. J.* **75** (1998), 294–320.

[*]Datar et al., "The roles of microtubules and membrane tension in axonal beading, retraction, and atrophy".

Stationary *in vitro* tethers: Front propagation

We begin by considering the measurements described by Bar-Ziv et al., [‡] in which a localized laser pulse is applied to artificial membrane tethers. As the tube is held stationary, the Scriven–Love number $\mathcal{SL} = 0$ in all experiments. In addition, before the laser is applied, the tether is stable and $\Gamma < \Gamma_c$. Upon application of the laser at time $t = 0$, the membrane tension is rapidly modified along the entire cylinder such that $\Gamma > \Gamma_c$ everywhere; the laser also disturbs the membrane shape at one location. [†] Accordingly, the system is well-characterized as an unstable tube with constant base tension, subject to a localized shape perturbation.

Interestingly, Bar-Ziv et al. report both the dimensionless tension and the dimensionless front speed in their study (see Fig. 11 of their manuscript). [‡] However, their characterization of the membrane dynamics did not include the intramembrane viscosity ζ, and thus their front velocity was non-dimensionalized with the shear viscosity μ of the surrounding fluid—taken to be $\mu = 10^{-3}$ pN $\cdot$ μsec/nm^2. To express the presented data in terms of the dimensionless numbers employed in the present study, namely the Föppl–von Kármán number Γ and the Scriven–Love number of the front $\mathcal{SL}_f$, we recognize

$$\Gamma = \frac{3}{4} \cdot \Big\{ \text{presented dimensionless tension} \Big\} \tag{249}$$

and

$$\mathcal{SL}_f = \frac{\zeta}{2\mu R} \cdot \Big\{ \text{presented dimensionless velocity} \Big\} , \tag{250}$$

where both quantities in curly braces refer to the experimentally reported measurements. [‡] For the choice $\zeta = 10$ pN $\cdot$ μsec/nm [*, §] used throughout this work, we reproduce the presented experimental data in terms of our own dimensionless quantities in Fig. 20. [♯]

From Fig. 20, we immediately notice several consistencies between our theory and the reported experimental data. First, for any choice of Γ, the data lie above the calculated value of $\mathcal{SL}_{ac}(\Gamma)$ predicted by the linear theory—as we expect for pushed fronts. Next, the experimental investigation reports that only pearled fronts were observed upon application of the laser. Since all data (to within experimental uncertainty) lie within the range $\Gamma \in (\Gamma_1, \Gamma_2)$, such a finding is again consistent with our theoretical prediction. Finally, we note that the nonlinear front speed converges to $\mathcal{SL}_{ac}(\Gamma)$ as $\Gamma \to \Gamma_c^+$, in which case we expect $\mathcal{SL}_f = \mathcal{SL}_{ac} \sim (\Gamma - \Gamma_c)^{1/2}$ near the instability threshold. Figure 20 indeed exhibits this power law scaling about Γ_c, and in this manner we justify the observed front speeds near the instability threshold—a behavior that was previously unexplained.

[‡] Bar-Ziv, Moses, and Nelson, "Dynamic excitations in membranes induced by optical tweezers"

[†] R.E. Goldstein et al. "Front propagation in the pearling instability of tubular vesicles". *J. Phys. II* **6** (1996), 767–796.

[*] Cicuta, Keller, and Veatch, "Diffusion of liquid domains in lipid bilayer membranes".

[§] Honerkamp-Smith et al., "Membrane viscosity determined from shear-driven flow in giant vesicles".

[♯] As mentioned previously, the ratio $\zeta/(\mu R)$ is a dimensionless quantity known as the Boussinesq number *Bo*, which contributes to the membrane behavior when the dynamics of the surrounding fluid are taken into account.

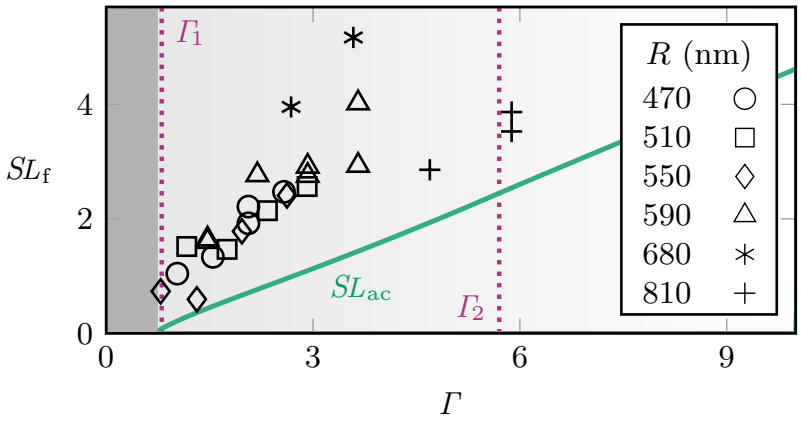

Figure 20: The dimensionless front velocity as a function of the dimensionless surface tension, for tubes of different radii R (see provided symbols), obtained from Fig. 11 of R. Bar-Ziv, E. Moses, and P. Nelson. "Dynamic excitations in membranes induced by optical tweezers". *Biophys. J.* **75** (1998), 294–320. The experimental data from this study are represented in terms of Γ and $SL_{\rm f}$ via Eqs. (249) and (250). In all cases, the measured front speed is larger than the absolute-to-convective transition speed $SL_{\rm ac}$ (solid green line)—as expected. The purple dashed lines delineate the range (Γ_1, Γ_2) within which fronts are predicted to pearl—a prediction again consistent with experimental measurements.

Front propagation in stationary axons

We next investigate the experimental study by Datar et al., [‡] which presents data on how axons respond to a variety of different local perturbations, from which outwardly propagating fronts ensue. Since there is initially no base flow of lipids before the neuron is disturbed, $SL = 0$ in these experiments. Moreover, as the study was primarily concerned with understanding molecular mechanisms, it often did not provide sufficient data for us to quantitatively calculate Γ and $SL_{\rm f}$ in experiments—especially when the tube was perturbed by a laser. Nonetheless, in what follows, we show the experimental measurments involving local drug treatments are consistent with our theoretical predictions.

We analyze experiments involving two different drug treatments: Nocodazole (Noco) and Latrunculin A (LatA), with all data reproduced from Table S2 of the Supplemental Material of Datar et al. [‡] At a low Noco concentration, the axons were either stable ($\Gamma < \Gamma_{\rm c}$, 16% of axons), formed fronts without pearls ($\Gamma \in [\Gamma_{\rm c}, \Gamma_1]$, 13% of axons), or formed fronts with pearls ($\Gamma \in (\Gamma_1, \Gamma_2)$, 71% of axons). We assume the Föppl–von Kármán number of all perturbed axons were close to one another in this experiment, and thus expect Γ to be closer to Γ_1 than Γ_2 in the pearled systems. Our hypothesis is consistent with experimental results where the Noco concentration was increased, thereby increasing the base tension and shifting the range of Föppl–von Kármán numbers upwards. In this case, all axons developed fronts ($\Gamma > \Gamma_{\rm c}$), with 5% not pearling ($\Gamma \in [\Gamma_{\rm c}, \Gamma_1]$) and 95% pearling [$\Gamma \in (\Gamma_1, \Gamma_2)$]. A similar result was observed with LatA, with fronts developing in all cases: at low concentrations, only 3% of axons pearled, while at higher concentrations 19% of axons pearled. Again, increasing

[‡]Datar et al., "The roles of microtubules and membrane tension in axonal beading, retraction, and atrophy"

the concentration of LatA caused the distribution of Föppl–von Kármán numbers to shift upwards, such that a higher proportion of axons satisfied $\Gamma > \Gamma_1$ and thus formed beads-on-a-string morphologies. In both cases, the experimental findings of local drug administration are qualitatively consistent with our theoretical results.

For a more quantitative analysis, we turn to Fig. S4 of the Supplemental Material of Datar et al. [‡] From part (A) of the figure, we see pearling front speeds vary from 70–200 nm/sec, while in part (B) monotonic fronts retract at speeds ranging from 10–70 nm/sec. Though sufficient data is not reported for us to calculate either Γ or SL_f, we can show the experimental observations are consistent with our theory. We begin by noting that for a range of characteristic values for the bending modulus, viscosity, and radius of an axon, we expect $SL_\mathrm{f} \ll 1$ over all reported front speeds. In this case, we also expect to be close to the instability threshold, such that $\Gamma - \Gamma_\mathrm{c} \ll 1$—a result consistent with the above analysis of Noco and LatA experiments. With this understanding, we recall that for Föppl–von Kármán numbers near the instability threshold, the fully nonlinear front speed is well-predicted by $SL_\mathrm{ac}(\Gamma)$. Moreover, as we predict a transition from monotonic to pearled fronts at $\Gamma = \Gamma_1 \approx 0.805$, we expect $SL_\mathrm{f}(\Gamma_1) \approx SL_\mathrm{ac}(\Gamma_1) \approx 0.08$ to be the dimensionless front speed at which the front morphology transitions. The corresponding dimensional front speed at which the transition was observed in experiments is $V_\mathrm{f} \approx 70$ nm/sec. We posit the following values of material parameters to be consistent with the observations: $R = 600$ nm, $\zeta = 300$ pN $\cdot$ μsec/nm, and $k_\mathrm{b} = 150$ pN $\cdot$ nm. With this hypothesis, we can then translate the entire range of observed velocities (10–200 nm/sec) to their dimensionless counterparts, and extract the corresponding range of Föppl–von Kármán numbers as $\Gamma \in (0.75, 1)$. Thus, despite not being able to make quantitative predictions based on the available data, our finding of a monotonic to pearled bifurcation in the front shape is consistent with the experimental data. However, the nonlinear morphologies observed in experiments (see, e.g. Figs. 1(a) and 3(a) of Datar et al. [‡]) are more atrophied than those in our simulations, suggesting additional phenomena arise in the neuronal environment—which is not surprising, given that neurons are significantly more complex than the membrane tubes considered in the present work.

(e). Supplemental movies

Here we describe several movies of the fully nonlinear membrane dynamics, as described in §8 (c). In all cases, the time is provided in units of $\tau = \zeta R^2/k_\mathrm{b}$ (107), the color indicates the surface tension, and the vertical black arrow indicates the location of an initially local perturbation. All movies can be found at the following case-sensitive hyperlink:

youtube.com/playlist?list=PLuzng8nroSCu-0pQE-PrhfwzdeSMfUeS6

M1. Local inward perturbation, with $\Gamma = 6$ and $SL = 0.25\,SL_\mathrm{ac}$. See also Figs. 16 and 17.

M2. Local inward perturbation, with $\Gamma = 6$ and $SL = SL_\mathrm{ac}$.

M3. Local inward perturbation, with $\Gamma = 6$ and $SL = 2\,SL_\mathrm{ac}$. See also Figs. 16 and 17.

[‡]Datar et al., "The roles of microtubules and membrane tension in axonal beading, retraction, and atrophy"

M4. Local inward perturbation, with $\Gamma = 0.77$ and $\mathcal{SL} = 0$. See also Fig. 18a.

M5. Early-time behavior in response to a local inward perturbation, with $\Gamma = 2$ and $\mathcal{SL} = 0$. The front appears to propagate monotonically. See also Fig. 18b.

M6. Late-time behavior in response to a local inward perturbation, with $\Gamma = 2$ and $\mathcal{SL} = 0$. Oscillations at the leading edge grow and saturate to form a pearled morphology in the near wake of the front, which connects the atrophied and unperturbed regions. See also Fig. 18b.

M7. Local inward perturbation, with $\Gamma = 6$ and $\mathcal{SL} = 0$. See also Fig. 18c.

References

[1] A. Agrawal and D.J. Steigmann. "Modeling protein-mediated morphology in biomembranes". *Biomech. Model. Mechan.* **8** (2009), 371–379

[2] R. Bar-Ziv and E. Moses. "Instability and "pearling" states produced in tubular membranes by competition of curvature and tension". *Phys. Rev. Lett.* **73** (1994), 1392–1395

[3] R. Bar-Ziv, E. Moses, and P. Nelson. "Dynamic excitations in membranes induced by optical tweezers". *Biophys. J.* **75** (1998), 294–320

[4] R. Bar-Ziv, T. Tlusty, and E. Moses. "Critical dynamics in the pearling instability of membranes". *Phys. Rev. Lett.* **79** (1997), 1158–1161

[5] E. Ben-Jacob et al. "Pattern propagation in nonlinear dissipative systems". *Physica D* **14** (1985), 348–364

[6] A. Bers and R.J. Briggs. "Criteria for determining absolute instability and distinguishing between amplifying and evanescent waves". *Bull. Am. Phys. Soc.* **9** (1963), 304

[7] G. Boedec, M. Jaeger, and M. Leonetti. "Pearling instability of a cylindrical vesicle". *J. Fluid Mech.* **743** (2014), 262–279

[8] C.V. Boys. *Soap Bubbles: Their Colors and the Forces Which Mold Them*. New York: Dover, 1959

[9] R.J. Briggs. *Electron-Stream Interactions with Plasmas*. MIT Press, 1964

[10] S. Chandrasekhar. *Hydrodynamic and Hydromagnetic Stability*. New York: Dover, 1981

[11] F. Charru. *Hydrodynamic Instabilities*. New York: Cambridge University Press, 2011

[12] J.-M. Chomaz. "Fully nonlinear dynamics of parallel wakes". *J. Fluid Mech.* **495** (2003), 57–75

[13] J.-M. Chomaz and A. Couairon. "Propagating pattern selection and causality reconsidered". *Phys. Rev. Lett.* **84** (2000), 1910–1913

[14] P. Cicuta, S.L. Keller, and S.L. Veatch. "Diffusion of liquid domains in lipid bilayer membranes". *J. Phys. Chem. B* **111** (2007), 3328–3331. arXiv: `cond-mat/0611492`

[15] P. Coullet, C. Elphick, and D. Repaux. "Nature of spatial chaos". *Phys. Rev. Lett.* **58** (1987), 431–434

[16] M. Cross and H. Greenside. *Pattern Formation and Dynamics in Nonequilibrium Systems*. New York: Cambridge University Press, 2009

[17] M.C. Cross and P.C. Hohenberg. "Pattern formation outside of equilibrium". *Rev. Mod. Phys.* **65** (1993), 851–1112

[18] D. Cuvelier et al. "Coalescence of membrane tethers: Experiments, theory, and applications". *Biophys. J.* **88** (2005), 2714–2726

[19] J.B. Dahl et al. "Experimental observation of the asymmetric instability of intermediate-reduced-volume vesicles in extensional flow". *Soft Matter* **12** (2016), 3787–3796

[20] J. Dai and M.P. Sheetz. "Axon membrane flows from the growth cone to the cell body". *Cell* **83** (1995), 693–701

[21] J. Dai and M.P. Sheetz. "Mechanical properties of neuronal growth cone membranes studied by tether formation with laser optical tweezers". *Biophys. J.* **68** (1995), 988–996

[22] A. Datar et al. "Dynamics of membrane tethers reveal novel aspects of cytoskeleton–membrane interactions in axons". *Biophys. J.* **108** (2015), 489–497

[23] A. Datar et al. "The roles of microtubules and membrane tension in axonal beading, retraction, and atrophy". *Biophys. J.* **117** (2019), 880–891

[24] G.T. Dee and J.S. Langer. "Propagating pattern selection". *Phys. Rev. Lett.* **50** (1983), 383–386

[25] G.T. Dee and W. van Saarloos. "Bistable systems with propagating fronts leading to pattern formation". *Phys. Rev. Lett.* **60** (1988), 2641–2644

[26] P.G. Dommersnes et al. "Marangoni transport in lipid nanotubes". *Europhys. Lett.* **70** (2005), 271–277

[27] C. Duprat et al. "Absolute and convective instabilities of a viscous film flowing down a vertical fiber". *Phys. Rev. Lett.* **98** (2007), 244502

[28] J. Eggers and E. Villermaux. "Physics of liquid jets". *Rep. Prog. Phys.* **71** (2008), 036601

[29] E.A. Evans and A. Yeung. "Hidden dynamics in rapid changes of bilayer shape". *Chem. Phys. Lipids* **73** (1994), 39–56

[30] J.-B. Fournier et al. "Chemically triggered ejection of membrane tubules controlled by intermonolayer friction". *Phys. Rev. Lett.* **102** (2009), 018102

[31] R.E. Goldstein et al. "Front propagation in the pearling instability of tubular vesicles". *J. Phys. II* **6** (1996), 767–796

[32] R. Granek and Z. Olami. "Dynamics of Rayleigh-like instability induced by laser tweezers in tubular vesicles of self-assembled membranes". *J. Phys. II* **5** (1995), 1349–1370

[33] K.L. Gurin, V.V. Lebedev, and A.R. Muratov. "Dynamic instability of a membrane tube". *J. Expl. Theor. Phys.* **83** (1996), 321–326

[34] F. Hecht. "New development in FreeFem++". *J. Numer. Math.* **20** (2012), 251–265

[35] A.R. Honerkamp-Smith et al. "Membrane viscosity determined from shear-driven flow in giant vesicles". *Phys. Rev. Lett.* **111** (2013), 038103. arXiv: 1308.6440

[36] R.M. Hornreich, M. Luban, and S. Shtrikman. "Critical behavior at the onset of $\vec{k}$-instability on the λ-line". *Phys. Rev. Lett.* **35** (1975), 1678–1681

[37] P. Huerre and P.A. Monkewitz. "Local and global instabilities in spatially developing flows". *Annu. Rev. Fluid Mech.* **22** (1990), 473–537

[38] P. Huerre and M. Rossi. "Hydrodynamic instabilities in open flows". *Hydrodynamics and Nonlinear Instabilities*. Ed. by C. Godrèche and P. Manneville. New York: Cambridge University Press, 1998, pp. 81–294

[39] S.C. Al-Izzi et al. "Hydro-osmotic instabilities in active membrane tubes". *Phys. Rev. Lett.* **120** (2018), 138102. arXiv: 1709.02703

[40] C. Kaether, P. Skehel, and C.G. Dotti. "Axonal membrane proteins are transported in distinct carriers: A two-color video microscopy study in cultured hippocampal neurons". *Mol. Biol. Cell* **11** (2000), 1213–1224

[41] V. Kantsler, E. Segre, and V. Steinberg. "Critical dynamics of vesicle stretching transition in elongational flow". *Phys. Rev. Lett.* **101** (2008), 048101

[42] G. Koster et al. "Membrane tube formation from giant vesicles by dynamic association of motor proteins". *Proc. Natl. Acad. Sci. U.S.A.* **100** (2003), 15583–15588

[43] L. Kramer et al. "New results on the electrohydrodynamic instability in nematics". *Liq. Cryst.* **5** (1989), 699–715

[44] K. Kupfer, A. Bers, and A.K. Ram. "The cusp map in the complex-frequency plane for absolute instabilities". *Phys. Fluids* **30** (1987), 3075–3082

[45] C. Leduc et al. "Cooperative extraction of membrane nanotubes by molecular motors". *Proc. Natl. Acad. Sci. U.S.A.* **101** (2004), 17096–17101

[46] C. Lee and L.-B. Chen. "Dynamic behavior of endoplasmic reticulum in living cells". *Cell* **54** (1988), 37–46

[47] L.-O. Merkine. "Convective and absolute instability of baroclinic eddies". *Geophys. Astro. Fluid* **9** (1977), 129–157

[48] S. Monnier et al. "Long-range protein coupling mediated by critical low-energy modes of tubular lipid membranes". *Phys. Rev. Lett.* **105** (2010), 028102

[49] F. Moser. "Convective and absolute instability of the positive column with longitudinal magnetic field". *Plasma Physics* **17** (1975), 821–840

[50] V. Narsimhan, A.P. Spann, and E.S.G. Shaqfeh. "Pearling, wrinkling, and buckling of vesicles in elongational flows". *J. Fluid Mech.* **777** (2015), 1–26

[51] P. Nelson, T. Powers, and U. Seifert. "Dynamical theory of the pearling instability in cylindrical vesicles". *Phys. Rev. Lett.* **74** (1995), 3384–3387

[52] J. Nixon-Abell et al. "Increased spatiotemporal resolution reveals highly dynamic dense tubular matrices in the peripheral ER". *Science* **354** (2016), aaf3928

[53] Y.A.D. Omar et al. "Non-axisymmetric shapes of biological membranes from locally induced curvature". *Biophys. J.* **119** (2020), 1065–1077

[54] R.T. Pierrehumbert. "Local and global baroclinic instability of zonally varying flow". *J. Atmos. Sci.* **41** (1984), 2141

[55] T.R. Powers et al. "Propagation of a topological transition: The Rayleigh instability". *Phys. Fluids* **10** (1998), 1052–1057. arXiv: cond-mat/9708169

[56] P.A. Pullarkat et al. "Osmotically driven shape transformations in axons". *Phys. Rev. Lett.* **96** (2006), 048104

[57] V. Rottschäfer and A. Doelman. "On the transition from the Ginzburg–Landau equation to the extended Fisher–Kolmogorov equation". *Physica D* **118** (1998), 261–292

[58] A. Roux et al. "A minimal system allowing tubulation with molecular motors pulling on giant liposomes". *Proc. Natl. Acad. Sci. U.S.A.* **99**.8 (2002), 5394–5399

[59] A. Rustom et al. "Nanotubular highways for intercellular organelle transport". *Science* **303** (2004), 1007–1010

[60] A. Sahu et al. "Arbitrary Lagrangian–Eulerian finite element formulation for curved and deforming surfaces. I. General theory and application to fluid interfaces". *J. Comp. Phys.* **407** (2020), 109253. arXiv: 1812.05086

[61] J. Sanborn et al. "Transient pearling and vesiculation of membrane tubes under osmotic gradients". *Faraday Discuss.* **161** (2013), 167–176

[62] B. Scheid, N. Kofman, and W. Rohlfs. "Critical inclination for absolute/convective instability transition in inverted falling films". *Phys. Fluids* **28** (2016), 044107

[63] Z. Shi et al. "Cell membranes resist flow". *Cell* **175** (2018), 1769–1779

[64] J. Tchoufag, A. Sahu, and K.K. Mandadapu. "Absolute vs convective instabilities and front propagation in lipid membrane tubes". *Phys. Rev. Lett.* **128** (2022), 068101. arXiv: 2008.13780

[65] M. Terasaki, L.B. Chen, and K. Fujiwara. "Microtubules and the endoplasmic reticulum are highly interdependent structures". *J. Cell Biol.* **103** (1986), 1557–1568

[66] S. Tomotika. "On the instability of a cylindrical thread of a viscous liquid surrounded by another viscous fluid". *Proc. R. Soc. Lond. A* **150** (1935), 322–337

[67] A. Torres-Sánchez, D. Millán, and M. Arroyo. "Modelling fluid deformable surfaces with an emphasis on biological interfaces". *J. Fluid Mech.* **872** (2019), 218–271. arXiv: 1812.02837

[68] A. Upadhyaya and M.P. Sheetz. "Tension in tubulovesicular networks of Golgi and endoplasmic reticulum membranes". *Biophys. J.* **86** (2004), 2923–2928

[69] W. van Saarloos. "Front propagation into unstable states". *Phys. Rep.* **386** (2003), 29–222. arXiv: cond-mat/0308540

[70] W. van Saarloos. "Front Propagation into Unstable States: Some Recent Developments and Surprises". *Nonlinear Evolution of Spatio-Temporal Structures in Dissipative Continuous Systems*. Ed. by F.H. Busse and L. Kramer. Boston: Springer US, 1990, pp. 499–508

[71] W. van Saarloos. "Front propagation into unstable states. II. Linear versus nonlinear marginal stability and rate of convergence". *Phys. Rev. A* **39** (1989), 6367–6390

[72] M. Yanagisawa, M. Imai, and T. Taniguchi. "Shape deformation of ternary vesicles coupled with phase separation". *Phys. Rev. Lett.* **100** (2008), 148102

[73] W. Zimmermann. "Propagating fronts near a Lifshitz point". *Phys. Rev. Lett.* **66** (1991), 1546–1546

Chapter X

Conclusions and Future Work

> *To those who do not know mathematics it is difficult to get across a real feeling as to the beauty, the deepest beauty, of Nature . . . Physicists cannot make a conversation to any other language. If you want to learn about Nature, to appreciate Nature, it is necessary to understand the language that She speaks in. She offers her information only in one form; we are not so unhumble as to demand that She change before we pay any attention.*
>
> —Richard P. Feynman, 1964 [‡]

In this thesis, we systematically studied the behavior of arbitrarily curved and deforming biological membranes. We first obtained the equations governing such materials through the framework of irreversible thermodynamics—which was applied in a differential geometric setting. [†] In particular, the local forms of the balance of mass, linear momentum, angular momentum, energy, and entropy were obtained, and the internal entropy production was subsequently determined. Recalling that the in-plane flow of lipids is irreversible, while the membrane deforms reversibly in the out-of-plane direction, our irreversible thermodynamic framework provided a natural way to develop constitutive relations for the stresses and couple-stresses in the material. The resultant equations of motion are identical to those of earlier studies that proposed constitutive forms of the viscous stresses. [*, §, ♯]

The lipid membrane equations are highly nonlinear, and exhibit intricate couplings between the in-plane and out-of-plane behavior. To probe this coupling, we determined and non-dimensionalized the equations governing small perturbations to three commonly occurring membrane geometries: flat patches, spherical vesicles, and cylindrical tubes. [‖] We found a new dimensionless number, namely the Scriven–Love number SL, comparing out-of-plane

[‡]R.P. Feynman. *The Character of Physical Law*. Cambridge: MIT Press, 1967.

[†]A. Sahu et al. "Irreversible thermodynamics of curved lipid membranes". *Phys. Rev. E* **96** (2017), 042409. arXiv: 1701.06495.

[*]D. Hu, P. Zhang, and W. E. "Continuum theory of a moving membrane". *Phys. Rev. E* **75** (2007), 041605.

[§]M. Arroyo and A. DeSimone. "Relaxation dynamics of fluid membranes". *Phys. Rev. E* **79** (2009), 31915–31931.

[♯]P. Rangamani et al. "Interaction between surface shape and intra-surface viscous flow on lipid membranes". *Biomech. Model. Mechan.* **12** (2012), 833–845.

[‖]A. Sahu et al. "Geometry and dynamics of lipid membranes: The Scriven–Love number". *Phys. Rev. E* **101** (2020), 052401. arXiv: 1910.10693.

viscous–curvature coupling forces to the well-known bending forces. Moreover, an analysis of past experiments revealed biologically relevant situations in which $\mathcal{SL} \geq 1$ in perturbed spheres and cylinders. In this manner, we demonstrated the in-plane flow of lipids cannot be ignored when characterizing biological membrane behavior. We hope our findings prompt future investigators to report characteristic velocities and surface tensions in experimental systems, as thus far such measurements are often omitted.

Our investigations into the stability of biological membranes motivate several theoretical extensions and numerical advancements. For example, we found both spherical vesicles and cylindrical tubes undergo a non-axisymmetric buckling instability when the base surface tension is negative. To determine the long-time response of biological membranes in such situations, advanced numerical methods are required to solve the membrane equations. [‡, †] Moreover, a linear stability analysis of planar membranes revealed the importance of including the surrounding fluid, which (i) provides another dissipative mode via the three-dimensional shear viscosity, and (ii) is especially relevant in the planar case, where to first order, the in-plane intramembrane viscosity does not affect the height modes. Once the hydrodynamics of the surrounding fluid are included, the normal stress jump $[\![p]\!]$ will no longer be constant: as the membrane deforms and displaces its surroundings, the bulk fluid stresses will have first-order corrections, which then enter the perturbed equations governing membrane dynamics. Moreover, when biological membranes undergo large deformations, the tractions they feel from the surrounding fluid can be significant. We thus expect bulk hydrodynamics to affect, for example, the long-time morphology of unstable membrane tubes subjected to either global or local disturbances—and the speed of the resultant fronts in the latter case. [*] Numerical methods that solve for the coupled membrane and fluid behavior are required to describe such phenomena.

References

[1] M. Arroyo and A. DeSimone. "Relaxation dynamics of fluid membranes". *Phys. Rev. E* **79** (2009), 31915–31931

[2] R.P. Feynman. *The Character of Physical Law*. Cambridge: MIT Press, 1967

[3] D. Hu, P. Zhang, and W. E. "Continuum theory of a moving membrane". *Phys. Rev. E* **75** (2007), 041605

[4] P. Rangamani et al. "Interaction between surface shape and intra-surface viscous flow on lipid membranes". *Biomech. Model. Mechan.* **12** (2012), 833–845

[‡] A. Sahu et al. "Arbitrary Lagrangian–Eulerian finite element formulation for curved and deforming surfaces. I. General theory and application to fluid interfaces". *J. Comp. Phys.* **407** (2020), 109253. arXiv: 1812.05086.

[†] A. Torres-Sánchez, D. Millán, and M. Arroyo. "Modelling fluid deformable surfaces with an emphasis on biological interfaces". *J. Fluid Mech.* **872** (2019), 218–271. arXiv: 1812.02837.

[*] J. Tchoufag, A. Sahu, and K.K. Mandadapu. "Absolute vs convective instabilities and front propagation in lipid membrane tubes". *Phys. Rev. Lett.* **128** (2022), 068101. arXiv: 2008.13780.

[5] A. Sahu et al. "Arbitrary Lagrangian–Eulerian finite element formulation for curved and deforming surfaces. I. General theory and application to fluid interfaces". *J. Comp. Phys.* **407** (2020), 109253. arXiv: 1812.05086

[6] A. Sahu et al. "Geometry and dynamics of lipid membranes: The Scriven–Love number". *Phys. Rev. E* **101** (2020), 052401. arXiv: 1910.10693

[7] A. Sahu et al. "Irreversible thermodynamics of curved lipid membranes". *Phys. Rev. E* **96** (2017), 042409. arXiv: 1701.06495

[8] J. Tchoufag, A. Sahu, and K.K. Mandadapu. "Absolute vs convective instabilities and front propagation in lipid membrane tubes". *Phys. Rev. Lett.* **128** (2022), 068101. arXiv: 2008.13780

[9] A. Torres-Sánchez, D. Millán, and M. Arroyo. "Modelling fluid deformable surfaces with an emphasis on biological interfaces". *J. Fluid Mech.* **872** (2019), 218–271. arXiv: 1812.02837